Springer Series in Optical Sciences 232

Alexander A. Bortsov
Yuri B. Il'in
Sergey M. Smolskiy

Laser Optoelectronic Oscillators

Springer

Springer Series in Optical Sciences

Volume 232

Springer Series in Optical Sciences is led by Editor-in-Chief William T. Rhodes, Florida Atlantic University, USA, and provides an expanding selection of research monographs in all major areas of optics:

- lasers and quantum optics
- ultrafast phenomena
- optical spectroscopy techniques
- optoelectronics
- information optics
- applied laser technology
- industrial applications and
- other topics of contemporary interest.

With this broad coverage of topics the series is useful to research scientists and engineers who need up-to-date reference books.

More information about this series at http://www.springer.com/series/624

Alexander A. Bortsov • Yuri B. Il'in
Sergey M. Smolskiy

Laser Optoelectronic Oscillators

Springer

Alexander A. Bortsov
Moscow Power Engineering Institute
National Research University
Moscow, Russia

Yuri B. Il'in
Moscow Power Engineering Institute
National Research University
Moscow, Russia

Sergey M. Smolskiy
Moscow Power Engineering Institute
National Research University
Moscow, Russia

ISSN 0342-4111 ISSN 1556-1534 (electronic)
Springer Series in Optical Sciences
ISBN 978-3-030-45699-3 ISBN 978-3-030-45700-6 (eBook)
https://doi.org/10.1007/978-3-030-45700-6

This Springer imprint is published by the registered company Springer Nature Switzerland AG
The registered company address is: Gewerbestrasse 11, 6330 Cham, Switzerland

The authors devote this book to the 90th anniversary of the National Research University "Moscow Power Engineering Institute," which is the alma mater of all coauthors as well as their place of work for their full scientific and pedagogic lives

At the very end of the final stage of the preparation of this book for publication, Prof. Sergey M. Smolskiy died. We, his other co-authors, and longtime colleagues grieve deeply about this and offer sincere compassion to all who knew Prof. Sergey M. Smolskiy and worked with this wonderful man. He was a highly qualified specialist in radio physics and many related fields of science and technology. Prof. Sergey M. Smolskiy had a rare ability to unite in creative teams a wide variety of scientists and teachers of higher education. Confined to a wheelchair for the past 20 years, he continued selflessly and successfully to engage in scientific work every day. Prof. Sergey M. Smolskiy had authored or co-authored 20 books and more than 350 published articles. He successfully collaborated with well-known people around the world and the publishing houses Springer, Artech, and others. The research and teaching activities of Prof. Sergey M. Smolskiy are a feat worthy of admiration.

Foreword

This book offered to readers is devoted to investigations of the optoelectronic oscillators (OEO) with the external electro-optical modulator (for instance, the Mach–Zehnder modulator) and with the direct electrical modulation. At simplest examination, the optoelectronic oscillator presents the analog fiber-optical communication line closed into a loop, in which, besides oscillation in the optical range with the help of the modern laser, the conditions are created for excitation of microwave or mm-wave radio-frequency oscillations.

At present, OEO is intensively investigated by several dozen laboratories in the world. OEO is the promising source of microwave and mm-wave oscillations with the ultralow level of the power spectral density of the phase noise. Record results of the obtained phase noise level, which are found in the laboratory conditions, give to authors a right to predict about the fast implementations of OEO into commercial civil and military projects. OEO is considered by authors as the promising low-noise oscillator for the radar technology, optical radars, in onboard transmitting stations of unmanned flying vehicles, as the measuring system of the angular velocity in gyroscopes, as a sensor of physical quantities, as the coding-decoding element of the information transmission systems with "masking" effects, etc.

One of the OEO advantages is its small overall dimensions. The optoelectronic oscillator can be made as a walnut in dimensions using the modern technologies. Small OEO dimensions facilitates to the high resistance to vibrations and loads.

First important researchings on OEO appeared more than 40 years ago (1980–1989) in USSR, USA and Japan. The new "burst" of interest to OEO investigation in microwave range was caused by an appearance in the market of commercially available "quantum-well" lasers with the small width of the spectral density line (less than 50 MHz) and the Mach–Zehnder modulators with the modulation bandwidth more than 10 GHz. At that, the research team of Maleki L. (Calteh) in 1999–2005, in a series of publication, was able to realize OEO with the record phase noise level (-143 dB/Hz at offset of 1–10 kHz from the carrier of 10 GHz).

Now, the flow of publications on OEO grows each year, more than 100 researchers from different countries (the USA, Russia, China, Italy, Iraq,

Pakistan, Iran, Egypt, etc.) participate in investigations. But, many interesting issues of the unique device operation are not yet discovered and not understandable to the wide circle of researchers till these days. It is caused by the fact that OEO combines two oscillating process, which flow in different ranges: radio-frequency and optical. It requires from the researcher the necessary store of knowledge not only in optics, quantum electronics, but in fundamentals of the nonlinear oscillations theory of the radio-frequency oscillators, statistical radio engineering, optimal reception approaches.

In this book, authors discover "mysteries" of this device to readers and describe of the OEO noise theory, explain the methods of ultralow phase noise oscillation obtaining. Not only descriptions of the basing structures of OEO are discussed in this book, but authors open the complicate physical phenomena occurring in the laser, and how they influence on characteristics and properties of OEO.

The new approach of authors to investigation of this device consists in *laser* examination in OEO as the main element: the energy source and the main source of then phase noise. At that, authors consider the laser (or the quantum-well laser diode—QWLD) physics on the base of semi-classical equations (Haken G.), together with the laser emission modulation methods. Then authors offer the fluctuation model of the OEO generation process, in which not only noises of the RF amplifier and the photodetector, but phase noises of the laser diode with Langevinian sources.

Authors expand before readers of the principal new picture for the truth search at the OEO investigation. They use different methods of the complicate quantum-electronic device research. On the one hand, authors enough fully and accurately described the study of the radio-frequency single-dimension OEO model as the oscillator with the high-Q delay line. On the other hand, authors examine of OEO as the random quantity correlator, in which the noise suppression occurs not only owing to the high-Q delay line, but due to the statistical process of combining of different optical harmonics. Authors propose to study the influence upon the frequency, the amplitude and noise properties of the complicate optoelectronic channel including the fiber-optical channel, which contains a laser, a modulator, and the optical fiber.

The specific issue of this book description is the offered theory (on the base of Epstein model of the electromagnetic oscillation representation) taking into account irregularities of different optical channels. Such a theory, based on Maxwell equations, gives representations about dependences of amplitude and phase of optical oscillations in the Mach–Zehnder modulator.

Authors investigated in this book of the power spectral density of the phase noise of two types of OEO and made important conclusions on its application and on technologies of low-noise sources of microwave and mm-wave oscillations. The advantage of this book is combination of the strict mathematical methods for analysis and solutions of differential equations based on the Evtianov method (developed at MPEI department) with the clear enough description supported by manifold illustrations (more than 150 figures).

In Chaps. 6 and 7, the descriptions of several original patents of authors, which concern to the automatic control of the frequency and the phase and measuring of various physical quantities, etc.

This book, addressing to various areas of knowledge, widens the scope of creating backgrounds of students, engineers, and of mature scientists, develops the researcher intellect by means of solution of complicate physical problems. Undoubtedly, this book will be interesting for experts in optoelectronics and photonics, since the new material on generation of microwave and mm-wave oscillations with the help of the optoelectronic generation methods is systemized in the similar manner for the first time.

Undoubtedly, on the base of offered book, the specials lecture course on optoelectronics and quantum electronics can be introduced in technical and classical universities.

NRU "MPEI", Moscow, Russia V. N. Kuleshov

Acknowledgements

Authors kindly thank our teachers and our colleagues from National Research University "Moscow Power Engineering Institute" for detailed discussion of several sections of this book and especially professors Kotelnikov V.A., Utkin G.M., Kapranov M.V., Kuleshov V.N., Udalov N.N., Grigoriants V.V., Dvornikov A.A., Chamorovskiy Yu.K., Tsarapkin D.P., Ph.D. Babkina T.v., Ph.D. Khrunov A.V., Ph.D. Kurochkina T.I. for the long-term support.

We thank Professor N.N. Udalov for his attentive and supporting attitude to this direction in 2006–2014 which was necessary for this book appearance. Professor M.V. Kapranov introduced the serious contribution in development of PLL methods for RF systems with fiber optical delay lines in (1988–1989). Professor V.V. Grigoriantz, Professor A.A. Dvornikov, Ph.D. V.N. Konstantinov, leading engineer V.A. Prokofiev are pioneers of founders of laser optical-electronic oscillators. V.N. Konstantinov, in his Ph.D. thesis (1985–1988) developed the base parts of theory of an optoelectronic oscillator with retarded feedback. The main aim of this thesis was directed to investigation of this source of the long-term stable oscillation without noises. V.N. Prokofiev created the first experimental sample of OEO, which operated in frequencies of 30–40 MHz. Prof. Tsarapkin D.P. is a pioneer in the field of Gunn diode oscillators with leuco-sapphire resonators, and Ph.D. Khrunov A.V. worked with IMPATT diode oscillators with leuco-sapphire resonators.

Our sincere gratitude to Sam Harrison, Editor in the Physics Books group at Springer, for his inestimable help to us at the stage of final manuscript preparation.

Moscow, Russia

Alexander A. Bortsov
Yuri B. Il'in
Sergey M. Smolskiy

Contents

List of Acronyms

A	Amplifier
AE	Active element
AFC	Amplitude-frequency characteristics
AM	Amplitude modulation, active medium
AN	Amplitude noise
AOM	Acoustic-optical modulator
APB	Amplitude and phase balance
C	Coupler
CE	Common emitter
CR	Cavity resonator
DC	Direct current, constant component
DDR	Disk dielectric resonator
DDRLS	Disk dielectric resonator from leuco-sapphire
DE	Differential equation
DM	Direct modulation (of the laser)
EMF	Electric-magnetic field, electromotive force
F	Filter
FB	Feedback
FBG	Fiber Bragg gratings
FC	Functional converter
FET	Field-effect transistor
FL	Fiber laser
FM	Frequency modulation
FODL	Fiber-optical delay line
FOL	Fiber-optical laser
FOLG	Fiber-optical light guide
FORL	Fiber-optical ring laser
FOS	Fiber-optical system
FSS	Femto-second synthesizer

IR	Infra-red
IRE	Institute of Radio Engineering and Electronics of Russian Academy of Sciences
LD	Laser diode
LDR	Laser Doppler radar
LED	Light-emitting diode
LPF	Low-pass filter
MLS	Modulated light source
MPEI	National Research University – Moscow Power Engineering Institute
MZ	Mach–Zehnder (modulator)
NA	Nonlinear amplifier
NE	Nonlinear element
OA	Optical amplifier
OC	Optical channel
ODR	Optical disk resonator
OEO	Opto-electronic oscillator
OEO DM	OEO with DM
OEO MZ	OEO with Mach–Zehnder modulator
OF	Optical filter
OPAA	Optical phased antenna array
OQO	Optical quantum oscillator
OTF	Operator transfer function
PAA	Phased antenna array
PD	Photodetector; photodiode
PFB	Positive feedback
PFC	Phase-frequency characteristic
PLL	Phase-locked loop
PM	Phase modulation
PN	Phase noise
PSD	Power spectral density
QFS	Quantum frequency standard
QR	Quartz resonator
QS	Quasi-stationary
QWLD	Quantum-well laser diode
RF	Radio frequency
RF FODL	The element of equivalent delay line for RF section of OEO
RFO	RF oscillator
ROR	Radio-optical radar
SAW	Surface acoustic wave
SE	Spontaneous emission, Schrodinger equation
SOS	Self-oscillation system
SSMB	Stimulated scattering of Mandelstam-Brillouin
TF	Transfer function
UMFV	Unmanned flying vehicle

VAC	Volt–Ampere characteristics
WAC	Watt–Ampere characteristic
WBA	Wideband amplifier
YIG	Yttrium-indium garnet

List of Symbols

Designation	Essence
A and B	Excitation coefficients of optical channels in differential delay line
A_1 and A_2	Dimensionless coefficients proportional to the oscillation amplitude of EMF strength of optical harmonic formed at modulation
C_{B}	Coupling coefficient
C_{L}	Laser diode capacitance
$_c$	Light speed
D	Vector of electrical displacement
D_{a}	Coefficient of the ambipolar diffusion
d_{e}	Electrical dipole moment
d_{ei}	Quantum-mechanical average value of the dipole moment in the space point in the time moment t
E_1	Lower energy level
E_2	Upper energy level
$_E\mathrm{L}$	Strength of electric component of EMF
$E_{\mathrm{LO,\ L}}$	Strength of laser local oscillator
$E(t)$	Optical emission from the laser
$E(t - T_{\mathrm{FOS}})$	Optical emission passed through the optical fiber
$E^2_{\mathrm{PD}}(t)$	Squared normalized EMF intensity on the PD area
$E_{\mathrm{L}\tau}$	Intensity delayed on some time $\Delta t = \tau$
e	Electron charge
e_{B}	Base voltage of the bipolar transistor
e_{C}	Collector voltage of the bipolar transistor
$e_{\mathrm{con,\ 0}}$	DC control voltage
e_{con1}	DC control voltage, which is applied to OF to change its natural optical frequency
e_{con2}	DC control voltage of the MZ modulator

F	RF frequency offset from RF carrier; electrostatic Coulomb force
f	RF frequency
f_0	DC part of RF frequency, steady-state RF frequency of OEO, modulation frequency OEO
f_{F0}	Natural frequency of the RF filter
f_{IF}	Intermediate frequency
$G_{opt,\ A}$	Gain of the optical amplifier
$G_{RF,\ A}$	The gain of the RF amplifier
G_0	Saturation coefficient; gain of the active layer
G_{non}	Nonlinear gain
h	Plank constant
hv	Energy of the one quantum
$I_M(t)$	Modulation current of the laser diode
I_0	DC pumping current of the laser diode, the bias current of the laser diode
$I_{PD}(t)$	Current in the PD output
i_B	Base current of the bipolar transistor
i_C	Collector current of the bipolar transistor
i_{1L}	AC component of the laser pumping current
$i_{PD}(t)$	Instantaneous PD current
J_L	Pumping current
J_{L0}	DC component of the pumping current
J_{1L}	AC component of the pumping current $J_{1L} = i_{1L}$
J_{0Lth}	DC component of the threshold pumping current of QWLD pumping current
J_{2k}	Bessel function
$K21$	Autocorrelation function of the random process
$K_{OA}(\nu)$	Module of AFC of the optical amplifier
$K_{OF}(\nu)$	Module of AFC of the optical filter
$K_{FOS}(\nu)$	Module of AFC of FOS
K_L	Complex transfer function of QWLD
$K^2_{\Gamma PN}$	Phase noise suppression factor
K^2_{AN}	Amplitude noise suppression factor
$K^2_{2\Gamma PN}$	Approximated phase noise suppression factor
K_{FOS}	Transfer function of FOS
K_{FBN}	Transfer function of feedback network (see text)
K_{DL}	Transfer function of feedback network (see text)
$K_{RF,\ F}$	Transfer function of the radio frequency filter
K_{FODL}	Transfer function of FODL
K_{LOC}	Complex transfer functions of OEO laser optical channel
k	Boltzmann constant
k_1 and k_2	Excitations coefficients of optical channel in MZ
k_{fb}	Feedback loop coefficient

L_a	Total thickness of quantum wells
L_w	Thickness of the laser wave-guiding layer
l_0	Dipole arm
$\lvert M_{eZ}\rvert$	Module of the MZ transfer function
m	Amplitude fluctuations, charge carrier mass, mass of the electron
$m_{RF,\ m}(t)$	RF amplitude fluctuations
$m_{Lm}(t)$	Laser amplitude noise component
$N(t)$	Population difference between levels
N_2	Quantity of carriers on the upper energy level
N_{sp}	Number of spontaneous photons obtained in PD
n	Refraction index
n_0	Refraction index of the medium material
P_0	Optical power
$_{POL}$	Optical power of the laser
P_{L0}	DC component of the photon flow density in the resonator
P_{RF}	RF power of OEO
P_n	Spatial component of the active medium polarization
$P(z, t)$	Polarization
P_{NL}	Nonlinear pumping
$p = \mathrm{d}/\mathrm{d}t$	Laplace operator
$Q_{RF,\ F}$	Q-factor of the RF filter
Q_n	Q-factor for the n-mode
q	Carrier charge
R	Distance
R_c	Controlling resistance
R_d	Laser diode resistance
$R(t, t + \tau)$	Autocorrelation function of the laser random field
$R_{MZ}(\tau)$	Autocorrelation function of the MZ modulator
r_{fi}	Matrix element
S, S_d	Spectrum, spectral density
S_{1L}	Slope of the Watt–Ampere characteristic; proportionality coefficient defining the dependence of photon flow density (in laser optical resonator)
$S_{12L}(F, R)$	Mutual spectral density of PSD
S_L	Optical oscillation spectrum with noises
S_{NY}	Nonlinear function of RF first harmonic of collector current of the RF amplifier
S_{RFL}	Spectrum of the electric signal
S_{RFMZ}	Current spectrum at the MZ input
$S_\xi(f)$	Spectral density of $\xi(t)$
$S_\eta(f)$	Spectral density of $\eta(t)$
$S_{\psi L}(\nu)$	Spectral density of the laser phase fluctuations
T_1	Lifetime of carriers on the upper excited level
T_{1FOS} and T_{2FOS}	Delay time in 1 and 2 channel

T_{FOS}	Time delay of fiber-optical system
T°_{OF}	Temperature of optical fiber in °K
T_c	Laser coherence time
T_F	Time constant of the RF filter
$T_{RF,\ F}$	Time constant of the RF filter
T_{L0}	Time constant of the laser cavity
T_M	The group delay time at the output of the optical channel with respect to the MZ input
T_{OF}	Time constant of the optical filter
$U(t)$	Amplitude of RF voltage of OEO
U_0	RF oscillation amplitude
U_{01}, U_{01MZ}	RF oscillation amplitude of the fundamental harmonic in the electrical input of the MZ modulator
U_{01C}	Oscillation amplitude of the fundamental harmonic in the coupler output
$U_{0M} = U_{0MZ}$	RF oscillation amplitude of the controlling (modulating); microwave voltage at the input of the MZ modulator
U_{0F}	RF oscillation amplitude of the output of RF filter
$U_f(t)$	Amplitude of RF oscillation
$U_M(t)$	Modulation voltage of the laser diode
$u(t)$	Instantaneous RF voltage
$u_{gen}(t)$	Instantaneous RF voltage generated by OEO
$u_s(t)$	Instantaneous signal voltage
u_{1MZ}	AC voltage component of the MZ modulator
$V(z)$	Potential well
V_{gr}	Group light speed
v	Frequency of optical emission
v_F	Natural frequency of the optical filter
v_0	Average optical frequency
$v \pm f$	Two subcarriers around optical frequency
x	Modulation index $x = U_{01MZ}/U_{0\pi}$, abscissa axis
$y(j\omega)$	Controlling symbolic conductivity
Z_{PD}	Load impedance of PD
z	Spatial coordinate

Greek Designations

α	Constant of the thin structure 1/132; constant width of the laser spectral line
α_B	Losses per the length unit in the Bragg grating
α_{0e}	Expansion coefficient of the nonlinear function of RF amplifier
α_{0L}	Expansion coefficient of the nonlinear function of laser
β_B	Propagation constant
β_{0e}	Expansion coefficient of the nonlinear function of RF amplifier

β_{0L}	Expansion coefficient of the nonlinear function of laser
Γ_a	Coefficient of the optical field limitation
$\gamma_k = \gamma = k_2/k_1$	Coefficient of excitation irregularity of MZ optical channels
$\gamma_{L\psi}$	Spatial constant of the phase fluctuations of the laser output emission
ε	Medium permittivity
ε_0	Vacuum permittivity
ε_{sh}	Nonlinearity coefficient of QWLD
$\delta(f)$	Delta-function (Dirac function)
K_n	Propagation constant for the mode
χ	Medium susceptibility
∇	Laplace operator
Δf_{gen}	Natural width of the RF spectral line
$\Delta\varphi$	Phase fluctuations
Δn_{OF}	Difference of refraction indices in the Bragg grating
ΔT_M	Delay difference in the phase detector channels (or in channels of the MZ
$\Delta\nu_L$	Laser emission spectrum width
$\Delta\nu_{R0}$	Half-width of the spectral line of the laser optical resonator
λ_B	Bragg grating period
μ	QWLD decay decrement, permeability
$\eta(t)$	Random process
$\varphi(\omega, A, B)$	PFC of the fiber-optical system (FOS)
$\varphi_{FODL,\ rem}$	PFC of the remaining part of FODL containing the MZ modulator, FODL and the photodetector
$\varphi_{RF,\ A}$	Phase incursion in the wideband RF nonlinear amplifier r
$\varphi_{em}(t)$	Phase fluctuations
φ_{Lm}	Laser phase noise component
$\varphi_{RF,\ F}(\omega)$	PFC of the narrowband RF filter
$\varphi_{OA}(\nu)$	Argument of PFC of the optical amplifier
$\varphi_{OF}(\nu)$	Argument of PFC of the optical filter
$\varphi_{FOS}(\nu)$	Argument of PFC of FOS
φ_{0L}	Initial constant phase shift
φ_{0Om}, φ_{1Om}, φ_{2Om}	Phase fluctuations of DC component, first and second harmonics
$\varphi_{opt,\ A}$	Phase-frequency characteristic of the optical amplifier
$\varphi_{opt,\ F}$	Phase-frequency characteristics of the optical filter
$\varphi_{opt,\ L}$	Phase of the optical laser
$\varphi_{opt,\ rem}$	Phase incursion in the remaining parts of the laser equivalent circuit (besides OF and NA)
φ_{MZ}	PFC of the MZ modulator
Φ	Phase
$\phi_{0,\ RF}$	Initial phase of the $u_g(t)$ RF voltage (the constant phase shift)
ϕ_{0O}, ϕ_{10O}, ϕ_{20O}	Constant phase shifts defining by the selective optical filter

ψ	Eigenfunction
$\psi_{\mathrm{m}}(t)$	Phase fluctuation
σ	Ohmic conductance
σ^2_{PD}	Phase dispersion at output of the phase detector (or in the photocurrent of the photodetector)
σ_{U}	Nonlinearity coefficient
σ^2_{E}	Dispersion of the laser phase noise
σ^2_{ξ}	Dispersion of Gaussian random process
$\sigma^2_{\Delta\psi_{\mathrm{m}}}$	Dispersion of the random phase difference
τ	Delay time
τ_{D}	Delay slope
τ_{n1}	Carrier lifetime in the active area
τ_{ce}	Time constant of the laser diode
τ_{c}	Local time of capture of carriers for the AC signal
τ_{e}	Local time of ejection of carriers for the AC signal
τ_{ph}	Photon lifetime in the resonator $\tau_{\mathrm{ph}} = T_1$
ξ_{N}	Dispersion of the carrier noise
$\xi(t)$	Gaussian random process $\xi(t)$ with σ^2_{ξ} dispersion
$\omega = 2\pi f$	Angular RF frequency
$\omega_{\mathrm{F}} = 2\pi f_{0\mathrm{F}}$	Angular natural resonance frequency of the RF filter
ω_{L0}	Frequency of the resonance peak
ω_{L00}	Own RF resonance frequency of QWLD

About the Authors

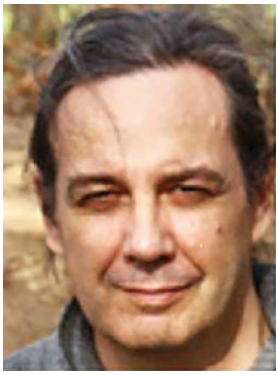

Alexander A. Bortsov was born in Moscow, completed his Ph.D. in Engineering, and graduated from MPEI. His Ph.D. thesis was on the theme "Opto-electronic oscillator with the QW laser diode" in 2005. He is the author of more than 40 scientific publications, among them 30 scientific papers, one book *Quantum Opto-Electronic Oscillator*, 3 USSR copyright certificates on invention, 4 Russian patents, and more than 20 technological reports on various conferences, including international ones. He was the first in Russia, who in 2004–2005 had got the generation of the opto-electronic oscillator with direct modulation in the microwave range (more than 8 GHz) and investigated of it experiment tally and theoretical in his Ph.D. thesis (2005). He is the first researcher in Russia in 2008–2009 to investigate the opto-electronic oscillator with the Mach–Zehnder modulator in the microwave range 8–10 Ghz. He delivers lectures to students on the fundamentals of the quantum electronics and quantum physics. He trains students in the probabilities theory, mathematical statistics, and many areas of the higher mathematics including mathematical methods of modeling in the MatLab system. Fields of current research: opto-electronic oscillator, photonics, lasers, QW lasers, phase noise, the probabilities theory, mathematical statistics, calculation methods in MatLab.

Yuri B. Il'in, born in 1939, Ph.D. in Engineering.

Professional education: Moscow State Mining University, Electromechanical Faculty (1958–1959)/Moscow Power Engineering Institute (National Technical University), Radio Engineering Faculty (1959–1964)/ Moscow State University, Faculty of Mechanics and Mathematics (1964–1968).

He graduated from Radio Engineering Faculty of MPEI since 1964 just after graduation before he left this institute of his own accord in 1997. At the beginning, he worked on Department of Radio Transmitting Devices, where engaged in the construction of masers, and theoretical study of steady-state and dynamic behavior of a multimode lasers with non-homogeneously broadened spectral line and practical questions of development of fiber-optic communication lines. After graduation of Ph.D. course and defending a Ph.D. thesis in 1986, he worked on Department of Performing of Oscillations and Signals in Radio Engineering Faculty of MPEI. At the same time, he was with SIMVOL Ltd. Company in Moscow, Russia. Here he led the pioneering works on the creation of Optoelectronic Oscillators and Magneto-Infrared Laser Diode Therapeutic devices. Since 1997, he was with OPTEN Ltd. Company in Moscow, Russia. Here he worked as a Department of Education Programs manager until 2005. At the same time, he was engaged in creating, organizing, and conducting courses in Russia and the United States of America (USTTI) of advanced training for senior engineering personnel of electric power companies in Russia and a number of countries. These courses were devoted to the technology of laying fiber-optic communication cables overhead the phase wires of long-height high-voltage power lines. From 2005 to the present time he works as a freelancer scientist. His academic experience spans over 30 years.

He worked as assistant professor, senior teacher and associate professor.

Sergey M. Smolskiy, born in 1946, Ph.D. in Engineering, Dr.Sc. in Engineering, full professor of Department of Radio Signals Formation and Processing of the National Research University "MPEI." He was engaged in theoretical and practical problems concerning the development of modern transmitting cascades including the short-range radar. In 1993, he defended the Doctor of Science thesis and now he works as a professor of Radio Signals Formation and Processing Dept. His academic experience spans over 40 years. The list of scientific works and inventions contains over 358 of scientific papers, 20 books, more than 100 technological reports on various conferences, including international ones. He is an active member of International Academy of Informatization, International Academy of Electrotechnical Sciences, International Academy of Sciences of Higher Educational Institutions, and IEEE. The scientific work for the latter 15 years is connected with conversion directions of short-range radar systems, radio measuring systems for fuel and energy complex, radio monitoring system, radar technology, radio transmitters, radio receivers, etc.

Chapter 1
Introduction

At present, one of the most important problem of radio electronics, on which the efforts of many worldwide leading labs and companies with $-millions budgets are concentrated, is the development, creation, and manufacture of commercially available high-stable oscillators of microwave and millimeter-wave ranges with the ultralow phase noise: less than −140 dB/Hz at offset of 1–100 kHz from a carrier [1–5].

Such precision devices for oscillation formation are necessary at development and design of mobile communications systems, aircraft and satellite communications, systems of data transmission for unmanned flying vehicles (UMFV), radar and optical coherent systems, antennas systems, and high-precision measuring equipment. Such oscillation sources are also called for UMFLs, including networks or swarms of UMFVs (20–100 small UMFVs launched simultaneously). Overall dimensions of such sources should be less that 1000 mm^3 taking into account modern requirements.

The short-term relative frequency instability (less that 10^{-12} at medium operating frequency 10 GHz) and ultralow phase noises (less that −140 dB/Hz at 10-kHz frequency offset from the average carrier operating frequency) should provide the wideband (up to 10–100 Gbit/s) ultrasecret transmission of coded information via a radio-channel on the long distance (100 km and above).

At present, in many worldwide countries, the development of *compact* low-noise frequency-stabilized radio-frequency (RF) oscillators [6–11], which operate in the 1–100-GHz range in integral or hybrid versions. The well-known traditional high-stable microwave oscillators, which are available at present, are unacceptable for some applications. Traditional oscillators with crystal resonators and oscillators on surface acoustic waves (SAW) with multiplication of frequency being generated do not enable to get the required level of the power spectral density (PSD) of the phase noise (PN) at the expense of the multiple phase noise increase at frequency multiplication in microwave and mm-wave oscillating devices. Such well-known

A. A. Bortsov et al., *Laser Optoelectronic Oscillators*, Springer Series in Optical Sciences 232, https://doi.org/10.1007/978-3-030-45700-6_1

oscillators have no the required level of the short-term frequency instability in the frequency range of 1–100 GHz.

Oscillators with the dielectric resonator (cavity) on ceramic alloys have the evident limitations on the phase noise level. At the expense of the relatively low Q-factor of such a cavity, which equals approximately 1000 (on the 10GHz generation frequency), the typical phase noise level of commercially available oscillators could not, as a rule, be less than −90 to −115 dBm/Hz at 1-kHz frequency offset from the nominal generation frequency 8–20 GHz.

Microwave oscillators with frequency stabilization by the solid-state leuco-sapphire dielectric cavity [12–17] have at present the most low registered phase noise level of −167 dBm/Hz at 1–10-kHz offsets. The operating frequency range of such oscillators is from 6 to 35 GHz and has, as a rule, the discrete range of frequency tuning. The leuco-sapphire cavity of such an oscillator has relatively large overall dimensions (a diameter is 30–100 mm) and a big weight (150–400 g). Due to large overall dimensions and a weight of a cavity in such oscillators, the oscillation frequency strongly depends upon mechanical loads. The serious disadvantage of an oscillator with leuco-sapphire cavity is the fact that in such oscillators, at the expense of relatively high dependence of material permittivity upon a temperature (10^{-4} 1/deg), systems of frequency heat-setting are complicate and expensive.

Recently, an developers' attention in the field of the high-stable oscillation sources is attracted to the new type of a source called an optoelectronic oscillator (OEO), which contains besides traditional elements of RF section (a nonlinear active element, high-Q frequency-selective element, the circuit of the positive feedback, auxiliary circuit for control and stabilization) the optical section (a laser as the source of optical oscillations, FODL in the optical section, auxiliary optical elements, for example, a modulator and a demodulator). At definite configurations of optical and RF sections and their parameters (see further chapters in this book), both optical and RF oscillations are excited, which interact in complicate manner and give to OEO some unique properties, which will be analyzed later in this book. These properties will be considered in detail later in this Introduction with the purpose of the first acquaintance of readers with OEO features.

One of the alternative approaches to creation of reliable compact and low-cost low-noise oscillators in the frequency range 1–100 GHz is an application in OEO of the stabilized low-noise fiber-optical delay line on the base of the fast-acting quantum-well laser diode, a photodiode, as well as at the expense of special low-dispersion optical fibers. These FODLs have a large delay for harmonic microwave oscillations. The delay time in these FODLs is from 1 ns to 50 μs (for a bandwidth of transmitted frequencies up to 100 GHz). At that, the power losses in these FODLs (at the expense of scattering and the optoelectronic conversion) are 10–18 dB and more in microwave and mm-wave ranges.

In the best samples of the microwave optoelectronic oscillators, which have a similar FODL in the feedback loop, a low power spectral density of the phase noise is already achieved equaled to −130 to −153 dBc/Hz at frequency offsets of 1–10 kHz [18–20]. The short-term frequency instability of this OEO is about 10^{-10}. The ultralow phase noise of this OEO is achieved at the expense of creation

(based on FODL) of high-Q optoelectronic resonator of the "traveling wave" with the loaded equivalent Q-factor of $Q = (0.2–0.8)\cdot 10^6$ in the frequency range 1–70 GHz.

This FODL consists of the series-connected quantum-well laser diode (QWLD) with the external electro-optical modulator of Mach–Zehnder (MZ) (or QWLD with direct modulation), the fiber-optical system (FOS) consisting of one or several optical fibers and a photodetector (PD).

In OEO with QWLD and compact FODLs, we can obtain the low relative *short-term* and *long-term* frequency instability of microwave oscillations of the order 10^{-8} to 10^{-11}. In this OEO, the generation frequency control can be performed by both optical and RF means. OEO can be used with the great promise in classical radar stations and in optical radars of new generation, in ultra-wideband regenerative FODL as generators of ultrashort optical pulses and radio-pulse signal with duration of 0.01–1 ps with the low "jitter" [21] (a random offset of the pulse leading edge), as well as in FODLs, for information transmission in systems with increased confidentiality using the masking interference.

OEO utilization with such record characteristic in the radar technology allows us the reliable determination of the small, hardly noticeable, and slow-moving targets on the interference background at large distances. Utilization of compact radars for UMFVs presents the special interest.

In the modern stage, the optoelectronic oscillator is a product of nanotechnologies. It uses the quantum-well (or nano-dimension) laser diodes, which have the small phase noises and the high output power of optical emission (1–10 mW). The optical fiber (OF) in miniature OEOs, is the special nanostructured fiber, which allows the provision of the small OF bending radius (down to 1–5 mm) with low optical losses per one bend (less than 0.001 dB).

We can say without overestimate that the appearance of commercially available miniature optoelectronic oscillators with a *walnut size* will probably make the next breakthrough in the radar technology, radio engineering, UMFVs, FODLs, and in the mobile radio-telephony.

Nevertheless, this type of the promising OEOs is insufficiently theoretically and experimentally studied at present. The main reasons of the ultralow phase noise values are not explained for RF oscillation type at using in OEO with FODL of the direct and external QWLD modulation type. In Russia, before 2004, none functioning laboratory sample of OEO (and an experimental breadboard) was developed in the frequency range 2–12 GHz and above. In different countries, at the beginning of 2000s, with the appearance of commercial microwave electro-optical modulators, the first experimental publications of Maleki and Steve Yao (Caltech) [22, 23] and other researchers appeared concerning OEO investigations with external modulation (using the electro-optical Mach-Zehnder modulator). In these publications, together with successful experimental results on the phase noise PSD, the OEO theory with fluctuations was not still formulated. It was not analyzed how the laser phase noise (determined by its spontaneous noises) affects the RF phase noise in OEO as a whole. A role of the laser phase noise [24] was not discussed in known publications

[19, 25–28]. Mentioned and other circumstances are one of the motivations for preparation and fulfillment of this book's investigations during 2005 through 2014.

Known publications (books, papers, reports at conferences) on OEO research [29–33] does not at once enable the determination of the OEO main properties in microwave range and methods of the frequency control. It is rather difficult to extract and to analyze factors, which influence on the frequency instability and on the phase noise of OEO. To authors' opinion, one of the advantages of this book is a construction of the physical and engineering theory of OEO taking into account fluctuations, and explanation of the phase noise influence of the spontaneous optical laser emission on the process of the RF resulting phase noise formation at intended generation in RF range.

We should note that, from the point of view of classical oscillations theory, OEO is concerned to oscillators with delayed feedback [34–36]. Oscillators with surface acoustic waves (SAW) delay lines [37, 38] are theoretically studied oscillators with delayed feedback, and they are close to OEO in its construction circuit. These research results form a base for theoretical investigations of the new class of precision oscillations—OEO with FODL and the present book is devoted to these oscillators research.

Intensive investigations (1970s–1980s) of fiber-optical communication lines and optical fibers with low optical losses give an impulse to fiber-optical systems' application in precision oscillating systems. During recent decades, researches were performed on theoretical and experimental investigations of modern fast-acting optoelectronic components: lasers, electro-optical modulators, photodiodes, as well as optoelectronic and fiber-optical systems with operating speed of 0.01–100 ps, with bandwidths of modulation frequencies up to 18–200 GHz.

Such researches gave an impulse to investigation of optoelectronic oscillators in microwave and mm-wave ranges. Such investigations are actively fulfilled in many countries including Russia. At present, under supervision of V.D. Kurnosov (Moscow, Russia), investigations and development of modern Russian quantum-well laser diodes and photodiodes are performed, which allow modulation and demodulation on frequencies up to 12 GHz [39, 40].

The appearance of such ultra-wideband QWLDs enables the practical development of OEO with FODL in 12 GHz-range. Further perspectives of OEO development, which operate in microwave and mm-wave ranges, are related to creation of modern optoelectronic devices and photonic nanotechnologies. Recently, the publications in experimental research of optoelectronic oscillator under supervision of professor M.E. Belkin appear in Russia, and we may tell about urgency of the problem of low-noise optoelectronic oscillator with FODL development [41].

As concerned to worldwide researchers in the field of OEO experimental investigations, we may note publications of Nakazava M. (NTT Transmission Systems Laboratories, Japan, 1984) [42], Yariv Amnon (Caltech, USA, 1984) [43], V.V. Grigoriants and Yu.B. Il'in (MPEI, USSR, 1982–1990) [44–46], Steve Yao and L. Maleki (Caltech, USA, 1994–1997) [22, 23, 47, 48], J. Lasri (the Electrical Engineering Dept., Technion, Israel, 2001) [49, 50] and E. Shumakher (Israel, 2008) [51].

Investigations of the Russian "quantum" team in National Research University "Moscow Power Engineering Institute" (MPEI) consisting of Y.B. Il'in, V.N. Konstantinov, and A.A. Bortsov seems to us as pioneering investigations with new theoretical and experimental researches, which were performed in 1981–1993 under supervision of professor V.V. Grigoriants (MPEI and Institute of Radio Engineering and Electronics of Russian Academy of Sciences) [44–46].

In these publications, OEO with FODL was studied and it was called the "laser oscillator with FODL."

An analysis of optoelectronic oscillator was performed by the last team under assumption of small excitation, and the ordinary differential equations were obtained for the autonomous OEO with the single optical fiber in FODL, and main concepts of OEO structure were formulated as the stabilized oscillator based of the lengthy optical fiber. One of the principal new statements of this Russian quantum team (and relevant for today) was the proved condition that the low-noise OEO can operate without the RF amplifier. This quantum team with direct participation of this book authors was firstly fulfilled theoretical and experimental investigations of OEO and published results in [52–58] about utilization of differential FODLs and recirculation (non-recursive and recursive) FODLs. New methods of the OEO frequency control were performed, and it was proved that FODL application leads to reduction of the short-term and long-term OEO frequency instability.

At modern stage, the intensive researches are performed in various countries on development of the ultracompact low-noise oscillator based on OEO with FODL dedicated for the onboard application in compact UMFVs and other systems of information transmission. Creation on ultralow-noise microwave and mm-wave oscillators on the OEO base in various areas of engineering, in warfare systems, and in special military systems persistently requires answers to many questions. First of all, the following questions can be concerned to them:

- How much the laser phase noise should be in low-noise OEO?
- How can we choose the spectral line width and QWLD power?
- How much the RF filter optimal bandwidth should be?
- Which interaction should be between laser optical phase noises and RF phase noises in OEO?
- Which methods of frequency control must be applied in OEO with FODL?
- How does a temperature of the FODL optical fiber influence on oscillation frequency offsets in OEO?
- How much the geometrical length of the optical fiber should be, and many other different questions.

At present, the known theoretical publications cannot answer to questions concerning OEO because in these publications, authors were limited by the OEO model analysis in the form of the circular oscillating system with delay chain (without an account of dispersion) in the positive feedback loop, which role, within the limits of this model, is played by FODL. A laser in this model was not considered as the independent optical oscillations' source with its own amplitude and phase noises, but it was represented as a linear ideal passive element.

At present, we cannot find a comparison of OEO technical characteristics with other oscillators. In such an oscillator, the main advantages and shortcomings were not analyzed in detail. The theoretical and experimental investigation of OEO with the direct and external QWLD modulation was not yet performed taking laser noises into consideration.

The above-mentioned allows formulation of this book purposes as follows.

The purposes of this book are:

- Familiarization of the *worldwide scientific community* with high-tech approach for development of new sources of high-precision low-noise high-stable oscillations of the different *physical nature.*
- *Examination of the new principle of ultralow-noise microwave and mm-wave oscillations' generation, which consists in application the self-modulation effect of laser emission in the optoelectronic loop of the positive feedback.*
- *Description of fundamentals of the phase noise theory of the optoelectronic oscillator based on the semiclassical laser model.*
- *Discussion of structures and technical characteristics of the experimental breadboard of the optoelectronic oscillator with the quantum-well laser diode as the primary source of the high-coherent emission.*
- *Demonstration that among various OEO phase noise sources, the spontaneous noise of laser emission is the determinative one for the level of the power spectral density of the phase noise.*
- *Elaboration of recommendations for a choice of OEO element base of microwave and mm-wave oscillations.*
- *Comparison of OEO various structures with direct and external modulation of laser emission.*

This book is organized as follows. After present Introduction, this book contains seven Chapters.

Chapter 2 is devoted to reader introducing in the optoelectronic oscillator theme. We discuss the operation principle of this comparably new and the source of microwave and millimeter-wave precision oscillations, which is studied yet a little. Features, advantages, and shortcomings of these oscillators are described for two types of optical emission modulation: direct modulation and external modulation with the special modulators. Possible applications of optoelectronic oscillators are discussed in brief with an emphasis to complexities of analysis and design of such systems.

Chapter 3 is devoted to an analysis of laser emission modulation methods and formulation of mathematical model of the autonomous optoelectronic oscillator (OEO) on the base of nonlinear differential equations. Sections of the Chap. 3 present two methods of laser emission modulation: the direct (internal) electrical method and the external modulation through the electro-optical modulator offered by Mach and Zehnder. Before beginning of material discussion, to explain a consequence and the logic of description, we briefly describe the structure of mathematical

analysis of the laser optoelectronic oscillator in Chap. 3 and in the following chapters.

After brief description of two principles operation for internal and external approaches, we discuss its structural realization. The complexity of both approaches is related to nonstandard way of description of nonlinear method modulation for internal (direct) structure and the utilization of specific Mach–Zehnder modulator for the first stage on external modulation: the phase modulation in the optical channels of the external MZ modulator, and (at the second modulation stage) conversion (after the fiber optical delay line) of the phase-modulated laser emission into the amplitude-modulated radio-frequency signal in the nonlinear photodetector.

Chapter 4 is the logical continuation of OEO investigation, in which we consider that the laser is the main element defining the dynamic and noise properties of OEO. In this interpretation, OEO is represented as the quantum generator spanned by the positive feedback: the optoelectronic network containing the optical fiber, the photodetector, the RF filter, and the RF amplifier.

Sections of the Chap. 4 are devoted to model formation of the quantum generator, for which we use the semiclassical theory based on the dipole representation of the laser in double-level approximation. For formation of differential equations (DE) in quasi-stationary mode, we consider the DE system, which consists of three differential equations. This DE system establishes a connection between the active medium polarization, the electromagnetic field strength, the inversed population of particles on upper and lower energy levels, and pumping, taking into account the Q-factors of the optical resonator and the emission spectral line of the active medium and the population inertial properties. Examination of this system of nonlinear DEs with inertial properties allows formation of the laser analog model in the dipole approximation.

The analysis of the self-oscillating system (SOS) of the laser model is performed, for which we introduce the operator transfer function, the nonlinear element (NE) and execute the analysis of nonlinear properties. The special role is paid at laser system analysis to investigation of inertial nonlinear QWLD at its operation in quasi-stationary mode with the high excess of pumping current over its threshold value. Investigation of oscillation excitation conditions and oscillation existence conditions in the OWLD steady-state is performed.

The one section of the Chap. 4 is devoted to results' presentation of the nonlinear fourth-order DE solution for the laser model in the dipole approximation. The plots of realizations of oscillating processes for two types of nonlinearities are analyzed. Results of computer solution for the quasi-stationary mode of laser generation are presented for fourth-order DE at linear-hyperbolic inertial nonlinearity of the active medium. Numerical calculation results on the base of the symbolic equation solution are discussed for determination of resonance characteristics in the steady-state mode. Results of nonlinear DE equations and resonance characteristics at high power density in the optical resonator are described. Section of the Chap. 4 contains the main conclusions.

Chapter 5 is devoted to the main features of OEO. The optoelectronic oscillator is considered as the self-oscillating laser system with modulation, which is spanned by

the positive feedback loop. We compose symbolic and abbreviated equations of OEO and examine the analog model of OEO taking into consideration the laser fluctuations. At first, we discuss the symbolic differential equations of OEO DM (with direct modulation) and OEO MZ and construct the OEO analog model on its base. Then we investigate the oscillation stability of OEO and analyze the self-oscillation conditions and oscillation existence conditions in OEO. Then we investigate the dynamics of transients in OEO DM.

After that, in this chapter, we describe the differential equation of OEO with Langevinian noise sources. The main positions of the fluctuation laser model are discussed and Langevinian noise sources are described for OEO oscillating system. Relying on the symbolic constitutive equations of the laser with fluctuations, we construct the analog models of OEO DM and OEO MZ taking into account the laser noises. We analyze the symbolic differential equations of the laser with fluctuations in the quasi-stationary mode for the small signal. The approach for calculation of the power spectral density (PSD) of the amplitude noise (AN) and the phase noise (PN) of OEO is presented. We estimate the effect of the spontaneous laser emission upon the PSD of PN in OEO. At that, at calculation of PSD noises we use the approach basing on the symbolic equation of OEO and on the method of abbreviated fluctuation equations of Evtianov–Kuleshov.

Then, in this chapter, we discuss the approach for calculation of PSD of noises at representation of OEO as the *correlator* of random quantities. We describe the base correlator structures and calculate the autocorrelation functions for oscillations of the laser field strength and the electrical voltage in OEO.

In Chap. 6, we perform an analysis of the laser optoelectronic oscillator with the fiber-optical delay line (FODL) as the system of two oscillators of optical and RF ranges and we study the formation of the RF generation spectrum in OEO MZ taking into account the influence of laser optical emission parameters including the laser spectral line width and its power. Then we discuss the general statement of the investigation task of OEO MZ and describe the structure and the operation principle of OEO MZ.

The principles of the OEO MZ mathematical model construction and components including in the OEO MZ structure are described. We describe characteristics and the transfer function of the MZ modulator in OEO MZ.

After that, we examine the differential fluctuation equations of OEO MZ and discuss results of the computer modeling of transient processes for oscillation formation in OEO MZ.

In Chap. 7, we examine OEO as the time and spatial correlator of random quantities. At first, we investigate the model of nonsymmetrical dielectric waveguide structure of the laser and the optical waveguide. Then, we analyze the OEO DM on the base of abbreviated differential equations and discuss the problems of the frequency control in OEO DM by the laser pumping current.

Then we examine the schemes of the frequency control in OEO DM with differential FODL. The problems of the parametric and long-term frequency instability of OEO with FODL are discussed. The fluctuation equations for PSD of AN

and PN in OEO DM are analyzed. Systems of frequency and phase automatic control in OEO are described.

The final Chap. 8 has two main tasks: (1) description of manifold experiment results on studying of various modes of the optoelectronic oscillators, which are realized both for small laser diodes and for powerful lasers; (2) examination of practical issues of the new optoelectronic oscillator applications including the retuned low-noise oscillators, sources of precision oscillations for on-board aircraft and space radar equipment on flying vehicles, including phase noise issues; lengthy fiber-optical communication links with increased secretiveness, sources of ultrashort pulses, fiber-optical sensors of various physical quantities on the base of OEO.

The book is finished by general conclusion with the list of main results obtained and with discussion of near prospects.

1.1 Brief History of OEO Investigation in MPEI[1] and IRE[2]

First scientific papers and authors certificates of Russian scientists from NRU MPEI [44–46, 52–58] were prepared and published in prestigious journals "Optical and Quantum Electronics," "Quantum and Quantum Electronics" (Springer Science group), and in Russian journals "Quantum Electronics," "Radio Engineering," "Radio Engineering and Electronics," etc. more than 30 years ago. During this period, OEO from the laboratory breadboard, which was interesting for scientists only, converted into the microwave technical device, which future can be compared with quantum frequency standards or semiconductor lasers. A number of publications in the world on the theme of OEO stabilized by the fiber-optical delay lines increase each year and the total number can be counted as hundreds per a year.

First OEO investigations can be concerned to 1984–1990 [44–46, 52–58]. They were performed by the researcher team in MPEI at the department of Radio Transmitters and in IRE.

In these initial publications [44–46, 52–58], OEO with a direct modulation of the laser diode on frequencies 30–60 MHz was experimentally studied. The first name in papers on OEO was "the laser oscillator with the fiber-optical delay line." The mathematical models of first OEO were suggested and the frequency instability, frequency temperature dependences of the optical fiber, phase-frequency dependences, etc. were considered. In the quantum research team for OEO investigations, which was headed by the Lab 228 Head of IRE and MPEI professor, Dr.Sci. (Phys-Math) Vil V. Grigoriants the following main persons were included:

– Yuri B. Il'in, Ph.D. Associate Professor
– Alexei A. Dvornikov, Ph.D., Dr.Sci. (1987), MPEI
– Victor N. Konstantinov, Ph.D, MPEI

[1]Russian National Research University "Moscow Power Engineering Institute" (NRU MPEI).

[2]Institute of Radio Engineering and Electronics of Russian Academy of Sciences (IRE).

– Vladimir A. Prokofiev, senior engineer, MPEI
– Alexander A. Bortsov, initially Ph.D.student, after Ph.D. (2005), MPEI.

We should note the pioneer publication (1985) [44], in which the OEO structure was substantiated, and with the help of the equation system based on amplitude and phase balance, the amplitude and frequency of OEO generation were theoretically calculated. Another publication [45] was devoted to the absolutely new variant of OEO with the external acousto-optical modulator on the base of the Mach–Zehnder interferometer with heterodyne mixing of optical harmonics of oscillations with different frequencies. In this case, the OEO circuit represents the laser, which emission was modulated by the electro-acoustic modulator and directed in two optical fibers, which were excited by laser emission passed through the acousto-optical modulator. After that, this emission passed to the photodetector after transfer through the optical fibers, and then the electric signal was amplified by the RF amplifier, passed through the narrowband RF filter to the input of the acousto-optical modulator.

In [46], the OEO structure with two optical fibers of different length was considered and dependences of frequency tuning at power variation, which passed into the optical channels were calculated. In essence, a construction presented an interferometer with the feedback loop. Publications [55, 56] are devoted to examination of transfer functions of the single multi-mode fiber and the fiber-optical delay line formed by two optical fibers of different lengths. An influence of mode content of the optical fiber and excitation degrees of various optical fibers of different lengths included in OEO were studied. A series of patents were obtained on examined OEO breadboards. In beginning of 1990s, investigations of OEO with the external modulator on the base of the electro-acoustic cell [59].

Researches of the optoelectronic oscillator continued in Russia and in NRU MPEI during 2003–2018. New method of frequency control was patented by using the phase-locked loop (PLL) system in OEO on the base of differential fiber-optical discriminator [60]. The OEO generation was obtained on the frequency 8–10 GHz using the quantum-well laser diode (2005) [61], OEO with the Mach–Zehnder modulator was investigated [62]. The new theoretical noisy model of OEO was created and examined, in which we took into consideration the laser with ultralow phase noises (less than −100 dB/Hz at offset of 10 kHz from the carrier) [63].

Many earlier misunderstandable phenomena and causal relations of OEO parameters (which were related to the mode choice of the double-channel optical Mach–Zehnder modulator) were explained. Developed methods of characteristics examination of FODL in OEO permitted to our quantum team from MPEI with colleagues from other Russian universities (for instance, Bauman State Technical University) to create and provide patenting of the new technology of the radiation-resistant optical fiber [64].

The optical fiber of such a type has relatively small loss variations (to 10%) at radiation affect.

References

1. A. Ly, V. Auroux, R. Khayatzadeh, Highly spectrally pure 90-GHz signal synthesis using a coupled optoelectronic oscillator. IEEE Photon. Technol. Lett. **30**(14), 1313–1316 (2018)
2. A.G. Correa-Mena et al., Performance evaluation of an optoelectronic oscillator based on a band-pass microwave photonic filter architecture. Radioengineering **26**(3), 642–646 (2017)
3. T. Sakamoto, T. Kawanishi, M. Izutsu, Optoelectronic oscillator using a $LiNbO_3$ phase modulator for self-oscillating frequency comb generation. Opt. Lett. **31**(6), 811–813 (2006)
4. C.X. Li et al., A novel optoelectronic oscillator with series-coupled double recirculating delay lines. Adv. Mater. Res. **986-987**, 1730–1733 (2014)
5. X. Zou, X. Liu, et al., Optoelectronic oscillators (OEOs) to sensing, measurement, and detection. IEEE J. Quantum Electron. **52**(1), 0601116 (2016)
6. D. Zhu, T. Du, S. Pan, A coupled optoelectronic oscillator with performance improved by enhanced spatial hole burning in an erbium-doped fiber. J. Lightwave Technol. **36**(17), 3726 (2018)
7. Z. Xiaobo et al., Low phase noise frequency-multiplied optoelectronic oscillator using a dual-parallel Mach–Zehnder modulator. Opt. Eng. **57**(8), 080101 (2018)
8. J. Lasri, P. Devgan, R. Tang, P. Kumar, Self-starting optoelectronic oscillator for generating ultra-low-jitter high-rate (100 GHz or higher) optical pulses. Opt. Exp. **11**(12), 1430–1435 (2003)
9. W. Li, J. Yao, An optically tunable optoelectronic oscillator. J Lightwave Technol. **28**(18), 2640–2645 (2010)
10. O. Okusaga, E.J. Adles, E.C. Levy, et al., Spurious mode reduction in dual injection-locked optoelectronic oscillators. Opt. Exp. **19**(7), 5839–5854 (2011)
11. W. Loh, S. Yegnanarayanan, J. Klamkin, et al., Amplifier-free slab-coupled optical waveguide optoelectronic oscillator systems. Opt. Exp. **20**, 19589–19598 (2012)
12. G.J. Dick, D.G. Santiago, R.T. Wang, Temperature compensated sapphire resonator for ultra-stable oscillator capability at temperatures above 77 kelvin. IEEE Trans. Microwave Theory Tech. **42**(7), 19–25 (2000)
13. G.J. Dick, R.T. Wang, Stability and phase noise tests of two cryo-cooled sapphire oscillators, IEEE Trans Ultrason Ferroelectr Freq Control. **47**(5),1098–1101 (2000)
14. G.J. Dick, R.T. Wang, Design of a cryocooled sapphire oscillator for the cassini Ka-Band experiment, The Telecommunications and Mission Operations Progress Report, TMO Progress Report. 42–134, 1–10 (1998)
15. P. Stockwell, C. McNeilage, M. Mossammaparast, D.M. Green, 3-Axis vibration performance of a compact sapphire microwave oscillator. IEEE Trans. Microwave Theory Tech. **46**(8), 123–199 (2002)
16. K.L. Ribeiro, E.N. Ivanov, D.G. Blair and etc, A proposal for improving the noise floor of the gravitational wave antenna Niobe. Classical and Quantum Gravity. **19**, 1967–1972 (2002)
17. R.A. Woode, E.N. Ivanov, M.E. Tobar, Application of the interferometric noise measurement technique for the study of intrinsic fluctuations in microwave isolators. Meas. Sci. Technol. **9**(NA), 1593–1599 (1998)
18. W. Zhou, G. Blasche, Injection-locked dual opto-electronic oscillator with ultra-low phase noise and ultra-low spurious level. IEEE Trans. Microwave Theory Tech. **53**(3I), 929–933 (2005)
19. C.W. Nelson, A. Hati, D.A. Howe, Microwave optoelectronic oscillator with optical gain, in Proceedings of the IEEE International Frequency Control Symposium (FCS '07), **31**(7), 1014-1019 (2007)
20. D. Strekalov, D. Aveline, N. Yu, R. Thompson, A.B. Matsko, L. Maleki, Stabilizing an optoelectronic microwave oscillator with photonic filters. J. Lightwave Technol. **21**(12), 3052–3061 (2003)
21. P. Devgan, J. Lasri, R. Tang, P. Kumar, Ultra-low-jitter multiwavelength synchronised optical pulse source for C-, Land U-bands. Electron. Lett. **39**(18), 1337–1339 (2003)

22. X.S. Yao, L. Maleki, High frequency optical subcarrier generator. Electron. Lett. **30**(18), 1525–1526 (1994)
23. X.S. Yao, L. Maleki, Optoelectronic oscillator for photonic systems. IEEE J. Quantum Electron. **32**(7), 1141–1149 (1996)
24. M. Yamanishi, T. Edamura, K. Fujita, N. Akikusa, H. Kan, Theory of the intrinsic linewidth of quantum-cascade lasers: hidden reason for the narrow linewidth and line-broadening by thermal photons. IEEE J. Quantum Electron. **44**, 12 (2008)
25. M. Shin, P.S. Devgan, V.S. Grigoryan, P. Kumar, Y.D. Chung, J. Kim, Low phase-noise 40 GHz optical pulses from a self-starting electroabsorption-modulator-based optoelectronic oscillator, in Proceedings of the Optical Fiber Communication Conference (OFC '06), Anaheim, Calif, USA, March 2006
26. J. Lasri, P. Devgan, V.S. Grigoryan, P. Kumar, Multiwavelength NRZ-to-RZ conversion with significant timing-jitter suppression and SNR improvement. Opt. Commun. **240**(4–6), 293–298 (2004)
27. Y.K. Chembo, K. Volyanskiy, L. Larger, E. Rubiola, P. Colet, Determination of phase noise spectra in optoelectronic microwave oscillators: a Langevin approach. IEEE J. Quantum Electron. **45**(2), 178–186 (2009)
28. M. Shin, P. Kumar, Optical microwave frequency upconversion via a frequency-doubling optoelectronic oscillator. IEEE Photon. Technol. Lett. **19**(21), 1726–1728 (2007)
29. J. Yu, X. Steve Yao, L. Maleki, Ultra low phase noise compact-sized optoelectronic oscillator. Jet Propulsion Laboratory. Opt. Lett. **22**(2), 37–45 (2001)
30. E. Rubiola, E. Salik, Y. Nan, L. Maleki, Flicker noise in high-speed p-i-n photodiodes. IEEE Trans Microwave Theory Tech **54**(2, Part 2), 816–820 (2006)
31. E. Rubiola, Phase Noise and Frequency Stability in Oscillators, Cambridge University Press, Cambridge, UK, 228p. (2010)
32. H. Peng, Y. Xu, R. Guo, D. Huayang, J. Chen, Z. Chen, High sensitivity microwave phase noise analyzer based on a phase locked optoelectronic oscillator. Opt. Exp. **27**(13), 18910–18927 (2019)
33. S. Pan, J. Yao, Optical clock recovery using a polarization modulator-based frequency-doubling optoelectronic oscillator. J. Lightwave Technol. **27**(16), 3531–3539 (2009)
34. D. Leeson, A simple model of feedback oscillator noise spectrum. Proc. IEEE **54**, 329–330 (1966)
35. D.B. Leeson, A simple model of feed back oscillator noise spectrum. Proc. IEEE **54**, 329–330 (1966)
36. M.X. Jeremy Everard, S. Bale, Simplified phase noise model for negative-resistance oscillators and a comparison with feedback oscillator models. IEEE Trans. Ultrason. Ferroelectr. Freq. Control **59**(3), 382–390 (2012)
37. T.E. Parker, G.K. Montress, et al., Precision surface-acoustic-wave (SAW) oscillators. IEEE Trans. Ultrason. Ferroelectr. Freq. Control **35**(3), 342–364 (1988)
38. A.A. Dvornikov, V.I. Ogurtsov, G.M. Utkin, On stationary states in two-dimensional networks of self-excited oscillators. Radiophys. Quantum Electron. **33**(9), 800–805 (1990)
39. V.S. Zholnerov, A.V. Ivanov, V.D. Kurnosov, R.V. Chernov, Parameters of a laser diode with a fiber Bragg grating at different fiber lengths. Tech. Phys. **59**, 416–420 (2014)
40. P.V. Gorlachuk, A.V. Ivanov, V.D. Kurnosov, R.V. Chernov, et al., Simulation of power current characteristics of high-power semiconductor lasers emitting in the range 1.5-1.55 μm. Quantum Electron. **44**(2), 149 (2014)
41. M.E. Belkin, Y. Semenova, et al., Tunable RF-band optoelectronic oscillator and optoelectronic computer-added design model for its simulation. Microwave Opt. Technol. Lett. **53**(11), 2474–2477 (2011)
42. M. Nakazawa, T. Nakashima, M. Tokuda, An optoelectronic self-oscillatory circuit with an optical fiber delayed feedback and its injection locking technique. J. Lightwave Technol. **2**(5), 719–730 (1984)
43. K.Y. Lau, A. Yariv, Self-sustained picosecond pulse generation in a GaAlAs laser at an electrically tunable repetition rate by optoelectronic feedback. Appl. Phys. Lett. **15**(45), 124–126 (1984)

44. V.V. Grigoriants, A.A. Dvornikov, Y.B. Il'in, V.N. Konstantinov, V.A. Prokof'ev, G.M. Utkin, A laser diode with feedback using a fibre delay line as a stable-frequency signal generator and potential fibre sensor. Opt. Quantum Electron. **17**(4), 263–267 (1985)
45. V.V. Grigoriaynts, Y.B. Il'in, Laser optical fibre heterodyne interferometer with frequency indicating of the phase shift of a light signal in an optical waveguide. Opt. Quantum Electron. **21** (5), 423–427 (1989)
46. A.A. Bortsov, V.V. Grigoriants, Y.B. Il'in, Effect of the lightguide excitation efficiency on the frequency of a self-excited oscillator with a differential fiber optic delay line. Telecommun. Radio Eng. **44**(8), 137–142 (1989)
47. X.S. Yao, L. Maleki, Optoelectronic microwave oscillator. J. Opt. Soc. Am. B **13**(8), 1725–1735 (1996)
48. Y.X. Steve, L. Maleki, Dual microwave and optical oscillator. Opt. Lett. **22**(24), 1867–1869 (1997)
49. J. Lasri, A. Bilenca, G. Eisenstein, D. Ritter, Optoelectronic mixing, modulation and injection locking in millimeter wave self-oscillating InP/InGaAs heterojunction bipolar photo transistors: single and dual transistor configurations. IEEE Trans. Microwave Technol. Theory **49**, 1934–1939 (2001)
50. J. Lasri, A. Bilenca, D. Dahan, et al., A self-starting hybrid optoelectronic oscillator generating ultra low jitter 10-GHz optical pulses and low phase noise electrical signals. IEEE Photon. Technol. Lett. **14**(7), 1004–1006 (2002)
51. E. Shumakher, G. Eisenstein, A novel multiloop optoelectronic oscillator. IEEE Photon. Technol. Lett. **20**(22), 1881–1883 (2008)
52. V.V. Grigoriants, A.A. Dvornikov, Y.B. Il'in, et al, Oscillators of the radio-frequency range with the optical carrier, in Proceeding of MPEI, Issue 607 (1983), pp. 76–79
53. A.A. Dvornikov, Y.B. Il'in, V.N. Konstantinov, About single-frequency modes of the oscillator with the fiber-optical delay line in the feedback loop. Radio Eng. Electron. **29**(11), 2234–2242 (1984)
54. V.V. Grigoriants, A.A. Dvornikov, Y.B. Il'in, et al., Radio signal generation in the system «laser optical delay line». Quant. Electron. **11**(4), 766–775 (1984)
55. A.A. Bortsov, V.V. Grigoriants, Yu. B. Il'in, ,V.N. Konstantinov. Transfer function of a composite fiber-optic delay line , Telecommun. Radio Eng. 43(9): 40-42, (1988)
56. A.A. Bortsov, V.V. Grigoriantz, Y.B. Il'in, Frequency tuning in a self-excited oscillator with a fiber-optic delay line. Telecommun. Radio Eng. **44**(4), 74–77 (1989)
57. T.V. Babkina, V.V. Grigoriantz, Y.B. Il'in, V.A. Prokof'iev, LASER APPLICATIONS AND OTHER TOPICS IN QUANTUM ELECTRONICS: Use of a laser oscillator heterodyne interferometer as an optical sensor of microdisplacements. Soviet J. Quantum Electron. **21** (12), 1384–1387 (1991)
58. T.V. Babkina, V.V. Grigoriantz, Y.B. Il'in, V.A. Prokof'ev, Self-sustained operation of a laser oscillating Mach-Zehnder interferometer. Soviet J. Quantum Electron. **21**(2), 230–231 (1991)
59. A.A. Bortsov, Y.B. Il'in, et al., Device for the functional transformation of acoustic pressure into frequency. Patent USSR 1,538,265, 1988,DOI: 10.13140/RG.2.2.10736.07688
60. Alexander A. Bortsov, Y.B. Il'in,Opto-electronic oscillator ,Generator of frequency-modulated signals, 2006-08-20, Patent RU2282302C1,2006, DOI: 10.13140/RG.2.2.29610.44488
61. A.A. Bortsov, Phase-frequency and amplitude-frequency characteristics of a mesa-adjusted laser diode with a modulation frequency band of up to 12 GHz. Radio Eng. (9), 43–47 (2006), DOI: 10.13140/RG.2.2.18285.82408
62. A.A. Bortsov, Y.B. Il'in, Laser spectral line widening effect on RF phase and amplitude noises of an optoelectronic oscillator OEO. J. Radio Eng. (2),21-31 (2010), DOI: 10.13140/RG.2.2.35665.07527
63. A.A. Bortsov, *The Influence of the Quality of Laser Resonator to Microwave Phase Noise in opto-electronic oscillator, Electromagnetic Waves and Electronic Systems, No.11* (Radiotekhnika, Moscow, 2012), DOI:10.13140/RG.2.2.28352.15361
64. A.A. Bortsov, Y.B. Il'in, V.E. Karasik, A. Karachev, et al., Method of manufacturing of work pieces for opticasing on nitrogen-doped quartz glass, Patent RU 2,537,450, 2015,DOI: 10.13140/RG.2.2.29191.01445

Chapter 2
Nanostructural Optoelectronic Oscillators with the Fiber-Optical Delay Line

We begin the description of a theory and application of the optoelectronic oscillator, which is the new nonlinear system combining units and methods of quantum electronics and radio electronics.

The main task of this chapter is to give the reader an initial information about operation principles of the optoelectronic oscillator, the principal issues, about complexities and suitable models for further discussion of advantages of this oscillator over the well-known devices for generation of precision microwave and mm-wave signals, and substantiate the problem statement of further theoretical and experimental analysis in this book.

In this chapter, we consecutively describe the main principal features and differences of the optoelectronic oscillator from the well-known traditional oscillators of precision oscillations. This chapter organizes as follows.

The chapter begins from examination of operation principles and the functional diagram of the optoelectronic oscillator (OEO) with the fiber-optical delay line (RF FODL) (Sect. 2.1). We formulate the methodological conception and discuss peculiarities of OEO theoretical investigations on the base of its representation as an ensemble of two nonlinear oscillating systems in the optical and radio-frequency (RF) ranges. We offer the reader the new approach for OEO examination, in which a laser (in the form of modern miniature laser diode) in the OEO structure is the key element. We emphasize that the basis for OEO mathematical description is the semiclassical laser theory with differential equations for electromagnetic field strength and the particle population on the upper energy level. At first, we introduce and discuss technical features and advantages of OEO with external and direct modulations (Sect. 2.2).

We introduce the most important functional diagrams reflecting the significant processes and describe of known from the theory of oscillating systems equations of phase balance for both OEO internal system: the optical-range modulating laser with the delay line and the internal microwave (or mm-wave) oscillator, which provides the microwave modulating signal for the optical part of OEO (Sect. 2.3). Further, we

A. A. Bortsov et al., *Laser Optoelectronic Oscillators*, Springer Series in Optical Sciences 232, https://doi.org/10.1007/978-3-030-45700-6_2

inform the readers and explain to them that in order to develop OEO with the low noise level on the RF carrier, the laser in the OEO structure should have low own noises (Sect. 2.4).

In Sect. 2.5, we discuss that the main reason of the laser noise is its spontaneous emission. To develop the theory (and further for experiment) we choose the modern quantum-dimension laser diode (the laser with a quantum well). Its role in OEO noise formation and its advantages and shortcomings are discussed further in Sect. 2.6 together with accomplished issues: the hybrid utilization of newest elements of optoelectronics and microwave and mm-wave techniques in OEO.

OEO with self-heterodyne mixing in the form of the oscillator consisting the phase fluctuations' correlator in the feedback loop; issues of OEO integration in future optical and optoelectronic systems; new methods of optical and optoelectronic control of the OEO microwave frequency. Then, in this section, we describe types on nonlinearities in OEO and study the dispersive fiber-optical delay line in OEO. The special attention is paid to types of optoelectronic oscillators based on the composition of modulated light sources, division of OEO according to topology of fiber-optical systems.

Section 2.7 is devoted to description of the modern elements of OEO: a laser, a modulator, the optical fiber, and the photodetector.

Comparison of technical OEO characteristics with other traditional oscillators: quartz oscillators, oscillators with surface acoustic waves (SAW), oscillators with resonator cavities for electromagnetic waves, performs in Sect. 2.8. The special attention at comparison is given to the Q-factors of oscillating systems, the phase noise of the RF carrier at small offsets.

Section 2.9 is devoted to description of technical characteristics of modern optoelectronic methods of formation of precision RF oscillations: commercial large-dimension and compact quantum frequency standards with optical pumping of the cesium and rubidium cells. Special attention is attracted to description of operation and characteristics of the frequency synthesizer with the optical microresonator.

At the end of this chapter, conclusions are offered necessary for further OEO analysis in Chaps. 3 through 7.

2.1 Operation Principle and Functional Diagram of OEO with RF FODL

This section is devoted to description of the operation principle, the functional diagram, and destination of OEO elements including RF FODL.

2.1.1 Optoelectronic Oscillator

OEO, which diagram is shown in Fig. 2.1a, from the scientific and engineering point of view is the self-oscillating system with delayed feedback, in which RF FODL is formed by the series-connected modulated light source (MLS), fiber-optical system (FOS), and photodetector (PD). In our case, the quantum-well laser diode (QWLD) is the MLS. The QWLD, which is described in detail in Chap. 4 of this book, has following serious features due to quantization of energy zones in the transition area:

- compared to the traditional micro-strip laser diode, it has the output optical power, which is several times more,
- its threshold pumping current is less by an order,
- less noises determined by the laser spontaneous emission, and
- less by the order bandwidth of the optical generation line.

The OEO block diagram presented in Fig. 2.1a consists of series-connected into a loop:

- the modulated light source on the base of QWLD,
- the FOS consisting of the one or several optical fibers,
- the PD,
- the nonlinear wideband amplifier for the RF signal,
- the narrowband RF filter (F) (the selective RF system), and
- the directional coupler for RF signal extraction.

At that, in this book, we consider OEO types, which differ on the modulation type: (1) OEO with direct modulation of QWLD emission [1], and (2) OEO with external QWLD emission modulation by the MZ electro-optical modulator (MZ in Fig. 2.1a). Both types of modulators are shown in upper insets in Fig. 2.1a. The OEO diagram with external modulation is constructed on the base of the electro-optical MZ modulator [2]. At that, the optical phase modulation (PM) is used in the one from two channels of MZ modulator. In addition, we can use the acousto-optical modulator with frequency modulation (FM) of laser emission for optical emission modulation in OEO. Application of various ways (direct and external) of optical modulation and its types: amplitude, phase, or frequency (AM, PM, FM) is defined by the OEO practical destination and its correspondence to technical specifications of the system.

For instance, in the high-frequency OEO, dedicated to systems for measurement of optical fiber parameters, in particular, at investigation of temperature dependences of the optical fibers, it is expedient to use the laser diode or the light-emitting diode (LED) with low-frequency internal modulation. In microwave OEO, suitable for application in the communication structures as, for example, low-noise devices for generation of reference oscillations with operation frequencies 5–73 GHz, it is expedient to use QWLD with direct and external modulation. In the ultralow-noise oscillators of microwave and mm-wave ranges (8–30 GHz) we need to use QWLD with the external MZ modulator.

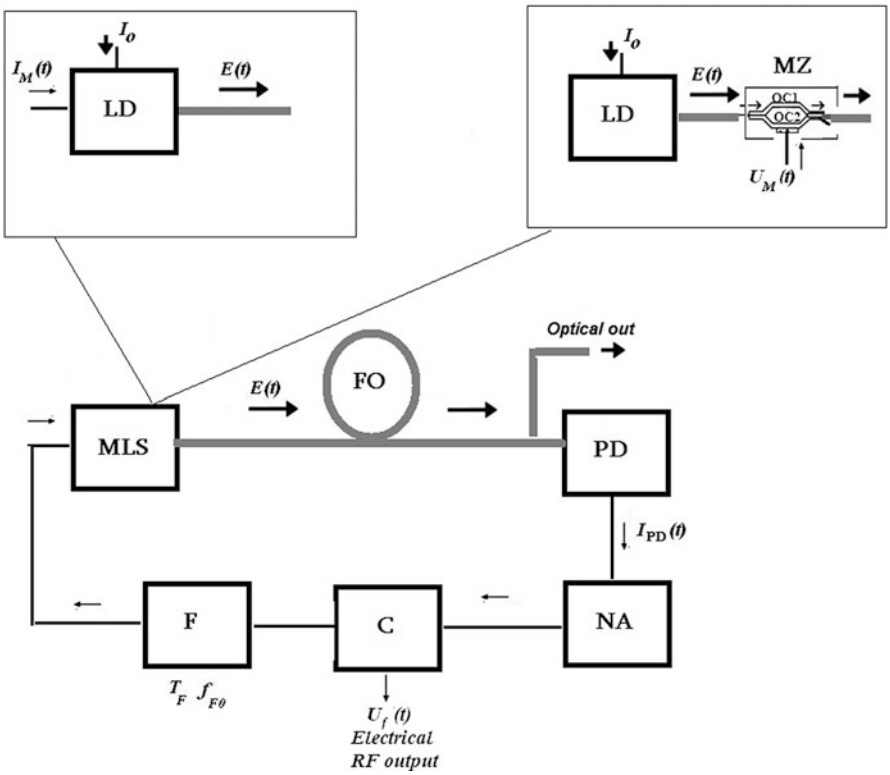

Fig. 2.1 (**a**) The OEO functional diagram with various modulated light sources: OEO with QWLD with direct modulation and OEO with QWLD with the external electro-optical modulator; (**b**) OEO oscillations spectra at optical and RF outputs, (**c**) the approximate view of the RF oscillation spectrum, which are generated by OEO with QWLD in the steady-state of single-frequency generation on 8.2-GHz frequency (observation time is 1 ms) (Hereinafter, in structural figures, thick lines in figures show the optical flows, while the thin lines show RF flows)

The quantum-dimension laser diode represents the nanostructural ultra-wideband mesa-strip injection semiconductor laser diode with the following high output indices:

- emission power 10–30 mW,
- modulation bandwidth due to utilization of photon technologies is 10–40 GHz, and
- the slope of the optical power transformation for pumping DC is 1 mW/10 mA.

QWLD is the nanostructural element since semiconductor material layers are formed in its active part, which have the de Broglie wave sizes of about 1–10 nm. From the point of view of modern oscillation theory, formation of such layers (or quantum zones) allows creation of original self-oscillating systems and resonators for electrons being the active particles in QWLD. In such oscillating systems,

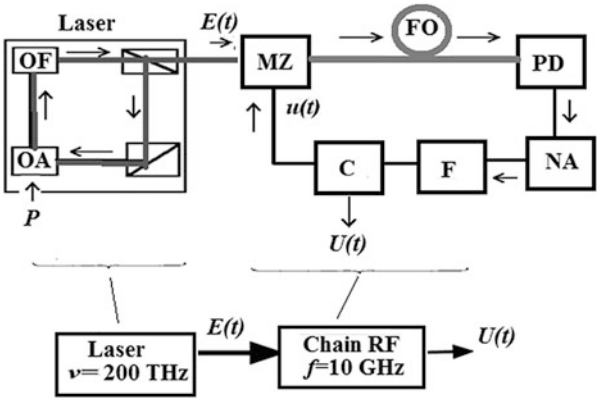

Fig. 2.2 The OEO structural diagram: Laser = the optical quantum oscillator (generator) (the laser or QWLD), MZ = the electro-optical MZ modulator, OA = the optical amplifier, OF = the optical filter, FOS = the fiber-optical system, PD = the photodetector, NA = the nonlinear amplifier, F = the RF filter, C = the RF coupler, Chain RF = the feedback radio-frequency chain of the oscillator

electrons begin to perform oscillating movements, and as a result, the function of the system amplification coefficient versus the optical frequency has the sharply expressed resonance peaks.

Figure 2.2 shows the real structural diagram of OEO. One of the main features of this OEO is simultaneous self-excitation of two oscillation processes of different frequency ranges: optical and RF. In Fig. 2.2, OEO consists of the separate blocks: a laser with the optical system (the left part of Fig. 2.2) and a loop with optoelectronic part (the right part in Fig. 2.2), in which there are RF elements (NA, F, C) closed in the loop and the MZ modulator at input of the optoelectronic part.

In the lower part of Fig. 2.2, the transmission of the optical signal $E(t)$ from a laser (optical part) to the input of optoelectronic part (the input of the MZ modulator) is conditionally shown.

The Fig. 2.3 shows a variant of the ultralow-noise RF oscillator implementation based on OEO, which can be used as the low-noise reference (master) oscillator for many standard and specific communication systems, radar systems, measuring systems, navigation systems with improved characteristics. In this diagram, excited RF oscillations pass to the external modulator of the laser and modulate the optical oscillations, which pass through the optical signal amplifier and then, through the double-channel fiber system, to the photodiode. This photodiode extracts the RF part of modulated optical oscillations and sends the RF signal into OEO feedback loop. As a result, the steady-state occurs with double-frequency process: optical and RF.

2.1.2 Methodic Conception and Features of OEO Theoretical Investigation

Let us extract the main components of investigation conception accepted by us in this book.

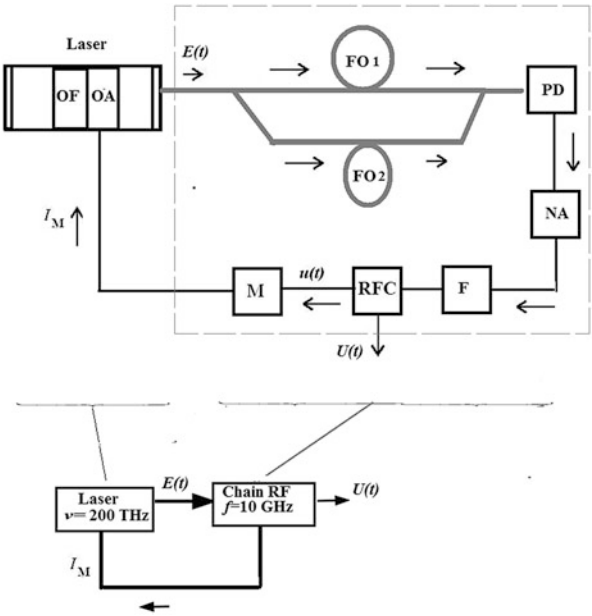

Fig. 2.3 The block diagram of the low-noise laser OEO with direct laser (or QWLD) amplitude optical modulation with two optical channels (FOS1 and FOS2). Laser = the optical quantum oscillator (generator) (the laser or QWLD), MZ = the electro-optical MZ modulator, OA = the optical amplifier, OF = the optical filter, FO = the optical fiber, PD = the photodetector, NA = the nonlinear amplifier, F = the RF filter, O = the RF coupler, Chain RF = the feedback radio-frequency chain of the oscillator

The subject of investigation is oscillation processes in OEO circuits (with external and direct modulation according to Figs. 2.1, 2.2, and 2.3), which contains in its basis the phase and amplitude principles of optical emission modulation. OEO represents the **double-range oscillating system** with the huge frequency difference, in which oscillations in optical and RF ranges are simultaneously formed according to their own laws and to nonlinear interaction, which we must study in this book.

In these OEOs, the radio frequency of QWLD modulation (it is the OEO output microwave frequency) is much more than the relative spectral line width of high-stable (according to physical principles) of laser emission. Moreover, in OEO, the optoelectronic conversion occurs on the photodetector at least of two optical harmonics into the low-frequency photocurrent (or the RF oscillation), and the heterodyne photodetection (of self-heterodyne mixing) takes place at the laser quasi-coherent oscillation. OEO structures under our investigation with direct and external modulation (as well as circuits with application of additional suppression of the one from three optical harmonics and with amplitude alignment of the rest remained harmonics) contain in its structure the initial base for utilization of the *correlation method of the phase noise suppression*. Potentially, these OEOs have the high degree of suppression of the spontaneous laser phase noise, the electronic noises of the photodetector and an amplifier. We may say that in OEOs under consideration, the practical *correlator* is implemented (together with utilization of the lengthy quartz RF FODL for stabilization of generated frequency and for phase noise suppression). In this case, the OEO operation mode is similar to operation of the difference oscillator, in which, thanks to generation of two frequencies, the essential reduction of power spectral density of the phase noise happens.

The main problems under solution of the theoretical of our investigation are: determination of QWLD parameter influence (the pumping current, the phase noise) and the optical fiber influence (the geometric length, the refraction index, the temperature dependence of the refraction index, etc.) onto characteristics of the oscillating RF process in OEO, determination of the laser noise influence on the OEO RF noise.

For mathematical modeling of the QWLD emission, we use, in particular, the well-known semiclassical laser theory, taking into consideration the phase relationships of the electrical field strength. This is caused by the circumstances discussed in the next sections.

2.1.3 Semiclassical Laser Theory

The semiclassical theory (of the semiclassical approximation) with account of phase relationships constitutes the one of methodic fundamentals of our approach. This means that for description of electromagnetic field (EMF) interaction with the active substance of QWLD we use the classical Maxwell equations, and substance properties are described by the polarization vectors and the carrier population level on the upper energy level. Further, we show that for the semiconductor QWLD, three equations (for the laser field intensity, for the active substance polarization, and for the population difference of energy levels) can be reduced to the system of two equations for the field intensity and the population difference. In some cases, in the present book (for instance, in Chap. 4), we use the balanced kinetic differential equations of Stats-de-Morse, in which the connection of the photon density in QWLD emission and the population difference level allows an analysis of dynamics and the laser (or QWLD) transfer function. Nevertheless, at utilization of the balanced equation method, as usually, we lose the *phase relationships*, which are the main at analysis of QWLD phase noises and its influence on the OEO RF output noises. Once more, we should note that most of OEO structures (with direct and external modulation) under investigation can be related to circuits with the phase and amplitude modulation of optical emission, and during photodetection with self-heterodyne mixing, an information about the subcarrier is contained in the phase of optical emission.

The following specific character influences on the model choice and its limitations at OEO investigations:

- the noise quantum nature,
- the temporal and spatial coherence,
- the presence of spatial distribution on the intensity amplitude $E_0(R)$, on the phase $\Phi_0(R)$ and on amplitude $m(R)$ and phase $\Delta\varphi(R)$ fluctuations (where R is the *spatial parameter*),
- the proportionality of overall sizes of optical channels and the phase detector area in the microwave range with the laser wavelength.

We must emphasize that the main aim of our research in this part is an analysis of laser characteristic influence (the optical power of stimulated emission, the spontaneous emission level, the laser phase noise, the *Q*-factor or the time constant of the laser optical cavity, the photon lifetime in the QWLD optical cavity, the carrier lifetime in QWLD) and the fiber-optical path (the geometric length of the fiber, the optical losses of emission in the fiber, etc.) on OEO characteristics as a whole. Therefore, the laser or QWLD is marked during analysis as *the main element*. The laser is the optical quantum generator, which generates oscillations using the forced transitions of the active substance between energy levels. The laser differs from traditional electronic oscillators by the nature of generation. It has features, one of which is the **quantum nature of the laser emission noise**. At that, *noises of spontaneous* output laser emission, which are determined by the lifetime of particles in excited state, essentially exceed thermal noises in the optical range.

In options of direct and external laser modulation, the low-noise OEO is built using the *phase and amplitude principles* of the laser emission modulation. In this case, the laser phase noise determines the total OEO phase noise level, taking into account a smallness of all remaining noises of the nonlinear amplifier and the phase detector.

2.1.4 Semiclassical Laser Approximation

The semiclassical approach to the laser theory (in particular, to QWLD) forms the one of the main methodic fundamentals of the present book. This means that for laser description (in Chaps. 6 and 7), which is a part of OEO with RF FODL, we use the classical Maxwell equations, but substance properties and properties of the active element material are described by polarization vectors. A peculiarity of this approach in semiclassical approximation is the fact that for specific laser type with narrowband QWLD cavity, we can express the substance polarization through the vector of the field strength. This allows reduction of three equations for the laser field strength, the active substance polarization, and the population difference of energy levels to the system of two equations for the field strength and the population difference (Chap. 3). The complete differential equations of the system obtained for this approach, permit so-called *abbreviation* (reduction of equation order) under assumption of band limitation or the high effective *Q*-factor. Abbreviation of our system of complete differential equations enables us to obtain a system from three equations for amplitude and phase of the optical oscillations strength and the equation for carrier population of active material. Such an approach is true for processes with the time constant of the optical cavity of 10^{-11} to 10^{-6} s, which is more than the time constant of longitudinal relaxation (substance polarization) 10^{-12} s. At that, for narrowband semiconductor QWLD (with the line width less than 1–1000 MHz), the time constant of the optical cavity is 10^{-9} to 10^{-6} s. The population settling process in the active substance plays an important role in the phase noise formation

process (determined by the spontaneous noise) and occurs with the time constant (or the carrier lifetime on the upper energy level) of 10^{-9} to 10^{-8} s.

Description of excitation and oscillation propagation in the OEO RF part (in the nonlinear amplifier, the filter and in electric circuits) is performed in this book by traditional methods using the apparatus of the circuit theory and the nonlinear oscillation theory. The time constant of OEO RF filter with the Q-factor of 100–1000 on the frequency, for example, of 10 GHz is about 10^{-8} to 10^{-7} s. At that, this time constant is much more or congruent than the time constant of the laser (or QWLD) optical, which is 10^{-12} to 10^{-6} s.

We may note that **two oscillating processes** are simultaneously developed and observed in OEO in different ranges: optical and RF with frequency ratio approximately 1:2800. In other words, we may separate two different oscillating processes in OEO on different frequencies or to say about different types of generators—the optical quantum generator with generating frequency about $\nu_0 = 128$ THz and the RF generator with generating frequency $f_0 = 1$–100 GHz. At that, the optical quantum generator in the OEO structure is as if the pumping source for the RF generator. If the laser or QWLD can be separated in OEO in the single unit (Fig. 2.2), then the RF generator includes the laser or QWLD. On the other hand, OEO may be represented at mathematical modeling in specific cases by the equivalent circuit of the traditional RF oscillator with laser presentation by various mathematical models, including the simplest one: the linear or nonlinear element with the relatively simple transfer function. For example, RF FODL in the OEO structure can be presented by the linear two-port circuit, which is described by the Y-matrix with given input and output admittance. In the further analysis in Chaps. 3 and 7, at OEO investigation, we use mathematical models based on differential equations.

Spectra of two oscillating processes in OEO are formed by *fluctuations* of different nature, and the final width of the OEO RF spectral line is determined by parameters of two resonant systems—the optical laser cavity and the RF filter in the OEO structure. The interesting OEO feature is that the RF oscillation spectrum is formed by not only noises, which have an electronic nature, but the phase fluctuations of the laser optical emission, which have the *quantum nature* and are determined by spontaneous laser emission.

In the optical range, in low-noise microwave OEOs, **transverse section sizes** of the photodetection area (or the emission "spot" on the light-sensitive area of the photodetector) are **commensurate with the laser wavelength**. As a result of interference on the photodetector area of two optical oscillations and photodetection, the useful electric signal is extracted on the photodetector load. In contrast to the RF range, in which transverse geometrical sizes of the detector chip (for instance, the semiconductor diode) are 10–1000 times less than the wavelength of electromagnetic oscillations, which fall to this detector. In the optical range sizes of the photodetector light-sensitive area (used in the low-noise OEOs, which operate on frequencies above 0.3 GHz) are comparable with the laser emission wavelength and are 1.5 μm. In this case, the model of the plane electromagnetic wave for the OEO optical units and the photodetector area must be applied with a big prudence.

These features are determinative at account of OEO phase noises in the circuits with direct QWLD amplitude modulation and external modulation with the help of the MZ modulator.

We can conclude that in optical range, the laser phase noise, because of mentioned reasons, cannot be cancelled, as it was made in all previous OEO publications of other authors [3–9] at the general phase noise analysis of RF oscillations.

Let us consider the OEO structure (Fig. 2.2) in detail.

2.1.5 A Laser in OEO Structure

The laser or QWLD in the OEO structure (Fig. 2.2) is formed by the optical amplifier, the narrowband optical filter, closed into a loop. The optical generating frequency ν in the laser (or QWLD) is determined (of course, under fulfillment of excitation conditions) by so-called equations of the amplitude (power) balance and the phase balance of steady-state optical oscillations. The phase balance equation has a form:

$$\varphi_{\text{optY}}(\nu) + \varphi_{\text{optF}}(\nu, e_{\text{Y1}}) + \varphi_{\text{optZ}}(\nu) = -2\pi n, \tag{2.1}$$

where $\varphi_{\text{optY}}(\nu)$ is the phase-frequency characteristics (PFC) of the nonlinear optical amplifier, $\varphi_{\text{optF}}(\nu, e_{\text{Y1}}) = \varphi_{\text{OF}}$ is PFC of the narrowband optical filter with the natural frequency $\nu_{0\text{L}} = \nu_{\text{OF}}$ with the time constant $T_{\text{OF}} = T_{\text{optF}}$; $\varphi_{\text{optZ}}(\nu)$ is the phase incursion in the remaining parts of the laser equivalent circuit (besides OF and NA); e_{Y1} is the DC control voltage, which is applied to OF to change its natural optical frequency, $n = 1, 2, \ldots$. The sign minus in the right side of Eq. (2.1) shows that the total PFC is the negative quantity.

On the other hand, OEO with the external MZ modulator (Fig. 2.2) represents the RF oscillator, which is formed by a laser and the electro-optical MZ modulator, the fiber-optical light guider, the photodetector, the nonlinear amplifier, the narrowband RF filter closed into a loop. The generating radio frequency ω in the RF part of OEO is determined by *fulfillment of excitation conditions* and the phase balance equation of steady-state self-modulated[1] oscillations:

$$\varphi_{\text{FODL}}(\omega) + \varphi_{\text{k}}(\omega) + \varphi_{\text{e}}(\omega) = -2\pi m, \tag{2.2}$$

where φ_{FODL} is PFC of the remaining part of RF FODL containing the MZ modulator, RF FODL and the photodetector, with total group optical time delay in

[1]Do not confuse yourself: speaking about self-modulation (or auto-modulation), we mean here not the spurious self-modulation of traditional oscillator, caused by wrong choice of inertial auto-bias circuit. We mean here the useful self-modulation of the optical oscillation by the RF output microwave oscillation of OEO, which is principal useful process for OEO.

this part of $T_{FODL} \approx T_{FOS}$; T_{FOS}—time delay in optical fiber; $\varphi_k = \arctan[2\pi(f - f_{eF})$ $T_{eF}]$ is PFC of the narrowband RF filter with the natural resonance frequency $\omega_F = 2\pi f_{0F}$ and the time constant $T_F = T_{eF} = T_{EF}$; $\varphi_e(\omega)$ is the phase incursion in the wideband electronic nonlinear amplifier, $m = 1, 2, \ldots$.

In the circuit of Fig. 2.2, a laser, on the one hand, performs the energy pumping of the RF oscillator, and on the other hand, is the main element of OEO with RF FODL.

2.1.6 MZ Modulator in OEO Structure

Laser optical emission (on the carrying optical frequency) passes to the input of the MZ modulator, in which the emission is modulated by the electric signal $u = u_g(t)$ at microwave frequency. Then, the optical emission passes to the light-sensitive area of the photodetector (the optical input of PD) through the optical modulator. RF oscillations (subcarrier) obtained on low-frequency PD load pass to the transistor nonlinear amplifier and to the frequency-selective RF filter and are directed to the microwave control input of the MZ modulator within this loop system through the directional coupler (C).

If OEO excitation conditions are satisfied for the "electronic" part of OEO (where exactly $u = u_g(t)$), then RF microwave oscillations of the electric voltage $u = u_g(t)$ arise, which are self-modulating for optical emission. The instantaneous value of this voltage can be written as

$$u_g(t) = U_0 \cos(2\pi f_0 t + \phi_{0e}), \tag{2.3}$$

where $U_0 = U_{0M} = U_{0F}$ is the oscillation amplitude of the controlling (modulating) microwave voltage at the input of the MZ modulator or at the output of the RF filter, f_0 is the microwave frequency of generated steady-state oscillations, ϕ_{0e} is an initial phase of the $u_g(t)$ voltage (the constant phase shift). When using of QWLD, which is controlled by the microwave component of the bias current, the direct amplitude modulation occurs and, as a consequence, the laser intensity modulation.

Let us consider now peculiarities of microwave generation in OEO at formation of modulated laser emission with a small modulation index for the case when the laser emission spectrum width $\Delta\nu_L$ is much less than a RF subcarrier frequency f_0: $\Delta\nu_L \ll f$. The spectrum of modulated optical emission represents the definite equidistant set of components, which is apart one from another by the subcarrier frequency (modulation frequency) of f_0. We are limited by consideration of the "mode with two sidebands", i.e., only three optical spectral components, which optical frequencies are, relatively, $\nu_1 = \nu_1 - f_0$, $\nu_2 = \nu_0$, $\nu_3 = \nu_3 - f_0$. Two of these optical frequencies ν_1 and ν_2 are spaced from the central optical laser frequency ν_0 by the subcarrier frequency f_0.

In the further discussion, we examine OEO with the modulated light source, in which the optical phase MZ modulator plays a role of the OEO modulator (or the intensity modulator, as it is often called).

The MZ modulator represents two optical channels OC1 and OC2 in the form of two strip optical waveguides connected at the input and the output by the optical Y-couplers (Fig. 2.1a). The input Y-coupler distributes the laser emission with the strength of electric component E_{L} of EMF between these two optical channels. In OC2, emission with the electric component strength $E_{2\mathrm{L}}$ of EMF is modulated due to the linear electro-optical effect in the optical phase by the microwave voltage $u = u_{\mathrm{g}}(t)$ from the output of the RF filter. In the optical channel OC1, emission of this component is not modulated. The group delay time at the output of the optical channel OC2 with respect to the MZ input depends on the instantaneous value of the control voltage: $T_{2\mathrm{M}} = T_{2\mathrm{M}}[u(t)]$. At the output of OC1, the delay time $T_{1\mathrm{M}}$ keeps constant. Optical emission from outputs of OC1 and OC2 with electric components strengths $E_{1\mathrm{L}}$ and $E_{2\mathrm{L}}$ of EMF are combined (summed) in the output X-coupler and pass to the input of the single optical fiber, in which they are delayed by the group time and, having passed through it, act on the light-sensitive area of the photodetector.

In the general case, output emission with electric component strengths $E_{1\mathrm{L}}$ and $E_{2\mathrm{L}}$ of EMF of the OC1 and OC2 channels of the MZ modulator may pass to the photodetector input not through the single mutual light guider, but each emission (from these two) through the own separate light guider. In this case, the delay difference will be:

$$\Delta T_{\mathrm{M}} = T_{2\mathrm{M}} - T_{1\mathrm{M}} + T_{2\mathrm{FOS}} - T_{1\mathrm{FOS}}. \tag{2.4}$$

In the case when the fiber-optical system is formed by the single optical fiber (from 100 m and to 1 km and more), $\Delta T_{\mathrm{M}} = T_{2\mathrm{M}} - T_{1\mathrm{M}}$. In the general case, optical fibers included into RF FODL are dispersive optical delay lines, i.e., the delay time in them is a function of the optical frequency. In the vicinity of the average laser generation frequency ν_0, a dependence of delay T_{FOS} versus the optical frequency ν is approximately the linear function:

$$T_{\mathrm{FOS}}(\nu) = T_{\mathrm{FOS}}(\nu_0) + T_{\mathrm{FOS}}(\nu_0) \cdot (\nu - \nu_0) \cdot \tau_{\mathrm{D}} \tag{2.5}$$

where τ_{D} is the delay slope and determines by the polarization, mode, material and waveguide dispersion of the fiber system in the time domain and by the spatial dispersion of the fiber-optical system and is at average the value of $\tau_{\mathrm{D}} = 2$–15 ps/(nm km) (or 10^{-7} s/GHz) for modern single-mode optical fibers. Thus, in the general case, OEO represents the oscillating system with dissipation, in which structure the dispersive delay line is included. But, taking into consideration that narrowband lasers with the spectral line width of 1 kHz to 1 MHz are used for operation in low-noise OEO, we neglect the optical fiber dispersion during the analysis of OEO. An influence of the optical fiber dispersion, when using the high-dispersive optical fibers in OEO, will be considered in Chap. 7 of the present book.

The control of the generation frequency ω in OEO with RF FODL under consideration is explained starting from the phase balance equations of the steady-state auto-modulated oscillations [10]:

$$\varphi(\omega, A, B) + \varphi_{\mathrm{k}}(\omega) + \varphi_{\mathrm{e}}(\omega) = -2\pi m, \quad m = 1, 2, \ldots \tag{2.6}$$

where $\varphi(\omega, A, B)$ is the PFC of the fiber-optical system (FOS), $\varphi_k = \arctan[2\pi(f - f_{eF})T_{eF}]$ is the PFC of the narrowband filter with natural frequency f_{eF} and the time constant $T_{eF} = T_{EF} = T_F$; $\varphi_e(\omega)$ is the phase incursion in the remaining (besides the filter) wideband RF part of OEO including a laser and a photodiode. A and B are excitation coefficients of the optical fiber OF1 and OF2, relatively (Fig. 2.3).

During varying of FOS PFC at variation of excitation factors of the OF various lengths, which are included into RF FODL structure, the frequency of OEO with RF FODL varies. Authors of this book offered [3, 10–24] and patented new methods of OEO microwave frequency control with the help of optical and optical-electronic methods [20, 21]. The steady-state frequency in the system of OEO with RF FODL with the directional coupler of Y-type (Fig. 2.3) at variation of A and $B = 1 - A$ is determined by the following equation (at approximate equality of A and B coefficients) [11]:

$$f = (f \cdot T_{eF} + m)/(T_{eF} + T_{0FOS} + AT_{1FOS} + BT_{2FOS}) \tag{2.7}$$

where $m = 1, 2, \ldots, T_{0FOS}, T_{1FOS}, T_{2FOS}$ are oscillation delays in the optical fibers FOS0, FOS1, and FOS2, relatively (Fig. 2.3). The frequency control in the system with the Y-type directional coupler, as it is shown in Chap. 5, is performed by variation of A and B coefficients in the one of the light guiders FOS1 or FOS2. From Eq. (2.7) it follows that at $A = 1$ and $B = 0$, the OEO frequency depends on the delay time in RF FODL. At large delays $T_{FOS} = T_{0FOS} + T_{1FOS}$, $T_{FOS} \gg T_{eF}$, the OEO generation frequency is stabilized at the expense of large delay in the feedback loop of RF FODL. The ultralow OEO phase noise is achieved at the expense of creation of the high-Q optoelectronic oscillator of the "traveling-wave" with the loaded equivalent Q-factor $Q = (0.2–0.8) \times 10^6$ (in the frequency range 1–70 GHz) on the base of RF FODL.

2.2 Technical Features and Advantages of OEO with External and Direct Modulation in Options with Self-Heterodyne Mixing

OEO can be subdivided into types of modulated light sources: with laser, which bandwidth $\Delta\nu_L \ll f$, where f is radio-frequency of modulation. At fulfillment of the condition $\Delta\nu_L \ll f$ at frequency and phase laser modulation, OEO is a system with coherent photo-heterodyne mixing or with the differential oscillator. In such a differential oscillator, we can perform the self-heterodyne mixing mode for optical emission at photodetecting, and to provide the effective noise suppression, which has the electronic and optical nature. The physical sense of this benefit can be explained by the "spectrum purification" of the differential from two optical harmonics of the detected (by the photodetector) oscillation similar to the traditional heterodyne receiving. Later, in one of the sections of this chapter, physical sense on this effect in OEO is described in detail.

Architectures of OEO can be distinguished according to modulation approach and to photodetection. In OEO with external modulation and with the direct amplitude modulation, the phase and amplitude (relatively) modulation of the optical emission and further photodetection at least two optical oscillation are used. The one of the optical oscillation is modulated in phase by the RF subcarrier signal. These architectures can be concerned to the circuits with heterodyne photodetection according to the approach to photodetection. In cases of the traditional heterodyne photodetection, which is used in the laser radar technology, at reception of the external optical emission, the oscillation *modulated in phase or frequency* is received with using the external optical generator or the heterodyne, which oscillations pass to the light-sensitive area of the photodetector together with the external receiving optical oscillation. In OEO with external or direct modulation, the *self-heterodyne-mixing* is used, i.e., on the photodetector area, two (or three) optical oscillations (or harmonics) with frequency (1) $\nu_1 = \nu_0 - f_0$, $\nu_2 = \nu_0$, $\nu_3 = \nu_0 + f_0$, or (2) $\nu_2 = \nu_0$, $\nu_3 = \nu_0 + f_0$, which pass from the one QWLD, are combined.

The most important advantage of the heterodyne conversion is its ability to save information in phase of the optical oscillations and its transfer into the electric signal of the photodetector current. But at that, at photoreception of the laser (or QWLD) emission, there is a transfer of phase fluctuations of the laser oscillations, which are determined by its spontaneous emission, into phase fluctuations of the RF microwave oscillations, and this is unpleasant and often inadmissible.

As a result of self-heterodyne mixing, in the photodetector, the RF subcarrier, and phase noises of QWLD (which plays the role of the heterodyne) are extracted. In this case, the oscillation spectrum of the photocurrent (under condition of smallness of the own noises of photodetector and the nonlinear amplifier) repeats the spectrum form of optical oscillations of the field strength of the signal wave, but with the frequency shift downward exactly by the frequency of the laser-heterodyne. In spectral representation this can be expressed as: the optical signal spectrum (or PSD of AN and PN noises) shifts almost without variations into the region of the RF subcarrier f_0 spectrum, and at finite spectrum width of the laser-heterodyne, the RF subcarrier f_0 spectrum (the electric signal) is additionally spread.

2.3 Spontaneous Laser and QWLD Emission and Its Role in OEO Noises' Formation

The main aim of this section is determination of the ratio of the spontaneous emission level and the level of stimulated laser emission at its output for different quantum generators (laser on ruby and neodymium, semiconductor quantum generators, and QWLDs). In essence, we below substantiate and prove the following statement: the contribution of spontaneous emission of the laser (or QWLD) is the main contribution into phase noise formation in OEO, and the power spectral density (PSD) of the phase noise is determined as a ratio of spontaneous emission level and

the level of stimulated laser emission, which depends mainly by a ratio of active carrier population in the upper "emissive" level and the total carrier population. The bandwidth of PSD of the phase noise line is determined by the spontaneous emission intensity, which depends on the carrier lifetime on the emissive level.

We emphasize that the influence on OEO phase noise formation, which is caused by a presence of the relatively large spontaneous emission level, is the one of the main distinctive properties of optical generators compared to traditional electronic oscillators. As it well known, the spontaneous emission level has a cubic dependence upon the photon emission frequency. At that, it essentially exceeds a noise in the optical range caused by thermal factors, which is proportional kT (where k is the Boltzmann constant, T is the temperature in Kelvin), and the flicker-noise and the shot noise, which are traditionally studied in radio physics. The issue of the OEO phase noise is considered in detail in Chaps. 4, 6, and 7. Here we substantiate the main relationships.

The new scantily investigated (in radio physics sense) noise source appears, which is caused by the QWLD spontaneous emission detected by the photodetector in OEO compared to traditional electronic oscillators investigated in the nonlinear oscillation theory. For the coherent system of formation and the heterodyne photodetection, to which OEOs are concerned, the spontaneous emission noise is determining because its level essentially exceeds the proper electronic noises of the photodetector and the nonlinear amplifier. Small spontaneous emission examination and the fact that it is not marked as the separate specific quantum noise in a majority pulse optoelectronic systems, which are widely used in RF FODLs, can be explained by the fact that they use the pulse mode of laser (or QWLD) operation. At that, the detection is usually performed without utilization of heterodyne-mixing. In systems for information transmission, for example, in usual pulse RF FODLs (in OEO, the large signal acts on the light-sensitive area of the photodetector) a small signal is applied to the photodetector area, and the pulse emission power is detected, while noises in RF FODL are determined by the photoreceiver noises.

A complexity of noise modeling and investigation, which is caused by QWLD spontaneous emission, can be explained by the fact that spontaneous emission has the pure quantum nature. Here under the quantum nature, we mean the "postulates," which are proved within the limits of the quantum mechanics theory about atom energy levels at transfer from upper "emissive" energy level E_2 onto the lower level E_1, the particle (an atom or an electron at recombination) emits a light quantum $h\nu = E_2 - E_1$ (ν is the optical frequency, h is the Planck constant) and stimulated emission happens at interaction of the particle with the electromagnetic field with this field frequency and the same phase of external EMF. We must at that to take in the consideration the process of spontaneous emission. The correct mathematical description of spontaneous emission is possible at using the quantum mechanics apparatus. We would like to remind that spontaneous and stimulated emission in impossible to describe within the limits of the ordinary electrodynamics. For example, during accelerated electron movement on an orbit around a nucleus, the light emission does not occur although, according to electrodynamics laws, in this case the electromagnetic wave must be emitted into a space. Dealing with quantum

mechanics equations is rather complicate, and the theoretical investigation practice shows that for accurate description of processes in the optical quantum generators is sufficient to use the semiclassical model in the dipole approximation. As we already mentioned, in this book, we use exactly such a semiclassical laser model in the dipole approximation for an analysis of the OEO PSD phase noise (Chaps. 4, 6, and 7). If to perform the investigation of OEO phase noise within the limits of this semiclassical laser model, we must add the traditional model built for electric field strength of the laser stimulated emission by the noise source also in the dimension of the electric field strength, which is proportional to the spontaneous emission level in the quasi-steady-state condition.

2.4 Hybrid Utilization of Up-to-Date Electro-Optical Elements and Microwave Elements in OEO

OEO as the oscillation source of new type has advantages caused by the combined use of up-to-date solid-state components and elements of optoelectronics and acoustic-optics, the optical fibers and the traditional element base of microwave and mm-wave engineering.

Application in OEO of the single optical fiber (together with the low-noise laser and the photodiodes) allows development of the compact (10 mm × 100 mm × 100 mm) low-noise RF FODL of high-Q (more than 1,000,000) with the delay more than 50 μs (at the fiber length of 10 km). Electric power losses of the transmitted signal in the frequency range from 0.1 Hz to 50 GHz are from −10 to −18 dB at the fiber length not more than several kilometers.

This low level of microwave losses occurs at the expense of the relatively high slope of laser and photodiode transformation, low optical attenuation in optical fibers and in directional couplers. Such a RF FODL is stable to high percussion and long-term dynamic overloads and acceleration (2–10 g), to long-term acoustic impacts. The nearest alternative solution of the microwave oscillator on the sapphire monocrystals [25] cannot endure of high percussive and dynamic loads more than 100–200 N/sm^2. On the other hand, the creation of oscillation delay more than 50 μs (at optical fiber length of 10 km) is possible in RF FODL. At that, due to raising of the geometric fiber length, the laser power growth, application of the low-noise lasers in RF FODL, we can achieve the OEO phase noise less than −120 dB/Hz at frequency offset 1 kHz from 10 GHz carrier.

Obtaining of the microwave phase modulation of the optical emission became possible at appearance of electro-optical phase modulators of the microwave oscillations. Effective reduction of the phase noise in OEO takes place at the expense of the RF FODL use with large delay time (10–50 μs for oscillations with frequencies 8–12 GHz), as well as at the expense of coherent photodetection use and the heterodyne mixing of two delayed optical oscillations. An opportunity to obtain the phase noise compensation at self-heterodyne mixing is caused by the high ratio

of the optical carrier frequency 128 THz to the frequency of the microwave subcarrier of 10 GHz, which is 12,800. Obtaining in OEO on the microwave subcarrier of 10 GHz of PSD of the phase noise less than −120 dB/Hz for offset 1 kHz is quite realizable.

2.5 OEO with Self-Heterodyne Mixing as the Oscillator Containing the Phase Fluctuation Correlator in the Feedback Loop

OEO with the direct and external modulation has a following feature: at application of two optical fibers or two optical channels (as in the case of OEO with the MZ modulator) and arrangement of optical filters, the suppression of the one harmonic happens together with alignment of undepressed harmonic amplitudes with the help of attenuators. In this case, OEO with RF FODL of such a type contains the frequency discriminator or a correlator (Fig. 2.4a). The frequency discriminator method is applied in radio electronics and optoelectronics to measure the phase noise and laser spectra. This method is a version of the phase detector method with the difference that here we need not the reference source. Figure 2.4a illustrates the principle of the frequency discriminator method, which uses a delay line. Here, the signal from the generator G is divided into two channels. The signal of the one channel is delayed with the respect of the second channel by the time $\Delta T_{\mathrm{M}} = |T_{2\mathrm{M}} - T_{1\mathrm{M}}|$. The delay line transforms the frequency fluctuations into phase fluctuations. The quadrature phase shift of signals passed to inputs of the mixer (phase-detector) (i.e., the 90°-phase shift between oscillations in channels) is settled by adjustment of the delay line or the phase shifter.

Then the phase detector transforms the phase fluctuations into the voltage fluctuations, which can be further interpreted by the spectrum analyzer in the bandwidth of the modulating signal as the frequency noise. The frequency noise is then transformed into phase noise values of the device under consideration. This method is perfectly used for the LC oscillators or the cavity oscillators [25–30].

OEO, shown in Figs. 2.1, 2.2, and 2.3 includes the above-mentioned circuit (Fig. 2.4), which illustrates operation principles of the correlator and the frequency discriminator methods. The laser is used as the reference generator in OEO, the optical fiber or channels in the MZ modulator is used as the delay line, the photodetector is used as the phase detector.

At small relative delays in Figs. 2.1, 2.2, and 2.3, the phase dispersion σ^2_{PD} at output of the phase detector (or in the photocurrent of the photodetector) is determined as $\sigma^2_{\mathrm{PD}} = \sigma^2_{1\mathrm{L}} + \sigma^2_{1\mathrm{L}} - 2\left(\frac{A_2}{A_1}\right)K_{21}\sigma_{1\mathrm{L}}\sigma_{2\mathrm{L}}$, where $\sigma^2_{1\mathrm{L}}$, $\sigma^2_{2\mathrm{L}}$ are dispersions of the optical phase fluctuations, relatively, at input of optical channels OC1 and OC2, K_{21} is the auto-correlation function of the random process $K_{21} \approx \exp(-2\Delta\nu_{\mathrm{L}} \cdot \Delta T_{\mathrm{M}}) = \exp(-2\Delta T_{\mathrm{M}}/T_{\mathrm{c}})$, $\Delta\nu_{\mathrm{L}} \approx 1/T_{\mathrm{c}}$ is the natural width of the spectral line of the reference generator (a laser) emission, T_{c} is the time of laser

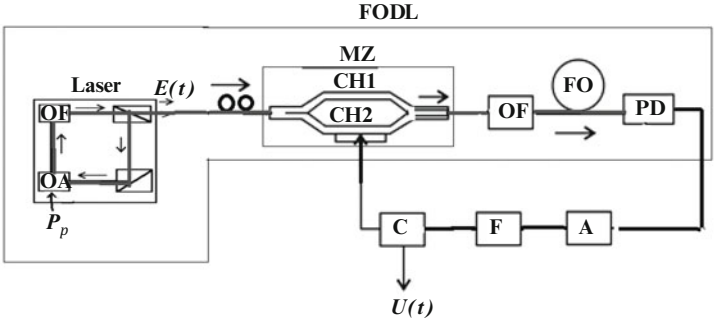

(a)

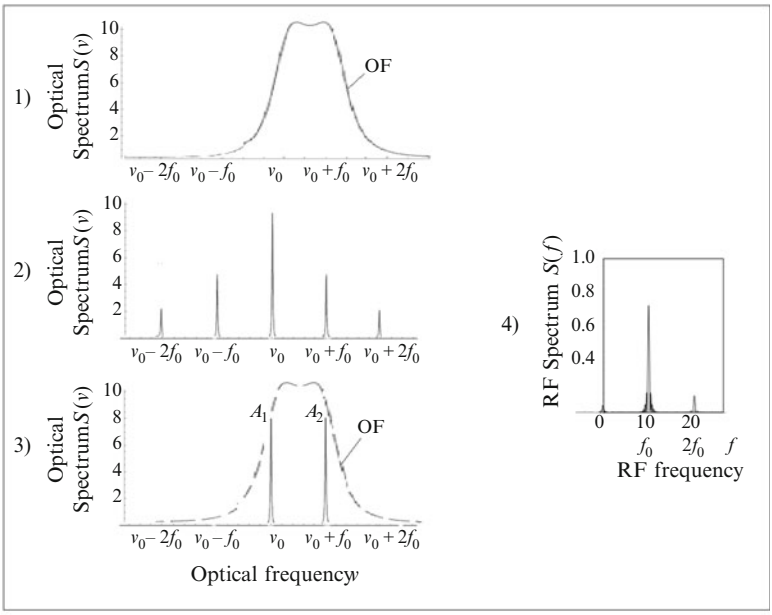

(b)

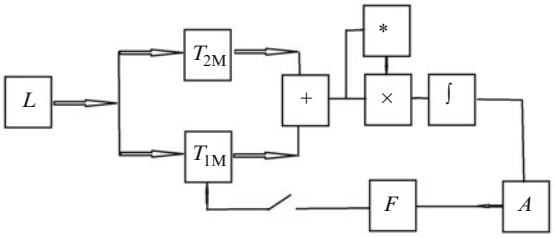

(c)

Fig. 2.4 The functional diagram illustrating principles of the correlator method and the frequency discriminator method in OEO with the MZ modulator and in the circuit with direct amplitude modulation at suppression of the one harmonic. (**a**) Laser = the optical quantum oscillator (generator) (the laser or QWLD), MZ = the electro-optical MZ modulator, OA = the optical amplifier, OF = the optical filter, OF = the optical fiber, P_p = the pumping power, PD = the

coherence, $\Delta T_M = |T_{2M} - T_{1M}|$ is the delay difference in the phase detector channels (or in OC1 and OC2 of the MZ modulator), $\nu_L = \nu$ is the laser frequency, A_2/A_1 is the ratio of quadrature amplitude of optical harmonics: the $\sqrt{A_1}E_{0L}$ and $\sqrt{A_2}E_{0L}$ in the first harmonic and second harmonic, relatively (Fig. 2.4b). At that, on the PD area, there is the process of statistical averaging in time of the interference result of two optical harmonics ν_{0L} and $\nu_{0L} + f_0$, which are applied to the PD area: $E_{10L}(t) = \sqrt{A_1}E_{0L}\cos[2\pi\nu_{0L}t + \varphi_{0L} + \varphi_{10Lm}(t)]$ and $E_{20L}(t) = \sqrt{A_2}E_{0L}\cos[2\pi(\nu_{0L} + f_0)t + \varphi_{0L} + \varphi_{20Lm}(t)]$, with the amplitudes of optical harmonics $\sqrt{A_1}E_{0L}$ and $\sqrt{A_2}E_{0L}$.

The suppression of the one from three optical harmonics is the necessary condition of the noise reduction.

1. At large difference $\Delta T_M = |T_{2M} - T_{1M}|$, i.e., at much larger (by 1000 times and more) time constant T_{L0} of the cavity (and the G oscillation period), the frequency discriminator plays a role of a converter of frequency fluctuations in the phase fluctuations. At that, the correlation coefficient tends to zero.
2. At small delay difference $\Delta T_M = |T_{2M} - T_{1M}|$, i.e., comparable to the cavity time constant T_c (and the G generator oscillation period), the frequency discriminator plays a role of a correlator or the phase fluctuation suppressor, its correlation coefficient tends to 1. The suppression degree is defined by the laser line width, the accuracy of channel alignment on the optical power (or irregularity coefficient of optical channel excitation), as well as the channel irregularity degree, which influences on relative phase delays in the transverse section of the channel. In the optical range, irregularity of the refraction index and micro-irregularities are determinative for the quality of phase fluctuation suppression. The phase irregularity account in the transverse section can be preformed by the irregularity coefficient, which depends on the transverse irregularity.

For instance, in OEO with a laser with the 3-kHz line width, for relative delay in the MZ modulator of $\Delta T_M = |T_{2M} - T_{1M}| = 10^{-13}$ to 10^{-12} s, $T_c = 10^{-9}$ to 10^{-6} s, and, as we show in Chaps. 6 and 7, the auto-correlation function value is $K_{21} \approx \exp(-2\Delta\nu_L \cdot \Delta T_M) = \exp(-2\Delta T_M/T_c) = 1$ with accuracy up to third character after a comma for frequency offset 1 kHz to 1 MHz from optical carrier.

At power alignment in optical channels with 0.1-accuracy, we obtain from the mentioned formula that the phase fluctuation dispersion in the photodetector photocurrent is less than the initial value by more than 10 times. There is a possibility of *phase modulation* arrangement of laser optical emission in the optical channel of OEO.

Fig. 2.4 (continued) photodetector, NA = the nonlinear amplifier, F = the RF filter, C = the RF coupler, CH1, CH2 = the optical channels of the MZ modulator; (**b**) diagrams (1–4) of optical frequency selection; (**c**) L = the laser, T_{1M} and T_{2M}, = delay lines have delay times in channels, "+" = (adding), "×" = (multiplication), "∗" = (conjugate operation), "∫" = (integration), F = the low-pass filter, A = the amplifier

We should note that small proper phase noises at RF FODL output are from −110 to −40 dB/Hz, which are determined by the laser phase noise. Phase noises of QWLD for the offset (1/10) kHz are −100 to −120 dB/Hz and hence, the coherence length is up to 50 km.

A possibility to achieve the high-accurate relative alignment (up to 10^{-1} to 10^{-3}) of the optical power in the channel of MZ modulator interferometer and in RF FODL directional optical couplers permits reduction of laser phase noises to values of electronic noises. This possibility can be granted by optical attenuators at self-heterodyne mixing on the photodetector. In QWLD OEO with the direct and external modulation, there is a possibility to reduce the OEO phase noises, which are determined by the quantum nature of spontaneous emission, more than an order thanks to self-heterodyne mixing.

From the analysis of above formulas, it follows that for phase noise reduction due to self-heterodyne mixing, it is necessary to suppress the "third" or the one from the "sideband optical harmonics", i.e., to provide the narrowband laser. Phase noise reduction at self-heterodyne mixing depends in this case on not only temporal but on the spatial source coherence in the transverse section.

Self-heterodyne mixing in OEO with application of the MZ modulator (Fig. 2.1), thanks to laser noises correlation, as is shown in Chap. 7, gives a possibility to suppress the OEO phase noise caused by detected laser noises by 10–15 dB/Hz.

2.6 Integration in Future Optical and Optoelectronic Systems

OEO has potentially two and more different input/output terminals: optical and electrical (in microwave range). A presence of two outputs broadens the functional possibilities of OEO application in optoelectronic systems of future generation of devices for high-stable precision oscillation formation. Oscillations on the microwave carrier pass from the electric microwave output to inputs of signal consumers—frequency multipliers, amplifiers, modulators, and the recording devices (the spectrum analyzer, frequency-meters etc.). From the optical output, the microwave-modulated/non-modulated optical emission of QWLD is applied (if necessary) to optical channel of data transmission, to systems of optical data processing, etc. When using the optical output, we can provide the full galvanic and microwave decoupling of OEO with its output load. For example, we must transmit the signal from OEO optical output to the external (outside the OEO structure) second photodetector of another device, and from the second photodetector output, the signal may pass to the output amplifier. Such a galvanic optical decoupling essentially (by 10–20 dB) reduces the OEO noise level, which are caused by external noise sources and be a signal reflected from the load.

2.6.1 New Methods of Optical and Optoelectronic Frequency Control of the RF Oscillators

One of the important OEO advantages is a possibility of generated frequency control with the help of optical and optoelectronic methods using the differential RF FODL and the fiber-optical discriminators. Authors of this book patented [3, 20, 21] and theoretically and experimentally investigated new types of OEO radio-frequency control including the variation of the pumping current and of the laser optical frequency. The OEO RF frequency control is performed at variation of the RF FODL phase-frequency response. One of the methods of OEO frequency control is the approach developed by authors and using RF FODL with various geometric lengths. Variations of the entry optical power into fibers with different lengths lead to the OEO microwave frequency variations. One of the important achievements of OEO revealed by authors is broadening of the RF frequency control possibilities by the purely optical and optoelectronic methods using for this of differential RF FODL and different fiber-optical discriminators.

2.6.2 Nonlinearities in OEO

OEO represents the oscillating system with various types of nonlinearities. Besides the "traditional" nonlinearity of the electronic amplifier in the OEO feedback loop, at studying of oscillation passing through the feedback loop, we need to keep in mind that potentially there are additional and enough complicate for investigations the nonlinearities of the photodiode, the laser, the modulator as well as nonlinearity of the fiber-optical light guider. In OEO, there are also the various versions of nonlinear laws: quadratic and cubic (the laser diode with internal modulation by the pumping current, and the photodiode), the cosine nonlinearity (the Mach–Zehnder modulator), and others. For instance, the cosine nonlinearity of the MZ modulator can be used for multiplication by the even number of times of the subcarrier frequency of optical oscillations [4].

The analysis and experimental results of the signal transmission system with the ultralow noise level (−100 dB/Hz at 1-Hz offset) are presented in [5]. Authors of this paper describe an expression for the transfer function of the MZ modulator for large oscillation amplitude on the electric MZ input. The transfer function in this paper is presented as a sum of terms of even and odd harmonics of Bessel functions. At that, the nonlinear function of the oscillation amplitude of the first harmonic is determined by the even and odd Bessel functions.

Nonlinearity in lengthy quartz single-mode optical fibers with the geometric length from 1 to 12 km is manifested at development of large power densities in the optical thread at the level of 20–500 mW/1 μ^2 at average continuous powers 20–200 mW of QWLD emission. The threshold power level, at which nonlinear effects begin to become apparent, depends on a type and a length of the optical fiber,

on the entry power of laser emission into the optical fiber, as well as on the spectral line width of QWLD emission and parameters of effective section of the fiber [6]. The multi-photon nonlinear effects arising due to direct and inverse Brillouin scattering [7, 8] are the most extensively studied. We can increase the threshold power of nonlinear optical effects by 10–20 times by means of use in RF FODL of specific micro-structured optical fibers, which transverse sections are represented in Fig. 2.13 (see later). In the optical disk resonators (ODR) with the diameter 1–10 mm, their nonlinearity is clearly demonstrated at entry powers 10–100 μW of optical emission. At that, nonlinear effects not only cause the spectral stochastic noises of oscillations, but lead to the high temperature instability of the natural ODR frequency. Unfortunately, this does not give a possibility to use ODR in OEO as the passive high-Q resonators and filters in RF FODL.

2.6.3 *Dispersion RF FODL in OEO*

In the general case, RF FODL is characterized by dispersion properties, i.e., its delay depends on the optical oscillation frequency generated by a laser. The modern small-dispersion optical fibers are characterized by the spectral linear delay of order (1–10) ps/(nm/km). On the other hand, there are specific dispersive optical fibers permitting to implement both negative and positive dispersion of 100–1000 ps/(nm/km).

The delay line dispersion leads to distortions of the generated signal spectrum, an appearance of additional spurious components in the RF signal spectrum (due to combination with nonlinear effects in FOS), which is accompanied by spreading of the laser spectral line. Nevertheless, as we show in Chap. 7, their level is demonstrated in small-dispersive optical fibers at the spectral line width of the modulated light sources more than 500 MHz and for fiber lengths more than 10 km.

2.6.4 *Types of Optoelectronic Oscillators by the Composition of Modulated Light Source*

Utilization of different types of the modulated light sources in OEO depends on the oscillator destination. For instance, in OEO of RF range (in the measuring fiber-optical systems), it is expedient to apply the laser diode (or the light-emitting diode) with low-frequency internal modulation. In OEO of microwave range (in devices for signal formation, say, for communication systems or for radar systems), the efficient QWLD with internal modulation or QWLD with the external absorption modulator are more promising. In low-noise microwave and mm-wave oscillators (8–30 GHz), QWLD with MZ modulator can be used.

2.6.5 OEO Division According to FOS Topology

Fiber-optical systems on the base of quartz single-mode optical fibers with low dispersion (t_d = 1–3 ps/(nm/km)) on the wavelength of 1.3 μm allows creation of low-dispersion delay lines for microwave signals with delay time T_d = 10–100 μs at relative time dispersion due to the frequency band of emitted frequencies of the modulated light source $t_d/T_d = (2–6) \times 10^{-7}$ $(nm)^{-1}$.

This means that the relative delay time for spectral line width on the optical signal at 30 GHz is $t_d/T_d = (2–6) \times 10^{-7}$.

The last circumstance gives us a possibility to implement delay lines with the low phase noise at output basing on the narrowband lasers with the spectral line width less than 1 MHz.

Application of RF FODL on the base of composite complicate fiber systems for selection of oscillation types (Fig. 2.5a) is the OEO feature. A rejection character of the frequency response of such RF FODLs allows a possibility to select the adjacent oscillation types and to suppress the amplitude of spurious types of oscillations. Methods of complicate FOSs implementation allow essential reduction of sideband components of the adjacent oscillation types down to the level −100 to −140 dB/Hz. A possibility of single-frequency mode in RF microwave range can be provided for large delay times T_{dt} = 1–50 μs in the fiber system. Application in OEO of recirculating FOSs with the single or several fibers in the feedback loop (Fig. 2.5b) is the one utilization of complicate fiber-optical systems in OEO. Such recirculating RF FODLs has a narrowband PFC of ridged type and can reduce by several ten times of the geometric length of the optical fiber in OEO. Figure 2.5 introduces the new designation: a wideband amplifier (WBA).

The linear topology of RF FODL differs favorably from the monolithic crystals of dielectric resonators in RF oscillators in their strengthening characteristic at destroying percussive impacts. According to own geometrical sizes, they are almost the same. This strengthening characteristic for the optical fiber constitutes 2000 N/cm^2 [9] (for monolithic crystals of the leuco-sapphire [31] type with disk diameter 5–8 cm and the 1-cm in thickness, this characteristics is usually one-two orders less) and it may be one of the governing factors at utilization of the low-noise OEOs in unmanned orbital stations and unmanned flying vehicles, in military applications, etc., where percussive and strength characteristics are governing.

The equivalent electric block diagram of OEO with the separate laser (the optical quantum generator) and the RF part of OEO is shown in Fig. 2.6. The linear part (LP) of the active element (NE) and RF FODL are also shown in Fig. 2.6, and we can see the nonlinear current sources of NE ($I_1(U_1)$ and $I(U_2)$). To study the frequency, amplitude, and time functions for OEO, in Chap. 3 of this book we use the mathematical model of RF FODL, in which we replace RF FODL by the equivalent two-port with the input conductance, which is equal to input conductance of the MZ modulator (for version with external modulation of QWLD emission) or to input conductance of QWLD (for version with direct modulation).

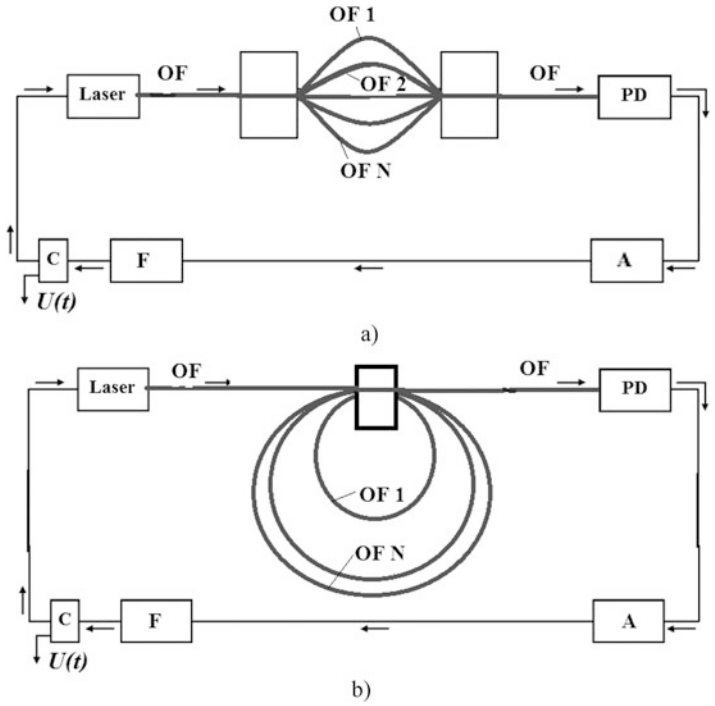

Fig. 2.5 Block diagrams of OEO with the complicate *composite* fiber-optical system (**a**) and with the *recirculating* fiber-optical system (**b**) with various geometric lengths of fibers

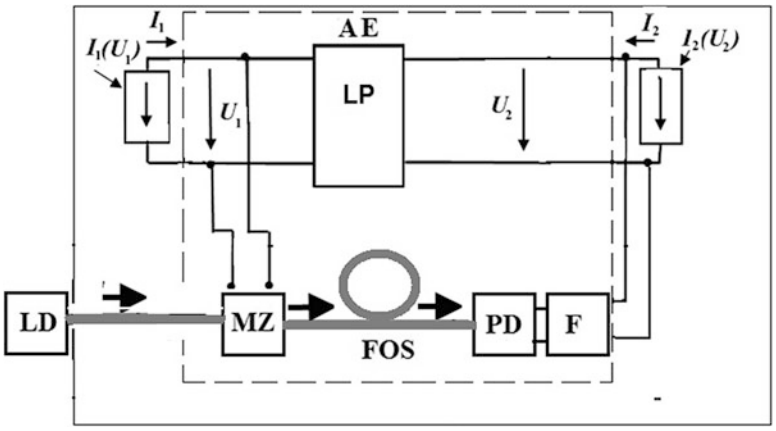

Fig. 2.6 The equivalent block diagram of OEO with RF FODL

The output conductance of this equivalent two-port is equal to the conductance of the photodetector with the transfer function of RF FODL. The more complicate mathematical model, in which a laser is presented by semiclassical equations and takes into consideration the laser optical emission noises and its conversion into the RF phase noise, is discussed in Chap. 7 of this book.

2.7 Modern Elements of OEO: A Laser, the Optical Fiber, and a Photodetector

In describing OEO system, the important role in achievement of the minimal phase noise level is played by RF FODL elements: the laser with included optical resonators and discriminator, the optical fiber, and the photodetector. In this section, we briefly discuss the most important key problems, which solution leads to the record minimal characteristic of the phase noise.

2.7.1 A Laser

Utilization as a laser of the nanostructured quantum-well laser diode in OEO leads to qualitatively new properties of OEO. Due to "quantization of zones in the transition," as we show in Chaps. 4 and 5 of this book, the quality of optical emission changes: the level of noisy spontaneous emission reduces more than 100 times, and due to this, phase and amplitude noises of the laser significantly reduce, the optical emission spectral line decreases from several gigahertz to several kilohertz. In addition, the emission directivity pattern becomes narrower and polarization characteristics improve.

Besides the transition from the 3D semiconductor structures to the quantum-well laser with minimal phase noises, the choice of optical resonator plays the significant role. At that, the line width (on the level of half-power) of the resonance curve of promising lasers should achieve 1–1000 kHz.

2.7.2 Optical Resonators and the Optical Fiber

Experimental characteristics of main modern optical resonators are illustrated in Table 2.1 and in Fig. 2.7. As shown in Table 2.1, disk resonators have the maximum Q-factor [32–36]: $Q = 8 \times 10^9$ on SiO_2, and $Q = 8 \times 10^{15}$ on CaF_2. Their disadvantages are:

Table 2.1 Q-factors and dimensions of various optical resonators applied in lasers and laser systems

	Time constant, not more than	Volume in cubic $(\mu m)^3$	Fabry–Perot	Fiber Bragg grating FBG	Disk optical resonator	Photon crystals
Medium-Q	1 ps	10,000	$Q = 2000$ Mirrors	$Q = 1.2 \times 10^6$ FBG	$Q = 7000$ $Q = 130{,}000$ $Q = 520{,}000$ (Painter)	$Q = 6 \times 10^5$ (Noda)
High-Q	1 ns	1000	$Q = 10^7$ Super-mirrors (Kembl)	$Q = 1.2 \times 10^6$ FBG (step 100 nm, Cell length 34 mm, length of delay 2 m, 16 MHz, SiO_2, TeraXion)	$Q = 2 \times 10^9$ disk (Vahala) $Q = 8 \times 10^9$ SiO_2	
Ultrahigh-Q	1 μs	100			$Q = 8 \times 10^{15}$ CaF_2 (Il'chenko)	

Note: Q is the Q-factor of the optical resonator (a product of the optical frequency and the time constant)

- the low coefficient of power entry under standard conditions (less than 5% of optical power),
- low threshold of optical power, at which optical nonlinear effects begin to become apparent, and
- strong temperature dependence of resonator characteristics.

Resonators on the optical distributed fiber Bragg gratings (FBG), for which the Q-factor of $Q = 1.2 \times 10^7$ is achieved, have got a special attraction in laser systems (Figs. 2.6, 2.7, 2.8, and 2.9).

If the phase-locked loop system for the laser optical frequency adjustment uses the Bragg grating as the optical discriminator (Fig. 2.8) (at the grating step of 100 nm and at the discriminator cell length of 34 mm), then we may implement the system, in which the QWLD emission happens with the narrow band (on half-power level) of the resonance peak of 15 MHz (Fig. 2.10) [37–41].

Experimental results of the phase noise measurement for QWLD emission with the discriminator on the base of high-Q diffraction grating (Fig. 2.9) are shown in Fig. 2.10. We can clearly see from these results that discriminator utilization in the negative feedback loop allows reduction of the laser phase noise by −15 to −20 dB/Hz at offset 0.1–10 kHz [37, 38].

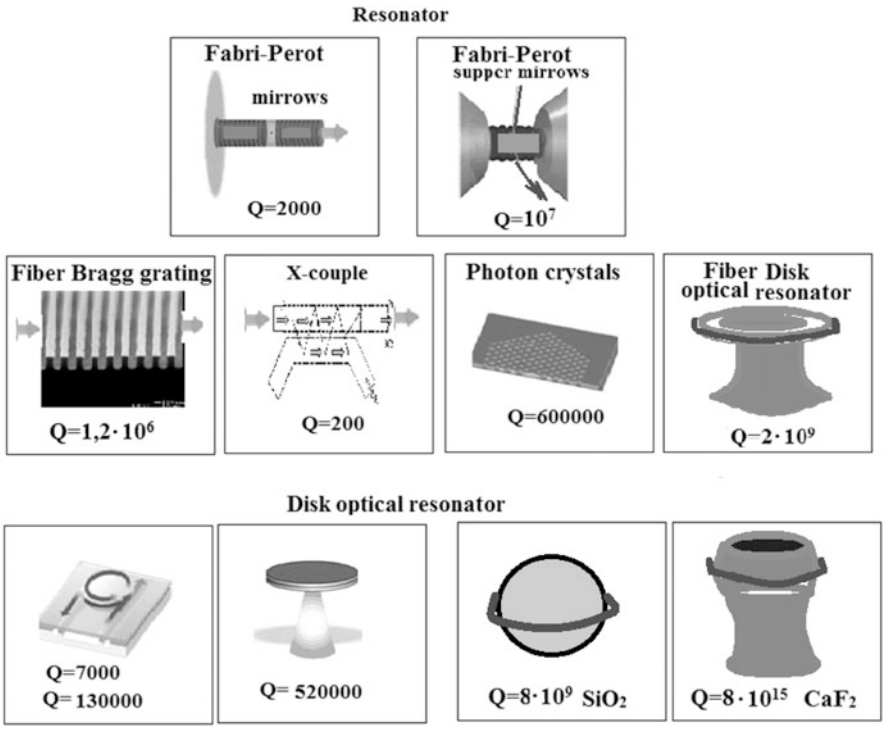

Fig. 2.7 Forms of optical resonator and delay optical structures applied in lasers and in fiber-optical systems

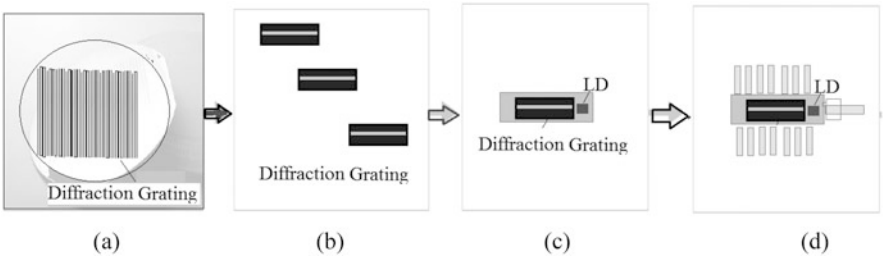

Fig. 2.8 Stages of a technological cycle for creation of the quantum-dimension laser diode with application of high-Q optical discriminators and resonators. (**a**) Creation of the diffraction grating on the substrate, (**b**) obtaining of the optical discriminator (a resonator), (**c**) combination of the laser and the resonator, (**d**) the finished laser

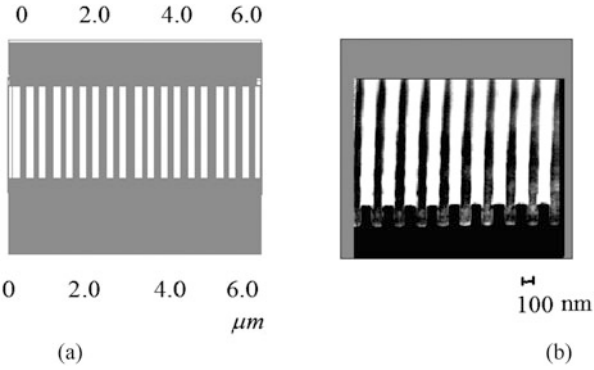

Fig. 2.9 Enlarged images of the primary "mask" on the substrate (**a**) and after technological cycle of the dry deposition of the diffraction grating of the discriminator optical resonator (**b**) with a grating half-period of 100 hm. The image is enlarged with the help of the electronic microscope

The high emission density is the feature of the high-Q devices on the base of such a diffraction grating at 10^6 Q-factor. Owing to this, the emission power, which is entered in such a device, is limited by the extreme power of nonlinear effect appearance. Resonators in the form of disks have the similar restriction.

The high power density applies a series of restrictions at utilization of high-Q optical resonators and discriminators in order to implement the ultra-miniature devices. This leads to the fact that we can only use resonators and discriminators on the "linear" mode as discriminators, which are in the feedback loops, and at input of which a part of the power applies from the total power acting in the main optical channel of OEO.

As at small sizes of such a resonator (the disk radius is 1 mm and the cross-section area of the light-guiding layer is 10^2 $(\mu m)^2$) and at the relatively high Q-factor of order $Q = 10^7$ (the equivalent length is 2 m), nonlinear effects begin to become apparent at entry power of the order several microwatt. That is why, we can attribute the solution search in micro-miniaturization of the linear RF FODL to promising methods of miniature resonator implementation. For instance, at fiber length in several kilometers, at wavelength 1.55 μm, the threshold power is about 100–200 mW.

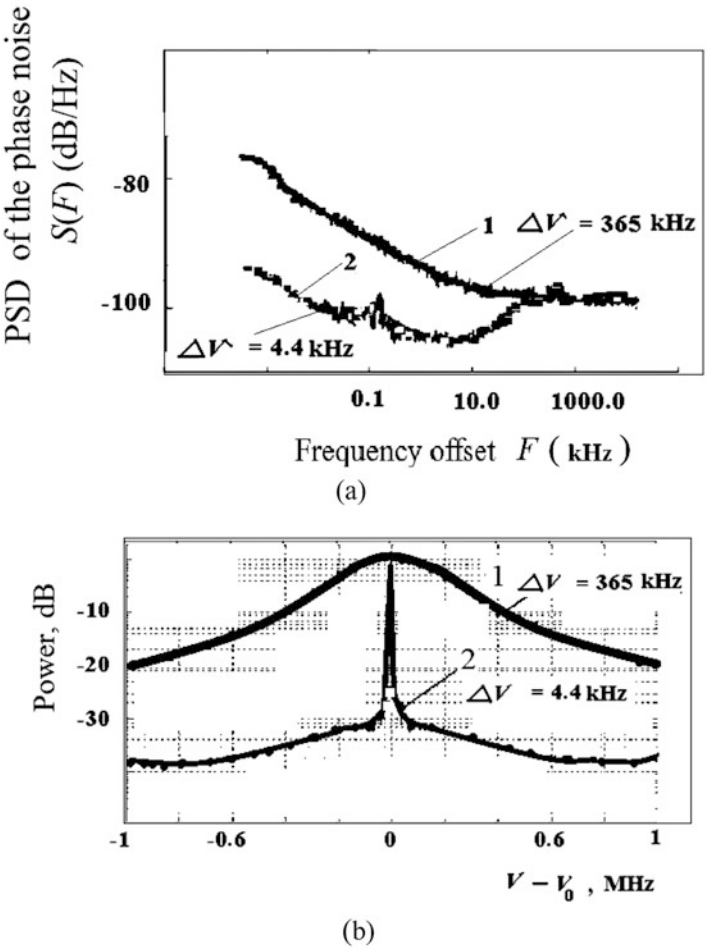

Fig. 2.10 (**a**) Experimental results of phase noise measurement of QWLD emission with the discriminator on the base of high-*Q* diffraction grating, which is used for reduction of the QWLD phase noise, and (**b**) the calculated function (based on QWLD phase noise measurement, see (**a**)) of the relative emission power vs. the offset from central frequency of the QWLD spectrum without and with a discriminator. Curve 1—QWLD without discriminator. Curve 2—QWLD with use of the high-*Q* resonator on the base of the high-*Q* diffraction grating. The analysis time is 1 ms (**b**)

2.7.3 Fiber Lasers

Application in OEO of low-noise fiber lasers (FL) is promising. The fiber lasers with activated erbium (Er) or ytterbium (Y) dopes (the wavelength is 1.55 μm) with the ultralow phase noise of the fiber laser optical emission [42–44] are commercially available. The construction of fiber lasers consists of the closed ring of the optical activated fiber, to which the optical pumping emission is applied with the help of the

fiber-optical coupler. Usually, the geometrical length of the optical activated fiber is 0.4–10 m. The optical emission power of the low-noise fiber lasers is 1–100 mW.

The power spectral density (PSD) of the phase noise in the fiber laser is −100 to −132 dB/Hz (at offsets from the optical carrier of 1–10 kHz). Such small parameters of the phase noise are obtained by means of the utilization of the phase-locked loop (PLL) system at optical frequency. Without PLL utilization (curve 1 in Fig. 2.10), the phase noise in the fiber laser are more by −10 to −15 dB/Hz at the same frequency offset. The line width of the optical emission in this fiber laser is about 1 kHz.

2.7.4 The Optical Modulator in OEO and Modules

Recently, the commercially available electro-optical Mach–Zehnder modulators in the planar implementation appears (Fig. 2.11) with high characteristics: the low control half-wave voltage of 0.3–1 V, the high entry optical power—up to 50 mW, with low optical power losses of −3 dB. Figure 2.12 shows the disk phase electro-optical modulator (Fig. 2.12a) with the control voltage less than 0.01 V, and the optical toroidal resonator (Fig. 2.12b) with Q-factor about 10^6 [45–47]. The construction of the phase RF modulator at 60 GHz has a special interest [48]. At that, for effective modulation, the principle of the phased antenna array is used. Several signal electrodes are deposited along the optical channel of a modulator. Excitation of such the "antenna array" is provided by the RF oscillator with the 60 GHz-frequency with the 20 mW power. The RF oscillator with the frequency of 60 GHz is located above the optical channel with signal electrodes.

On the base of modern QWLD and modulators, new integrated photonic elements with optical amplifiers and micro-resonators are developed. The commercially available integrated module consists of the quantum-well laser (with the emission line width of 1 MHz) with the MZ modulator with modulation frequency band of 15 GHz and the half-wave voltage 2 V. This laser is attended with the electro-optical Mach–Zehnder modulator. The overall dimensions of this combined module is about 30 mm × 50 mm × 100 mm, and its cost is about $2500–$5000. Figure 2.13a–d shows profiles of commercial "perforated" optical fibers with the nano-dimension structure of the light-guiding thread.

2.7.5 Optical Fibers for OEO and Photodiodes

Such optical fibers (Fig. 2.13) are used in optoelectronic devices for formation of microwave and mm-wave oscillations foe obtaining of the second harmonic of the optical frequency at nonlinear optical transformation.

Plots of optical losses for different types of optical fibers are shown in Fig. 2.13d. From this plot we can make conclusion fibers with the perforation of the HALF type

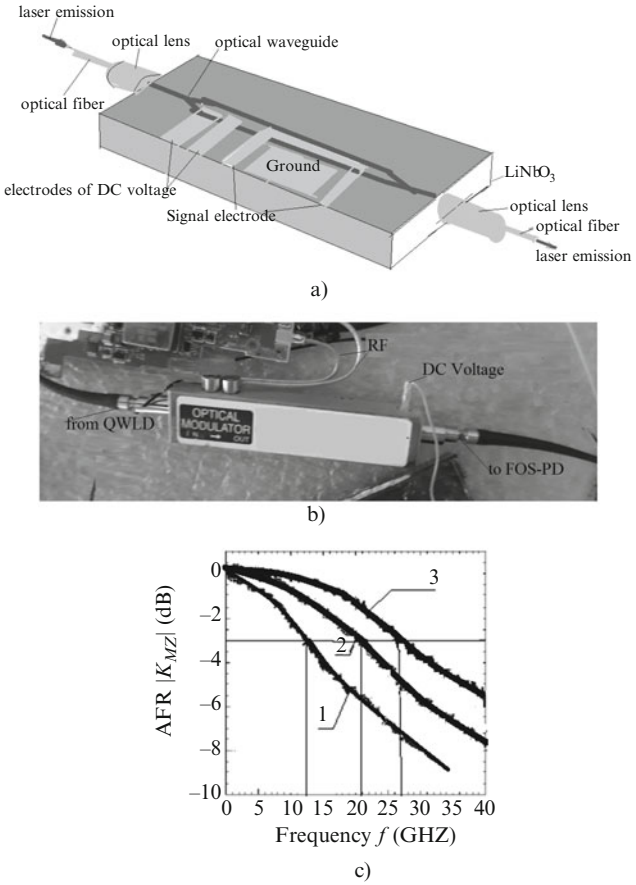

Fig. 2.11 (**a**) Planar implementation of the electro-optical Mach–Zehnder modulator (MZ section length is 10 mm), (**b**) the external view of the MZ modulator, (**c**) its experimental AFC for MZ modulator with the RF modulation bandwidth 12 GHz (curve 1), 21 GHz (2), 27 GHz (3); the laser wavelength is $\lambda = 1550$ nm

are promising for development of small-size delay lines. Application of special or nano-dimension optical fibers (Fig. 2.13d, e) with low losses at small bend radii (1–3 mm) (0.001 dB/one bend) allows creation of miniature delay lines (1–50 μs) with overall sizes from 10 to 30 mm [49, 50].

At present, in many countries, commercially available photodiodes with the bandwidth of 12, 18, and 60 GHz are manufactured [51–55].

Their natural output photocurrent phase noises are ultralow and are less than −120 to −130 dB/Hz at offsets 1–10 kHz from the nominal frequency in the microwave range [52–56]. The photodiode construction allows its mating with the optical fiber. A coefficient of optoelectronic conversion of photodiodes is up to 0.5 A/W. One of features of modern photodiodes of microwave range is the small

Fig. 2.12 The disk electro-optical modulator (the disk radius is 2 mm) on the crystal of $LiNbO_3$ (**a**) and the optical nano-toroidal resonator (the disk radius is 50 μm) from SiO_2 (**b**) with Q-factor more than 1,000,000

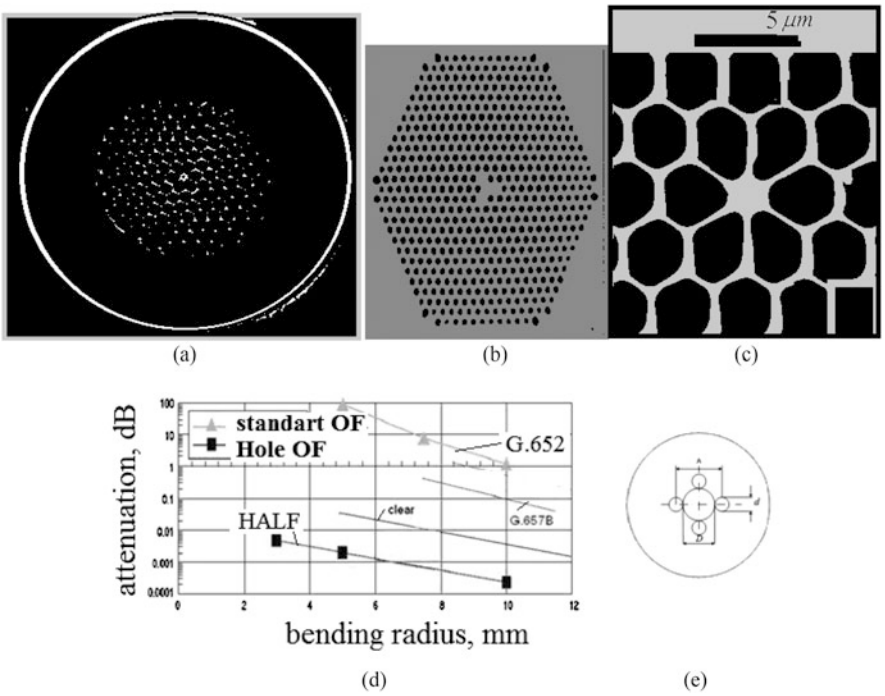

Fig. 2.13 Profiles of commercial micro-structured "perforated" optical fibers with the nano-dimension structure of the light-guiding core (**a**–**c**). (**d**) The plot of functions of traditional optical fiber damping and photo-crystal (or perforated) fibers vs. the bend radius for different fibers: (1) The traditional fiber of G.652 type. The single-mode fiber with core diameter about 10 μm. Variants of this fiber without water peak: All Wave (company OSF), SMF-28e (Corning), SMR (Pirelli) within the limits of G.652C recommendation; (2) The fiber of G.657 type with reduced bend damping. Similar fibers are developed by Corning and OFS; (3) Clear—fibers from Corning of SMF-28e XB (Extra Bend) type with decreased bend attenuation, and the fiber with nanostructured core ClearCurve with strongly reduced bend attenuation; (4) The third type of perforated fibers—the light guided fiber with additional holes (CBBO), or hole-assisted light guided fiber (HALF); (**e**) The structure of HALF–PCF fiber

size of the light-sensitive area. Its sizes are approximately the same as the wavelength of arriving optical emission. It is necessary to take this into account at mathematical modeling of RF FODL. If we consider the model of electromagnetic emission in the form of the plane wave, which falls into the photodiode light-sensitive area, we must take into consideration that in the general case, non-axially symmetric plane wave falls into this area. The electromagnetic laser emission wave, which amplitude and phase are not constant at coordinate x and y variations in the cross-section, falls into the photodiode.

Photodiode constructions with channel separation are developed for coherent photodetection with optical and RF amplifiers using of selective optical filters in order to suppress of the laser spontaneous emission noise, etc.

The listed characteristics of new laser elements with low output noises, high-Q optical resonators and discriminators, nanofibers and wideband photodetectors for OEO allow the following important conclusion. Application of these elements in OEO leads to qualitatively new levels of development the optoelectronic generation, as a whole, and to high OEO characteristics, which made them competitively capable compared to traditional RF precision oscillators.

2.8 Comparison of OEO Characteristics with Other Traditional Oscillators

2.8.1 Traditional Electronic Oscillators

At present, generation techniques for RF and microwave oscillations with the small noise are sufficiently developed. A market for commercially available various oscillation sources is open in many countries.

The crystal (quartz) and SAW oscillators without and with frequency multiplication, oscillators with YIG-resonators, Gunn-diode oscillators, low noise oscillators with dielectric resonators on ceramics and with dielectric resonators with whispering-gallery waves and on the leuco-sapphire crystal, etc. can be attributed to the widely spread claiming models of precision oscillators. Such oscillators are used for frequency stabilization in electronic systems, computer engineering, navigation systems, etc. Several specific tasks on long-term frequency stabilization can be solved with the help cesium and rubidium frequency standards Some special tasks on long-term frequency stabilization are solved using cesium and rubidium frequency standards, which are also commercially available, although rather expensive devices. There appear publications on compact frequency standards [57–61]. Last time, in communication systems and also in radio-electronic systems of miniature unmanned flying vehicles on frequencies 2–60 GHz, grows the need in microwave and mm-wave oscillators in miniature implementation. In scientific publications, the papers appear on investigation of optoelectronic methods of generation in microwave and mm-wave ranges with application of laser, fiber-optical, and micro-

resonator technologies. For main characteristic comparison of OEO with traditional electronic and optoelectronic oscillators, Table 2.2 shows their technical characteristics. The carrier frequency, the retuning range, the long-term frequency stability, the power spectral density of the phase noise, overall dimensions can be concerned to these characteristics. In this Table 2.2, the main types of oscillators are presented, and for them the following designations are introduces: (1) Osc QR—an oscillator with quartz resonator, (2) Osc SAW—an oscillator on surface acoustic waves, (3) Osc DDR—an oscillator with disk dielectric resonator from ceramic alloys, (4) Osc DDRLS—an oscillator with the disk dielectric resonator from the leuco-sapphire, (5) Osc YIG—an oscillator with the YIG resonator, (6) OEO RF FODL—an optoelectronic oscillator with RF FODL, (7) OEO ODR—an oscillator with the optical disk resonator, (8) Laser FSS—a laser femtosecond synthesizer, (9) QFS on Cz—the quantum frequency standard of the cesium cell.

Basing on mechanisms of oscillations delay and of energy accumulating in oscillators with various types of resonators, they can be conditionally divided on acoustic (quartz [62] and SAW [63, 64]), electromagnetic (YIG, DQR, and DDRLS [25, 28–30]), and optoelectronic (RF FODL, ODR—optical disk resonators ODR [32–36]). Oscillators of laser femtosecond synthesizer (FSS) and the quantum frequency standard (QFS) can be also attributed to optoelectronic converters according to formation methods of radio-frequency oscillation.

In Table 2.2 the following abbreviation are used: "PSD PN"—power spectral density of phase noise at offset 1 kHz/10 kHz from the 10 GHz-carrier. "Long-term freq. instab."—long-term frequency instability. "Tuning range"—the range of frequency tuning, "Comm. name"—Commercial name.

In the quantum frequency standard, the transformation of the optical frequency, which is equal to about 200 GHz, into the RF frequency 6.4 GHz is performed using quantum resonance properties of the cesium atom. In the oscillator "Laser FSS," the transformation of the optical frequency 438 THz into the frequency 10 GHz is performed using beats of two "phased" optical frequencies on the photodetector.

With RF frequency growth, the increase of acoustic losses occur in the quartz and SAW resonators (or delay lines). This leads to resonator Q-factor reduction in the microwave range. Among "electromagnetic" resonators, in which the electrical oscillations conversion into the electromagnetic microwave field is provided. At that, the disk dielectric resonator from the leuco-sapphire has the maximal Q-factor.

The main shortcoming of the dielectric resonator from the leuco-sapphire is its strong dependence of the resonance frequency and its phase-frequency response upon temperature (the temperature instability of the resonance frequency of the leuco-sapphire resonator is about 10^{-4} 1/°C and is determined by the temperature dependence of permittivity and the loss angle tangent of material).

We note for comparison that in OEO, in contrast to the oscillator on the leuco-sapphire resonator, the stabilized RF FODL on the optical quartz fiber is applied. The own frequency instability of OEO (without external devices for frequency tuning) is 10^{-5} to 10^{-6} 1/°C [13] and is determined by the temperature dependence of the quartz refraction index. The frequency tuning range of OEO with RF FODL for

Table 2.2 Characteristics of high-stable oscillators

	1	2	3	4	5	6	7	8	9
Oscill. type	Osc. QR	Osc. SAW	Osc. DDR	Osc. DDRLS	Osc. YIG	OEO FODL	OEO ODR	Laser FSS	QSF on Cz
Comm. names	OCXO A260 MTI	SAO	DRO PLO-3000	SBox	YIG	OEWave, QUANT	OEO	FSC	HP 5071
Carr. freq., GHz	(0.032–30) 10^{-3}	0.3–2	10–22	10	7 and 32	1–33	1–22	10	4.8
Tuning range, GHz	Fixed.	0.01	12	0.01	2.0 and 8.0	14	14	Fixed.	Fixed.
Long-term. freq. instabil.	10^{-9}	10^{-7}	10^{-6}	10^{-7}	10^{-5}	10^{-7}	10^{-7}	10^{-7}	10^{-13}
PSD PN., dB/Hz	−115/−145	−118/−149	−110/−115	−140/−160	−74/−98	−129/−153	−86/ −100	−140/−145	−120/−145
Dimen., mm^3	38 × 50 × 50	53 × 56 × 56	53 × 50 × 27	53 × 50 × 27	25 × 25 × 25	80 × 50 × 30	5 × 5 × 5	200 × 450 × 550	135 × 425 × 523

external modulation in the MZ modulator is from 0.1 to 40 GHz and exceeds tuning ranges of other types of oscillators.

The primary cesium frequency standard (Agilent 5071A from Hewlett-Packard Company) is the oscillator having the best long-term frequency stability. We should note that the cost of such commercial oscillators approaches to several ten thousand dollar depending on complete set.

Power spectral density of the oscillator phase noise is the most suitable characteristics, which reflects of its noisy properties. Noises in oscillators participate in formation of its spectral liney. The most of known methods for noise measurement are useless concerning the reference oscillator due to their inability to analyze extra-narrowband signals. The oscillator noise can be described more convenient with the help of such concepts as power spectral densities of amplitude $S_a(f)$, W/Hz, and phase $S_\varphi(f)$, rad^2/Hz, noises, which are functions of the analysis frequency f. The power spectral density of the oscillator phase noise defines the short-term frequency instability. So, the low-noise oscillator with the disk dielectric resonator from the leuco-sapphire, which has a generation frequency about 10–12 GHz, has the best short-term frequency instability [25, 29, 30, 65] (Table 2.3).

YIG oscillators and oscillators on Gunn diodes, which are electrically tuned in the wide ranges, have the high output power of 40–400 mW [66], small dimensions ($20 \times 40 \times 40$ mm^3) and the low cost ($300–$3000) and have advantages in this regard over low-noise oscillators on the leuco-sapphire dielectric resonators. But these oscillators have the low short-term and long-term frequency stability and have low quality of spectrum purity. Their PSD of the phase noise is −50 to 70 dB/Hz at standard offset 10 kHz from the carrier in the range 2–8 GHz. The utilization of modern CAD tools allows optimization for the accurate YIG oscillator, which results in a phase noise performance below −133 dBc/Hz at the frequency offset of 100 kHz over the entire range of 6–12 GHz [66].

Oscillators on dielectric resonators from ceramics can be attributed to more efficient models. Their PSD of the phase noise of frequency offset 10 kHz from the carrier in the range 2–22 GHz is −100 to −90 dBc/Hz [67, 68]. Their cost is from $2000 to $15,000. SAW oscillators with frequency multiplication take the intermediate place between quartz oscillators and oscillators with dielectric resonators in their technical specifications. Their cost is from $100 to $7000.

PSD of phase noises in traditional electronic oscillators is determined by the resonator or the delay line Q-factor. Overall dimensions of oscillators depend on resonator sizes, because active element (transistors) used in such oscillators have the overall dimensions by 100 and 1000 times less than the resonator dimensions.

2.8.2 Q-*factors of Oscillator Resonance Systems*

For comparison, Fig. 2.14a shows the loaded Q-factors of resonators of traditional oscillators and OEO with RF FODL, and Fig. 2.14b shows the normalized (to delay time) power losses at oscillation propagation. From analysis of resonator (and delay

Table 2.3 Characteristics of various oscillators

Type of oscillating system	Fiber-optical delay line with the modulator on $LiNbO_3$ crystal	Dielectric toroidal resonator from the microwave ceramic or disk torodial resonator from the leuco-sapphire	SAW resonator, on quartz monocrystal or $LiNbO_3$	Quartz piezoelectric resonator
Power spectral density of the phase noise at offset 1 kHz from the operating frequency, dB/Hz	−(130/135)	−(115/145)	−(105/110)	−(100/110)
Range of relative electronic tuning of frequency, relative units	$(2/3) \times 10^{-3}$	$(2/3) \times 10^{-1}/(2/3) \times 10^{-5}$	$(2/3) \times 10^{-4}$	$(2/3) \times 10^{-4}$
Long-term frequency stability, relative units	$(2/3) \times 10^{-6}$	$(2/3) \times 10^{-6}$	$(1/2) \times 10^{-5}$	$(2/3) \times 10^{-8}$
Sensitivity of generation frequency to cyclic mechanical loads (vibrations), relative units	$(1.5/5.0) \times 10^{-10}$	2.0×10^{-9}	–	$1 \times 10^{-11}/1 \times 10^{-9}$
Sensitivity of frequency to platform acceleration (1 kHz), relative units	$2 \times 10^{-28}/1.5 \times 10^{-24}$	–	–	$3 \times 10^{-27}/1 \times 10^{-23}$
Delay line or resonator durability to strong mechanical shocks, N/cm^2	2000–5000 High linear topology of RF FODL and ultralow dimensions of the micro-resonator	100–200 Low—large dimensions of the resonator 100 × 100 × 20 mm	2000–5000 High, small dimensions of the resonator 100 × 100 × 20 mm	2000–5000 High, small dimensions of the resonator 100 × 100 × 20 mm

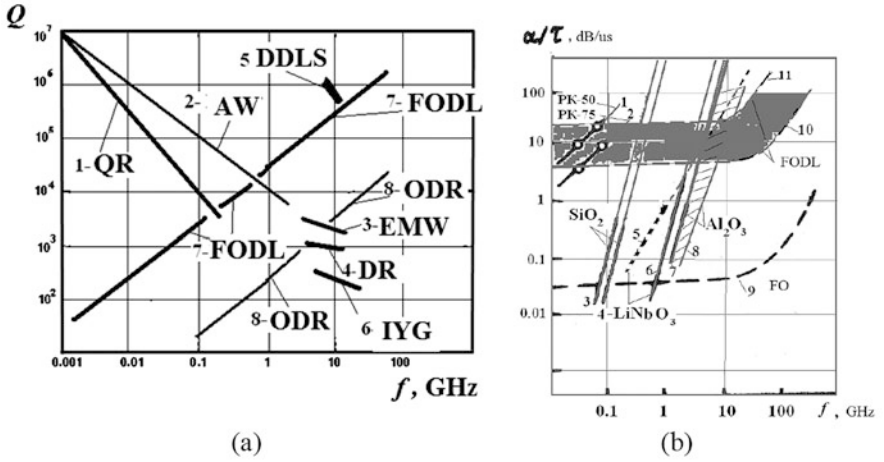

Fig. 2.14 (**a**) *Q*-factors of resonators and delay lines used in the modern stable RF and microwave oscillators. (1) QR—quartz resonator, (2) SAWR—the resonator on surface acoustic waves, (3) CR—the cavity resonator of electromagnetic waves, (4) DCR—the disk dielectric resonator from ceramic alloys, (5) DDRLS—the disk dielectric resonator from the leuco-sapphire, (6) YIGR—the resonator from the yttrium-aluminum garnet, (7) RF FODL—the fiber-optical delay line (delay time 50 μs), (8) ODR—the optical disk resonator. (**b**) Normalized (to the delay time) power losses at signal (oscillation) propagation in: (1, 2) in RF cables RC-50 and RC-75; (3, 4) in acoustic crystals in quartz SiO_2 of *Y*- and *Z*-cuts; (5, 6) the Rayleigh electric wave and the longitudinal wave in the crystal $LiNbO_3$ (without account losses in electro-acoustic converters); (7, 8) the longitudinal wave and the surface wave of "whispering gallery" in the leuco-sapphire; (9) losses in the optical fiber (losses are about 0.2 dB/km on wavelengths 1.3 and 1.55 μm); (10, 11) at different losses in RF FODL taking into account losses on electro-optical conversion in QWLD and on optoelectronic conversion in the photodetector and losses on mating of the optical fiber with the laser diode and photodetector

lines) *Q*-factors in Fig. 2.14 and normalized power losses we may make the following conclusions:

- application of OEO with RF FODL as the low-noise oscillator should have undoubted advantages over oscillators with quartz and SAW resonators on frequencies above 5–7 GHz [63, 64],
- OEO with RF FODL becomes competitive on frequencies above 5–7 GHz with regard to the oscillator on leuco-sapphire,
- OEO with RF FODL has advantages with regard of the leuco-sapphire oscillator on frequency 12–70 GHz and above.

From Fig. 2.14, we see that with frequency growth, the *Q*-factor of the quartz and SAW resonators decreases due to losses of the acoustic wave in the resonator material, which is made from a quartz. For OEO, the RF FODL *Q*-factor, which can be calculated as $Q = f_0 T_{BC}$, where f_0 is the average OEO oscillation frequency, T_{BC} is the delay time of oscillations (a signal) in RF FODL and is the linearly growing function. Oscillator resonators can be divided into acoustic (quartz and

SAW resonators), electromagnetic (YIG, DDR, CR, and DDRLS) and optoelectronic (RF FODL and ODR) according to mechanisms of oscillation delay and energy accumulating. With radio-frequency growth, acoustic losses increases in the "acoustic-electronic" quartz and SAW resonators, and this leads to reduction of their Q-factor in microwave frequencies. Among "electromagnetic" resonators, in which the conversion of electrical oscillations into the microwave electromagnetic field occurs, the disk dielectric resonator from the leuco-sapphire has the maximal Q-factor.

The main shortcoming of the dielectric resonator from the leuco-sapphire is its strong dependence of the resonance frequency and its phase-frequency response upon temperature (the temperature instability of the resonance frequency of the leuco-sapphire resonator is about 10^{-4} 1/°C). The alternative approach for Q-factor increase is application mechanisms of optoelectronic conversion and usage of RF FODL and optical disk resonators. The Q-factor of RF FODL on frequencies 5–100 GHz is about $Q = 10^5$ to 10^6.

At present, the Q-factor value (which can be estimate approximately by the ratio of the own filter natural frequency on the laser generation frequency to the resonance peak width on the 0.7 level) of optical disk resonators, at which nonlinear optical effects are not manifested, is $Q = 10^4$ to 10^7. The overall dimensions of resonators, at which the transmission of one transverse optical mode is provided, approach to dimensions of several tens of optical wavelengths or several tens of microns. Nonlinear optical effects such as three- and four-photon interaction, the Brillouin scattering, etc. have a threshold character, and are manifested in the disk optical resonators due to high power density in the cross-section (of the order more than 50 mW/(μm)^2) in the ultralow micro-volumes of the resonator. Owing to high power density in ODR, the material temperature sharply increases due to emission absorption in the quartz or the paratellurite, which leads to complicate temperature compensation of such a resonator.

2.8.3 *Dimensions of Oscillator Resonance Systems*

At first, we would like to note that in RF FODL with geometric length of the optical fiber of 1–5 km, the useful volume (in which emission propagates in the regime of one transverse mode) is not more than 1 cm^3.

Figure 2.15a shows maximal overall dimensions of resonators and delay lines used in the modern high-stable OEOs and microwave and mm-wave oscillators. Here we see that the optical disk resonator (ODR) is a leader of minimal dimensions. Its linear dimensions with input/output emission devices are less than 1 mm. The plot of maximal overall dimensions of the optical fiber reel with the length 5–10 km is presented in Fig. 2.15b over years. The empiric function of the reel size reduction, and appearance of nano-dimension fibers in the market with minimal losses of 0.001 dB per one bend of radius of 2–3 mm guarantees appearance in the market

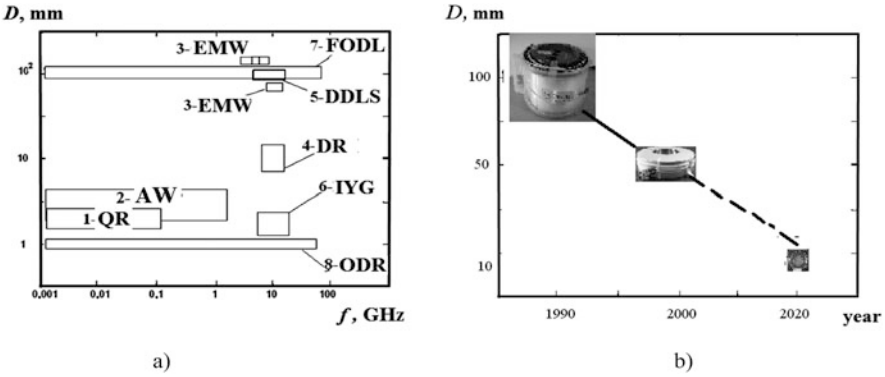

Fig. 2.15 (**a**) Maximal dimensions of resonators and delay lines used in modern high-stable OEOs and microwave oscillators. (**b**) The plot of maximal overall dimensions' variations of the fiber reels in years. Dependence of the resonator size in years (delay time is 50 μs). (1) QR—the quartz resonator, (2) SAWR—the resonator on surface acoustic waves, (3) CR—the caviar resonator of electromagnetic waves, (4) DCR—the disk dielectric resonator from ceramic alloys, (5) DDRLS—the disk dielectric resonator from leuco-sapphire, (6) YIGR—the YIR resonator, (7) RF FODL—the fiber-optical delay line (delay time is 10–50 μs), (8) ODR—the optical disk resonator

of delay lines with overall dimensions 10–50 mm with delay times 1–50 μs within the next 5-years period.

Authors of this book are initiators and pioneers of the idea to use the heating of the support tube in the range from 1000 to 1950 °C for manufacture of miniature RF FODL for microwave oscillators with reduction of settling time of required temperature and with increased accuracy of temperature adjustment [3].

A progress of technologies of crude product manufacture for optical fibers with application of high-temperature automated methods of heating of the quartz glass blanks alloyed by a nitrogen, and synchronic displacement of plasma columns along the blanks using of stabilized microwave oscillators will lead to creation of ultra-miniature RF FODLs with overall dimensions less that 0.5 cm^3 with effective delay more than 50 μs at transmitted oscillation bandwidth of 1–100 GHz.

For comparison, Figs. 2.15 and 2.16 show dimensions and types of RF FODL with the optical fiber length of 10 km with dimensions used in OEOs.

We note (Figs. 2.15 and 2.16) that RF FODL geometric dimensions for the length of 10 km with the delay 50 μs is about 100 × 100 × 20 (mm^3), and dimensions of the optical disk resonator are 100 × 100 × 100 $(\mu m)^3$. The record small dimensions of RF FODL and optical disk resonators allow manufacturing of microwave and mm-wave oscillators in the miniature implementation with relatively high characteristics in noises and frequency tuning.

At the modern stage of OEO technology development, the RF FODL overall dimension almost coincide with overall dimensions of the disk dielectric resonator from the leuco-sapphire with generation frequencies in the range of 10–12 GHz.

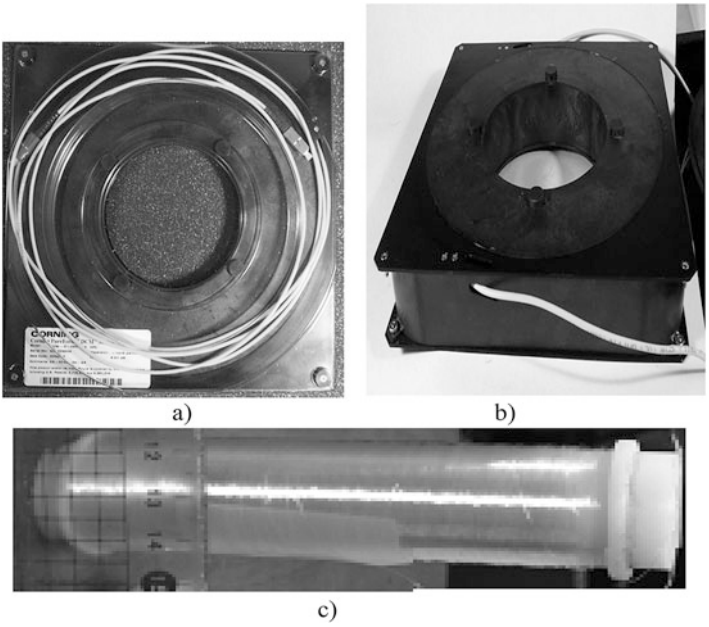

Fig. 2.16 Views of RF FODL with thee optical fiber length of 10 km with dimensions $100 \times 100 \times 20$ $(\text{mm})^3$ (**a**, **b**). View of RF FODL with optical fiber length of 0.2 km with dimensions 20×100 mm (**c**)

We note that RF FODLs have relatively small dimensions and the linear topology (the optical fiber is packed up on "a coil after a coil" principle to the disk reel). The useful volume of the fiber is 10–20% from the total RF FODL volume.

Therefore, it is relatively simple to perform in RF FODL the stabilization in temperature compared to resonators from leuco-sapphire. Owing to specific methods to pick up the optical fiber [69], we can achieve good mechanical strength of RF FODL. Such RF FODLs are much less than monolithic crystals from the leuco-sapphire, which have approximately the same overall dimensions as the RF FODL maximal dimensions. They are subjects to destructive shocking impacts with accelerations in several g, which happens at exploitation of radio-electronic systems accommodated in the flying vehicles (piloted and unmanned). In other words, it is necessary to note this special important property of delay lines in OEO with RF FODL. Such RF FODLs and oscillators as a whole are subjects to the lesser degree to mechanical, acoustical impacts and shocking loads than oscillators with the disk dielectric resonator from the leuco-sapphire monocrystal. Figure 2.17 shows experimental results of spectral density $S(F)$ of the phase noise of the low-noise traditional electronic oscillators and optoelectronic oscillators of various types.

From curves presented in Fig. 2.17 we can conclude that OEO with RF FODL [69] is competitive with known electronic oscillators, and concerning noises, they yield yet by 10–15 dB/Hz to the oscillator on the sapphire (DDRLS) [29, 30] in the offset area of 1 kHz from the carrier of 10 GHz.

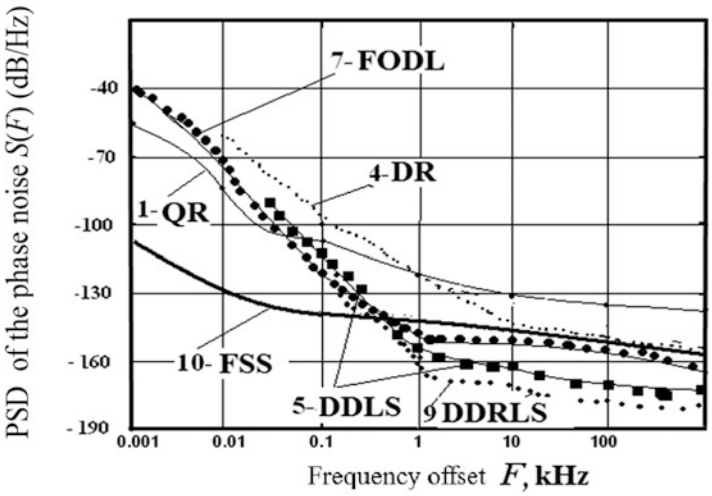

Fig. 2.17 Experimental results of the spectral density of phase noises $S(F)$ of low-noise oscillators with different types of resonators and RF FODL. The central (mean) generation frequency is 10 GHz. F is the offset in radio frequency from the central frequency. (1) QR—the quartz resonator, (4) DDR—the disk dielectric resonator from ceramic alloys. (5) DDRLS—the disk dielectric resonator from the leuco-sapphire, (7) RF FODL—OEO with RF FODL with the MZ modulator (delay in RF FODL is 90 μs), (9) SDDR—the special disk dielectric resonator, (10) FSS—the femtosecond synthesizer on the base of the highly stabilized laser and the frequency divider

2.8.4 Phase Noises and PSD of Precision RF Oscillations

Compared to oscillators with quartz and SAW [70] resonators (Fig. 2.17), OEO with RF FODL has a benefit by 10–20 dB/Hz in the area of frequency offsets 1–10 kHz from the carrier of 10 GHz.

The FSS oscillator is the undisputable leader in the area of small offsets 0.001–0.1 Hz. It is necessary to note that at present, in OEO, the potentially possible ultralow noises and the ultrasmall compact construction are not yet implemented.

As we already mentioned, traditional oscillators of RF oscillations can be divided into the following two classes: constructed on the base of (1) electromagnetic and (2) acoustic resonators. Oscillators with dielectric and ceramic dielectric resonators and oscillators with leuco-sapphire resonators (DDRLS) can be concerned to oscillators with electromagnetic resonators. Oscillators with quartz resonators (QR) and oscillators with resonators (or delay lines) on surface acoustic waves (SAW) can be concerned to oscillators with acoustic resonators.

Experimental results of the spectral density of the phase noises $S(F)$ for commercially available low-noise oscillators on DDR are presented in [71], and DDRLS are presented in [72]. The overall dimensions of DDR are about 70 mm × 60 mm × 30 mm. Overall dimensions of the oscillator on the sapphire (DDRLS) is much more than DDR and are about 100 mm × 120 mm × 130 mm.

At analysis of presented characteristics, we can see that in the offset area of 1–10 kHz from the carrier frequency 10 GHz, the oscillator on the leuco-sapphire has the noises on the level −140 to −160 dB/Hz. Such minimal values of the phase noise are achieved not only owing to the high Q-factor of the leuco-sapphire resonator, but thanks to application of PLL systems for frequency adjustment [73]. The oscillator with DCR has the appropriate dependences at mentioned offsets, and we have as result of phase noise −90 to −100 dB/Hz. We note that overall dimensions of such oscillators (not taking into account of regulated power supply units) are about 200 × 100 × 50 mm. Such relatively small sizes play critical importance at placing of oscillators in the onboard complexes of flying vehicles.

From fulfilled analysis, we may conclude that OEO with RF FODL is able to compete with well-known electronic oscillators with DCR and DDRLS by all main characteristics. Although OEO with RF FODL yields in PSD of the phase noise in the area of frequency offsets 1–10 kHz from the nominal carrier frequency 10 GHz by 5–15 dB/Hz to the oscillator with the leuco-sapphire resonator (DDRLS). Nevertheless, OEO with RF FODL [69] has quite noticeable advantages: less (almost two-orders) frequency dependence on the temperature variations and higher mechanical resistance and almost less to one order the frequency dependence on mechanical loads.

2.9 Modern Optoelectronic Methods for Precision RF Oscillation Formation

Together with usual electronic methods of oscillation formation, optoelectronic methods of precision RF oscillation formation in microwave and mm-wave ranges are successfully developed. Utilization of *electromagnetic emission of the optical frequency range* with wavelengths of 0.4–2.0 μm besides RF oscillation is the main difference from traditional electronic methods.

In addition to the laser optoelectronic oscillator investigated in this book, which can be concerned to the modem type, we can mark out several types of such formation devices of microwave and mm-wave oscillations: the quantum frequency standard, the laser femtosecond synthesized on the base of the high-stabilized laser and the frequency divide, the synthesizer with the optical micro-resonator, and the laser oscillator with optical synchronization of two lasers [74].

2.9.1 Commercial Bulky and Compact Frequency Standards with Optical Pumping on Cesium and Rubidium Cells

The commercially available quantum frequency standard (QFS) on the Cs cell, which has the long-term frequency stability of 10^{-12}, possesses large dimensions

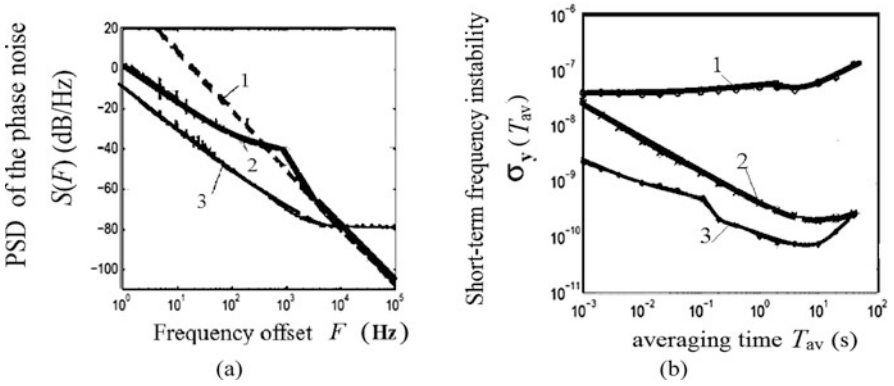

Fig. 2.18 (**a**) Experimental measurement results of PSD of phase noises $S(F)$ of commercial quantum frequency standard on the cesium cell. (**b**) Experimental measurement results of short-term frequency instability of QFS on the cesium cell. Curves in plots corresponds to: (1) QFS in the autonomous generation mode, (2) QFS with system of frequency automatic control, (3) QFS with the PLL system. T_{av} is the averaging time [58]

and a weight, and it is not an oscillator, which can be used in onboard equipment of unmanned flying vehicles (UMFV) and the specific flying vehicles. As in OEOs, the laser is one of the main elements of QFS. It is used for tuning of the generated RF frequency to the average frequency of the Cs cell absorption. The QFS operation as a whole and, in particular, its phase noises, depends in many aspects upon laser characteristics including the spectral line width, which is about 1 MHz, and the laser phase noise level. The last note also concerns to OEO with RF FODL. And these two devices are similar in this sense. Figure 2.18 shows dependences of PSD of the phase noise $S(F)$ of QFS (Fig. 2.18a) and the short-term frequency instability (T_{av} is the averaging time (observation or integration)) (Fig. 2.18b). From presented plots we see that the short-term frequency instability for standard offsets of 1 kHz from the nominal carrier frequency 4.6 GHz is not quite satisfactory and is −50 to −70 dB/Hz [57–60].

Investigations and development of the *compact* QFS for utilization in UNFV and in special apparatuses were begun recently. A construction and the functional diagram of the *compact* QFS on the cesium cell are presented in Fig. 2.19a, b [57]. In Fig. 2.19 the following designation are introduced: “5 MHz QO”—the quartz oscillator, PD—the photodiode, “Lock-in”—the mixer, the phase detector, “530 Hz”—the oscillator operation at the frequency 530 Hz, “10 kHz”—the oscillator operating at the frequency 10 kHz.

Figure 2.19c, d shows a diagram of operation energy levels of cesium and rubidium, relatively, with optical pumping. A peculiarity of modern cells with cesium and rubidium is its compactness. Dimensions of QFS unit, which contains the cesium capsule placed in the permanent magnetic field and located between the laser with wavelength 0.85 μm and the photodetector, are 20 × 20 × 50 mm. At that, the output power of RF oscillations with the frequency 4.6 GHz, extracted from the

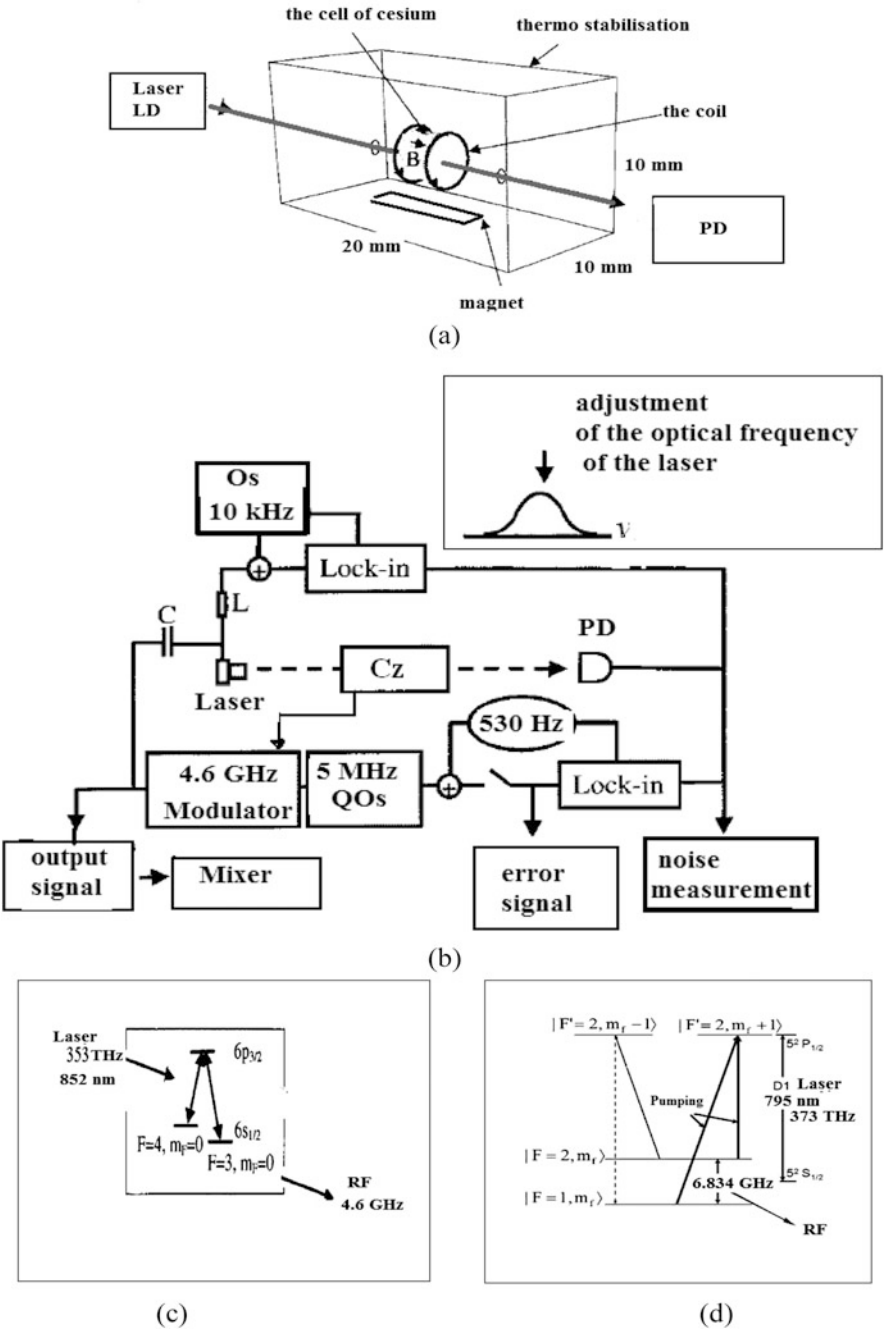

Fig. 2.19 Functional scheme of the *compact* quantum frequency standard on the cesium (or rubidium) cell. "5 MHz QO"—the quartz oscillator, PD—the photodiode, "Lock-in"—the mixer, the phase detector, "530 Hz"—the oscillator with frequency of 530 Hz, "10 kHz"—the

cesium cell, is not less than 0.1 μW, while the long-term stability is 10^{-10}. In QFS, oscillations with the frequency 4.6 GHz are extracted by the resonator, in which the cesium cell is placed.

These oscillations pass on the modulator. Control of laser optical frequency is performed with the modulator. In the compact rubidium QFS, oscillations are formed by the almost similar control scheme as in QFS on cesium. We can conclude that in the compact rubidium QFS the *adjustment* happens with the help of "input" laser emission with the wavelength 0.795 μm (with generation frequency of 373 THz) on the "output" radio frequency 6.8 GHz (Fig. 2.19d). Here, with some reservation, QFS represents the "black box", and we may speak about conversion of the laser emission of 373 THz into the radio frequency of 6.8 GHz.

2.9.2 A Synthesizer with the Fabry–Perot High-Q Resonator

In the laser synthesized FSS, the stabilized laser, made on the laser base (optical operating frequency $\nu_o = 456$ THz, the wavelength is 658 nm) with the stabilizing Fabry–Perot high-Q resonator, and the femtosecond laser operating in the synchronous mode of longitudinal laser mode (or "mode-locking") are used. Control of the optical frequency with utilization the Fabry–Perot high-Q optical resonator provides the spectral line width 0.2 Hz of the master laser optical emission, which is the record index. PSD of the phase noise of the laser optical emission with the frequency 456 THz is −17 dB/Hz at the offset 1 Hz from the optical carrier [61, 75].

The basis of QFS creation, which circuit is shown in [61, 75], is the principle of radio-frequency oscillation formation by means of adding on the photodetector area of two synchronized optical oscillations spaced in the frequency by 1 GHz. Modern lasers operating in this mode are usually constructed according to the diagram shown in [61, 75]. This diagram contains series-connected into a loop the amplitude electro-optical modulator (or absorption cell with saturation), the pass-band optical filter, the directional isolator, and the active nonlinear optical element for emission amplification.

Types of the optical spectra at output of the femtosecond laser and the RF spectrum at output of FSS are shown in [61, 75].

The FSS structure represents the ideal optoelectronic divider-converter of the optical frequency of 456 THz (the wavelength in the air is 0.65 μm) by a number $N = 53{,}200$. At the "divider" output, the RF signal of 10 GHz is formed, which PSD of the phase noise at offset frequency 1 Hz is −112 dB/Hz. This result is record at frequency offset 1–300 Hz. This synthesizer surpasses by −50 dB/Hz in phase

Fig. 2.19 (continued) oscillator with frequency of 10 kHz. (**a**) The equivalent diagram of the optoelectronic part of the quantum frequency standard with cesium cell. (**b**) Functional diagram of QFS of cesium cell. (**c**) Cesium energy levels. (**d**) Rubidium energy levels [57]

noises the best microwave oscillators with the leuco-sapphire resonator. Measured time jitter (time incursions of the pulse front edge due to fluctuations) is 0.8 fs. FSS represents the optoelectronic converter of optical emission frequency of 456 THz into RF oscillations of 10 GHz, This converter uses the scheme of photodetection of double-frequency optical oscillations using self-heterodyne mixing on the photodetector area. Exactly as a result self-heterodyne mixing, the record level of phase noise PSD is obtained in the FSS.

We should note that, thanks to utilization of a laser with low phase noise with the high-stability optical resonator, the record ultralow phase noises of RF oscillation are obtained in FSS. On 10-GHz frequency, at offset 0.001 kHz from RF carrier, its levels is less than −110 dB/Hz. Such extremely low low-frequency phase noises are explained not only by extremely low susceptibility of the optical resonator in the femtosecond laser to the low-frequency noises due to small geometrical sizes.

2.9.3 A Synthesizer with the Optical Micro-Resonator

In the synthesizer with the optical micro-resonator (SOMR), which block diagram is shown in Fig. 2.20a the *synthesis* of RF oscillations of 10 and 89 GHz occur [76–78].

The main formation principle, as in FSS, is double-frequency optical conversion with self-heterodyne emission mixing on the photodetector into microwave oscillations. Exactly due to self-heterodyne mixing, in the SOMR, one obtains the relatively low level (although not record) of PSD of the phase noise and good short-term 10 GHz-frequency instability.

The distinctive feature of SOMR is utilization of the nonlinear optical conversion in the optical micro-resonator (shown in Fig. 2.20b) for formation of two optical frequencies. The optical emission enter in the micro-resonator input at relatively high power of 200 mW from the narrowband laser with ultralow laser optical phase noises (with wavelength 1.55 μm and the spectral line width of 3 kHz). At that, the *optical Q*-factor of the micro-resonator (i.e., the ratio of the own natural optical frequency to the resonance peak width on 0.7-level) is 10^9.

Thanks to the large optical power of 200 mW and the narrow spectral line of optical emission of 3 kHz, the multifrequency oscillations are formed at the microtoroid output, which spectrum is shown in Fig. 2.20d. In this system, on the frequency 8.57 GHz, the short-term frequency stability 10^{-12} is obtained. The laser pumping block consists of the high-coherent laser with the line width of 3 kHz synchronized by the more powerful laser with the optical amplifier with automatic frequency control. SOMR, as we see from description of its functional diagram, is also concerned to optoelectronic devices of RF oscillation formation, and the conversion of optical frequencies of 200 THz into oscillations of 10 GHz-frequency occurs. Phase noises of RF oscillation in this system are determined by the laser phase noises. We also see in this device much similar with OEO with RF FODL, for instance, extraction of subcarrier oscillation in the photocurrent of the photodetector.

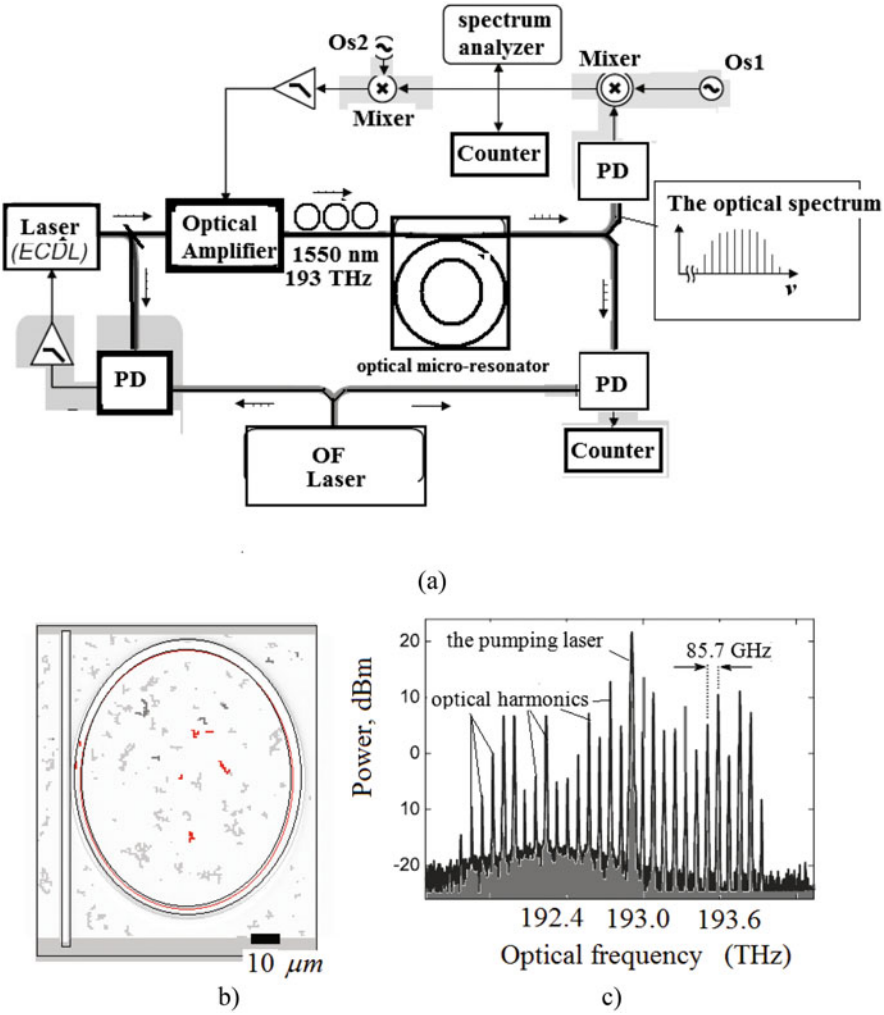

Fig. 2.20 Formation of RF oscillation of 10 and 89 GHz in the synthesizer with the optical micro-resonator (**a**) in the optical frequency synthesizer on the base of optical frequency synthesizer with micro-toroid (**b**) using the nonlinear optical conversion. The optical emission spectrum at the output of the optical circular resonator of the micro-toroid (**c**). Components of the pumping laser and optical harmonics are shown (wavelength is 1570 nm). The difference of wavelengths between adjacent harmonics is about 0.71 nm (which corresponds to frequency difference of adjacent harmonics of about 85.7 GHz) [78]

Together with described circuits for formation of microwave and mm-wave oscillations with heterodyne-mixing, one may use the mode of mutual synchronization of two laser diodes (LD1 and LD2). In this case, the optical frequencies difference is the final formed oscillation frequency, for instance, 10 GHz. For synchronization of these laser diodes LD1 and LD2 we can use either the continuous

multifrequency laser, or the laser with passive or active synchronization of longitudinal modes. We may also notice circuits for RF oscillation formation with the frequency of 40 GHz using the nonlinear Brillouin effect in the specific perforated optical fiber. The cross-section of such an optical fiber is shown in Fig. 2.13a, b [79].

Table 2.4 Methods of oscillation formation in RF oscillators, lasers (OQG), and in the optoelectronic oscillator

	Traditionally RF oscillators	OEO as the laser with the positive feedback loop	The laser or the optical quantum generator
Oscillation frequency f_0 and ν_0	$f_0 = 0.001$–100 GHz	$f_0 = 0.001$–100 GHz $\nu_0 = 100$–280 THz	$\nu_0 = 100$–280 THz
The main construction circuit	The RF van-der Pol oscillator	The RF van-der Pol oscillator + RF FODL	OQG—the van-der Pol oscillator
Resonator or delay lines, their Q-factor and time constants	Electronic: QR, SAW, DCR, YIG, DDRLS. $Q = 10^6$, $T_{ep} = 10^{-4}$ s	Electronic: QR, SAW, DCR, YIG, DDRLs Optical: {Fabry–Perot, DOptR, BraggR, FtCr} + RF FODL + Cz cell $Q_{REFODL} = 10^6$ $Q_e = 10^6$, $T_{ep} = 10^{-4}$ s	Optical: {Fabry–Perot, DOptR, FtCr, FOS, BraggR} $Q_O = (2 \times 10^3)/10^{10}$ $T_{op} = 10^{-11}$ s
Natural width of the RF spectral line and laser generation	$\Delta f_G = \left(\frac{f_0}{Q_e}\right)^2 \frac{kT_B}{2P_e}$	Defined by laser noises, which have the quantum nature, and by noises of the electronic amplifier	$\Delta\nu = \frac{\nu_0^2 h\nu_0}{Q_O^2 2P_{OL}}$
Active elements and their noises	RF amplifier {Thermal noise and shot noise, flicker noise ($1/f$) etc.}	RF amplifier + laser + photodetector {Spontaneous quantum noise} + {noise of photodetector} + {thermal noise and shot noise, flicker-noise ($1/f$)}	Active optical medium with inverse population. Spontaneous quantum noise. Noises of carriers, the pumping current
Restrictions on Q-factor improvement of the oscillating system	Sound-wave dispersion and losses in the resonator	RF FODL light dispersion, nonlinear effects in the optical resonator, thermal effects	Dispersion of the optical amplifier, laser and optical fiber system
$S = \frac{f_0^2 kT_B}{Q_e^2 P_e} \frac{D_Y}{4F^2}$	PSD of phase noise is determined by phase noises of a laser, the electronic amplifier, and the photodetector.		$S(F) = \frac{\nu_0^2 h\nu_0 D_{0Y}}{4Q_O^2 F^2 P_{OL}}$

The following designations are introduced in Table 2.4: QR—the quartz resonator, DCR—the disk dielectric resonator from ceramic alloys, DDRLS—the disk dielectric resonator from the leuco-sapphire, SDDR—the disk dielectric stabilized resonator, FSS—the femtosecond synthesizer on the base of the highly stabilized laser and the frequency divider, RF FODL—the fiber-optical delay line, DOptR—the disc optical resonator, FOS—the fiber-optical system, BraggR—the optical Bragg resonator, Fabry–Perot—the optical resonator Fabry–Perot, PhCr—photon crystals, h—the Planck constant, k—the Boltzmann constant, $T_B = T_{FO}^0$—temperature in Kelvin, D_Y—the amplification factor, Q_e—the Q-factor of the electronic filter in OEO, P_e—the power of the OEO oscillator, F—the frequency offset from the carrier, ν_0—the optical frequency of the laser (or OQG) generation, $h\nu$—an energy of the one quantum, D_{0Y}—The optical amplification factor of the laser optical amplifier, P_{OL}—the laser optical power, Q_O—the Q-factor of the optical resonator.

The analysis result of various oscillating circuits and their characteristics is the information presented in Table 2.4, in which we compare of oscillation formation methods in RF and optical ranges. From Table 2.4 we see that OEO is the modem oscillator with self-heterodyne mixing by its characteristics, in which we may use (together with traditional electronic oscillators) both filters, delay lines and optical delay lines and resonators. Phase noise levels and PSD of the phase noise in this OEO oscillating system is defined by spontaneous emission, "electronic" noises of the photodetector and the electronic amplifier.

We note that for traditional oscillators and optical quantum generators, the basing fundamental relationships for coupling of the natural line width and PSD of the phase noise with the main characteristics of the oscillating systems are already determined in many publications [20–24, 63, 64, 70, 80–83]. For OEO with RF FODL, which is the result of synthesis of two oscillating processes, lying in the optical and RF ranges (or two oscillators), these relationships are defined in publications of authors and described in Chaps. 3–7 on this book. This is exactly one of the tasks of further analysis OEO with RF FODL.

2.10 Conclusions

Here we briefly list the main results of this chapter.

1. OEO represents the double-range oscillating system, in which oscillations in optical and RF ranges are developed. Methods of direct and external modulation of the laser narrowband emission of QWLD (with additional suppression of optical harmonics), which are examined in this book, basically, use the phase (amplitude or frequency) optical modulation of the carrier. The photodetection process with extraction in the photocurrent of a subcarrier with phase noises in these OEO systems is the process of the heterodyne mixing or the self-heterodyne mixing. One of the problem solved in this book, is the issue that the laser noise affects the OEO RF noise.

Therefore, for mathematical modeling of QWLD, we use the semiclassical theory. When using the method of laser balanced (kinetic) equations the *phase relationships* are lost, which are the most important for analysis of laser phase noise influence on the RF noises of OEO. It is necessary to note once more that the most of OEO schemes under consideration with direct and external modulations can be attributed to schemes with phase or amplitude modulation of optical emission, while in the process of photodetection with self-heterodyne mixing, information about the subcarrier is contained in the phase of optical emission.

2. In this book, OEO is the main object under investigation. One of the tasks of this investigation is the understanding of the basing operation mechanisms of the complicate oscillating system, which determine the OEO phase noise. At that, the main attention is attracted not so much to the OEO RF part (this is well-developed in traditional RF oscillators) as to influence of laser emission characteristics on the OEO frequency and amplitude, as well as to influence of amplitude and phase noises of laser spontaneous emission on the OEO RF phase noise.
3. Solution of problem stated in this book on OEO investigation should be matched with the specificity of the laser emission, which relates with the noise quantum nature, the temporal and spatial coherence, the presence of the spatial distribution on strength amplitude $E_0(R)$, on phase $\Phi_0(R)$, and on fluctuations of amplitude m (R) and phase $\Delta\varphi(R)$, the adequacy with the laser wavelengths of overall dimensions of optical channels and the photodetector area in the microwave range.
4. Methods of direct and external modulation of the QWLD laser narrowband emission (with additional suppression of optical harmonics), used in OEO, potentially have the high degree of laser phase noise suppression, on the one hand, due to utilization of *lengthy low-dispersive optical fiber*, the narrowband QWLD laser emission, while, on the other hand, due to utilization of methods of the phase noise compensation at self-heterodyne mixing on the photodetector, the transmission of two optical harmonics (with suppression of the third optical harmonic) through the optical channel and alignment of these harmonics in amplitude.
5. An approach to OEO examination as to the system where two oscillating processes are developing in the optical and RF ranges with scattering, the energy transformation, taking into consideration of spontaneous emission generation in the laser, to our opinion, is new and effective. Such an approach enables to analyze of laser element influence of OEO RF noises, to examine the RF frequency control by the laser optical frequency (and vice versa), to provide the control of the laser optical frequency varying the OEO RF frequency. In the future, this permits to study the OEO synchronization by the external optical emission source, to perform the analysis of PLL systems for OEO by modulated laser oscillations, to investigate OEO as the master microwave oscillator for different laser systems, for instance, the laser with synchronization of longitudinal modes with the pulse duration 1–10 ps with low jitter, etc.
6. As a result of the review fulfilled and the analysis of various oscillators in this chapter, we can conclude that the phase noise level in OEO approaches to the phase noise of the "best low-noise oscillator" on the leuco-sapphire. Difference in

the microwave frequencies of the range 8–12 GHz is approximately 5–15 dB/Hz. But, at that, OEO has the wider potential operating microwave range up to 70–100 GHz at keeping of low phase noises. The principal moment is that OEO with RF FODL has potential possibilities of phase noise reduction due to optimization of the laser and RF FODL as a whole.

Other important OEO advantages compared to the leuco-sapphire oscillator are higher strength characteristics due to application of lengthy laid by rings RF FODL structure, the potentially smaller weight and overall dimensions of the RF FODL useful volume, in which laser emission propagates in the optical fiber. The RF FODL useful volume is less than 1 cm^3 at application in RF FODL of 1 km of the optical fiber length.

Other advantages of OEO are the weaker dependence on temperature (by two orders) of the RF FODL phase-frequency response and stronger (by the order and more) resistance to external mechanical influences and to accelerations due to linear topology of laying of the quartz fiber thin thread in the RF FODL reel.

7. One of the analysis results of various optoelectronic structures for creation of high-stable oscillations is the conclusion that modern optical micro-resonators (Bragg, disks, etc.) can be used in OEO only as the optical discriminators in systems on automatic phase control and the optical frequency due to low thresholds of the entry power of optical emission (5–20 μW), which is caused by nonlinear optical effects.
8. The key moment at manufacture of stable oscillators in microwave and mm-wave ranges is the reasonable transition from the completely RF oscillator and from the completely optical oscillator to the hybrid structure of OEO containing both optical and RF parts. Only in this case, the possibility appears of high-effective selective suppression of spurious harmonics, spaced from the useful harmonic by the interval less than 1–100 kHz by RF high-Q filters at increase of the geometric length of RF FODL of the order 2–10 km. Fundamental reason of this restriction is the fact that Q-factors of RF microwave and mm-wave filters are restricted by a million (due to loss increase in the material at reduction of wavelength), while the Q-factor of optical filters (without presence of nonlinear effects) is restricted by 10–1000 due to high power density owing to wavelength smallness, approximately, 1 μm. As a consequence of such a transition to the hybrid OEO structure, the inevitable power losses arise, which are circulated in the oscillator loop. At double optoelectronic conversion, the power decreases not less than by 10 times. Moreover, the additional phase noises of spontaneous laser emission arise, which are essentially higher of natural electronic noises, taking into account this conversion. Nevertheless, development of technology of quantum-dimension low-noise laser diodes with optical phase adjustment, using high-Q micro-resonators (with line width less than 10 MHz on the optical carrier) (the phase noise is less than −100 dB/Hz), and manufacture of commercially available low-dispersive optical fibers with lengths of 2–10 km wounded into the compact reels (with overall dimensions 5 × 5 × 5 cm) is guarantees the revolutionary breakthrough in the field of stable microwave and mm-wave oscillators.

9. As the results of an analysis of various oscillating structures and their characteristics, we may conclude that OEO is the modern oscillator with self-heterodyne mixing according to its characteristics, in which, together with traditional RF resonators, filters and delay lines, we may apply optical delay lines and optical resonators. Phase noises in this OEO oscillating system are determines by spontaneous laser noises, RF phase noise of the laser, the photodetector, and the RF nonlinear amplifier.

References

1. A.A. Bortsov, Y.B. Il'in, New low-noise UHF oscillator with the pumping by the quantum-well laser diode. Radio-optical technologies in instrumentation: (In Russian), in Proceedings of II Scientific Conference, 14–21 of September 2004. Sochy (2004), pp. 70–71
2. A.A. Bortsov, Y.B. Il'in, Nanostructured opto-electronic oscillator of frequency-modulated signals, Patent RU: 103431 (2010) DOI: 10.13140/RG.2.2.19544.11524
3. A.A. Bortsov, Y.B. Il'in, V.E. Karasik, A. Karachev, et al., Method of manufacturing of work pieces for opticasing on nitrogen-doped quartz glass, Patent RU 2,537,450, 2015, DOI:10.13140/RG.2.2.29191.01445
4. Alexander A. Bortsov and Sergey M. Smolskiy, Opto-Electronic Oscillator with Mach-Zender Modulator. Infocommunications Journal, Vol. XI, No 1, 45-53, (2019), DOI:10.13140/RG.2.2.20992.69126
5. G. Qi, J. Yao, J. Seregelyi, et al., Phase-noise analysis of optically generated millimeter-wave signals with external optical modulation techniques. J. Lightwave Technol. **24**(12), 4861–4875 (2006)
6. A.R. Chraplyvy, Limitations on lightwave communications imposed by optical fiber nonlinearities. J. Lightwave Technol. **8**, 1548–1557 (1990)
7. Y.X. Steve, Brillouin selective sideband amplification of microwave photonic signals. IEEE Photon. Technol. Lett. **10**(1), 138–140 (1998)
8. S.K. Turitsyn, A.E. Bednyakova, et al., Inverse four-wave-mixing and self-parametric amplification effect in optical fibre. Nat. Photon. **9**(9), 608–614 (2015)
9. P.J. Lezzi, M. Tomozawa, An overview of the strengthening of glass fibers by surface stress. Appl. Glass Sci. **6**(1), 34–44 (January 2015)
10. A.A. Bortsov, V.V. Grigoriants, Y.B. Il'in, Effect of the lightguide excitation efficiency on the frequency of a self-excited oscillator with a differential fiber optic delay line. Telecommun. Radio Eng. **44**(8), 137–142 (1989)
11. V.V. Grigoriants, A.A. Dvornikov, Y.B. Il'in, V.N. Konstantinov, V.A. Prokof'ev, G.M. Utkin, A laser diode with feedback using a fibre delay line as a stable-frequency signal generator and potential fibre sensor. Opt. Quantum Electron. **17**(4), 263–267 (1985)
12. V.V. Grigoriaynts, Y.B. Il'in, Laser optical fibre heterodyne interferometer with frequency indicating of the phase shift of a light signal in an optical waveguide. Opt. Quantum Electron. **21**(5), 423–427 (1989)
13. V.V. Grigoriants, A.A. Dvornikov, Y.B. Il'in, et al, Oscillators of the radio-frequency range with the optical carrier, in Proceeding of MPEI, Issue 607 (1983), pp. 76–79
14. A.A. Dvornikov, Y.B. Il'in, V.N. Konstantinov, About single-frequency modes of the oscillator with the fiber-optical delay line in the feedback loop. Radio Eng. Electron. **29**(11), 2234–2242 (1984)
15. V.V. Grigoriants, A.A. Dvornikov, Y.B. Il'in, et al., Radio signal generation in the system «laser optical delay line». Quant. Electron. **11**(4), 766–775 (1984)
16. A.A. Bortsov, V.V. Grigoriants, Y.B. Il'in, V.N. Konstantinov, Transfer function of a composite fiber-optic delay line. Telecommun. Radio Eng. **43**(9), 40–42 (1988)

17. A.A. Bortsov, V.V. Grigoriantz, Y.B. Il'in, Frequency tuning in a self-excited oscillator with a fiber-optic delay line. Telecommun. Radio Eng. **44**(4), 74–77 (1989)
18. T.V. Babkina, V.V. Grigoriantz, Y.B. Il'in, V.A. Prokof'iev, LASER APPLICATIONS AND OTHER TOPICS IN QUANTUM ELECTRONICS: Use of a laser oscillator heterodyne interferometer as an optical sensor of microdisplacements. Soviet J. Quantum Electron. **21** (12), 1384–1387 (1991)
19. T.V. Babkina, V.V. Grigoriantz, Y.B. Il'in, V.A. Prokof'ev, Self-sustained operation of a laser oscillating Mach-Zehnder interferometer. Soviet J. Quantum Electron. **21**(2) (1991)
20. A.A. Bortsov, Y.B. Il'in, et al., Device for the functional transformation of acoustic pressure into frequency. Patent USSR 1,538,265, 1988,DOI: 10.13140/RG.2.2.10736.07688
21. Alexander A. Bortsov, Y.B. Il'in,Opto-electronic oscillator ,Generator of frequency-modulated signals, 2006-08-20, Patent RU2282302C1,2006, DOI: 10.13140/RG.2.2.29610.44488
22. A.A. Bortsov, Phase-frequency and amplitude-frequency characteristics of a mesa-adjusted laser diode with a modulation frequency band of up to 12 GHz. Radio Eng. (Radiotekhnika, Moscow),vol.9, 43–47 (2006),DOI: 10.13140/RG.2.2.18285.82408
23. A.A. Bortsov, Y.B. Il'in, Laser spectral line widening effect on RF phase and amplitude noises of an optoelectronic oscillator OEO. J. Radio Eng. (2), 21-31 (2010), DOI: 10.13140/RG.2.2.35665.07527
24. A.A. Bortsov, The Influence of the Quality of Laser Resonator to Microwave Phase Noise in opto-electronic oscillator, Electromagnetic Waves and Electronic Systems,(Radiotekhnika, Moscow), vol.11, 48-55(2012),DOI:10.13140/RG.2.2.28352.15361
25. R.A. Woode, E.N. Ivanov, M.E. Tobar, Application of the interferometric noise measurement technique for the study of intrinsic fluctuations in microwave isolators. Meas. Sci. Technol., vol.9 ,1593–1599 (1998)
26. G.J. Dick, D.G. Santiago, R.T. Wang, Temperature compensated sapphire resonator for ultra-stable oscillator capability at temperatures above 77 kelvin. IEEE Trans. Microwave Theory Tech. **42**(7), 19–25 (2000)
27. G.J. Dick, R.T. Wang, Stability and phase noise tests of two cryo-cooled sapphire oscillators. TMO Progress Report, vol. 42-1542 (1999), pp. 34–45
28. G.J. Dick, R.T. Wang, Design of a cryocooled sapphire oscillator for the cassini Ka-Band experiment. TMO Progress Report, vol. 42-134 (1998), pp. 176–189
29. P. Stockwell, C. McNeilage, M. Mossammaparast, D.M. Green, 3-Axis vibration performance of a compact sapphire microwave oscillator. IEEE Trans. Microwave Theory Tech. **46**(8), 123–199 (2002)
30. K.L. Ribeiro, E.N. Ivanov, D.G. Blair and etc, A proposal for improving the noise floor of the gravitational wave antenna Niobè,Classical and Quantum Gravity ,vol.19 , 1967–1972 (2002)
31. V.G. Thomas, N. Daneu, et al., The internal structure of hydrothermally grown leucosapphire crystals. CrystEngComm **21**(5), 1122–1129 (2019)
32. V.S. Ilchenko, M.L. Gorodetsky, Y.X. Steve, L. Maleki, Microtorus: a high finesse microcavity with whispering-gallery modes. IEEE Photon. Technol. Lett. **26**(5), 256–258 (2001)
33. K.R. Hiremath, V.N. Astratov, Perturbations of whispering gallery modes by nanoparticles embedded in microcavities. Opt. Exp. **16**(8), 5421–5426 (2008)
34. G.S. Murugan, J.S. Wilkinson, M.N. Zervas, Selective excitation of whispering gallery modes in a novel bottle microresonato. Opt. Exp. **17**(14), 11916–11925 (2009)
35. K.J. Vahala, Optical microcavities. Nature **424**, 839–846 (2003)
36. L. Maleki, V.S. Ilchenko, A.A. Savchenkov, A.B. Matsko, Crystalline whispering gallery mode resonators in optics and photonics, in *Practical applications of microresonators in optics and photonics*, ed. by A. B. Matsko, (CRC Press, New York, 2009)
37. L. Stolpner, S. Lee, S. Li, A. Mehnert, P. Mols, S. Siala. Low noise planar external cavity laser for interferometric fiber optic sensors, in Proceedings of SPIE 7004, 19th International Conference on Optical Fibre Sensors (2008), pp. 700451–700457
38. K. Numata, J. Camp, M.A. Krainak, L. Stolpner, Performance of planar-waveguide external cavity laser for precision measurements. Opt. Exp. **18**(22), 22781–22788 (2010)

39. R.E. Bartolo, C.K. Kirkendall, V. Kupershmidt, S. Siala, Achieving narrow linewidth, low phase noise external cavity semiconductor lasers through the reduction of 1/f noise, in Proceedings of SPIE 61333, 6133OI (2006)
40. R.E. Bartolo, C.K. Kirkendall, V. Kupershmidt, S. Siala, Achieving narrow linewidth, low phase noise external cavity semiconductor lasers through the reduction of 1/f noise, in *Novel In-Plane Semiconductor Lasers V*, ed. by C. Mermelstein, D.P. Bour, Proceedings of SPIE, vol. 6133, 61330I (2006)
41. M. Morin, S. Ayotte, C. Latrasse, et al., What narrow-linewidth semiconductor lasers can do for defense and security? in Proceedings of SPIE—The International Society for Optical Engineering 7677, April 2010
42. P. Qin, Y. Song, H. Kim, J. Shin, D. Kwon, M. Hu, C. Wang, J. Kim, Reduction of timing jitter and intensity noise in normal-dispersion passively mode-locked fiber lasers by narrow bandpass filtering. Opt. Exp. **22**(23), 28276–28283 (2014)
43. S.-Y. Wu, W.-W. Hsiang, Y. Lai, Laser dynamics and relative timing jitter analysis of passively synchronized Er- and Yb-doped mode-locked fiber lasers. J. Opt. Soc. Am. B **31**(7), 1508–1515 (2014)
44. Y. Wang, H. Tian, et al., Timing jitter reduction through relative intensity noise suppression in high-repetition-rate mode-locked fiber lasers. Opt. Exp. **27**(8), 11273–11280 (2019)
45. M. Bortz, M. Arbore, M. Fejer, Quasi-phase-matched optical parametric amplification and oscillation in periodically poled LiNbO3 waveguides. Opt. Lett. **20**(1), 59–60 (1995)
46. D. Jeffrey, N.A. Bull, J. Hiroshi, K. Show, et al., 40 GHz electro-optic polarization modulator for fiber optic communication systems, in Proceedings of SPIE, December 2004, pp. 133–143
47. M. Bremer, Periodically poled ridge waveguides in LiNbO3, PhD in physics, TritaFYS **30**, 17–44 (2012)
48. H.M. Naohiro, K. Okamura, Y. Okamura, 60 GHz-band electro-optic modulators using array antenna electrodes and polarization-reversed structures for SDM wireless systems, 2014, in 44th European Microwave Conference (EuMC), October 2014
49. G. Keiser, *Optical fiber communications*, 4th edn. (McGraw Hill, New York, 2008)
50. S.N. Prajwalasimha, V.N. Kamalesh, Macro bending loss in single mode optical fibre cable for long haul optical networks. Int. J. Emerg. Technol. Adv. Eng. **4**(6), 863–865 (2014)
51. H. Ito, S. Kodama, Y. Muramoto, T. Furuta, T. Nagatsuma, T. Ishibashi, High-speed and high-output InP-InGaAs uni-traveling carrier photodiodes. IEEE J. Sel. Top. Quantum Electron. **10**, 709–727 (2004)
52. A. Beling, A.S. Cross, Q. Zhou, Y. Fu, J.C. Campbell, High-power flip-chip balanced photodetector with >40 GHz bandwidth, in Photonics Conference (IEEE, 2013) (2013), pp. 352–353
53. C. Park, T.S. Rappaport, Short-range wireless communications for next-generation networks: UWB, 60 GHz millimeter-wave WPAN, and ZigBee. IEEE Wireless Commun. **14**, 70–78 (2007)
54. K. Li, X. Xie, Q. Li, Y. Shen, M.E. Woodsen, Z. Yang, et al., High-power photodiode integrated with coplanar patch antenna for 60-GHz applications. IEEE Photon. Technol. Lett. **27**, 650–653 (2015)
55. A. Beling, X. Xie, J.C. Campbell, High-power, high-linearity photodiodes. Optica **3**(3), 328–338 (2016)
56. J. Kim, J.A. Cox, J. Chen, F.X. Kartner, Drift-free femtosecond timing synchronization of remote optical and microwave sources. Nat. Photon. **2**, 733–736 (2008)
57. A. Brannon, Z. Popovic, et al., in Self-Injection Locking of a Microwave Oscillator by Use of Four-Wave Mixing in an Atomic Vapor, Conference: Frequency Control Symposium, 2007 Joint with the 21st European Frequency and Time Forum. IEEE International, IEEE-Xplore, 1-4244-0647-1/07/ (2007), pp. 275–278
58. J. Kitching, S. Knappe, L. Hollberg, Miniature vapor-cell atomic frequency references. Appl. Phys. Lett. **81**, 553–555 (2002)
59. V. Gerginov, V. Shah, S. Knappe, L. Hollberg, J. Kitching, Atomic-based stabilization for laser-pumped atomic clocks. Opt. Lett. **31**, 1851–1853 (2006)

60. V.B. Gerard, Atomic frequency standards using optical pumping of rubidium-87 and caesium-133 in gas cells. Br. J. Appl. Phys. **13**(8), 409 (2002)
61. D.S. Makarov, M.Y. Tretyakov, A.P. Shkaev, A.M. Kiselev, A.N. Stepanov, V.V. Parshin, Femtosecond laser comb based subterahertz synthesizer. Appl. Phys. Lett. **105**, 063502 (2014)
62. Y.S. Shmaliy, A.P. Kurotchka, E.G. Sokolinskiy, A.V. Marienko, Quartz crystal oscillator with an effective aging rate compensation, in Conference: 12th European Frequency and Time Forum (EFTF'98), 1998
63. T.E. Parker, G.K. Montress, et al., Precision surface-acoustic-wave (SAW) oscillators. IEEE Trans. Ultrason. Ferroelectr. Freq. Control **35**(3), 342–364 (1988)
64. A.A. Dvornikov, V.I. Ogurtsov, G.M. Utkin, On stationary states in two-dimensional networks of self-excited oscillators. Radiophys. Quantum Electron. **33**(9), 800–805 (1990)
65. E. Rubiola, *Phase Noise and Frequency Stability in Oscillators* (Cambridge University Press, Cambridge, UK, 2009)
66. W. Stein, F. Huber, S. Bildik, M. Aigle, M. Vossiek, An improved ultra-low-phase noise tunable YIG oscillator operating in the 6–12 GHz range, in 2017 47th European Microwave Conference (EuMC), IEEE Xplor,21 December, 2017
67. Ultra-Low Noise Dielectric Resonator Oscillator, www.microwavejournal.com/articles/18794-ultra-low-noise-dielectric-resonator-oscillator, December 12, 2012
68. J.G. Hartnett, N.R. Nand, C. Lu, Ultra-low-phase-noise cryocooled microwave dielectric-sapphire-resonator oscillators with 1 x 10^-16 frequency instability. Appl. Phys. Lett. **100**, 183501 (2012)
69. C.W. Nelson, A. Hati, D.A. Howe, Microwave optoelectronic oscillator with optical gain, in Proceedings of the IEEE International Frequency Control Symposium (FCS '07), vol. 31 (7) (2007), pp. 1014–1019
70. M.X. Jeremy Everard, S. Bale, Simplified phase noise model for negative-resistance oscillators and a comparison with feedback oscillator models. IEEE Trans. Ultrason. Ferroelectr. Freq. Control **59**(3), 382–390 (2012)
71. J.L. Everard, K. Theodoropoulos, Ultra-low phase noise ceramic based dielectric resonator oscillators, in IEEE International Frequency Control Symposium, 2006
72. J.J. McFerran, E.N. Ivanov, A. Bartels, G. Wilpers, C.W. Oates, S.A. Diddams, L. Hollberg, Low-noise synthesis of microwave signals from an optical source. Electron. Lett. **41**(11), 650 (2005)
73. E.N. Ivanov, M.E. Tobar, Low phase-noise sapphire crystal microwave oscillators: current status. IEEE Trans. Ultrason. Ferroelectr. Freq. Control **56**(2), 263–269 (2009)
74. W. Seitz, T.R. Schibli, U. Morgner, F.X. Kärtner, C.H. Lange, W. Richter, B. Braun, Passive synchronization of two independent laser oscillators with a Fabry–Perot modulator. Opt. Lett. **27**(6), 454–456 (2002)
75. S. Schilt, N. Bucalovic, L. Tombez, V. Dolgovskiy, C. Schori, G. Di Domenico, M. Zaffalon, P. Thomann, Frequency discriminators for the characterization of narrow-spectrum heterodyne beat signals: Application to the measurement of a sub-hertz carrier-envelope-offset beat in an optical frequency comb. Rev Sci Instrum **82**(12), 123116 (2011)
76. A.S. Raja, A.S. Voloshin, et al., Electrically driven photonic integrated soliton microcomb, 3–7 March 2019, in Optical Fiber Communication Conference (OFC), 2019 OSA Technical Digest (Optical Society of America, 2019), paper W1C.1
77. T.J. Kippenberg, S.M. Spillane, K.J. Vahala, Kerr-nonlinearity optical parametric oscillation in an ultrahigh-*Q* toroid microcavity. Phys. Rev. Lett. **93**, 083904 (2004)
78. T.J. Kippenberg, R. Holzwarth, S.A. Diddams, Microresonator-based optical frequency combs. *Science* **332**(6029), 555–559 (2011)
79. G.-F. Shen, X. Zhang, X. Zhang, et al., Microwave/millimeter-wave generation using multi-wavelength photonic crystal fiber Brillouin laser. Prog. Electromagnet. Res. **80**, 307–320 (2008)
80. D. Leeson, A simple model of feedback oscillator noise spectrum. Proc. IEEE **54**, 329–330 (1966)

81. D.B. Leeson, A simple model of feed back oscillator noise spectrum. Proc. IEEE **54**, 329–330 (1966)
82. V.S. Zholnerov, A.V. Ivanov, V.D. Kurnosov, R.V. Chernov, Parameters of a laser diode with a fiber Bragg grating at different fiber lengths. Tech. Phys. **59**, 416–420 (2014)
83. P.V. Gorlachuk, A.V. Ivanov, V.D. Kurnosov, R.V. Chernov, et al., Simulation of power current characteristics of high-power semiconductor lasers emitting in the range 1.5-1.55 μm. Quantum Electron. **44**(2), 149 (2014)

Chapter 3
Modulation Methods of Laser Emission in Optoelectronic oscillator (OEO) and OEO Differential Equations

This chapter is devoted to an analysis of laser emission modulation methods and formulation of mathematical model of the autonomous optoelectronic oscillator (OEO) on the base of nonlinear differential equations. Section 3.1 presents two methods of laser emission modulation: the direct (internal) electrical method and the external modulation through the electro-optical modulator offered by Mach and Zehnder. Before beginning of material discussion, in order to explain a consequence and the logic of description, we briefly describe the structure of mathematical analysis of the laser optoelectronic oscillator in this chapter and in the following chapters.

After brief description of two operation principles for internal and external approaches, we discuss its structural realization (Sect. 3.1.2). The complexity of both approaches is related to the nonstandard way of description of the nonlinear method modulation for the internal (direct) structure and the utilization of the specific Mach–Zehnder modulator for the first stage on external modulation: the phase modulation in the optical channels of the external MZ modulator, and (at the second modulation stage) conversion (after fiber optical delay line) of the phase-modulated laser emission into the amplitude-modulated radio-frequency signal in the nonlinear photodetector.

Methods, which permit to achieve excellent technical RF characteristics of OEO in microwave and mm-wave ranges, include:

- utilization the specific quantum-well laser diodes (QWLD) with the low phase noise level;
- active low-noise delay line on the base of the optical fiber;
- heterodyning (spectrum transformation) of the phase noise in the light-sensitive area of the nonlinear photodetector (Sect. 3.1.3);
- application of the laser emission modulation method with the single sideband (in the optical region) with suppression of the optical carrier frequency in the optical channel.

A. A. Bortsov et al., *Laser Optoelectronic Oscillators*, Springer Series in Optical Sciences 232, https://doi.org/10.1007/978-3-030-45700-6_3

Obviously, almost all mentioned features are very complicated from the point of view of its mathematical description due to nonstandard models, nonlinear optical and RF sections of the different OEOs, and complicated interaction of optical and microwave oscillation, which are principal for normal OEO operation. Mentioned complications force to undertake the very nonstandard mathematical models of all optical and RF component of OEO.

Because one of our purposes is the accurate investigation of the ultralow phase noise of OEO, which is the most important property for the source of microwave and mm-wave oscillations, it is necessary for us to understand up-to-date details of the quantum nature of the laser noises in OEO, which can be influenced for the phase noise of RF section. Section 3.1.4 is devoted to research these issues. For this, we use standard and nonstandard approaches to the laser theory.

After that (Sect. 3.1.5), we discuss the *functional diagrams* of OEO with direct and external modulation of laser emission, introduce the mathematical description of OEO principal components: the laser, the optical fiber, the photodetector, the RF amplifier, the optical amplifier, the RF and optical filters, directional couplers, auxiliary blocks, power sources, and so on.

Section 3.2 is devoted to detailed investigations of both methods of the laser emission modulation and the approaches for heterodyning of the useful laser emission. Our principal position here is the laser representation as the main source of fluctuations, which have the quantum nature.

We consequently describe the theory of OEO with direct modulation (Sect. 3.2.1) and the external modulation (Sect. 3.2.2) in detail.

Before the construction of main OEO DM and OEO MZ differential equations, which will be chosen for investigation in this book, at first, we must specify the mathematical models of principal OEO component. These problems are considered in Sect. 3.3. After that, we go on to so-called equations of amplitude and phase balance (Sect. 3.4), which are well-known to specialists in nonlinear oscillation theory. In Sect. 3.4.3, we describe the symbolic and then "abbreviated" differential equations of OEOs of different types.

Main results of this chapter are summed in Sect. 3.5.

3.1 Direct and External Laser Modulation in OEO

Before discussing of this chapter materials, we describe at first the main structure of the OEO mathematical analysis as a whole in this book to explain the text sequence and the logic of future materials.

3.1.1 The Structure of OEO Analysis

First of all, we would like to accent the reader's attention on several methods of oscillation generations, which allow obtaining the extremely low level of the phase noise in OEO and gives the right to speak about the ultralow-noise mode of microwave and mm-wave oscillators. These methods include:

- utilization in OEO of so-called quantum-well lasers with the low level of the phase noise;
- application of the low-noise active delay line on 10–50 μs on the base of the optical fiber;
- the self-heterodyning of the phase noise of two optical oscillation in the PD area and their effective statistical suppression;
- utilization in the optical channel of the modulation method with the optical single side frequency;
- transmission of modulated oscillations without optical carrier;
- application of single-frequency generation methods of the microwave and mm-wave autonomous retarded oscillators.

Each from listed approaches cannot be considered as unknown, and their description can be found in manifold books and scientific and engineering papers. Nevertheless, there are not yet the theoretical descriptions of these methods' utilization for generation in the aggregate of RF oscillations in OEO in known publications.

These methods *applied in the aggregate* allow obtaining of the record-breaking low levels of the phase noise spectral density in experimental OEO models: less than −150 dBm/Hz at frequency offsets 1–10 kHz from carrier frequency of 10–30 GHz. This has indisputably the universal importance in radio physics and quantum electronics.

Starting from described methods of OEO generation, the theoretical analysis in this book is performed by means of the mathematical description separately for the laser model with fluctuations and for RF OEO itself taking into consideration of noisy impacts. The laser analysis is executed on the base of the semiclassical model in dipole approximation. We use the velocity (kinetic, balanced, or probabilistic) equations. The semiclassical laser model is added also by the Langevinian noise sources.

For OEO modeling, we use equations of phase and amplitude balance, the symbolic "abbreviated" equations, the statistical fluctuation description of the autonomous RF oscillator, which are well-known in the nonlinear oscillation theory. The special attention in our investigations is attracted to the mathematical model of fluctuation correlator, which is formed by optical channels of the Mach–Zehnder modulator and the photodetector. In OEO with direct amplitude modulation (DM), this correlator is created specially in the optical channel. The main formulas and functions are derived for DC components, first and second harmonics of laser optical oscillations in OEO taking into account the laser phase noise. Then we discuss

problems of achievement of extremely admissible phase noises in different OEO structures at the specified level of the spontaneous laser emission.

The adequate OEO model with fluctuations cannot be created, to our minds, without addressing to the fundamental laser theory with account of the carrier noise. In classical laser model, its emission field is described with the help of classical electrodynamics (Maxwell equations). The semiclassical theory is able to take into consideration phase relationships, phase fluctuations of the laser emission, and then to transform them into the OEO phase noise. This theory describes the laser with the help of classical electrodynamics, and the atom system is described by the quantum-mechanical approach, the kinetic equations are analyzed, the phase and (if necessary) frequency relationships are calculated. For spontaneous emission description, we use the quantum theory, in which the field and the atom system are determined from the quantum mechanics.

Authors use the different approaches of OEO mathematical modeling: on the base of amplitude and phase balance equations, on the base of abbreviated equations, on the base of kinetic laser equations, and on the base of semiclassical laser differential equations taking into account the equation for optical carrier phase. At solution of different tasks (for instance, finding of the steady-state amplitude and OEO frequency), the OEO laser is represented as the passive one-port network of the two-port network, which is characterized by amplitude-frequency characteristic (AFC) and phase-frequency characteristics (PFC) and its watt–ampere characteristic (WAC). For other tasks, for example, obtaining of the OEO phase noise spectral density or the analysis of transient dynamics, time-functions of emission intensity, the optical emission frequency and phase, the laser should be represented by more complicate models on the base of semiclassical description in the dipole approximation of the double-level model.

To obtain the dependence of PSD of the phase noise of OEO RF oscillations from the laser phase noise level, we consider fluctuation differential equations for the strength squared, the population and the phase of optical oscillations, and equations for the positive feedback network.

We hope that the autonomous delayed oscillator theory is well known to the reader, because it is discussed in many books and papers. The features of OEO modulation methods and methods of the noise suppression are studied in lesser degree. Therefore, in our OEO analysis we begin from description of structures with direct and external modulation of laser emission taking into consideration the phase fluctuations of the laser emission.

3.1.2 Variants with Direct and External Modulations

Following the approach described in [1–3] for the OEO noise analysis, we consider the system (Fig. 3.1), in which two different oscillating processes are developed: in the laser with oscillation frequency about 200 THz and in a closed into a loop RF

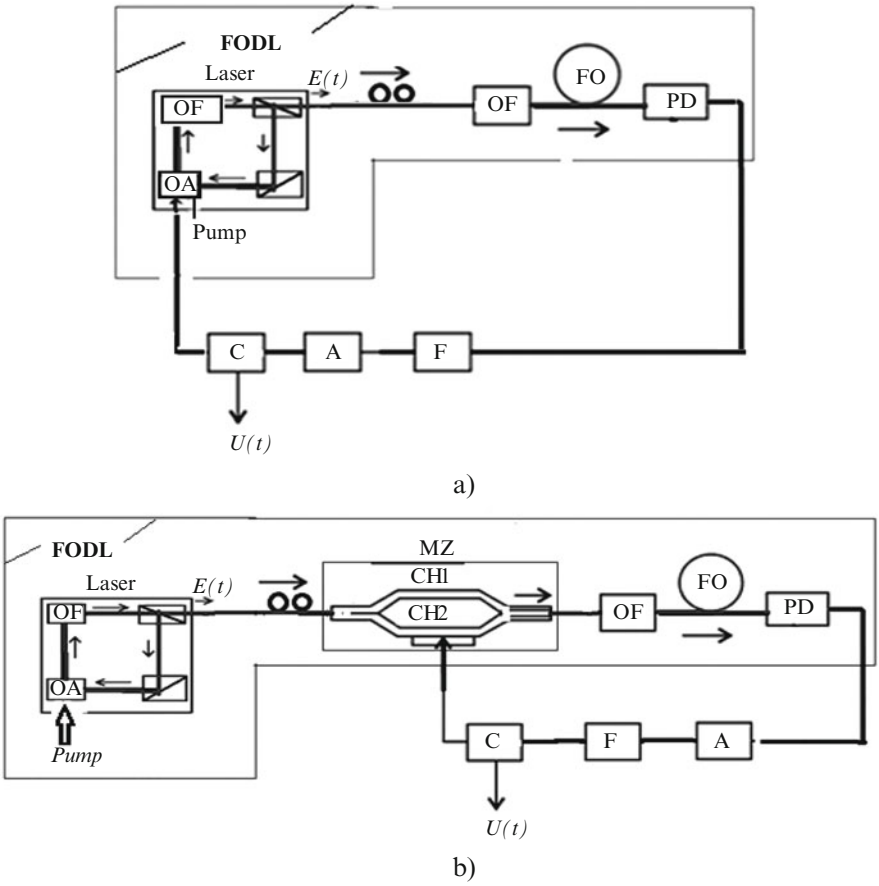

Fig. 3.1 Structural diagrams of the optoelectronic oscillator (**a**) with the direct modulation by current and (**b**) with external Mach–Zehnder modulator

network, in which oscillations with frequency about 10 GHz are generated. The multiplicity of these frequencies is about 20,000.

The laser (quantum-well laser diode) is the pumping source for closed into a loop RF network formed by a modulator, the optical fiber, the photodetector, the RF amplifier, the RF filter, and the directional coupler. In result of oscillating processes, the spectra with fluctuations are formed, which have the different nature, and the spectral line width of RF oscillations is defined by parameters of both self-oscillating interacting systems: the laser and the RF oscillator. The interesting OEO feature is the fact that the generating spectrum of RF oscillations is formed not only by noises, which have the electronic nature, but also by phase fluctuations of the laser optical emission. Laser fluctuations have the quantum nature and are defined by the laser spontaneous emission. OEO can be represented as the system providing the division of optical frequency of 200 THz to the RF values of 10 GHz.

3.1.2.1 OEO Construction and Its Operation Principle

The feature of OEO diagrams with the direct modulation (Fig. 3.1a) is the possibility of operation in the mode of amplitude (or intensity) modulation of the QWLD emission. Structural diagrams of OEO with external modulation (Fig. 3.1b) operate in the mode of phase modulation of QWLD emission. At that, the phase modulation of QWLD emission is performed in one of optical channels of the MZ modulator.

In the OEO DM structure (Fig. 3.1a), the following elements are included sequentially closed in the loop: the laser, which is the modulated light source on the base, for example, QWLD; the single-mode low-dispersion optical fiber (OF); the photodetector (PD); the nonlinear wideband amplifier (A) of microwave or mm-wave ranges; and the RF high-Q filter (F) of microwave or mm-wave ranges, for instance, on the base of the dielectric microwave resonator.

The main difference of the diagram with the external laser modulator (Fig. 3.1b) compared to OEO DM is a presence of the external electro-optical MZ modulator. OEO *with external modulation* [2] or OEO MZ is formed by the laser and the following elements are sequentially closed into a loop: the Mach–Zehnder (MZ) modulator; the fiber optical system (FOS) containing the optical filter (OF) and the single-mode optical fiber (FO); the photodetector (PD), for example the quantum-dimension photodiode; and the narrowband RF filter (F), the nonlinear amplifier (A) and directional coupler (C). When sequentially connected with the laser, MZ, OF, FO, and PD form the block of fiber optical delay line (RF FODL), whose electric input is the MZ input (input voltage of MZ), and its electric output coincides with the electric output of PD (we mean the output voltage on the PD load resistance).

The optoelectronic oscillator *made according to the diagram with external modulation* can be considered as the oscillator with the retarded feedback, in which RF FODL for RF oscillation is active. RF FODL has its own amplitude and phase noises, which are the laser noises reduced on the RF FODL output (or passed from the laser output through MZ, OF, FO).

The quantum-well laser diode or the fiber laser with activating dopes of erbium, ytterbium, etc. can be served as the OEO laser. Figure 3.2a shows the laser represented by the closed into a loop optical amplifier (OA) and the optical filter (OF). This structure corresponds to the laser with the "traveling-wave" resonator. The optical pumping power P_p passes to the active amplifier. If the excitation conditions are satisfied, laser produces optical oscillations, which pass to MZ from the laser output, then pass through two optical channels with different delays, then integrate together and through OF and FO act in the light-sensitive area of PD. The effective MZ modulation in the microwave range is possible only for single-mode single-frequency and linearly polarized emission of the highly coherent laser. Quantum-well laser diodes and fiber lasers with polarizers on their outputs are such emission sources and therefore, we fulfill the theoretical analysis for this case only.

Figure 3.2 presents the structural diagrams of OEO DM (Fig. 3.2b) and OEO MZ (Fig. 3.2c). In the structure of OEO DM, we see the following blocks, which are

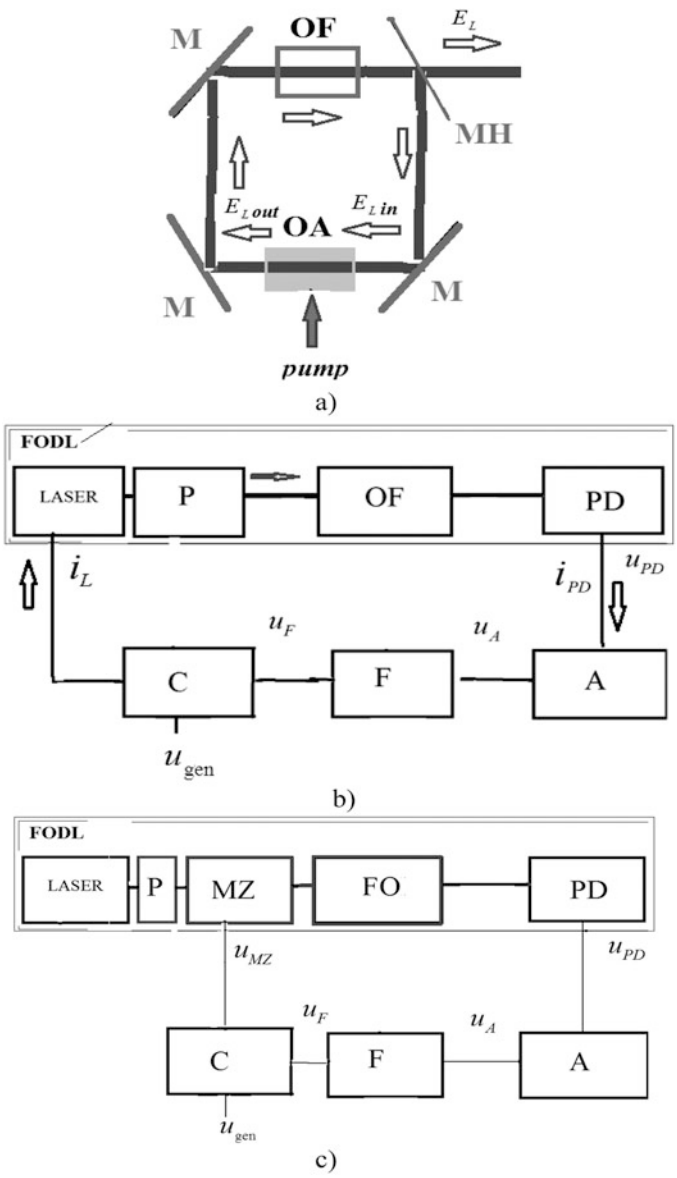

Fig. 3.2 The diagram of the laser (**a**) OA is the optical amplifier, OF is the optical filter. This diagram corresponds to the laser with the traveling-wave resonator. The optical pumping power passes to the active amplifier, (**b**) the block diagram for representation of OEO DM and OEO MZ for amplitude and phase balance equations formation, (**c**) OEO MZ. Designations: OA is the optical amplifier, OF is the optical filter, M is the mirror, MH is the output mirror, Pump is the laser energy pumping, P is the optical gate, Laser is QWLD, P is the polarizer, FO is the optical fiber, PD is the photodetector, A is the RF amplifier, F is the RF filter, C is the RF coupler, and MZ is the Mach–Zehnder modulator

series-connected in the loop: a laser, a polarizer, the optical fiber, a photodetector, the RF amplifier, the RF filter, and the RF directional coupler. In the structure of OEO MZ are included: a laser, a polarizer, the Mach–Zehnder modulator, the optical fiber, a photodetector, the RF amplifier, the RF filter and the RF coupler. (All designations are explained in the figure caption.)

Considering that the laser is high-coherent, i.e., the spectral line width is significantly less than 100 MHz at average generation frequency of 200 THz, we assume that oscillations of the electromagnetic field (EMF) intensity are close to harmonic with the noisy phase component $\varphi_{\mathrm{Lm}}(t)$[1] at the laser output and amplitude noises $m_{\mathrm{Lm}}(t)$:

$$E_{\mathrm{L}}(t) = [E_{0\mathrm{L}} + m_{\mathrm{Lm}}(t)] \cos [2\pi\nu_{0\mathrm{L}} t + \varphi_{0\mathrm{L}} + \varphi_{\mathrm{Lm}}(t)], \tag{3.1}$$

where $E_{0\mathrm{L}}$ is the amplitude of EMF intensity, ν_0 is the average oscillation frequency, $\varphi_{0\mathrm{L}}$ is the initial constant phase shift, and t is the current time.

In OEO system, at fulfillment of excitation conditions, in the RF part of such an oscillator, RF oscillations $u = u_{\mathrm{g}}(t) = u_{\mathrm{c}}(t)$ occur. At that, the RF signal from the nonlinear amplifier output passes to the electrical input of MZ through the coupler C during the oscillation generation, and the instantaneous voltage of this signal is

$$u_{\mathrm{g}}(t) = [U_{10} + m_{\mathrm{em}}(t)] \cos [2\pi ft + \phi_{0\mathrm{e}} + \varphi_{\mathrm{em}}(t)], \tag{3.2}$$

where $U_{01} = U_{01\mathrm{MZ}} = U_{01\mathrm{C}}$ is the oscillation amplitude of the fundamental harmonic in the electrical input of the MZ modulator and at the coupler output, f is the RF oscillation frequency, $\phi_{0\mathrm{e}}$ is the constant phase shift, $\varphi_{\mathrm{em}}(t)$ are the phase fluctuations, and $m_{\mathrm{em}}(t)$ are the amplitude fluctuations. These expressions for a signal will be used later.

3.1.3 *Heterodyne Transformation and Self-Heterodyning in OEO*

Let us consider the features of the heterodyne reception of the laser emission with phase fluctuations in OEO.

As an illustration to the discussing issue, Fig. 3.3 shows the diagrams of the heterodyne reception (Fig. 3.3a) and the self-heterodyning mode in OEO (Fig. 3.3b). The picture on the spectrum "transfer" from the optical range into the RF range is presented in Fig. 3.3c.

Figure 3.3a shows the laser local oscillator, which plays the role of the heterodyne block. The signals mixing of the laser and the laser local oscillator is performed in the photodetector, which is the nonlinear element for heterodyning.

[1] Here and later, indices L show the relation to the laser in OEO.

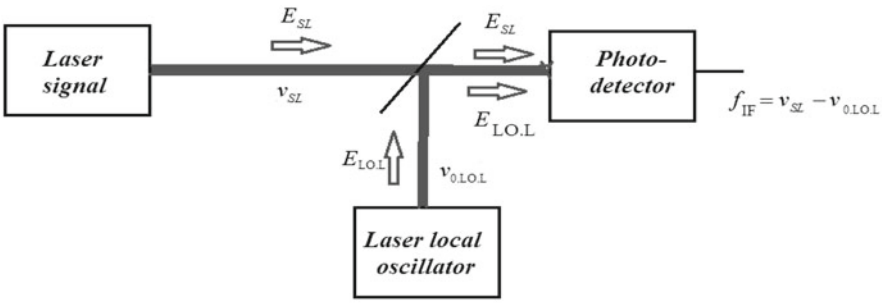

a)

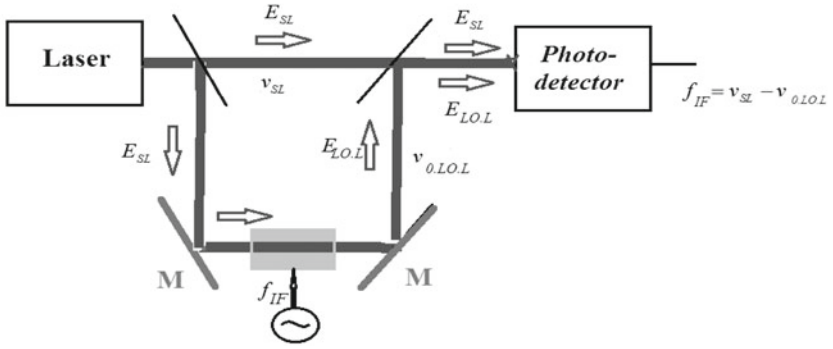

b)

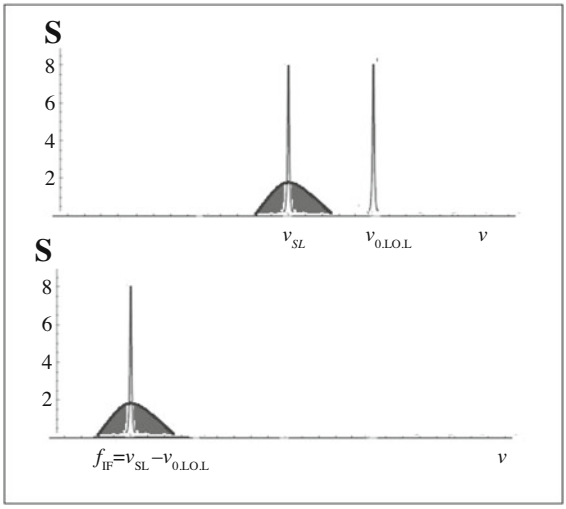

c)

Fig. 3.3 Diagrams of the heterodyne processing (**a**) and the self-heterodyning in OEO (**b**). Representation of the spectrum transfer from the optical range into the RF range (**c**)

At heterodyne transformation, the optical oscillation spectrum with noises S_L (S_L designates the power spectral density, which is determined by amplitude and phase noises) is shifted to the spectrum region of the electric signal S_{RFL} on the intermediate frequency (IF). If to add the slow fluctuation supplements $\varphi_{Lm}(t)$ to oscillation phases of the signal and the local oscillator, then in the phase of the electric signal on intermediate frequency, the phase fluctuations $\varphi_{Lm}(t)$ arise on the IF frequency f_{IF}. The signal oscillation with noises is described in the frequency domain by the spectrum, which density is concentrated in the vicinity of the ν_{SL} frequency.[2] The local oscillator signal with noises is described by the spectrum, which density is concentrated in the vicinity of the local oscillator frequency $\nu_{0LO.L}$.

The value of the squared normalized EMF intensity $E^2_{PD}(t)$ on the PD area, at combined action of signal oscillation with intensity E_{SL} and the local oscillator signal with intensity $E_{LO.L}$, is defined as:

$$E^2_{PD}(t) = K_C \cdot \langle [E_{SL}(t) + E_{LO.L}(t)] \cdot [E^*_{SL}(t+\tau) + E^*_{LO.L}(t+\tau)] \rangle. \tag{3.3}$$

Here the symbol "$*$" designates of the conjugate operation, and the symbol $\langle\rangle$ designates the mathematical expectation (or the mean value) operation.

We note several features of heterodyning of the laser emission in OEO. In this case, the laser plays both the roles: as the source of the *signal oscillations* and as the *local oscillator*, therefore, we may speak about "self-heterodyning" of the laser emission.[3] The intermediate frequency $f_{IF} = \nu_{SL} - \nu_{0LO.L}$ is in OEO the average oscillation frequency and, as a rule, it may be, say, 10 GHz. We should add that in the low-noise OEO, lasers are used, which operate in the single-frequency mode and have the narrow spectral line of emission with the width $\Delta\nu_L$ = 10–1000 kHz, therefore, for the optical "frequencies of analysis" ν the following relation is true: $f_{IF} \gg \nu - \nu_{0LO.L}$, where $\nu = \nu_L$ is the optical analysis frequency.

One of features of heterodyning in OEO is the fact that the laser coherence time and the spectral line width of laser emission are defined the spectrum of RF oscillations. This can be proved if to consider the photodetection process in OEO MZ, to calculate the autocorrelation function $R(t, t+\tau)$ of the laser random field $E_L(t)$ and the spectrum of RF oscillation in OEO.

Let two emissions (Fig. 3.3b), which propagate in different optical channels of the MZ modulator, have different delays. These emissions pass on the PD area. The laser intensity $E_L = E_L(t)$ and the intensity delayed on some time $\Delta t = \tau$ or $E_{L\tau} = E_L(t - \Delta t)$ are the random correlative *dependent* magnitudes. As the result of photodetection of two optical oscillations $E_L = E_L(t)$ with different frequencies, for example, ν_{0L} and $\nu_{0L} + f$, the photocurrent oscillation arises in the PD load with the average frequency f. The spectrum of the electrical oscillation in the PD load represents the convolution of two spectra S_{L1} and S_{L2}. Let us determine the autocorrelation function at

[2]Here and later, indices S show the relation to "signals" in OEO.

[3]In radio electronics, the device in such self-heterodyning mode has a special name: the self-oscillation mixer (SOM) or in Russian publication "autodynes."

photodetection and obtain formulas for oscillation spectrum in the photodetector output taking into account phase fluctuations.

3.1.3.1 The Autocorrelation Function of the Random EMF of Laser Emission

The autocorrelation function $R(t, t + \tau)$ of the random EMF of the laser emission $E_L(t)$ depends on the laser coherence time T_{coh} and is defined as $R_L(t, t + \tau) = R_L(\tau)$:

$$R_L(\tau) = \left\langle E_L(t) \cdot E_L^*(t-\tau) \right\rangle = \int_{-\infty}^{\infty} E_L(t) \cdot E_L^*(t-\tau) \mathrm{d}t. \tag{3.4}$$

Substituting in the expression for $R_L(t, t + \tau)$ oscillations of the normalized intensity $E_L(t) = E_{L0} \exp[j2\pi \cdot \nu t + \psi_m(t)]$ and oscillations of conjugated quantity and delayed quantity by τ. $E_L^*(t-\tau) = E_{L0} \exp[-j2\pi \cdot \nu t - j2\pi \cdot \nu\tau - \psi_m(t-\tau)]$, we can write the expression for $R(t, t + \tau)$ in the form:

$$\begin{aligned} R(t,t+\tau) &= \int_{-\infty}^{\infty} E_{L0} \exp[\, j2\pi \cdot \nu t + \psi_m(t)] \cdot E_{L0} \exp[-j2\pi \cdot \nu t + j2\pi \cdot \nu\tau - \psi_m(t-\tau)] \mathrm{d}t \\ &= E_{L0}^2 \int_{-\infty}^{\infty} \exp[\, j2\pi \cdot \nu\tau + \psi_m(t) - \psi_m(t-\tau)] \mathrm{d}t. \end{aligned} \tag{3.5}$$

We should note that in the last formula, the phase fluctuation difference $\psi_m(t) - \psi_m(t - \tau)$ is defined by the laser coherence time T_{coh} After integration, we have the expression for $R(t, t + \tau)$ as $R(t, t+\tau) = E_{L0}^2 \exp\left(-\frac{\tau}{T_{coh}}\right) \cdot \exp(\, j2\pi \cdot \nu\tau)$.

To calculate the required power spectral density of the laser S_L, we must use the Wiener–Khinchin formula

$$\begin{aligned} S_L &= 4 \int_0^{\infty} R_L(\tau) \cos(2\pi f\tau) \mathrm{d}\tau \\ &= 4 \int_0^{\infty} E_L^2 \exp\left(-\frac{\tau}{T_{coh}} + j2\pi\nu\tau\right) \cos(2\pi f\tau) \mathrm{d}\tau \end{aligned} \tag{3.6}$$

After integration, we have: $S_{\mathrm{L}} = T_{\mathrm{coh}}/\{1 + [T_{\mathrm{coh}}(\nu - \nu_{\mathrm{L0}})]^2\}$, where ν_{L0} is the average frequency of the laser generation. The spectrum of laser emission S_{L} is Lorentzian, and its spectral line width $\Delta\nu_{\mathrm{L}} = 1/T_{\mathrm{coh}}$ and for S_{L} we may write:

$$S_{\mathrm{L}} = \frac{1/(\Delta\nu_L)}{1 + [(\nu - \nu_{\mathrm{L0}})/\Delta\nu_{\mathrm{L}}]^2} = \frac{\Delta\nu_{\mathrm{L}}}{\Delta\nu_{\mathrm{L}}^2 + [(\nu - \nu_{\mathrm{L0}})]^2}. \tag{3.7}$$

Mathematical formulas and the correlation issues of two oscillations with fluctuations in OEO are presented in detail in Chaps. 5–7 of this book. Here we make use of obtained formulas derived in mentioned chapters in order to show the sense of the suppression process of the laser phase noise in the oscillation system of OEO.

Figure 3.4a shows OEO MZ with the delay in the optical section. The equivalent block diagram with the delay in OEO is presented in Fig. 3.4b, in which the equivalent delay line is located in the electrical part of OEO after PD. The switch Sw is shown in both figures. When the switch Sw is closed, the oscillation generation occurs in the closed loop, if the excitation conditions are satisfied. In opened position of the Sw switch, the generator of RF oscillations is connected to the electrical input of the MZ modulator.

Let us list the main positions at the theoretical analysis of fluctuations in OEO in heterodyning including examination of the influence of intensive optical oscillations with fluctuations on the photodetector, which is the nonlinear element. The process of photodetection is represented as the process of multiplication (Fig. 3.5) of *optical oscillations* $E_{\mathrm{L}} = E_{\mathrm{L}}(t)$ and $E_{\mathrm{L}\tau} = E_{\mathrm{L}}(t - \Delta t)$. The system, in which the delay line and a multiplier (Fig. 3.5) are present, is adopted to refer as the correlator of two random quantities. Electrical current oscillation in the PD load represents the convolution of two spectra of *two optical oscillations* S_{L} and S_{RFL}.

The correlator is presented in Fig. 3.5 by the delay line and the multiplier. The Gaussian random process $\xi(t)$ with σ_ξ^2 dispersion affects the correlator input. At multiplier output, the low-pass filter (LPF) is included and at its output, the random process $\eta(t)$ acts.

3.1.3.2 Autocorrelation Function of OEO MZ at the Open Feedback Loop

Let us consider the block diagram presented in Fig. 3.4a. Let the Sw switch be open, and the electrical oscillation with the average frequency f_0, which spectrum presents the delta-function $\delta(f)$, passes from the generator to the electrical input of the MZ modulator. At that, as in the previous case, *two optical oscillations* $E_{\mathrm{L}} = E_{\mathrm{L}}(t)$ and $E_{\mathrm{L}\tau} = E_{\mathrm{L}}(t - \Delta T_{\mathrm{MZ}})$, which are delayed with regard to each other by the time ΔT_{MZ}, are added on the PD area.

In this case, the autocorrelation function $R_{\mathrm{MZ}}(\tau)$ at the analysis time $\tau > \Delta T_{\mathrm{MZ}}$ is $R_{\mathrm{MZ}}(\tau) \approx \exp\left(-\frac{\Delta T_{\mathrm{MZ}}}{T_{\mathrm{coh}}}\right)\cos(2\pi \cdot f_0)$. Accordingly, the current spectrum at the PD output for $\tau > \Delta T_{\mathrm{MZ}}$ is defined as:

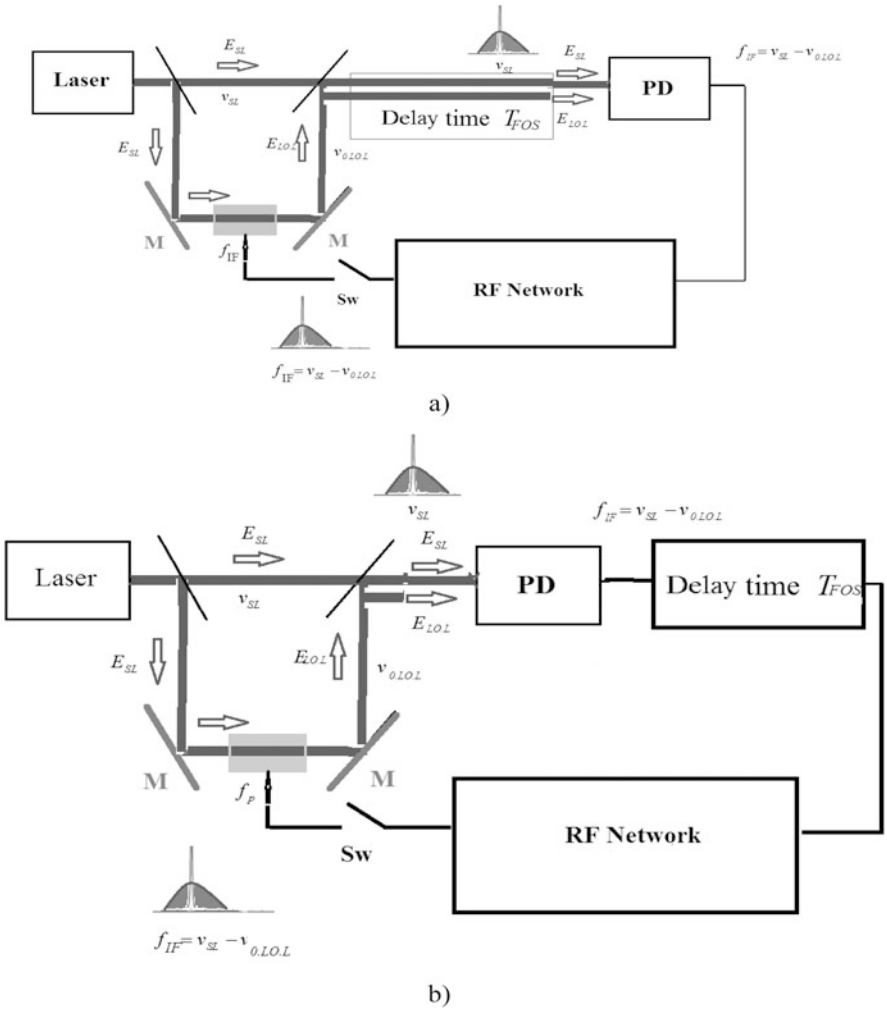

Fig. 3.4 (**a**) The block diagram represented the heterodyning with delay in OEO, in which the laser is the noise source. (**b**) The block diagram representing OEO, in which the equivalent delay line is located in the electrical part of OEO after PD. New designations: Laser is the optical amplifier, delay time T_{FOS} is the block of the delay time by T_{FOS}, RF Network is the RF circuit consisting of the RF amplifier, the RF filter and the RF coupler, and Sw is a switch

$$S_{\mathrm{RFMZ}} = \exp\left(-\frac{\Delta T_{\mathrm{MZ}}}{T_{\mathrm{coh}}}\right) \cdot S_{0\mathrm{RFL}} * \frac{\Delta\nu_{\mathrm{L}}}{\Delta\nu_{\mathrm{L}}{}^2 + [(f - f_0)]^2}, \tag{3.8}$$

where "$*$" is operation of the convolution, $S_{0\mathrm{RFL}}$ the RF spectrum input MZ, $F = f - f_0$ is the frequency offset from the average radio frequency f_0 of voltage oscillations, which passes to the MZ electric input. *Thus, at the open feedback loop,* the spectrum

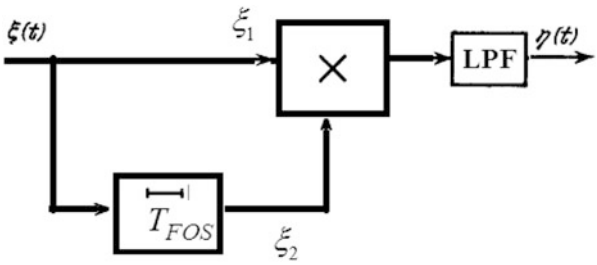

Fig. 3.5 The structure of the correlator on the base of PD at modeling of the statistical process in OEO

S_{RFMZ} has the Lorentzian view and is defined by the laser phase noise, and the maximal value of S_{RFMZ} is defined by the ratio $\Delta T_{\mathrm{MZ}}/T_{\mathrm{coh}}$. As a rule, $\Delta T_{\mathrm{MZ}}/T_{\mathrm{coh}}$ is small, i.e., less than 0.001 and $\exp\left(-\frac{\Delta T_{\mathrm{MZ}}}{T_{\mathrm{coh}}}\right) \approx 1$.

3.1.3.3 Oscillation Spectrum at the Closed Feedback Loop

At closed Sw switch in Fig. 3.4a, at fulfillment of OEO excitation conditions, the amplified electrical oscillation passes to the electrical input of the MZ modulator from the PD output. We note that this oscillation is delayed by the time of fiber optical system T_{FOS} relative to the laser oscillation arriving to PD.

At that, on the PD area, there is the process of statistical averaging in time of the interference result of two optical harmonics $\nu_{0\mathrm{L}}$ and $\nu_{0\mathrm{L}} + f$, which are applied to the PD area:

$$E_{10\mathrm{L}}(t) = A_1 E_{0\mathrm{L}} \cos\left[2\pi\nu_{0\mathrm{L}} t + \varphi_{0\mathrm{L}} + \varphi_{10\mathrm{Lm}}(t)\right] \tag{3.9}$$

and

$$E_{20\mathrm{L}}(t) = A_2 E_{0\mathrm{L}} \cos\left[2\pi(\nu_{0\mathrm{L}} + f_0)t + \varphi_{0\mathrm{L}} + \varphi_{20\mathrm{Lm}}(t)\right], \tag{3.10}$$

with the amplitudes $A_1 E_{0\mathrm{L}}$ and $A_2 E_{0\mathrm{L}}$.

As shown in Chaps. 5 and 6 of this book, in this case, the RF spectrum at the PD output $S_{\mathrm{RFL}}(F)$ is defined by the formula:

$$S_{\mathrm{RFL}}(F) = K^2_{2\Gamma\mathrm{PN}}(F) \cdot \frac{1/(\Delta\nu_{\mathrm{L}})}{1 + [(F - \nu_{\mathrm{L0}})/\Delta\nu_{\mathrm{L}}]^2} \cdot \left\{1 - \frac{A_2}{A_1} \exp\left(-\frac{T_{\mathrm{FOS}}}{T_{\mathrm{coh}}}\right)\right\}, \tag{3.11}$$

in which $K^2_{2\Gamma\mathrm{PN}}(F)$ is the coefficient of phase noise suppression, which depends on T_{FOS}, on the laser optical power $P_{0\mathrm{L}}$, σ_{U} is the nonlinearity coefficient, and T_{F} is the time constant of the RF filter. The analytical formula for the RF FODL transfer function $K^2_{2\Gamma\mathrm{PN}}(F)$ is defined and investigated in Chap. 6 of this book.

Thus, at the *closed feedback loop* in OEO MZ (Fig. 3.4a), the spectrum in PD output has the Lopentzian shape, is defined by the laser phase noises, and its

maximal value depends on the ratio T_{FOS}/T_c. At long length of the optical fiber (1 km and longer), the ratio T_{FOS}/T_c is not small and is about $T_{FOS}/T_c \approx 1$ and more. The noise suppression effectiveness in OEO is not only defined by the fiber length, but it also depends on the ratio of the laser coherence time to the delay time in the optical fiber. When the Sw switch closes, in the case of steady-state mode in OEO, the effective statistical suppression occurs in the case, if the laser coherence time T_c is comparable to the delay time in the optical fiber T_{FOS}, i.e., $T_c \approx N \cdot T_{FOS}$, where for instance, $N = 1$–5. In this case, statistically related phase fluctuations of laser oscillations will be suppressed. At small T_{FOS} delays, when $T_c \gg T_{FOS}$, the noise suppression does not happen; i.e., the correlator, as a device, does not fulfill its functions of the phase noise suppression. When $T_c \ll T_{FOS}$, the noise suppression is not effective as well. In this case, the correlation coefficient is close to zero and the correlator effectiveness is low.

In experimental investigations of OEO, the minimal level of the noise spectral density can be achieved at utilization of high-coherent lasers (with the spectral line width of 10–100 kHz) and at geometrical lengths of optical fibers of 1–2 km, which provides the delay in the optical fiber of 10^{-5} s and more.

3.1.3.4 Comparison of OEO and the Multi-Tapped Delay Line

The OEO structure can be compared in the noise suppression mechanism with the structure of the multi-tapped delay line, which has N taps through time intervals (Fig. 3.6). Such multi-tapped networks for delays are used for radio-frequency signal processing in radar technologies. Let these time intervals be equal to the time delay T_{FOS}. If at the electrical input of such the delay line, the stationary random process $\xi(t)$ with zero mean value affects (passes), which is defined by the correlation function $R_\xi(\tau)$ with the spectral density $S_\xi(f)$, then the spectral density $S_\eta(f)$ of the $\eta(t)$ process in the adder output is defined as:

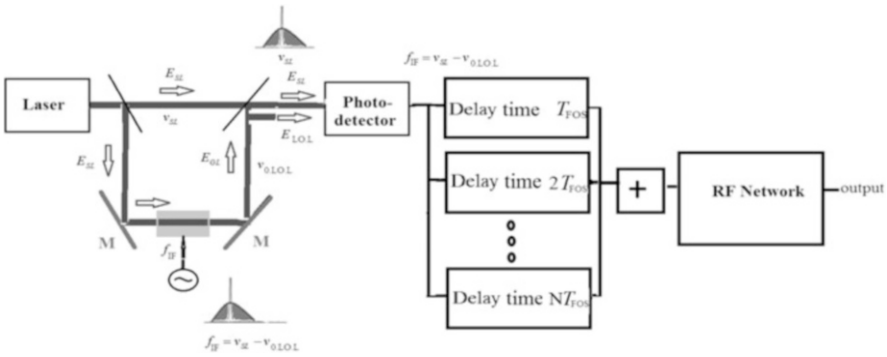

Fig. 3.6 The block diagram of RF signal processing on the base of the laser, the MZ modulator, the photodetector, the combined delay line from N delay elements and the adder (+)

$$S_\eta(f) = S_\xi(f) \cdot \frac{1}{N^2} \cdot \frac{\sin^2(T_{FOS} \cdot N \cdot f/2)}{(T_{FOS} \cdot N \cdot f/2)^2}. \tag{3.12}$$

This formula shows that the larger a number of delay lines N, the more effectively the input noise impact will be suppressed.

Our analysis is directed to the determination of the laser phase fluctuation connection with the OEO phase fluctuations. The laser phase fluctuations are defined by the quantum nature of spontaneous emission. Let us devote the next section to this physical phenomenon.

3.1.4 Quantum Nature of Laser Noises in OEO

Usually, the quantum-well semiconductor lasers are used in OEO as the optical source. In the quantum-well lasers, the special conditions have been created for the charge carriers, and at these conditions, the moving charge demonstrates the quantum properties. At that, the carrier moving in the electrostatic field can be characterized by the de Broglie wavelength, which has the order in tens nanometers. In the volumetric semiconductor crystal, the quantum wells or spatial resonators are created by means of evaporation of special layers with thickness from one nanometer to several tens nanometers. An electron, which falls in these "nano-resonators," acquires properties of the particle with the sharply defined energy states. In other words, the energy spectrum of carriers is quantizing.

The calculation of the laser spontaneous emission, which plays the important role in formation of OEO phase noises, is performed with the help of quantum-mechanic Schrodinger equations (SE). The energy of the charge carriers and eigenfunctions are obtained by the electric field operator supplement in SE. The particle lifetime at specified energy level and the energy level width are determined. The calculation of the lifetime in the quantum well is similar the same calculation for the particle in the single atom, which is located in the electrical field. In the stationary SE with the potential energy $V(z)$, which defines the quantum-well shape, the term $-qFz$ is added, which takes into consideration the electric field influence:

$$-\frac{(2\pi)^2 h^2}{2m}\frac{\mathrm{d}^2\psi}{\mathrm{d}^2 z} + (V(z) - qFz)\psi = E\psi, \tag{3.13}$$

where ψ is the eigenfunction, z is the spatial coordinate, q is the carrier charge, F is the electrostatic Coulomb force, m is the charge carrier mass, ħ is the Planck constant. Eigenfunctions for the single-dimension task are defined by Airy functions. Specifying the shape of the potential well $V(z)$ and the Coulomb force of the electrical field F, which affects the charged particle, we determine from SE the positions of the energy levels, coefficient of well passage by the particle, the energy level widths, the particle lifetime at each level, and the probability of the photon

emanation. At that, the complete probability of the phonon emanation (or the spontaneous emission) in time unit is defined as

$$P_{\text{sp}} = C_{\text{k}} \frac{2}{3} \alpha \left(\frac{r_{\text{fi}}}{c} \right)^2 (2\pi\nu)^3, \tag{3.14}$$

where ν is optical emission frequency, α is the constant of the thin structure 1/132, and r_{fi} is the matrix element, which of the order equal to $e^2/h\nu$, for atoms, e is the electron charge, C_{k} is some constant. The lifetime of an atom in excited state depends on the electron mass and charge and inversely proportional of the emitted frequency ν. A behavior of the carrier (particle) of the electron in the quantum-well zone is similar to the atom behavior in excited state. For example, for the simplest case—for the hydrogen atom, for the transfer between states $2p$ to $1S$, the lifetime T_1 is expressed as

$$T_1 = 1/P_{\text{sp}} = \frac{3^{11}}{2^{17}} \frac{c^3 m^2 e^2}{h^3 (2\pi\nu)^3}, \tag{3.15}$$

where m is the electron mass, c is the light speed in vacuum. For the frequency $\nu = 2 \times 10^{14}$ 1/s, the lifetime is approximately $T_1 \approx 1.3 \times 10^{-9}$ s.

The dispersion of the laser phase noise σ_{E}^2 is defined by the dispersion of the carrier noise ξ_{N} and depends on lifetime on the excited level

$$\sigma_{\text{N}}^2 = \langle \xi_{\text{N}}(t) \xi_{\text{N}}(t-\tau) \rangle - \left\langle [\xi_{\text{N}}(t)]^2 \right\rangle \approx C_{\text{N}} N_2 / T_1, \tag{3.16}$$

where C_{N} is a constant, N_2 is a quantity of carriers on the upper energy level (in two-level laser model). The important fact is that the phase noise level in OEO is defined by the phase noise of the laser, which depends on the lifetime T_1.

Figure 3.7 illustrates the active zone and the diagram of energy levels (Fermi quasi-levels) of QWLD on the base of InGaAsP. The bandgap of QWLD is approximately 1303 MeV. The arrow upward shows the pumping level. The lifetime of carriers in the excited state is about $T_1 \approx 10^{-9}$ s.

In this chapter (Sect. 3.4.3), we form differential equations of OEO MZ on the base of laser presentation as the "black box" using the output normalized strength, its amplitude, frequency, and its width of the spectral line of emission.

Now we show another useful OEO structures, in which, as before, the laser is chosen as the main element.

3.1.5 *Variants of OEO Operating Structures*

External views and structural variants of different operating structures of the low-noise laser OEO of the microwave range with the average generated frequency

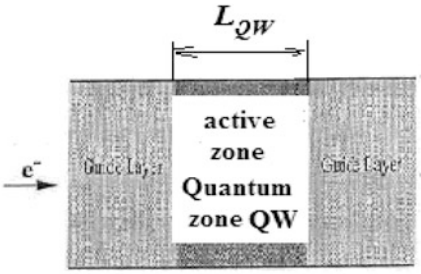

a)

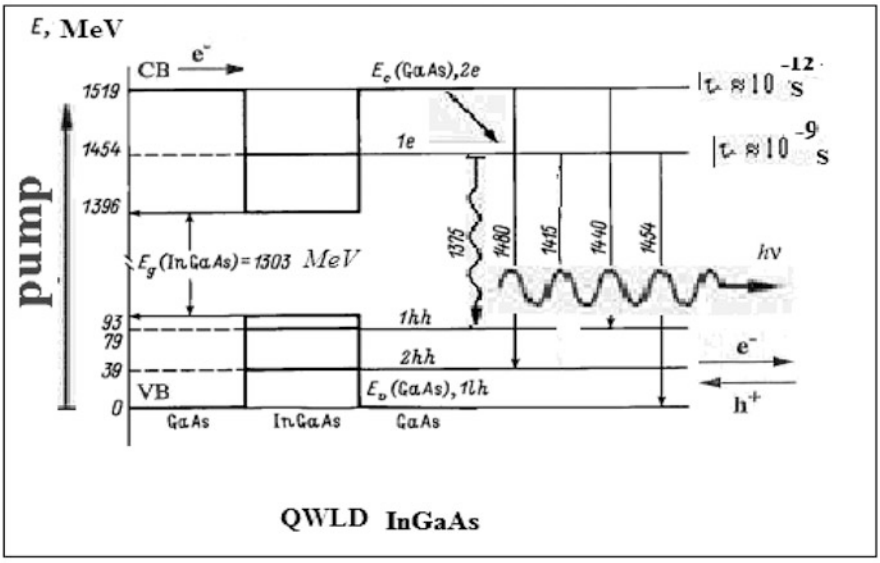

b)

Fig. 3.7 The view of the active QW zone (**a**) of the quantum-well laser on the base of InGaAsP and the diagram of energy levels of QWLD (**b**). On the active QW zone (**a**), at reduction of its width down to the value L_{QW} = 1–45 nm, the quantization of the electron and hole energy states occurs

8–10 GHz, which are useful for a practice, are presented in Figs. 3.8 and 3.9. Figure 3.8 shows the photo-pictures of experimental OEO models with direct modulation (Fig. 3.8a) and external MZ modulation (Fig. 3.8b).

Three different OEO structures, studying of which broadens the knowledge of OEO possibilities as the device intended for generation of microwave and mm-wave oscillations with ultralow phase noises, are shown in Fig. 3.9.

In the structure in Fig. 3.9a, the second photodetector PD2 is anticipated, and the laser emission passes to PD2 and detected. This constructive solution allows the galvanic decoupling of the electrical port, which decreases requirements on the networks' matching.

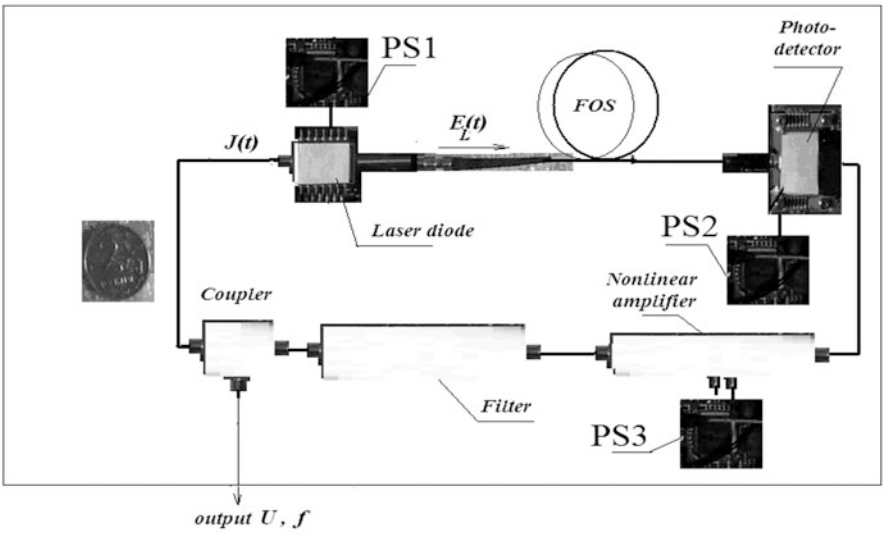

a)

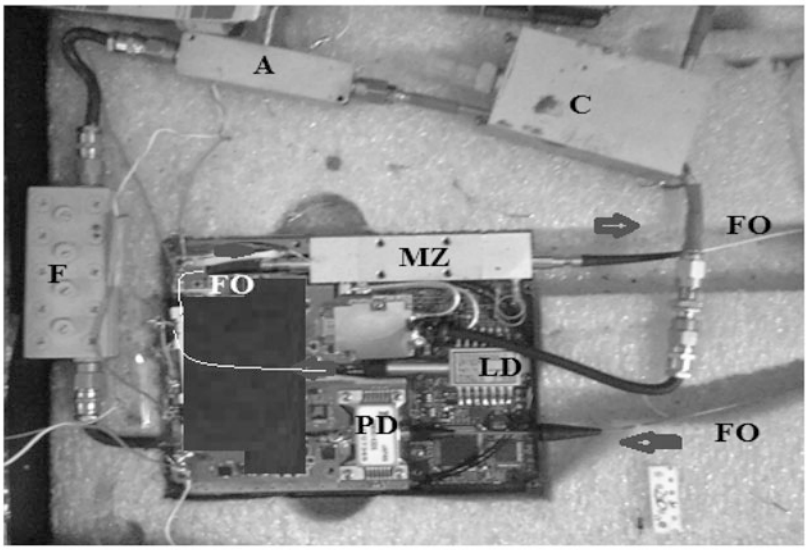

b)

Fig. 3.8 General view of experimental models of the low-noise laser optoelectronic oscillator of the microwave range (on the left, the usual Russian coin). The average generation RF frequency is 8–10 GHz: OEO with the direct modulation (**a**), the photo-picture of OEO with external MZ modulation (**b**). PS1 is the power supply 1, PS2 is the power supply 2, PS3 is the power supply 3

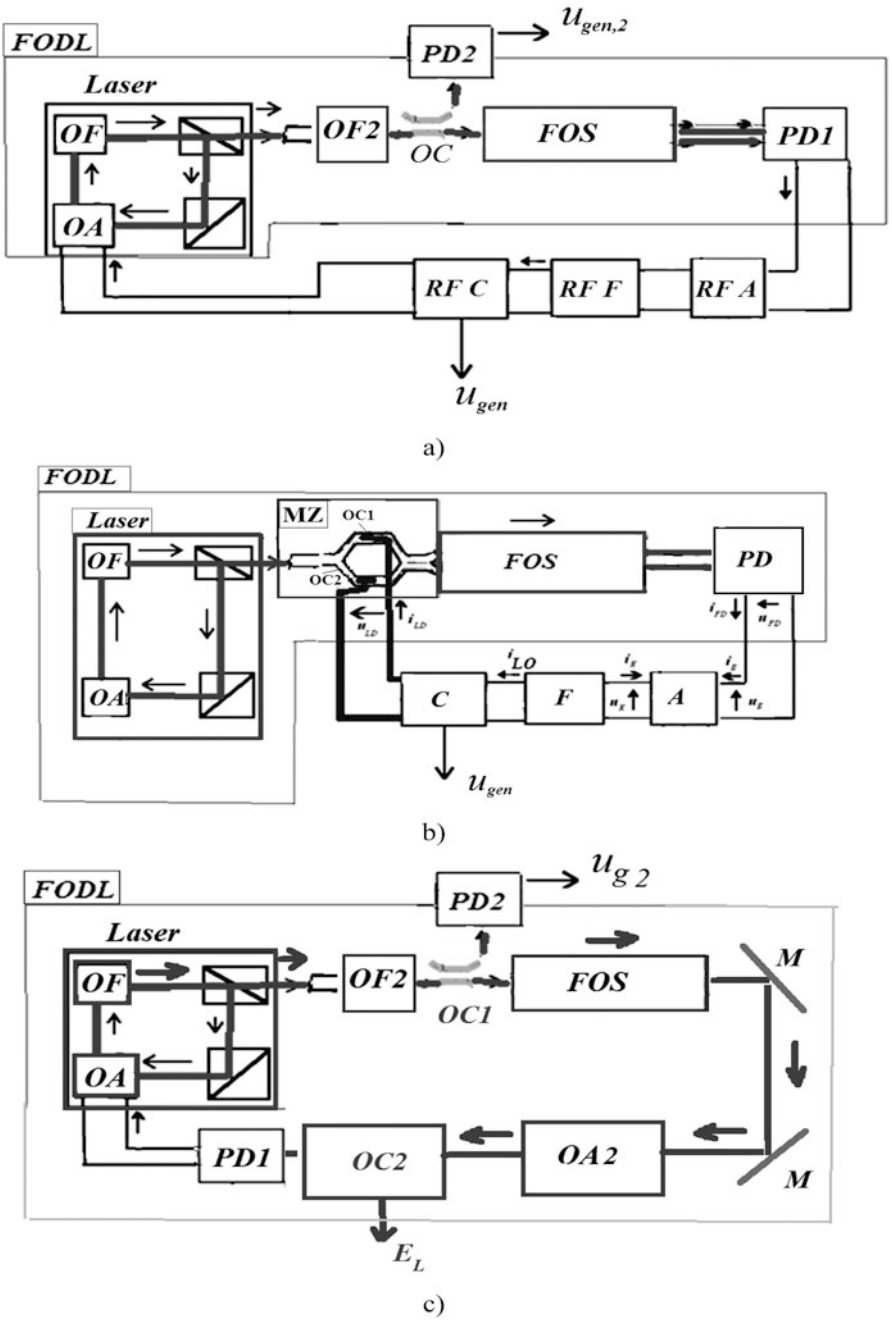

Fig. 3.9 Different variants of OEO structural diagrams: (**a**) with direct modulation of the laser pumping current and with the external photodetector PD2; (**b**) with external electro-optical Mach–Zehnder modulator with modulation of the laser emission in both MZ optical channels (OC1 and OC2); (**c**) OEO structure without RF amplifier, but with optical amplifier OA2 mounted in the fiber

One of the features of the structure shown in Fig. 3.9b is a presence of the fiber optical system of the differential type. It is formed by two optical fibers having the different delay time T_1 and T_2. The presence of such FOS allows, as it is shown below and in Chap. 6, not only performing the selection of optical harmonics and execution of the mode with the single sideband frequency, but the essential reduction of the phase noise of RF oscillations.

The promising OEO structure with the direct modulation by the pumping current *without RF amplifier* is presented in Fig. 3.9c. Oscillation amplification is performed in the optical OEO part by the optical amplifier A2 in FOS. The output RF oscillation is formed in the output by the external photodetector PD2. Such a structure has a series of advantages, which will be discussed in Chap. 6. The potentially possible reduction of the phase noise owing to elimination of the RF amplifier noises can be attributed to the one from these advantages. The absence of RF matching blocks, compactness, and manufacturability are concerned to another advantages.

Mentioned OEO structures are integrated into the single class—they contain the main OEO element—the optical quantum generator with external or internal modulator (installed in the laser resonator) and the optoelectronic network of the positive feedback, which covers the modulated source of the laser emission. The given optoelectronic network contains the optical fiber, the photodetector, the RF amplifier and the RF filter. The different elements operating in the radio-frequency and optical frequency ranges can be included into the optoelectronic section.

Let us analyze the operation of mentioned OEO structures (Fig. 3.1). The primary analysis consists in formation of equations of amplitude and phase balance, formation of symbolic and abbreviated differential equations of OEO. For this, it is necessary, as usual in any dynamic systems, to offer a description of modulation methods of laser emission and to determine the transfer functions for components included in OEO. Because the OEO under consideration represents the device with low phase noise, we shall at once pay attention to noise when providing description of modulation methods.

3.2 Methods of Modulation and Heterodyning of Laser Emissions at DM and MZ Modulations

Let us consider structures with direct internal modulation of the quantum-well laser diode (QWLD). The intensity modulation of QWLD is performed by variation of the pumping current. In OEO MZ structures, the emission modulation of QWLD is performed by the external Mach–Zehnder modulator.

Fig. 3.9 (continued) optical system of OEO and external photodetector PD2. OF2 is the optical filter 2, OC2 is the optical coupler 2, PD1 is the photodetector 1, PD2 is the photodetector 2

3.2.1 Method of Direct Amplitude Modulation

Let us consider the case on direct amplitude modulation (DM) of the laser emission by the pumping (bias) current. Structures of DM of the laser included in the OEO structure are shown in Fig. 3.10a, b. In the structure of direct modulation of laser emission, the pumping current can be presented in the form $J_L = J_{L0} + J_{L1} \cdot \mathrm{Re}[\exp(j2\pi f_0)]$, where J_{L0} and J_{L1} are the DC and AC components of the pumping current, relatively. The slope S_{1L} of the watt–ampere characteristic and the complex transfer function of QWLD $K_L(j2\pi f_0, J_{0L}, J_{0Lth})$, which depends on the modulation frequency f_0, the DC component of the pumping current J_{0L}, where J_{0Lth} is the threshold value of QWLD pumping current, are attributed to the main QWLD characteristics.

3.2.1.1 Watt–Ampere Characteristics of QWLD

The watt–ampere characteristics (WAC) of the laser diode is the function of the normalized power of the photon flow density on the QWLD output $P_L = E_{LL}^2$ versus the DC pumping current J_{L0}. If we assume that spontaneous intensity noises are small, WAC is approximated by the piecewise-linear curve: $P = P_L = 0$, at $I = J_{0L} < J_{0Lth}$, $P = P_L = S_{1L} \cdot (J_{0L} - J_{0Lth})$, at $J_{0L} > J_{0Lth}$, where S_{1L} is the slope of WAC at $J_{0L} > J_{0Lth}$. Let the intensity of output laser emission be described at modulation absence by the last formula.

To obtain the harmonic amplitudes of the oscillation spectrum of the normalized QWLD intensity, we present $E_L(J_{0L})$ by the function:

$$E_L(J_{0L}) = \begin{cases} 0, & \text{at} I = J_{0L} < J_{0Lth} \\ S_{0EL}(J_{0L} - J_{0Lth}) + S_{2EL}(J_{0L} - J_{0Lth})^2 - S_{3EL}(J_{0L} - J_{0Lth})^3, & \text{at} J_{0L} > J_{0Lth} \end{cases} \tag{3.17}$$

where S_{0EL}, S_{2EL}, S_{3EL} are slopes of the nonlinear characteristics $E_L(J_{0L})$ at $J_{0L} > J_{0Lth}$. The normalized emission power $P_L = E_{LL}^2$ is $P_L(t) = E_L^2(t) = K_C \cdot \langle E_L(t) \cdot E_L^*(t - \tau) \rangle$.

The power $P_L = E_L^2$ at the resonator output can be presented in the form $P_L = P_{L0} + P_{L1} \cdot \cos(2\pi f_0 t)$, where $P_{L0} = E_{0L}^2$, $P_{L1} = E_{10L}^2$ are DC and AC components on the optical QWLD output, $2\pi f_0$ is the radio frequency of the QWLD modulation current.

Figure 3.10 illustrates the principle of the direct modulation of the single-frequency narrowband laser by means of the pumping current variations. This method is called, for short, DM.

Figure 3.10 shows the experimental watt–ampere characteristic of the high-speed QWLD (with the modulation radio-frequency band of 12 GHz) operating on the

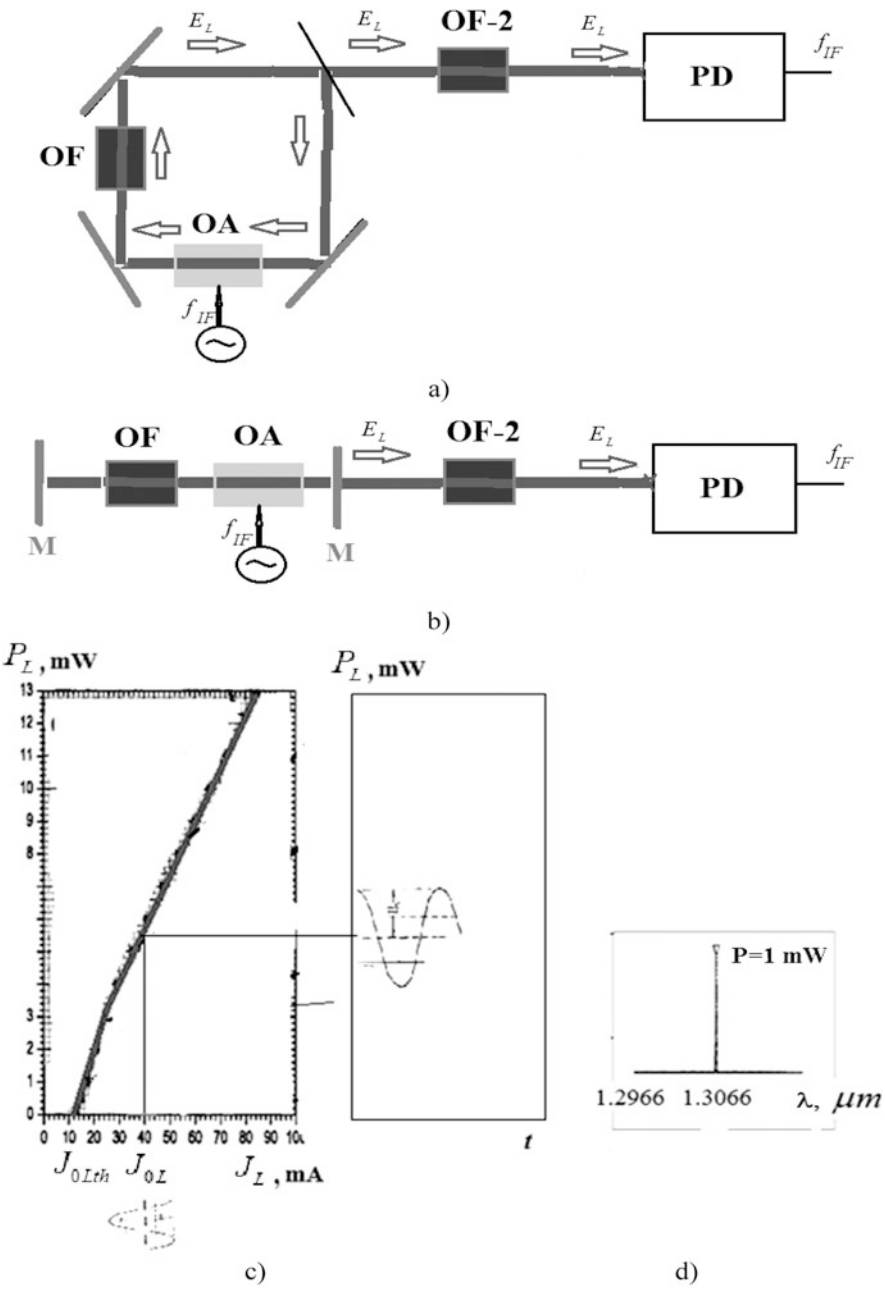

Fig. 3.10 The principle of the direct modulation (DM) of laser emission in the laser with the traveling-wave resonator (for instance, fiber optical laser) (**a**) and in the laser in the resonator with the standing wave (**b**). The experimental watt–ampere characteristic of QWLD at modulation of the harmonic signal (**c**). The optical spectrum of the laser without modulation, the wavelength at signal-frequency single-mode emission mode is 1.3 μm, the power is 1 mW (**d**)

average optical frequency of oscillations about 231 THz (the average wavelength is 1.3 μm).

Let us calculate the level of optical harmonics in the spectrum of the intensity square of the output emission at modulation of the pumping current according to the sine law.

At constant laser pumping current (bias current), for instance, 30–50 mA, and at AC component amplitude, for example, 5–10 mA (Fig. 3.10a), the intensity (or power) modulation of the laser output emission occurs. If to analyze the optical spectrum of the laser output emission, then the square on output emission intensity will represent the set of harmonics.

Let us determine the side harmonic levels at variation of the laser pumping (bias) current according to the structure of Fig. 3.10 and the law $J_L = J_{L0} + J_{L1} \cdot \cos(2\pi f_0 t)$ and, for instance, at values of normalized values $J_{L0} = 5$, $J_{L1} = 1$, $2\pi f_0 = 10$. To calculate the harmonic level of the power spectral density S_L of the laser, we may apply the Wiener–Khinchin formula. For simplicity, to illustrate the principle of DM, we make use the approximation by the function: $E_L = 0$, at $I = J_{0L} < J_{0Lth}$, $E_L = S_{2L}(J_{0L} - J_{0Lth})^2$, at $J_{0L} > J_{0Lth}$.

Let us determine the side harmonic level at modulation by the harmonic oscillation (restricting by two harmonics on the left and right from the central frequency) as:

$$\begin{aligned} S_L &= \sqrt{1/2\pi} \int_{-\infty}^{\infty} (J_{L0} + J_{L1} \cdot \cos(2\pi f_0 t))^2 \cdot \exp(-2\pi\nu_0 t)\mathrm{d}t \\ &= \frac{1}{2}\sqrt{\pi/2}(\delta(2\pi\nu_0 - 2 \cdot 2\pi f_0) + 20\delta(2\pi\nu_0 - 2\pi f_0) \\ &\quad +102 \cdot \delta(2\pi\nu_0) + 20\delta(2\pi\nu_0 + 2\pi f_0) + \delta(2\pi\nu_0 + 2 \cdot 2\pi f_0)). \end{aligned} \tag{3.18}$$

The calculated spectrum of the QWLD squared emission intensity at modulation absence is presented in Fig. 3.11a (second plot), Fig. 3.11b (second plot). Figures 3.11a, b shows the calculated spectrum at modulation by the harmonic oscillation. As we see, in the optical spectrum of intensity square, together with the carrier frequency ν_0, harmonics $\nu_0 \pm f_0$, $\nu_0 \pm 2f_0$ and so on arise at modulation by the current, which are spaced from the carrier by the multiples of the f_0 microwave frequency of the harmonic modulation.

3.2.1.2 Harmonic Selection by the OF-2 Optical Filter

The optical filter OF-2 is shown in Fig. 3.10. In the pictures presented in Fig. 3.12 the operation of the OF-2 optical filter located on the QWLD optical output is demonstrated: from five harmonics of the laser optical emission, the only two are extracted (the carrier ν_0 and the right harmonic $\nu_0 - f_0$), and other harmonic are suppressed.

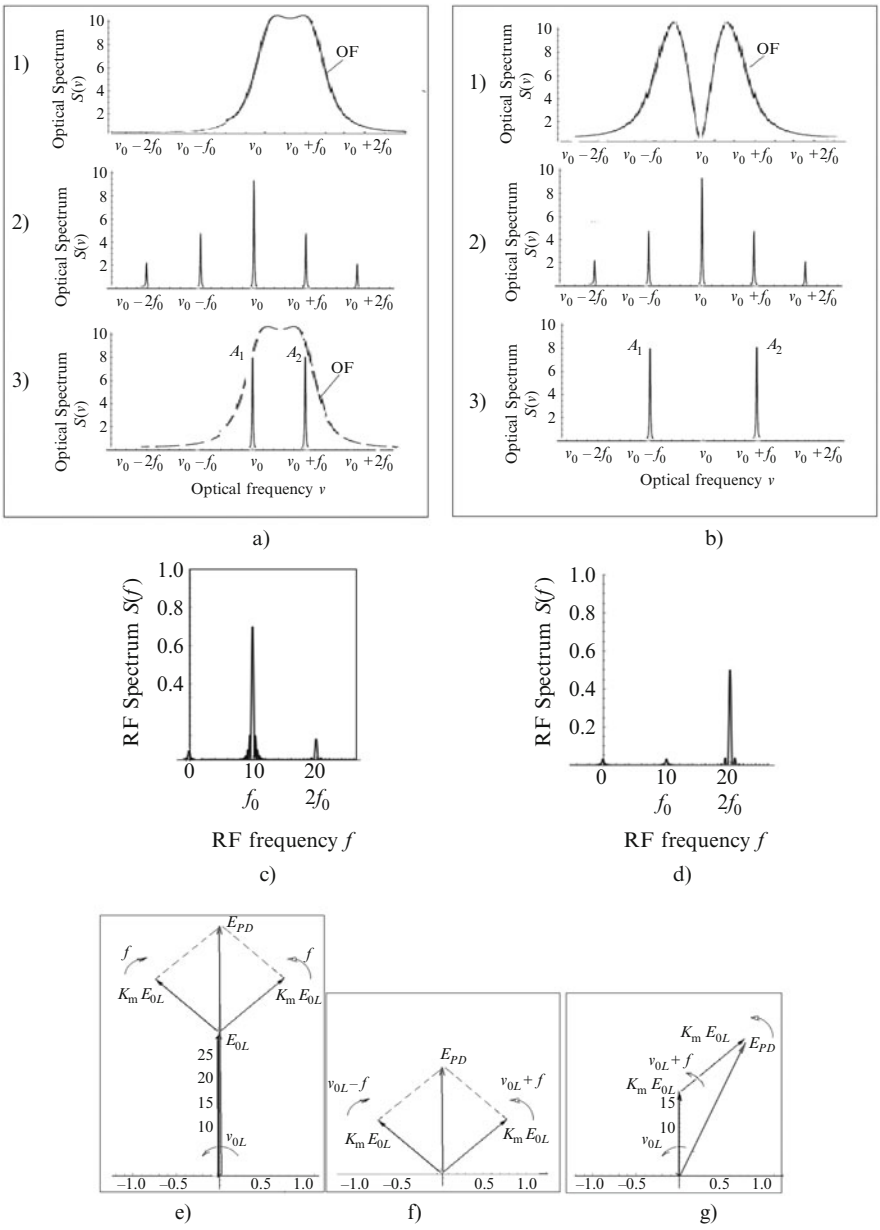

Fig. 3.11 Selection of optical harmonics in the spectrum of output emission intensity of laser oscillations with the help of narrowband (**a**) and the rejection (**b**) optical filters, and relatively, spectra of current oscillations in the PD load (**c**) and (**d**). The vector presentation of EMF amplitude summation on PD: without selection of the optical harmonic (**e**), with summation of two side harmonics at carrier suppression (**f**), with summation of carrier and one of side harmonics (**g**)

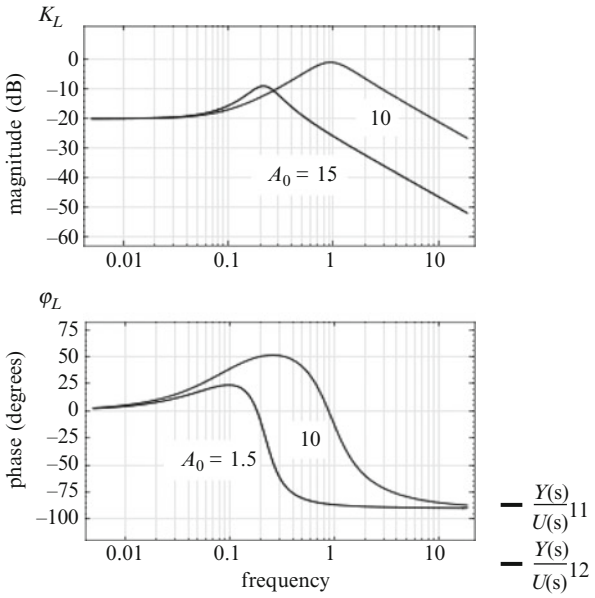

Fig. 3.12 The module K_L and argument φ_L of QWLD transfer function for two different assesses $A_0 = J_{0L}/J_{0Lth}$ of the pumping (bias) current J_{0L} above the threshold value J_{0Lth}. Values $A_0 = 1.5; 10$

The mode of two optical frequency transfer, for example, ν_0 and $\nu_0 - f_0$ and their summation on PD with extraction in its load of electrical oscillation with the f_0 frequency can be implemented. We remind that such a mode is called the OEO mode with the single sideband optical frequency from the optical carrier ν_0. In this mode, the ultralow level of oscillation phase noise and high short-term stability of generated frequency are provided owing to interference of two hard-correlated optical oscillations of the light-sensitive PD area. In OEO, there is a possibility to add on PD and to obtain in its load of oscillations with the frequency $2f_0$ and with more order at selection of the appropriate optical frequencies in the optical channel. As it is shown below, utilization of harmonics of the laser modulated oscillations with the frequency $\nu_0 - 2f_0$ expands possibilities of phase noise suppression in OEO.

3.2.1.3 Complex Transfer Function of QWLD

The complex transfer function (TF) (for small signal) of QWLD for the single-frequency generation mode (with the optical emission frequency ν_L) is determined from the kinetic equations (considered in Chap. 4) by the ratio: $K_L(j2\pi f, \nu_L) = [P_{1L}(j2\pi f, \nu_L)/J_{1L}(j2\pi f)]$ At such limitations, the complex transfer function of QWLD can be written as:

$$K_L(\, j2\pi f) = \omega_{L0}^2 / \left\{ (1 + j\omega C_L R_d)(1 + j\omega\tau_{ce}) \left[\left(\omega_{L0}^2 - \omega^2 \right) + j\omega\mu \right) \right] \right\} \qquad (3.19)$$

where $\omega = 2\pi f$, the square of the own RF resonance frequency of QWLD ω_{L00}^2 and the QWLD decay decrement μ are functions of the quantum-well parameters. Values of laser diode capacitance C_L, the laser diode resistance R_d, the time constant τ_{ce} are determined by constructive features of the laser diode and are described in Chap. 4. The fundamental resonance radio frequency is: $\omega_{L0}^2 = \frac{\Gamma_a U_{gr} g_0 P_{L0}}{(1+R_\tau r_D)(1+\varepsilon_{sh} P_{L0})\tau_{ph}}$; and QWLD decay decrement μ can be written as

$$\mu = \frac{1}{(1+R_\tau r_D)\tau_{n1}} + \omega_{L0}^2 \left[\tau_{ph} + \frac{(\varepsilon_{sh} + \varepsilon_{ce})(1 + R r_D)}{\Gamma_a U_{gr} g_0} \right]; \tag{3.20}$$

where $\tau_{ce} = r_D \tau_c + \tau_e$; $R_\tau = \frac{\tau_c}{\tau_e}$; $r_D = \frac{L_w}{L_a}$; $\varepsilon_{ce} = \frac{R r_D \Gamma_a U_{gr} g_0 \tau_{ce}}{(1+R_\tau r_D)^2}$; $\tau_D = \frac{(L_w - L_a)^2}{8 D_a}$; L_a is the total thickness of the quantum well; L_w is the thickness of the laser waveguiding layer; $P_{L0} = S_{1L} \cdot (J_{0L} - J_{0Lth})$ is the DC component of the photon flow density in the resonator; Γ_a is the coefficient of the optical field limitation; V_{gr} is the group light speed; D_a is the coefficient of ambipolar diffusion; τ_c, τ_e are the local time of capture and ejection of carriers for the AC signal, ε_{sh} is the nonlinear gain; g_0 is the gain of the active layer; τ_{ph} is the photon lifetime in the resonator; S_{1L} is the proportionality coefficient defining the dependence of photon flow density (in laser optical resonator) versus the DC pumping current in QWLD; J_{0L}, J_{0Lth} are the DC of QWLD pumping current and its threshold value; τ_{n1} is the carrier lifetime in the active area.

The module K_L and argument φ_L of the QWLD transfer function for two different excesses $A_0 = J_{0L}/J_{0Lth}$ of the pumping (bias) current J_{0L} above the threshold value J_{0Lth} are presented in Fig. 3.12. From Fig. 3.12 we see that at growth of DC pumping current J_{0L}, the frequency of the resonance peak ω_{L0} is shifted to the right, and the peak line width of the transfer function modulus increases, which is related to the growth of the expression $G_L = \Gamma_a U_{gr} g_0 P_{L0}$, which is in the numerator, at increase of the laser DC optical power P_{L0}. The frequency square is defined by the expression $\omega_{L0}^2 = \frac{1}{T_1^2} G_L \cdot (A_0 - 1)$, where T_1 is lifetime of carriers on the upper excited level.

Let us pay attention to the modulation type in DM. In OEO DM, the emission intensity or the photon flow is modulated. At wave approach, we consider the laser optical emission as oscillations of normalized EMF strength. Therefore, we speak not only about the modulation intensity, but also about amplitude modulation of the strength, i.e., about AM. The mathematical expression of E_{LL} for interfering five harmonics of the laser EMF on the PD area without application of selection by the optical filter can be written in the form:

$$\begin{aligned} E_{LL} \quad &= \{E_{0L} \cdot I_0(A_0) \cos[2\pi\nu t + \phi_{0O} + \varphi_{0Om}(t)] \\ &+ E_{0L} \cdot I_1(A_0) \cos[2\pi\nu t + 2\pi f t + \phi_{10O} + \varphi_{1Om}(t)] \\ &+ E_{0L} \cdot I_1(A_0) \cos[2\pi\nu t - 2\pi f t - \phi_{10O} + \varphi_{1Om}(t)] \\ &+ E_{0L} \cdot I_2(A_0) \cos[2\pi\nu t + 2 \cdot 2\pi f t + 2\phi_{20O} + 2\varphi_{2Om}(t)] \\ &+ E_{0L} \cdot I_2(A_0) \cos[2\pi\nu t - 2 \cdot 2\pi f t - 2\phi_{20O} - 2\varphi_{2Om}(t)]\} \end{aligned}, \tag{3.21}$$

where ϕ_{0O}, ϕ_{10O}, ϕ_{20O} are constant phase shifts defining by the selective optical filter, φ_{0m}, φ_{10m}, φ_{20m} are phase fluctuations of DC component, first and second

harmonics: $I_0(A_0)$, $I_1(A_0)$, $I_2(A_0)$, where coefficients depend on pumping and are defined with the help of the Fourier transform, for instance, as it is shown in example of WAC approximation by the quadratic function.

The effective operation is performed with zero or small cutoff angles and at large excesses of the pumping current above the threshold values, since for the laser diodes, the mode with negative pumping currents leads to the QWLD failure. The modulation index defining as the ratio of the amplitude of AC component of the fundamental harmonic to the DC component is from 0.1 to 0.2.

The constant phase incursions ϕ_{0O}, ϕ_{10O}, ϕ_{20O} of harmonics play the special role in analysis of the OEO DM system. Their values on the PD area are determined by the phase-frequency characteristic shape (we mean the PFC for optical harmonics) of the laser and the PFC of the optical filter applied for selection. The fundamental harmonic level (on the radio frequency f) in the PD photocurrent $I_1(A_0)$ is proportional to $\cos(\phi_{10O} - \phi_{0O})$. At that, for optical phases ϕ_{0O}, ϕ_{10O}, ϕ_{20O} and their differences, the following relation is true: $\phi_{0O} = 2\pi\nu_0 T_{OF20}$, $\phi_{10O} = 2\pi(\nu_0 + f)T_{OF10}$, $\Delta\phi_{0e} = \phi_{10O} - \phi_{0O} = 2\pi\nu_0 T_{OF20} - 2\pi(\nu_0 + f)T_{OF10}$. Here we specially introduce the fictive constant delays T_{OF10} and T_{OF20} in order to be more clear to understand how self-heterodyning occurs in OEO with QWLD DM.

The mathematical expression E_{LL} for the sum of EMF two harmonics on the PD area after selection by the optical filter can be written as:

$$\begin{aligned} E_{LL} &= E_{0L} \cdot k_0 \cdot I_0(A_0) \cdot \cos\left(2\pi t\nu_0 + \phi_{0e} + \varphi_{em}(t)\right) \\ &+ E_{0L} \cdot k_1 \cdot I_1(A_0) \cdot \cos\left(2\pi t(\nu_0 - f) - \phi_{0e} - \varphi_{em}(t)\right) \end{aligned}, \tag{3.22}$$

Now we find the ratio: $K_p = E_{PD}/[2E_{0L} \cdot k_0 \cdot I_0(A_0)]$. Assuming that amplitudes of harmonics ν_0 and $\nu_0 - f$ after passing through the optical filter are equal: $E_{0L} \cdot k_0 \cdot I_0(A_0) = E_{0L} \cdot k_1 \cdot I_1(A_0)$, and using the trigonometric formula for adding the cosines of different angles, we obtain:

$$\begin{aligned} K_P &= \{\cos[2\pi t\nu_0 + \phi_{0e} + \varphi_{em}(t)] + \cos[2\pi t(\nu_0 - f) - \phi_{0e} - \varphi_{em}(t)]\} \\ &= 2\cos\left[\frac{2\pi t\nu_0 + \phi_{0e} + \varphi_{em}(t) + 2\pi t(\nu_0 - f) - \phi_{0e} - \varphi_{em}(t)}{2}\right] \cdot \\ &\times \cos\left[\frac{2\pi t\nu_0 + \phi_{0e} + \varphi_{em}(t) - [2\pi t(\nu_0 - f) - \phi_{0e} - \varphi_{em}(t)]}{2}\right] \end{aligned} \tag{3.23}$$

Transforming the last expression for K_p, we have:

$$\begin{aligned} K_P &= 2\cos\left[\frac{2 \cdot 2\pi t\nu_0 - 2\pi tf + \Delta\phi_{0e} + \varphi_{em}(t) - \varphi_{em}(t)}{2}\right] \\ &\cdot \cos[2\pi tf + \Delta\phi_{0e} + \varphi_{em}(t)]. \end{aligned} \tag{3.24}$$

The first multiplier in Eq. (3.23) is the oscillating term in time with the average value equaled to 1.

Having used the last formula, we obtain the expression for connection of squared amplitude of the field strength E_{PD} on the PD area (the PD optical input) with the squared field amplitude on the laser output E_{0L}:

$$E_{PD} = 2E_{0L} \cdot k_0 \cdot I_0(A_0)\langle \cos[\Delta\phi_{0e}]\rangle \exp[-\Delta\nu_L \cdot t]. \tag{3.25}$$

Here we used the formula for mathematical expectation calculation:

$$\begin{aligned}\langle \cos[2\pi tf + \Delta\phi_{0e} + \varphi_{em}(t)]\rangle &= \langle \cos[2\pi tf] \cdot \cos[\Delta\phi_{0e} + \varphi_{em}(t)]\rangle \\ &\quad -\langle \sin[2\pi tf] \cdot \cos[\Delta\phi_{0e} + \varphi_{em}(t)]\rangle\ , \\ &= \langle \cos[\Delta\phi_{0e}]\rangle \exp[-\Delta\nu_L \cdot t]\end{aligned} \tag{3.26}$$

where $\langle\rangle$ designate the operation of average value finding (averaging in time).

The output electrical current of the PD is defined as $i_{PD}(t) = E_{PD} \cdot E_{PD}^*$. If nonlinearity of PD is not taken into account, the output current of PD is defined by the second multiplier with the fluctuating DC component and the first harmonic of current:

$$i_{PD}(t) = I_{PD0} \cdot \cos[\Delta\phi_{0e} + \varphi_{em}(t)] + I_{PD10} \cdot \cos[2\pi ft + \Delta\phi_{0e} + \varphi_{em}(t)]. \tag{3.27}$$

The output current of PD (taking into account the PD nonlinearity) includes the DC component I_{PD0} defining by the level of DC component of the laser emission on the PR area and by components of the first I_{PD10}, second I_{PD20} (in the general case, the other possible harmonics), which level is determined by nonlinear characteristics of PD is:

$$\begin{aligned}i_{PD}(t) &= I_{PD0} \cdot \cos[\Delta\phi_{0e} + \varphi_{em}(t)] \\ &\quad + I_{PD10} \cdot \cos[2\pi ft + \Delta\phi_{0e} + \varphi_{em}(t)] \\ &\quad + I_{PD20} \cdot \cos[2 \cdot 2\pi ft + 2 \cdot \Delta\phi_{0e} + 2 \cdot \varphi_{em}(t)]\end{aligned}\ . \tag{3.28}$$

At selection by the rejection optical filter (Fig. 3.12b), the DC component is suppressed, and the radio frequency of the photocurrent is multiple to 2: $2 \cdot 2\pi f$, and constant components I_{PD0} and I_{PD10} are close to zero:

$$i_{PD}(t) = I_{PD20} \cdot \cos[2 \cdot 2\pi ft + 2\Delta\phi_{022e} + 2\varphi_{em}(t)], \tag{3.29}$$

From the last mathematical formulas, we can make the following conclusions. We should note the main point: the suppression of the optical carrier frequency ν_0 significantly decreases the phase fluctuations. A degree of the fluctuation suppression is defined by the level of the carrier suppression. The PD photocurrent in OEO DM is a result of self-heterodyning; the level of harmonic components is defined by the difference phase incursion of the first and second optical harmonics $\Delta\phi_{0e}$, and laser phase fluctuations $\varphi_{em}(t)$, in the end are defined by the spectrum of

RF oscillation in the load of PD. We would like to remind that in the beginning, we here neglected the laser amplitude fluctuations $m_{em}(t)$ in the analysis, assuming that they are small in the mode with the large excess of the pumping current above the threshold value. The fluctuating phases in the last formula define the oscillation spectrum.

Further, we analyze the QWLD emission modulation in OEO at using of the external Mach–Zehnder modulator.

3.2.2 Modulation and Heterodyning in OEO MZ

The electro-optical MZ modulator is concerned to a class of modulators for electromagnetic field intensity. The phase modulation of optical emission oscillations is performed in the one from two optical channels in the MZ modulator. The interference of the phase-modulated and non-phase-modulated EMF oscillations delayed with regard to each other and passed through the first and second optical channels of MZ (Fig. 3.13).

Let the laser optical emission with phase fluctuations be fed to the MZ optical input. The influence of the $u_g(t)$ voltage in the one from two optical MZ channels (Fig. 3.1) upon the material refraction index (usually, the lithium niobate is used), from which the MZ optical channels are made, leads to the phase modulation of the optical oscillation. And adding of two emissions passed through different MZ optical channels leads to intensity modulation of laser emission on the PD area, where their interference occurs. Delayed output emissions of the first and second channels of MZ modulator E_{1L} and E_{2L}, in the general case, pass to the input of PD. When the fiber optical system (FOS) is formed by the single lengthy optical fiber, the difference in delay is defined as $\Delta T_M = T_{M20} - T_{M10}$.

We take into consideration that EMF oscillations $E_{1L} = k_{01}E_{0L}$ and $E_{2L} = k_{02}E_{0L}$ (where k_{01} and k_{02} are excitation coefficients: $k_{01} + k_{02} \approx 1$) propagate through different MZ optical channels. Designating E_{0L}^2 as the normalized intensity in the optical MZ input (or the power reduced to the unitary normalized area), we introduce the coefficient of excitation irregularity of MZ optical channels $\gamma = (k_{02}/k_{01}) \approx 1$ (in the experiment $k_{01} \approx k_{02} \approx 0.5$), then for the result of interfering oscillations after MZ E_{12L}, extracting their module $|E_{12L}|$ and argument $\arg(E_{12L})$, we can write expressions:

- for $(E_{12L})^2$

$$|E_{12L}|^2 = E_{0L}^2\left\{{k_{01}}^2 + {k_{02}}^2 - 2k_{01}k_{02}\cos\left[\varphi_{0L1}\left(u_g\right) - \varphi_{0L2}\right)\right], \tag{3.30}$$

- for $\arg E_{12L}$

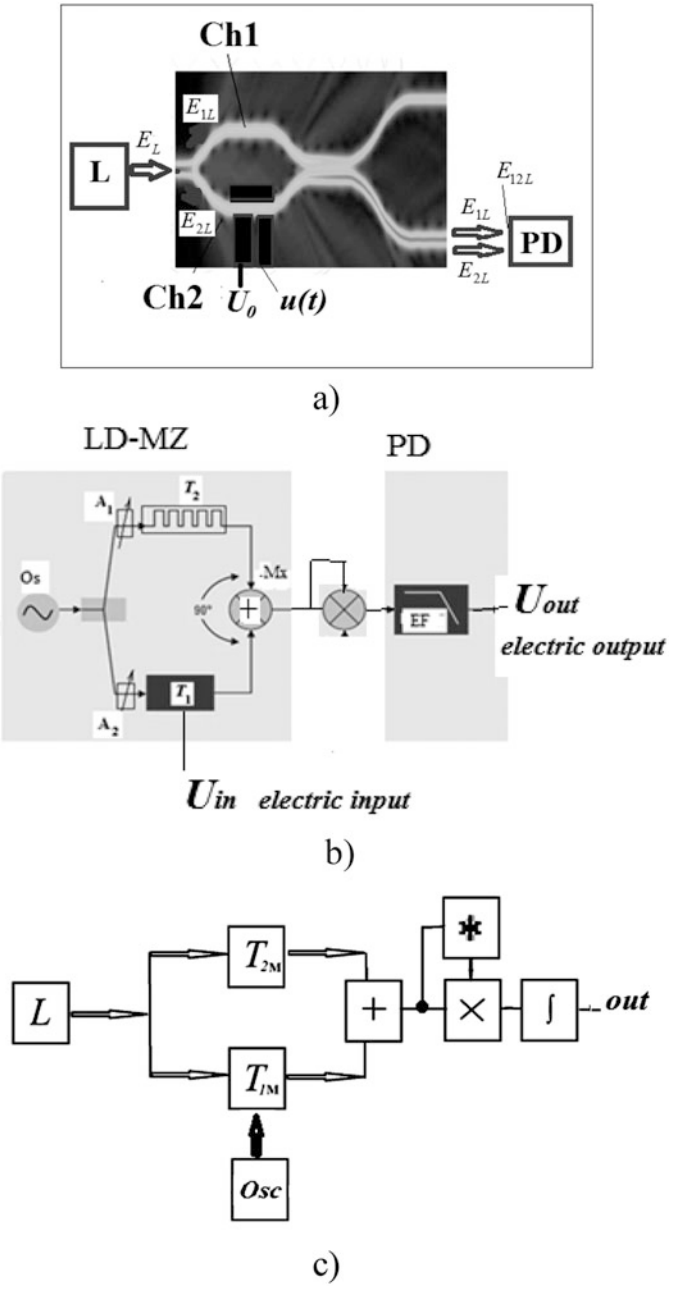

Fig. 3.13 The MZ modulator (**a**) and the equivalent modulator diagrams by electrical networks (**b**) and by blocks of mathematical operations, which represent (in the aggregate) the correlator of the fluctuating quantities

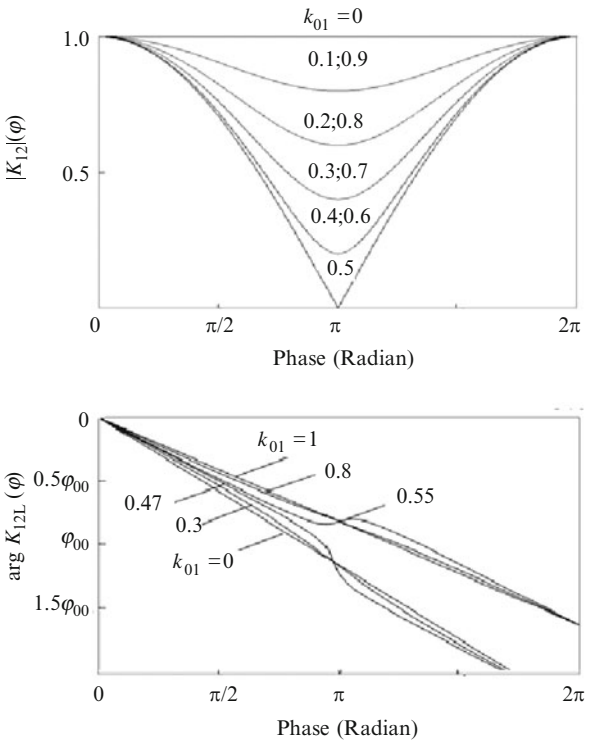

Fig. 3.14 The plot of module and argument of the transfer function of the MZ modulator

$$\arg E_{12L} = \operatorname{arctg}\left\{\frac{k_{01}\sin\varphi_1 + k_{02}\sin\varphi_2}{k_{01}\cos\varphi_1 + k_{02}\cos\varphi_2}\right\} = \operatorname{arctg}\left\{\frac{\sin\varphi_1 + \gamma\sin\varphi_2}{\cos\varphi_1 + \gamma\cos\varphi_2}\right\} \quad (3.31)$$

Plots of the module and arguments of the transfer function of MZ modulator are presented in Fig. 3.14.

We attract the reader's attention that in the expression for $|E_{12L}|^2$ the phase $\varphi_{0L1}(u_g)$ is modulated by the harmonic oscillation $u_g(t) = U_{1MZ}\cos[2\pi f_0 t + \phi_{0e} + \varphi_{em}(t)]$:

$$|E_{12L}|^2 = \frac{E_{0L}^2}{2}\gamma\left\{\frac{(1+\gamma^2)}{2\gamma} - \cos\left[\varphi_{0L1}(u_g) - \varphi_{0L2}\right]\right. . \quad (3.32)$$

If to assume that excitation of MZ optical channels is uniform, we may suppose that $\frac{(1+\gamma^2)}{2\gamma} \approx 1$ and using the trigonometric formula of the double angle, we can write:

$$|E_{12L}|^2 = \frac{E_{0L}^2}{2}\left\{1 - \cos\left[\varphi_{0L1}(u_g) - \varphi_{0L2}\right]\right\}$$
$$= \frac{E_{0L}^2}{2} 2\sin^2\left[\varphi_{0L1}(u_g) - \varphi_{0L2}\right]. \quad (3.33)$$

From the last formula, it follows that

$$|E_{12L}| = |E_{0L}| \cdot \sin\left[\varphi_{0L1}(u_g) - \varphi_{0L2}\right]. \quad (3.34)$$

In other words, we derived the connection formulas both for the EMF amplitude squared and for the amplitude. These formulas allows formation of expressions for $|E_{12L}|^2$ and also for $|E_{12L}|$ at utilization of expansions on the Bessel functions.

The function $(E_{12L})^2$ of oscillation amplitude U_{0M} depends upon the MZ operation point choice or the DC bias voltage U_{0MZ}. The DC bias changes and regulates of the phase incursion φ_{0L2}. The MZ operation point can be varied by the constant bias voltage U_{0MZ}. Let us designate $x = U_{1MZ}/U_{0MZ\pi}$, $\varphi_{0MZ} = \frac{\pi U_{0MZ}}{U_{0MZ\pi}}$.

Now we can present Fig. 3.15, which shows the functions of DC component of the optical emission and AC component of fundamental harmonic in the MZ output.

From Fig. 3.15 we see that the laser emission modulation can be performed in two modes: "quadrature" and "non-quadrature," at DC bias there is the minimum at $x = U_{1MZ}/U_{0MZ\pi} = 1$.

In OEO, the optical filter is used, which effectively suppresses the optical harmonics with carriers higher than second $\nu_2 = \nu_0 \pm 2f$. Therefore, we present below the expressions for E_{12L} with limited number of harmonics without the account of higher harmonics. The expression for $(E_{12L})^2$ can be wrote using the expansion to even J_{2k} and odd J_{2k-1} Bessel functions. Let us introduce the constant half-wavelength bias voltage on MZ $U_{0MZ\pi}$, which provides the phase difference φ_{0L2} in 180° between optical oscillations of the first and second MZ channels. Now we use the trigonometric formula for the cosine of two angle sum for carrier, the first and second harmonics and we can write:

$$\begin{aligned}(E_{L12})^2 &= \frac{E_{0L}^2}{2}\gamma\{\frac{(1+\gamma^2)}{2\gamma} \cdot \cos(2\pi\nu t + \phi_{0e}) \\ &- \cos(\varphi_{0MZ}) \cdot J_0(x) \cdot \cos(2\pi\nu t + \phi_{0e}) \\ &- \sin(\varphi_{0MZ}) \cdot J_1(x) \cdot \cos(2\pi\nu t + 2\pi f t + \phi_{0e}) \\ &- \sin(\varphi_{0MZ}) \cdot J_1(x) \cdot \cos(2\pi\nu t - 2\pi f t - \phi_{0e}) \\ &- \cos(\varphi_{0MZ}) \cdot J_2(x) \cdot \cos(2\pi\nu t + 2 \cdot 2\pi f t + 2 \cdot \phi_{0e}) \\ &- \cos(\varphi_{0MZ}) \cdot J_2(x) \cdot \cos(2\pi\nu t - 2 \cdot 2\pi f t - 2 \cdot \phi_{0e})\}\end{aligned} \quad (3.35)$$

Figure 3.16 shows the spectrum of optical harmonics in the optical harmonics in the optical channel of OEO with MZ at modulation index $x = U_{1MZ}/U_{0MZ\pi} = 1$ (Fig. 3.16a), and also the values of Bessel functions of differential orders, which are defined the harmonic amplitudes at variation of the modulation index (Fig. 3.16b). The optical harmonic spectrum at $x = U_{1MZ}/U_{0MZ\pi} = 2.4$ is presented in Fig. 3.16c.

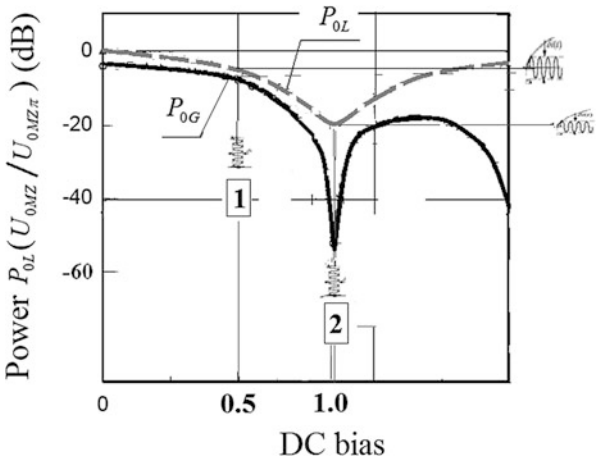

Fig. 3.15 Functions of DC component of the optical emission and AC component of fundamental harmonic in the MZ output. Numbers "1" and "2" designates the values of DC bias voltage in the "quadrature" and "non-quadrature" modes, they are equal relatively 0.5 and 1.0 and correspond in this figure to phases $\varphi_{0MZ} = \frac{\pi U_{0MZ}}{U_{0MZ\pi}} = \pi/2$ and π, relatively

From these spectra, we see that at this AC voltage amplitude $U_{1MZ} = 2U_{0MZ\pi}$ (the fundamental harmonic) applied to the MZ modulator, the central optical harmonic disappears in the spectrum (or PSD level becomes equal to zero on the optical frequency). The spectrum of optical harmonics in the optical channel of OEO MZ at the modulation index $x = U_{1MZ}/U_{0MZ\pi} = 2.4$ is presented in Fig. 3.16a, c.

The vector presentation of the EMF amplitude summation on PD is shown without selection of the optical harmonic (Fig. 3.16d) and with summation of two side harmonics at the carrier suppression (Fig. 3.16e) and with summation of the carrier and the one of side harmonics (Fig. 3.16f). Figure 3.16d–f is the vector diagrams, which clearly show the process of the central harmonic suppression with the frequency ν_0 (or the constant optical emission with E_{0L}). Here E_{PD} is the field strength on the photodetector area. In Fig. 3.16d we see the non-suppressed central harmonic with the frequency ν_0. Figure 3.16e illustrates the suppression condition of the harmonic with the frequency ν_0. Here E_{0L}, E_{PD} are laser field strengths in the optical input of the MZ modulator and on the PD area, relatively. The coefficient K_m introduced in Fig. 3.16d–f clearly shows that the amplitude of harmonics on the left $(\nu_0 - f)$ and on the right $(\nu_0 + f)$ with respect to the central optical frequency ν_0 represents the product $K_m E_{0L}$. In the case shown in Fig. 3.16f, at nonsymmetric suppression, for example, of the left harmonic $(\nu_0 - f)$ suppression, the total vector E_{PD} is determined by both AC and DC components.

3.2.2.1 Approximation of Bessel Functions by Quadratic and Cubic Functions

We take into consideration in calculations of the first and second harmonics only for appropriate Bessel functions the following approximation for small $x = U_{1MZ}/U_{0MZ\pi}$, and $x \in [0;1]$: $J_0(x) \approx 1 - \frac{x^2}{4}$; $J_1(x) \approx \frac{x}{2} - \frac{x^3}{16}$ and $J_2(x) \approx \frac{x^2}{8}$. Assumed approximation allows obtaining of the relatively simple expression for AC

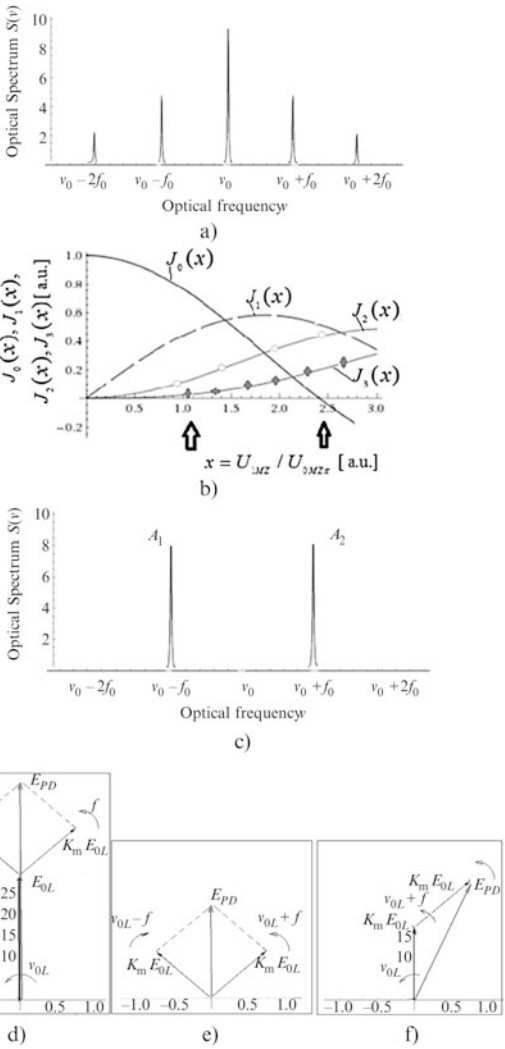

Fig. 3.16 The spectrum of optical harmonics in the optical channel of OEO with MZ at modulation index $x = U_{1MZ}/U_{0MZ\pi} = 1$ (**a**). The values of Bessel functions of differential orders, which are defined the harmonic amplitudes at variation of the modulation index (**b**). The spectrum of optical harmonics in the optical channel of OEO MZ at the modulation index $x = U_{1MZ}/U_{0MZ\pi} = 2.4$ (**a**). (**c**) The vector presentation of EMF amplitude summation on PD: without selection of the optical harmonic (**d**), with summation of two side harmonics at carrier suppression (**e**), with summation of carrier and one of side harmonics (**f**)

component $(E_{12L})^2$. We must take into account that on the PD area, the AC component of intensity is present on the background of DC component.

Let us introduce coefficients a_0, a_1, a_2: $a_0 = \frac{E_{0L}^2}{2}\gamma\left[\frac{(1+\gamma^2)}{2\gamma} - \cos(\varphi_{0MZ}) \cdot \left(1 - \frac{x^2}{4}\right)\right]$; $a_1 = -\frac{E_{0L}^2}{4}\gamma \sin(\varphi_{0MZ})$; $a_2 = -\frac{E_{0L}^2}{8}\gamma \cos(\varphi_{0MZ})$. Taking into account that $I_{PD} = S_{PD} \cdot \left(E_{L12} \cdot E_{L12}^*\right)$ and introducing ϕ_{0eMZ}, which is total phase incursion of the photocurrent, we get following expressions for photocurrent harmonics: $I_{0PD} = a_0 - (a_2/2)x^2$; $I_{1PD} = a_1\left(\frac{x}{2} - \frac{x^3}{16}\right) \cdot \cos(2\pi ft + \phi_{0eMZ})$; $I_{2PD} = a_2 x^2 \cos^2(\pi ft + \phi_{0eMZ})$. As we see, at the choice of $\varphi_{0MZ}(U_{0MZ}) = m\pi/2$, $m = \pm 1, \pm 2, \ldots$, the function

of photocurrent versus the input voltage in the MZ electrical input is linear-cubic, the slope of phase fluctuation is about 1, and at $\varphi_{0L2}(U_{0M}) = m\pi$ this function is quadratic, but at that, the transformation slope of phase fluctuations in MZ increases by several times. Since at nonuniform excitation of MZ optical channels, for instance, $k_{02} \approx 0.55$ and $k_{01} \approx 0.45$, the phase-frequency MZ function (Eq. 3.31) has the local maximum at $\varphi_{0MZ}(U_{0MZ}) = 0.95m\pi$. Therefore, in this operating point, the MZ slope of phase fluctuation transformation is minimal and, as it follows from the further analysis, the transformation slope of MZ phase fluctuations is small. But at that, the second harmonic level essentially exceeds the level of the first harmonic.

Thus, PD photocurrents in the open loops of OEO DM and OEO MZ at nodulation, relatively, of the QWLD pumping current (OEO DM) and of the MZ voltage (in OEO MZ) are results of self-heterodyning, the level of harmonic components is defined by the difference phase incursion of two optical harmonics $\Delta\phi_{0e}$, which pass to PD area, and phase fluctuations of the laser $\varphi_{em}(t)$ define the spectrum of RF oscillations in the PD load.

In OEO DM and in OEO MZ, the mode of *radio-frequency doubling* is possible at DC component suppression, which significant level degrades of the OEO phase noise. In this case, it is necessary to introduce the optical rejection filter tuned on the suppression of DC component in OEO DM. And in OEO MZ, the ratio $U_{1MZ}/U_{0MZ\pi}$ should be $x = U_{1MZ}/U_{0MZ\pi} = 2.4$. The tasks of power spectral density determination for the OEO phase noise, which are defined by laser phase fluctuations $\varphi_{em}(t)$, will be solved in Chaps. 5–7. Further, in order to derive the amplitude and phase balance equations and OEO differential equations, we present below the mathematical description of transfer functions of various OEO components: the photodetector, the RF amplifier and the RF filter, as well as the optical fiber and the optical amplifier.

3.3 Mathematical Description of Transfer Functions of OEO Components

3.3.1 The Optical Amplifier for the Laser

The expression for the *transfer function* of the optical amplifier for a laser represents the ratio of the intensity amplitude (with the optical frequency ν) in the OA output E_{Lout} to its value in the input E_{Lin}: $K_{OA} = E_{Lout}/E_{Lin}$.

For the double-level laser model (the point model in space without taking into consideration the OA linear dimensions), TF of OA is obtained from the equation solution of interaction of the plane monochromatic wave with the active medium. The transfer function of the laser optical amplifier in the small-signal mode in linear approximation can be written as:

$$K_{\mathrm{OA}} = \frac{1}{3 \cdot 2\pi h} \cdot \frac{(2\pi\nu_{21}) T_2 d_{\mathrm{e}}^2 N_0}{\left[(2\pi\nu_{21})^2 - (2\pi\nu)^2\right] + j2\pi\nu\mu_{000}}, \tag{3.36}$$

where ν_{21} is the transition frequency, T_2 is longitudinal relaxation time, d_{e}^2 is the dipole moment, $\mu_{000} = (1/T_2)$ is the damping decrement, which is defined by total losses in the active medium, N_0 is the population difference on upper and lower operation levels, which is related with pumping $\alpha_{\mathrm{N0}} = N_0/T_1$.

3.3.1.1 Nonlinear Characteristic of the Optical Amplifier

During analysis of different watt–ampere characteristics of QWLD and lasers used in OEOs, we can find out that WAC is linear at currents, which are higher than the threshold value. The significant deviation from linearity is demonstrated at large DC pumping currents, which cannot be considered as normal for operation. Nonlinear optical effects, such as doubling of the optical frequency, the double-photon absorption, stimulated scattering of Mandelstam–Brillouin (SSMB), etc. are demonstrated only at ultrahigh power densities, which are unachievable in OEO lasers.

At future analysis of the semiclassical double-level laser model in Chap. 4, it is shown that the "main nonlinearity" at normal operating densities (in the laser active medium in OEO) is the nonlinearity in the form of a product of population and the field intensity amplitude $N_0 \cdot \left[E_{\mathrm{L}} \cdot E_{\mathrm{L}}^*\right]$. Such nonlinearity is caused by interaction of external pumping and a field. The continuous regulation of the field amplitude by the level of population difference occurs in the laser. The population grows at decrease of field oscillation amplitude and decreases at its growth. The regulation system is similar with the control system in amplifiers on electronic tubes and transistors with the auto-bias mode. The radio-frequency oscillators with the inertial auto-bias network operate on the similar principle.

3.3.2 Optical Filter of a Laser

3.3.2.1 Fabry–Perot, Bragg and Disc Resonators, Their Mathematical Models

In this section, we briefly describe the main transfer functions for optical resonators and filters for lasers in the OEO structure.

Figure 2.7 shows types of optical resonators and the slow-wave optical structures for lasers and OEO.

The Fabry–Perot resonator is formed by two mirrors with reflection factors $R_{1\mathrm{OF}}$ and $R_{2\mathrm{OF}}$ and, relatively, transfer factors $K_{1\mathrm{OF}}$ and $K_{2\mathrm{OF}}$, located on the L_{OF} distance, which is filled by the medium with the refraction index n_{OF}, α_{OF} is the absorption coefficient. The transfer function of the Fabry–Perot resonator defines as a ratio of

the input oscillation E_{Lin} to the output oscillation E_{Lout} of the emission field strength, is

$$K_{\mathrm{OF}} = \frac{E_{\mathrm{Lout}}}{E_{\mathrm{Lin}}} = \frac{K_{1\mathrm{OF}} \cdot K_{2\mathrm{OF}} \exp\left(\alpha_{\mathrm{OF}} L_{\mathrm{OF}} + j2\pi\nu L_{\mathrm{OF}} n_{\mathrm{OF}}/c\right)}{1 - R_{1\mathrm{OF}} \cdot R_{2\mathrm{OF}} \exp\left(\alpha_{\mathrm{OF}} L_{\mathrm{OF}} + j2\pi\nu L_{\mathrm{OF}} n_{\mathrm{OF}}/c\right)} \tag{3.37}$$

where c is the light speed in vacuum.

The Bragg resonator is formed by the optical structure, in which the refraction index periodically varies or by the multilayer structures with different refraction indices (Fig. 2.7). The extreme Q-factors are restricted by the length and losses of the periodic structure and achieve a million at geometrical length about 3 cm. The high power density of emission at high Q-factors (10^6) [4–8] does not permit to use them as the linear devices for input powers more than 20–100 μW. Evolution of nonlinear optical effects and the temperature instability prohibits from qualitative oscillation selection. Nevertheless, they are acceptable as frequency discriminators (with the conversion slope 1/Hz) in devices for frequency and phase automatic control of semiconductor lasers, if the small optical power of 20–100 μW is applied to the input. The transfer function of the Bragg resonator can be obtained from solution of two coupled differential equations for the forward and backward waves and this function is determined as

$$K_{\mathrm{OF}} = \frac{E_{\mathrm{Lout}}}{E_{\mathrm{Lin}}}$$

$$= \frac{-(\gamma_{\mathrm{B}} + \alpha_{\mathrm{B}} - j\Delta\beta_{\mathrm{B}}) \cdot \exp\left(\gamma_{\mathrm{B}} L_{\mathrm{B}}/2\right) + (-\gamma_{\mathrm{B}} + \alpha_{\mathrm{B}} - j\Delta\beta_{\mathrm{B}}) \cdot \exp\left(-\gamma_{\mathrm{B}} L_{\mathrm{B}}/2\right)}{(-\gamma_{\mathrm{B}} + \alpha_{\mathrm{B}} - j\Delta\beta_{\mathrm{B}}) \cdot \exp\left(\gamma_{\mathrm{B}} L_{\mathrm{B}}\right) - (\gamma_{\mathrm{B}} + \alpha_{\mathrm{B}} - j\Delta\beta_{\mathrm{B}}) \exp\left(-\gamma_{\mathrm{B}} L_{\mathrm{B}}\right)}, \tag{3.38}$$

where $\gamma_{\mathrm{B}} = \sqrt{{C_{\mathrm{B}}}^2 + \left(\beta_{\mathrm{B}} - 2\pi n_{0\mathrm{B}}/\lambda_{0\mathrm{B}}\right)^2}$, $C_{\mathrm{B}} = j(\Delta n_{0\mathrm{F}}/\lambda_{\mathrm{B}})$ is the coupling coefficient, α_{B} are losses per the length unit in the Bragg grating, $\Delta\beta_{\mathrm{B}} = \beta_{\mathrm{B}} - 2\pi n_{0\mathrm{B}}/\lambda_{0\mathrm{B}} = 2\pi\nu n_{0\mathrm{B}}/c - 2\pi n_{0\mathrm{B}}/\lambda_{0\mathrm{B}}$, $\beta_{\mathrm{B}} = 2\pi\nu n_{0\mathrm{B}}/c$ is the propagation constant, λ_{B} the Bragg grating period, $\Delta n_{0\mathrm{F}}$ is the difference of refraction indices in the Bragg grating.

Cylindrical disc resonators [9–11] have higher Q-factors at excitation of waves of whispering gallery in them. At present, the Q-factors of dielectric cylindrical resonators in the optical range, which are produced by methods of integrated technology from silicon, achieve 5×10^6. Both in microwave and in optical ranges, disc resonators are usually made from materials with relatively large permittivity (with large refraction index). So, the sapphire discs in the mm-wave range have the permittivity approximately 12, while for a silicon on the wavelength 1.55 μm, where it is transparent, and the refraction index $n \approx 3.48$.

The Q-factor of optical disc resonators is defined by the simple expression: $Q = 2\pi n/(\alpha_1 \lambda)$, where the refraction index $n = 1.4$–1.5, and α_1 corresponds to losses

per one passage or per the length unit of the bean path. Considered optical resonators provide the selective functions and decrease the spectral density level of the laser emission phase noise.

Since we are interested in OEO in resonator operation near the natural frequency within the limits of triple excess of the pass band, we assume that, for optical resonators used in OEO, their transfer function is defined by the following expression, which describes well their characteristics in the specified frequency band: $K_{\mathrm{OF}} = \frac{E_{\mathrm{Lout}}}{E_{\mathrm{Lin}}} = \frac{(\ j2\pi\nu)(1/T_{\mathrm{OF}})}{(\ j2\pi\nu)^2+(1/T_{\mathrm{OF}})(\ j2\pi\nu)+(2\pi\nu_{0\mathrm{OF}})^2}$, where T_{OF} is the time constant of the optical resonators, $\nu_{0\mathrm{OF}}$ is the natural frequency of the resonator.

3.3.3 The Photodetector in OEO

The photodetector in OEO is the quantum-dimension device (QWPD) [12, 13]. The effectiveness of transformation of optical emission intensity into the electrical current in modern PDs is close to 100%. In this section, we do not pay attention of readers to the issue of nonlinear light transformation in PD and consider it as the inertial linear element. The PD current i_{PD} is proportional to emission intensity (or the square of field strength) on the PD area multiplied by the PR transformation slope $K_{0\mathrm{PD}}$, and the following expression is true: $i_{\mathrm{PD}} = K_{0\mathrm{PD}} \cdot \mathrm{Re}\left[E_{\mathrm{L}} \cdot E_{\mathrm{L}}^{*}\right]$, where "·" is the complex conjugation operation of the field strength $E_{\mathrm{L}} = E_{0\mathrm{L}} \cdot \mathrm{Re}[\exp(j2\pi\nu \cdot t)]$, where ν is the optical frequency of laser generation.

In OEO, the single-frequency optical oscillations, which are modulated by the RF oscillation (with the radio frequency $\omega = 2\pi f$), pass on the PD area. Let us represent the emission power as a sum of constant P_{L0} and alternate P_{L1} (the first harmonic $2\pi f$) components $P_{\mathrm{L}} = P_{\mathrm{L0}} + P_{\mathrm{L1}}\,\mathrm{Re}[\exp(j2\pi f \cdot t)]$, where $P_{\mathrm{L0}} = (E_{0\mathrm{L}})^2 = (E_{12\mathrm{L}})^2$. At that, the current in the PD load is a sum of constant $I_{0\mathrm{PD}}$ and alternate $I_{1\mathrm{PD}}$ component of the photocurrent $I_{\mathrm{FD}} = I_{0\mathrm{PD}} + I_{1\mathrm{PD}}\,\mathrm{Re}[\exp(j2\pi ft)]$.

The complex transfer function of PD (on first harmonic) for the linearized system can be defined as the ratio: $K_{1\mathrm{PD}}(j\omega) = [I_{1\mathrm{PD}}(j\omega)/P_{\mathrm{L1}}(j\omega)]$.

The voltage on the load impedance Z_{PD} of PD is $u_{\mathrm{PD}} = Z_{\mathrm{PD}} \cdot i_{\mathrm{PD}}$. The transfer function of PD $K_{1\mathrm{PD}}$ is defined as $K_{1\mathrm{PD}} = \frac{K_{0\mathrm{PD}}}{1+j(2\pi fT_{\mathrm{PD}})} = |K_{1\mathrm{PD}}| \cdot \exp\left[-j\mathrm{Arg}(K_{1\mathrm{PD}})\right]$, in which we extract the module $|K_{1\mathrm{PD}}| = \frac{K_{0\mathrm{PD}}}{\left[1+(2\pi fT_{\mathrm{PD}})^2\right]^{1/2}}$, and the argument $\mathrm{Arg}(K_{1\mathrm{PD}}) = \mathrm{arctg}(2\pi fT_{\mathrm{PD}})$, where T_{PD} is the time constant of the photodetector.

3.3.4 The Transfer Function of the Fiber Optical System

The complex transfer function of the fiber optical system (FOS) on the amplitude of the field strength $E_{\mathrm{L}} = E_{0\mathrm{L}} \cdot \mathrm{Re}[\exp(j2\pi\nu \cdot t)]$, which acts in the FOS optical input, we define as a ratio of the amplitude on the FOS optical output $E_{0\mathrm{Lout}}$ to the

amplitude on the FOS optical input $E_{0\mathrm{Lin}}$. For this transfer function $K_{\mathrm{FOS}}(j2\pi\nu)$ the following expression is true: $K_{\mathrm{FOS}}(\ j2\pi\nu) = \frac{E_{0\mathrm{Lout}}}{E_{0\mathrm{Lin}}} = \frac{K_{\mathrm{FOS}}}{1+j(2\pi\nu T_{\mathrm{FOS}})}$, where T_{FOS} is the time constant of FOS. Let us extract the module $|K_{\mathrm{FOS}}(\ j2\pi\nu)| = \frac{K_{\mathrm{FOS}}}{\left[1+(2\pi f T_{\mathrm{FOS}})^2\right]^{1/2}}$, and the argument $\mathrm{Arg}[K_{\mathrm{FOS}}(j2\pi\nu)] = \arctan(2\pi f T_{\mathrm{FOS}})$.

We note that at examination of OEO, we consider FOS as nondispersion linear passive element, in which oscillations are delayed by the delay time T_{FOS}.

3.3.5 The Radio-Frequency Filter

In the OEO system, the narrowband high-Q RF filter is intended for filtering the one type of oscillation from the variety of possible oscillations. The transfer function of the radio-frequency filter on current can be defined as

$$K_{\mathrm{FE}} = \frac{I_{\mathrm{FEout}}}{I_{\mathrm{FEin}}} = \frac{(\ j2\pi f)(1/T_{\mathrm{eF}})}{(\ j2\pi f)^2 + (1/T_{\mathrm{eF}})(\ j2\pi f) + (2\pi f_{0\mathrm{e}})^2}, \tag{3.39}$$

where I_{FEout}, I_{FEin} are amplitudes of AC components of electric currents (the first harmonic) in output and input of electrical filter, relatively, δ_{e} is the damping factor of the RF filter: $\delta_{\mathrm{e}} = 1/T_{\mathrm{eF}} = f_{0\mathrm{e}}/f_{0\mathrm{e}}T_{\mathrm{eF}} = f_{0\mathrm{e}}/Q_{\mathrm{eF}}$, $T_{\mathrm{eF}} = T_{\mathrm{F}}$ is the filter time constant, Q_{eF} is the filter Q-factor, $f_{\mathrm{F0}} = f_{0\mathrm{e}}$ is the filter natural frequency, relatively.

3.3.6 The Nonlinear RF Amplifier in OEO

Let us consider the bipolar transistor amplifying stage on the common emitter (CE) scheme as the nonlinear amplifier. The static characteristics of the CE transistor are the input characteristics (the base electrode) $i_{\mathrm{B}} = f_{\mathrm{B}}(e_{\mathrm{B}})$ and the output characteristics (the collector electrode) $i_{\mathrm{C}} = f_{\mathrm{C}}(e_{\mathrm{C}})$. Here i_{B}, e_{B} are instantaneous values of the base current and voltage; i_{C}, e_{C} are instantaneous values of the collector current and voltage; I_{C0}, e_{C0} are DC components of the collector current and voltage; and I_{B0}, e_{B0}, are DC components of the base current and voltage.

Now we examine the mode, in which the harmonic signal acts at the transistor input (between base and emitter electrodes) at constant bias on the base and the collector. The static transfer characteristics in the CE stage have a form: $i_{\mathrm{C}} = f_{\mathrm{CB}}(u_{\mathrm{B}})$ and can be approximated by the polynomial of third order (for simplicity): $i_{\mathrm{C}} = \alpha u_{\mathrm{B}} - \beta u_{\mathrm{B}}^3$. The amplifier consisting of the series-connected transistor stages will have the total characteristic in the form of combination of nonlinearities. The difficulty of obtaining

the total, so-called, oscillating characteristic[4] is defined by existence of blocking interstage connections, which extracts the DC components of signals. In other words, if the first transistor "falls" into the nonlinear mode, we shall have the dependence of the DC component of the output voltage of the amplitude of the input signal, which will lead to the operating point displacement on the transfer characteristic. In the future, for simplicity sake, we consider the single amplifier stage with the transfer characteristic, $i_C = \alpha u_B - \beta u_B^3$. The transfer slope of the nonlinear amplifier can be defined as $S_{NA} = i_C/u_B = \alpha - \beta u_B^2$. Let the harmonic signal in the form $u_B = U_B \cos(\omega t - \phi_0)$, where U_B is the amplitude, ω, φ are frequency and phase, acts in the stage input. At that, the oscillating characteristic defined as the function of the first harmonic amplitude of the collector current $I_C = f(U_B)$, is obtained as the average value or as the ratio of the integral on $\xi = \omega t - \phi_0$ parameter to π, and it is equal:

$$I_K = \frac{1}{\pi} \int_{-\pi}^{\pi} \left[\alpha u_B \cos\xi - \beta(u_B \cos\xi)^3\right] \cos\xi d\xi = \alpha U_B - (3/4)\beta U_B^3. \quad (3.40)$$

The average (during the period) slope on the first harmonic amplitude can be defined as: $S_{NA1} = I_C/U_B = \alpha - (3/4)\beta U_B^2$. In the general case, the active element (AE) can be inertial. The expression for the instantaneous value of the u_{PD} voltage in the PD output or in the NA input can be written in the form: $u_{PD} = K_{PD} E_{0L}^2 K_{FODL} U_{0M} \exp(j2\pi f_0 t)$, where the transfer function K_{FOLD} is defined as

$$K_{FODL} = K_{PD} M_Z^2 B_{1M} \exp[j2\pi f_0 (T_{FOS} + T_{1M} + \Delta T_M/2)] \quad (3.41)$$

where T_{2M}, T_{1M} are delays in the optical channels OC2 and OC1, relatively, in the MZ modulator T_{2M}, $\Delta T_M = T_{1M} - T_{2M}$.

The expression for the instantaneous value of NA output voltage u_{NA} or in the input of RF filter can be written as: $u_{NA} = S_{NA}\left[E_{0L}^2 K_{BLZ} u_{PD}(t - T_{FOS})\right]$.

3.3.7 The Feedback Network in OEO

3.3.7.1 The Positive Feedback Network in OEO (Spanned a Laser)

The series-connected fiber optical system (FOS) including in general case the optical filters, the optical amplifiers and the optical modulators, the photodetector, the nonlinear RF amplifier, and the RF filter with the natural frequency and the

[4]Under "oscillating characteristic" of the RF amplifier we understand the function of the *first harmonic* of the output (collector) current versus the amplitude of the *first harmonic* of input (base) voltage.

directional coupler are included in the positive feedback network covering the QWLD in OEO.

The transfer function of the feedback network K_{FBN} can be defined as:

for OEO DM: $K_{\mathrm{FBN}} = i_{\mathrm{mod}}/E_{\mathrm{L}}^2$,
for OEO MZ: $K_{\mathrm{FBN}} = u_{\mathrm{mod}}/E_{\mathrm{Lin}}^2$,

where E_{L}^2 is the normalized squared strength in the QWLD output, which is equal in magnitude to the value in the FOS input, i_{mod} is the AC current modulation component in the QWLD in the OEO DM and u_{mod} is the AC voltage modulation component in the MZ input on the OEO MZ structure.

3.4 Equations of Amplitude and Phase Balance for the Laser and for OEO

Before operations with OEO differential equations, let us analyze the OEO operation on the base of the stationary (steady-state) algebraic equations, which are called in the theory of nonlinear oscillations as the equations of *amplitude and phase balance* (APB). Simplified structural (blocks) representation of the laser and complete OEO structures, shown in Fig. 3.2, gives us a possibility to form the APB equations.

3.4.1 Equations of Amplitude and Phase Balance for the Laser

The laser including in the OEO structure is formed by the closed in the loop of optical nonlinear amplifier OA, the narrowband optical filter OF, and the fiber optical delay line (RF FODL) in the form of lengthy (0.3 mm to 1 m) optical channel. The optical oscillation frequency $\nu_{0\mathrm{L}}$, which is generated by the laser in the free steady-state mode, can be obtained (of course, at satisfaction of the self-oscillation conditions) from the solution of the amplitude and phase balance equations for steady-state optical oscillations of the field strength in the optical resonator and in the active laser element:

$$\begin{cases} K_{\mathrm{OA}}(\nu)K_{\mathrm{OF}}(\nu)K_{\mathrm{FOS}}(\nu) = 1, \\ \varphi_{\mathrm{OA}}(\nu) + \varphi_{\mathrm{OF}}(\nu) + \varphi_{\mathrm{FOS}}(\nu) = -2\pi n \end{cases}, \tag{3.42}$$

where $K_{\mathrm{OA}}(\nu)$, $\varphi_{\mathrm{OA}}(\nu)$ are the module (AFC), and the argument (PFC) of the optical amplifier; $K_{\mathrm{OF}}(\nu)$, $\varphi_{\mathrm{OF}}(\nu)$ are the module (AFC) and the argument (PFC) of the optical filter with the natural frequency $\nu_{0\mathrm{OF}}$ and with the time constant T_{OF}; $K_{\mathrm{FOS}}(\nu)$, $\varphi_{\mathrm{FOS}}(\nu)$ are the module (AFC) and the argument (PFC) of the other laser

part (the optical channel of the laser resonator) apart of the optical filter and the nonlinear optical amplifier, $n = 1, 2, \ldots$.

At satisfaction of self-excitement conditions, the emission is generated on the laser output, which EMF strength is equal: $E_{\mathrm{L}}(t) = E_{0\mathrm{L}} \cos(2\pi\nu_{0\mathrm{L}} t + \varphi_{0\mathrm{L}})$.

3.4.2 Equations of Amplitude and Phase Balance for the RF Part of OEO DM and OEO MZ

3.4.2.1 OEO MZ in the "First Harmonic" Mode

Determination of the generated radio frequency $2\pi f$ in the RF part of OEO MZ can be explained from the equations of the amplitude and phase balance of the steady-state auto-modulated oscillations as:

$$\begin{cases} K_{\mathrm{L}}(f, U_{0\mathrm{MZ}}, \nu_{0\mathrm{L}}) K_{\mathrm{FOS}}(f) K_{\mathrm{PD}} K_{\mathrm{EF}}(f) K_{\mathrm{EA}}(f) = 1, \\ \varphi_{1\mathrm{MZ}}(f, U_{0\mathrm{MZ}}, \nu_{0\mathrm{L}}) + \varphi_{\mathrm{FOS}}(f) + \varphi_{\mathrm{PD}}(f) + \varphi_{\mathrm{EF}}(f) + \varphi_{\mathrm{EA}}(f) = -2\pi m \end{cases}, \tag{3.43}$$

where $K_{1\mathrm{MZ}}(f)$, $K_{\mathrm{FOS}}(f)$, K_{PD}, $K_{\mathrm{EF}}(f)$, $K_{\mathrm{EA}}(f)$ are the modules (AFC), relatively, of the MZ modulator, the fiber optical system, the photodetector, the RF filter, the RF amplifier; $\varphi_{1\mathrm{MZ}}(f)$, $\varphi_{\mathrm{FOS}}(f)$, $\varphi_{\mathrm{PD}}(f)$, $\varphi_{\mathrm{EF}}(f)$, $\varphi_{\mathrm{EA}}(f)$ are arguments (PFC), relatively, of the MZ modulator, the fiber optical system, the photodetector, the RF filter, the RF amplifier; $U_{0\mathrm{MZ}}$ is DC bias voltage of MZ; $\nu_{0\mathrm{L}}$ is the optical laser frequency, $m = 1, 2, \ldots$.

If the self-excitation conditions are satisfied in the closed loop, the oscillation will be generated on the OEO electrical output, which voltage (or current) is: $U_{\mathrm{e}}(t) = U_{0\mathrm{e}} \cos(2\pi f_{0\mathrm{e}} t + \phi_{0\mathrm{e}})$ where $U_{0\mathrm{e}}$ is the amplitude, $f_{0\mathrm{e}}$ is the average optical generated frequency, $\phi_{0\mathrm{e}}$ is the constant initial phase shift. In this case, we do not take into consideration the amplitude and phase fluctuations m_{e} and ψ_{me}.

3.4.2.2 OEO DM in the "First Harmonic" Mode

The system of AFB equations for OEO DM in the "first harmonic" mode can be written in the similar manner as for OEO MZ:

$$\begin{cases} K_{\mathrm{L}}(f, J_0, \nu_{0\mathrm{L}}) K_{\mathrm{FOS}}(f) K_{\mathrm{PD}} K_{\mathrm{EF}}(f) K_{\mathrm{EA}}(f) = 1, \\ \varphi_{\mathrm{L}}(f, J_0, \nu_{0\mathrm{L}}) + \varphi_{\mathrm{FOS}}(f) + \varphi_{\mathrm{PD}}(f) + \varphi_{\mathrm{EF}}(f) + \varphi_{\mathrm{EA}}(f) = -2\pi m, \end{cases} \tag{3.44}$$

where $K_{\mathrm{L}}(f, J_0, \nu_{0\mathrm{L}})$, $K_{\mathrm{FOS}}(f)$, K_{PD}, $K_{\mathrm{EF}}(f)$, $K_{\mathrm{EA}}(f)$ are modules (AFC), relatively, of the MZ modulator, the fiber optical system, the photodetector, the RF filter, the RF amplifier; $\varphi_{1\mathrm{L}}(f, J_0, \nu_{0\mathrm{L}})$, $\varphi_{\mathrm{FOS}}(f)$, $\varphi_{\mathrm{PD}}(f)$, $\varphi_{\mathrm{EF}}(f)$, $\varphi_{\mathrm{EA}}(f)$ are arguments (PFC),

relatively, of the laser modulator, the fiber optical system, the photodetector, the RF filter, the RF amplifier, J_0 is the DC current of the laser pumping, ν_{0L} is the laser optical frequency, $m = 1, 2, \ldots$.

The diagram for determination of the QWLD frequency of generation and RF frequency of generation frequency is shown in Fig. 3.17a, b for OEO DM.

From Fig. 3.17a, b, we see that the increase of the pumping current leads to appearance of the laser generation and radio-frequency generation at fulfillment of amplitude and balance equations. These equations allow determination of frequency and amplitude dependence for the laser and for OEO of the pumping current and system parameters in the steady-state mode. APB equations cannot solve the issues of dynamics, excitation and phase noises. Therefore, we must pass to formation of differential equations (DE) on the base on the structural block model.

3.4.3 *Differential Equations of OEO MZ with the Single Optical Fiber*

In this section, we pay the main attention to the effects of laser and MZ modulator parameters on OEO operation. Therefore, we assume in this section that all RF networks are wideband besides the RF narrowband filter (F in Fig. 3.2c) in order to accent the OEO properties related to MZ modulator and the laser. We do not take into consideration the photodetector and amplifier lags and suppose that the directional coupler C represents the ideal ("without electrical power reflection") connector with the transfer function (from input to output connected with the electrical input of MZ modulator) close to 1. The PD load and the internal resistance of the MZ electrical input are supposed to be active (we assume that the reactive component of the complex load impedance is equal to zero). In RF networks, the complete matching occurs from PD to the MZ electric input (i.e., the standing-wave ratio in networks is zero). To the optical PD input, the delayed laser emission $(E_{12L})^2$ passes:

$$E_{12L}^2 = E_{01L}^2\left(1+\gamma^2\right) + \gamma 0.5\, E_{01L}^2 \cos\left[\left(\pi U_{0MZ}/2U_{0MZ\pi}\right) - \left(U_{10MZ}/U_{0MZ\pi}\right)\cos\left(2\pi ft + \varphi_{0L}\right)\right]. \tag{3.45}$$

Figure 3.17a–c shows the total amplitude-frequency characteristic, $K_{OA} \cdot K_{OF}$ (Fig. 3.17a) of the laser optical amplifier and the optical filter, as well as the phase-frequency characteristics of the optical amplifier φ_{OA} and the optical filter φ_{OF} (Fig. 3.17b) for different values of the laser pumping current excess over its threshold value $A_0 = J_{0L}/J_{0Lth}$ (curve 1 corresponds to $A_0 = 1.5$, curve 2—$A_0 = 3$, curve 3—$A_0 = 5$).

The graphical solutions for obtaining the laser steady-state frequency for the pumping current $A_0 = 5$ (curve 3) are shown in Fig. 3.17c. The point of the

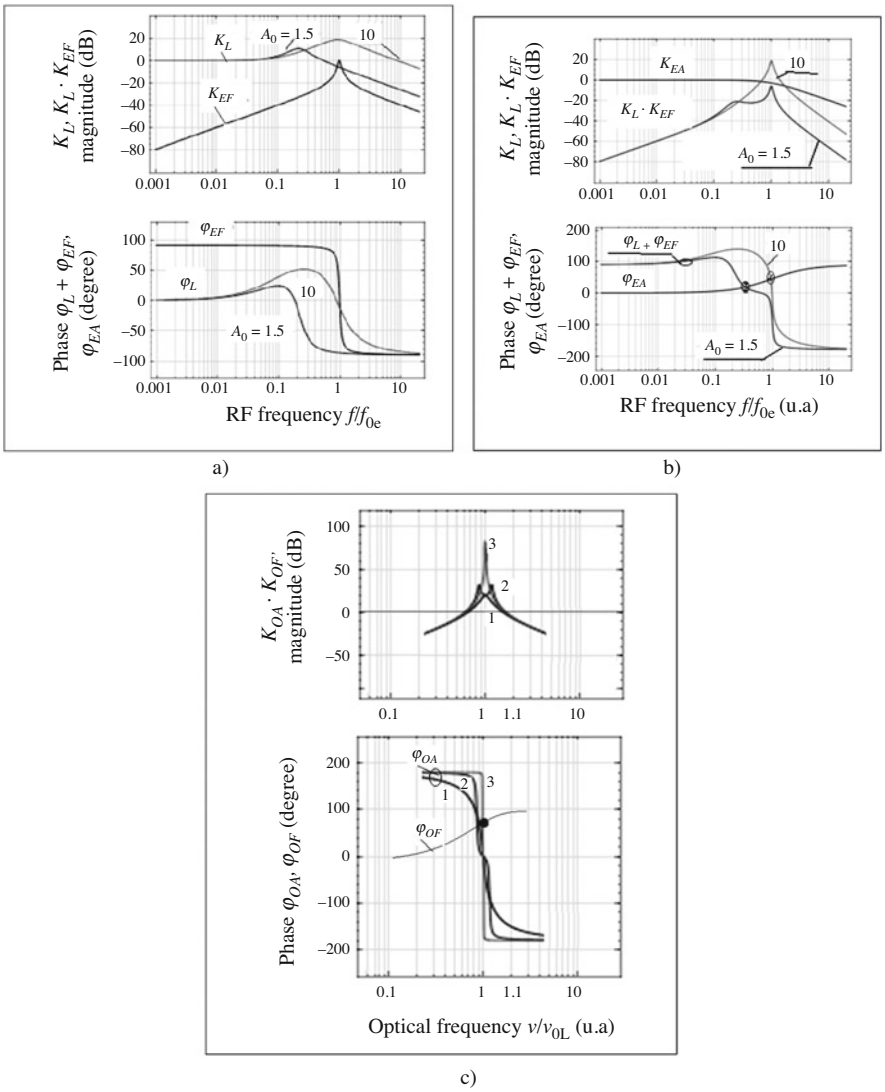

Fig. 3.17 The example of the graphical solution of APB equation for OEO DM. (**a**) The module K_L and the argument φ_L of QWLD for two excess values $A_0 = J_{0L}/J_{0Lth}$ ($A_0 = 1.5$; 10) of the pumping (bias) current J_{0L} above the threshold value J_{0Lth}, and also the module K_{EF} and the argument φ_{EF}. (**b**) The module $K_L \cdot K_{EF}$ and the argument $\varphi_L + \varphi_{EF}$ for $A_0 = 1.5$; 10. The module K_{EA} and the argument φ_{EA}. The normalized frequency f/f_{0e}, which is 1, corresponds to the natural frequency of the RF filter. (**c**) The example of graphical solution of APB equations for the laser in OEO. The module and the argument of the gain for QWLD with the resonator Q-factor of 100 at different pumping current. The module and the argument of the optical channel of the laser. Normalized frequency ν/ν_{0L}, which is 1, corresponds to the natural frequency of the optical filter

steady-state frequency can be found at the solution of the phase and amplitude balance equations (Eq. 3.44). At that, the laser generation frequency (the intercept point of plots φ_{OA} and φ_{OF} is shown by the point in Fig. 3.17c) slightly exceeds the value of the own natural resonance frequency.

Let us represent the instantaneous values of voltages (Fig. 3.2c) $u_{PD}(t)$, $u_F(t)$, $u_A(t)$, $u_C(t)$ in the time form: for MZ input $u_{MZ} = U_{10MZ}\,\mathrm{Re}[\exp(j2\pi ft - \Phi_{MZ})]$; for PD output $u_{PD} = U_{10PD}\,\mathrm{Re}[\exp(j2\pi ft - \Phi_{PD})]$; for RF filter output $u_F = U_{10F}\,\mathrm{Re}[\exp(j2\pi ft - \Phi_F)]$; for amplifier output $u_A = U_{10A}\,\mathrm{Re}[\exp(j2\pi ft - \Phi_A)]$; for coupler output $u_C = U_{10C}\,\mathrm{Re}[\exp(j2\pi ft - \Phi_C)]$; where U_{10MZ}; U_{10PD}; U_{10F}; U_{10A}; U_{10C} are amplitudes of the first harmonics, Φ_{MZ}; Φ_{PD}; Φ_F; Φ_A; Φ_C are the appropriate phase incursions.

We designate[5] as $\boldsymbol{U}_{MZ}$, $\boldsymbol{U}_{PD}$, $\boldsymbol{U}_F$, $\boldsymbol{U}_A$, $\boldsymbol{U}_C$ the complex quantities of the appropriate variables of $u_{PD}(t)$, $u_F(t)$, $u_A(t)$, $u_C(t)$. We introduce the complex transfer function of RF FODL $\boldsymbol{K}_{FODL}$: $\boldsymbol{K}_{FODL} = \boldsymbol{U}_{PD}/\boldsymbol{U}_{MZ} = |K_{FODL}|\exp(-j2\pi fT_{FOS} - j\Phi_{FOS})$, where T_{FOS} is the delay time in the optical fiber system, Φ_{FOS} is the PFC of FODL without account of the phase incursion in FOS, $|K_{FODL}|$ is the module of RF FODL transfer function. Let us introduce the complex transfer functions for blocks F, A, C, relatively, $\boldsymbol{K}_F$, $\boldsymbol{K}_A$, $\boldsymbol{K}_C$: $\boldsymbol{K}_F = \boldsymbol{U}_F/\boldsymbol{U}_{PD}$; $\boldsymbol{K}_A = \boldsymbol{U}_A/\boldsymbol{U}_F$; $\boldsymbol{K}_C = \boldsymbol{U}_{MZ}/\boldsymbol{U}_A$.

At that, for the RF filter F, we have:

$$\boldsymbol{K}_F = \boldsymbol{U}_F/\boldsymbol{U}_{PD} = (j\omega)(1/T_{EF})/\left[(j\omega)^2 + (1/T_{EF})(j\omega) + (2\pi f_{0e})^2\right], \tag{3.46}$$

where the current oscillation frequency $\omega = 2\pi f$, δ_e is loss in the RF filter, $\delta_e = 1/T_{EF} = f_{0e}/f_{0e}T_{EF} = f_{0e}/Q_{EF}$, T_{EF} is the time constant of the RF filter, Q_{EF} is the filter Q-factor, $f_{F0} = f_{0e}$ is the natural or resonance frequency of the RF filter (or the resonance circuit), relatively. We take the single "ideal" (i.e., without influence account of the output voltage of the stage on the current at the stage input) non-inertial amplifying stage as the RF amplifier A (Fig. 3.2c). At that, the tube triode connected on the common anode scheme (or the stage on the field-effect transistor (FET) connected on the common source scheme) can be such an ideal amplifying stage. For the amplifying stage, we neglect the electron inertia, the reaction of the grid current (input current) upon the RF filter (circuit) and the anode reaction.

Then the OEO generator equation (Fig. 3.2c), which connects the instantaneous values of the amplifier input voltage u_{PD} and the output current $i_A(u_{PD})$, can be written as

$$y(j\omega)u_{PD} = i_A(u_{PD}), \tag{3.47}$$

[5]Hereinafter, we shall designate the complex amplitudes (input and output) of currents, voltages and the complex functions by the bold symbols.

where $y(j\omega)$ is the control symbolic conductivity, which is (for the typical RF oscillator) the ratio of the symbolic load conductivity y_1 to the feedback coefficient k_{fb}; $\omega = 2\pi f$, $j\omega$ is the symbolic operator of differentiation[6] [14]. Having introduced the time constant T_{EF} and the natural frequency $f_{0\text{e}}$ for the RF filter F (Fig. 3.2c), we can write for the symbolic load conductance y_1 of the A amplifier the following expression:

$$y_1(j\omega) = \left[(j\omega)^2 + (1/T_{\text{EF}})(j\omega) + (2\pi f_{0\text{e}})^2\right]/[(j\omega)(1/T_{\text{EF}})]. \tag{3.48}$$

If we will combine Eq. (3.47) and Eq. (3.48) and change the symbolic operator $j\omega$ to the differentiation operator in the time domain d/dt and $(j\omega)^2$ to d^2/dt^2, we shall have the differential nonlinear equation of the second order.

Now we take into consideration that in our structural diagram the feedback coefficient k_{fb} is the transfer function of RF FODL, i.e., $\boldsymbol{k}_{\text{fb}} = \boldsymbol{K}_{\text{FODL}} = \boldsymbol{U}_{\text{PD}}/\boldsymbol{U}_{\text{MZ}}$.

For simplicity, we assume that the module of the RF FODL transfer function is constant and equal to $K_{0\text{FODL}}$, and then $K_{0\text{FODL}} = E_{0\text{L}}^2 K_{\text{FODL}}$. We take into consideration that the directional coupler C has the transfer function on the voltage and the current, which is 1, then $u_{\text{F}} \approx u_{\text{MZ}}$. Having considered $j\omega$ as the differentiation operator d/dt, we write the OEO equation in the operator:

$$\left[p^2 + (1/T_{\text{EF}})p + (2\pi f_{0\text{e}})^2\right] u_{\text{MZ}} = (1/T_{\text{EF}}) K_{0\text{FODL}} p i_{\text{A}}(u_{\text{PD}}) \exp(-pT_{\text{FOS}}); \tag{3.49}$$

and in the time domain:

$$\frac{\text{d}^2 u_{\text{MZ}}}{\text{d}t^2} + \frac{1}{T_{\text{EF}}} \cdot \frac{\text{d}u_{\text{MZ}}}{\text{d}t} + (2\pi f_{\text{F0}})^2 u_{\text{MZ}} = (1/T_{\text{EF}}) K_{0\text{FODL}} \frac{\text{d}i_{\text{A}}(u_{\text{PD}} - T_{\text{FOS}})}{\text{d}t}. \tag{3.50}$$

As it was shown earlier, at the choice of the operating point, the function of AC component of the MZ output emission power versus the u_{MZ} voltage or the function of AC component of FODL output voltage $u_{\text{PD}} = f(u_{\text{MZ}})$ is close to linear function, if the MZ modulator operates "in quadrature" at small amplitude of electric voltage in its electrical input. Figure 3.15 shows functions of the DC component of the optical emission and the AC component of the fundamental harmonic in the MZ output. Numbers "1" and "2" mark the values at constant relative DC bias voltage in the "quadrature" and "non-quadrature" modes. They are equal relatively 0.5 and 1.0 and corresponds in Fig. 3.15 to the phase $\varphi_{0\text{MZ}} = \frac{\pi U_{0\text{MZ}}}{U_{0\text{MZ}\pi}} = \pi/2$ and π, relatively.

The MZ function becomes nonlinear, for instance, at large oscillation amplitude in the MZ input at constant bias equaled to "π."

[6]Detailed information about the Evtianov method and about abbreviation of the differential equations you can find in the book Komarov I.V., Smolskiy S.M. *Fundamentals of Short-Range FM Radar*. Norwood: Artech House, 2003. DOI: 10.1109/MAES.2004.1346903.

For simplicity sake, we consider OEO as the generator with the single nonlinear element, i.e., in our oscillator structure, the only one nonlinear is present. We analyze two variants of modes. In the first mode, we consider that the OEO nonlinearity is present only in the RF amplifier, and "small amplitude oscillations" pass at the electrical input of the MZ modulator and the MZ modulator operates "in quadrature." In the second mode, the RF amplifier A operates in the linear mode with amplification, and the nonlinear MZ characteristic $i_{PD} = f(u_{MZ})$ is used as the OEO nonlinearity.

3.4.3.1 The Nonlinear Element Is the RF Amplifier A

The instantaneous value of the output current of the amplifying stage is equal to $i_A = \left(\alpha_e u_{PD} - \beta_e u_{PD}^3\right)$, where u_{PD} is the instantaneous values of the input voltage, which coincides with the voltage on the PD output. Then the nonlinear dependence of the i_A current and differential equation (Eq. 3.50) in time domain are written as: $i_A = \left(\alpha_e u_{PD} - \beta_e u_{PD}^3\right)$.

3.4.3.2 The Nonlinear Element Is the Mach–Zehnder Modulator

The instantaneous output PD voltage is equal $u_{PD} = R_{PD} i_{PD}$, where i_{PD} is the instantaneous "output" photocurrent of PD, R_{PD} is the active load resistance of PD. The nonlinear function $i_{PD} = f(u_{MZ})$ takes a form:

$$i_{PD} = 0.5\gamma (E_{0L})^2 K_{0FOS.MZ} \cos\left[(\pi U_{0MZ}/2U_{0MZ\pi}) - u_{MZ}\right] \tag{3.51}$$

and Eq. (3.50) in the time domain is written as: $i_A = \alpha_e R_{PD} i_{PD} - \beta_e (R_{PD} i_{PD})^3$.

Equation (2.50) is a nonlinear differential equation of the second order. For arbitrary nonlinearities they cannot be solved in general case, for the specific cases (for instance, the high Q-factors) these equation can be simplified or "abbreviated" till the one order less.

3.4.3.3 Abbreviated Equations of OEO MZ with the Single Optical Fiber

In order to obtain the abbreviated equations of OEO MZ with the single optical fiber, we write differential equations for OEO in operator form:

$$\left[p^2 + (1/T_{\text{EF}})p + (2\pi f_{0\text{e}})^2\right] u_{\text{MZ}} = (1/T_{\text{EF}}) K_{0\text{FODL}} p i_{\text{A}}(u_{\text{PD}}) \exp(-j2\pi f_{0\text{e}} T_{\text{FOS}}); \tag{3.52}$$

in which the instantaneous voltage on the load resistance R_{PD} of PD is $u_{\text{PD}} = R_{\text{PD}} \cdot i_{\text{PD}}$, and the instantaneous PD current i_{PD} is

$$i_{\text{PD}} = 0.5\,(E_{0\text{L}})^2 K_{0\text{FOS.MZ}} \cos\left[\pi(U_{0\text{MZ}} - u_{\text{MZ}})/2U_{0\text{MZ}\pi})\right], \tag{3.53}$$

where $(E_{0\text{L}})^2$ is the power of laser emission, $U_{0\text{MZ}}$ is the DC bias voltage of the MZ modulator, and $K_{0\text{FOS.MZ}}$ is the FODL transfer function on the frequency $f_{0\text{e}}$.

Following the Evtianov approach to abbreviation of differential equations [14, 15], in the first approximation for slowly changing amplitude $U_{10\text{MZ}}$ and phase Φ_{MZ} of oscillations in the OEO output we have: $u_{\text{MZ}} = U_{10\text{MZ}}$ Re[exp $(j2\pi ft - \Phi_{\text{MZ}})$].

Let us perform a normalization dividing the right and left parts of Eq. (3.52) equation by $(2\pi f_{0\text{e}})^2$, $p/(2\pi f_{0\text{e}})$, and introduce the Q-factor $Q_{\text{EF}} = T_{\text{EF}} \cdot f_{0\text{e}}$:

$$\frac{\left[(p/2\pi f_{0\text{e}})^2 + (1/Q_{\text{EF}}) \cdot (p/2\pi f_{0\text{e}}) + 1\right] u_{\text{MZ}}}{(p/2\pi f_{0\text{e}})} = \frac{K_{0\text{FODL}}}{Q_{e\text{F}}} i_{\text{A}}(u_{\text{PD}}) \exp(-j2\pi f_{0\text{e}} T_{\text{FOS}}); \tag{3.54}$$

According to Evtianov method, we must find the biased operator. In order to obtain the abbreviated differential equations of the first approximation, it is necessary [14]: to represent a solution in the form of harmonic oscillation with slowly changing amplitude and phase and to substitute it into the initial Eq. (3.47) or (3.54). The current should be represented by the Fourier series keeping on the right the main harmonic only. Then we use the bias theorem of the operation calculus; then we expand the biased operators in the Taylor on $p/(2\pi f_{0\text{e}})$, keeping the first (nonzero) terms in this expansion.

We choose $2\pi f_{0\text{e}}$ as the reference frequency. Replacing p to $j2\pi f_{0\text{e}} + p_1$, combining terms in groups according to the smallness order, keeping only the first order of smallness terms, we obtain the expression for the abbreviated conductance in the first approximation in the left part of Eq. (3.54) [14]:

$$\frac{\left[(p/2\pi f_{0\text{e}})^2 + (1/Q_{\text{EF}})(p/2\pi f_{0\text{e}}) + 1\right]}{(p/2\pi f_{0\text{e}})} \overset{j2\pi f_{0\text{e}}+p_1}{\rightarrow} \left(\frac{1}{Q_{\text{EF}}} + 2p_1\right) \tag{3.55}$$

where the arrow "$\overset{j2\pi f_{0\text{e}}+p_1}{\rightarrow}$" designates the representation of the control conductance in the abbreviated form. At abbreviation, we expand the current in the right part $I_{1\text{A}}$ into in-phase and quadratic components:

$$i_{\mathrm{A}}(u_{\mathrm{PD}})\exp\left(-j2\pi f_{0\mathrm{e}}T_{\mathrm{FOS}}\right) \overset{j2\pi f_{0\mathrm{e}}+p_1}{\longrightarrow} \times\left[I_{1\mathrm{A}}\cos\left(2\pi f_{0\mathrm{e}}T_{\mathrm{FOS}}\right)+jI_{1\mathrm{A}}\sin\left(2\pi f_{0\mathrm{e}}T_{\mathrm{FOS}}\right)\right] \tag{3.56}$$

Now we write the abbreviated equation of the first approximation

$$\left(\frac{1}{Q_{\mathrm{EF}}}+2p_1\right)\cdot\exp\left[j\Phi_1\right]\cdot U_{10\mathrm{MZ}}=\frac{K_{0\mathrm{FODL}}}{Q_{\mathrm{EF}}} \times\left\{I_{1\mathrm{A}}\cos\left[2\pi f_{0\mathrm{e}}T_{\mathrm{FOS}}\right]+jI_{1\mathrm{A}}\sin\left[2\pi f_{0\mathrm{e}}T_{\mathrm{FOS}}\right]\right\} \cdot\exp\left[j\Phi_1\right] \tag{3.57}$$

Performing differentiation and separation of real and imaginary parts, we have system of two real equations:

$$\begin{cases}\left(\dfrac{1}{Q_{\mathrm{EF}}}+2p_1\right)\cdot U_{10\mathrm{MZ}}=\dfrac{K_{0\mathrm{FODL}}}{Q_{\mathrm{EF}}}\cdot I_{1\mathrm{A}}\cos\left[2\pi f_{0\mathrm{e}}T_{\mathrm{FOS}}\right],\\ 2U_{10\mathrm{MZ}}p_1\Phi_1=\dfrac{K_{0\mathrm{FOLD}}}{Q_{\mathrm{EF}}}\cdot I_{1\mathrm{A}}\sin\left[2\pi f_{0\mathrm{e}}T_{\mathrm{FOS}}\right])\end{cases} \tag{3.58}$$

Let us write equations in the time domain replacing p_1 by d/dt:

$$\begin{cases}\dfrac{\mathrm{d}U_{10\mathrm{MZ}}}{\mathrm{d}t}=2\pi f_{0\mathrm{e}}\dfrac{K_{0\mathrm{FODL}}}{2Q_{\mathrm{EF}}}I_{1\mathrm{A}}\cos\left[2\pi f_{0\mathrm{e}}T_{\mathrm{FOS}}\right]-2\pi f_{0\mathrm{e}}\cdot\dfrac{U_{10\mathrm{MZ}}}{2Q_{\mathrm{EF}}}\\ \dfrac{\mathrm{d}\Phi_{10\mathrm{MZ}}}{\mathrm{d}t}=2\pi f_{0\mathrm{e}}\dfrac{K_{0\mathrm{FODL}}}{2Q_{\mathrm{EF}}}\dfrac{I_{1\mathrm{A}}}{U_{10\mathrm{MZ}}}\sin\left[2\pi f_{0\mathrm{e}}T_{\mathrm{FOS}}\right])\end{cases} \tag{3.59}$$

where $I_{1\mathrm{A}}=(S_{1\mathrm{A}}/2U_{0\mathrm{MZ}\pi})\sin[\pi(U_{0\mathrm{MZ}}-U_{10\mathrm{MZ}})/(2U_{0\mathrm{MZ}\pi})]$.

The first Eq. (3.59) defines the oscillation amplitude transient, while the second Eq. (3.59) defines the frequency amendment in the first approximation. The system of Eq. (3.59) allows determination of the amplitude $U_{10\mathrm{MZ}}$ upon the generated frequency.

3.4.3.4 Amplitude and Frequency in OEO MZ in the Steady State

In the steady state, $\frac{\mathrm{d}U_{10\mathrm{MZ}}}{\mathrm{d}t}=0$ and $\frac{\mathrm{d}\Phi_{10\mathrm{MZ}}}{\mathrm{d}t}=0$ and we have the system of equations two algebraic equations:

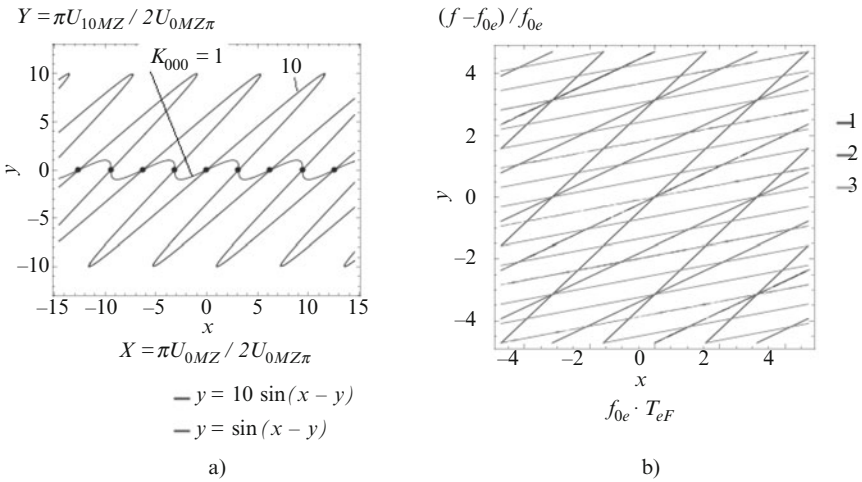

Fig. 3.18 Dependence of normalized amplitude Y of the first harmonic versus the constant bias voltage of MZ X (**a**) and the oscillation frequency of OEO (**b**)

$$\begin{cases} U_{10\mathrm{MZ}} = K_{0\mathrm{FODL}}(S_{1\mathrm{A}}/2U_{0\mathrm{MZ}\pi}) \cos[2\pi f_{0\mathrm{e}} T_{\mathrm{FOS}}] \cdot \sin[\pi(U_{0\mathrm{MZ}} - U_{10\mathrm{MZ}})/2U_{0\mathrm{MZ}\pi}], \\ \sin[2\pi f_{0\mathrm{e}} T_{\mathrm{FOS}}] = 0. \end{cases} \tag{3.60}$$

The first equation of the system (Eq. 3.60), at introducing of the following variables $X = \pi U_{0\mathrm{MZ}}/2U_{0\mathrm{MZ}\pi}$, $Y = \pi U_{10\mathrm{MZ}}/2U_{0\mathrm{MZ}\pi}$, $K_{000} = K_{0\mathrm{FODL}} \cdot (S_{1\mathrm{A}}/2U_{0\mathrm{MZ}\pi}) \cdot \cos[2\pi f_{0\mathrm{e}} T_{\mathrm{FOS}}]$, has a form $X = K_{000} \cdot \sin(X - Y)$, and can be solved graphically (Fig. 3.18). The second equation defines the grid of possible frequencies f of OEO together with APB equations ($m = \pm 1, 2, \ldots$):

$$(f - f_{0\mathrm{e}})/f_{0\mathrm{e}} \cong \left(\frac{m + f_{0\mathrm{e}} \cdot T_{\mathrm{EF}}}{T_{\mathrm{FOS}} + T_{\mathrm{EF}}} - f_{0\mathrm{e}}\right)/f_{0\mathrm{e}} \tag{3.61}$$

Figure 3.18a shows plots depicted at solution of the equation $X = K_{000} \cdot \sin(X - Y)$ at the values $K_{000} = 1$; 10. In Fig. 3.18b, the plots are presented, which are calculated on Eq. (3.61). Possible deviations of the generation frequency $(f - f_{0\mathrm{e}})/f_{0\mathrm{e}}$ are given at three different values of delay $T_{\mathrm{FOS}} = T_{\mathrm{BZ}}$ in the optical fiber: curves 1 corresponds to $T_{\mathrm{BZ}}/T_{\mathrm{eF}} = 1$; curves 2—$T_{\mathrm{BZ}}/T_{\mathrm{eF}} = 2$; curves 3—$T_{\mathrm{BZ}}/T_{\mathrm{eF}} = 5$.

In the similar manner, we can obtain the abbreviated differential equations for OEO with the active element nonlinear characteristic $i(u) = S_{01}u - S_{03}u^3$. For mentioned nonlinear characteristic (the average slope on the first harmonic $S_1(U) = S_{01} - (3/4)S_{03}U^2$) we obtain the expression for amplitude $U_{10\mathrm{MZ}}$ of oscillations in OEO MZ:

$$U_{10\mathrm{MZ}} = \sqrt{4S_{01}/3S_{03}} \cdot \left(1 - \frac{1}{S_{01}P_{0\mathrm{L}} \cdot R_{\mathrm{FD}}|K_{\mathrm{FODL}}|}\right)^{1/2} \tag{3.62}$$

If the transfer functions of MZ optical channels $k_{01} = A$ and $k_{02} = B = 1 - A$ are equal about 0.5, the irregularity coefficient of MZ channels' excitation $\gamma \approx 1$, the formula for radio-frequency deviations $\Delta f = \Delta f_{\mathrm{gen}}$ at OEO generation from its average value at variation of the optical frequency of the laser $\Delta\nu$ can be written in the form:

$$\Delta f_{\mathrm{gen}} \cong \frac{m + f_{\mathrm{EF}} \cdot T_{\mathrm{EF}}}{\frac{T_{2\mathrm{MZ}}+T_{1\mathrm{MZ}}}{2} + \frac{T_{2\mathrm{MZ}}-T_{1\mathrm{MZ}}}{2} \cdot (1-\gamma) \cdot \frac{\Delta\nu}{f_{\mathrm{F}}} + T_{\mathrm{eMZ}} + T_{\mathrm{FOS}} + T_{\mathrm{EF}}} \tag{3.63}$$

From Eq. (3.63), the one important OEO features follows: the dependence of radio-frequency deviations Δf versus deviations of the laser optical generation frequency $\Delta\nu$ will be less at lesser delay differences in optical channels $T_2 - T_1$, at lesser ratio of optical frequency deviations from the average frequency $\Delta\nu/f_{\mathrm{EF}}$, at lesser difference in transfer functions of optical channels $k_{01} = A$ and $k_{02} = B = 1 - A$, i.e., $\gamma \approx 1$, $(1 - \gamma) \approx 0$, and at larger the T_{EF} time constant and at larger the delay time in FOS T_{FOS}.

Figure 3.19 shows the graphical solution for the OEO steady-state mode. Point are shown determination of the OEO generation frequency as point of interception of two functions: the PFC of the resonance circuit and the PFC of the optical fiber under condition of amplitude balance fulfillment. The generation frequency in the OEO steady-state mode defines its amplitude.

3.4.3.5 Resonance Characteristics of OEO with Nonlinearity in the Form of Cosine

OEO investigation and analysis with the nonlinearity in the form of cosine will be performed using the symbolic equations (Eq. 3.49) and replacing the operator $p/2\pi f_{0\mathrm{e}}$ by $s = j(f/f_{0\mathrm{e}})$, where $j = \sqrt{-1}$. Such a replacement means the transition to the normalized generation frequency of OEO, which is represented on the complex parameter plane along the abscissa axis.

Let us perform the replacement of the normalized current i_{A}, $x = U_{1\mathrm{MZ}}/U_{0\mathrm{MZ}\pi}$, which will be represented along the ordinate axis. Then the solution of the algebraic equation in the form

$$\left[s^2 + (1/Q_{\mathrm{eF}}) \cdot s + 1\right] \cdot x = (K_{0\mathrm{FODL}}/Q_{\mathrm{EF}}) \cdot s \cdot \cos\left[(m_{00}\pi/2) + \beta_{00}x\right]; \tag{3.64}$$

depends upon two variables s and x and constant parameters $K_{0\mathrm{FODL}}$, Q_{EF}, $m_{00}\pi/2$, β_{00}. These functions of OEO normalized oscillation amplitude x versus its normalized frequency s are called resonance characteristics (resonance curves) of OEO. Solutions are constructed, for example, in WA operation system at specification of

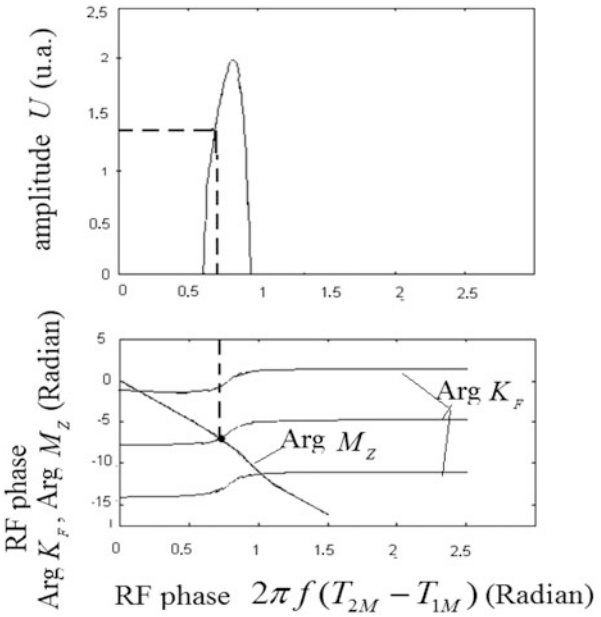

Fig. 3.19 The graphical method for frequency and amplitude determination in the OEO steady-state mode

the appropriate codes. Figure 3.20a shows the example of solution (Eq. 3.64) with values of $K_{0FODL}/Q_{EF} = 3$, $1/Q_{EF} = 0.05$, $m_{00}\pi/2 = 0$, $\beta_{00} = 5.1$. The example of (Eq. 3.64) solution for $K_{0FODL}/Q_{EF} = -2.5$, $1/Q_{EF} = 0.05$, $m_{00}\pi/2 = \pi/2$, $\beta_{00} = -10.5$ is presented in Fig. 3.20b.

The example of (Eq. 3.64) solution is shown in Fig. 3.21a for values: $K_{0FODL}/Q_{EF} = 5$, $1/Q_{EF} = 0.05$, $m_{00}\pi/2 = 0$, $\beta_{00} = 10.1$. From solution analysis we can make a conclusion that at sine nonlinearity or at MZ "quadrature" mode, the "soft" self-excitation mode of OEO is possible, which is caused by the disturbance of OEO stability conditions. We can also conclude that at cosine nonlinearity, there is the "rigid" self-excitation mode only or at MZ operation in the "non-quadrature" mode. At large modulation indices (Fig. 3.21b, c), $\beta_{00} = 10.5$, and at the gain $K_{0FODL}/Q_{EF} = 2.5$, the nonlinearity $\cos[m_{00}\pi/2 + \beta_{00}x]$, $m_{00}\pi/2 = \pi/4$, for $1/Q_{EF} = 0.01$, there is the rigid OEO self-excitation only. At that, zones of possible steady-state values broaden, and their transients depend on initial conditions.

Plots of the resonance characteristics of OEO MZ i.e., functions of the oscillation amplitude U_{10MZ} of OEO MZ versus the generation frequency $s = j(f/f_{0e})$ are presented in Figs. 3.20 and 3.21. Figure 3.15 shows functions of the DC component of the optical emission and the AC component of fundamental harmonic in the MZ output. Numbers "1" and "2" designate the values of constant relative DC bias voltage in the "quadrature" and "non-quadrature" modes. They are equal, relatively, 0.5 and 1.0 and correspond in Fig. 3.15 to phases $\varphi_{0MZ} = \frac{\pi U_{0MZ}}{U_{0MZ\pi}} = \pi/2$ and π, relatively. At that, we should note that at OEO MZ excitation in the quadrature mode, when the excitation conditions are fulfilled, OEO MZ begins to generate at the cosine nonlinearity. We may speak about the soft mode of excitation. In this case, in

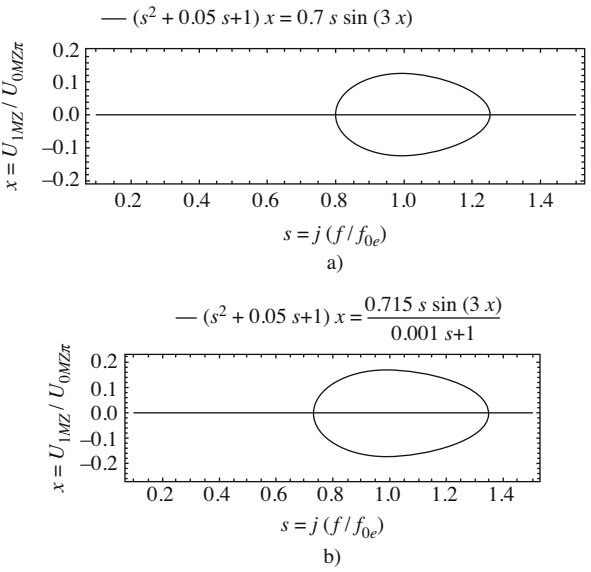

Fig. 3.20 Functions of oscillation amplitude versus the OEO MZ frequency at constant bias voltage of MZ at modulator operation in the quadrature mode ($m_{00}\pi/2 = \pi/2$) at gains $K_{0FOLD}/Q_{EF} = 0.7$ (**a**), $K_{0FOLD}/Q_{EF} = 0.715$ (**b**). Figures show solvable equations at $1/Q_{EF} = 0.05$, nonlinearity $\cos[m_{00}\pi/2 + \beta_{00}x]$, $m_{00}\pi/2 = \pi/2$, the modulation index $\beta_{00} = 3$

the diagram of Fig. 3.20, we see two symmetric branches, which tells that generation begins from the zero level of amplitude. At "non-quadrature" mode or the mode of "π"-generation of OEO MZ oscillation may be excited only in the "rigid" mode. At that, in the diagram in Fig. 3.21, the only non-symmetrical branches or the closed contours are presented with regard to the abscissa axis. The number of closed contours begins to grow with the modulation index growth (Fig. 3.21e, f). In Fig. 3.21d–f we can observe both quasi-symmetric closed contours with regard to origin coordinate (Fig. 3.21d), and the complete symmetric contours with regard to the ordinate axis (Fig. 3.21e, f). The presence of additional differentiating link "s", to which the operator $p/2\pi f_{0e}$ corresponds (Fig. 3.21d), make the resonance curves picture more manifold. The described method of construction and analysis of resonance curves, which is offered by this book authors (on the base of the nonlinear differential equations), to clarify the possibilities of self-excitation and operation in the steady state, is not only the new method but the promising because it takes into consideration many parameters at analysis of the exit to the steady-state mode of generation. Such a method of oscillator analysis supplements the known method of the phase trajectories. Clearness on this method is possible at fast computer solution of nonlinear differential equations.

Examples of OEO differential equations' solutions with sine and cosine nonlinearity are presented in Fig. 3.22. Examples of the OEO MZ differential equation solution with the cosine nonlinearity are presented for $Q_{EF} = 100$ at different values of the MZ constant bias voltage and at different gains. It is shown that at small gains and the low modulation index, the formation of the limit cycle in the soft excitation mode depends on the initial conditions, and for large enough gains and modulation indices, the steady-state oscillations have the high nonlinear

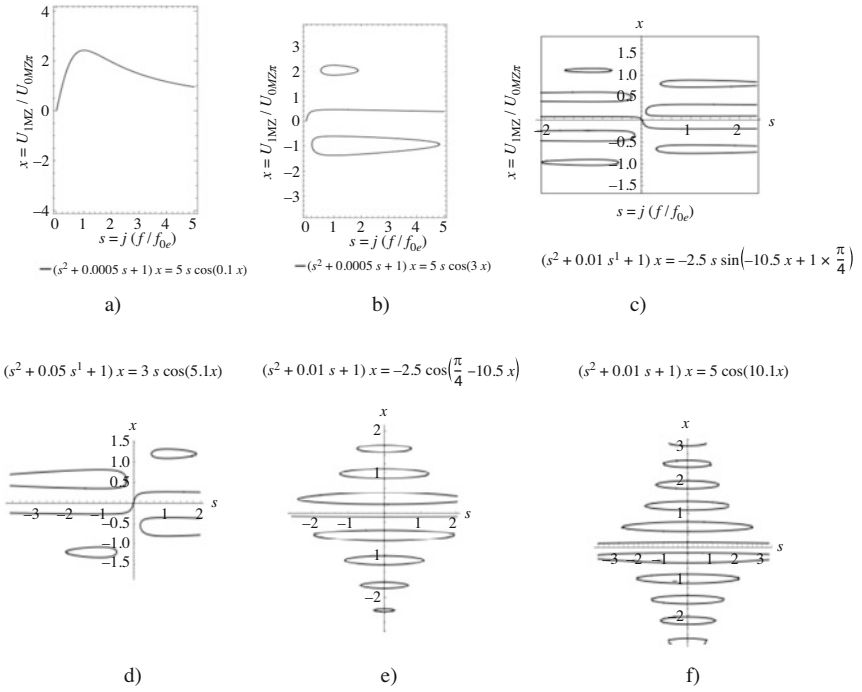

Fig. 3.21 Functions of amplitude versus frequency in OEO MZ at constant MZ bias voltage at modulator operation in the "non-quadrature" mode ($m_{00}\pi = \pi$) for gains $K_{0FOLD}/Q_{EF} = 5$ (**a**), $K_{0FOLD}/Q_{EF} = 5$ (**b**). In figure the solvable equations are shown at $1/Q_{EF} = 0.0005$ (**a**), at nonlinearity $\cos[\beta_{00}x]$, at the modulation index $\beta_{00} = 0.1$ (**a**). For the gain $K_{0FOLD}/Q_{EF} = 5$ and the nonlinearity $\cos[\beta_{00}x]$, $\beta_{00} = 3.0$ for $1/Q_{EF} = 0.0005$ (**b**). For the gain $K_{0FOLD}/Q_{EF} = 2.5$ and the nonlinearity $\cos[\varphi_0 + m_{00}\pi/2 + \beta_{00}x] = -\cos[(\pi/4) + (\pi/2) - 10.5x]$, for $\beta_{00} = 10.5$, $1/Q_{EF} = 0.01$ (**c**). Functions of amplitude versus frequency in OEO MZ at different values of constant MZ bias voltage at different gains. Above figures, there are solvable equations (**d–f**)

distortions. Remarkably, that the level of nonlinear distortions depends upon the initial conditions. The differential second-order equation solutions with the cosine nonlinearity, which are presented in Fig. 3.22 for different $K_{0FODL}/Q_{EF} = 5$, $\beta_{00} = 2.0$ and various initial conditions. These plots allow estimation how the modulation index β_{00} of the MZ modulator influences on development of oscillating processes. In particular, we may speak the growing of the modulation index from $\beta_{00} = 2.0$ to $\beta_{00} = 10.5$ leads not only to the growth of the second harmonic (Fig. 3.22c), but to the frequency doubling (Fig. 3.22d).

Thus, we perform the primary analysis of the modulation methods and investigate the main modes of OEO MZ taking into consideration the OEO block-representation on the base of the amplitude and phase balance equations, the symbolic and abbreviated differential equations. This analysis permits to answer the questions about the oscillation amplitude and frequency in the steady-state modes. The derived differential equations allow investigation of transients of OEO amplitude and

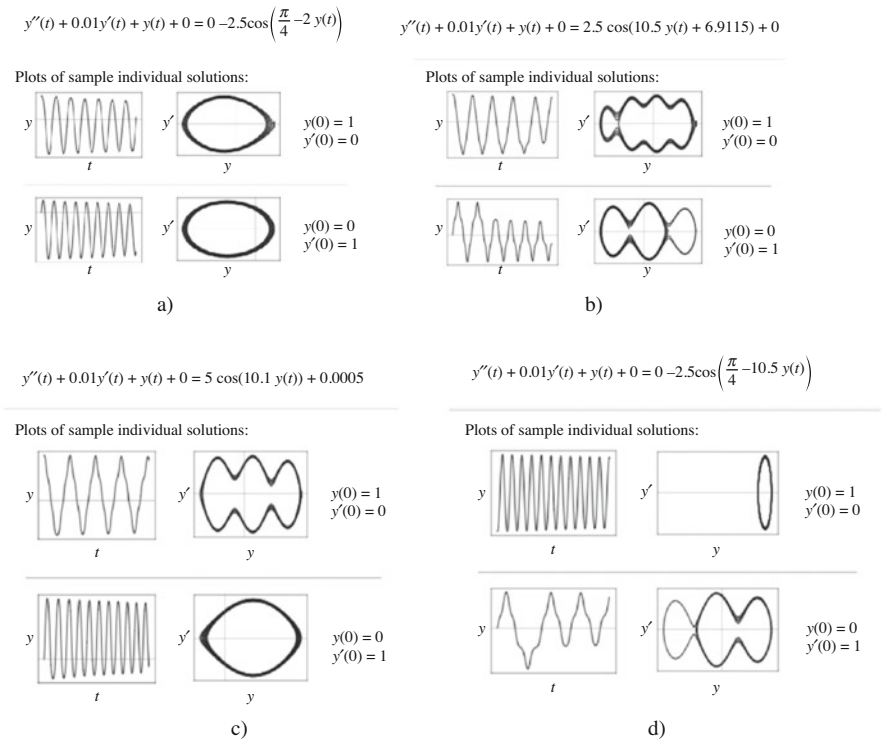

Fig. 3.22 Examples of OEO MZ differential equations solution with the cosine nonlinearity at $Q_{EF} = 100$ at different values of MX bias DC voltage for various gains. Above figures, there are the solvable equations for $K_{0FOLD}/Q_{EF} = 5$, nonlinearity $-\cos[\pi/4 - \beta_{00}x]$, $\beta_{00} = 2.0$ (**a**), $K_{0FOLD}/Q_{EF} = 2.5$, nonlinearity $\cos[\beta_{00}x + 6.91]$, $\beta_{00} = 10.5$ (**b**), $K_{0FOLD}/Q_{EF} = 5$, nonlinearity $\cos[\beta_{00}x]$, $\beta_{00} = 10.1$ (**c**), $K_{0FOLD}/Q_{EF} = 5$, nonlinearity $-\cos[\pi/4 - \beta_{00}x]$, $\beta_{00} = 10.5$ (**d**)

frequency. To this moment, the problems of OEO oscillation stability and self-excitation, the research of the laser parameters' influence on the OEO oscillations. In the future, for solution of mentioned problems, we shall address to OEO differential equations examination taking into account the laser presence at its consideration in quasi-classical approximation on the base of the double-level model in the dipole assumption.

3.5 Conclusions

This chapter is devoted to investigation of modulation methods of laser emission, to formation of the mathematical model of the autonomous OEO on the base of differential equations. We describe some methods, which allow obtaining of the extremely low phase noise level in OEO or to "transform" it into the ultralow-noise

oscillator of microwave or mm-wave ranges. Utilization of the quantum-well laser diodes in OEO with the low phase noise level; the active low-noise delay line on the base of the optical fiber; the phase noise heterodyning on the phase-detector area; application the modulation methods with the single sideband optical frequency at suppression of the optical carrier in the optical channel can be attributed to these methods.

In this chapter beginning, the OEO *functional diagrams* with direct and external modulation of optical emission are presented, the mathematical description of components including in OEO is given: a laser, the optical fiber, the photodetector, the RF amplifier, the RF filter. Furthermore, to widen knowledge about OEO functional possibilities, the various OEO variants, which improve its operation characteristics, are presented.

The variant with direct modulation of the laser pumping current and the external photodetector; the variant with external electro-optical Mach–Zehnder modulator for laser emission; the variant with laser emission modulation in both MZ optical channels; the variant of OEO without the RF amplifier but with optical amplifier located in the OEO fiber optical system and with the external photodetector can be attributed to these variants of improvement. It is proved that the special interest can be demonstrated by variants with the external photodetector, since requirements to elements of electrical matching essentially decrease, and the same situation with the variants with double modulation in both MZ optical channels.

The special role in this chapter is derived to the laser representation in OEO as the main source of fluctuations which have the quantum nature. It is shown that the dispersion on the laser phase noise is defined by the carrier noise dispersion and depends on the lifetime at the excited level. The level of the OEO phase noise is defined by the laser phase noise, which depends on the lifetime.

The OEO model is considered taking into account of the correlator of the laser phase noise, which is formed by the laser, the optical MZ modulator and the photodetector. It is shown that at the *closed feedback loop* in OEO MZ, the spectrum at the photodetector output has the Lorentzian shape, is defined by the laser phase noises, while its maximal value depends on the ratio of time constants. Effectiveness of noise suppression in OEO is not only defined by the fiber length, but also depends on the ratio of the laser coherence time and the delay line in the optical fiber.

At consideration of the modulation methods in OEO, we showed that the transfer mode in realized (from the laser and the modulator to the photodetector area) of two optical harmonics of laser emission with optical frequencies of ν_0 and $\nu_0 - f_0$. The transmission mode with the single sideband optical frequency, which is shifted from the optical carrier, is examined. In this mode, the ultralow phase noise level of RF oscillations in microwave and mm-wave ranges and the high short-term frequency stability are provided, owing to the interference of two rigidly correlated optical oscillations on the light-sensitivity photodetector area. Another important conclusion is the fact that in OEO DM and OEO MZ, the mode of radio-frequency doubling is possible. In this mode, the significant possibility of DC optical *component* suppression of laser emission is provided; the essential level of this component degrades the OEO phase noises. In this case, we must introduce in OEO DM the

optical rejection filter tuned on suppression of DC component. In OEO MZ the relation of $U_{1MZ}/U_{0MZ\pi}$ should be 2.4.

To form the equations of amplitude and phase balance separately for the laser and for OEO, and also for formation and solution of symbolic and abbreviated differential equation of OEO, we considered the mathematical formulas for the complex transfer functions of OEO elements (optical and RF parts). As the result of modulation method analysis of the complex transfer functions of OEO components, the symbolic and abbreviated equations have been formed.

The special attention is attracted to formation and solution of abbreviated equations for OEO with the single optical fiber. Solutions allowed revealing of amplitude and frequency functions versus the Q-factor of the RF filter, the delay time in the optical fiber, the laser power, etc.

On the base of formed symbolic equations, the resonance curves are constructed and discussed for OEO dependences of the amplitude-frequency at modulator operation with the different DC bias voltage of OEO MZ. From the analysis of symbolic equation solutions and from the analysis of resonance curves at different OEO parameters, some interesting conclusions can be made. So, at sine nonlinearity (or MZ operation in "quadrature") the soft excitation OEO mode is possible, which is caused by disturbance of OEO stability conditions in the initial state. On the contrary, at cosine nonlinearity of the MZ modulator (or at MZ operation in the mode "non-quadrature"), there is the rigid excitation mode only of the autonomous oscillator. At modulation index grows and at the module of the transfer function increases, there is the OEO rigid excitation only, and at that, zones of possible steady-state values of amplitude are broadening and their transients depend on initial conditions. Several examples of differential equation solutions with cosine and sine nonlinearities are presented for different Q-factors of the RF filters (100 and higher) at different DC bias voltages for MZ.

The problems of the laser parameters' influence (the Q-factor of the optical filter, the Q-factor of the spectral amplification line of the laser active medium, the nonlinear function of the laser active medium, the lifetime of carriers on the upper level, etc.) on the amplitude and the frequency of OEO. Some these problems will be considered in future chapters.

References

1. V.V. Grigoriants, A.A. Dvornikov, Y.B. Il'in, et al, Oscillators of the radio-frequency range with the optical carrier, in Proceeding of MPEI, Issue 607 (1983), pp. 76–79
2. A.A. Dvornikov, Y.B. Il'in, V.N. Konstantinov, About single-frequency modes of the oscillator with the fiber-optical delay line in the feedback loop. Radio Eng. Electron. **29**(11), 2234–2242 (1984)
3. V.V. Grigoriants, A.A. Dvornikov, Y.B. Il'in, et al., Radio signal generation in the system «laser optical delay line». Quant. Electron. **11**(4), 766–775 (1984)

4. L. Stolpner, S. Lee, S. Li, A. Mehnert, P. Mols, S. Siala. Low noise planar external cavity laser for interferometric fiber optic sensors, in Proceedings of SPIE 7004, 19th International Conference on Optical Fibre Sensors (2008), pp. 700451–700457
5. K. Numata, J. Camp, M.A. Krainak, L. Stolpner, Performance of planar-waveguide external cavity laser for precision measurements. Opt. Exp. **18**(22), 22781–22788 (2010)
6. R.E. Bartolo, C.K. Kirkendall, V. Kupershmidt, S. Siala, Achieving narrow linewidth, low phase noise external cavity semiconductor lasers through the reduction of 1/f noise, in Proceedings of SPIE 61333, 6133OI (2006)
7. R.E. Bartolo, C.K. Kirkendall, V. Kupershmidt, S. Siala, Achieving narrow linewidth, low phase noise external cavity semiconductor lasers through the reduction of 1/f noise, in *Novel In-Plane Semiconductor Lasers V*, ed. by C. Mermelstein, D.P. Bour, Proceedings of SPIE, vol. 6133, 61330I (2006)
8. M. Morin, S. Ayotte, C. Latrasse, et al., What narrow-linewidth semiconductor lasers can do for defense and security? in Proceedings of SPIE—The International Society for Optical Engineering 7677, April 2010
9. V.S. Ilchenko, M.L. Gorodetsky, Y.X. Steve, L. Maleki, Microtorus: a high finesse microcavity with whispering-gallery modes. IEEE Photon. Technol. Lett. **26**(5), 256–258 (2001)
10. K.R. Hiremath, V.N. Astratov, Perturbations of whispering gallery modes by nanoparticles embedded in microcavities. Opt. Exp. **16**(8), 5421–5426 (2008)
11. G.S. Murugan, J.S. Wilkinson, M.N. Zervas, Selective excitation of whispering gallery modes in a novel bottle microresonato. Opt. Exp. **17**(14), 11916–11925 (2009)
12. K. Li, X. Xie, Q. Li, Y. Shen, M.E. Woodsen, Z. Yang, et al., High-power photodiode integrated with coplanar patch antenna for 60-GHz applications. IEEE Photon. Technol. Lett. **27**, 650–653 (2015)
13. A. Beling, X. Xie, J.C. Campbell, High-power, high-linearity photodiodes. Optica **3**(3), 328–338 (2016)
14. I.V. Komarov, S.M. Smolskiy, *Fundamentals of short-range FM radar* (Norwood, Artech House, 2003)
15. V. Zhalud, V.N. Kuleshov, *Noise in Semiconductor Devices. Under Edition of A.K. Naryshkin* (Sovetskoe Radio, 416 p. (in Russian), Moscow, 1977)

Chapter 4
Semiclassical Theory and Laser Differential Equations for Optoelectronic oscillator (OEO) Analysis

This chapter is the logical continuation of OEO investigation, in which we consider that the laser is the main element defining the dynamic and noise properties of OEO. In this interpretation, OEO is represented as the quantum generator spanned by the positive feedback: the optoelectronic network containing the optical fiber, the photodetector, the RF filter, and the RF amplifier.

Section 4.1 is devoted to model formation of the quantum generator, for which we use the semiclassical theory based on the dipole representation of the laser in double-level approximation. For formation of differential equations (DE) in quasi-stationary mode, we consider in Sect. 4.2 the DE system, which consists of three differential equations. This DE system establishes a connection between the active medium polarization, the electromagnetic field strength, the inversed population of particles on upper and lower energy levels, and pumping, taking into account the Q-factors of the optical resonator and the emission spectral line of the active medium and the population inertial properties. Examination of this system of nonlinear DEs with inertial properties allows formation of the laser analog model in the dipole approximation.

The analysis of the self-oscillating system (SOS) of the laser model is performed in Sect. 4.3, for which we introduce the operator transfer function, the nonlinear element (NE) and execute the analysis of nonlinear properties. The special role is paid (Sect. 4.4) at laser system analysis to investigation of inertial nonlinear QWLD at its operation in quasi-stationary mode with the high excess of pumping current over its threshold value. Investigation of oscillation excitation conditions and oscillation existence conditions in the OWLD steady-state is performed in Sect. 4.5.

Section 4.6 is devoted to results' presentation of the nonlinear fourth-order DE solution for the laser model in the dipole approximation. The plots of realizations of oscillating processes for two types of nonlinearities are analyzed. Results of computer solution for the quasi-stationary mode of laser generation are presented for fourth-order DE at the linear-hyperbolic inertial nonlinearity of the active medium. Numerical calculation results on the base of the symbolic equation solution are

A. A. Bortsov et al., *Laser Optoelectronic Oscillators*, Springer Series in Optical Sciences 232, https://doi.org/10.1007/978-3-030-45700-6_4

discussed for determination of resonance characteristics in the steady-state mode. Results of nonlinear DE equations and resonance characteristics at high power density in the optical resonator are described in Sect. 4.7. Section 4.8 contains the main conclusions on this chapter.

4.1 Semiclassical Laser Equations and OEO Differential Equations

In this chapter, we continue to develop the *main idea of this book*: in OEO, the laser is the main element defining the dynamic and noise properties of OEO (Fig. 3.2a–c).

We address for the analysis of the quantum generator, which plays a role in OEO of the main energy source, to the semiclassical laser theory based on the dipole representation in the double-level approximation. The classical theory uses the Maxwell equations connecting the polarization of the laser active medium and the oscillation field strength for description of the electromagnetic field of laser emission. At that, the model of *complete* nonlinear DEs is traditionally considered consisting of three equations, which connect the medium polarization, the field strength and the particle population difference in upper and lower levels. This system of nonlinear DEs of fourth order with inertial oscillation control allows formation of the laser analog model.

In the classical model, the laser emission field is described with the help of the classical electrodynamics (Maxwell equations). In kinetic equations, which are constructed on the base of constitutive law (on the phenomenological approach), the emission field is characterized by the average number of photons, and the atom system is represented on the language of mathematical expectation of level populations.

Although the method of kinetic equations permits to analyze of dynamics and to find out the intensity and thresholds of emission, this method does not allow calculation of phase relationships. The semiclassical theory is able to take into consideration phase relationships, phase fluctuations of laser emission and then to transform it into the phase noise of OEO. This quasi-classical theory describes the laser with the help of the classical electrodynamics, and the atom system is described in the quantum mechanics manner, kinetic equations are analyzed and specified, the phase relations are calculated and (if necessary) the frequency relations. To describe the spontaneous emission, we can use the quantum theory, in which the field and the atom system are determined from the quantum mechanics manner.

Here we deal not only with description (available for students and engineers) of known positions developed in the 1960s–1980s by Haken [1–3], Haug [4], Lamb [5], and others, but we analyze of the laser system from positions of the nonlinear oscillation theory for QWLD.

At our analysis, as will be shown in further sections of this chapter, we sequentially perform the following:

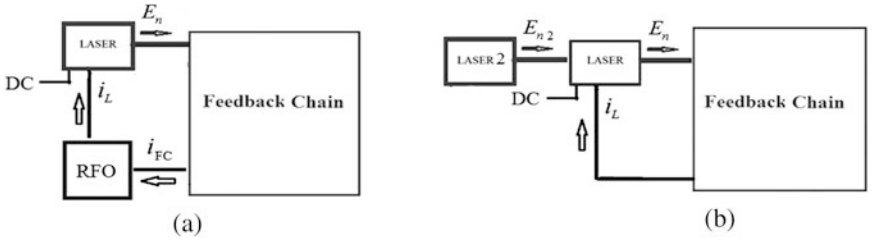

Fig. 4.1 OEO structure as the laser spanned by the positive FB: (**a**) OEO structure with external synchronizing radio-frequency oscillator (RFO); (**b**) OEO structure with the reference "Laser2," which synchronizes the "Laser" spanned by the positive FB

- Determine the order of DEs,
- Extract the operator controlling transfer function in SOS,
- Study the control law of oscillation amplitude of EMF in the laser with the help of the saturation effect or the inversed population variation,
- Analyze the nonlinear function of NE,
- Investigate oscillation excitation conditions and oscillation existence condition for QWLD in steady-state modem,
- Determine the existence condition of the limit cycle on the phase plane of generalized parameters and their bifurcations.

The special attention in the laser system analysis is attracted to the nonlinear QWLD element. In contrast to kinetic equations, the *phase relations are saved* in this DE system.

Since the main practical purpose of OEO systems is the creation of ultralow-noise oscillators of microwave and mm-wave ranges, we must pay attention to features of fluctuation and phase noise investigations in OEO.

At examination of noises, which is performed in Chap. 5, we supplement of DEs (and the analog model considering and analyzing in this chapter) of the laser in dipole approximation by Langevinian noise sources and we form the basing symbolic fluctuation DEs for OEO with the *direct and external modulation*.

Recently, QWLD with the spectral line width less than 10 kHz become commercially available. Such lasers have ultralow levels of PSD of the amplitude noise (AN) and the phase noise (PN). Figure 4.1d shows the typical experimental function of PSD of AN and PN of the semiconductor QWLD with the spectral line width of 10 kHz at power of 15 mW. Applying such lasers in OEO MZ and analyzing its operation, we must have the appropriate adequate analog fluctuation dynamic and static models.

This approach on the base of constitutive equations with formation of Langevinian noise sources enables better understanding of how does oscillation process develop in the laser, helps to obtain the phase and amplitude noises of its emission. Such an approach gives an opportunity to connect functionally of the laser with external (not included into the laser) optical and RF components: optical filters

(resonators), delay lines and filters on the base of optical fibers and disks, the photodetector (or detectors).

In the further chapters, owing to this theoretical approach, we write the DE system of the laser taking into account the noisy Langevinian fluctuation sources [6]. The noise of spontaneous (radiation) emission having the quantum nature plays the role of the main one among such sources. Then we develop the method based on the OEO representation as the unified oscillating system, in which the motion processes develop in optical and radio-frequency ranges taking fluctuations into account.

The analog fluctuation model of the laser formed on the base of constitutional equation with utilization of Langevinian noise sources allows determination of phase and amplitude noise in OEO MZ. In this interpretation, OEO is the quantum generator spanned by the positive feedback or opto-electronic network containing the optical fiber, the photodetector, the RF filter, and the RF amplifier

4.1.1 OEO as the Laser Spanned by the Feedback Loop

We remind once more that at analysis of OEO DM and OEO MZ, we consider them as systems, in which the laser is spanned by the positive feedback (FB) loop, which consists of series-connected the optical fiber, the photodetector, the RF amplifier, the RF amplifier, and the RF filter (Fig. 4.1a, b). In OEO DM, the loop of positive feedback is closed (connected) through the coupler C to the laser, while in OEO MZ the FB loop connects through the coupler C to the Mach–Zehnder modulator.

4.1.1.1 The Positive Feedback Loop in OEO DM Spanned the Laser

The closed loop of positive FB contains (Fig. 4.1a) series-connected the "polarizer" P, the optical fiber OF, the photodetector PD, the amplifier A, the filter F, and the coupler C.

For simplicity, we neglect by actions of the optical polarizer (P), by dispersion of the optical fiber, and we consider that PD is wideband, and the RF amplifier has no inertial properties. The transfer function of FB loop K_{BZ} we define for OEO DM and OEO MZ as: $K_{\mathrm{FB}} = \frac{E_{1\mathrm{L}}^2}{i_{1\mathrm{L}}}$ or $K_{\mathrm{FB}} = \frac{E_{1\mathrm{L}}^2}{u_{1\mathrm{MZ}}}$, where $E_{1\mathrm{L}}^2$ is the normalized strength square (laser power), $i_{1\mathrm{L}}$ is AC component of the laser pumping current, $u_{1\mathrm{MZ}}$ is AC voltage component of the MZ modulator. In this case, the operator controlling transfer function of this FB loop has a form: $K_{\mathrm{FB}} = K_{\mathrm{BZ}} = \frac{E_{1\mathrm{L}}^2}{i_{1\mathrm{L}}} = \frac{(1/T_{\mathrm{EF}})p}{p^2+(1/T_{\mathrm{EF}})p+(2\pi f_{0\mathrm{e}})^2} K_{\mathrm{OF}} \exp(-pT_{\mathrm{OF}}) K_{\mathrm{PD}} S_{\mathrm{NY}}$, where $p = \mathrm{d}/\mathrm{d}t$ is the Laplace operator, $f_{0\mathrm{e}}$ is the fundamental frequency of the RF filter, T_{EF} is the time constant of the RF filter, T_{OF} is time delay in the optical fiber, K_{OF} is the transfer function of OF, K_{PD} is

the transfer function of PD, S_{NY} is the nonlinear function of RF first harmonic of collector current of the RF amplifier: $S_{NY} = i_C/u_B = \alpha u_B - \beta u_B^3$ at $u_B = u_{PD}$.

The connection of the current first harmonic with the normalized strength E_{1L}^2 is evident: $i_{1L} = \frac{\left[p^2+(1/T_{EF})p+(2\pi f_{0e})^2\right]\exp(-pT_{OF})}{(1/T_{EF})pK_{OF}K_{PD}S_{NY}} E_{1L}^2$. With the purpose to substantiate the great attention to investigation of the quantum generator in Chap. 3, Fig. 4.1 shows the other OEO structures, in which the laser is covered by the positive FB loop. The OEO structure (Fig. 4.1a) with the external synchronizing radio-frequency oscillator (RFO) can be attributed to these structures (without which the representation of OEO cannot be complete). The OEO structure (Fig. 4.1b) with the reference "Laser 2," which synchronizes the first laser spanned by positive FB, can be also attributed to these structures. Operation of structures in Fig. 4.1 cannot be understood and investigated without the deep knowledge of processes, which takes place in the laser, taking into consideration the fluctuations. Fundamentals of the theory presented in the present chapter allow determination of the complete DE system and its analysis not only for OEO DM and OEO MZ (Fig. 3.2), but from the point of view of standard approaches of nonlinear oscillation theory, which is approved in radio electronics and the communication theory. Developed laser theory on the base of symbolic equations is relevant for many laser systems, in which the laser synchronization from the external laser (Fig. 4.1b) and the modulation of the laser optical frequency by variation of the OF Q-factor are used. The laser spanned by delayed FB, the laser with the set of optical filters including the optical disks with the high Q-factor, and also with the set of inertial optical components, the laser with control system for optical frequency, the laser with the PLL system, etc. can be attributed to these systems.

4.1.2 Quasi-Classical Laser Theory

In spite of literature plenty, the transition from the electromagnetic field equations in the laser to dynamical DEs for the separate longitudinal mode often causes many problems, therefore, we discuss it in detail. The relative simplicity of our approach is explained by the fact that we consider the laser operating in the single-mode regime with generation of the single optical frequency. At that, the laser spectral line width in OEO we consider as narrow and close to the Lorentzian curve. This is true, for example, for single-mode single-frequency semiconductor QWLDs with the Bragg optical filter, which has the spectral line width of less than 50–300 MHz, and the oscillation frequency is about 150–250 THz. Such a condition is satisfied in the fiber-optical lasers (FOL) with the active medium on erbium, ytterbium, neodymium, etc.

4.1.2.1 Quasi-Classical Laser Representation and Description of the Two-Level Model

Let us consider a laser model containing the active medium (optical amplifier) and the single-mode resonator of "traveling-wave" formed by mirrors, as shown in Fig. 3.2a.

An electromagnetic field affects the active medium and produces the electric polarization of the medium. According to the electric dipole model of interaction (based on Maxwell equations), the OA polarization is the energy source for induced EMF. Amplitude and phase of possible field self-oscillations defined from the field self-consistent conditions (or from the phase and amplitude balance equations for EMF) states that the field is excited (or induced) should be equal to the initial field.

Figure 4.2 shows the laser model with the traveling-wave resonator, in which the active medium (OA) under the influence of energetic pumping is schematically shown. The EMF oscillation is applied into an optical input of OA. The optically active medium (OA) is presented in Fig. 4.2a, while the two-level pumping scheme is presented in Fig. 4.2b. Figure 4.2c shows the dipole representation of the OA atom.

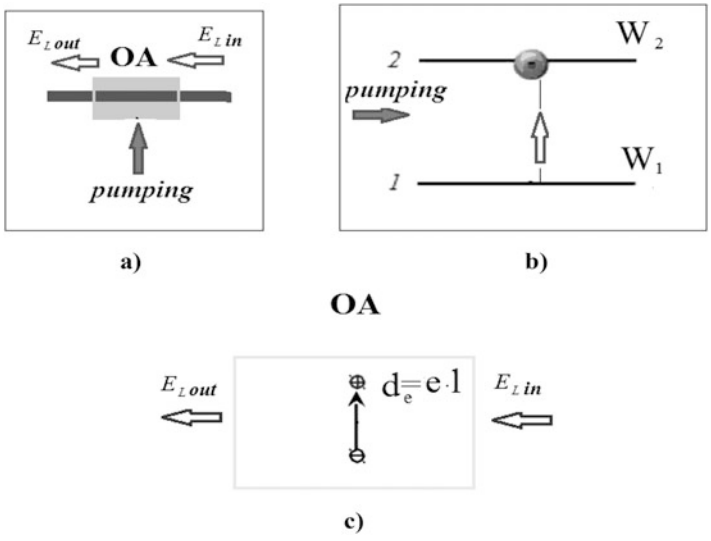

Fig. 4.2 The laser model under the influence of energetic pumping. The EMF oscillation is applied in the OA input. (**a**) optical amplifier, (**b**) double-level pumping scheme of OA, (**c**) the dipole representation of the active medium atom

Limitations of a Model

Lifetime in excited state of an atom or a particle is ten thousand periods of the EMF wave. In the general case, during lifetime, the atom (or the particle) can pass (in the space) several wavelengths. We neglect by the atom (particle) motion under action of the electrostatic field and we neglect also by the atom motion due to the thermal motion, and we use an analysis of the solid-state laser.

We suppose that the laser system of energy zones consists of only two states: 1 (main) and 2 (excited). For simplification, we neglect by the vector character of EMF and consider that EMF propagates only in the single polarization plane. The resonator is assumed as the high-Q system and it provides the single-frequency generation mode.

In the model, we consider a variety of atoms as a medium, in which its electrical state is described by the macroscopic polarization. A polarization is a sum of particle (charge carriers or atoms) dipole moments normalized to the volume V_0 : $P = \sum_i d_{ei}/V_0$,: where d_{ei} is the quantum-mechanical average value of the dipole moment in the space point in the time moment t, V_0 is the small volume of average near the point under consideration, $d_e = e \cdot l_0 = d_{ei}$ is the electrical dipole moment, e is the electric charge of the electron, and l_0 is the dipole arm. The total electrical dipole moment of an atom represents a sum of all atom electrons.

The problem of boundary conditions in the considered model is avoided by consideration of the absorbing medium with a conductance (the ohmic or wave conductance) σ, which is chosen so as to provide the observable damping of natural oscillation owing to reflections and the diffraction.

Let us extract the high-Q mode of the laser resonator. Let it be the plane EMF wave and propagates along the z-axis or along the i_z vector and is polarized along the x-axis or along the i_x vector, and the EMF strength with amplitude E_0 and the wavelength λ is:

$$E = E_0 \exp\left[jz(2\pi/\lambda)\right] \cdot i_x. \tag{4.1}$$

In electrodynamics, the absolute value of Poynting vector is expressed through the normalized wave strength E_{0L}^2. For simplicity, we use dimensionless normalized values of the strength square E_L^2, which has a sense of the field intensity (or field power) on the standard area. The connection of normalized E_L^2 and factual E^2, as well as E_{0L}^2 and E_0^2 is specified as

$$E_L^2 = \frac{c}{n_0}\frac{\varepsilon\varepsilon_0}{2}E^2, \quad E_{0L}^2 = \frac{c}{n_0}\frac{\varepsilon\varepsilon_0}{2}E_0^2. \tag{4.2}$$

Here ε is the medium permittivity, ε_0 the vacuum permittivity, n_0 is the refraction index of the medium material. The normalized strength used in this book can be defined as $E_L = \sqrt{E_L^2}$.

4.1.3 Wave Differential Equation of the Laser

At the complex field representations in the form:

$$E(r = z, t) = E(z, t) \cdot \exp(-j2\pi\nu t), \tag{4.3}$$

where $r = z$ is a radius-vector; here we assume that the transfer to the real fields is performed as:

$$\begin{aligned} E(r = z, t) &= \operatorname{Re} E(z, t) \\ &= \frac{1}{2}[E(t, r) \cdot \exp(-j2\pi\nu t) + E(t, r) \cdot \exp(\ j2\pi\nu t)]. \end{aligned} \tag{4.4}$$

Dynamical equations for the field amplitude of the laser mode can be obtained starting from the electrodynamics equation [7]:

$$\nabla \times \nabla \times E + \mu_0 \frac{\partial^2 D}{\partial t^2} = 0, \tag{4.5}$$

where $\nabla = i_x \frac{\partial}{\partial t} + i_y \frac{\partial}{\partial t} + i_z \frac{\partial}{\partial t}$ is the Laplace operator, E is the strength vector, and μ_0 is the permeability, i_x, i_y, i_z are unit vectors, D is the vector of electrical displacement connected with the polarization P, the permittivity ε_0 and E as:

$$D = \varepsilon_0 E + P. \tag{4.6}$$

This equation can be rewritten in the form:

$$\nabla \times \nabla \times E + \frac{1}{c^2} \frac{\partial^2 E}{\partial t^2} = -\frac{1}{\varepsilon_0 c^2} \frac{\mathrm{d}^2 P}{\mathrm{d}t^2}. \tag{4.7}$$

Equation (4.7) is the general form of the wave equation in the medium, because the term in the right part, which plays a role of the exciting force, permits to take into consideration the *pumping*, *nonlinearity* and *dispersion* in the *medium*. The first term in the left side of Eq. (4.7) is:

$$\nabla \times \nabla \times E = \nabla(\nabla \cdot E) - \nabla^2 E. \tag{4.8}$$

In the general nonlinear case, this equation cannot be reduced to the single vector Laplace operator, because $\nabla \cdot E \neq 0$ due to nonlinear connection of D and E vectors. In some cases, we can neglect by the first term in the right part of Eq. (4.8) because of its smallness.

If to separate from the polarization a part connected with pumping P_{P} and a part connected with nonlinearity P_{NL}, then the wave equation can be rewritten in the form:

$$\nabla \times \nabla \times E + \frac{1}{c^2}\frac{\partial^2 E}{\partial t^2} = \frac{1}{\varepsilon_0 c^2}\frac{d^2 P_{\mathrm{P}}}{\mathrm{d}t^2} - \frac{1}{\varepsilon_0 c^2}\frac{d^2 P_{\mathrm{NL}}}{\mathrm{d}t^2}, \tag{4.9}$$

where P_{P} describes a polarization caused by the pumping field taking into account a population: $P_{\mathrm{NL}} = \varepsilon_0 \chi^3(\nu) N |E|^2 \cdot E$, where χ is the medium susceptibility (here we consider the cubic nonlinearity). As a rule, we can neglect by nonlinearity P_{NL} in connection with its smallness. It manifests at nonlinear optical phenomena, for instance, at harmonic doubling, at two- and three-photon nonlinear interaction, the Brillouin dispersion, etc. Such phenomena have the threshold character and are demonstrated at high power densities (more than 10^{10} mW/m^3).

At pumping action, the polarization P_{P} is proportional the population difference between levels $N(t)$ and depends on the dipole moment $p_{\mathrm{e}}^2 = d_{\mathrm{e}}^2 : P_{\mathrm{P}} = \frac{d_{\mathrm{e}}^2}{2 \cdot 2\pi h} \cdot N \cdot E$. We assume that non-excited field for the **main** (or zero) mode is described by the equation in the linear case:

$$\nabla \times \nabla \times e_{\mathrm{m}} - \frac{\nu^2 \cdot n^2(\nu)}{c^2} \quad e_{\mathrm{m}} = 0, \tag{4.10}$$

Note that the e_{m} vector defining the polarization plane of oscillations is normalized to the maximum so as $\max(e_{\mathrm{m}}) = 1$, and integration of $|e_{\mathrm{m}}|^2$ over the volume V is: $V_0 = \int |e_{\mathrm{m}}|^2 \mathrm{d}V$.

Let us represent the main mode field in the form:

$$E = \frac{1}{2} \times [E_{0\mathrm{n}}(t) \cdot e_{\mathrm{m}}(r) \cdot \exp(-j2\pi\nu t + j\varphi_{\mathrm{L}}(t)) + E_{0\mathrm{n}}(t) \cdot e_{\mathrm{m}}(r) \cdot \exp(j2\pi\nu t + j\varphi_{\mathrm{L}}(t))], \tag{4.11}$$

where ν is the mode optical frequency close to the natural frequency $\nu_{0\mathrm{L}}$ of the laser resonator, $r = z$ is the radius-vector, $E_{0\mathrm{n}}(t)$ and $\varphi_{\mathrm{L}}(t)$ is slowly changing amplitude and phase.

4.1.4 Differential Equations of QWLD

We substitute Eq. (4.11) into Eq. (4.9), multiply it by e_{m} and integrate over the whole volume. As the result, we obtain DEs connecting strengths and polarizations:

$$\frac{\mathrm{d}^2E}{\mathrm{d}z^2}+\mu_0\varepsilon_0\frac{\mathrm{d}^2E}{\mathrm{d}t^2}+\mu_0\sigma\frac{\mathrm{d}E}{\mathrm{d}t}=\mu_0\frac{\mathrm{d}^2P}{\mathrm{d}t^2}-\mu_0\frac{\mathrm{d}^2P_{\mathrm{NL}}}{\mathrm{d}t^2}, \tag{4.12}$$

where σ is the ohmic conductance.

At presence of the required polarization, the quasi-stationary stimulated oscillations of the electrical field *can be expanded on eigenfunctions of the fundamental modes*. We are interested only by a solution for the *main mode for the single-frequency oscillation mode* of generation. But for solution of the more general task for the fundamental mode, we have the eigenfunction $U_{\mathrm{n}}(z) = \sin K_{\mathrm{n}}z$ (non-normalized for $r = z$), and at adding over all modes n, we obtain the expansion formula:

$$E(z,t)=\sum_n E_n(t)\cdot\sin K_{\mathrm{n}}z, \tag{4.13}$$

where $\mathrm{K_n}$ is the propagation constant for the mode. Amplitudes of all fundamental oscillations are finite, and solution will be in the form of a series over eigenfunctions. We assume that the Q-factor of the main type of oscillations is much more than 1. And one term of such a series prevails and therefore, a sum is replaced by the single term $E(z,t) = E_{\mathrm{n}}(t)\cdot E_{\mathrm{n}}(z)$.

The polarization of the operating transition steps forward as the exciting force (or current, as in generators). Using the integration formula along to resonator length L, we obtain P_{n}:

$$P_{\mathrm{n}}(t)=(2/L)\int_0^L(P(z,t)\sin\mathrm{K_n}z))\mathrm{d}z. \tag{4.14}$$

Introduced conductance σ is chosen so that to obtain the necessary Q-factor for the n-mode (main mode) Q_{n}, then the ohmic conductance is:

$$\sigma=\varepsilon_0 2\pi\nu_{0\mathrm{n}}/Q_{\mathrm{n}}=\varepsilon_0(1/T_{\mathrm{OF}}). \tag{4.15}$$

If to represent the polarization $P(z,t)$ in the form of a series: $P(z,t)=\sum_n P_{\mathrm{n}}(t)\cdot P_{\mathrm{n}}(z)$ for the field strength E_{n} (with the slowly changing amplitude $E_{0\mathrm{n}}(t)$ and phase $\varphi_{\mathrm{L}}(t)$). We obtain that E_{n} satisfies to DE with the exciting term for stimulated oscillations of the harmonic oscillator with damping:

$$\frac{\mathrm{d}^2E_{\mathrm{n}}}{\mathrm{d}t^2}+(1/T_{\mathrm{OF}})\frac{\mathrm{d}E_{\mathrm{n}}}{\mathrm{d}t}+(2\pi\nu_{0\mathrm{n}})^2E_{\mathrm{n}}=(\varepsilon_0)^{-1}\cdot\frac{\mathrm{d}^2P_{\mathrm{n}}}{\mathrm{d}t^2}, \tag{4.16}$$

in which P_{n} is the spatial component of the active medium polarization. We would like to attract attention to the fact that in the right part of DE, there is the second derivative $\frac{\mathrm{d}^2P_{\mathrm{n}}}{\mathrm{d}t^2}$ because the electromagnetic field of the excited dipole is defined by

the acceleration of dipole charges (or the second derivative of the dipole charge displacement).

Further, we shall address to the known system of semiclassical equations, in which the first equation is already defined by us.

4.2 Constitutive Equations of a Laser

4.2.1 *DE for the* Single-Frequency *Single-Mode Regime*

The generally accepted DE system for the *single-frequency* single-mode (the only type of spatial oscillations) laser generation regime [8]. The system of stimulated oscillation equations of the resonator filled by the active medium has a form for the dimensionless normalized strength of EMF for the main mode E_n:

$$\begin{cases} \dfrac{d^2E_n}{dt^2} + \dfrac{1}{T_{0F}}\dfrac{dE_n}{dt} + (2\pi\nu_{0n})^2 E_n = \dfrac{1}{\varepsilon_0}\dfrac{d^2P_n}{dt^2} \\ \dfrac{d^2P_n}{dt^2} + \dfrac{1}{T_2}\dfrac{dP_n}{dt} + (2\pi\nu_{12})^2 P_n = \dfrac{2d_e^2}{3\cdot 2\pi h} N E_n, \\ \dfrac{dN}{dt} = \alpha_{N0} - \dfrac{N}{T_1} - G_{00}N \cdot \mathrm{Re}\left[P_n \cdot E_n^*\right] \end{cases} \tag{4.17}$$

where $G_{00} = \frac{1}{T_1}\frac{G_0}{\left(1+\kappa E_n E_n^*\right)}$, G_0 is the gain, κ is the nonlinear coefficient. Variables including in Eq. (4.17) are listed in Table 4.1.

Solution of the system of "complete" differential equations Eq. (4.17) even with utilization of numerical methods and modern computers is the labor-intensive but solvable task. This is explained by the fact that the ratio of particle lifetime on the upper level T_1 to the oscillation period of the laser field $T_L = 1/\nu_L$ (where ν_L is the oscillation frequency) is about $T_1/T_L = 10^5$, and the total number of calculated values may exceed 10^8–10^{12}. The solution of Eq. (4.17) is possible to perform applying the analog modeling.

4.2.2 *Nonlinear Symbolic Differential Equations for QWLD*

Introducing the operator $p = \frac{d}{dt}$, taking $p = j2\pi\nu$, where ν is the oscillation frequency of the laser fundamental harmonic, we perform the Laplace transform for our equations. Then we introduce $K_D = \frac{2d_e^2}{3\cdot 2\pi h}$ and fulfilling the algebraic transformations, we have:

Table 4.1 Variables and parameters

Variable	Essence	Formula
E_n	Dimensionless normalized EMF strength of the main mode $E_n = E_L$	$E_L^2 = \frac{c}{n_0}\frac{\varepsilon\varepsilon_0}{2}E^2 \approx 3 \cdot 10^{-3}E^2$, E [V/m]
T_{0F}	Time constant of the optical resonator	$T_{OF} = 10^{-12} - 10^{-8}$ s
$\nu_{0n} = \nu_{0OF}$	Fundamental optical frequency of the resonator	$\nu_{0n} = 231 \cdot 10^{12}$ [1/s]
P_n	Polarization of the active material of the main mode	
T_2	Time constant of the transverse relaxation (polarization)	For QWLD $T_2 = 10^{-12}$ s
ν_{12}	The optical frequency of transition	$\nu_{12} \approx 231 \cdot 10^{12}$ [1/s]
$p_e = d_e$	Dipole moment	$d_e = p_e = 10^{-30}$ [C · m]
N	Population difference between excited and non-excited levels	$N = 10^{16} - 10^{18}$[1/м^3]
T_1	Lifetime of excited particles on upper energy level	$T_1 = 10^{-9}$ s
α_{N0}	$\alpha_{N0} = N_{00}/T_1$, where N_{00} is the average population difference produces by the pumping	
$\hbar = 2\pi h$ ε_0	The Planck constant Permittivity	$\hbar = 6.6 \cdot 10^{-34}$ J · s $\varepsilon_0 = 8.85 \cdot 10^{-12}$ C^2/(N · m^2)

$$\begin{cases} E_n = \dfrac{1}{\varepsilon_0}\dfrac{p^2}{p^2 + \dfrac{1}{T_{0F}}p + (2\pi\nu_{0n})^2}P_n \\ P_n = K_D \cdot \dfrac{1}{p^2 + (1/T_2)p + (2\pi\nu_{12})^2}N \times E_n \cdot \\ pN = \alpha_{N0} - \dfrac{N}{T_1} - G_{00} \cdot N \times \text{ Re}\left[E_n \cdot E_n^*\right] \end{cases} \tag{4.18}$$

We introduce the operator transfer functions (OTF) $K_P(p)$ и $K_E(p)$:

$$K_{E0}(p) = \frac{1}{\varepsilon_0}\frac{p^2}{p^2 + (1/T_{2OF})p + (2\pi\nu_{0n})^2}, \tag{4.19}$$

$$K_{P0}(p) = K_D \cdot \frac{1}{p^2 + (1/T_2)p + (2\pi\nu_{12})^2}. \tag{4.20}$$

The total OTF $K_E \cdot K_P$ is:

$$K_E \cdot K_P = \frac{K_D}{\varepsilon_0}\frac{p^2}{p^2 + (1/T_{2OF})p + (2\pi\nu_{0n})^2} \cdot \frac{1}{p^2 + (1/T_2)p + (2\pi\nu_{12})^2}, \tag{4.21}$$

where $K_{D0} = K_{00} = \frac{2d_e^2}{3 \cdot \varepsilon_0 2\pi h}$.

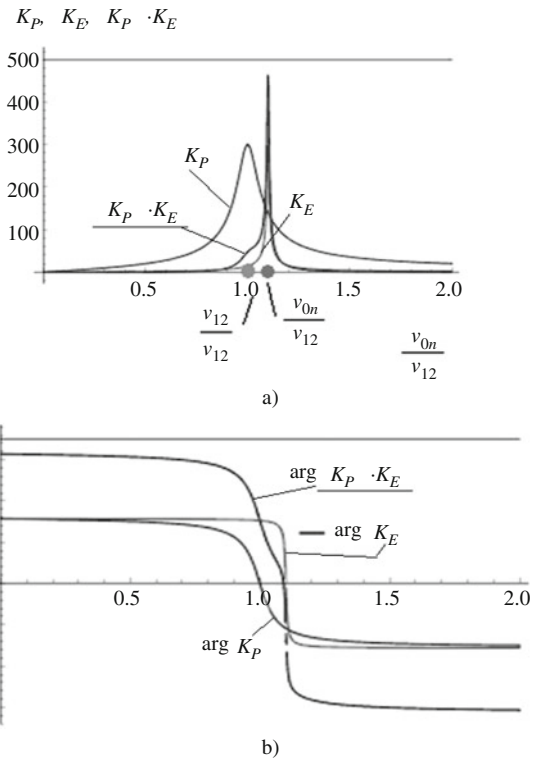

Fig. 4.3 Modules and arguments of OTF of QWLD K_P, K_E,$K_\mathrm{P} \cdot K_\mathrm{E}$ at Q-factor values of the optical resonator $Q_\mathrm{OF} = 100$ and the Q-factor of the spectral line of the active medium $Q_{02} = 10$. The detuning of natural frequencies $(\nu_{0\mathrm{n}} - \nu_{12})/\nu_{12} = 0.1$ is given for clearness

For the analysis convenience, reminding that we consider the quasi-harmonic oscillations in nonconservative oscillating system, we introduced the normalized OTF $K_\mathrm{E}(p) = K_{\mathrm{E}0}(p)/p$ and $K_\mathrm{P}(p) = p \cdot K_{\mathrm{P}0}(p)$. Then, the DE system is written in the compact form as:

$$\begin{cases} E_\mathrm{n} = K_\mathrm{E}(p) \cdot P_n \\ P_\mathrm{n} = K_\mathrm{P}(p) \cdot N \times E_\mathrm{n} \\ pN = \alpha_{\mathrm{N}0} - \dfrac{N}{T_1} - N \times \mathrm{Re}\left[E_\mathrm{n} \cdot P_\mathrm{n}^*\right] \end{cases}, \tag{4.22}$$

Figure 4.3 shows plots of modules and arguments of OTF of QWLD K_P, K_E, $K_\mathrm{P} \cdot K_\mathrm{E}$ for the values of the optical resonator Q-factor $Q_\mathrm{OF} = 100$ and the Q-factor of the spectral line of the active medium $Q_{02} = 10$. The detuning of the natural frequencies $(\nu_{0\mathrm{n}} - \nu_{12})/\nu_{12} = 0.1$ is presented for clearness. In the real QWLDs, the tuning is less than 0.001.

Plots of OTF modules and arguments of the laser at Q-factors of the optical resonators $Q_\mathrm{OF} = 100$ and the spectral line of the active medium $Q_{02} = 10$ demonstrate the narrow spectral line of the module of the total OTF, which in this example is defined by the high-Q optical resonator.

4.2.3 Q-*Factors of Spectral Lines of Amplification of Quantum-Well Laser Diodes*

On the example of examination of two types of lasers, we prove that the Q-factor of the spectral line of the active medium in QWLD is commensurable on the value of the Q-factor of the optical resonator.

Q-factors of the spectral line of QWLD amplification are defined by the structure of the semiconductor. In the modern semiconductor lasers, the materials on the base of the quantum-well structures with three and several quantum wells (or the quantum-dimension zones) are used. At creation of quantum zones in the junction, the laser demonstrates the new qualitative properties: the selection rules in states at junction begin to be performed and the gain of QWLD has the typical peak-shaped curves. Figure 4.4 shows typical functions of the gain g of optical emission versus the energy E_{eff} for the injection semiconductor laser on the *bulk crystal* (a) and QWLD (b) on the base of PInGaAs.

The plot in Fig. 4.4 shows that the Q-factor of the separate "peak" of the spectral line of QWLD amplification (Fig. 4.4b) more than ten times exceeds the Q-factor of the spectral line of amplification of the injection semiconductor laser on the hetero-structure on the bulk crystal (Fig. 4.4a). In modern QWLD, Q-factors of the optical resonators Q_{OF} and Q-factors of the spectral line of the active medium Q_{02} may be quantities of the same order. In the general case, at analysis of the laser model, we cannot consider the Q-factor of the spectral line of amplification as much less than the Q-factor of the optical resonator. Therefore, the QWLD model must be considered as the oscillating system with two degrees of freedom.

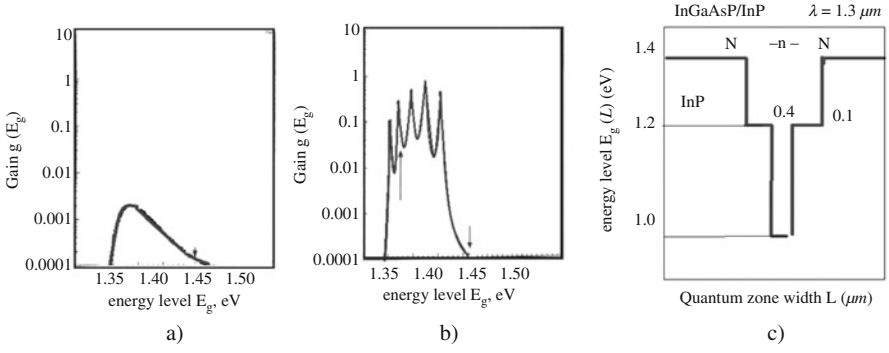

Fig. 4.4 Typical experimental functions of the gain g of the optical emission versus the energy level E_g (Fermi quasi-levels) of the injection semiconductor laser on the hetero-structure (on the bulk crystal) (**a**); of QWLD on the base of PInGaAsP structure with the quantum well with the quantum zone width about 50 nm; the average wavelength of laser emission is $\lambda = 1.3$ μm (**b**). Diagrams of the Fermi quasi-levels of QWLD on the base PInGaAsP (**c**)

4.2.4 Abbreviated Equations of QWLD

The laser of the mentioned DE system (4.17) we represent as SOS, in which oscillations are close to harmonic that is defined by high Q-factors of the resonator and the amplification line. Methods of the approximate analysis developed in the nonlinear oscillation theory include the method of abbreviated equation, which can be used for the QWLD analysis. Using the described in [9] Evtianov method, we can obtain the abbreviated DEs from Eq. (4.22) for the first harmonic of slowly changing amplitudes of P_{10n} and E_{10n}: for the EMF strength $E_n(t) = E_{0n}(t)\cos[2\pi\nu_n t + \varphi_{Ln}(t)]$, for the polarization $P_n(t) = P_{10n}(t)\cos[2\pi\nu_n t + \varphi_{Ln}(t)]$.

According to the Evtianov method, we must find the biased differential operator by choosing the optical frequency $2\pi\nu_{0n}$ as the reference frequency. After normalization of DEs, replacing p_{00} by $j2\pi\nu_{0n} + p_{001}$, we group equation terms in smallness order keeping only the terms of the first smallness order, we obtain the expression for abbreviated OTF in the first approximation [9]. At that, we neglect by the small detuning $\beta = [(\nu_{0n} - \nu_{12})/\nu_{12}]^2 \approx 0.01 \div 0.001$. Then we introduce the dimensionless time τ and the system of abbreviated differential equations takes a form:

$$\begin{cases} \dfrac{dE_{10n}}{d\tau} = K_{D1}P_{10n} - \dfrac{1}{Q_{0F}}E_{10n} \\ \dfrac{dP_{10n}}{d\tau} = K_{D0}\cdot N \times E_{10n} - \dfrac{1}{Q_{02}}P_{10n} \\ \dfrac{dN}{d\tau} = \alpha_{N0} - \dfrac{N}{T_1} - N \times \mathrm{Re}\left[E_n \cdot P_n^*\right] \end{cases}. \tag{4.23}$$

Solutions for *population* and *amplitudes of EMF strength and polarization* are presented in Fig. 4.5 (at abbreviation, the fundamental frequency of the optical resonator is taken as the reference frequency).

Plots in Fig. 4.5 show that the population growth on the upper operating level leads to appearance of the EMF generation with the delay, which is defined by the particle lifetime T_1 on the upper level. The delay defines the time inertia of the laser pumping system. Transient processes of the stationary values of amplitudes of polarization P_{0n} and strength E_{0n} have the oscillating character and qualitatively insignificantly differs one from another. Transient of the stationary value of E_{0n} delays with regard to P_{0n}.

Comparison of QWLD DEs with the RF autonomous oscillator with double-resonance circuits. The first two equations of the DE system (4.17) in many respects coincide with DE of RF oscillator with two resonance circuits and the single active element [10]. The third equation of (4.17) for population reflects inertial regulation of the strength E_n and the polarization P_n. The main difference DEs of QWLD from the RF oscillator with two circuits is the presence of the term $N \times E_n$, which is caused by the laser nonlinearity character.

From the classical oscillation theory, we know that in the system with two freedom degrees, oscillations with two different frequencies are possible as well as oscillations with the single frequency. In such nonconservative SOS with the single

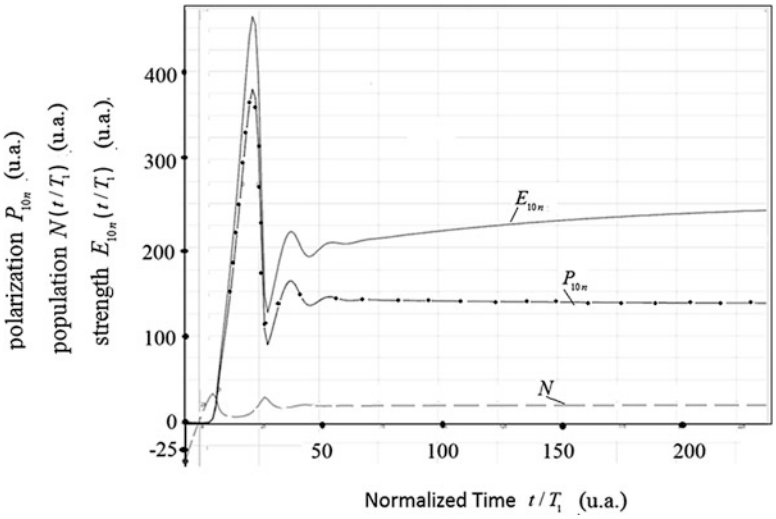

Fig. 4.5 Solutions of abbreviated equations for population N and for normalized slowly changing amplitudes of the first harmonics of strength E_{10n} and polarization P_{10n} for pumping excess by seven times than the threshold value. The time is normalized to the carrier lifetime on the upper operating level T_1. The frequency detuning ν_{0n} and ν_{12} is 0.01, Q-factors are $Q_{OF} = 50$ and $Q_{02} = 33$. The normalized time t/T_1 is on the abscissa axis

nonlinearity (nonlinear element) with detuned resonance circuits, there is a phenomenon of frequency pulling by the circuit with the higher Q-factor. Figure 4.6 shows the typical fragmentation of the phase plane at $Q_1 > Q_2/2$ (b) and at $Q_2 > Q_1/2$ (c). At $Q_1 > Q_2/2$ the double-frequency mode with amplitudes U_{10}, U_{20} is established in the system (b), while at $Q_2 > Q_1/2$ the single-frequency mode with amplitudes U_{20} and $U_{10} = 0$ (c) occurs. The feature of our investigation of the QWLD model is the fact that we only consider the case of the single-frequency generation at equality of fundamental frequency of both circuits.

4.2.5 Analog Laser DEs Model

The analog model (AM) of the DE system (4.17) with utilization of operator transfer functions (4.18)–(4.22) is presented in Fig. 4.7. The analog model contains of two closed feedback loops: for strength E_n and for population. There are three multipliers in this model. In the moment $t = 0$, the "stepped" pumping pulse passes in the input of an adder. From this moment, the population increases to the threshold value and at achievement of this threshold, the laser generation occurs. In the closed FB loop, oscillations excite and then it passes to the output.

The analog model reflects the functional connection of the laser model parameters. This model gives us the understanding how the oscillation amplitude is settled

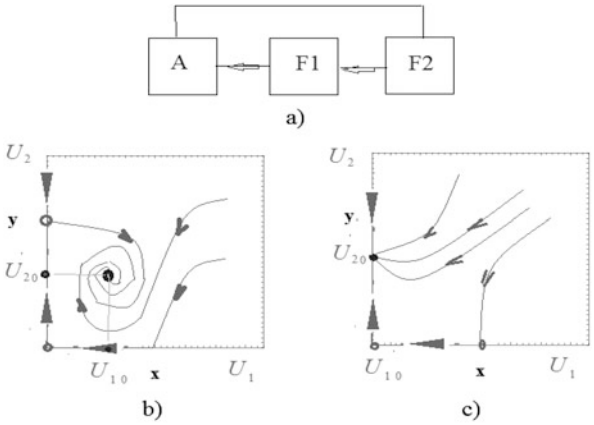

Fig. 4.6 Typical fragmentation of the phase plane for the double-circuit RF oscillator with the active amplifier A and two resonance circuits F1 and F2 with close (but not equal) fundamental frequencies (**a**). Q-factors of the first and second resonance circuits are Q_1 and Q_2, relatively. At $Q_1 > Q_2$/2the double-frequency mode with amplitudes U_{10}, U_{20} is established in the system (**b**), while at $Q_2 > Q_1/2$ the single-frequency mode with amplitudes U_{20} and $U_{10} = 0$ (**c**)

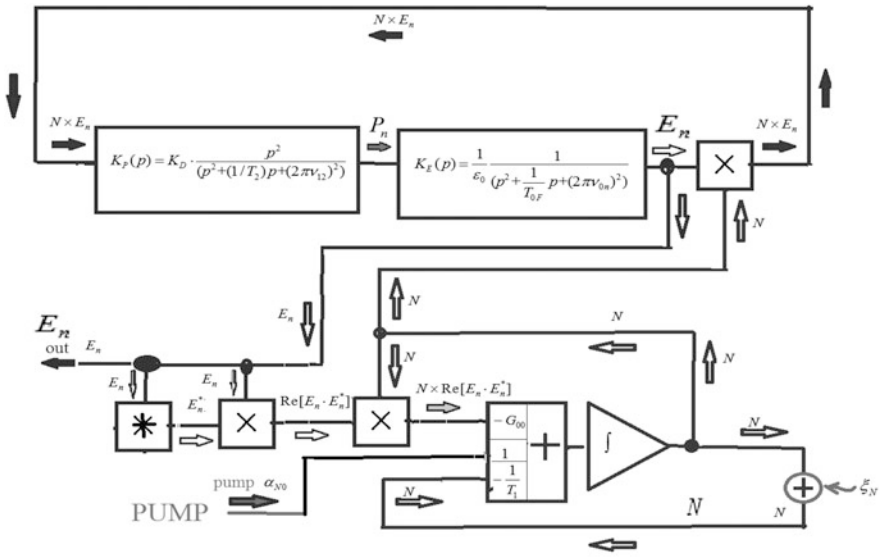

Fig. 4.7 The analog QWLD model formed by DEs (4.23). We used designations: " $\int$"—the integrator, "×"—the multiplier, "+"—the adder, "∗"—the operation of complex conjugation, "PUMP"—α_{N0}. The adder is shown with the noise component of the population ξ_N

during transients and how the time constants T_{0F}, T_2, T_1 and the difference between frequencies ν_{0n} and ν_{12} influence on dynamics. The analog model permits to estimate the influence of coefficients K_{D0}, G_{00} and to perform clearly the analysis of different types of lasers used in OEO: the injection laser diodes with "volumetric" (not quantum-well) active media, QWLD with several quantum wells and quantum points, fiber-optical lasers with the active media (erbium, ytterbium, Nd^{3+} etc,). In contrast to balance kinetic equations, which are presented below and derived from the DE system, this DE system *saves the phase relationships*. As we shall prove in the future, DE are added by the *fluctuation sources*, for instance, the population ξ_N, to solve the task on determination of spectral densities of the phase noise of the laser oscillations and PSD of the phase noise in OEO.

With the help of the correlation analysis adopted in radio engineering, it is not rather complicate to obtain the spectral density of phase and amplitude noises of QWLD. This model allows an analysis of the laser synchronization by the reference laser and investigation of frequency control system in the dynamic mode including PLL systems for lasers used in OEO.

4.2.6 Kinetic Equations of a Laser

To analyze the transients, we address to kinetic equations. At $Q_{0F} \gg Q_{02}$, we use the representation $P_{10n} = Q_{02}K_D \cdot N \times E_{10n}$ considering that $\beta = [(\nu_{0n} - \nu_{12})/\nu_{12}]^2 \approx 0$, then we introduce the dimensionless time τ и multiply E_n by the complex-conjugate quantity E_n^*, and obtain the system of kinetic equations for the square of the first harmonic amplitude (normalized power) of electromagnetic field $E_{10n}^2 = \mathrm{Re}\left[E_n \cdot E_n^*\right]$:

$$\begin{cases} \dfrac{dE_{10n}^2}{d\tau} = G_{00} \cdot N \times E_{10n}^2 - \dfrac{1}{Q_{0F}} E_{10n}^2 \\ \dfrac{dN}{d\tau} = \alpha_{N0} - \dfrac{N}{T_1} - G_{00} \cdot N \times E_{10n}^2 \end{cases}, \tag{4.24}$$

where $G_{00} = Q_{02}K_{00}$ is the gain. Let us consider the features of transients at pumping modulation by stepped and sine signals.

4.3 Laser Kinetic Equations and the Pumping System

With the purpose of pumping effect (taking into account time delays) and other features, we represent the plots of laser transients of the field strength and the inversed population on the base of balance kinetic equations at pumping activation (stepped pumping pulse) and at sine pumping modulation.

4.3.1 Laser Pumping System

The population difference $N(t) = N_2 - N_1$ (where N_2 and N_1 are populations of the second and first levels, relatively) is determined from the third DE (4.17) for particles being under impact of pumping α_{N0}, it follows that at pumping variation $\alpha_{N0}(t)$ in the form of the stepped pulse:

$$\alpha_{N0}(t) = \begin{cases} 0, & t < 0 \\ N_{0P}/T_1, & t > 0 \end{cases}, \tag{4.25}$$

before the moment of generation beginning (i.e., stimulated laser emission $E_n = 0$) the population difference N increases obeying

$$N(t) = N_0[1 - \exp(-t/T_1)], \tag{4.26}$$

where lifetime on the upper level T_1 defines the growth constant, and $1/T_1$ is a probability of stimulated transition. At achievement of the threshold value, in the quasi-stationary mode, the population depends on the amplitude square E_{0n}^2, i.e., $E_{0n}^2 = \mathrm{Re}\left[E_n \cdot E_n^*\right]$, where "$*$" is the operation of conjugation. In stationary (or quasi-stationary) mode $\frac{dE_{10n}^2}{d\tau} = 0$, $\frac{dN}{d\tau} = 0$ and from Eq. (4.24), it follows that $N = \frac{1}{G_{00}Q_{0F}}$ and $0 = \alpha_{N0} - \frac{N}{T_1} - G_{00} \cdot N \times E_{10n}^2$.

At achievement of the threshold, the laser transfers in the generation state. Variables values in the steady-state mode are $E_{10n}^2 = E_0^2$ and $N = N_0$:

$$N = \frac{N_{0P}}{\left[1 + T_1 G_{00} E_{10n}^2\right]}. \tag{4.27}$$

Figure 4.8 shows the transient scenario in the laser at stepped variation of the normalized pumping level $\alpha_{N0} = J_0 = 20$. The steady-state point is the interception point (Fig. 4.8d) of the plot 1 $N = \frac{1}{G_{00}Q_{0F}}$ and the plot 2 calculated on Eq. (4.27).

4.3.1.1 Laser Modulation by Sine Oscillation

At laser modulation of the harmonic oscillation, the population difference $N(t)$ delays relative the pumping pulse $\alpha_{N0}(t)$. This delay is determined by the lifetime T_1 on the operating level. At pumping variation on the harmonic law (the case of DM in OEO) with some radio frequency f_o and the modulation index m_0 in the form:

$$\alpha_{N0}(t) = \begin{cases} 0, t < 0 \\ (N_0/T_1) \cdot [1 + m_0 \cos(2\pi f_o t)], t > 0 \end{cases}.$$

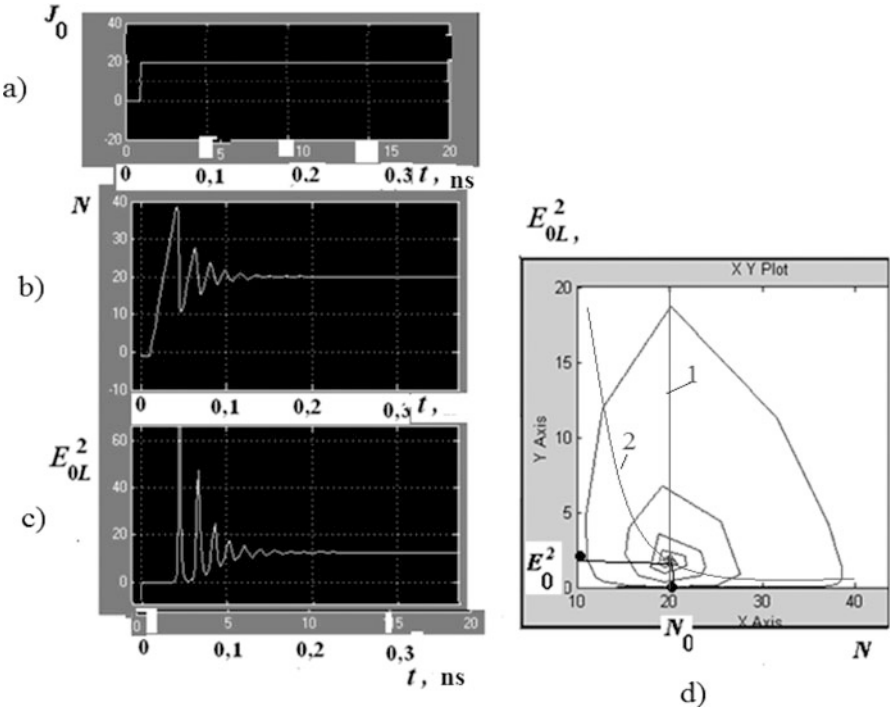

Fig. 4.8 The transient scenario in the laser at stepped variation of the normalized pumping level $\alpha_{N0} = J_0 = 20$. Time-functions for normalized values of the pumping currents J_0 (**a**), and population difference N (**b**), (**c**) normalized strength square $(E)^2 = (E_{0L})^2$, (dimensionless quantity), (**d**) time-function of E_{0L}, N_0

In quasi-stationary mode, $N(t)$ varies on the harmonic law with some delay in phase $2\pi f_0 T_1$. For $N(t)$we have: $N(t) = N_{00} \cdot \left[1 + \frac{m_0}{\sqrt{1+(2\pi f_0 T_1)^2}} \cos(2\pi f_0 t + 2\pi f_0 T_1)\right]$. The pumping current contains DC and AC components and is equal $J_L = J_{L0} + J_{L1}$. The AC component J_{L1} of the pumping current is modeled by the generator of harmonic oscillations, the DC component of the pumping current J_{0L} is modeled by the generator of stepped current variation of by a jump. The transient scenario in the laser at sine variation of the pumping level (by the amplitude of the *first harmonic* $J_{01} = 15$) at the constant pumping level $J_0 = 30$ is presented in Fig. 4.9. In presented time-functions, we see that nonlinear transient in the oscillating system is close to the sine process, which is interpreted in the phase portrait in the form of a cycle.

From presented plots of modulation by the sine signals, we see that at increase of the oscillation amplitude (the modulation index), the nonlinear distortions arise connected with appearance of harmonics in the spectrum.

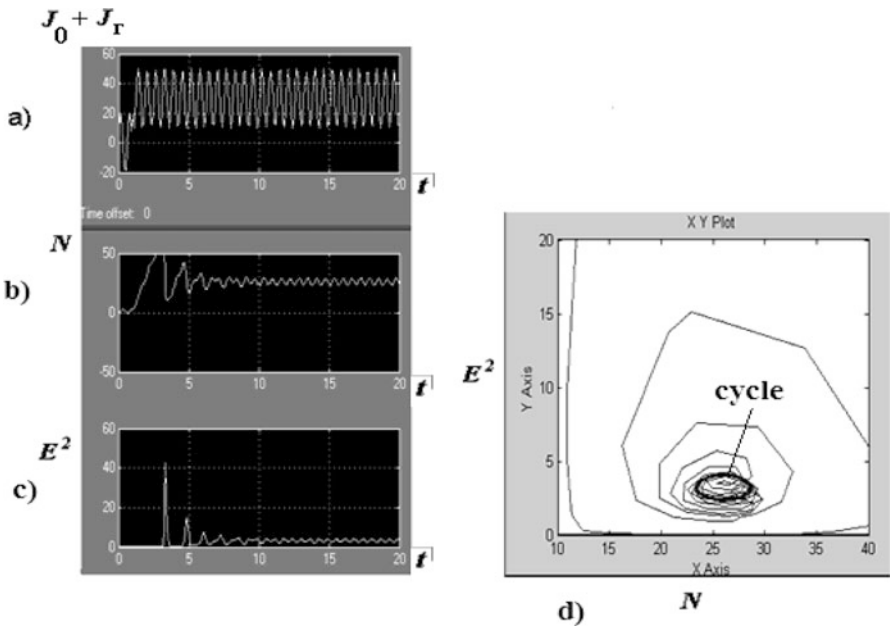

Fig. 4.9 Laser modulation by the sine pumping signal of the *small* amplitude with the constant bias from the external generation. The transient scenario in the laser at sine variation of the pumping level (by the amplitude of the first harmonics) at constant pumping level. Time-functions for normalized values (**a**) the pumping current $J_0(1)$, (**b**) the population difference N (10^{16} 1/cm^3), (**c**) the normalized strength square $(E)^2 = (E_{0L})^2(1)$, (**d**) the time-function E_{0L}, N_0. The limit cycle in the time diagram E_{0L}, N_0 (**d**) is shown

4.3.1.2 Oscillation Delay in the FB Channel of the Optical Resonator

It is necessary to bear in mind that in the laser, there may exist the delay of the field oscillations in the optical FB channel besides inertial properties, which are defined by carriers' lifetime T_1 on the upper operating level. In the laser, the resonator length exceeds the optical wavelength of laser oscillations, and the light delay is T_R per one passage through the FB loop. We note that having passed through the FB loop, oscillations again pass in the optical amplifier input with the delay by time of resonator passing (here we mean the resonator of traveling-waves): $T_R = n_0 L_R / c$.

We emphasis that the mentioned system of three differential equations (two equations of second order and the one equation of first order) is complicate for engineering calculations of QWLD characteristics and is not optimal for investigation OEO as a whole (Fig. 4.10).

We would like to note that the traditional laser analysis, as a rule, is based on the transfer to balance kinetic equations and its examinations. However, at that, we loose the valuable information about phase relationships, i.e., information on the phase of field strength oscillations and phase noises. At that, we cannot estimate the effects of many other parameters upon the generation development. In the future, we shall

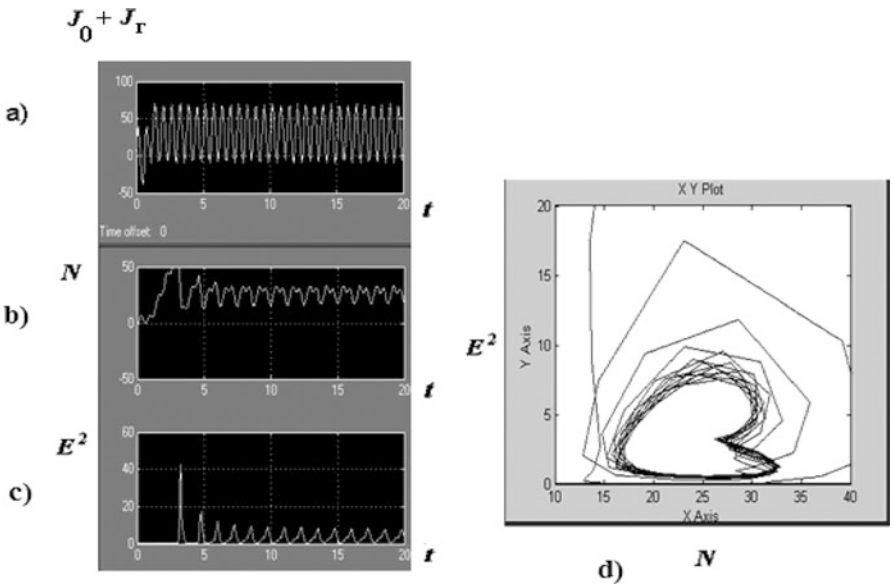

Fig. 4.10 Laser modulation by the sine signal of the *large* amplitude with the constant bias from the external RF generator. The transient scenario in the laser at sine variation of the pumping level (by the amplitude of the *first harmonic* $J_{01} = 40$) for constant pumping level $J_0 = 30$. Time-functions for normalized values (**a**) the pumping current $J_0(1)$, (**b**) the population difference, (**c**) the normalized strength square $(E)^2 = (E_{0L})^2(1)$, (**d**) the time diagram E_{0L}, N_0. The limit cycle in the time diagram E_{0L}, N_0 is shown

perform the analysis of the laser model on the base of classical scheme adopted in the oscillation theory. For this, we transfer from the above-mentioned system from three equations to the DE system consisting of two nonlinear symbolic differential equations. Further, we reduce the system to the single differential symbolic equation, which in quasi-stationary mode takes into account features and parameters of the laser constitutive model, which are necessary for OEO investigation including the phase noise analysis.

4.3.2 Nonlinear Symbolic DEs for QWLD

Let us obtain the system of **nonlinear symbolic differential equations**:

$$\begin{cases} \left(p^2 + \dfrac{1}{T_{0F}}p + (2\pi\nu_{0n})^2\right)\left[p^2 + (1/T_2)p + (2\pi\nu_{12})^2\right]E_n = K_\alpha p^2 S_L(N \cdot E_n) \\ pN = \alpha_{N0} - \dfrac{N}{T_1} - G_{00}N \cdot \mathrm{Re}\left[E_n E_n^*\right] \end{cases}. \tag{4.28}$$

The first equation of the mentioned system is the nonlinear equation of the fourth order for the instantaneous value of the normalized field strength. The second equation is the equation of the first order for the population.

The main parameters of such a system of DE are the time constant T_2 (or the Q-factor of the spectral line of laser emission $Q_{02} = \nu T_{02}$) and the time constant T_{0F} (or the Q-factor of the optical resonator $Q_{OF} = \nu T_{OF}$), the lifetime of carriers on the upper operating level T_{1n}, and the gain (of the saturation coefficient) G_{00}. We note that this SOS system has double-circuit (or double-resonance) network with the inertial pumping (energy feed). The operation feature is the presence of automatic control of the laser generation level by means of variation of laser pumping (or feed). At decrease or increase of the laser generation amplitude, pumping provides its recovering up to steady-state value. This control mode is similar to regulation of the laser power at sensing with the help of the photodetector. The power control is performed by variation of the pumping current.

The term in the right side of the first equation describes of the exciting force, which is proportional to the product $N \cdot E_n$. At that, oscillations of the field strength E_n are the "fast" function. The "slow" function N reflects the population difference on the upper level and depends on pumping.

From the second equation, we can express the function $\boldsymbol{N(p)}$ transferring to the formal symbolic notation: $\boldsymbol{N}(\boldsymbol{p}) = \alpha_{N0} / \left\{ p + \frac{1}{T_i} + G_{00} \cdot \text{Re}\left[E_n E_n^*\right] \right\}$. With the purpose to determine the nonlinearity in this system of DEs, we write the product of the field strength by population in the time domain: $N(t) \cdot E_n(t) = N_{00} \cdot E_{0n}(t) \cos(2\pi\nu_n t + \varphi_{Ln}(t) + 2\pi\nu_n T_{OY})$.

The laser in this equation can be interpreted as the generator with the active element, which is characterized by the gain K_α and the nonlinearity $S_L(E_n)$. In the general case, at large densities of the field strength, the function $S_L(E_n)$ has inertial properties: $S_{LT}(E_n) = S_L(E_n) \cdot \exp(-j2\pi\nu_{0n} T_{OY})$. By the mathematical notation, these equations are similar to differential equations of the autonomous RF oscillator with two stages, each of which is loaded on the oscillating circuit.

The natural frequencies of oscillating circuits are equal (up to thousandth parts). The DE system is also similar to the equation of the autonomous oscillator with inertial feed [9]. The laser pumping plays a role of the laser "power supply." To take into consideration the delay in the FB loop, the right term can be supplemented by the multiplier $\exp(-j2\pi\nu_{0n} T_R)$. In differential equations, we can take into account the nonlinearity and inertial properties of the active medium arising at strong fields.

Let us write the term in the right side of the first DE introducing the gain:

$$K = \frac{2 \cdot 2d_e^2}{3 \cdot \varepsilon_0 2\pi h} N_{00}. \tag{4.29}$$

Then we extract the nonlinear function $S_L(N \cdot E_n) = (N/N_{00}) \cdot E_n$. Now we can write the right term in DE as:

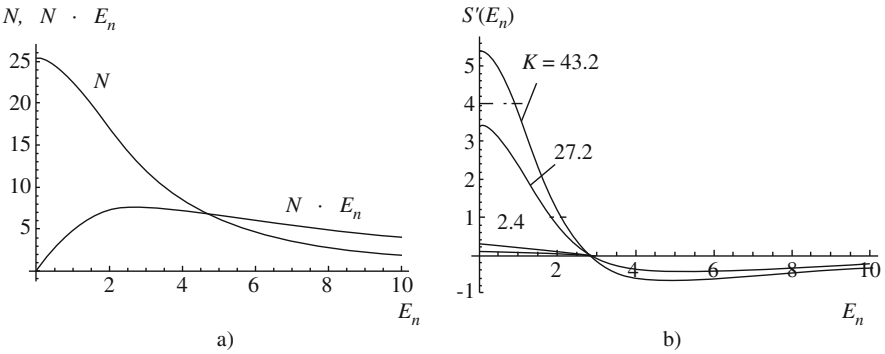

Fig. 4.11 Functions of population difference N and the product $N \cdot E_\mathrm{n}$ versus amplitude E_n as the function of amplitude E_n (**a**), and the derivative $(N \cdot E_\mathrm{n})'$ (the slope of the nonlinear characteristic) for different values of pumping (**b**)

$$\frac{1}{\varepsilon_0}\frac{2d_\mathrm{e}^2}{3\cdot 2\pi h}p^2 N\cdot E_\mathrm{n} = \frac{1}{\varepsilon_0}\frac{2d_\mathrm{e}^2 N_{00}}{3\cdot 2\pi h}p^2\frac{N}{N_{00}}\cdot E_\mathrm{n} = K_\alpha p^2\frac{N}{N_{00}}\cdot E_\mathrm{n}$$
$$= K_\alpha p^2 S_\mathrm{L}(N\cdot E_\mathrm{n}). \tag{4.30}$$

At values $N_{00} = 10^{+16} - 10^{+17}$ m^{-3} and $d_\mathrm{e} = 1.2\cdot 10^{-30}$ [C · m], the gain, which is defined by the difference of N_0 and the dipole moment d_e, is approximately equal: $K = \frac{2\cdot 2d_\mathrm{e}^2}{\varepsilon_0 2\pi h}N_{00} = \frac{2\cdot 2\cdot\left(1.2\cdot 10^{-30}\right)^2\cdot 10^{+16}-10^{+17}\cdot 10^{+17}}{8.85\cdot 10^{-12}\cdot 6\cdot 6.6\cdot 10^{-34}} \approx 1-10$. Now we obtain for N the formal notation at $p = 0$. We call the extracted nonlinear function $S_\mathrm{L}(E_\mathrm{n}) = N\cdot E_\mathrm{n}$ as the linear-hyperbolic function of the nonlinear element of the laser model. For it, the following formula is true:

$$S_\mathrm{L}(E_\mathrm{n}) = N\cdot E_\mathrm{n} = \frac{T_1\alpha_{\mathrm{N}0}E_\mathrm{n}}{1+T_1 G_{00}\cdot \mathrm{Re}\left[E_\mathrm{n}E_\mathrm{n}^*\right]} = \frac{T_1\alpha_{\mathrm{N}0}E_\mathrm{n}}{1+T_1 G_{00}\cdot\left(E_{0\mathrm{n}}\right)^2}. \tag{4.31}$$

Figures 4.11 and 4.12 show the functions of population difference N versus E_n, as well as its derivative for different values of pumping K.

Presented functions of the amplitude $E_{0\mathrm{n}}$ (a), the product $N\cdot E_{0\mathrm{n}}$ and the derivative $(N\cdot E_\mathrm{n})'$ permit the determination of oscillation amplitude in the steady-state mode.

Figure 4.12 shows the functions of the product $N\cdot E_\mathrm{n}$ in the laser versus the amplitude E_n for different values of pumping K.

From Figs. 4.11 and 4.12, we see that steady-state points of the generator (the laser model) correspond to interception points of plots E_n and $N\cdot E_\mathrm{n}$. At weak pumping, i.e., when the threshold inversed population does not achieve, these interception points are absent. At pumping growth, on the branch, where the slope of the nonlinear function $N\cdot E_\mathrm{n}$ is less than zero, functions have the interception point. From the plot, it is clear that one of conditions of laser generation existence

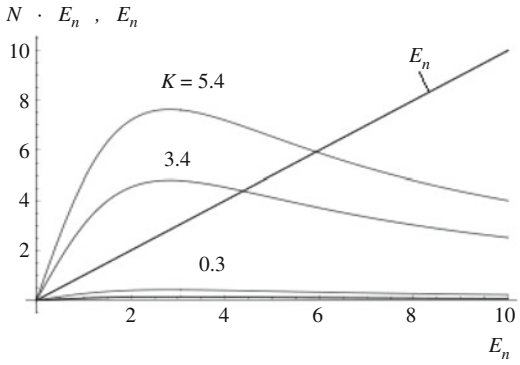

Fig. 4.12 Functions of the product $N \cdot E_\mathrm{n}$ in the laser versus the amplitude E_n for different values of pumping. To determination of the steady-state point of the laser

(or self-excitation) is $N \cdot E_\mathrm{n} > E_\mathrm{n}$, and one of conditions of oscillations' existence is the fulfillment of inequality $(N \cdot E_\mathrm{n})' < 0$. From the previous plot, it can be seen that for specified values, the point of the sign changing of derivative is $E_\mathrm{n} = 2.75$. Let us continue to analyze the DE system and transfer to simplification of the laser analog model.

The laser analog model, which presented at Fig. 4.11 on the base of the constitutive equations in the dipole approximation, contains the operator transfer functions K_E and K_P. The pumping block in Fig. 4.11 is shown in the mutual block with the operator transfer function K_N and marked by the blue color. Operator transfer functions are:

$$K_\mathrm{E} = \frac{1}{\varepsilon_0} \frac{p^2}{p^2 + \frac{1}{T_{0\mathrm{F}}} p + (2\pi\nu_{0\mathrm{n}})^2}, \quad K_\mathrm{P} = \frac{K_\mathrm{D}}{p^2 + \frac{1}{T_2} p + (2\pi\nu_{12})^2},$$

$$K_\mathrm{N} = \frac{1}{1 + \frac{1}{T_1} + G_{00}\,\mathrm{Re}\left[E_\mathrm{n} \cdot E_\mathrm{n}^*\right]}. \tag{4.32}$$

We note that introduction into the analog model of the formal coefficient $K_{E1} = 1$ (or slightly more than unit) allows solution of the task of transformation of the external pumping network in the laser analog model (see Fig. 4.7), which is shown in Fig. 4.13.

With the purpose of obtaining and analyzing of DEs for the quasi-stationary mode, we continue transformation of structures presented in Fig. 4.7. The quasi-stationary mode of laser operation is the laser operation mode with the high excess of pumping over its threshold value. In the following Section we shall give the expression for population in the frequency domain $N(j2\pi(\nu - \nu_0))$ in quasi-stationary mode.

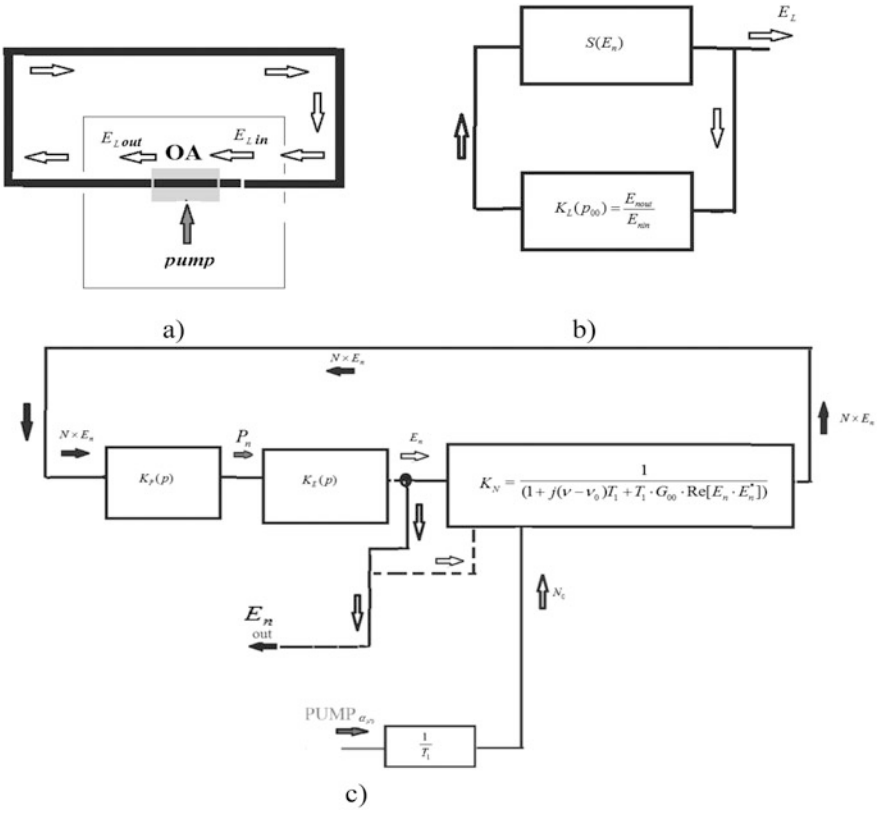

Fig. 4.13 (**a**) The structure of the laser model with the closed loop of the positive feedback and the active medium (OA). The optical oscillations of the field strength $E_{\mathrm{L.\ in}}$ affect to the OA input. After amplification we have in the optical OA output $E_{\mathrm{L.\ out}}$. (**b**) The laser analog model in quasi-stationary mode presented with the help of the control operator transfer function $K_{\mathrm{L}}(p_{00}) = E_{\mathrm{L.\ out}}/E_{\mathrm{L.\ in}}$ and the nonlinear element $S(E_{\mathrm{n}})$. (**c**) The laser analog model in the dipole approximation in the quasi-stationary small-signal mode

4.3.3 Population and the Laser Analog Model in the Quasi-Stationary Mode

The structures of the laser analog model (Figs. 4.7 and 4.13) show that the pumping system is the system of the negative feedback with inertia for the control or restriction of the oscillation amplitude of the field strength taking into consideration the laser power $E_{0\mathrm{n}}^2 = \mathrm{Re}\left[E_{\mathrm{n}}E_{\mathrm{n}}^*\right]$. At that, the following expression is true for the population:

$$N[\,j2\pi(\nu-\nu_0)] = \frac{1}{1+T_1\cdot j2\pi(\nu-\nu_0)}\cdot\frac{N_0}{1+\frac{T_1\cdot G_{00}\cdot E_{0n}^2}{1+T_1\cdot j2\pi(\nu-\nu_0)}}. \tag{4.33}$$

We introduce the coefficient $K_N[j2\pi(\nu - \nu_0)]$, which we define as: $K_N[\,j2\pi(\nu-\nu_0)] = \frac{N[\,j2\pi(\nu-\nu_0)]}{N_0}$. The last representation allows the solution of the task on transformation of external pumping block in the laser analog model (Fig. 4.7) into the laser analog models shown in Fig. 4.13.

The laser analog model in the dipole approximation in the quasi-stationary mode is presented in Fig. 4.13c. Its peculiarity consists in the fact that the pimping block is located into a loop (a circuit) of the positive feedback. Restrictions of such a "single-loop" (or single-circuit) laser model are discussed later. To find out solutions of the symbolic differential equations, we perform the normalization of the laser symbolic DE.

In the laser analog model presented in Fig. 4.13a, the closed loop of the positive FB with the active medium (OA) is shown. The optical oscillations of the strength $E_{L.\ in}$ act in the OA input. Amplified strength oscillations $E_{L.\ out}$ act in the optical output of OA. The laser analog model in the quasi-stationary mode is presented in Fig. 4.13b with the help of the control operator transfer function $K_L(p_{00}) = E_{L.\ out}/E_{L.\ in}$ and the nonlinear element $S(E_n)$.

4.3.4 *Normalized Differential Equations of the Laser*

We introduce the operator $p_{00} = p/(2\pi\nu_{0n})$ and normalized variables: $G_{0n} = \frac{G_0}{2\pi\nu_{0n}T_1N_{00}}$, $\tau = t\cdot 2\pi\nu_{0n}$, $T_{1n} = 2\pi\nu_{0n}T_1$, $N_n = \frac{N}{N_{00}}$, $\alpha_{nN0} = \frac{\alpha_{N0}}{N_{00}2\pi\nu_{0n}}$ and use the approximation of N_n in the vicinity of optical frequencies $2\pi(\nu - \nu_{0n})$:

$$N_n = \frac{N_0}{1+j[(\nu/\nu_{0F})-1)]T_{1n}+T_{1n}G_{00n}\,\mathrm{Re}\left[E_n\cdot E_n^*\right]}. \tag{4.34}$$

Now we introduce the designation of the operator function:

$$Y(p_{00}) = \frac{1}{{p_{00}}^2} \times\left[p_{00}^4+\left(\frac{1}{Q_{0F}}+\frac{1}{Q_{02}}\right)p_{00}^3+\left(2+\frac{1}{Q_{0F}}\cdot\frac{1}{Q_{02}}\right)p_{00}^2+\left(\frac{1}{Q_{0F}}+\frac{1}{Q_{02}}\right)p_{00}+1\right]. \tag{4.35}$$

After performing of the **normalization** at $\beta = [(\nu_{0n}-\nu_{12})/\nu_{12}]^2 \approx 0.001$, the last expression can be written in the compact form:

$$Y(p_{00})E_{\mathrm{n}} = K_{00}N_{\mathrm{n}}E_{\mathrm{n}}. \tag{4.36}$$

In the time domain $\tau = t \cdot 2\pi\nu_{0\mathrm{n}}$ and dividing the equation by the threshold value of the population N_{00}, we may write equations in the final form:

$$\begin{cases} a_{00}\dfrac{\mathrm{d}^4E_{\mathrm{n}}}{\mathrm{d}\tau^4} + a_{10}\dfrac{\mathrm{d}^3E_{\mathrm{n}}}{\mathrm{d}\tau^3} + a_{20}\dfrac{\mathrm{d}^2E_{\mathrm{n}}}{\mathrm{d}\tau^2} + a_{30}\dfrac{\mathrm{d}E_{\mathrm{n}}}{\mathrm{d}\tau} + a_{40}E_{\mathrm{n}} = K_{00}\cdot\dfrac{\mathrm{d}^2}{\mathrm{d}\tau^2}N_{\mathrm{n}}\cdot E_{\mathrm{n}}(\tau) \\ N_{\mathrm{n}} = \dfrac{N_0}{\left[1 + j[(\nu/\nu_{0\mathrm{F}}) - 1]T_{1\mathrm{n}} + T_{1\mathrm{n}}G_{0\mathrm{n}}\,\mathrm{Re}\left[E_{\mathrm{n}}\cdot E_{\mathrm{n}}^*\right]\right.}, \end{cases} \tag{4.37}$$

where coefficients a_{00}, a_{10}, a_{20}, a_{30}, a_{40} for $\nu_{0\mathrm{n}} \approx \nu_{12} \approx \nu_{0\mathrm{F}}$ are included into Tables 4.1, 4.2, and 4.3. Initial conditions for differential equations are: $E_{\mathrm{n}}(t=0) = E_{\mathrm{n}000}$, $N_{\mathrm{n}}(t=0) = N_{000}$ and $E_{\mathrm{n}000} > 0$.

Let us discuss the **model restrictions** at introduction in the FB loop of the nonlinearity, which is caused by the population saturation effect, as it is shown in Fig. 4.13c (which is built on the base of Eq. (4.37)). The question is put: will the motion laws, which were laid in the original system of three differential equations of the laser in the quasi-stationary mode, be disturbed at transfer of the pumping block in the FB loop or not? The nonlinearity, which is introduced in the positive FB loop of the laser model, restricts the oscillation amplitude of the field strength and produces the higher-order harmonics of the field strength, which examination goes out of limits of this book because we assume that their amplitudes are small due to the high Q-factor of the laser SOS. The second question during the transfer of the pumping block into the positive FB loop is the issue about dynamics and field fluctuations and population fluctuations filtering, which will be considered in Chap. 5. The investigation of obtained DEs (4.37) fulfilled by authors for the quasi-stationary mode gives the time-functions and conditions of oscillation stability in the steady-state point (which are discussed later) and confirm that the Eq. (4.37) enough accurate in qualitative and quantitative sense describe the influence of main parameters and characteristics at small and moderate field amplitudes at large excess of pumping over the threshold values. The calculation of the laser phase noise is performed in the steady-state point with much more values than the threshold one. At that, the effect of population fluctuations on the phase noise of the field strength is taken into account. Discrepancy of results of equation solution for quasi-stationary mode and results of the complete DE system is observed only in the region of small pumping (1.01–1.1). We can add that the modern commercially available QWLDs have the small threshold pumping current (less than 10 mA at normal operating currents 50–70 mA). Therefore, an analysis of discussing differential equations (4.37) of the laser model is relevant and significant.

From analysis of Table 4.4, we can make conclusions: for different resonance systems of examined lasers, coefficients $a_{00} = 1$, $a_{40} = 1$, coefficient with the accuracy to one thousandth part are approximately equal: $a_{10} \approx a_{30}$ and depends

Table 4.2 Values of parameters for different types of lasers

Types of lasers	Laser diodes without quantum wells	QWLD without Bragg resonator (InGaAlAs/InP[a])	QWLD (InGaAlAs/InP[a]) with Bragg resonator	Fiber-optical laser Yt, Nd3+	QWLD (InGaAlAs/InP[a]) with toroid resonator (SiO_2)
Time constant of optical resonator T_{0F}, s	$1.2 \cdot 10^{-12}$	$1.2 \cdot 10^{-12}$	10^{-8}	10^{-9}	$10^{-8}/10^{-5}$
Q-factor of optical resonator (filter) $Q_{0F} = 2\pi\nu_{0n} \cdot T_{0F}$ at natural optical frequency $\nu_{0n} = 2.3 \cdot 10^{14}$ 1/s	$2.76 \cdot 10^2$	$2.76 \cdot 10^2$	$2.3 \cdot 10^6$	$2.3 \cdot 10^5$	$2.3 \cdot 10^6$ $/2.3 \cdot 10^9$
Time constant T_2, s	10^{-12}	$7.2 \cdot 10^{-12}$	$7.2 \cdot 10^{-12}$	10^{-12}	$7.2 \cdot 10^{-12}$
Q-factor of spectral line at optical frequency $\nu_{0n} = 2.3 \cdot 10^{14}$ 1/s$Q_{02} = 2\pi\nu_{0n} \cdot T_2$	$2.3 \cdot 10^2$	$1.6 \cdot 10^3$	$1.6 \cdot 10^3$	$2.3 \cdot 10^3$	$1.6 \cdot 10^3$
Lifetime T_1 of carrier on upper level	10^{-9}	$0.5 \cdot 10^{-9}$	10^{-9}	10^{-4} – 10^{-6}	$0.5 \cdot 10^{-9}$
Maximal gain $K_\alpha = \frac{2 \cdot 2p_e^2}{\varepsilon_0 2\pi h} N_{00}$	10^1	10^1	10^1	10^1	10^1

[a]InGaAlAs/InP is QWLD with the wavelength 1.3 μm

on total losses in the system, their values vary for various laser types from 0.008 to 0.000439. The coefficient a_{20} is equal $a_{20} \approx 2$ with accuracy of thousandth and less.

For laser diodes without quantum wells (taking into account that at $\nu_{0n} \approx \nu_{12}$ coefficients are mentioned in Table 4.3), we can write in Eq. (4.37): $a_{00} = 1$, $a_{40} = 1$, $a_{10} \approx a_{30} = 0.008$, $a_{20} \approx 2$.

4.4 Abbreviated DE for the Laser in Quasi-Stationary Mode

4.4.1 Approximation of the Complex Nonlinearity $\mathbf{E}_n \times \mathbf{N}_n$ *by Cubic Polynomial*

We may approximate of linear-hyperbolic nonlinearity of laser "saturation" by the third-order polynomial for convenience of calculation of analytical functions:

$$S(E_n) = E_n \times N_n = \frac{E_n \times N_0}{1 + j2\pi(\nu - \nu_0)T_{1n} + T_{1n}G_{0n}\,\mathrm{Re}\left[E_n \cdot E_n^*\right]} \approx \alpha_{0L}E_n - \beta_{0L}E_n\,\mathrm{Re}\left[E_n \cdot E_n^*\right], \tag{4.38}$$

Table 4.3 Values of parameters and **normalized** coefficients in DE for various types of lasers

Laser type	Laser diodes without quantum wells	QWLD without Bragg resonator (InGaAlAs/InP[a])	QWLD (InGaAlAs/InP[a]) with Bragg resonator	Fiber-optical laser Yt, Nd3+	QWLD (InGaAlAs/InP[a]) with toroid resonator (SiO_2)
$a_{10} = a_{30} = \left(\frac{1}{Q_{0F}} + \frac{1}{Q_{02}}\right)$	0.008	0.004248	0.000625	0.000439	0.000625
$a_{20} \approx 2 + \frac{1}{Q_{0F}Q_{02}}$	$2.0 + 1.57 \cdot 10^{-5}$	$2 + 2.26 \cdot 10^{-6}$	$2 + 2.71 \cdot 10^{-10}$ $= 2.000000000271$	$2 + 1.89 \cdot 10^{-9}$ $= 2.00000000189$	$2.0 + 2.72 \cdot 10^{-12}$ $= 2.000000000000272$

Table 4.4 Normalized coefficient of DE

Normalized coefficient of DE	Values of coefficients
a_{00}	1
a_{10}	$\left(\frac{1}{Q_{0F}}+\frac{1}{Q_{02}}\right) \xrightarrow{Q_{0F}\gg Q_{02}} \frac{1}{Q_{02}}$
a_{20}	$2+\frac{1}{Q_{0F}Q_{02}} \xrightarrow{Q_{0F}\gg 1, Q_{02}\gg 1} 2$
a_{30}	$\left(\frac{1}{Q_{0F}}+\frac{1}{Q_{02}}\right) \xrightarrow{Q_{0F}\gg Q_{02}} \frac{1}{Q_{02}}$
a_{40}	1

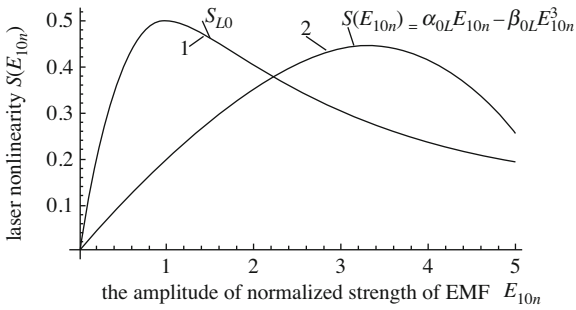

Fig. 4.14 Approximation of the laser nonlinearity $S_{L0} = N_0 E_{10n}/\left(1 + T_{1n}G_{00}E_{10n}^2\right)$ (curve 1) by the cubic polynomial $S(E_{10n}) = \alpha_{0L}E_{10n} - \beta_{0L}E_{10n}^3$ (curve 2)

where coefficients α_{0L} and β_{0L} are inertial and express the pumping "action." Such a representation enables to perform the extraction of the inertial part in nonlinearity and execute easier algebraic actions during finding of oscillation amplitude in abbreviated equations. Figure 4.14 shows an explanation to approximation of laser nonlinearity by the cubic function.

The algebraic replacement is presented below. Let us represent the product $E_{10n} \times N_n$, in which E_{10n} is the amplitude of the field first harmonics, as:

$$E_{10n} \times \frac{N_0}{1 + j2\pi(\nu - \nu_0)T_{1n} + T_{1n}G_{00}E_{10n}^2} = \frac{1}{1 + j2\pi(\nu - \nu_0)T_{1n}} \cdot \frac{E_{10n}N_0}{1 + [1 + j2\pi(\nu - \nu_0)T_{1n}]^{-1} + T_{1n}G_{00}E_{10n}^2}. \tag{4.39}$$

Now we extract the real and imaginary parts in the last expression

$$\frac{N_0}{1 + j2\pi(\nu - \nu_0)T_{1n} + T_{1n}G_{00}E_{0n}^2} = \frac{N_0\left[1 + T_{1n}G_{00}E_{0n}^2\right]}{\left(1 + T_{1n}G_{00}E_{0n}^2\right)^2 + [2\pi(\nu - \nu_0)T_{1n}]^2} - j\frac{N_0[2\pi(\nu - \nu_0)T_{1n}]}{\left(1 + T_{1n}G_{00}E_{0n}^2\right)^2 + [2\pi(\nu - \nu_0)T_{1n}]^2}. \tag{4.40}$$

In order to obtain the first and second derivative over E_{10n}, we represent S_L as:

$$S_{\mathrm{L}} = N_0 \left\{ \frac{E_{10\mathrm{L}}}{\left(1 + T_{1\mathrm{n}} G_{00} E_{10\mathrm{n}}^2\right)^2 + \left[2\pi(\nu - \nu_0) T_{1\mathrm{n}}\right]^2} \right\} \cdot \left\{ \left(1 + T_{1\mathrm{n}} G_{00} E_{0\mathrm{n}}^2\right) - j[2\pi(\nu - \nu_0) T_{1\mathrm{n}}] \right\}. \tag{4.41}$$

Now we obtain the following expression:

$$S_{\mathrm{L}} = N_0 \frac{E_{10\mathrm{L}}}{\left\{ \left(1 + T_{1\mathrm{n}} G_{00} E_{10\mathrm{n}}^2\right)^2 + \left[2\pi(\nu - \nu_0) T_{1\mathrm{n}}\right]^2 \right\}^{1/2}} \exp\left[-j \mathrm{Arctan} \frac{2\pi(\nu - \nu_0) T_{1\mathrm{n}}}{1 + T_{1\mathrm{n}} G_{00} E_{0\mathrm{n}}^2} \right]. \tag{4.42}$$

With the aim to ensure notation compactness for S_{L}, we introduce the module S_{L0}: $S_{\mathrm{L0}} = N_0 \frac{E_{10\mathrm{L}}}{\left(1 + T_{1\mathrm{n}} G_{00} E_{10\mathrm{n}}^2\right)^2 + \left[2\pi(\nu - \nu_0) T_{1\mathrm{n}}\right]^2}$. Then, the formula for S_{L} takes a form:

$$S_{\mathrm{L}} = S_{\mathrm{L0}} \cdot \exp\left[-j \mathrm{Arctan} \frac{2\pi(\nu - \nu_0) T_{1\mathrm{n}}}{1 + T_{1\mathrm{n}} G_{00} E_{0\mathrm{n}}^2} \right]. \tag{4.43}$$

Having approximated S_{L} by the fifth-order polynomial and taking sequentially the first and second derivative on $E_{10\mathrm{L}}$, we obtain the expression for the nonlinearity slope on the stationary mode for the laser model in the dipole approximation.

For the second derivative (on $E_{10\mathrm{L}}$) we obtain after some transformations:

$$\begin{aligned} S_{\mathrm{L}}'' = & -E_{10\mathrm{L}} \frac{6 N_0 T_{1\mathrm{n}} G_{00}}{\left[\left(2\pi(\nu - \nu_0) T_{1\mathrm{n}}\right)^2 + 1 \right]^2} \left[1 - 2j 2\pi(\nu - \nu_0) T_{1\mathrm{n}}\right] \\ & -(E_{10\mathrm{L}})^3 \frac{20 N_0 (T_{1\mathrm{n}} G_{00})^2}{\left\{ \left[2\pi(\nu - \nu_0) T_{1\mathrm{n}}\right]^2 + 1 \right\}^3} \left[1 - 3j \cdot 2\pi(\nu - \nu_0) T_{1\mathrm{n}}\right]. \end{aligned} \tag{4.44}$$

The last expression can be presented (using the Euler formula) in the form. Then, in the compact notation of the expression $S_{\mathrm{L}}'' = \alpha_{0\mathrm{L}} E_{\mathrm{n}} - \beta_{0\mathrm{L}} E_{\mathrm{n}} \mathrm{Re}\left[E_{\mathrm{n}} \cdot E_{\mathrm{n}}^*\right]$, coefficients of the first $\alpha_{0\mathrm{L}}$ and third $\beta_{0\mathrm{L}}$ powers of the S_{L}'' polynomial, relatively, are equal:

$$\alpha_{0\mathrm{L}} = \frac{6 N_0 T_{1\mathrm{n}} G_{00}}{\left\{ \left[2\pi(\nu - \nu_0) T_{1\mathrm{n}}\right]^2 + 1 \right\}^2} \sqrt{5} \exp\left\{ -j \mathrm{Arctan}[4\pi(\nu - \nu_0) T_{1\mathrm{n}}] \right\} \tag{4.45}$$

and

$$\beta_{0\mathrm{L}} = \frac{20 N_0 (T_{1\mathrm{n}} G_{00})^2}{\left\{ \left[2\pi(\nu - \nu_0) T_{1\mathrm{n}}\right]^2 + 1 \right\}^3} \sqrt{10} \exp\left\{ -j \mathrm{Arctan}[6\pi(\nu - \nu_0) T_{1\mathrm{n}}] \right\} \tag{4.46}$$

In last expressions, arguments of exponential functions represent phase shifts due to population inertial properties or the carriers' lifetime on the upper energy level.

The oscillation amplitude in the steady-state point, as it follows for the solution of the laser abbreviated equations at low losses of the high Q-factors (of the optical resonator and the spectral line of laser emission), is determined by the approximate expression:

$$\frac{\alpha_{0L}}{\beta_{0L}} = \frac{\left\{[2\pi(\nu-\nu_0)T_{1n}]^2 + 1\right\}\exp\{-j[2\pi(\nu-\nu_0)T_{1n}]\}}{3.3\sqrt{2}T_{1n}G_{00}}. \tag{4.47}$$

For $\nu \approx \nu_0$, we obtain: $\alpha_{0L} = 6N_0T_{1n}G_{00}$ and $\beta_{0L} = 20\sqrt{10}\cdot N_0\cdot(T_{1n}G_{00})^2$, then the last formula is $\frac{\alpha_{0L}}{\beta_{0L}} \approx \frac{1}{3.3\sqrt{2}T_{1n}G_{00}}$. Figure 4.14 shows plots explaining the fulfilled approximation of the laser nonlinearity $S_{L0} = N_0\frac{E_{10L}}{1+T_{1n}G_{00}E_{10n}^2}$ by the cubic polynomial (curve 2) $S(E_n) = \alpha_{0L}E_n - \beta_{0L}E_{10n}^3$.

4.4.2 *Abbreviated DEs for the Laser in the Quasi-Stationary Mode*

According to Evtianov approach, we can introduce the operator p_{001} and obtain the differential equations for slowly changing amplitudes and phases. As the initial, we take Eq. (4.28) and introduce parameters $K = K_\alpha$ and $S(E_n)$, taking into account Eqs. (4.38), (4.45) and (4.46). We make use the ready expressions for abbreviated immitance of single circuits. As the reference frequency, we choose $2\pi\nu_{0n}$. Changing p_{00} by $j2\pi\nu_{0n} + p_{001}$, grouping terms on the smallness order, and keeping only the first order of smallness terms, we obtain an expression for the abbreviated conductance in the first approximation in the left part [9]. Here we take into consideration that the detuning of the laser generation frequencies ν_{0n} and the natural frequency ν_{12} of the amplification loop (or the natural frequency of the spectral emission line of the laser active material) β is small for QWLD and fiber lasers $\beta = [(\nu_{0n} - \nu_{12})/\nu_{12}]^2 \approx 0.001$.

Performing the differentiation and assuming that $(p_{001})^2 = 0$ and $\beta = 0$, we obtain the system of two real differential equations:

$$\begin{cases} \dfrac{dE_{10L}}{dt} = \dfrac{2\pi V_{0F}K_{0L}N_0}{Q_{12}+Q_{0F}}\dfrac{\partial}{\partial E}\left\{\dfrac{E_{10L}\left(1+T_{1n}G_{00}E_{0n}^2\right)}{\left(1+T_{1n}G_{00}E_{0n}^2\right)^2 + [2\pi(\nu-\nu_{0F})T_{1n}]}\right\} - \dfrac{2\pi\nu_{0F}E_{10L}}{Q_{12}+Q_{0F}} \\ E_{10L}\dfrac{d\Phi_{1L}}{dt} = -2\pi\nu_{0F}\dfrac{K_{0L}N_0}{Q_{12}Q_{0F}}\dfrac{\partial}{\partial E}\left\{\dfrac{E_{10L}(2\pi(\nu-\nu_{0F})T_{1n}}{\left(1+T_{1n}G_{00}E_{0n}^2\right)^2 + [2\pi(\nu-\nu_{0F})T_{1n}]^2}\right\} \end{cases}. \tag{4.48}$$

The abbreviated laser equations allow determination of the first harmonic amplitude.

4.4.3 Steady-State Analysis

At $\frac{dE_{10L}}{dt} = 0$ and $\frac{d\Phi_{1L}}{dt} = 0$, we have the system of steady-state equation from (4.48). If $\nu \approx \nu_{0F}$, then from the first equation, the formula for the amplitude square E_L (where $E_L = E_{10L} = E_{10n}$) follows: $E_{0L}^2 = \frac{1}{T_{1n}G_{00}}(K_{0L}N_0 - 1)$.

The calculation results with utilization of steady-state equation from (4.48) are presented below. Figure 4.15 gives the functions of the amplitude square and the oscillation frequency amendment.

Plots presented in Fig. 4.15 are obtained from the solution of abbreviated equations (4.48) for the laser at utilization of the nonlinearity in the form $S(E_n) = \frac{E_{10n}}{1+T_{1n}G_{00}E_{10n}^2E_{10n}}$. An analysis of these plots of E_{10L} permits to conclude that at increase of the coefficient $K_{0L} = K$, which plays the role of energy pumping in the laser, we come to the "saturation" of the strength amplitude E_{10L}. This is the general property for oscillators.

The plot of the function $E_{0L}^2(K)$ is, in essence, the well-known for laser experts watt–ampere characteristic of the laser. The shape change of the curve $E_{0L}^2(K)$ for different values of the G_0 coefficient gives us understanding that the linearity of the watt-ampere characteristic is determined by the G_0 coefficient.

The G_0 coefficient including into the nonlinear laser function defines the oscillation amplitude in the steady-state mode. An analysis of the plot of frequency deviation from the steady-state value (Fig. 4.15b) allows making conclusion that the increase of the G_0 coefficient leads to the growth of the generation frequency deviations from the steady-state values. Presented plots of the laser nonlinearity $S_{L0}K_{0L}N_0 = \frac{E_{10L}}{1+T_{1n}G_{00}E_{10n}^2}K_{0L}N_0$ (Fig. 4.15c, d), as the function of $E_{10L} = E_n$, allows clearly interpretation for the laser of self-excitation conditions and the steady-state conditions. The arrow shows the tangent to the plot (Fig. 4.15c) in the point of the generation start, which coincides with the origin point. The laser generation is possible (or the self-excitation conditions are satisfied) when the inequality $(S_{L0}K_{0L}N_0) > 1$ is fulfilled. The second arrow in the plot in Fig. 4.15c corresponds to the tangent of the nonlinearity function in the steady-state point. For instance, at $K_{0L} = K = 5.4$, the normalized oscillation amplitude is equal about $E_{10L} = E_n = 6$. Remarkably that the nonlinearity function has a maximum: $(S_{L0}K_{0L}N_0)_{max} = \frac{K_{0L}N_0}{2\sqrt{T_{1n}G_{00}}}$ in the point $E_{10L} = E_n = \frac{1}{\sqrt{T_{1n}G_{00}}}$. Figure 4.15 shows the plot of the derivative of nonlinear function $S_{L0}K_{0L}N_0$. It is notable that the derivative minimum corresponds to the point $E_{10L} = E_n = \frac{\sqrt{3}}{\sqrt{T_{1n}G_{00}}}$. Thus, addressing to abbreviated equations permitted to obtain enough exact information about the laser at its representation by the model in the dipole approximation and at utilization of the Evtianov method, which is developed for the radio-frequency oscillators, for the analysis of the quantum generators.

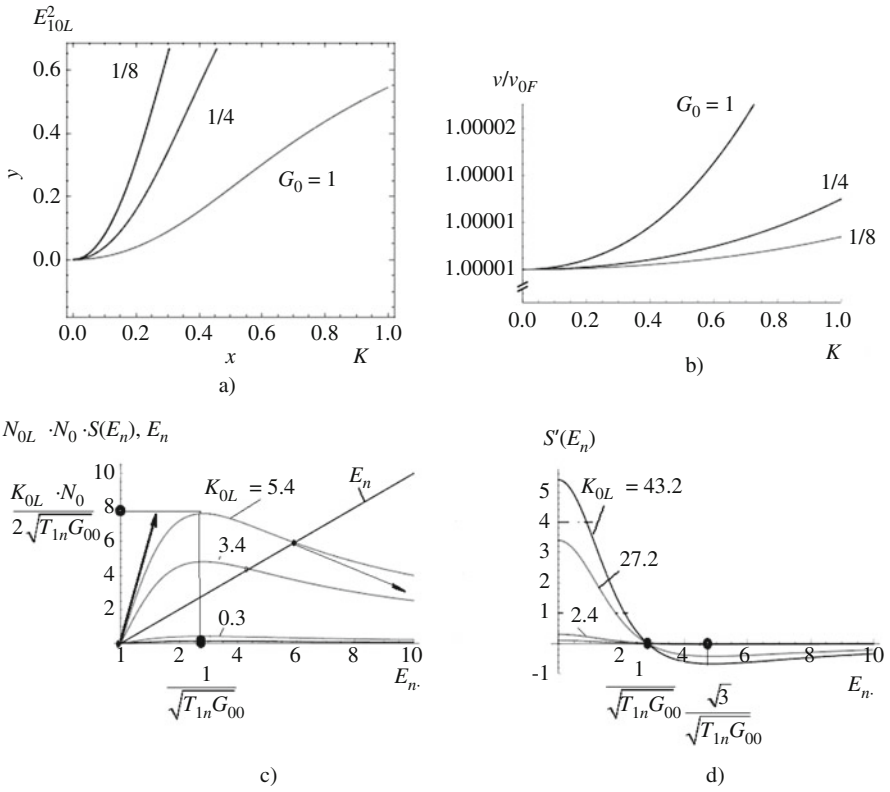

Fig. 4.15 The functions of the amplitude square (**a**) and the oscillation frequency amendment (**b**) of the laser versus $K_{0L} = K$ for$T_{1n}G_{00} = 0.125, 0.25, 1$ for $K_{0L}N_0S(E_n) = K_{0L}N_0 \frac{E_{10n}}{1+T_{1n}G_{00}\cdot E^2_{10n}}$. Functions of the product $N \cdot E_n$ in the laser versus the amplitude E_n (**c**) and (**d**) for different pumping

4.4.4 *Analytical Functions for the Amplitude* $\mathbf{E}_{10L}$ *and the Laser Frequency Amendment* ($\nu - \nu_{0n}$)

Now we obtain the analytical functions for an amplitude and the frequency amendment at approximation of the laser model of nonlinearity by the five-power polynomial. The equation for the amplitude in the steady-state mode E_{10L} can be deduced for the second approximation with utilization of the second derivative of the nonlinear function:

$$0 = \frac{E_{10\mathrm{L}} K_{0\mathrm{L}} N_0 T_{1\mathrm{n}} G_{00}}{\left\{[2\pi(\nu-\nu_0)T_{1\mathrm{n}}]^2+1\right\}^2}\left[1-(E_{10\mathrm{L}})^2\frac{20(T_{1\mathrm{n}}G_{00})}{6\left\{[2\pi(\nu-\nu_0)T_{1\mathrm{n}}]^2+1\right\}}\right] - E_{10\mathrm{L}}. \tag{4.49}$$

The equation for the frequency amendment takes the following form:

$$0 = -2\pi\nu_{0\mathrm{F}}\frac{K_{0\mathrm{L}}N_0}{Q_{12}Q_{0\mathrm{F}}}\frac{\partial^2}{\partial E}\left\{\frac{E_{10\mathrm{L}}[2\pi(\nu-\nu_{0\mathrm{F}})T_{1\mathrm{n}}]}{\left(1+T_{1\mathrm{n}}G_{00}E_{0\mathrm{n}}^2\right)^2+[2\pi(\nu-\nu_{0\mathrm{F}})T_{1\mathrm{n}}]^2}\right\}. \tag{4.50}$$

Now we simplify these equations substituting in them the approximate expression for the nonlinearity in the form of the third power polynomial. In this case, the equation under the analysis takes a form:

$$0 = E_{10\mathrm{L}}\frac{6N_0T_{1\mathrm{n}}G_{00}[\,j4\pi(\nu-\nu_0)T_{1\mathrm{n}}]}{\left\{[2\pi(\nu-\nu_0)T_{1\mathrm{n}}]^2+1\right\}^2} - (E_{10\mathrm{L}})^3\frac{20N_0(T_{1\mathrm{n}}G_{00})^2[\,j6\pi(\nu-\nu_0)T_{1\mathrm{n}}]}{\left\{[2\pi(\nu-\nu_0)T_{1\mathrm{n}}]^2+1\right\}^3}. \tag{4.51}$$

For values close to $\nu = \nu_0$, we obtain for the amplitude and the frequency amendment the following formulas:

$$(E_{10\mathrm{L}})^2 = \frac{1}{3.3(T_{1\mathrm{n}}G_{00})}\left[1-\frac{1}{K_{0\mathrm{L}}N_0T_{1\mathrm{n}}G_{00}}\right], \tag{4.52}$$

$$(\nu-\nu_{0\mathrm{n}}) = \frac{1}{2\pi T_{1\mathrm{n}}}\sqrt{5\cdot(E_{10\mathrm{L}})^2(T_{1\mathrm{n}}G_{00})-1} \tag{4.53}$$

These formulas coincide with the calculated functions obtained at computer modeling. From Eq. (4.52) we deduce the inequality: $K_{0\mathrm{L}}N_0T_{1\mathrm{n}}G_{00} > 1$. Equation for the frequency amendment has the real solution for: $(E_{10\mathrm{L}})^2 > \frac{1}{5\cdot(T_{1\mathrm{n}}G_{00})}$. This condition is satisfied in the steady-state point at $\frac{\mathrm{d}S(E_{10\mathrm{n}})}{\mathrm{d}E_{10\mathrm{n}}} < 0$. For the linear-hyperbolic nonlinearity of the form $S(E_{\mathrm{n}}) = \frac{E_{10\mathrm{n}}}{1+T_{1\mathrm{n}}G_{00}\cdot E_{10\mathrm{n}}^2}$, the derivative value $S'(E_{\mathrm{n}})$ should satisfy to the inequality: $S'(E_{\mathrm{n}}) = \frac{1-T_{1\mathrm{n}}G_{00}E_{10\mathrm{n}}^2}{\left(1+T_{1\mathrm{n}}G_{00}\cdot E_{10\mathrm{n}}^2\right)^2} < 0$. From last it follows that in the steady-state point $E_{10\mathrm{n}}^2 > \frac{1}{T_{1n}G_{00}}$.

Our analysis of the linear-hyperbolic function of the nonlinear laser model allows performing of its approximation with the help of polynomial of third and fifth power taking into account the inertial properties (or the lifetime of carriers). The transfer to approximate expressions for nonlinearity essentially simplifies the deduction of

abbreviated DEs of the laser and obtaining of steady-state values of oscillation amplitudes and the laser frequency.

Further, we perform investigations of oscillation excitation and existence conditions for QWLD in the steady-state mode. At that, we shall use the Gurvitz criterion for characteristic equations of fourth order.

4.5 Oscillations' Self-Excitation and Existence in QWLD

4.5.1 Conditions of Oscillations' Self-Excitation of QWLD

Differential equations allow considering a question about laser self-excitation. The modern QWLDs operate at low threshold currents (less than 10 mA) at average operating pumping currents of 50–80 mA and transient time of quasi-stationary mode is small (less than 10 ns).

The self-excitation peculiarity is the fulfilling of two conditions following from the first and second equation of (4.28), (4.37). For the first equation, we use the Gurvitz stability criterion. For the second equation, we find the laser self-excitation boundary in the steady-state point $\frac{\mathrm{d}^i E_n}{\mathrm{d}\tau^i} = 0 \quad (i = 1, 2, 3, 4)$ and $\frac{\mathrm{d}N}{\mathrm{d}\tau} = 0$. From the last condition, we see that pumping should be higher than the threshold value, i.e., the population difference on the upper operation level must be higher than the threshold value: $\alpha_{\mathrm{N0}} > N \cdot \frac{1}{T_1}$.

Now we write the characteristic equation for our DEs transferring the term from the right side into the left side and assuming for simplicity $\exp[-j(2\pi\nu_{0\mathrm{n}}T_{\mathrm{R}})] = 1$ and introducing the average slope $S'(E_{\mathrm{n}})$ for the first harmonic $K_{000} = K \cdot S'(E_{\mathrm{n}})$. Now we write the final characteristic equation:

$$a_0\lambda^4 + a_1\lambda^3 + a_{20}\lambda^2 + a_3\lambda + a_4 = 0, \tag{4.54}$$

where λ is the complex root of characteristic equation and the new coefficient a_{20} at λ^2 is equal: $a_{20} = (2\pi\nu_{0\mathrm{n}})^2 + (2\pi\nu_{12})^2 + [1/(T_{0\mathrm{F}}T_2)] - K_{000}$.

The Rauth–Gurvitz stability conditions for the steady-state mode (for small amplitudes) for DE (4.37) are: $a_i > 0 (i = 0, \ldots, 4)$, $\Delta_2 = a_1a_2 - a_0a_3 > 0$, $\Delta_3 = a_1a_2a_3 - a_1^2a_4 - a_0a_3^2 > 0$, $\Delta_4 = a_4 > 0$. The laser **self-excitation condition** following from the mentioned Gurvitz stability conditions and from the pumping threshold condition for QWLD takes a form:

$$K_{000} = K \cdot N_{00}S'(E_{10\mathrm{n}}) > \frac{\nu_{12}^2 - \nu_{0\mathrm{n}}^2}{\nu_{0\mathrm{n}}^2} + \frac{1}{(2\pi\nu_{0\mathrm{n}})^2}\frac{1}{T_{0\mathrm{F}}}\frac{1}{T_2}, \tag{4.55}$$

where $S'(E_{10\mathrm{n}})$ is a derivative of $S(E_{10\mathrm{n}})$. From Eq. (4.55), the condition of the threshold inversed population follows (the value of the population difference between levels, when generation occurs).

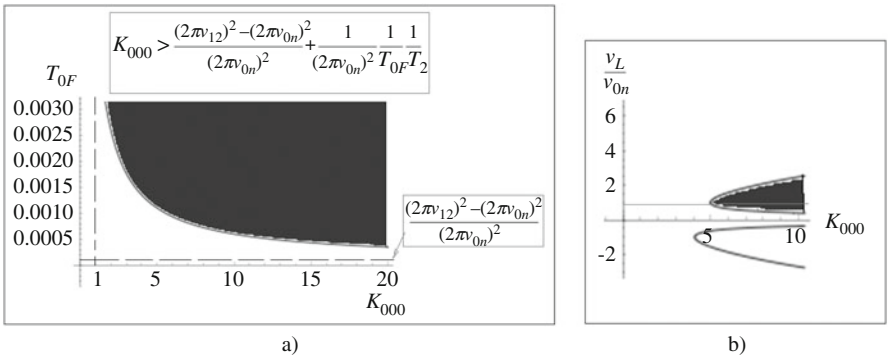

Fig. 4.16 (**a**) The function of the time constant of the optical filter T_{0F} versus the gain $K_{000} = K \cdot S'(E_{10n})$. (**b**) The function of the normalized laser oscillation frequency ν_L/ν_{0n} versus the gain K_{000}. The region, where the laser self-excitation conditions are satisfied, is marked by black

Figure 4.16 shows the function on the time constant of the optical filter T_{0F} (a) and the function of normalized laser oscillation frequency ν_L/ν_{0n} (b) versus the gain $K_{000} = K \cdot S'(E_{10n})$. Presented plots of functions (Fig. 4.16) show that the laser self-excitation conditions (the laser model in the dipole approximation) are fulfilled at condition that the value $K \cdot N_{00}S'(E_{10n})$ exceeds losses, which are determined by losses in the optical resonator and in the material of the laser active element, or $\frac{1}{(2\pi\nu_{0n})^2}\frac{1}{T_{0F}}\frac{1}{T_2}$. The laser self-excitation is possible in the wide range of values T_{0F}, $K_{000} = K \cdot S'(E_{10n})$. The generation region is covered by red. Calculated plots (Fig. 4.16) of the function of the normalized frequency ν_L/ν_{0n} versus $K_{000} = K \cdot S'(E_{10n})$ allow to clearly define the laser generation zone.

4.5.2 *Stability of the Steady-State Mode of Large Amplitude*

Let us analyze the conditions of oscillation stability in the steady-state point (the point of large oscillation amplitude). We introduce the averaged slope in the first (fundamental) harmonic for the steady-state point with large amplitude. Calculating the first derivative of the averaged slope and taking into account the condition of the steady-state mode, we obtain the stability condition as:

$$\frac{dS(E_{10n})}{dE_{10n}} < 0. \tag{4.56}$$

Geometric interpretation of this condition is shown in Fig. 4.15.

The operator control function in the small-signal mode can be defined at $\nu \approx \nu_{0F}$ as:

$$K_{\mathrm{L}}(p_{00}) = \frac{K_{\mathrm{L}00}{p_{00}}^2}{p_{00}^4 + a_{10}p_{00}^3 + [a_{20} - S(E_{10\mathrm{n}})K_{00}N_{00}]p_{00}^2 + a_{30}p_{00} + 1}, \tag{4.57}$$

where $K_{\mathrm{L}00} = \frac{K_{00}T_1G_{00}N_0E_{\mathrm{n}0}}{1+T_1G_{00}(E_{\mathrm{n}0})^2}$, $N_{00} = \frac{N_0}{1+G_{00}\,\mathrm{Re}\left(E_{\mathrm{n}}\cdot E_{\mathrm{n}}^*\right)}$; and $a_{10} = a_{30} = \left(\frac{1}{Q_{0\mathrm{F}}} + \frac{1}{Q_{02}}\right)$, $a_{20} \approx 2 + \frac{1}{Q_{0\mathrm{F}}Q_{02}}$, $a_{20} \approx 2$, $a_{10} \approx a_{30}$ and depend on the total losses in the system (their values are varied from 0.008 to 0.00004 for different types of lasers).

The characteristic Eq. (4.54) can be obtained from the operator DE (4.36) or (4.29).

Substituting in it $a_{10} = a_{30} = \left(\frac{1}{Q_{0\mathrm{F}}} + \frac{1}{Q_{02}}\right)$; $a_{20} = \left[2 + \frac{1}{Q_{0\mathrm{F}}Q_{02}} - K_{00}\cdot N_{00}\right]$, where $a_{10} \approx a_{30}$, we have:

$$\lambda^4 + \left(\frac{1}{Q_{0\mathrm{F}}} + \frac{1}{Q_{02}}\right)\lambda^3 + \left[2 + \frac{1}{Q_{0\mathrm{F}}Q_{02}} - S_0(E_{10\mathrm{n}})K_{00}\cdot N_{00}\right]\lambda^2$$

$$+\left(\frac{1}{Q_{0\mathrm{F}}} + \frac{1}{Q_{02}}\right)\lambda^1 + 1 = 0. \tag{4.58}$$

We can write the Rauth–Gurvitz stability conditions for the steady-state mode of large amplitude. We determine the *conditions of laser oscillation* existence following from mentioned Gurvitz stability conditions and investigations of laser equation of the fourth order for the nonlinearity of the form:

$$S_{\mathrm{L}} = S_{\mathrm{L}0}\exp\left\{-j\mathrm{Arctan}\frac{2\pi(\nu-\nu_0)T_{1\mathrm{n}}}{1+T_{1\mathrm{n}}G_{00}E_{0\mathrm{n}}^2}\right\}, \tag{4.59}$$

where

$$S_{\mathrm{L}0} = N_0\frac{E_{10\mathrm{L}}}{\left(1+T_{1\mathrm{n}}G_{00}E_{10\mathrm{n}}^2\right)^2 + [2\pi(\nu-\nu_0)T_{1\mathrm{n}}]^2}. \tag{4.60}$$

Let us write the condition of oscillation existence in the steady-state mode in the form of inequalities, which connect the laser SOS parameters and the square of the strength amplitude $(E_{10\mathrm{L}})^2$:

$$K_{0\mathrm{L}}N_0T_{1\mathrm{n}}G_{00} > 1; \quad (E_{10\mathrm{L}})^2 > \frac{1}{(T_{1\mathrm{n}}G_{00})}. \tag{4.61}$$

From these inequalities, it follows that for oscillations existence should be: $K_{0\mathrm{L}}N_0T_{1\mathrm{n}}G_{00} > 1$. We remind that here $E_{10\mathrm{L}}$ is the dimensionless value—the amplitude of the normalized field strength, therefore, we have the formula of possible values of $E_{10\mathrm{L}}$ amplitudes.

The laser self-excitation conditions following from the Gurvitz stability conditions (taking into consideration that $1-\frac{\nu_{12}^2}{\nu_{0n}^2}$ is small), takes the form:

$$K_{000} = K \cdot N_{00} S''(E_{10n}) > \frac{\nu_{12}^2 - \nu_{0n}^2}{\nu_{0n}^2} + \frac{1}{(2\pi\nu_{0n})^2}\frac{1}{T_{0F}}\frac{1}{T_2} = \frac{1}{(2\pi\nu_{0n})^2}\frac{1}{T_{0F}}\frac{1}{T_2}. \tag{4.62}$$

This condition takes a form: $Q_{0F}Q_{02}K \cdot N_{00}S''(E_{10n}) > 1$. The last inequality can be interpreted as similar to well-known from the oscillation theory the excitation condition of RF oscillators: $SR_c > 1$.

In $SR_c > 1$, the slope of the nonlinear function of the nonlinear element is equal to the derivative: $S = S'(E_{10n})$, and the control resistance R_c is: $R_c = Q_{0F}Q_{02}KN_{00}$.

At that, the normalized value of the oscillation amplitude square in the steady-state mode depends on the lifetime T_{1n} and the saturation coefficient (or the gain) G_{00} and is defined by inequalities: $(E_{10L})^2 > \frac{1}{T_{1n}G_{00}}$.

Figure 4.17a shows the dependence of the gain $K_{000} = K_{00}N_{00}S'(E_n)$ upon the Q-factor of the optical filter Q_{0F} at the value of $Q_{02} = 10$; Fig. 4.17b shows the same function at $Q_{02} = 100$.

On the base of these investigations, we can give the brief conclusions. For the soft excitation mode (when the excitation happens just after the activation of the system from zero oscillations) and the further oscillation stability in the steady-state mode of large amplitudes, the slope of the nonlinear function in the initial (zero) point must be positive, but in the steady-state mode of large amplitudes, this slope must be negative, and the slope module in the initial state should be more than the module of the slope of nonlinear function in the steady-state point.

4.5.3 *The Operator Control Function of the Laser at Small Oscillations in the Quasi-Stationary Mode*

We use the preliminarily written symbolic equation on the base of QWLD DE considering it in the quasi-stationary small-signal mode ($E_n = E_{n0} + e_L$ and $N = N_{00} + n_L$ and $2\pi\nu_{0n}$):

$$\begin{cases} \left[a_{00}P_{00}^4 + a_{10}P_{00}^3 + a_{20}P_{00}^2 + a_{30}P_{00} + a_{40}\right](E_{n0} + e_L) = K_{00}P_{00}^2(N_{00} + n_L)(E_{n0} + e_L) \\ p_{00}(N_{00} + n_L) = \alpha_{N0} - \dfrac{N_{00} + n_L}{T_1} - G_{00}(N_{00} + n_L)(E_{n0} + e_L)^2 \end{cases}. \tag{4.63}$$

Then at $n_L e_L \approx 0 : n_L = (\alpha_{N0} - G_{00}N_{00}E_{n0}e_L)/\left[p_{00} + \frac{1}{T_1} + G_{00}(E_{n0})^2\right]$ or

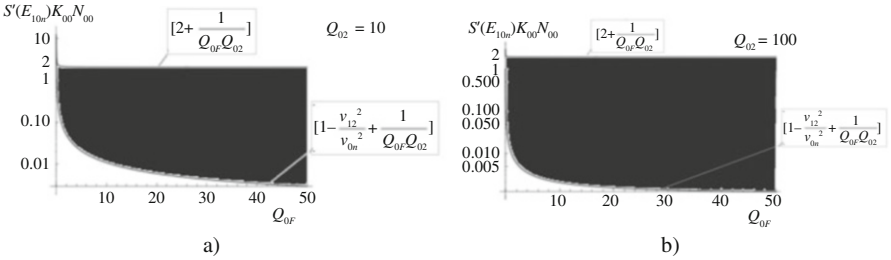

Fig. 4.17 (**a**) The gain $K_{000} = K_{00}N_{00}S'(E_n)$ versus the Q-factor of the optical filter Q_{OF}, while $Q_{02} = 10$. (**b**) The same plot for $Q_{02} = 100$. The region, where laser self-excitation conditions are satisfied, is marked by black

$$n_L = \frac{T_1\alpha_{N0} - T_1G_{00}N_{00}E_{n0}e_L}{j[T_1(\nu - \nu_{0F})/\nu_{0F}] + 1 + T_1G_{00}(E_{n0})^2}. \tag{4.64}$$

The operator control function in the small-signal mode can be defined as:

$$K_L(p_{00}) = \frac{K_{L00}p_{00}^2}{p_{00}^4 + a_{10}p_{00}^3 + (a_{20} - K_{00}N_{00})p_{00}^2 + a_{30}p_{00} + 1} \tag{4.65}$$

or in normalized frequency notation:

$$K_L[\,j(\nu/\nu_{0F})] = \frac{K_{L00}\cdot(\nu/\nu_{0F})^2}{(\nu/\nu_{0F})^4 - ja_{10}(\nu/\nu_{0F})^3 - (a_{20} - K_{00}N_{00})(\nu/\nu_{0F})^2 + ja_{30}(\nu/\nu_{0F}) + 1}, \tag{4.66}$$

where

$$K_{L00} = \frac{K_{00}T_1G_{00}N_{00}E_{10n}}{j[T_1(\nu - \nu_{0F})/\nu_{0F}] + 1 + T_1G_{00}\cdot(E_{10n})^2}. \tag{4.67}$$

If $\nu \approx \nu_{0F}$ in Eq. (4.67), $K_{L00} = \frac{K_{00}T_1G_{00}N_{00}E_{10n}}{1+T_1G_{00}(E_{10n})^2}$, $K_{00} = \frac{2d_a^2}{3\cdot\varepsilon_0 2\pi h}$. In Eq. (4.66) $a_{10} = a_{30} = \left(\frac{1}{Q_{0F}} + \frac{1}{Q_{02}}\right)$; $a_{20} \approx 2 + \frac{1}{Q_{0F}Q_{02}}$, $a_{20} \approx 2$, $a_{10} \approx a_{30}$ and depend on the total losses in the system. Their values are varied from 0.008 to 0.0004 for different types of lasers.

Figure 4.18 shows the poles diagram of the laser operator control function in the state of the thermal equilibrium at the population difference less than (a) and higher than (b) of the threshold value, at different Q-factors of the optical resonator and the spectral line.

The plots of the module and argument of the operator control function for three types of lasers (1—without quantum wells, 2—QWLD with the low resonator Q-

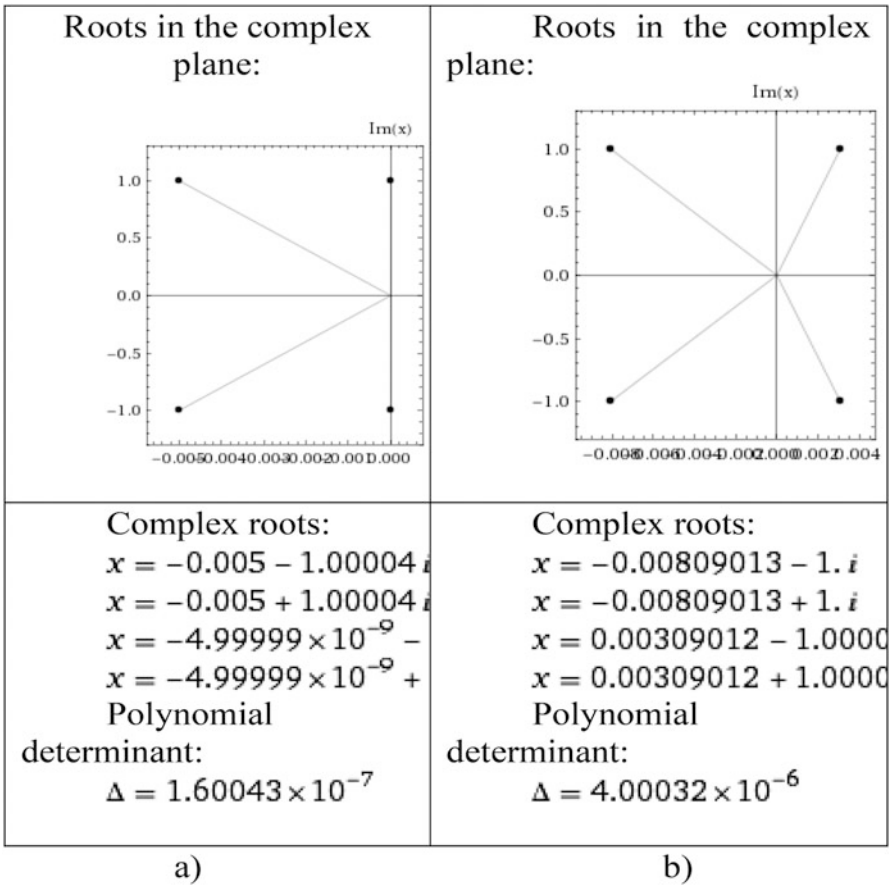

Fig. 4.18 The poles diagram of the operator control function of the laser in the state of the thermal equilibrium at the population difference below (**a**) and higher (**b**) than the threshold value, at Q-factors of the laser optical resonator and of the spectral line. (To solution and analysis of the nonlinear DE of fourth order for QWLD in quasi-stationary mode)

factor, 3—QWLD with the high Q-factor of the Bragg resonator) are presented in Fig. 3.17c (in Chap. 3).

We consider the laser model in the dipole approximation. Symbolic equations coincide with equations of the double-circuit RF oscillator with the inertial nonlinearity with the soft oscillation characteristics, which permit to analyze the steady-state mode stability of the laser model not only using AFC and PCF but with utilization of the Nyquist locus method.

4.5.3.1 The Locus Method for Obtaining of QWLD Steady-State Modes

This method uses the superposition in the complex plane of the oscillating system locus and the dynamic locus of the active element (the laser). The last locus is built on the base of the function:

$$S_{\mathrm{L}} = S_{\mathrm{L}}[\, j(\nu/\nu_{0\mathrm{F}}), E_{10\mathrm{L}}, K_{0\mathrm{L}}N_0] = S_{\mathrm{L\,Re}} + jS_{\mathrm{LIm}}, \tag{4.68}$$

where $E_{10\mathrm{L}}$ is determined from the steady-state equation. The oscillating system locus of *QWLD* can be constructed on the formula:

$$Y_{\mathrm{L}}[\, j(\nu/\nu_{0\mathrm{F}})] = (\nu/\nu_{0\mathrm{F}})^4 - ja_{10}(\nu/\nu_{0\mathrm{F}})^3 - a_{20}(\nu/\nu_{0\mathrm{F}})^2 + ja_{30}(\nu/\nu_{0\mathrm{F}}) + 1 \tag{4.69}$$

We represent this formula as

$$Y_{\mathrm{L}}[\, j(\nu/\nu_{0\mathrm{F}})] = Y_{\mathrm{L\,Re}} + jY_{\mathrm{LIm}}(\nu/\nu_{0\mathrm{F}}). \tag{4.70}$$

The intersection of two these loci (at satisfying of the geometrical stability criterion) determines the points of the laser steady-state mode. Figure 4.19 illustrates an application of the locus method to investigation of the steady-state stability of the laser model in the dipole approximation. Positive directions of loci are shown by arrows and correspond to the current frequency ν growth. In the general case, the locus of the active element is considered as dynamic. Modes are stable for those part of the loci, where the derivative $\frac{\mathrm{d}S(E_{10\mathrm{n}})}{\mathrm{d}E_{10\mathrm{n}}} < 0$. This is the condition of the amplitude stability of steady-state mode.

As we see from Fig. 4.19, the unstable modes fall in those part of the locus, where $\frac{\mathrm{d}Y_{\mathrm{LIm}}}{\mathrm{d}\nu} < 0$. Such points are designated in Fig. 4.19 by numbers 1 and 2. This is the condition of phase or frequency instability. The point 3 in this figure happens to be unstable. The phase stability condition takes the form: $\frac{\mathrm{d}Y_{\mathrm{LIm}}/\mathrm{d}\nu}{\mathrm{d}Y_{\mathrm{L\,Re}}/\mathrm{d}\nu} > \frac{\mathrm{d}S_{\mathrm{LIm}}/\mathrm{d}E_{10\mathrm{n}}}{\mathrm{d}S_{\mathrm{L\,Re}}/\mathrm{d}E_{10\mathrm{n}}}$. According to this criterion, the part of the locus with the negative slope of Y_{LIm} can become the stable and on the contrary, the phase instability can appear on those parts where $\frac{\mathrm{d}Y_{\mathrm{LIm}}}{\mathrm{d}\nu} < 0$, even if this function has no parts with the negative slope.

The module (1) and the argument (2) of the oscillating system and the laser inertial nonlinearity and its loci for two different values of the gain (the pumping levels) are presented in Fig. 4.20 for demonstration of the locus method.

The investigation of oscillation excitation conditions from small amplitudes and the oscillation existence of the large steady-state amplitudes leads to the following brief conclusions. These investigations with utilization of the Gurvitz criterion enable to write a system of inequalities for main parameters of the oscillating systems. Regions of gain values in the laser feedback loop, of Q-factors of the optical resonators and of the spectral line of laser emission are extracted. Special attention in the analysis of the laser system is paid to examination of the inertial nonlinear QWLD and studying of laser operation in the quasi-stationary mode with the large exceed of the pumping current over its threshold value. Utilization of the

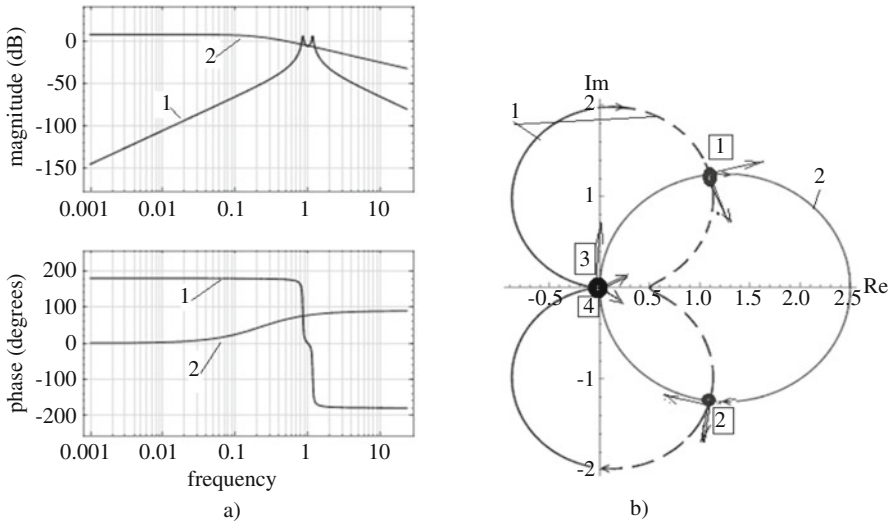

Fig. 4.19 The module and argument (**a**) of the operator control function (curve 1) and the laser inertial nonlinearity (curve 2) in the form $S_L[j(\nu/\nu_{0F}), E_{10L}, K_{0L}N_0] = S_{LRe} + jS_{LIm} = 0.5/[0.2 + j0.9(\nu/\nu_{0F})]$, $s = j(\nu/\nu_{0F})$, and loci of the active elements (**b**). Points 1, 2, 3, 4 on the locus (**b**) are shown by numbers in squares

locus method and the Nyquist criterion at determination of DE solutions for the laser model gives a possibility to more accurate analyze the oscillations self-excitation conditions taking into account the inertial properties, which are defined by the carrier lifetime. We can make the important conclusion that to earlier considered conditions of self-excitation and steady-state conditions we must add by conditions of the phase and amplitude stability of the laser oscillation system. To examine the self-excitation issue of the laser model on the base of DE of fourth order, we can use the Neimark **D-fragmentation method** of the **Nyquist locus method**. The internal zone is well seen in Fig. 4.20, which is restricted by the "internal loop." For this loop, the self-excitation of the laser model is impossible. For internal values of this zone the stability conditions are satisfies for the system with closed FB "according to Nyquist": i.e., the amplitude-frequency curve of the Nyquist locus does not span the point with coordinates (Re = 1; Im = 0) in the complex plane.

Thus, the self-excitation conditions and large oscillation existence conditions for the laser model in the dipole approximation must be added by conditions of phase and amplitude stability.

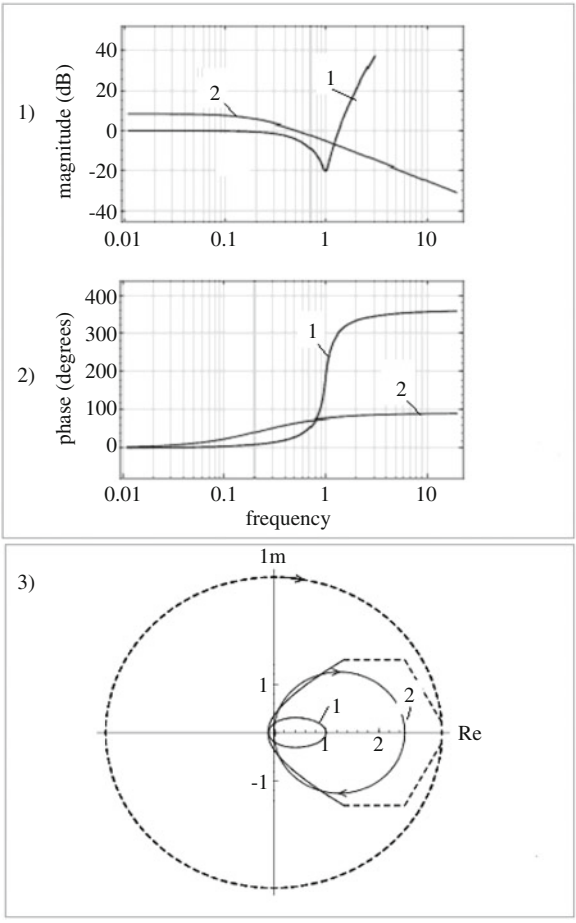

Fig. 4.20 The module (1) and the argument (2) of the oscillating characteristics (the curve 1) and the laser inertial nonlinearity (the curve 2) and its loci

4.6 Solutions of Nonlinear DEs of Fourth Order and Second Order for the Laser

4.6.1 Results on Nonlinear DE Solution of Fourth Order for the Laser Model

Results of DEs solution (4.37) for the QWLD model in the quasi-stationary mode in the dipole approximation foe different values of the gain in the positive feedback loop (or different pumping values) are presented in Figs. 4.21 and 4.22. At that, the polynomial coefficients of the characteristic equations are: $a_{00} = 1$, $a_{10} = 0.01$, $a_{20} = 2.0001$, $a_{30} = 0.01$, $a_{40} = 1.0001$, (1) $K_{00} = 0.5$; (2) $G_{n00} = 0.01$.

These figures allow the following conclusions.

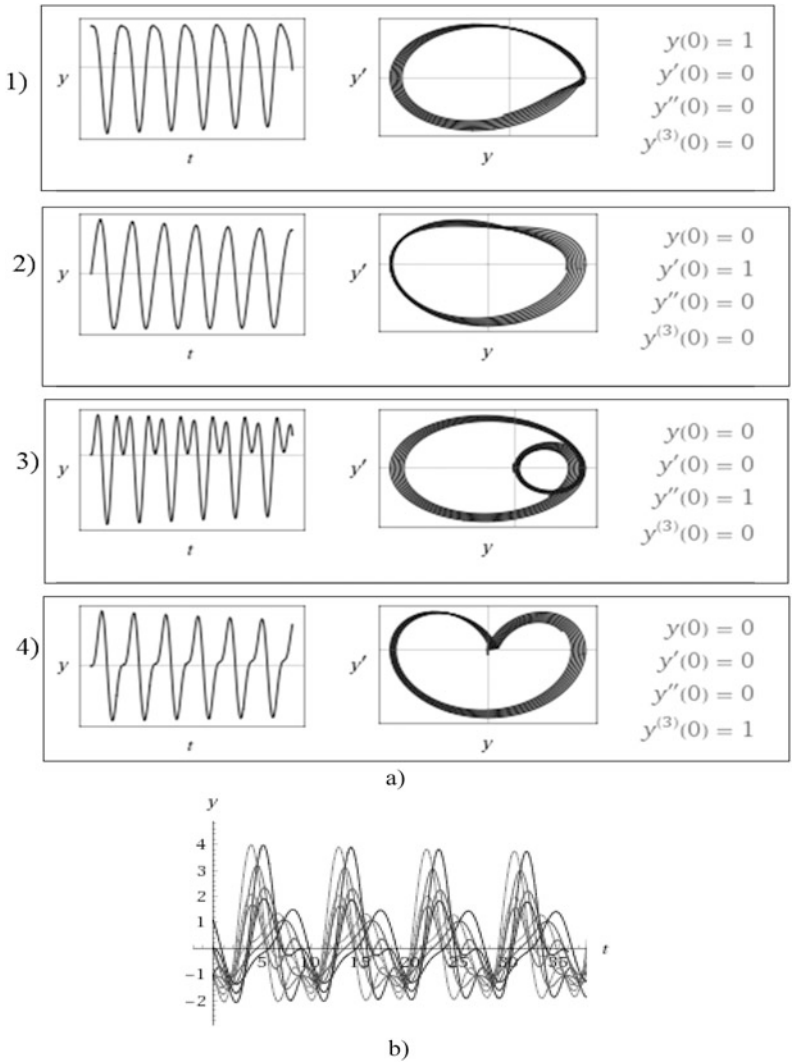

Fig. 4.21 An example of the nonlinear differential equation (DE) solution of fourth order for QWLD in the quasi-stationary mode *without taking into account the lag* in the optical channel (DE (4.37)). (**a**) Instantaneous values of the EMF strength $E_n(t)$, $y(t) = E_n(t)$ for different initial conditions and phase portraits $\{y(t), y'(t)\}(1,2,3,4)$; (**b**) Instantaneous values of the EMF strength $y(t) = E_n(t)$ for different initial conditions in one plot for normalized time. The DE (4.37) for $y(t) = E_n(t)$: $y^{(4)} + 0.01y^{(3)} + 2.0001y'' + 0.01y' + 1.0001y = -0.5 \cdot \frac{\partial^2}{\partial t^2} \frac{y}{1+0.01y^2}$

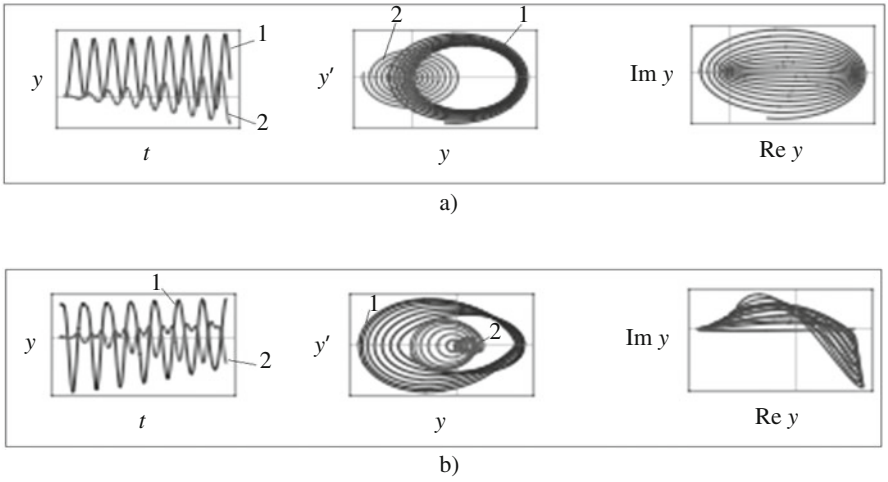

Fig. 4.22 An example of the nonlinear differential equation solution of fourth order for QWLD in quasi-stationary mode **with** *account of the total large inertial properties.* At account of inertia as the large oscillation delay in phase with introduction in the right part of equation by the multiplier plots (**a**). At account of inertia of the nonlinear element (**b**). Instantaneous values of strength $E_n(t)$, $y(t) = E_n(t)$ in black (curve1) is a real part, in gray (curve2) is an imaginary part are shown and phase portraits $\{y(t), y'(t)\}$; $\{\mathrm{Re}y(t), \mathrm{Im}y(t)\}$. The DE for (**a**): $y^{(4)} + 0.00001y^{(3)} + 2.01y'' + 0.00001y' + 1.01y = -100.9 \cdot \exp(-j100.5) \cdot \frac{\partial^2}{\partial t^2} \frac{y}{1+0.125y^2}$; The DE for (**b**): $y^{(4)} + 0.01y^{(3)} + 2.0001y'' + 0.01y' + 1.0001y = -0.5 \frac{\partial^2}{\partial t^2} \frac{y}{1+j0.1(y'/y)+y^2}$

Solutions of the differential equations illustrated in Figs. 4.21 and 4.22 permit to analyze the development of the oscillating process in the quasi-stationary mode for the double-level laser model in the dipole approximation. The limit cycle of the single-frequency oscillations of the laser model exists in the limited range of pumping at fulfillment of the condition $K_{000} > 1$, which is defined by the double-resonance SOS with two equivalent resonance circuits formed by the spectral line of laser emission and its optical resonator. Inertial properties of the laser nonlinear element caused by the saturation effect are defined by the carriers' lifetime on the upper excited state. At examination of the dynamic picture of oscillations, we can note that together with the in-phase component, the essential role is played by the quadratic component in field oscillations. At that, the exit to the limit cycle is accompanied by ripples caused by the nonlinear interaction of harmonics. The oscillating process with the cubic nonlinearity and with the nonlinearity in the form of the "inertial network of the saturation effect" differs in many respects from each other.

Computer modeling results of the laser generation in the quasi-stationary mode for the differential equation of the fourth order at inertial nonlinearity are presented at absence of these inertial properties of the active medium caused by the saturation effect. The analysis of obtained time-functions gave new information about possible

laser parameters, at which the stable oscillations exist for the field strength, which are close to harmonic ones. Phase portraits built on the base of the DE solution have a series of interesting features, for instance, the loop-shaped phase portrait and the cycloid symmetric closed trajectories with singularities.

In particular, it is stated that at absence of inertial properties (in the laser model, the carrier lifetime on the upper level is zero) for the linear-hyperbolic nonlinearity, there exists the restricted region of values of the normalized pumping (or values of the gain). For example, for the optical resonator and the spectral line of laser emission Q-factors equaled to 100, for the coefficient $G = 10$, the region of normalized pumping, for which the quasi-harmonic oscillations are excited and existed, is about from 1 to 2. If the carriers' lifetime is nonzero, the region of pumping values (at generation of quasi-harmonic oscillations) essentially widens from 1 to 15–20, which is caused by expansion of the region, in which conditions of single-frequency existence are satisfied at fulfillment of amplitude and phase balance conditions.

4.6.2 Resonance Characteristics for Laser DE of Fourth Order

Before the presentation start in this section, which is devoted to the analysis of the QWLD resonance characteristics, we would like to tell several words about this problem relevance. It is known that in the LIGO interferometer (International project on investigation of gravitation waves) the ultrahigh-Q (the Q-factor $Q_{0F} = 10^{10} - 10^{20}$) disk optical resonators are used for registration of gravitation waves (LIGO) [11, 12]. The problem of ultrahigh-Q optical resonator application as the discriminator in optoelectronic measuring equipment for ultrasmall physical quantities is the extremely relevant. The influence of the field characteristic upon the behavior is weakly theoretically studied. The Russian physicist Gorodetskiy M.L. (1966–2019), the participant of the LIGO project [13, 14], has theoretically investigated the phenomenon of parametric instability of the optical disk resonator (with the geometrical radius about 20–120 μm) at the ultrahigh Q-factor $Q_{0F} = 10^{10} - 10^{20}$ and at relatively high introducing power into the optical resonator $P_{in} = 10^{-6} - 10^{-4}$ W.

The mathematical model of the optical resonator (Fig. 2.7) is complicate. So, at ultrahigh power densities of the light in the ultralow volume about $V_D = 10^{-15}$ m^3, several processes occur:

- Nonlinear interactions of the field and the material,
- Quadratic or cubic variation of the resonator Q-factor versus the field strength amplitude,
- The temperature heating of the resonator material due to the losses of the optical power.

In the optical range, the task solution becomes complicate by the fact that the propagation condition of the plane wave is not satisfied in the general case. It can be explained by commensurability of the emission wavelength 1.55 μm with the geometric overall dimensions of the disk, the ball-shaped or the "ring" toroid with the radius about 5–20 μm.

Let us consider the case of the ball-shaped resonator and perform the rough estimation of the power density. We must bear in mind that only the part of emission is inside the material of the optical resonator (Fig. 2.7). We estimate the density of the optical power in the optical resonator with the volume $V_D = 10^{-15}$ m^3 at introduced of the initial optical power of $P_{opt} = 10^{-6} - 10^{-4}$ into the resonator: $P_{opt}/V_D = \frac{10^{-6}-10^{-4}}{V_D} = \frac{10^{-6}-10^{-4}}{10^{-15}} = 10^9 - 10^{19}$ W/m^3.

The circulation of the optical emission in the optical resonator with the Q-factor, for example, $Q_{0F} = 10^{10}$, gives the power density value in the optical resonator in the steady-state mode: $Q_{0F}P_{opt}/V_D = 10^{19} - 10^{29}$ W/m^3. The one from the simple models of the optical disk resonator at its excitation by the external optical field is the model of the oscillator, which is under the effect of external force or the strength with the amplitude E_{100} of the electromagnetic field.

Let us pass to creation of QWLD resonance characteristics: dependences of the oscillation amplitude versus the frequency $E_{10n}(\nu/\nu_{0F})$. Sometimes, they are called the Cartesian functions because they can be found out from solutions of algebraic Cartesian equations.

On the one hand, these functions $E_{10n}(\nu/\nu_{0F})$ are obtained from algebraic equations of the laser *steady-state mode*. On the other hand, we offer the second approach to construction of $E_{10n}(\nu/\nu_{0F})$. This approach consists in these functions construction during the solution of the laser symbolic DEs. The second approach for obtaining of $E_{10n}(\nu/\nu_{0F})$ is more evident and informative, because the plots of solutions of the laser symbolic DEs are constructed only at laser self-excitation condition satisfaction. At that, on the complex plane of parameters [$y = \mathrm{Re}(.) = E_{10n}$, $x = \mathrm{Im}(.) = j(\nu_n/\nu_{0L})$], the axis of $x = \mathrm{Im}(.)$ corresponds to the normalized laser optical frequency $j(\nu_n/\nu_{0L}) = p_{00} = s$, where the p_{00} operator is the normalized operator of the laser symbolic equation. The ordinate axis $y = \mathrm{Re}(.) = E_{10n}$ corresponds to the axis of strength amplitude values E_{10n}. At first, we consider the construction of the laser resonance characteristics by the first traditional approach.

4.6.2.1 Results of Steady-State Equations' Solution

Functions presented in Fig. 4.23a, b are built at solution of the steady-state mode equations for nonlinear characteristic of the laser active medium $S(E_n) = \alpha_{01}E_n - \beta_{03}E_n^3$. The DE solution in the steady-state gives the approximate expression (under the condition that the generation frequency is close to the natural frequency of the optical resonator) for the first harmonic amplitude E_{10n} in the steady-state mode:

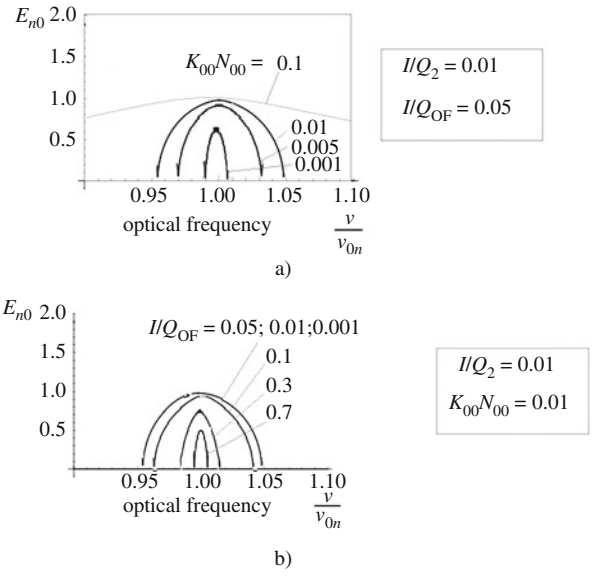

Fig. 4.23 The resonance characteristics of QWLD at different values of the Q-factor of the optical resonator. Plots of the first harmonic amplitude $E_{n0} = E_{10n}(\nu/\nu_{0F})$ (**a**) for $Q_{0F} = 20$, $Q_{02} = 100$ for different values of $N_{00}K_{00} = N_0K_{00}$; (**b**) for $N_{00}K_{00}$= 0.01, $Q_{02} = 100$ for different values of $1/Q_{0F}$

$$E_{10n} = \sqrt{4\alpha_{01}/3\beta_{03}} \cdot [1 - 1/(\alpha_{01}|K_L|)]^{1/2}, \tag{4.71}$$

where $|K_L|$ is the module of the operator transfer function which takes into consideration the Q-factors of the optical resonator and the spectral line of the laser active medium.

Figure 4.23a shows the plots of $E_{10n}(\nu/\nu_{0F})$ for different values of $K_{00}N_0 = K_{00}N_{00} = 0.001$–$0.1$ for Q-factors of the spectral line of emission $Q_{02} = 100$ and of the optical resonator $Q_{0F} = 20$, and Fig. 4.23b shows the plots of $E_{10n}(\nu/\nu_{0F})$ at the Q-factor $Q_{02} = 100$ and $N_{00}K_{00} = 0.1$ for different values $1/Q_{0F} = 0.7 - 0.001$.

As the initial symbolic equations of the laser model, we take equations of fourth order taking into account the inertial property T_{1n}, considered earlier:

$$\left[p_{00}^4 + \left(\frac{1}{Q_{0F}} + \frac{1}{Q_{02}}\right)p_{00}^3 + \left(2 + \frac{1}{Q_{0F}}\frac{1}{Q_{02}}\right)p_{00}^2 + \left(\frac{1}{Q_{0F}} + \frac{1}{Q_{02}}\right)p_{00} + 1\right]E_n = p_{00}^2 \frac{K_{00}N_0E_n}{1 + T_{1n}G_{00}(E_n)^2}. \tag{4.72}$$

4.6.2.2 Construction of the QWLD Resonance Characteristics by Solution of Symbolic Equations

OEO investigations and analysis with the linear-hyperbolic function, we perform with utilization of the symbolic equation (4.72) replacing the $p_{00} = p/(2\pi\nu_{0F})$ operator by $s = j(\nu/\nu_{0F})$, where $j = \sqrt{-1}$. Such a replacement means the transfer to the normalized frequency s of OEO generation, which is presented in the plane of complex variables along the abscissa axis. Now we perform the replacement $E_{10n}(\nu/\nu_{0F}) = x$, which will be presented in the ordinate axis.

The solution of the algebraic equation of the type *linear-hyperbolic nonlinearity* $S(E_{10n}) = (E_{10n})K_{00}N_0/\left[1 + T_{1n}G_{00}E_{10n}^2\right]$ is:

$$\begin{aligned}&\left[s^2 + (1/Q_{0F})s + 1\right]\left[s^2 + (1/Q_{02})s + 1.001\right]x\\&\quad = s^2K_{00}N_0x/\left[1 + T_{1n}G_{00}x^2\right]\end{aligned} \tag{4.73}$$

for *quadratic-hyperbolic nonlinearity* $S(E_{10n}) = (E_{10n})^2K_{00}N_0/\left[1 + T_{1n}G_{00}E_{10n}^2\right]$:

$$\begin{aligned}&\left[s^2 + (1/Q_{0F})s + 1\right]\left[s^2 + (1/Q_{02})s + 1.001\right]x\\&\quad = s^2K_{00}N_0x^2/\left[1 + T_{1n}G_{00}x^2\right].\end{aligned} \tag{4.74}$$

Similarly, for Eq. (4.72), we consider the resonance characteristics for the differential equation on the second order:

$$\left[p_{00}^2 + \frac{1}{Q_{0F}}p_{00} + 1\right]E_n = p_{00}S(E_{10n}). \tag{4.75}$$

The solution of the algebraic equation of the type for *linear-hyperbolic nonlinearity*:

$$\left[s^2 + (1/Q_{0F})s + 1\right]x = s \cdot K_{00}N_0x/\left[1 + T_{1n}G_{00}x^2\right] \tag{4.76}$$

for *quadratic-hyperbolic nonlinearity*:

$$\left[s^2 + (1/Q_{0F})s + 1\right]x = s \cdot K_{00}N_0x^2/\left[1 + T_{1n}G_{00}x^2\right]. \tag{4.77}$$

The resonance characteristics in the case of parametric dependence of the optical resonator Q-factor versus the field strength E_{10n} are analyzed in specific manner. We can consider the quadratic-hyperbolic function: $Q_{0F} = \frac{1}{0.1\cdot\left(1-A\cdot E_{10n}{}^2\right)}$, and the cubic hyperbolic function: $Q_{0F} = \frac{1}{0.1\cdot\left(1-A\cdot(E_{10n})^3\right)}$, where A is the small parameter: $A \ll 1$.

These functions depend on two variables s and x, and also on constants $T_{1n}G_{00}$, $K_{00}N_0$, Q_{0F}, Q_{02} included in Eq. (4.73). These functions of the normalized oscillation

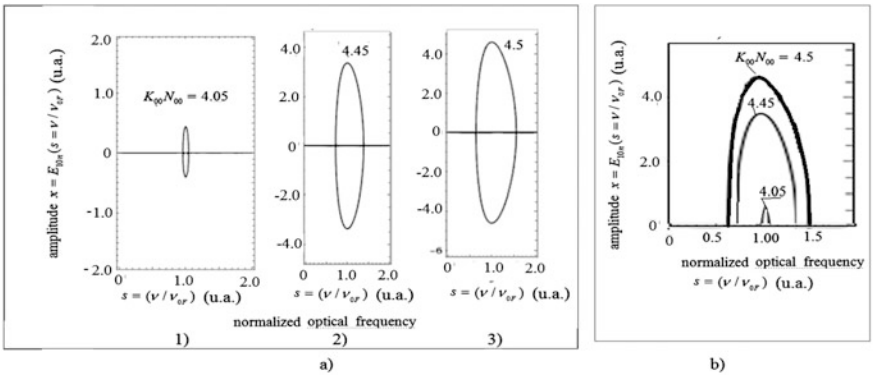

Fig. 4.24 The resonance characteristic of QWLD $E_{10n}(\nu/\nu_{0F})$ at different pumping values for the nonlinearity $S(E_{10n}) = \frac{E_{10n}K_{00}N_0}{1+T_{1n}G_{00}E_{10n}^2}$. (**a**) Plots of $E_{10n}(\nu/\nu_{0F})$ for different values of $N_{00}K_{00} = 4.05$, 4.45, and 4.5 at $T_{1n}G_{00} = 0.125$, Q-factors $Q_{02} = 10000$ and $Q_{0F} = 10,000$. The operator in the right part of DE has the second power of $p_{00}^2 = s^2$. Functions of the QWLD oscillation amplitude $E_n = E_{10n}$ versus the normalized frequency (ν/ν_{0n}) at $Q_{0F} = 100$, $Q_{02} = 100$, $K_{00}N_0 = 4.05$ (plot 1), 4.45 (plot 2) and 4.50 (plot 3). (**b**) The plot contains all three functions at $K_{00}N_0 = 4.05$, 4.45 and 4.50

amplitude x of OEO upon its normalized frequency s are the resonance characteristics (curves) of OEO. These curves can be constructed with the help of any computer software.

Figure 4.24 show the QWLD resonance characteristic at different pumping values, different Q-factors Q_{02}, Q_{0F}, $K_{00}N_0 = K_{00}N_{00}$, and $T_{1n}G_{00} = 0.125$ for the nonlinear approximation $S(E_{10n}) = E_{10n}K_{00}N_0/\left[1 + T_{1n}G_{00}E_{10n}^2\right]$.

The resonance characteristics for the linear-hyperbolic characteristic are presented in Fig. 4.24 for different values of $N_{00}K_{00} = 4.05$, 4.45, and 4.5 for $T_{1n}G_{00} = 0.125$, and at Q-factors $Q_{02} = 10,000$ and $Q_{0F} = 10,000$.

From analysis of plots in Fig. 4.24, it is stated that variations of $N_{00}K_{00}$ lead to increase of $E_{10n}(\nu/\nu_{0F})$, the resonance curve shape does not change and has the bell curve. The existence of the mirror part of functions at negative amplitudes speaks about the fact that for given nonlinearity, the conditions of the soft laser excitation are satisfied.

4.6.2.3 Investigation of Resonance Characteristics for the Quadratic-Hyperbolic Nonlinearity Taking into Account of the Population Inertial Properties

Figure 4.25 shows the resonance characteristics for the *quadratic-hyperbolic nonlinearity* ***taking into account*** the *population inertial properties* $S(E_{10n}) = \frac{(E_{10n})^2K_{00}N_0}{1+j(\nu/\nu_{0F})T_{1n}G_{00}+T_{1n}G_{00}E_{10n}^2}$.

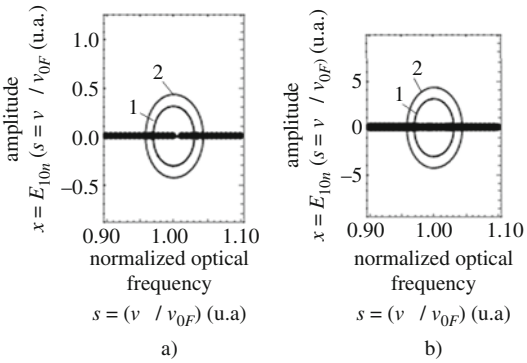

Fig. 4.25 The resonance characteristics of QWLD $E_{10n}(s = \nu/\nu_{0F})$ for different values of the normalized lifetime T_{1n}. The $x = E_{0n}$ parameter is the normalized strength amplitude, and the $s = j(\nu/\nu_{0F})$ parameter is the normalized optical frequency. The function of the amplitude $x = E_{0n}$ versus the laser optical frequency at $Q_{0F} = 100$, $Q_{02} = 100$ for $K_{00}N_0 = 4.05$: (**a**) for $T_{1n}G_{00} = 0.01$, (**b**) for $T_{1n}G_{00} = 0.0001$, for $[s^2 + (1/Q_{0F})s + 1][s^2 + (1/Q_{02})s + 1.001]x = s^1 \frac{K_{00}N_0x}{1+0.001\cdot s+T_{1n}G_{00}x^2}$ (curve 1). $[s^2 + (1/Q_{0F})s + 1][s^2 + (1/Q_{02})s + 1.001]x = s^1 \frac{K_{00}N_0x}{1+0.0001\cdot s+T_{1n}G_{00}x^2}$ (curve 2)

From analysis of plots in Fig. 4.25, we state that variations of $T_{1n}G_{00}$ lead to the growth of $E_{10n}(\nu/\nu_{0F})$, but the resonance curve shape does not change and has the shape of the semicircle.

Functions of the amplitudes $E_{10n}(\nu/\nu_{0F})$ versus the QWLD model optical frequency $y = E_{0n}$ or $s = j(\nu/\nu_{0F})$ are presented in Fig. 4.26 for the linear-hyperbolic nonlinearity of $S(E_{10n}) = (E_{10n})K_{00}N_0/\left[1 + T_{1n}G_{00}E_{10n}^2\right]$ type for (a) and (c) and for the *quadratic-hyperbolic nonlinearity* of $S(E_{10n}) = (E_{10n})^2K_{00}N_0/\left[1 + T_{1n}G_{00}E_{10n}^2\right]$ type for (b) at different values of $K_{00}N_{00} = 0.2$.

The comparison of plots in Fig. 4.26 shows that the nonlinearity type influences on the laser excitation type. Plots in Fig. 4.26a, c with the linear-hyperbolic nonlinearity $S(E_{10n}) = (E_{10n})K_{00}N_0/\left[1 + T_{1n}G_{00}E_{10n}^2\right]$ show that the mirror reflections of the positive values of amplitudes are present. In this case, we have the soft type of the laser self-excitation. In the plot in Fig. 4.26b with the quadratic nonlinearity of the $S(E_{10n}) = (E_{10n})^2K_{00}N_0/\left[1 + T_{1n}G_{00}E_{10n}^2\right]$ type, the mirror functions $E_{10n}(\nu/\nu_{0F})$ are absent and these functions have the closed character and have no interceptions with the abscissa axis. The resonance peaks for the last plots in Fig. 4.26b are evident.

4.6.2.4 Investigation of Resonance Characteristics at Quadratic-Hyperbolic Nonlinearity of the $S(E_{10n}) = (E_{10n})^2K_{00}N_0/\left[1 + T_{1n}G_{00}E_{10n}^2\right]$ Type

Figure 4.27 shows the resonance characteristics of QWLD with the ***quadratic-hyperbolic nonlinearity*** at different pumping values and various parameter

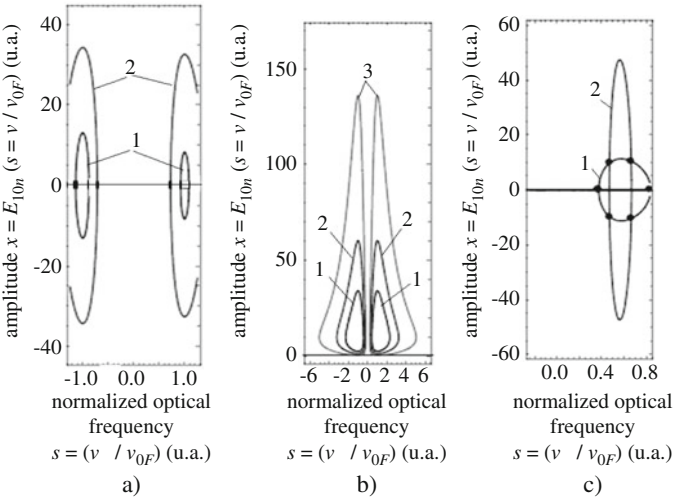

Fig. 4.26 The function of the amplitude $x = E_{10n}$ versus the QWLD optical frequency $s = (\nu/\nu_{0F})$ $E_{10n}(\nu/\nu_{0F})$ for the *linear-hyperbolic nonlinearity* $S(E_{10n}) = \frac{(E_{10n})K_{00}N_0}{1+T_{1n}G_{00}E_{10n}^2}$ for (**a**) and (**c**) and for the *quadratic-hyperbolic nonlinearity* $S(E_{10n}) = \frac{(E_{10n})^2K_{00}N_0}{1+T_{1n}G_{00}E_{10n}^2}$ for (**b**) for different $K = 0.2$: (a) $Q_{0F} = 10{,}000$, $Q_{02} = 100$, $K_{00}N_0 = 4.05$ (curve 1), 4.45(curve 2), for $T_{1n}G_{00} = 0.0001$, for $[s^2 + (1/Q_{0F})s + 1][s^2 + (1/Q_{02})s + 1.001]x = s^1\frac{K_{00}N_0x}{1+T_{1n}G_{00}x^2}$; (b) $Q_{0F} = 0.5$, $K_{00}N_0 = 1.5$ (curve 1), 2.5 (curve 2), and 5.5 (curve 3) for $T_{1n}G_{00} = 0.01$, for $[s^4 + 2.01s^2 + 1.01]x = s^2 \cdot \frac{K_{00}N_0x^2}{1+T_{1n}G_{00}x^2}$; (c) $Q_{0F} = 100$, $Q_{02} = 100$, for $T_{1n}G_{00} = 0.001$, $K_{00}N_0 = 3.5$ (curve 1); $Q_{0F} = 10$, $Q_{02} = 10$, $T_{1n}G_{00} = 0.00001$, $K_{00}N_0 = 3.45$ (curve 2), for $[s^2 + (1/Q_{0F})s + 1][s^2 + (1/Q_{02})s + 1.001]x = s^1\frac{K_{00}N_0x}{1+T_{1n}G_{00}x^2}$

$T_{1n}G_{00}$, while Fig. 4.28 shows the QWLD resonance characteristics with the ***quadratic-hyperbolic nonlinearity*** at variation of the right part of Eq. (4.73) at saving of the left part unchanged. In Fig. 4.28a at solution of Eq. (4.73) for values $T_{1n}G_{00} = 0.0001$, the right part of (4.79) has the form $S(E_{10n} = x) = s^2\frac{K_{00}N_0 \cdot x}{1+T_{1n}G_{00}(x)^2}$.

Figure 4.27 shows plots of the QWLD resonance characteristics with: *quadratic-hyperbolic nonlinearity* $S(E_{10n}) = \frac{(E_{10n})^2K_{00}N_0}{1+T_{1n}G_{00}E_{10n}^2}$ for the second-order differential equation for $Q_{0F} = 0.4975$: at quadratic-hyperbolic parametric dependence of the Q-factor: $Q_{0F} = 1/[2.01 - A \cdot (E_{10n})^3]$, where A is the small parameter $A = 10^{-9}$.

From plots presented in Fig. 4.27 we can conclude that at the quadratic nonlinearity $S(E_{10n})$ at extremely small influence on Q_{0F} of the amplitude E_{10n}, QWLD at $A = 10^{-9}$ transfers into the mode of chaotic oscillations, and its resonance characteristic having regular branches at $A = 10^{-10}$ (Fig. 4.27c) is completely destroyed at $A = 10^{-9}$ (Fig. 4.27d).

From an analysis of plots in Figs. 4.27 and 4.28 with the quadratic-hyperbolic nonlinearity, we can make a conclusion that the laser exits on the mode of the steady-state generation only in the rigid self-excitation mode. These functions $E_{10n}(\nu/\nu_{0F})$ differ qualitatively from the function at the linear-hyperbolic nonlinearity. In the plot

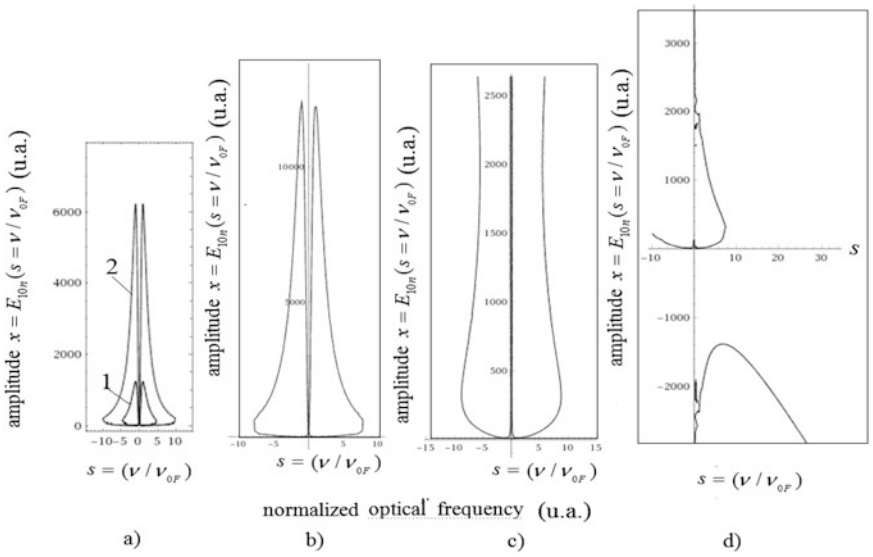

Fig. 4.27 Resonance characteristics of QWLD or functions of the oscillation amplitude $x = E_{10n}$ versus the laser optical frequency $s = j(\nu/\nu_{0F})$and for the *quadratic-hyperbolic nonlinearity* $S(E_{10n}) = \frac{(E_{10n})^2 K_{00} N_0}{1+T_{1n} G_{00} E_{10n}^2}$ for $[s^4 + 2.01s^2 + 1.01]x = s^2 \cdot \frac{K_{00} N_0 x^2}{1+T_{1n} G_{00} x^2}$: (**a**) $K_{00}N_0 = 0.5$ (curve 1), $K_{00}N_0 = 2.5$ (curve 2), for $T_{1n}G_{00} = 0.0001$; (**b**) $K_{00}N_0 = 0.5$, $T_{1n}G_{00} = 0.00001$, $A = 0$; (**c**) $K_{00}N_0 = 0.5$, $T_{1n}G_{00} = 0.00001$, the parameter $A = 10^{-10}$, (**d**)$T_{1n}G_{00} = 0.0001$, $K_{00}N_0 = 0.5$, $T_{1n}G_{00} = 0.00001$, the parameter $A = 10^{-9}$

in Figs. 4.27 and 4.28 with the quadratic nonlinearity of the $S(E_{10n}) = \frac{(E_{10n})^2 K_{00} N_0}{1+T_{1n} G_{00} E_{10n}^2}$ type, the mirror functions $E_{10n}(\nu/\nu_{0F})$ are absent and these functions have the closed character and have no interception with the abscissa axis. Resonant peaks in plots in Figs. 4.27 and 4.28 are evident. Closed curves in plots shown in Fig. 4.28 are interesting at changing in the right part of Eq. (4.73) depending on the power of the parameter $s = j(\nu/\nu_{0F})$.

4.6.2.5 Investigation of Resonance Characteristics for High Power Density in the Optical Resonator and in the Laser Active Medium

Figure 4.29a, b show the *resonance characteristics at quadratic function* of the resonator Q-factor versus the field amplitude $(E_{10n})^2$: $(1/Q_{0F}) + (1/Q_{02}) = 0.001 \cdot (1 - AE_{10n}{}^2)$ (Fig. 4.29a); $(1/Q_{0F}) + (1/Q_{02}) = 0.0001 \cdot (1 - AE_{10n}{}^2)$ (Fig. 4.29b).

From an analysis of plots (Fig. 4.29a), we state that branches of unstable and stable operation of the generator in the steady-state mode *come together from above and from below* at growth of the A coefficient, which achieves the critical magnitude

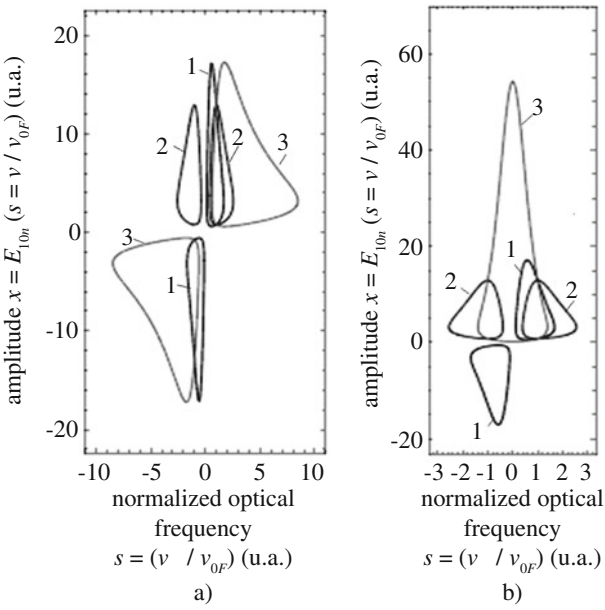

Fig. 4.28 Resonance characteristics with different nonlinearities of the type for $K_{00}N_0 = 5.5$, for $T_{1n}G_{00} = 0.1$: (**a**) $[s^4 + 2.01s^2 + 1.01]x = s \cdot \frac{K_{00}N_0x^2}{1+T_{1n}G_{00}x^2}$ (curve 1); $[s^4 + 2.01s^2 + 1.01]x = s^2 \cdot \frac{K_{00}N_0x^2}{1+T_{1n}G_{00}x^2}$ (curve 2); $[s^4 + 2.01s^2 + 1.01]x = s^3 \cdot \frac{K_{00}N_0x^2}{1+T_{1n}G_{00}x^2}$ (curve 3). (**b**) $[s^4 + 2.01s^2 + 1.01]x = s^1 \cdot \frac{K_{00}N_0x^2}{1+T_{1n}G_{00}x^2}$ (curve 1); $[s^4 + 2.01s^2 + 1.01]x = s^2 \cdot \frac{K_{00}N_0x^2}{1+T_{1n}G_{00}x^2}$ (curve 2); $[s^4 + 2.01s^2 + 1.01]x = s^0 \cdot \frac{K_{00}N_0x^2}{1+T_{1n}G_{00}x^2}$ (curve 3)

of $A = 0.0081$ at parametric growth of the Q-factor. The further growth of A leads to instability (the chaotic generation). At that, the amplitude values are defined ambiguously for the same values of the frequency. From an analysis of plots (Fig. 4.29b), we state that branches of unstable and stable operation of the generator in the steady-state mode *come together from above and from below* at growth of the A coefficient, which achieves the critical magnitude of $A = 0.082$ at parametric growth of the Q-factor. The further growth of A leads to instability (the chaotic generation).

4.6.2.6 The Cubic Parametric Function of the Resonator Q-factor

Figure 4.30 shows the resonance characteristics at cubic function of the resonator Q-factor versus the field amplitude E_{10n}^2: $(1/Q_{0F}) + (1/Q_{02}) = 0.0001 \cdot (1 - A \cdot (E_{10n})^3)$ (Fig. 4.30a) and $(1/Q_{0F}) + (1/Q_{02}) = 0.1 \cdot (1 + A \cdot (E_{10n})^3)$ (Fig. 4.30b).

From the analysis of plots in Fig. 4.30a, we state that branches of unstable and stable operation of the generator in the steady-state mode come close *only from above* at growth of the A coefficient, which achieves the critical value of $A = 0.0034$ at parametric growth of the Q-factor. The further growth of A leads to

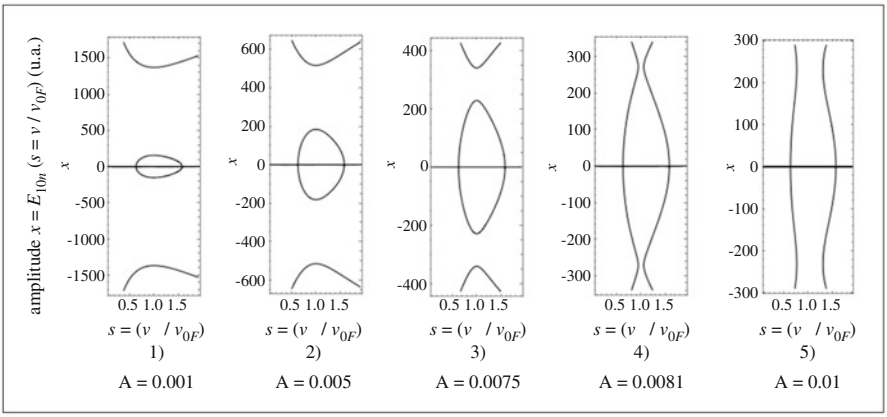

a)

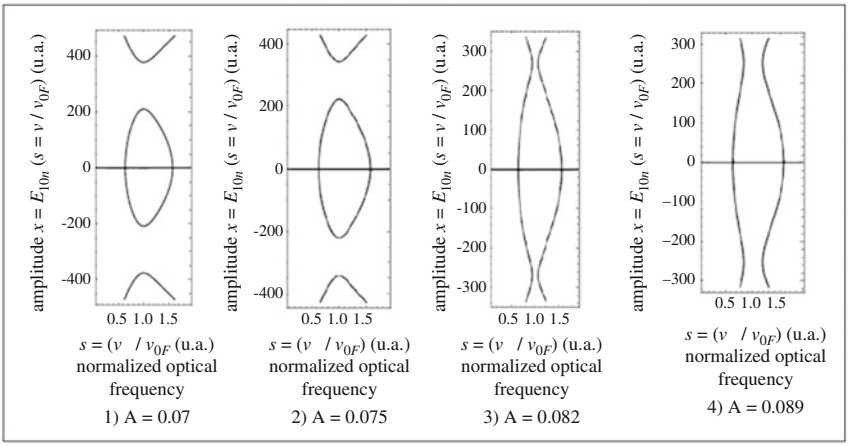

b)

Fig. 4.29 The resonance characteristic of QWLD at nonlinear parametric variation of the resonator Q-factor $Q_{0F} = 1/[0.001(1 - Ax^2)]$. The function of amplitude $x = E_{10n}$ versus the laser optical frequency $s = j(\nu/\nu_{0F})$ at $K_{00}N_0 = 4.9$, $T_{1n}G_{00} = 0.00001$. For (**a**)$[s^4 + 0.001(1 - Ax^2)s^3 + 2.001s^2 + 0.001(1 - Ax^2)s + 1]x = s^2 \cdot K_{00}N_0x/(1 + T_{1n}G_{00}x^2)$; $(1/Q_{0F} + 1/Q_{02}) = 0.001 \cdot (1 - Ax^2)$. For (**b**) $[s^2 + 0.01s + 1.001] \cdot [s^2 + 0.0001(1 - Ax^2)s + 1.001]x = s^2 \cdot K_{00}N_0x/(1 + T_{1n}G_{00}x^2)$; $(1/Q_{0F} + 1/Q_{02}) = 0.0001 \cdot (1 - Ax^2)$

instability (or to chaotic generation). At that, the amplitude and frequency are defined ambiguously for the same conditions.

4.6.2.7 The Cubic Parametric Function for Odd Powers of the Characteristic Polynomial

From an analysis of plots in Fig. 4.30b we state that at the cubic parametric function for odd powers of the characteristic polynomial, the branches of unstable and stable

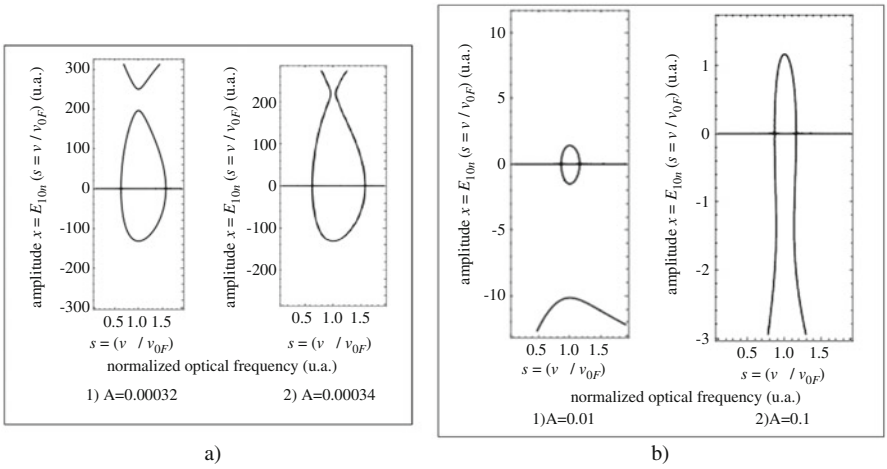

Fig. 4.30 The resonance characteristics of QWLD at nonlinear parametric variations of the resonator Q-factor $(1/Q_{0F} + 1/Q_{02}) = 0.0001 \cdot (1 - Ax^3)$ (**a**) and $(1/Q_{0F} + 1/Q_{02}) = 0.1 \cdot (1 + Ax^3)$ (**b**). The function of the amplitude $x = E_{10n}$ versus the laser optical frequency $s = j(\nu/\nu_{0F})$. (**a**) at $K_{00}N_0 = 4.9$, $T_{1n}G_{00} = 0.00001$ for (1) $A = 0.00032$; (**2**) $A = 0.00034$. $[s^2 + 0.01s + 1.0] \cdot [s^2 + 0.0001(1 - Ax^3)s + 1.001]x = s^2 \cdot K_{00}N_0x/(1 + T_{1n}G_{00}x^2)$ (**b**) at $K_{00}N_0 = 4.3$, $T_{1n}G_{00} = 0.01$; for (1) $A = 0.01$; (2) $A = 0.1$. For $[s^4 + 0.1(1 + Ax^2)s^3 + 2.001s^2 + 0.1(1 + Ax^2)s + 1]x = s^2 \cdot K_{00}N_0x/(1 + T_{1n}G_{00}x^2)$; $(1/Q_{0F} + 1/Q_{02}) = 0.1 \cdot (1 + Ax^3)$

operation in the steady-state mode come close *only from below* (or for the zone of negative amplitudes) at growth of the A coefficient, which achieves the critical value of $A = 0.1$ at parametric increase of the Q-factor. The further growth of A leads to the slight increase of oscillation amplitude in the region of positive amplitudes, at saving the generation stability. At that, for the given frequency values, the amplitude values are determined *unambiguously*.

Resonance characteristics of the laser model in the dipole approximation, which are presented in Figs. 4.24, 4.25, 4.26, 4.27, 4.28, 4.29 and 4.30, differ quantitatively from the functions, which were constructed on the base of algebraic equations presented in Fig. 4.30 without taking into account of the nonlinearity.

In the steady-state mode, at constant pumping amplitude and frequency, equations describe the nonlinear resonance characteristic of the resonator. Formally, we add losses, which include losses on absorption and scattering and which can be obtained introducing the imaginary part of permittivity or the finite specific resistance of the material, losses in the coupling element, which take into consideration the coupling effectiveness and the power entered in the resonator.

To compare with the previous plots in Figs. 4.29 and 4.30 at parametric dependence of the Q-factor versus the QWLD strength amplitude, Fig. 4.31 presents the plots of resonance curves constructed at utilization of the algebraic equation [13–15], which deduction is presented below:

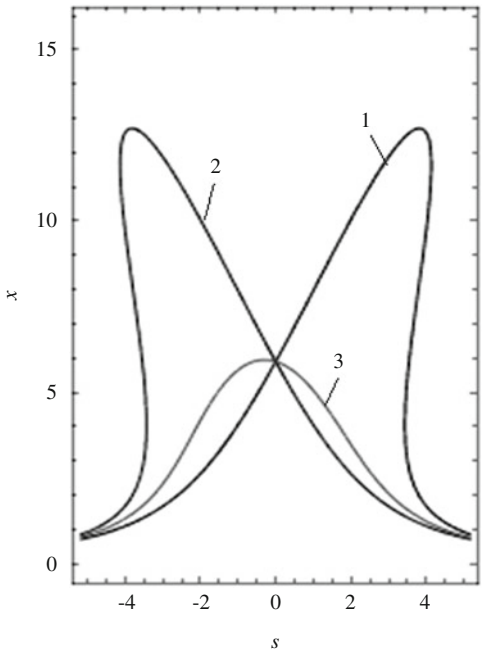

Fig. 4.31 Resonance characteristics of QWLD. The function of oscillation amplitude $x = E_{0n}$ versus the laser optical frequency at pumping $K = 20.5$. Plots are depicted for the following functions: curve 1: $0.1x^3 - 0.6s \cdot x^2 + 0.1xs^2 = 20.5$, curve 2: $0.1x^3 + 0.6s \cdot x^2 + 0.1xs^2 = 20.5$, curve 3: $0.1x^3 + 0.1s \cdot x^2 + 0.1xs^2 = 20.5$

$$\mu_{\text{opt}}^2 E_{10n}^3 + 6\pi\mu_{\text{opt}} \cdot \Delta\nu \cdot E_{10n}^2 + \left(\Delta\nu^2 + \frac{1}{Q_{0F}^2}\right) E_{10n} = E_{100in}. \tag{4.78}$$

which in our variables $x = E_{10n}$ and $s = j(\nu/\nu_{0F})$ has a form: $\mu_{\text{opt}}^2 x^3 \pm 6\pi\mu_{\text{opt}} s \cdot x^2 + xs^2 = E_{100in}$. For the whispering-gallery modes: $\mu_{\text{opt}} = \frac{6 \cdot 2\pi\nu}{8n^2}\chi^{(3)}$, where $\chi^{(3)}$ is the susceptibility of the optical resonator material, n is the refraction index of the resonator material, ν is the laser optical frequency.

The plots (4.78) are presented in Fig. 4.31 for the following functions: (1) curve 1: $0.1x^3 - 0.6s \cdot x^2 + 0.1xs^2 = 20.5$, (2) curve 2: $0.1x^3 + 0.6s \cdot x^2 + 0.1xs^2 = 20.5$, (3) curve 3: $0.1x^3 + 0.1s \cdot x^2 + 0.1xs^2 = 20.5$.

Plots presented in Fig. 4.31 describe the nonlinear amplitude-frequency characteristic of the resonator. The main difference from the previous plots in Figs. 4.29 and 4.30 is the pronounced incline of the amplitude-frequency characteristic at μ_{opt} growth. This incline is caused, firstly, by utilization for Fig. 4.31 of the first-order differential equation only and, secondly, by changing of the imaginary part $\mu_{\text{opt}} E_{10n}^2$ of the complex quantity $\delta_{\text{opt}} = \frac{1}{Q_{0F}} - j\mu_{\text{opt}} E_{10n}^2$. The imaginary part is defined by the imaginary part of the permittivity of the optical resonator material and it is related to the susceptibility $\chi^{(3)}$ of the optical resonator material.

We briefly present the deduction of the algebraic equation (4.78), which was used for construction of the nonlinear amplitude-frequency characteristics of the disk resonator. The simplest oscillator model under influence of the external field with the constant amplitude E_{100in} has the appropriate symbolic equation:

$$E_{10n}^3 p_{00}^2 + \delta_{opt} E_{10n}^2 p_{00} + E_{10n} = p_{00} S(E_{10n}). \tag{4.79}$$

where δ_{opt} has both the real and the imaginary parts: $\delta_{opt} = \frac{1}{Q_{0F}} - j\mu_{opt} E_{10n}^2$. For the whispering-gallery modes: $\mu_{opt} = \frac{6 \cdot 2\pi\nu}{8n^2}\chi^{(3)}$, where $\chi^{(3)}$ is the susceptibility of the optical resonator material.

The abbreviated equation for (4.79) at $S(E_{10n}) = E_{100in}$ takes the form:

$$p_{00} E_{10n} + \left[-j\mu_{opt} E_{10n}^2 + \frac{1}{Q_{0F}}\right] E_{10n} = jE_{100in}. \tag{4.80}$$

From Eq. (4.80), the algebraic equation follows, which was used for construction of plots in Fig. 4.31:

$$\mu^2 E_{10n}^3 + 6\pi\mu \cdot \Delta\nu \cdot E_{10n}^2 + \left(\Delta\nu^2 + \frac{1}{Q_{0F}^2}\right) E_{10n}^2 = E_{100in}. \tag{4.81}$$

Calculated functions of the QWLD oscillation amplitude versus frequency (resonance characteristics) allow determination of the threshold pumping values, regions of steady-state laser generation existence, as well as to determine how does the oscillation amplitude depend upon the pumping level, the gain, the lifetime, the saturation coefficient and Q-factors of the resonator and the spectral line of amplification. The nonlinear parametric impact depends on the variation of resonator losses as $1/Q_{0F} = 0.001\left(1 - AE_{10n}^2\right)$. Modeling of the high emission power density is performed by means of the increase of the A parameter. At critical value of $A = 0.0081$, the valleys of stability and instability are "collapsed," which leads to the sharp growth of amplitude and to disordered oscillation motions in the wide frequency area. Such types of stability loss of the single-frequency generation are manifested at the cubic parametric impact $1/Q_{0F} = 0.001\left(1 - AE_{10n}^3\right)$.

The special role in the analysis is featured to investigation of resonance characteristics of the laser model in the dipole approximation.

Results of symbolic equation solutions of the laser model in the dipole approximation at parametric variation of the resonator Q-factor under influence of the high optical power, which passes into the optical resonator or in the laser active medium, are relevant and original. Such a process of the Q-factor growth up to ultrahigh values (10^8–10^{12}) is observed in modern experimental researches of QWLD at utilization of disk resonators in lasers and resonators on the base on the Bragg optical lattices, which description was made in Chaps. 2 and 3 of this book.

At that, one of the purposes of an analysis is determination of cause-effect relations of critical values of Q-factors, at which the stable single-frequency

oscillation are disturbed. The results of numerical calculations on the base of solution of the resonance characteristic equations in the steady-state laser mode for the linear-hyperbolic, quadratic-hyperbolic, and linear-cubic nonlinearities.

Calculated functions of the QWLD oscillation amplitudes versus frequency (resonance characteristics) allow determination of the threshold values of the A coefficient, the region of stable steady-state single-frequency laser generation. We offer the research method, which allows determination for the laser model how does the amplitude-frequency function change at the power level growth in the optical resonator or on the active medium. These functions obtained from solution of symbolic equations take into account the gain on the feedback loop, the lifetime, the saturation coefficient, Q-factors of the resonator, and the spectral emission line of the active medium. The modeling of optical emission power variation in the optical resonator is executed by means of introduction of the A parameter, at variation of which the Q-factor of the resonator varies in nonlinear manner. We considered the quadratic and cubic parametric variation of the resonator Q-factor. Laws on Q-factor variation are determined for quadratic Q-factor variation as $Q_{0F} = 1/\left[0.001 \cdot \left(1 - A \cdot E_{10n}^2\right)\right]$, and for cubic equations $Q_{0F} = 1/[0.001 \cdot (1 - A \cdot E_{10n}{}^3)]$. As the result of symbolic equation solutions in quasi-stationary mode, we show that at critical value of $A = 0.0081$, branches of stable operation and branches of unstable operation "merge into one node" corresponding to disordered oscillation motions in the wide frequency region. The stability loss of the single-frequency generation is also manifested at growth of the A parameter at *cubic parametric impact*. At that, critical value of the A parameter is about $A = 0.0034$.

Determination of critical values is the important contribution in the theory of ultrahigh-Q disk resonators and Bragg resonators.

Fulfilled investigation of resonance characteristics widens our knowledge about oscillation processes and enables to make the well-founded conclusion. It consists in the fact that growth of Q-factors cannot increase without limit in ultrasmall volumes of optical structures. Decrease of the spectral line width and reduction of the laser phase noises can be performed with utilization of optical frequency control systems and PLL systems with application of ultrahigh-Q resonators as discriminators in the additional laser optical channel. At that, the power density in resonators can be significantly decreases by several ten times.

4.7 Solution of Nonlinear DE of Second Order for the Laser

4.7.1 Equation of Second Order for the Laser with the Nonlinear Element in the Form $S(E_{10n}) = E_{10n}/\left(1 + T_{1n}G_{00}E_{10n}^2\right)$

At the high-Q optical resonator in the laser (when the Q-factor exceeds the Q-factor of the spectral emission line by several hundred times and more), the conditions are created for transfer from the nonlinear differential equation of fourth order for

QWLD in the quasi-stationary mode to the differential equation of second order and to appropriate symbolic differential equations of the type:

$$\left[p_{00}^2 + \left(\frac{1}{Q_{0F}} + \frac{1}{Q_{02}}\right)p_{00} + 1\right]E_n = p_{00}^2 \frac{K_{00}N_0E_n}{1 + T_{1n}G_{00}j[(\nu_n/\nu_{0L}) - 1] + T_{1n}G_{00}{E_n}^2} \tag{4.82}$$

which allows to obtain functions of the generated amplitude versus frequency $E_{10n}(\nu/\nu_{0F})$ at different pumping and gains using the operator representation $s = j(\nu_n/\nu_{0L})$.

Let us explain the sense of Eq. (4.82) for EMF strength E_n from the point of view of the oscillation theory. Its left part represents an expression for laser resonator with the natural frequency of $2\pi\nu_{0n}$and losses expressed through the time constant T_{OF}. In the right part of considered differential equations, there is an expression for exciting force in the form of pumping α_{N0}, where the reduced gain $K = K_{00}N_0 = \frac{2\cdot 2p_e^2}{\varepsilon_0 2\pi\hbar}N_0$ is inertial with the term equaled to $\exp[-j2\pi\nu_{0n}T_R]$, which characterizes the delay in the feedback loop.

Figure 4.32a–d show solutions of Eq. (4.82) after scaling performed in the similar manner earlier for DE of second order; for different values of the DC component of scaled pumping $K = 0.1, 0.3, 3.4, 5.4$.

Figure 4.32e shows the QWLD resonance characteristics at representation of the laser nonlinearity in the form $S(E_n) = E_{10n}/\left(1 + T_{1n}G_{00} \cdot E_{10n}^2\right)$ for different values of the DC component of scaled pumping $K = K_{00}N_{00} = 18.4, 24.0, 32.0$.

Further, Fig. 4.33a, b show results of resonance characteristic investigations at the high power density in the optical resonator and in the laser active medium for the case of the cubic parametric function of the laser resonator Q-factor $(1/Q_{0F}) = 0.06 \cdot (1 - A \cdot (E_{10n})^3)$ *without and with the account of inertial* properties of the nonlinear element: $S(E_n) = E_{10n}/\left(1 + T_{1n}G_{00} \cdot E_{10n}^2\right)$ (Fig. 4.33a). Figure 4.33b shows solutions for the *cubic* $(1/Q_{0F}) = 0.06 \cdot [1 - A \cdot (E_{10n})^3]$ *taking into account inertial properties* $S(E_{10n}) = E_{10n}/\left\{1 + T_{1n}G_{00}j[(\nu_n/\nu_{0L}) - 1] + T_{1n}G_{00} \cdot E_{10n}^2\right\}$ of the nonlinear element.

4.7.2 *Equation of Second Order for the Laser with the Nonlinearity of the Cubic Polynomial* $S(E_n) = \alpha_{00}E_n - \beta_{00}E_n^3$

Solutions of differential equations for the laser are presented in Fig. 4.34 for the pumping level growth $K = \alpha_0$ for the normalized amplitude of the EMF strength:

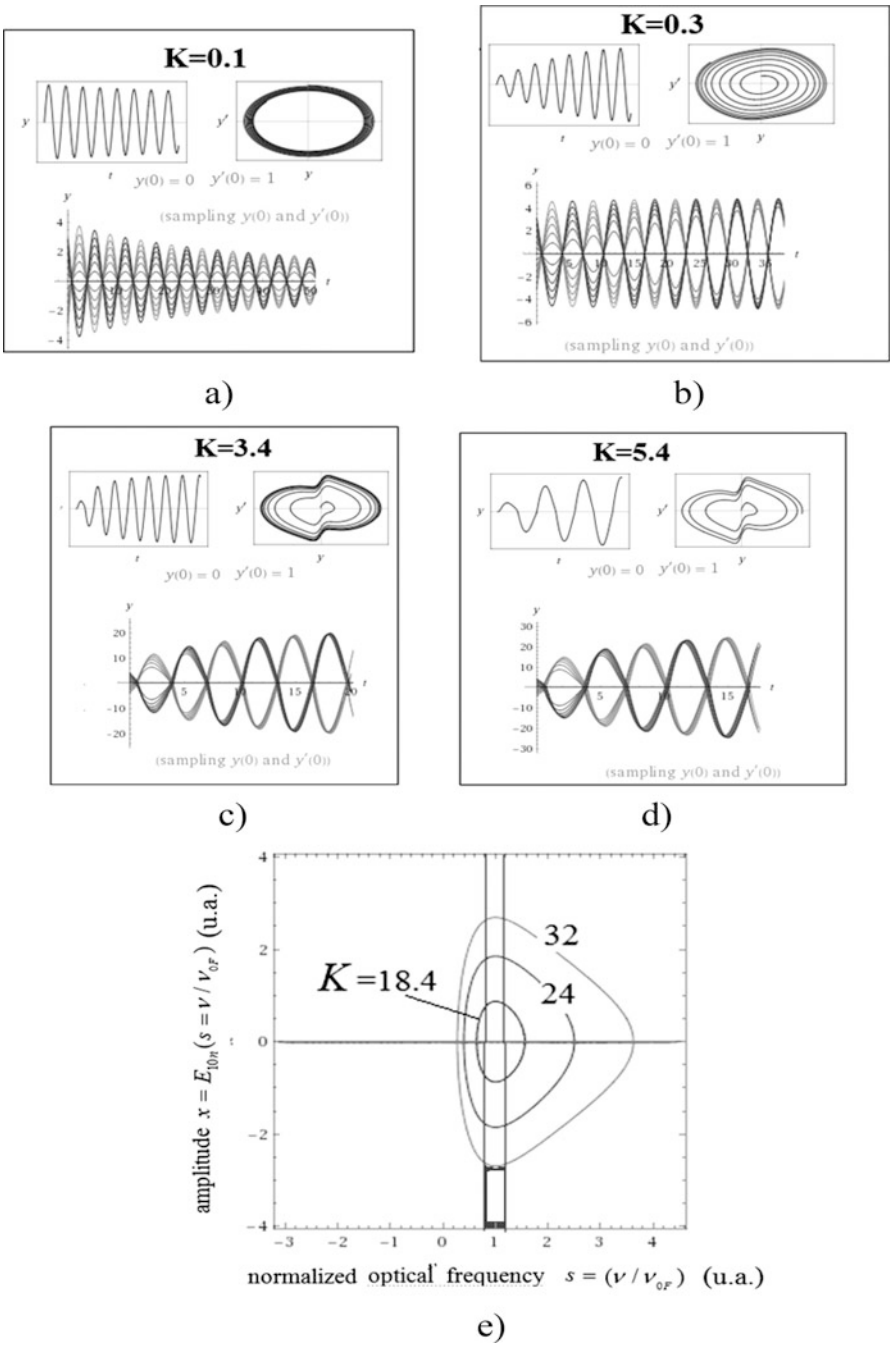

Fig. 4.32 Solution of the laser differential equation for EMF strength (4.83): at representation in the form of $S(E_n) = E_n/\left(1 + T_{1n}G_{00}E_n^2\right)$ for the scaled value $T_{1n}G_{00} = 0.01$ $k_0 = T_{1n}G_{00} = 0.125$, $2\pi\nu_{0n} = 1$, $\left(1/T'_{OF}\right) = 0.1$ for different values of the DC component of scaled pumping $K = 0.1$ (**a**), 0.3 (**b**), 3.4 (**c**), 5.4 (**d**). Initial conditions at the above-mentioned equation solution are the

$$\frac{d^2E_n}{dt^2} + (1/T_{OF})\frac{dE_n}{dt} + (2\pi\nu_{0n})^2 E_n = K_{00}N_0\frac{dS(E_n)}{dt} \tag{4.83}$$

for the nonlinearity in the form of the cubic polynomial $S(E_n) = \alpha_{00}E_n - \beta_{00}E_n^3$ for $\alpha_{00} = 0.5$, $\beta_{00} = 0.125$, $E_n = E_{10n}$and scaled values $2\pi\nu_{0n} = 1$, $(1/T_{OF}) = 0.1$ and pumping values $K = 0.2$ (a), 0.4 (b), 2.4 (c).

Figure 4.34 shows resonance characteristics of QWLD for $S(E_n) = \alpha_{00}E_n - \beta_{00}E_n^3$ at $\alpha_{00} = 0.5$,$\beta_{00} = 0.125$ and scaled values $\nu_{0n}/\nu_{0OF} = 1$, $(1/T_{OF}) = 0.1$ and the pumping values $K = 0.2$ (a), 0.4 (b), 2.4 (c).

Thus, we considered the features of the laser differential equations and discussed one of examples of OEO application on the base of constitutional equations in the dipole approximation for double-level pumping system. Let us proceed to examination of laser differential equations and OEO for triple-level pumping system on the base of the quantum-dimension structure.

Figure 4.35 shows resonance characteristics of QWLD (the Eq. (4.75)) for $S(E_n) = \alpha_{00}E_n - \beta_{00}E_n^3$ at $\alpha_{00} = 0.5$, $\beta_{00} = 0.125$ and scaled values $\nu_{0n}/\nu_{0OF} = 1$, $(1/T_{OF}) = 0.1$ and the pumping values $K = 0.2$ (a), 4.4 (b), 5.4 (c).

4.8 Conclusions

At analysis of the quantum generator, we used the semiclassical theory based on dipole representation of the laser model in two-level approximation. The evident urgency and necessity of laser theory development for OEO investigation are readily result from the key idea of this book: ***the quantum generator or the laser in OEO is the main energetic element defining amplitude and phase noises of OEO and its most important characteristics, features, and properties.***

The theoretical analysis of the quantum generator in this chapter is based on the system of three differential equations, which connect the medium polarization, the field strength and the inverted population of particles on upper and lower energy levels. This DE system is complicate for engineering calculations of QWLD characteristics and, unfortunately, it cannot be accepted for OEO investigation as a whole.

As a rule, the traditional laser analysis is based on transition to balance kinetic equation and its examination. However, at that, we loose the valuable information about phase relations, i.e., phase noises. At this approach, we cannot estimate the effect of many other parameters of laser generation development. We offer in this chapter to use for our problem of the classic approach of the nonlinear oscillation

Fig. 4.32 (continued) following: $y'(0) = E_n'(0) = 0$. The function of the laser oscillation amplitude $x = E_{0n}$ versus frequency at pumping $K = 18.4$, 24, 32 for representation in the form $S(E_n)$ (**e**). The frequency interval boundary is marked by lines (**e**)

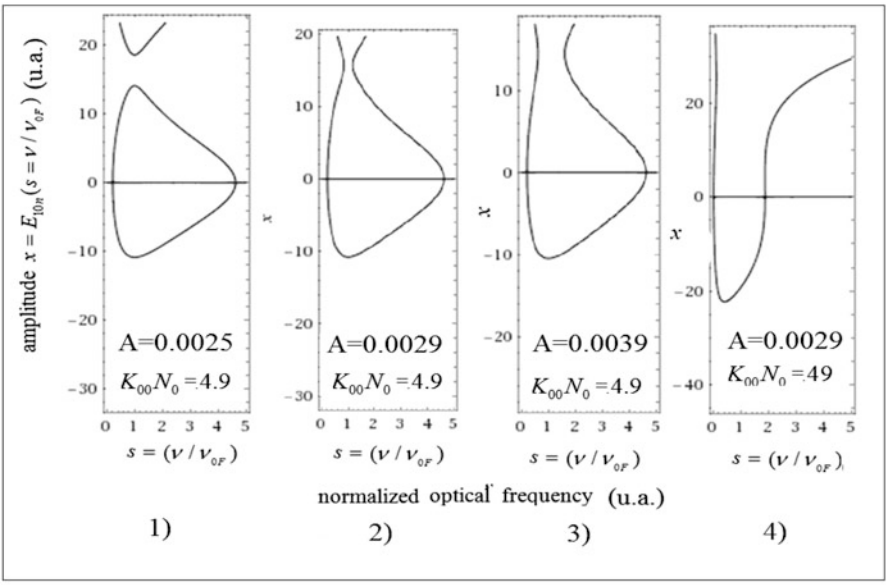

a)

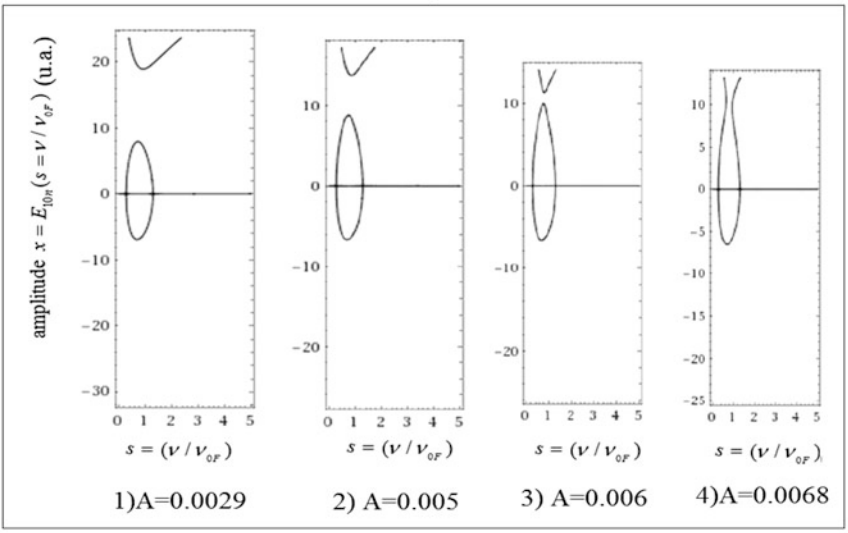

b)

Fig. 4.33 The QWLD resonance characteristic at nonlinear parametric variations of the resonator Q-factor. The $x = E_{0n}$ parameter is the normalized strength amplitude, and the $s = j2\pi\nu_L = j2\pi\nu_n$ parameter is the scaled laser oscillation frequency. (**a**) at $K_{00}N_0 = 4.9$, $T_{1n}G_{00} = 0.01$; $(1/Q_{0F}) = 0.06 \cdot (1 - Ax^3)$ for (1) $A = 0.0025$; (2) $A = 0.0029$; (3) $A = 0.0039$; (4) $A = 0.0029$; The equation for (**a**) (1–3): $[s^2 + 0.06(1 - Ax^3)s + 1.001]x = s \cdot 4.9x/(1 + T_{1n}G_{00}x^2)$. The equation for (**a**) (4): $[s^2 + 0.06(1 - Ax^3)s + 1.001]x = s \cdot 49x/(1 + s + T_{1n}G_{00}x^2)$. (**b**) at $K_{00}N_0 = 4.9$, $T_{1n}G_{00} = 0.01$;$(1/Q_{0F}) = 0.06 \cdot (1 - Ax^3)$ for (1) $A = 0.0025$; (2) $A = 0.0029$; (3) $A = 0.0039$; (4) $A = 0.0029$; The equation $[s^2 + 0.06(1 - Ax^3)s + 1.001]x = s \cdot 4.9x/(1 + s + 0.01x^2)$

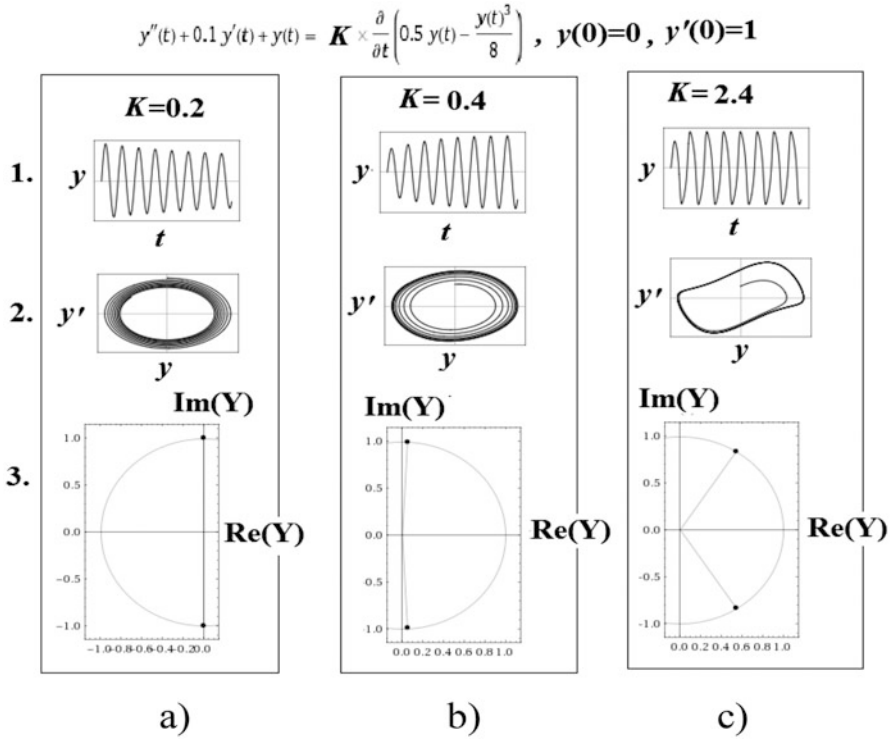

Fig. 4.34 Solutions of the differential equation for QWLD (4.83) at growth of the pumping level $K = \alpha_0$ for the scaled EMF strength $y = E_n$ for nonlinearity of the cubic polynomial $S(E_n) = \alpha_{00}E_n - \beta_{00}E_n^3$, $E_n = E_{10n}$, for $\alpha_{00} = 0.5$, $\beta_{00} = 0.125$ and scaled values $2\pi\nu_{0n} = 1$, $(1/T_{OF}) = 0.1$ and $K = 0.2$ (**a**), 0.4 (**b**), 2.4 (**c**)

theory: to transfer to the system of two nonlinear DE in ordinary derivatives, first of each has the fourth order for field strength, while the second is DE of the first order for population. Main parameters of these Des are the laser and the optical resonators Q-factors, the carrier lifetime on the upper level and gain. This DE system can be concerned to two-resonance system with inertial pumping.

Owing to studying of the population saturation effect on upper energy level under pumping action, we extract the main nonlinear element in the form of linear-hyperbolic function with inertia property caused by carrier time delay on upper level. The analysis of this two-resonance system allowed determination of the small-signal operator transfer function and the characteristic equation describing the oscillation stability. DEs obtained permitted to form the laser analog structure with two feedback loops for the field strength and a population.

After this, we obtained the abbreviated DEs, which show the oscillating transients. The transient of the field strength has a time delay with regard to population transient, which is caused by the carrier lifetime.

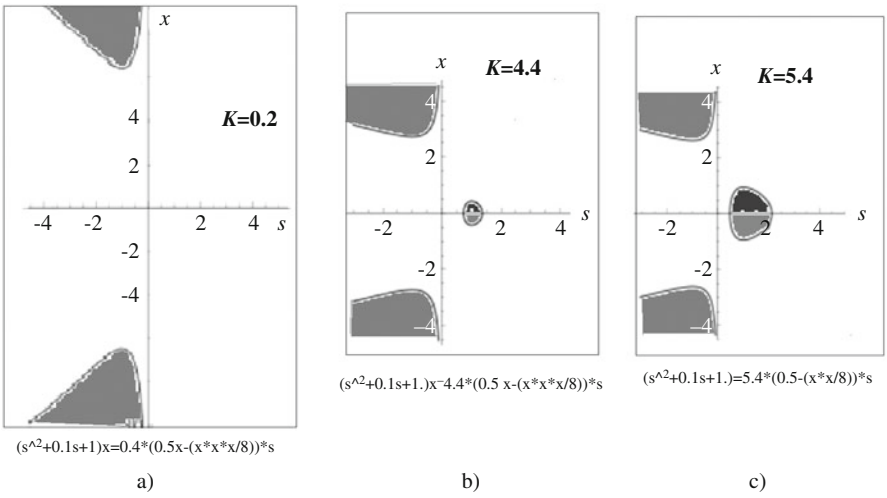

Fig. 4.35 Resonance characteristics of QWLD (the Eq. (4.75)) for representation of $S(E_n)$ in the form of the cubic polynomial $S(E_n) = \alpha_{00}E_n - \beta_{00}E_n^3$, $E_n = E_{10n}$, $\alpha_{00} = 0.5$, $\beta_{00} = 0.125$ and scaled values $\nu_{0n}/\nu_{0OF} = 1$, $(1/T_{OF}) = 0.1$ and pumping values $K = 0.2$ (**a**), 0.4 (**b**), 2.4 (**c**). The amplitude-frequency function $x = E_{0n}$ at growth of $K = 0.2$ (**a**), 4.4 (**b**), 5.4 (**c**). The $x = E_{0n}$ parameter is the normalized strength amplitude, and the $s = j2\pi\nu_L = j2\pi\nu_n = j2\pi\nu_{OF}$ parameter is the scaled laser oscillation frequency. Stimulated oscillation arise at pumping exceed above the threshold value

The investigation of oscillation excitation conditions in QWLD, positions of steady-state points and the limit cycle existence in the phase plane of generalized parameters is performed. It enables to obtain the system of inequalities for main parameters, which is important for the laser system analysis in the quasi-linear mode with high exceed of the pumping current over its threshold value. Utilization of the locus method and the Nyquist criterion help us to analyze more accurate conditions of excitation taking inertia property into account.

Modeling results are presented in quasi-stationary mode of laser generation at inertial nonlinearity. Analysis of time-functions gives new information about stable laser generation close to harmonic. Phase portraits are built, which have interesting features, for instance, the loop-type phase portrait and the cycloid symmetric closed trajectories and curves with singularities. In particular, at inertial property absence, at linear-hyperbolic nonlinearity, there is restricted region of values of pumping. The limit cycle of single-frequency oscillations exists in the restricted range of pumping, which defines by the two-resonance system formed the laser and its optical resonator.

At examination of the dynamic oscillation picture, taking into consideration the inertia property of laser nonlinear element, together with the in-phase component in existing oscillating motions of field strength the quadratic component plays the significant role. At that, exit to the limit cycle is accompanied by oscillations caused by nonlinear interaction of harmonics. The special role in analysis is attracted to

investigation of the resonance characteristics of the laser model in dipole approximation.

Results of solution of symbolic equations for laser model in dipole approximation at parametric variation of the resonator Q-factor are actual and original under action of the high optical power, which passes into optical resonator of the laser active medium. Such a process of Q-factor growth up to ultrahigh values in the optical resonator ($10^8...10^{12}$) is observed now in modern experimental QWLD investigations at utilization of disk resonators and on the base of Bragg optical lattices described in Chaps. 2 and 3.

One of the analysis purposes in this chapter was determination of cause–effect relations between critical values of Q-factor, at which single-frequency oscillation stability is lost. These results of numerical calculation are obtained for linear-hyperbolic, quadratic-hyperbolic and linear-cubic nonlinearities of the laser.

The investigation method is offered, which allows determination how the laser AFCs are changed at growth of power level in the optical resonator or in the laser active medium. We consider quadratic and cubic parametric variation of the resonator Q-factor. As the result of symbolic equation solution, we obtained that at critical parameters, branches of stable and unstable operation "confluent" into the single branch, which corresponds to disordered oscillating motions in the wide frequency region. The determination of critical values of parameters is the significant contribution in the theory of ultrahigh-Q disk resonators and Bragg resonators.

The main result OF Chap. 3, which is new in the laser analysis, is substantiation and investigation of DE of fourth order of the laser model in dipole approximation in quasi-stationary mode with high exceed of pumping over the threshold value. This approach leads to the new glance, which is suitable for the laser engineer and the expert in quantum electronics. The new glance at the quantum generator as the generator with the nonlinear inertial property containing two resonance circuits in the oscillating system, in contrast to traditional investigation of laser balance kinetic equations, widens the scientific scope of scientist. During analysis of the quantum generator, we reduced the complicate laser system with DE of fifth order, which in the most cases is incomprehensible for students and young scientists, to DE of second or third order, and we presented analog structures of the laser model. Mentioned issues significantly facilitate the development of OEO theory, as the reader will see from the following chapters.

References

1. H. Haken, *Laser Theory, Encyclopedia of Physics*, vol XXY/2c (Springer, Berlin, 1970)., 2nd corr.ed., 1984
2. H. Haken, *Introduction to lasers and masers* (McGraw-Hill, New York, 1971)
3. H. Haken, H. Sauerman, Z. Phys. **173**, 261 (1963).; 176, 47 (1963)
4. H. Haug, H. Haken, Theory of noise in semiconductor laser emission. Z. Physik **204**, 262 (1967)
5. W.E. Lamb,Theory of optical masers, Jr., Phys. Rev. **134A**, 1429 (1964)

6. M. Lax, *Fluctuation and Coherence Phenomena in Classical and Quantum Physics* (Gordon and Breach, New York, 1968)
7. D. Marcuse, *Light Transmission Optics* (Van Nostrand Reinhold, New York, 1972)
8. I. Hanin, *Quantum Radiophysics. Dynamics of Quantum Generators*, vol 2 (Sovetskoe Radio, Moscow, 1975)., (In Russian)
9. I.V. Komarov, S.M. Smolskiy, *Fundamentals of short-range FM radar* (Norwood, Artech House, 2003)
10. N. Yoshida, *Oscillation Theory Of Partial Differential Equations* (World Scientific Publishing, Singapore, 2008)
11. B.P. Abbott, R. Abbott, T.D. Abbot, M.L. Gorodetsky, et al., Observation of gravitational waves from a binary black hole merger. Phys. Rev. Lett. **116**(6), 061102 (2016)
12. B.P. Abbott, R. Abbott, T. Alford, et al., Search for transient gravitational-wave signals associated with magnetar bursts during advanced LIGO's second observing run. Astrophys. J. **874**(2), 163 (2019)
13. V.B. Braginsky, M.L. Gorodetsky, V.S. Ilchenko, Quality-factor and nonlinear properties of optical whispering gallery modes. Phys. Lett. A. V. **137**, 393–397 (1989)
14. M.L. Gorodetsky, A.A. Savchenkov, V.S. Ilchenko, Ultimate Q of optical microsphere resonators. Opt. Lett. **21**, 453–455 (1996)
15. M.L. Gorodetsky, A.E. Fomin, Whispering gallery modes in axisymmetric dielectric bodies, in Laser and Fiber-Optical Networks Modeling, 2005. Proceedings of LFNM 2005. 7th International Conference (2005), pp. 537–543

Chapter 5
Optoelectronic oscillator (OEO) Differential Equations as the Laser System with Modulation and Positive Feedback

This chapter is devoted to main features of OEO. The optoelectronic oscillator is considered as the oscillating system with modulation, which is spanned by the positive feedback. We form the symbolic and abbreviated equations of OEO. The analog model of OEO is examined taking into account the laser fluctuations.

In Sect. 5.1, we discuss the symbolic DEs of OEO DM and OEO MZ and the analog model of OEO, which is constructed on its base. The oscillation stability of the OEO oscillating system is investigated in Sect. 5.2, and OEO self-excitation and oscillation existence conditions are analyzed.

In Sect. 5.3, we investigate the transient dynamics in OEO DM. On the base of OEO abbreviated equations, we estimate the time for oscillation setting of laser strength and oscillations of the pumping current. Solutions are considered for the OEO DM field strength, for the population, and the pumping current in transients.

Section 5.4 is devoted to description of OEO differential equation with the Langevinian noise sources. The main regulations of the laser fluctuation model are described, and the Langevinian noise sources are examined for the OEO oscillating system. On the base of laser symbolic constitutive equations with fluctuations, we construct the analog models of OEO DM and OEO MZ with account of laser noises. The symbolic DEs of the laser with fluctuations in the quasi-stationary mode for the small signal are analyzed.

In Sect. 5.5, we describe the approach to calculation of the power spectral density of the amplitude and phase noise of OEO. The influence of the spontaneous laser emission on PSD of OEO phase noise is described. At PSD of the noise calculation, we use the approach based on the symbolic equations of OEO. For this, the method of abbreviated fluctuation equations of Evtianov–Kuleshov is used. The approach for PSD of OEO noises is described at OEO representation as the *correlator* of random quantities. The main correlator structures are discussed, and autocorrelation functions for oscillations of the laser field strength and the electrical voltage in OEO are calculated.

Main results of this chapter are summarized in Sect. 5.6.

A. A. Bortsov et al., *Laser Optoelectronic Oscillators*, Springer Series in Optical Sciences 232, https://doi.org/10.1007/978-3-030-45700-6_5

5.1 Symbolic and Abbreviated Equations of OEO

To construct the analog models of OEO DM and OEO MZ, we consider structural diagrams (Figs. 3.2 and 5.1a, b) and form and analyze of symbolic DEs of OEO.

At first, we take the symbolic differential equations of the laser, which we described in Chap. 4.

In the diagram of Fig. 3.2, the structures of OEO DM and OEO MZ with allocation of Feedback Chain and RF FODL are presented. For OEO MZ, two different approaches of the positive feedback spanned of modulated laser emission source "Laser-MZ" are shown in Fig. 5.1b, c. In the case of Fig. 3.2b, the one-port Feedback Chain has the optical input and electrical output. In the case of Fig. 3.2c, the one-port RF FODL has the electrical input and the electrical output. In the structure of Fig. 3.2b, "Laser" is enclosed by the feedback by the "DC" block, which fulfills the function of the laser optical frequency of the output power with utilization of adjustment by the laser DC pumping current. On the structure of OEO DM in Fig. 3.2a, instantaneous values of voltages, relatively, on the load resistance Z_L of photodetector $u_{PD}(t)$, on electrical output of the RF amplifier $u_A(t)$, of the RF filter $u_F(t)$, of the RF coupler $u_C(t)$, and instantaneous values of the laser pumping current $i_L = u_L/Z_L$ are shown. In the structure of OEO MZ in Fig. 3.2b, the instantaneous values of the field oscillation strength in the optical input of MZ (or in the laser output) E_n and in the optical output of E_{nMZ}, and the instantaneous voltage values in the electrical input u_{MZ} are shown. In the structure of OEO MZ in Fig. 3.2c, the instantaneous voltage values, relatively, in the load resistance Z_L of PD $u_{PD}(t)$, in electrical outputs of the RF amplifier $u_A(t)$, of the RF filter $u_F(t)$, of the RF coupler $u_C(t)$, and instantaneous voltage value on the electrical input of MZ are shown.

In order to obtain the connection of the AC pumping current $i_{1L} = J_{1L}$ with the AC component of the strength E_{1n} (or intensity E_{1n}^2), we transfer to more detailed description of parameters of the positive feedback circuit.

5.1.1 Symbolic Laser Equations in the OEO Structure

In Chap. 4, we examined and analyzed the symbolic differential equations (Eq. 4.28) and the abbreviated DEs for the laser model in the dipole approximation.

Let the strength of linear-polarized electrical field of optical carrier, which passes in the optical input of the optical fiber from the laser output, be expressed as (Fig. 3.2a): $E_n(t) = E_L(t) = E_{0L} \cos(2\pi\nu_{0L}t + \varphi_{0L})$, where $\nu_{0L} = \nu_{0n}$ is the average frequency of laser generation, and E_{0L} is the amplitude of the laser oscillation. φ_{0L} is the initial phase. The pumping current α_{N0} affects the laser electric input (Fig. 3.2a).

According to Eq. (4.28), for E_n and the population N of the model in dipole approximation, we have the following system of symbolic DEs (p is the symbolic operator of differentiation):

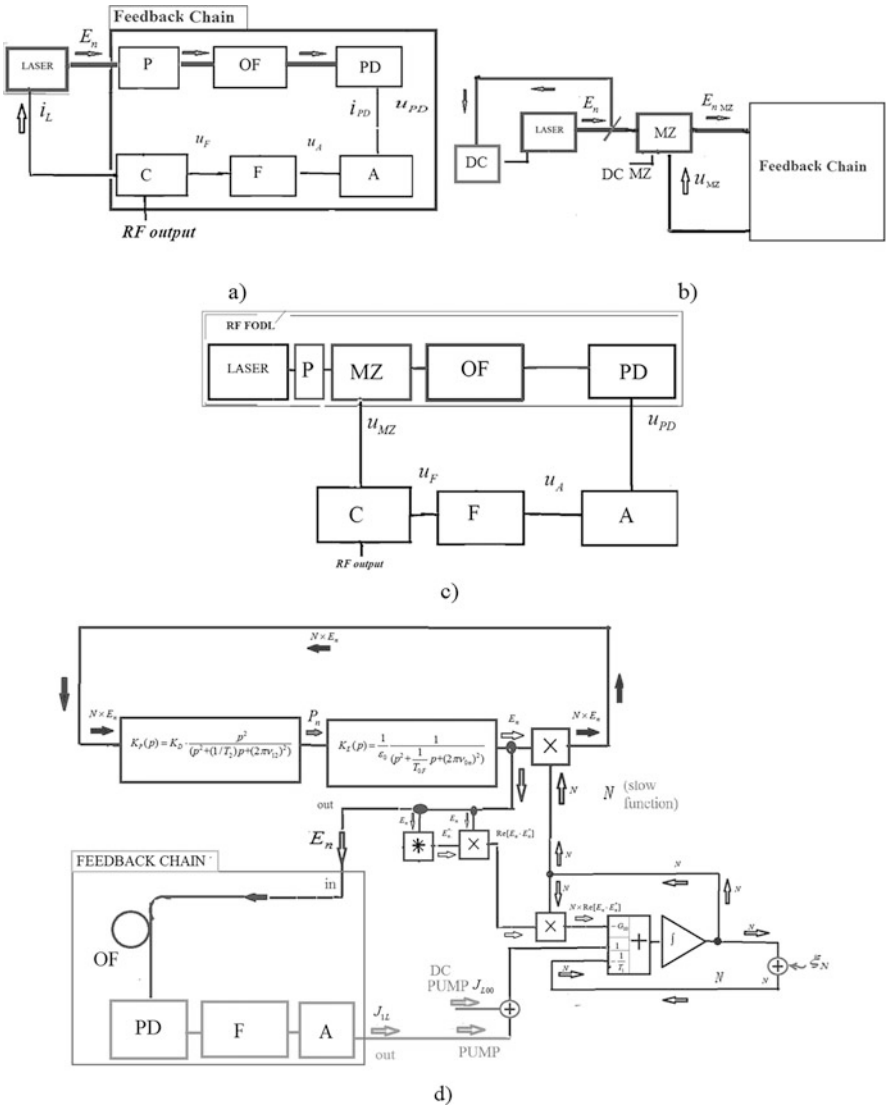

Fig. 5.1 OEO DM representation as a laser spanned by the positive Feedback Chain: (**a**) The structural diagram of OEO DM, (**b**) The diagram of OEO MZ with the block "Feedback Chain," (**c**) The structure diagram of OEO MZ with the block "PF FOLD." Laser is QWLD, P is a polarizer, OF is the optical filter, PD is the photodetector, A is the RF amplifier, F is the RF filter, C is the RF coupler, DC is the block for laser optical frequency stabilization or the output power with utilization of adjustment by the laser DC pumping current. (**d**) The analog model of OEO DM as QWLD enclosed by the positive feedback "Feedback Chain." The laser model is presented in the dipole approximation with the controlling element. "Feedback Chain" consists of the optical fiber (OF), the photodetector (PD), the RF filter (F), RF amplifier (A). We use designations: "$\int$" is the integrator, "$\times$" is the multiplier, "+" is the adder, "$*$" is the operation of complex conjugation, "PUMP" is the pumping α_{N0}

$$\begin{cases} \left[p^2 + \dfrac{1}{T_{0F}}p + (2\pi\nu_{0n})^2\right]\left[p^2 + (1/T_2)p + (2\pi\nu_{12})^2\right]E_n = K_\alpha p^2 S_L(N \cdot E_n), \\ pN = \alpha_{N0} - \dfrac{N}{T_1} - G_{00}N \cdot \mathrm{Re}\left[E_n E_n^*\right]. \end{cases} \tag{5.1}$$

The left part of the first DE in Eq. (5.1) represents the laser oscillating system. The right part of the first DE contains the nonlinear function $S_L(N \cdot E_n)$, which (at using of the N_n approximation in the vicinity of ν frequencies, which are close to the average optical frequency ν_{0n} of the laser), takes a form:

$$S_L(N \cdot E_n) = \frac{E_n N_0}{\left\{1 + j[(\nu - \nu_{0F})]T_1 + T_1 G_{00}\,\mathrm{Re}\left[E_n \cdot E_n^*\right]\right\}}, \tag{5.2}$$

where T_1 is the carrier lifetime, ν_{0F} the natural optical frequency of the laser resonator, G_{00} is the coefficient of amplification (or saturation).

The second DE in the system (Eq. 5.1) represents the equation for the population N. The pumping α_{N0}, which has the DC component $\alpha_{N00} \cdot J_{0L}$ and the AC component $\alpha_{N01} = \alpha_{N001} \cdot i_L$, where α_{N001} is the constant coefficient, is included in the right part of the second DE. The pumping α_{N0} in (Eq. 5.2) can be expressed as: $\alpha_{N0} = \alpha_{N00} \cdot J_{0L} + \alpha_{N01} \cdot i_L$, where α_{N00} and α_{N01} are constants, $J_{0L} = I_{0L}$ is DC component of the pumping current, i_L is the AC component of the pumping current.

In the general case, the AC component of the pumping current i_L is defined by the current sum of the first i_{1L}, second i_{2L}, third i_{3L}, ..., nth i_{nL} harmonics: $i_L = i_{1L} + i_{2L} + i_{3L} + \cdots + i_{nL}$. But since we examine the case of the narrowband RF filter in OEO DM, we consider that the harmonic amplitudes (besides first) are neglibly small: $i_{2L} + i_{3L} + \cdots + i_{nL} = 0$. Therefore we consider that $i_L = i_{1L} = J_{1L}$.

Now we form the system of differential equations (Eq. 5.1) for OEO DM (Fig. 5.1) for the square of strength amplitude E_n of electrical component of the electromagnetic field with the amplitude of the first harmonic E_{10L} and the AC electrical component i_{1L} with the amplitude of the first harmonic of the laser pumping current : $J_{1L} : E_{1n} = E_{10L}\,\mathrm{Re}\,[\exp(2\pi\nu_0 t - \Phi_{10L})]$, $i_{1L} = J_{10L}\,\mathrm{Re}\,[\exp(2\pi f_0 t - \Phi_{10L})]$.

For formation of OEO DM differential equations (Fig. 3.2a), the system (Eq. 5.1) must be added by the equation for the circuit of the positive feedback (PFB), which encloses the laser (QWLD). The series-closed in the loop, the optical filter (OF), the photodetector (PD), the RF amplifier (A), the RF filter (F), and the RF coupler (C) are included into the PFB circuit (Fig. 3.2a). In order to obtain the expression, which couples of the AC component of the pumping current $i_{1L} = J_{1L}$ of the laser with the AC component of the strength E_{1n} (or intensity E_{1n}^2), we transfer to the more detailed description of PFB circuit parameters.

5.1.2 Closed PFB Circuit

Let us consider the circuit of positive feedback in OEO DM presented in Figs. 3.1a and 3.2b. The laser pumping current can be written as the instantaneous value of the pumping current $i_L = J_{1L}$ (the first harmonic) in the electric laser input (or in the output of the RF filter F). Now we present the instantaneous voltage values (mentioned on the OEO DM diagram (Fig. 5.1a) $u_{PD}(t)$, $u_F(t)$, $u_A(t)$, $u_C(t)$, $u_L(t)$ in the time domain: for the photodetector (PD) $u_{PD} = U_{10PD}$ Re [exp($j2\pi ft - \Phi_{PD}$)]; for the RF filter (F) $u_F = U_{10F}$ Re [exp($j2\pi ft - \Phi_F$)]; for the RF amplifier (A) $u_A = U_{10A}$ Re [exp($j2\pi ft - \Phi_A$)]; for the RF coupler $u_C = U_{10C}$ Re [exp ($j2\pi ft - \Phi_C$)]; for the laser $u_L = Z_L i_L = U_{10L}$ Re [exp($j2\pi ft - \Phi_L$)]; here U_{10MZ}; U_{10PD}; U_{10F}; U_{10A}; U_{10C}; U_{10L} are amplitudes of first harmonics, Φ_{MZ}; Φ_{PD}; Φ_F; Φ_A; Φ_C; Φ_L are appropriate phase incursions), Z_L is the input resistance of the laser, and i_{1L} is the AC of the current in the QWLD input.

We introduce designation U_{PD}, U_F, U_A, U_C, U_L, E_L as the complex quantities of the appropriate variables $u_{PD}(t)$, $u_F(t)$, $u_A(t)$, $u_C(t)$, $u_L(t)$. We introduce the complex transfer function of RF FOLD K_{FOLD} : $K_{FOLD} = U_{PD}/U_L = |K_{FODL}| \exp(-j2\pi fT_{FOS} - j\Phi_{FS})$ where T_{FOS} is the delay time in the fiber-optical system (FOS), Φ_{FS} in the phase incursion in RF FODL without the account of the phase incursion in FOS, $|K_{FODL}|$ is the module of the RF FODL transfer function.

Let us introduce the complex transfer functions for blocks F, A, C, relatively, K_F, K_A, K_C: $K_F = U_F/U_{PD}$; $K_A = U_A/U_F$; $K_C = U_L/U_A$. At that, for RF filter, we have: $K_F = U_F/U_{PD} = \frac{(j\omega)(1/T_{EF})}{(j\omega)^2+(1/T_{EF})(j\omega)+(2\pi f_{0e})^2}$, where the current oscillation frequency $\omega = 2\pi f$, δ_e is the losses in the filter F, $\delta_e = 1/T_{EF} = f_{0e}/(f_{0e}T_{EF}) = f_{0e}/Q_{EF}$, $T_{EF}$is the time constant of the RF filter, Q_{EF} is the Q-factor of the RF filter, $f_{F0} = f_{0e}$ is the natural frequency of RF filter (or the resonance circuit), relatively. As the RF amplifier (A), we take the only "ideal" (i.e., without account the output voltage of the stage on the current in the stage input) non-inertia amplifying stage (Fig. 5.1a). At that, the tube triode connected on the common anode circuit (or the stage on the field-effect transistor (FET) connected on the common source circuit) can be such an ideal amplifying stage. For simplicity, we neglect by the electron inertia and the reaction of the grid current (input current) upon the RF filter and the anode reaction. Then the equation of OEO (Fig. 3.2a), which couples the instantaneous values of the amplifier input voltage and the output current $i_A(u_{PD})$, can be written in the form:

$$y(j\omega)u_{PD} = i_A(u_{PD}), \tag{5.3}$$

where $y(j\omega)$ is the symbolic control conductance, which is (for typical RF oscillator) a ratio of the symbolic load conductance y_l to the FB coefficient k_{fb}; $\omega = 2\pi f$, $j\omega$ is the symbolic operator of differentiation [1].

Introducing the time constant T_{EF} and the natural frequency f_{0e} for the RF filter (Fig. 5.1a), we can write for the symbolic load conductance of the amplifier the following equation (Eq. 3.48): $y_l(j\omega) = (j\omega)^2 + (1/T_{EF})(j\omega) + (2\pi f_{0e})^2/[(j\omega)(1/T_{EF})]$.

If we combine Eq. (5.3) and the formula (Eq. 3.48) for $y_l(j\omega)$ and replace the symbolic operator $j\omega$ by the differential operator in the time domain d/dt and $(j\omega)^2$ by d^2/dt^2, we obtain the differential nonlinear equation of the second order.

Now we take into consideration that in our structural diagram, the feedback coefficient is the transfer function of RF FODL, i.e., $k_{fb} = K_{RFFODL} = U_{PD}/U_L$.

For simplicity we shall consider that the module of the RF FODL transfer function is constant and equals to K_{0FODL}, and $K_{0FODL} = E_{0L}^2 K_{FODL}$. We take into account that the directional coupler C has the transfer function on voltage and on current, which are equal to 1, and then $u_F \approx u_{MZ.}$ Having considered $j\omega$ as the differentiation operator d/dt, and taking into account that $u_L = Z_L i_{1L}$, we can rewrite the OEO equation in the operator form as:

$$\left[p^2 + (1/T_{EF})p + (2\pi f_{0e})^2\right] i_L = [1/(Z_L T_{EF})] K_{0FOLD} p i_A(u_{PD}) \exp(-pT_{FOS}); \tag{5.4}$$

and in the time domain as:

$$\frac{d^2 i_L}{dt^2} + \frac{1}{T_{EF}} \cdot \frac{di_L}{dt} + (2\pi f_{F0})^2 i_L = \left(\frac{1}{Z_L T_{EF}}\right) K_{0FODD} \frac{di_A(u_{PD} - T_{FOS})}{dt}. \tag{5.5}$$

At closed positive feedback loop in OEO, the instantaneous AC current value (in the electric laser input) from Eq. (5.4) $i_L = \frac{|E_n|^2 (1/T_{0EF}) K_{OF} \cdot K_{PD} \cdot p \cdot \exp(-pT_{FOS}) \cdot S_{NY}(u_{PD})}{\left[p^2 + (1/T_{0EF}) \cdot p + (2\pi f_{0e})^2\right]}$.

Let us remind that we can determine (as we already mentioned in Chap. 3 of this book) the feedback circuits "from the laser optical fiber to its electrical input" and the transfer function of this feedback. The transfer function of the feedback network $K_{FBN} = K_{DL}$ for OEO DM can be defined as: $K_{DL} = K_{FBN} = \frac{i_L}{|E_n|^2} = \frac{i_L}{|E_L|^2}$, where E_L is the normalized strength in the QWLD output, which is equal in magnitude to the value in the FOS input, $i_L = i_m$ is the AC current modulation component in the QWLD in the OEO DM.

Taking into account Eq. (5.4) in the PFB loop, we transfer to determination of symbolic equations for OEO DM.

5.1.3 Symbolic Equations for OEO DM

Let us examine the single-frequency mode of the laser generation and the dynamic single-frequency mode of the radio-frequency generation. Taking into attention Eq. (5.4), the system of differential equations for the strength amplitude E_n of electrical component of the electromagnetic field (outside the optical resonator) of the QWLD output emission and for the instantaneous value of the pumping current i_L is:

$$\begin{cases} \left(p^2+\dfrac{1}{T_{0\mathrm{F}}}p+(2\pi\nu_{0\mathrm{F}})^2\right)\left[p^2+\dfrac{1}{T_2}p+(2\pi\nu_{12})^2\right]E_{\mathrm{n}} \\ =p^2\left[\alpha_{\mathrm{N01}}\cdot J_{1\mathrm{L}}\cdot E_{\mathrm{n}}+\alpha_{00}E_{\mathrm{n}}-\beta_{00}E_{\mathrm{n}}|E_{\mathrm{n}}|^2\right], \\ \left[p^2+(1/T_{\mathrm{eF}})\cdot p+(2\pi f_{0\mathrm{e}})^2\right]i_{\mathrm{L}} \\ =p\cdot\cos\left[\Delta\phi_{\mathrm{OF}}\right]\cdot|E_{\mathrm{n}}|^2(1/T_{\mathrm{eF}})K_{\mathrm{OF}}\cdot K_{\mathrm{PD}}\cdot\exp\left(-pT_{\mathrm{FOS}}\right)\cdot S_{\mathrm{NY}}(u_{\mathrm{PD}}), \end{cases} \tag{5.6}$$

where coefficients α_{00} and β_{00} are (in first approximation): $\alpha_{00}=N_0\frac{2p_{\mathrm{e}}^2}{\varepsilon_0 h}\eta_{00}$; $\beta_{00}=\frac{2p_{\mathrm{e}}^2}{\varepsilon_0 h}N_0G_{0\mathrm{n}}T_1\eta_{00}^2$; where $\eta_{00}=\frac{T_1\exp(-j2\pi\nu_0T_1)}{\sqrt{1+(2\pi\nu_0T_1)^2}}$. Coefficients $\alpha_{00}=\alpha_{0\mathrm{L}}$ and $\beta_{00}=\beta_{0\mathrm{L}}$ in the second approximation (at consideration of nonlinearity approximation with account of the fifth-order polynomial and at calculation of the second partial derivative) are: $\alpha_{0\mathrm{L}}=\frac{6N_0T_1G_{00}}{\left[(2\pi(\nu-\nu_0)T_1)^2+1\right]^2}\sqrt{5}\exp\left[-j\mathrm{Arctan}[2\cdot(2\pi(\nu-\nu_0)T_1\right]$ and $\beta_{0\mathrm{L}}=\frac{20N_0(T_1G_{00})^2}{\left[(2\pi(\nu-\nu_0)T_1)^2+1\right]^3}\sqrt{10}\exp\left[-j\mathrm{Arctan}[3(2\pi(\nu-\nu_0)T_1\right]$.

The system of Eq. (5.6) allows calculation in the specified quasi-stationary mode of the instantaneous values of E_{L}, the amplitude, the frequency, and the phase of laser oscillations, and of OEO DM, and to take into consideration the influence of different parameters in Eq. (5.6) upon the formation of current oscillations of the first harmonic of OEO DM. The specific feature of the equation system (Eq. 5.6) is the fact that these equations are similar in their form to well-studied radio electronics equations for the double-circuit autonomous oscillator (the first equation of the system) with the inertial auto-bias circuit. Nevertheless, the coefficient included in Eq. (5.6) are expressed through the laser variable parameters: the population, the dipole moment, the lifetime on the upper operating level, and the time constant of the laser optical filter.

The equation system (Eq. 5.6) reflects the laser properties as the oscillating system in the operation mode, which is upper than a threshold at modulation of the variable pumping current $i_{\mathrm{L}}=i_{1\mathrm{L}}$. In the left part of Eq. (5.6), there is the operator "conductance." It is defined by laser physical quantities: the transition frequency between the first and second energy levels ν_{12}, the natural frequency of the optical filter included in the laser and this frequency $\nu_{0\mathrm{F}}$ is much more than the time constant of the active medium polarization T_2, the time constant of the optical filter $T_{0\mathrm{F}}$. Oscillations of E_{n} in Eq. (5.6) occur only at the definite threshold pumping value α_{N00}. In the right part of Eq. (5.6), the following expression is located: $S_{\mathrm{L}}=\alpha_{00}E_{\mathrm{n}}-\beta_{00}E_{\mathrm{n}}|E_{\mathrm{n}}|^2$, which defines the laser nonlinearity in the quasi-stationary mode.

We must note that the equation system of OEO DM (Eq. 5.6) may take into consideration the heterodyning. As we discussed in Chap. 3, the heterodyning in OEO is performed by multiplication oscillations with different delays. For this, the multiplier $\cos[\Delta\phi_{\mathrm{OF}}]$ is added to the second equation in Eq. (5.6) into its right part. At that, $\Delta\phi_{\mathrm{OF}}$ is defined by the difference of optical phases of optical calculations, which pass to PD after passing of the optical filter (Fig. 3.1). The contribution into

the phase difference is made not only by the phase-frequency characteristics of the optical filter, but the phase-frequency characteristic of QWLD.

Thus, it is shown that the complicate system from three constitutive equations (Eq. 4.17), considered in Chap. 4, spanned by the positive feedback, is reduced in the quasi-stationary mode to the system of two DEs (Eq. 5.6). It is similar to the equation of double-circuit oscillator with inertial feeding, which was solved many times in the specific tasks of the nonlinear oscillation theory. Specific properties of this Eq. (5.6), which introduce new property, from the point of view of the oscillation theory of RF and optical oscillators, exactly the inertial multiplicative laser nonlinearity. The nonlinear functions are concretized for different pumping schemes, for instance, for three- and four-level systems for laser pumping.

5.1.4 *The Analog Model of DEs for* OEO *DM*

On the base of CE system (Eq. 5.12), the analog model of OEO DM was built, which is presented in Fig. 5.1. The model of OEO DM is constructed using the approach to OEO consideration as the QWLD, which is spanned of the positive feedback as it is shown in Fig. 5.1. "Feedback Chain" in this figure consists of the optical fiber OF, the photodetector PD, the RF filter F, and the RF amplifier.

5.1.5 *Abbreviated Equations of* OEO *DM*

To analyze processes in the optoelectronic oscillator, we must take into consideration that the spectrum of processes is located in the relatively narrow vicinity of the resonance frequency of the RF filter in the linear part of the system. Therefore, the AC current in the input of the RF amplifier (A) (or in the filter (F) input) (Fig. 3.2a) (the active element of the RF circuit) we consider as quasi-harmonic and present in the form: $u_F = U_{10F}\ \mathrm{Re}\ [\exp(2\pi f_0 t)]$, where U_{10F}, Φ_F are the slowly changing amplitude and phase, relatively, $\Delta f = f - f_0$ is the amendment on the oscillating frequency. Then the voltage U_{10F}, is equal to $U_{10F} = U_{10F}\ \mathrm{Re}\ [\exp(2\pi\Delta f \cdot t - \Phi_F)]$.

The voltage U_{10F} (compared to the instantaneous value u_F) has the slowly changing complex amplitude. In OEO DM, the ratio of the frequency amendment to the frequency $\Delta f/f_0 \ll 1$. We use the Evtianov method [1] and apply the bias theorem of the operational calculus and the similar considerations, which were used for the deduction of abbreviated equation of OEO MZ in Chap. 3.

Let us write the second equation of the system (Eq. 5.6) in the form:

$$\left[p^2 + (1/T_{eF})p + (2\pi f_{0e})^2\right] i_L = p\cos[\Delta\phi_{OF}]|E_n|^2(1/T_{eF})K_{OF}K_{PD} \exp(-pT_{FOS})S_{NY}(u_{PD}). \tag{5.7}$$

We introduce the designation $K_{DL} = \cos[\Delta\phi_{OF}](1/T_{eF})K_{OF}K_{PD}$, and divide the numerator and denominator of the left part of the equation by $(2\pi f_{0e})^2$:

$$\frac{\left[(p/2\pi f_{0e})^2 + (1/Q_{EF})(p/2\pi f_{0e}) + 1\right]}{(p/2\pi f_{0e})} i_L = |E_n|^2 K_{DL} \exp(-j2\pi f_{0e}T_{FOS}) \cdot S_{NY}(u_{PD}). \tag{5.8}$$

We choose $2\pi f_{0e}$ as the reference radian frequency. Replacing p by $j2\pi f_{0e} + p_1$, combining terms in groups according to the smallness order, keeping only the first order of smallness terms, we obtain the expression for the abbreviated conductance in the first approximation in the left part of Eq. (5.18) [1]:

$$\frac{\left[(p/2\pi f_{0e})^2 + (1/Q_{EF})(p/2\pi f_{0e}) + 1\right]}{(p/2\pi f_{0e})} \xrightarrow{j2\pi f_{0e}+p_1} \left(\frac{1}{Q_{EF}} + p_1\right), \tag{5.9}$$

where the arrow "$\xrightarrow{j2\pi f_{0e}+p_1}$" designates the representation of the controlling conductance in the abbreviated form. At abbreviation, we expand the current in the right part I_{1A} into in-phase and quadratic components:

$$i_A(u_{PD}) \exp(-j2\pi f_{0e}T_{FOS}) \xrightarrow{j2\pi f_{0e}+p_1} [I_{1A}(U_{PD}) \cos(2\pi f_{0e}T_{FOS}) + jI_{1A}(U_{PD}) \sin(2\pi f_{0e}T_{FOS})]. \tag{5.10}$$

Now we write the abbreviated equation for the current J_{10L} (where J_{10L} is the slowly changing amplitude of the first harmonic of the pumping current oscillations i_L) of the first approximation, taking into account R_L, which is the resistance of the electrical input of the laser:

$$\left(\frac{1}{Q_{EF}} + 2p_1\right) \exp[j\Phi_1] \cdot J_{1L} = \frac{K_{0DL}}{R_L Q_{EF}} \{I_{1A} \cos[2\pi f_{0e}T_{FOS}] + jI_{1A} \sin[2\pi f_{0e}T_{FOS}]\} \exp[j\Phi_1]. \tag{5.11}$$

We act in the similar manner as we acted in Sect. 2.4.3 (Chap. 3). For the first equation of the system (Eq. 5.6), we shall obtain the abbreviated equations for slowly changing amplitude E_{10L} and the phase Φ_{1L}, taking into account that $K_{0L} \cdot N_0(J_{1L}) = \alpha_{00} \cdot J_{0L} + \alpha_{N01} \cdot J_{1L}$, R_L is the input resistance of the laser, and

$J_{0L} = I_{0L}$ is the DC pumping current. Such abbreviated equation has the following form:

$$\frac{dE_{10L}}{dt} = 2\pi\nu_{0F} \cdot \frac{K_{0L} \cdot N_0}{Q_{12} + Q_{0F}} \frac{d^2}{dE_{10L}^2} [S_{LCOS}(E_{10L})] - 2\pi\nu_{0F} \cdot \frac{E_{10L}}{Q_{12} + Q_{0F}}, \quad (5.12)$$

$$E_{10L} \frac{d\Phi_{1L}}{dt} = -2\pi\nu_{0F} \cdot \frac{K_{0L} N_0}{Q_{12} Q_{0F}} \frac{d^2}{dE_{10L}^2} [S_{LSIn}(E_{10L})], \quad (5.13)$$

where nonlinear functions $S_{LCOS}(E_{10L})$ and $S_{LSIN}(E_{10L})$ have the form as in Chap. 4: $S_{LCOS}(E_{10L}) = \frac{E_{10L}\left[1+T_{1n}G_{00}E_{0n}^2\right]}{\left[\left(1+T_{1n}G_{00}E_{0n}^2\right)^2+(2\pi(\nu-\nu_{0F})T_{1n})^2\right]}$ and $S_{LSIN}(E_{10L}) = \frac{E_{10L}[2\pi(\nu-\nu_{0F})T_{1n}]}{\left[\left(1+T_{1n}G_{00}E_{0n}^2\right)^2+(2\pi(\nu-\nu_{0F})T_{1n})^2\right]}$.

Now we take into consideration that in our structural diagram the feedback coefficient k_{fb} is the transfer function of RF FODL, i.e., $K_{RFFODL} = U_{PD}/U_L$. But the transfer function of the feedback network $K_{FBN} = K_{DL}$ for OEO DM can be defined as, $K_{DL} = K_{FBN} = \frac{i_L}{|E_n|^2} = \frac{i_L}{|E_L|^2}$, where E_L is the normalized strength in the QWLD output, which is equal in magnitude to the value in the FOS input, $i_L = i_m$ is the AC current modulation component in the QWLD in the OEO DM.

For simplicity, we assume that the module of the RF FODL transfer function is constant and equal to K_{0FODL}, and then $K_{0FODL} = E_{0L}^2 K_{FODL}$.

Taking into consideration Eqs. (5.11)–(5.13), we write the complete system of abbreviated equations for OEO DM:

$$\begin{cases} \frac{dE_{10L}}{dt} = 2\pi\nu_{0F} \frac{K_{0L} N_0(J_{10L})}{Q_{12} + Q_{0F}} S_{LCOS}(E_{10L}) - 2\pi\nu_{0F} \cdot \frac{E_{10L}}{Q_{12} + Q_{0F}}, \\ E_{10L} \frac{d\Phi_{1L}}{dt} = -2\pi\nu_{0F} \frac{K_{0L} N_0(J_{10L})}{Q_{12} Q_{0F}} S_{LSIN}(E_{10L}), \\ \frac{dJ_{1L}}{dt} = 2\pi f_{0e} \frac{E_{10L}^2 K_{FOLD}}{2R_L Q_{EF}} I_{1A}(E_{10L}) \cos[2\pi f_{0e} T_{FOS}] - 2\pi f_{0e} \frac{J_{1L}}{2Q_{EF}}, \\ \frac{d\Phi_{10E}}{dt} = 2\pi f_{0e} \frac{E_{10L}^2 K_{FOLD}}{2Q_{EF}} I_{1A}(E_{10L}) \sin(2\pi f_{0e} T_{FOS}). \end{cases} \quad (5.14)$$

We obtain the system of abbreviated equations (Eq. 5.14), owing to which we can investigate transient and steady-state processes in OEO DM. The analysis of these equations is much simpler than the symbolic equation. The AC component of the laser pumping current (or the current first harmonic in the laser input) J_{1L} influences on the population $N_0(J_{1L})$, which determines solutions for the amplitude E_{10L} and phase Φ_{1L} of the laser field strength in the first and second equations. The laser power (or the square of the normalized amplitude) E_{10L}^2 is included in the third and fourth equations of the system (Eq. 5.14) and, relatively, determines its solutions for J_{1L} and the phase Φ_{10E}. The peculiarity of this self-oscillating system is the presence of the laser nonlinearities $S_{LCOS}(E_{10L})$, $S_{LSIN}(E_{10L})$ and the RF amplifier nonlinearity $I_{1A}(U_{PD})$. In OEO DM, the presence of mentioned nonlinearities complicates the

dynamics of oscillation processes. A choice of optimal type of the nonlinear function $I_{1A}(U_{PD})$ for realization of the "soft" self-excitation mode, for instance, as the polynomial of third and fifth order, becomes more complicate. This is caused by the fact that this choice must be connected with the linear-hyperbolic (in algebraic form) multiplicative (in the physical basis as the product of the field strength and the population) nonlinearity of the laser.

Another feature is the fact that the equations system unifies motions for the laser EMF in the optical range and electrical oscillations existing in the RF circuit of the positive feedback in the radio-frequency range.

Taking into account equations for oscillations phase Φ_{1L} of the laser electromagnetic field and phase Φ_{10E} of the electrical oscillations of the pumping current, the two modes exist: the in-phase mode and the mode of beats. With the growth of radio frequency, theoretically, there is a possibility of the optical oscillations synchronization by the electrical oscillations. In this case, the full phase incursion of optical and electrical oscillations in the closed loop in OEO DM must be multiple of 2π only for "electrical oscillations" (with account that the laser emission is modulated with the radio frequency) in the closed loop of OEO DM.

Steady-state laser modes in OEO DM will be discussed in Chaps. 6 and 7.

We should note that the system (Eq. 5.14) is obtained for the quasi-stationary (QS) operation mode of the laser, i.e., for values of DC pumping, which is higher than the threshold level. Owing to nonlinear functions $S_{LCOS}(E_{10L})$ and $S_{LSIN}(E_{10L})$, this system (Eq. 5.14) takes into consideration the inertia properties of the laser pumping, which is determined by the lifetime T_{1n} on the upper operation level. But the system (Eq. 5.14) have no separate differential equation for population. In this, there are significant restrictions of utilization of Eq. (5.14) for the quasi-stationary mode for investigation, for example, the transients.

Before the deduction of abbreviated equations with fluctuations, which is one of the main tasks of Chap. 5, we consider features of the abbreviated equation of OEO DM taking into account the equation for population $N(t) = N_{0L}(t)$.

5.1.5.1 Symbolic and Abbreviated Equations of OEO DM with Account of the Population Equation

We performed the system abbreviation process of initial constitutive equation (Eq. 4.17) according the Evtianov method [1], as for Eq. (5.14), which was discussed in Chap. 3. At that, we took into consideration the equation for population $N(t) = N_{0L}(t)$ in the complete form and differential equations (Eqs. 5.4 and 5.5) for the circuit of the positive feedback (Fig. 5.1a). We took the approximation of functions $S_{LCOS}(E_{10L})$ and $S_{LSIn}(E_{10L})$ included in Eq. (5.14) with the help of the third-order polynomials as it was performed in Chap. 3. For slowly changing time-functions E_{0n}, Φ_{10L}, Φ_{10J}, and the population $N(t) = N_{0L}(t)$, we present the system of abbreviated equations deduced from the considered differential equations for the laser and the positive feedback circuit of OEO DM (Fig. 2.2):

$$\begin{cases} \mathrm{d}E_{10\mathrm{L}}^2/\mathrm{d}t = G_0 E_{10\mathrm{L}}^2 N_{0\mathrm{L}} - E_{10\mathrm{L}}^2/T_{0\mathrm{F}}, \\ \mathrm{d}N_{0\mathrm{L}}/\mathrm{d}t = \alpha_{00}\cdot J_{0\mathrm{L}} + \alpha_{\mathrm{N}01}\cdot J_{1\mathrm{L}} - \dfrac{N_{0\mathrm{L}}}{T_{1\mathrm{L}}} - G_0 N_{0\mathrm{L}} E_{10\mathrm{L}}^2, \\ \mathrm{d}\Phi_{10\mathrm{L}}/\mathrm{d}t = 2\cdot\pi\cdot\nu_{0\mathrm{P}}(N_{0\mathrm{L}}) - 2\pi\nu_0 + \sigma_{0\mathrm{L}} - \rho_{0\mathrm{L}}\cdot E_{10\mathrm{L}}^2, \\ \dfrac{\mathrm{d}J_{10\mathrm{L}}}{\mathrm{d}t} = 2\pi f_{0\mathrm{e}} \dfrac{E_{10\mathrm{L}}^2 K_{\mathrm{DL}}}{2R_{\mathrm{L}} Q_{\mathrm{EF}}} I_{1\mathrm{A}}\left(U_{\mathrm{PD}}, E_{10\mathrm{L}}^2\right)\cos[2\pi f_{0\mathrm{e}} T_{\mathrm{FOS}}] - 2\pi f_{0\mathrm{e}}\cdot\dfrac{J_{10\mathrm{L}}}{2Q_{\mathrm{EF}}}, \\ \dfrac{\mathrm{d}\Phi_{10\mathrm{J}}}{\mathrm{d}t} = 2\pi f_{0\mathrm{e}} \dfrac{E_{10\mathrm{L}}^2 K_{\mathrm{DL}}}{2Q_{\mathrm{EF}}} I_{1\mathrm{A}}\left(U_{\mathrm{PD}}, E_{10\mathrm{L}}^2\right)\sin[2\pi f_{0\mathrm{e}} T_{\mathrm{FOS}}]), \end{cases} \tag{5.15}$$

where the coefficient K_{DL} is $K_{\mathrm{DL}} = \cos[\Delta\phi_{\mathrm{OF}}](1/T_{\mathrm{eF}})K_{\mathrm{OF}}K_{\mathrm{PD}}$.

The transfer function of the feedback network $K_{\mathrm{FBN}} = K_{\mathrm{DL}}$ for OEO DM can be defined as $K_{\mathrm{DL}} = K_{\mathrm{FBN}} = \frac{i_{\mathrm{L}}}{|E_{\mathrm{n}}|^2} = \frac{i_{\mathrm{L}}}{|E_{\mathrm{L}}|^2}$, where E_{L} is the normalized strength in the QWLD output, which is equal in magnitude to the value in the FOS input, $i_{\mathrm{L}} = i_{\mathrm{m}}$ is the AC current modulation component in the QWLD in the OEO DM.

The presented system of abbreviated equations (Eq. 5.15) from five equations gives a possibility to obtain the steady-state quantities of $E_{10\mathrm{L}}^2$, $N_{0\mathrm{L}}$, $\Phi_{10\mathrm{L}}$, $J_{10\mathrm{L}}$, $\Phi_{10\mathrm{J}}$, as well as the frequency deviations of the laser optical emission and the OEO radio frequency from their reference values. The system (Eq. 5.15) gives a possibility to investigate the dynamics of the transients in OEO DM. The second equation for the population $N_{0\mathrm{L}}$ in the system (Eq. 5.26) complicates the analysis but takes into account the generation development more accurately.

The analog model of QWLD, which is obtained on the base of abbreviated equations deduced in this section, is presented in Fig. 2.2. The pumping block is modeled by the circuit, as shown in Fig. 2.2.

The description of the main components of the analog model (Fig. 2.2) is presented in Chap. 3. We remind that the laser model consists of two closed loops, in one of which the oscillations of the strength E_{n} and the polarization P_{n} are circulated, while in the other loop, the population is circulated. The analog laser model reflects the functional connection of the laser model parameters. The model gives understanding how the oscillation amplitude establishes and how the time constants $T_{0\mathrm{F}}$, T_2, T_1 differences between frequencies $\nu_{0\mathrm{n}}$ and ν_{12}, and also the Q-factor of the RF filter Q_{EF} and its natural frequency $f_{\mathrm{F0}} = f_{0\mathrm{e}}$ affect laser dynamics.

Now we transfer to the stability analysis of OEO oscillating system and investigate the self-excitation conditions and existence conditions in OEO DM.

5.2 Stability Conditions: Self-Excitation and Oscillation Existence Conditions in OEO DM

For stability analysis of differential equations system, we consider oscillations of E_{n} and i_{L} with average frequencies ν_0 and f_0. As initial, we take the system of differential equations of OEO DM for the strength amplitude square E_{n}^2 of the

electrical component of EMF with the amplitude of the first harmonic E_{10L} of $E_n = E_{10L}$ Re [exp($2\pi\nu_0 t$)] and the AC electrical component $i_L = J_{10L}$ Re [exp ($2\pi f_0 t$)] with the amplitude of the first harmonic of the laser pumping current $J_{1L} = J_{10L}$.

We write the laser abbreviated equation taking into account the population equation for slowly changing functions E_{0n}, φ, the population difference $N(t)$, and we present the types of abbreviated equations, which are deduced from the considered differential equation for the laser:

$$\begin{cases} dE_{0L}^2/dt = G_0 E_{0L}^2 N_{0L} - E_{0L}^2/T_{0F}, \\ dN_{0L}/dt = \alpha_{N00} \cdot J_{0L} + \alpha_{N01} \cdot J_{1L} - \dfrac{N_{0L}}{T_1} - G_0 N_{0L} E_{0L}^2, \\ d\varphi/dt = 2\pi\nu_{0P}(N_{0L}) - 2\pi\nu_0 + \sigma_{0L} + \rho_{0L} E_{0L}^2. \end{cases} \tag{5.16}$$

We must add this system by differential equations for the circuit of the positive feedback.

5.2.1 The Circuit of the Positive Feedback Spanned the Laser: Differential Equations of OEO

The circuit of the positive feedback covered of QWLD consists of series-connected the fiber-optical system (FOS), which includes optical filters, optical amplifiers, and optical modulators; the photodetector (FD), the nonlinear RF amplifier, the RF filter with the natural frequency, and the coupler. The transfer function K_{FB} of the "Feedback Chain" circuit (Fig. 5.1a) can be defined as for OEO DM: $K_{DL} = K_{FB} = \frac{i_{1L}}{E_n^2} = \frac{J_{1L}}{E_n^2}$, where $E_n = E_L$ is the normalized strength in the QWLD output, which is equal to the value of the FOS input, $i_{1L} = i_m$ is the AC current component in the QWLD input in the structure of OEO DM and u_m is the AC component of the voltage in MZ input in the structure of OEO MZ. Now we have the following symbolic equation:

$$J_{1L} = \frac{[\cos(\Delta\phi_{OF})]|E_n|^2 (1/T_{EF}) K_{OF} K_{PD} p \exp(-pT_{DL}) S_{NY}(J_{1L})}{\left[p^2 + (1/T_{EF})p + (2\pi f_{0e})^2\right]}. \tag{5.17}$$

Taking into consideration the circuit of positive FB, we transfer to equation system in the time domain for OEO DM:

$$\begin{cases} \mathrm{d}E_{0\mathrm{L}}^2/\mathrm{d}t = G_0 \cdot E_{0\mathrm{L}}^2 \cdot N_{\mathrm{L}} - E_{0\mathrm{L}}^2/T_{0\mathrm{F}}, \\ \mathrm{d}N_{\mathrm{L}}/\mathrm{d}t = \alpha_{\mathrm{N}00} \cdot J_{0\mathrm{L}} + \alpha_{\mathrm{N}01} \cdot J_{1\mathrm{L}} - \dfrac{N_{0\mathrm{L}}}{T_1} - G_0 N_{\mathrm{L}} E_{0\mathrm{L}}^2, \\ \mathrm{d}\varphi/\mathrm{d}t = 2\pi\nu_{0\mathrm{P}}(N_{\mathrm{L}}) - 2\pi\nu_0 + \sigma_{0\mathrm{L}} + \rho_{0\mathrm{L}} E_{0\mathrm{L}}^2, \\ \dfrac{\mathrm{d}^2 J_{1\mathrm{L}}}{\mathrm{d}t^2} + \dfrac{1}{T_{\mathrm{F}}}\dfrac{\mathrm{d}J_{1\mathrm{L}}}{\mathrm{d}t} + (2\pi f_{\mathrm{eF}0})^2 J_{1\mathrm{L}} = S_{\mathrm{NY}}\left[E_{0\mathrm{L}}^2 K_{\mathrm{FOS}} K_{\mathrm{PD}}, J_{1\mathrm{L}}(t - T_{\mathrm{DL}})\right]\dfrac{\mathrm{d}J_{1\mathrm{L}}(t - T_{\mathrm{DL}})}{\mathrm{d}t}, \end{cases} \tag{5.18}$$

where the transfer function $K_{\mathrm{DL}} = K_{\mathrm{FOS}} K_{\mathrm{PD}}$, K_{FOS} is the transfer function of FOS, which contains the optical fiber of two fibers of different length, K_{PD} is the transfer function of the photodetector, which were defined in Chap. 2.

Now we present for comparison similar to Eq. (5.18) system from four time-equation for OEO MZ with QWLD:

$$\begin{cases} \mathrm{d}E_{0\mathrm{L}}^2/\mathrm{d}t = G_0 E_{0\mathrm{L}}^2 N_{\mathrm{L}} - E_{0\mathrm{L}}^2/T_{0\mathrm{F}}, \\ \mathrm{d}N_{\mathrm{L}}/\mathrm{d}t = \alpha_{\mathrm{N}00} \cdot J_{0\mathrm{L}} - \dfrac{N_{\mathrm{L}}}{T_{1\mathrm{L}}} - G_0 N_{\mathrm{L}} E_{0\mathrm{L}}^2, \\ \mathrm{d}\varphi/\mathrm{d}t = 2\pi\nu_{0\mathrm{P}}(N_{\mathrm{L}}) - 2\pi\nu_0 + \sigma_{0\mathrm{L}} + \rho_{0\mathrm{L}} E_{0\mathrm{L}}^2, \\ \dfrac{\mathrm{d}^2 U}{\mathrm{d}t^2} + \dfrac{1}{T_{\mathrm{F}}}\dfrac{\mathrm{d}U}{\mathrm{d}t} + (2\pi f_{\mathrm{eF}0})^2 U = S_{\mathrm{NY}}[E_{0\mathrm{L}}^2 K_{\mathrm{MZ}} K_{\mathrm{FOS}} K_{\mathrm{PD}} \cdot U(t - T_{\mathrm{FODL}})]\dfrac{\mathrm{d}U(t - T_{\mathrm{FODL}})}{\mathrm{d}t}. \end{cases} \tag{5.19}$$

5.2.1.1 The Symbolic Form of the Equation System of OEO DM and OEO MZ

Now we introduce the Laplace operator $p = \frac{\mathrm{d}}{\mathrm{d}t}$ in Eq. (5.19) and obtain the system of three symbolic equations for OEO DM with QWLD:

$$\begin{cases} pE_{0\mathrm{L}}^2 = G_0 E_{0\mathrm{L}}^2 N_{0\mathrm{L}} - E_{0\mathrm{L}}^2/T_{0\mathrm{F}}, \\ pN_{\mathrm{L}} = \alpha_{\mathrm{N}00} \cdot J_{0\mathrm{L}} + \alpha_{\mathrm{N}01} \cdot J_{1\mathrm{L}} - (1/T_1) N_{\mathrm{L}} - G_0 N_{\mathrm{L}} E_{0\mathrm{L}}^2, \\ \left[p^2 + \dfrac{1}{T_{\mathrm{F}}} p + 2\pi(\, f_{\mathrm{eF}0} \pm \nu_{0\mathrm{F}})^2\right] J_{1\mathrm{L}} = p S_{\mathrm{NY}}\left[E_{0\mathrm{L}}^2 K_{\mathrm{FOS}} K_{\mathrm{PD}} J_{1\mathrm{L}}\right]. \end{cases} \tag{5.20}$$

Below we present for comparison the similar to Eq. (5.20) system of three symbolic equations for OEO MZ with QWLD:

$$\begin{cases} pE_{0L}^2 = G_0 E_{0L}^2 N_{0L} - E_{0L}^2/T_{0F}, \\ pN_{0L} = \alpha_{N0}(J_{0N} + J_{10}) - (1/T_1)N - G_{00}N_{0L}E_{0L}^2, \\ \left[p^2 + \frac{1}{T_F}p + 2\pi(f_{eF0} \pm \nu_{0F})^2\right] U = pS_{NY}\left[E_{0L}^2 K_{MZ} K_{FOS} K_{PD} U\right]. \end{cases}, \quad (5.21)$$

The main difference of OEO MZ system (Eq. 5.21) from the OEO DM (Eq. 5.20) system is the full independence of the third equation with regard to the first and second. At the opened FB loop in OEO, i.e., at $J_{10} = 0$, two first symbolic equations of the system describe the QWLD without modulation of the optical emission by the AC component of the pumping current and at DC independent pumping current J_{0N}.

5.2.1.2 Self-Excitation Conditions of OEO DM

Let us analyze the self-excitation conditions for the OEO DM model (Fig. 5.1a). For this, we add the system of symbolic equations (Eq. 3.28) for the strength E_n of QWLD, which are considered in Chap. 3, by the differential equation for the circuit of the positive FB. We use the system of symbolic equations (Eq. 3.28) of QWLD examining the laser operation not only in the quasi-stationary (QS) mode but also in the small-signal mode. We would like to remind that in Chap. 3, the QS mode we referred the laser operation mode at pumping currents, which are much more than the threshold mode.

Let us consider the laser oscillating process in the vicinity of the optical resonator frequency $\nu_{0n} = \nu_{0F}$ in the point of the steady-state mode with values of the strength E_{n0} and the population N_{00}. Now we define the stability of the steady-state modes E_{0L}^2, N and J_{0L} with regard to small deviations e_L^2, n_L and i_{mL} of variables from the appropriate steady-state values E_{00L}^2, N_{00}, and J_{0L} (the Lyapunov stability). Let it be for the ***small deviations*** from these steady-state values: $E_{0L}^2 = E_{00L}^2 + e_L^2$ and $N = N_{00} + n_L$, $i_L = J_{00L} + i_{mmL}$.

Now we substitute E_{0L}^2, N, and i_L in the last expression (Eq. 5.21) of the system under investigation and neglect by the terms containing the product $e_L^2 \cdot n_L$ due to its smallness. In this case, the linearization on the equations system is achieved. As a result, instead of the initial system, we obtain the system of the first approximation formed by three symbolic equations for variables e_L^2, n_L, and i_{mmL}:

$$\begin{cases} pe_L^2 = G_0(N_{00}e_L^2 + n_L E_{0L}^2) - e_L^2/T_{0F}, \\ pn_L = \alpha_{N0} i_{mmL} - (1/T_1)n_L - G_0(N_{00}e_L^2 + n_L E_{n0}^2), \\ [p^2 + \frac{1}{T_F}p + (2\pi(f_{eF0} \pm \nu_{0F})^2] i_{mmL} = p|E_{10L}|^2 K_{0DL} S_{NY0}(e_L^2). \end{cases} \quad (5.22)$$

We introduce the designation $Q_{00E} = p^2 + \frac{1}{T_F}p + 2\pi(f_{eF0} \pm \nu_{0F})^2$. Now we may express n_L from the second equation of the system: $n_L = \frac{\alpha_{N0} i_{mmL} - G_0 N_{00} e_L^2}{p + (1/T_1) + E_{n0}^2}$.

We substitute n_L in the first equation of Eq. (5.22). Then we obtain the system of two symbolic equations of:

$$\begin{cases} (p + 1/T_{0F} - G_0 N_{00})\left(p + (1/T_1) + E_{n0}^2\right) e_L^2 = G_0 E_{0L}^2 \left(\alpha_{N0} i_{mmL} - G_0 N_{00} e_L^2\right), \\ Q_{00E} i_{mmL} = p|E_{10L}|^2 K_{0DL} S_{NY0}\left(e_L^2\right). \end{cases} \tag{5.23}$$

Now we take into consideration that:

$$\begin{aligned} &(p + 1/T_{0F} - G_0 N_{00})\left(p + (1/T_1) + E_{n0}^2\right) \\ &= p^2 + \left[(1/T_{0F}) + (1/T_1) + E_{n0}^2 - G_0 N_{00}\right] p + (1/T_{0F} - G_0 N_{00})\left[(1/T_1) + E_{n0}^2\right]. \end{aligned} \tag{5.24}$$

We introduce designations: $\omega_{0L}^2 = [(1/T_{0F}) - G_0 N_{00}]\left[(1/T_1) + E_{n0}^2\right]$, and $\alpha_P = (1/T_{0F}) + (1/T_1) + E_{0L}^2 - G_0 N_{00}$, $\omega_{0e}^2 = [2\pi(\, f_{eF0} \pm \nu_{0F})]^2$.

Then Eq. (5.23) can be written as:

$$\begin{cases} \left[p^2 + \alpha_P p + \omega_{0L}^2\right] e_L^2 = G_0 E_{0L}^2 \alpha_{N0} i_{mmL} - G_0^2 E_{0L}^2 N_{00} e_L^2, \\ i_{mmL} = [Q_{00E}]^{-1} p E_{0L}^2 K_{0DL} S_{NY0}\left(e_L^2\right). \end{cases} \tag{5.25}$$

Substituting i_{mL} into the first equation of Eq. (5.25), we obtain for the variable e_L^2, which has a sense of the AC component of the laser optical emission intensity, the OEO symbolic equation of fourth order in the small-signal mode:

$$\begin{aligned} &\left(p^2 + \alpha_P p + \omega_{0L}^2\right)\left(p^2 + \frac{1}{T_{eF}} p + \omega_{0e}^2\right) e_L^2 \\ &= p^2 \alpha_{N0} G_0 E_{0L}^4 K_{0DL} S_{NY0}\left(e_L^2\right) - Q_{00E} G_0^2 E_{0L}^2 N_{00} e_L^2. \end{aligned} \tag{5.26}$$

Finally, we obtain the symbolic equation of OEO DM, which coincides in mathematical notation with the equation for the tube or transistor autonomous oscillator with two resonators (with different and not-multiple natural frequencies) located in the feedback circuit .

The left part of the obtained equation (Eq. 5.26) is the oscillating characteristic. It consists of two multipliers, each of which can be called the operator conductance. Here ω_{0e}^2 and ω_{0L}^2 are the natural resonance frequencies, relatively, in the RF filter and in QWLD. The ω_{0L}^2 frequency is determined by laser parameters and depends on the DC pumping level. The second frequency ω_{0e}^2 is the natural frequency of the RF resonator. It is desirable to note that the damping decrement α_P, which is $\alpha_P = [(1/T_{0F}) + (1/T_1) - G_0 N_{00}]$, depends on the level of the inversed population N_{00} and the lifetime T_1 and T_{0F}. In the right part of Eq. (5.26), the first term reflects the action of the nonlinear RF amplifier (A), the circuit of positive FB consisting of

the optical fiber and the photodetector. The first term can be added by a multiplier, which takes into account the delay in the optical fiber. The second term in the right part of Eq. (5.26) takes into consideration the action of the multiplicative nonlinearity of the laser. By analogy with autonomous oscillators on transistors, the second term of the right part of Eq. (5.26) reflects the gain of the base current in the transistor connected with the common emitter circuit of the grid current (in tube oscillator). At examination of stability problems, we can neglect by this term due to its smallness, which is similar to the tube or transistor oscillator at discussing of stability problems for the influence of grid or based current.

We introduce designations $\delta_{\mathrm{L}} = \alpha_{\mathrm{P}}$, $\delta_{\mathrm{e}} = 1/T_{\mathrm{eF}}$, then the last considered differential equation can be written as:

$$\begin{aligned}&\left\{p^4 + p^3(\delta_{\mathrm{e}} + \delta_{\mathrm{L}}) + p^2\left(\omega_{0\mathrm{e}}^2 + \omega_{0\mathrm{L}}^2 + \delta_{\mathrm{e}}\delta_{\mathrm{L}}\right) + \left(\omega_{0\mathrm{L}}^2\delta_{\mathrm{e}} + \omega_{0\mathrm{e}}^2\delta_{\mathrm{L}}\right)p + \omega_{0\mathrm{L}}^2\omega_{0\mathrm{e}}^2\right\}e_{\mathrm{L}} \\ &= p^2\alpha_{\mathrm{N0}}G_0E_{0\mathrm{L}}^4K_{0\mathrm{DL}}S_{\mathrm{NY00}}\left(e_{\mathrm{L}}^2\right).\end{aligned} \tag{5.27}$$

For convenience of estimation of stability conditions, we introduce the operator $p_{00} = p/\omega_{0\mathrm{e}}$ and we take into account that the natural frequency detuning of $\omega_{0\mathrm{e}}$ and $\omega_{0\mathrm{L}}$ is: $\beta_{0\mathrm{L}} = \left(\omega_{0\mathrm{L}}^2 - \omega_{0\mathrm{e}}^2\right)/\omega_{0\mathrm{e}}^2$. We introduce Q-factors $Q_{0\mathrm{L}} = \omega_{0\mathrm{L}}/\alpha_{\mathrm{P}}$ and $Q_{0\mathrm{EF}} = \omega_{0\mathrm{e}}T_{\mathrm{eF}}$, then the normalized differential equations of OEO DM take the following form:

$$\begin{aligned}&\left[p_{00}^4 + \left(\frac{1}{Q_{0\mathrm{EF}}} + \frac{1}{Q_{0\mathrm{L}}}\right)p_{00}^3 + \left(2 + \beta_{0\mathrm{L}} + \frac{1}{Q_{0\mathrm{EF}}Q_{0\mathrm{L}}}\right)p_{00}^2 + \left(\frac{1+\beta_{0\mathrm{L}}}{Q_{0\mathrm{EF}}} + \frac{1}{Q_{0\mathrm{L}}}\right)p_{00} + 1 + \beta_{0\mathrm{L}}\right]\cdot \\ &e_{\mathrm{L}}^2 = p_{00}^2\alpha_{\mathrm{N0}}G_0E_{0\mathrm{L}}^4K_{0\mathrm{FODL}}S_{\mathrm{NY00}}\left(e_{\mathrm{L}}^2\right)\exp\left(-j2\pi T_{\mathrm{FOLD}}\cdot f_{0\mathrm{e}}\right).\end{aligned} \tag{5.28}$$

5.2.1.3 The Rauth–Gurvitz Stability Conditions for the Steady-State Mode Without Account of Inertia Properties

At first, we investigate the differential equation of OEO DM (Eq. 5.28) on stability in the steady-state points for appropriate stationary values of $E_{00\mathrm{L}}^2$, N_{00}, and $J_{0\mathrm{L}}$ at $e_{\mathrm{L}}^2 = 0$ without account of inertia properties. For this, we take the nonlinear function $S_{\mathrm{NY00}}\left(e_{\mathrm{L}}^2\right)\exp\left(-jT_{\mathrm{DL}}\cdot f_{0\mathrm{e}}\right)$ equal to the average slope S_{NY00}. Such a representation is true at small values of $T_{\mathrm{DL}}\cdot f_{0\mathrm{e}}$. Since the feedback circuit width is narrow, in the spectrum of e_{L}^2, it is enough to take into consideration only first harmonics. To estimate the excitation conditions, we present the nonlinearity $S_{\mathrm{NY0}}\left(e_{\mathrm{L}}^2\right)$ in the form $S_{\mathrm{NY00}}\left(e_{\mathrm{L}}^2\right) \approx \mathrm{d}S_{\mathrm{NY0}}/\mathrm{d}e_{\mathrm{L}}$, which has a sense of the average slope of the nonlinear dependence of the RF amplifier AE in the point of the steady-state mode.

Let us consider the characteristic equation for the fourth-order differential equation describing the dynamic system: $a_0\lambda^4 + a_1\lambda^3 + a_2\lambda^2 + a_3\lambda^1 + a_4 = 0$, where coefficients $a_0 = 1, a_1 = \left(\frac{1}{Q_{0EF}} + \frac{1}{Q_{0L}}\right), a_2 = \left(2 + \beta_{0L} + \frac{1}{Q_{0EF}} \cdot \frac{1}{Q_{0L}} - \alpha_{N0} G_0 E_{0L}^4 K_{0FODL} S_{NY00}\right)$, and also $a_3 = \left(\frac{1+\beta_{0L}}{Q_{0EF}} + \frac{1}{Q_{0L}}\right), a_4 = 1 + \beta_{0L}$.

We form the Gurvitz matrix

$$\begin{pmatrix} a_1 & a_0 & 0 & 0 \\ a_3 & a_2 & a_1 & a_0 \\ 0 & a_4 & a_3 & a_2 \\ 0 & 0 & 0 & 0 \end{pmatrix} = \begin{pmatrix} \left(\frac{1}{Q_{0EF}} + \frac{1}{Q_{0L}}\right) & 1 & 0 & 0 \\ \left(\frac{1+\beta_{0L}}{Q_{0EF}} + \frac{1}{Q_{0L}}\right) & a_2 & \left(\frac{1}{Q_{0EF}} + \frac{1}{Q_{0L}}\right) & 1 \\ 0 & 1+\beta_{0L} & \left(\frac{1+\beta_{0L}}{Q_{0EF}} + \frac{1}{Q_{0L}}\right) & a_2 \\ 0 & 0 & 0 & 0 \end{pmatrix}. \tag{5.29}$$

The Rauth–Gurvitz stability conditions can be written for the steady-state mode in the point $e_L^2 = 0$ for the differential equation (Eq. 5.28):

$$a_i > 0 (i = 0, \ldots, 4), \qquad \Delta_2 = \begin{vmatrix} a_1 & a_0 \\ a_3 & a_2 \end{vmatrix} = a_1 a_2 - a_0 a_3 > 0,$$
$$\Delta_3 = \begin{vmatrix} a_1 & a_0 & 0 \\ a_3 & a_2 & a_1 \\ 0 & a_4 & a_3 \end{vmatrix} = a_1 a_2 a_3 - a_1^2 a_4 - a_0 a_3^2 > 0, \qquad \Delta_4 = a_4 > 0. \tag{5.30}$$

Now we write the inequality system following from *stability conditions*. The system of two inequalities describing the stability region, in which oscillation will not be excited, will be: $\left(2 + \beta_{0L} + \frac{1}{Q_{0EF}} \frac{1}{Q_{0L}}\right) > \alpha_{N0} G_0 E_{0L}^4 K_{0DL} S_{NY00}$.

It follows from Eq. (5.30) that *self-excitation conditions* of OEO DM take the form of the two inequality system: $\alpha_{N0} G_0 E_{0L}^4 K_{0DL} S_{NY00} > \left(2 + \beta_{0L} + \frac{1}{Q_{0EF}} \cdot \frac{1}{Q_{0L}}\right)$,

$$\alpha_{N0} G_0 E_{0L}^4 K_{0FODL} S_{NY00} > 2 + \beta_{0L} + \frac{1}{Q_{0EF}} \cdot \frac{1}{Q_{0L}} - \left(\frac{1}{Q_{0EF}} + \frac{1}{Q_{0L}}\right)(1 + \beta_{0L})^2. \tag{5.31}$$

The analysis of mentioned inequalities shows that the sufficient condition of the *self-excitation* of OEO DM is the single second inequality (Eq. 5.31).

The self-excitation condition (Eq. 5.31) has the clear physical sense: the equivalent gain in the feedback loop of OEO $\alpha_{N0}G_0E_{0L}^4K_{0DL}$ multiplied by the average slope of the RF amplifier S_{NY00} should exceed losses in the resonator of the RF amplifier $\frac{1}{Q_{0EF}}$ and the reduced losses in the optical resonator of the laser $\frac{1}{Q_{0L}}$. The slope of the nonlinear dependence should be more than zero: $S_{NY00}\left(e_L^2=0\right)>0$, and the detuning of the natural frequencies $\beta_{0L}=\left(\omega_{0L}^2-\omega_{0e}^2\right)/\omega_{0e}^2$ introduces in the OEO self-excitation conditions of small correction: the increase of β_{0L} leads to the growth of the excitation threshold of OEO.

We should note that in the case, if the right part of DE (Eq. 5.28), i.e., the operator controlling transfer function, contains the operator in the first order p_{00} or the third order p_{00}^3, the self-excitation conditions take the form, which is traditional for RF oscillators: $\alpha_{N0}G_0E_{0L}^4K_{0DL}S_{NY00}>\frac{1}{Q_{0EF}}+\frac{1}{Q_{0L}}$,$\alpha_{N0}G_0E_{0L}^4K_{0DL}S_{NY00}>\frac{1+\beta_{0L}}{Q_{0EF}}+\frac{1}{Q_{0L}}$. These conditions take a form: $Q_{0EF}>Q_{0L}$:$Q_{0L}\alpha_{N0}G_0E_{0L}^4K_{0DL}S_{NY00}>1$.

The last inequality can be treated by analogy with the well-known (from the oscillation theory) self-excitation condition of RF oscillator as: $S\cdot R_{cont}>1$.

In $S\cdot R_{cont}>1$, the slope S of the nonlinear function of the nonlinear element is equal to the derivative of $S=S_{NY00}$, and the controlling resistance R_{cont} is: $R_{cont}=Q_{0L}\alpha_{N0}G_0E_{0L}^4K_{0DL}$.

We note that R_{cont} is the product of terms reflecting the transfer function on the closed feedback loop of OEO: the Q-factors Q_{0L}, pumping α_{N0}, the saturation coefficient G_0, the square of intensity E_{0L}^4, the transfer function on the feedback loop K_{0FODL}. Remarkably that the function of the normalized field strength of the laser has the fourth order.

Oscillation stability conditions of OEO DM in the steady-state point $e_L^2=e_{L0}^2$ for the appropriate stationary values of E_{00L}^2, N_{00}, and J_{0L} are found in the similar manner and have the form of inequality:

$$\alpha_{N0}G_0E_{0L}^4K_{0DL}S_{NY00}<2+\beta_{0L}+\frac{1}{Q_{0EF}}\frac{1}{Q_{0L}}-\left(\frac{1}{Q_{0EF}}+\frac{1}{Q_{0L}}\right)(1+\beta_{0L})^2. \quad (5.32)$$

For inequality (Eq. 5.31) fulfillment, the necessary condition is the condition $S_{NY00}\left(e_{L0}^2\right)<0$ fulfillment in the steady-state point $e_L^2=e_{L0}^2$, and the slope module in the initial state must be more than the slope module of the nonlinear function in the steady-state point.

We note that in the case when the right part of Eq. (5.28), i.e., the controlling operator transfer function, contains the operator in the first order p_{00} or in the third order p_{00}^3, and the oscillation *stability conditions* in the steady-state point take the form, which is traditional for the RF oscillators at $S_{NY00}\left(e_{L0}^2\right)<0$: $\alpha_{N0}G_0E_{0L}^4K_{0DL}S_{NY00}<\frac{1}{Q_{0EF}}+\frac{1}{Q_{0L}}$, and $\alpha_{N0}G_0E_{0L}^4K_{0DL}S_{NY00}<\frac{1+\beta_{0L}}{Q_{0EF}}+\frac{1}{Q_{0L}}$.

5.2.2 *Plots of Oscillation Stability Regions*

Now we construct the plots of oscillation *stability regions* of OEO DM. For this, we introduce coefficients $A = a_2$ and $B = a_3$ and use designations: $A = a_2 = \left(2 + \beta_{0L} + \frac{1}{Q_{0EF}}\frac{1}{Q_{0L}} - \alpha_{N0}G_0E_{0L}^4K_{0DL}S_{NY00}\right)$, and $B = a_3 = \left(\frac{1+\beta_{0L}}{Q_{0EF}} + \frac{1}{Q_{0L}}\right)$. Let us write the inequality system, which is deduced from the stability conditions. The system of two inequality describing the *stability region* (i.e., the zone of the steady-state point), which oscillations will not be excited, will take the following for: $\Delta_2 > 0$, $\Delta_3 > 0$. Now we have the inequalities:

$$\begin{cases} \left(\frac{1}{Q_{0EF}} + \frac{1}{Q_{0L}}\right)A - B > 0, \\ \left(\frac{1}{Q_{0EF}} + \frac{1}{Q_{0L}}\right)\left[AB - \left(\frac{1}{Q_{0EF}} + \frac{1}{Q_{0L}}\right)(1 + \beta_{0L})\right] - B^2 > 0. \end{cases} \tag{5.33}$$

The variety of points, which are above the straight line $A = \left(\frac{1}{Q_{0EF}} + \frac{1}{Q_{0L}}\right)^{-1} \cdot B$, satisfies the inequality $A > \left(\frac{1}{Q_{0EF}} + \frac{1}{Q_{0L}}\right)^{-1} B$. As a result, the solution of the whole system is the region of values A and B only, which satisfies the inequality (Eq. 5.33) having the form:

$$A > \left(\frac{1}{Q_{0EF}} + \frac{1}{Q_{0L}}\right)(1 + \beta_{0L}) \cdot \frac{1}{B} + \left(\frac{1}{Q_{0EF}} + \frac{1}{Q_{0L}}\right)^{-1} B. \tag{5.34}$$

Figure 5.2 shows plots of the *oscillation stability* regions of OEO DM without account of the inertial nonlinearity. The *stability* region of values A and B is located in the right upper quadrant (at $A > 0$ and $B > 0$) and shown in blue in Fig. 5.2. This region in the plane (B,A) represents the region of the *asymptotic stability* of the initial equation.

If we take into consideration the nonlinear inertia property in Eq. (5.28), we must expand the function $S_{NY00}\left(e_L^2\right)\exp\left(-jT_{FOS} \cdot f_{0e}\right)$ on the in-phase and quadrature components and to use the locus method or the Nyquist criterion as we performed in Chap. 3. It is shown in Chap. 3 that the self-excitation conditions and the oscillation stability conditions for the similar symbolic equation (Eq. 5.28) in the steady-state point must be added by conditions of amplitude and phase stability.

Now we can make a conclusion: for the soft OEO excitation mode and for the oscillation stability in the steady-state point, the slope of the nonlinear function in the initial state $e_L^2 = 0$ must be positive, and in the steady state $e_L^2 = e_{L0}^2$, this slope must be negative, and the slope module in the initial state must be more than the slope module in the steady-state point.

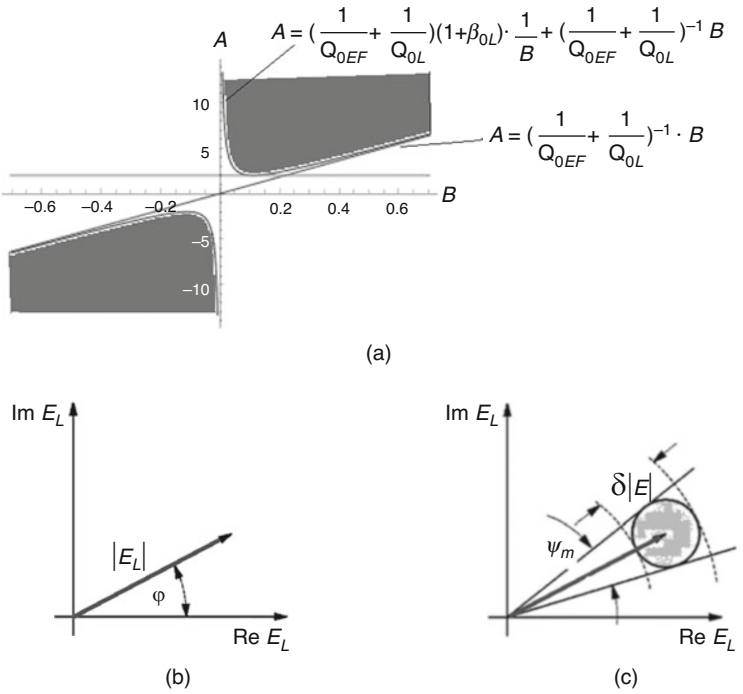

Fig. 5.2 Plots of quantities A and B region of OEO DM oscillation stability for $Q_{0L} = 10$, $Q_{0EF} = 100$ and $\beta_{0L} = 0.01$ without account of the nonlinear inertia property of the OEO nonlinear element (**a**). Representation of the laser field strength as the vector with the module $|E_L|$ and the argument without account of fluctuation $\varphi =$ arg E_L ($E_n = E_L$) (**b**). The same with account of fluctuations (**c**)

5.3 Dynamics of Transients in OEO DM and the Oscillation Amplitude

Let us determine the expression for the OEO oscillation amplitude in the small-signal single-frequency mode with the help of abbreviated equation obtained in Sect. 5.1.3, and analyze the main features of transients' dynamics in OEO DM.

We shall use deduced differential equations (Eq. 5.18) for the laser enclosed by the positive feedback loop. For analysis convenience, we write once more the system of differential equation (Eq. 5.18) with specified values of the slowly changing functions of the normalized square strength E_{0L}^2, phase φ and the population difference $N(t)$, as well as the AC component of the laser pumping current J_L:

$$\begin{cases} \mathrm{d}E_{0\mathrm{L}}^2/\mathrm{d}t = G_0 E_{0\mathrm{L}}^2 N - E_{0\mathrm{L}}^2/T_{0\mathrm{F}}, \\ \mathrm{d}N/\mathrm{d}t = \alpha_{\mathrm{N}00} \cdot J_{0\mathrm{L}} + \alpha_{\mathrm{N}01} \cdot J_{1\mathrm{L}} - \dfrac{N}{T_{1\mathrm{L}}} - G_0 N E_{0\mathrm{L}}^2, \\ \mathrm{d}\varphi/\mathrm{d}t = 2\pi\nu_{0\mathrm{P}}(N) - 2\pi\nu_0 + \sigma_{0\mathrm{L}} - \rho_{0\mathrm{L}} E_{0\mathrm{L}}^2, \\ \mathrm{d}^2 J_{1\mathrm{L}}/\mathrm{d}t^2 + \dfrac{1}{Q_{\mathrm{EF}}}\mathrm{d}J_{1\mathrm{L}}/\mathrm{d}t + (2\pi f_{0\mathrm{e}})^2 J_{1\mathrm{L}} = \dfrac{E_{00\mathrm{L}}^2 K_{\mathrm{FOS}} K_{\mathrm{PD}}}{Q_{\mathrm{EF}}} \dfrac{\mathrm{d}E_{0\mathrm{L}}^2(J_{1\mathrm{L}}, t - T_{\mathrm{FOS}})}{\mathrm{d}t}. \end{cases} \tag{5.35}$$

Variables included in the DE system were defined earlier. The distinguished feature of this system of differential equations is the fact that they connect the intensity $E_{0\mathrm{L}}^2$ of laser emission with the AC component of the current.

5.3.1 OEO Oscillation Amplitude in the Small-Signal Single-Frequency Mode

Let the excitation condition be fulfilled in the laser and in OEO and the single-frequency mode of the OEO RF generation in the frequency *f*. Considering the modulation of the pumping current in the form $J_{\mathrm{L}} = J_{\mathrm{L}00} + J_{1\mathrm{L}}$ and $J_{\mathrm{L}1} = J_{1\mathrm{OL}} \cos(2\pi ft + \varphi_{\mathrm{L}})$, where $J_{1\mathrm{L}}$ is much lesser than $J_{\mathrm{L}00}$, we shall find the solution of the differential equation system (Eq. 5.35).

We investigate DE (Eq. 5.35) of the laser under conditions of the quasi-stationary mode, i.e., with the steady-state values $E_{00\mathrm{L}}^2$, $N_{00\mathrm{L}}$, $\varphi_{00\mathrm{L}}$. For example, in the point A on the phase portrait in Fig. 5.2. In the small-signal mode of the OEO laser modulation in the DE system (Eq. 5.64), we take the variable change: (1) $E_{0\mathrm{L}}^2 = E_{00\mathrm{L}}^2 + e_{\mathrm{L}}^2$, (2) $N_{0\mathrm{L}} = N_{00\mathrm{L}} + n_{\mathrm{l}}$, (3) $\varphi = \varphi_{00\mathrm{L}} + \varphi_{\mathrm{L}}$, where $E_{00\mathrm{L}}^2$, $N_{00\mathrm{L}}$, $\varphi_{00\mathrm{L}}$ are solutions of differential equations (Eq. 5.64) in the steady state, and e_{L}^2, n_{l}, φ_{L} are small deviations from the steady-state values $E_{00\mathrm{L}}^2$, $N_{00\mathrm{L}}$, $\varphi_{00\mathrm{L}}$, relatively.

We assume that in the small-signal mode $E_{00\mathrm{L}} \gg e_{\mathrm{l}}$, $N_{00\mathrm{L}} \gg n_{\mathrm{l}}$, $\varphi_{00\mathrm{L}} \gg \varphi_{\mathrm{L}}$. We introduce in differential equations (Eq. 5.35) the normalized time $\tau = t/T_{1\mathrm{L}}$ and suppose that $G = G_0 T_{1\mathrm{L}}$. We take into consideration that in the steady-state mode the following equalities are fulfilled: $G_0 E_{00\mathrm{L}}(N_{00\mathrm{L}} - 1/T_{0\mathrm{P}}) = 0$, $A_2 = \frac{\hbar\nu J_{\mathrm{L}0}}{eV_{\mathrm{a}}} - \frac{N_{00\mathrm{L}}}{T_{1\mathrm{L}}} - G_0 N_{00\mathrm{L}} E_{00\mathrm{L}}^2 = J_{\mathrm{L}00}$.

Then, differential equations for small deviation of laser parameters e_{l}, n_{l}, and φ_{L} in the single-frequency mode, at positive feedback, without account of noises, will be written as:

$$\begin{cases} \mathrm{d}e_1/\mathrm{d}t = G_0 e_1 n_1 - e_1/T_{0\mathrm{P}}, \\ \mathrm{d}n_1/\mathrm{d}t = \alpha_{\mathrm{N}00} \cdot J_{0\mathrm{L}} + \alpha_{\mathrm{N}01} \cdot J_{1\mathrm{L}} - \dfrac{n_1}{T_{1\mathrm{L}}} - G_0 n_1 e_1, \\ \mathrm{d}\varphi_{\mathrm{L}}/\mathrm{d}t = 2\pi\nu_{0\mathrm{P}} - 2\pi\nu_0 + \sigma_{0\mathrm{L}} + \rho_{0\mathrm{L}} e_1, \\ \mathrm{d}^2 J_{1\mathrm{L}}/\mathrm{d}t^2 + \delta_{\mathrm{e}}\mathrm{d}J_{1\mathrm{L}}/\mathrm{d}t + (2\pi f_{0\mathrm{e}})^2 J_{1\mathrm{L}} = (\mathrm{d}e_{\mathrm{L}}/\mathrm{d}t)\delta_{\mathrm{e}} K_{0\mathrm{DL}} \mathrm{d}e_{\mathrm{L}}(t - T_{\mathrm{FOS}})/\mathrm{d}t. \end{cases} \tag{5.36}$$

Taking into account the last transformations in DE (Eqs. 5.35 and 5.36), supposing that the nonlinear element slope is constant in the vicinity of small amplitude deviations from the steady-state value, we obtain the following expression for amplitude of AC component of QWLD emission intensity $|e_{1\mathrm{l}}|$ in the OEO closed loop:

$$|e_{1\mathrm{l}}| = \frac{K_{\mathrm{DL}} G S_{\mathrm{HY}} P_{\mathrm{L}0}}{\left\{ (P_{\mathrm{L}0} G K_{\mathrm{DL}} S_{\mathrm{HY}})^2 \cos^2(\omega T_{\mathrm{FOS}}) + G^2 \left[1 + T_{0\mathrm{P}}^2 (\omega - \omega_{0\mathrm{L}})^2\right] \left[1 + T_{0\mathrm{e}}^2 (\omega - \omega_{0\mathrm{e}})^2\right] \right\}^{1/2}}. \tag{5.37}$$

The analysis of the last expression shows that the amplitude of AC component of the square intensity of the laser optical emission $|e_{1\mathrm{l}}|$ (relatively, the amplitude of the AC component of pumping current $J_{1\mathrm{L}} = K_{\mathrm{DL}} e_{\mathrm{L}}$) in OEO depends not only on RF circuit parameters, the time constant of the RF filter $T_{0\mathrm{e}}$, the natural frequency of the filter $\omega_{0\mathrm{e}}$, the average value of the nonlinear function slope S_{NF}, but on the laser or QWLD parameters. It depends also on the DC component of the QWLD output power $P_{\mathrm{L}0}$, the laser gain G, the natural frequency $\omega_{0\mathrm{L}}$ of laser relaxation oscillations (determined by the lifetime of active particles on the upper excited level, the pumping excess over the threshold value and the gain), the photon lifetime in the laser resonator $T_{0\mathrm{P}}$. At that, at delay time T_{DL} changing in the feedback circuit, the phase incursion ωT_{DL} changes of RF oscillations with ω, and the function $|e_{1\mathrm{l}}|$ is periodic of the argument ωT_{DL}. Expression (Eq. 5.37) well agrees with the expression for the amplitude of the oscillation square intensity (as well as for the expression for gain) of QWLD presented in Chap. 3.

5.3.2 *Simplified Estimation of the Setting Time of $E_{0\mathrm{L}}^2$ intensity and the Pumping Current $\mathbf{J}_L$ on the Base of OEO Abbreviated Equations*

In the primary analysis of dynamic features, we use abbreviated equations for the laser enclosed by the positive feedback loop. The initial equation system for solution of this problem is presented in this chapter under numbers (Eqs. 5.14, 5.15, and 5.18).

From the system of abbreviated differential equations (Eq. 5.25) (or taking into account equations for the population from the system of abbreviated DEs (Eq. 5.26)), using an analogy with traditional RF oscillators with inertial active element and with retarded feedback, we are able to obtain relatively simple the ***approximated*** equations for transients of variables E_{0L}^2 and J_L.

In order to have the exact solutions for variables E_{0L}^2 and J_L, we must (using the computer modeling) solve the DEs system (Eq. 5.18), which consists of four differential equations. At first, we make the rough estimations of oscillation setting time of E_{0L}^2 and J_L for the simple case.

We suppose in Eq. (5.25) that the quadrature component is equal to zero: $S_{LCOS}(E_{10L}) = 0$, and the in-phase component can be approximated by the "soft" dependence on the oscillation amplitude E_{10L} (by means of the third-order polynomial): $S_{LCOS}(E_{10L}) = \alpha_{0E} - (3/4)\beta_{0E}(E_{10L})_{10L}^2$. We suppose in Eq. (5.14) that the quadrature component is zero: $I_{1A}\left(U_{PD}, E_{10L}^2\right)\sin\left[2\pi f_{0e}T_{FOS}\right] = 0$, and the in-phase component $S_{COS} = I_{1A}\left(U_{PD}, E_{10L}^2\right)/U_{1A}$ can be approximated by the "soft" dependence (by means the third-order polynomial) on the oscillation amplitude J_{10L} : $S_{COS}(J_{10L}) = \alpha_J - (3/4)\gamma_J J_{10L}^2$.

Then, introducing the dimensionless amplitude $x(t) = E_{10L}/E_{10M}$, where $E_{10M} = \sqrt{4\alpha_{0E}/(3\beta_{0E})}$, and $y(t) = J_L/J_{10m}$, where $J_{10m} = \sqrt{4\alpha_J/(3\gamma_J)}$, from Eq. (5.14) we obtain the system of differential equations for variables $x(t) = E_{10L}/E_{10M}$ and $y(t) = J_L/J_{10m}$:

$$\begin{cases} \dfrac{dx}{dt} = \alpha_{0E}R_{contE}\left[\dfrac{\alpha_{0EN} + \alpha_{1EN}(y) - 1}{R_{contE}} - x^2\right]x, \\ \dfrac{dy}{dt} = \alpha_J R_{contJ}\left[\dfrac{\alpha_{JN}(x) - 1}{R_{contJ}} - y^2\right]y, \end{cases} \tag{5.38}$$

where $R_{cont} = 2\pi\nu_{0F}\cdot\frac{K_{0L}N_0(J_{10L})}{Q_{12}+Q_{0F}}$, $R_{contE} = \frac{E_{10L}^2 K_{FODL}}{2R_L Q_{EF}}$, α_{0EN} is the DC component of pumping, $\alpha_{1EN}(y)$ is the AC component of the pumping current, $\alpha_{JN}(x)$ is the AC component of the normalized current in the input of the RF amplifier.

In the general case, the system of differential equations (Eq. 5.35) has no analytical solution. But for estimation of the laser oscillation setting time, it is enough to take in the first equation of Eq. (5.35) $\alpha_{JN}(y) = 0$, and to find $x(t)$. This is true since without the existence of the laser optical generation, there is not the RF generation in the positive feedback loop of OEO.

Assuming that $\alpha_{JN}(y) = 0$ in Eq. (5.38), we obtain the time-variation law $x(t) = E_{10L}/E_{10M}$:

$$x(t) = E_{10L}/E_{10M} = \frac{x_0\exp\left(\delta_0 t/T_1\right)}{\sqrt{1 + \frac{\alpha_J R_{cont}x_0^2}{\delta_0}\left[x_0\exp\left(\delta_0 t/T_1\right) - 1\right]}}, \tag{5.39}$$

where $\delta_{0E} = \alpha_{EN} - 1$ is the laser pumping excess over the threshold normalized value equaled to 1, x_0 is the initial dimensionless amplitude at time moment $t = 0$. The expression (Eq. 5.39) allows determination of the plot $x(t)$ for values of initial dimensionless amplitude x_0 and the setting time T_X. For definite values of initial dimensionless amplitude y_0, the DE system (Eq. 5.35) permits to determine the time plot and the setting time T_Y. We assume in the second equation of Eq. (5.35) that $\alpha_{JN}(x)$ is the constant value equaled to the normalized value of strength oscillation amplitude in the steady-state mode, and we find the time-variation law of $y(t) = J_L/J_{10m}$:

$$y(t) = J_L/J_{10m} = \frac{y_0 \exp\left(\delta_{0J} t/T_{FOS}\right)}{\sqrt{1 + \frac{\alpha_J R_{cont} y_0^2}{\delta_{0J}}\left[y_0 \exp\left(\delta_{0J} t/T_{FOS}\right) - 1\right]}}, \tag{5.40}$$

where $\delta_{0J} = \alpha_{JN} - 1$ is the self-excitation reserve of OEO, y_0 is the initial dimensionless amplitude of AC component of the pumping current at $t = 0$. Expressions (Eqs. 5.39 and 5.40) allow estimation the total time of the transient $T_X + T_Y$ for the laser strength $x(t) = E_{10L}/E_{10M}$ and the pumping current $y(t) = J_L/J_{10m}$ on the closed loop of OEO DM: $T_X = \frac{1}{2(\alpha_{EN}-1)} T_1 \cdot F_1(x_0)$, $T_Y = \frac{1}{2(\alpha_{JN}-1)} T_{FOS} \cdot F_2(y_0)$, where $F_1(x_0)$, $F_2(y_0)$ are functions depending on the initial conditions x_0 and y_0, relatively, at $t = 0$ $F_1(x_0)$ and $F_2(y_0)$ are equaled to about 1.

Thus, the total setting time $T_X + T_Y$ of OEO auto-oscillations is determined not only by the delay time in the OEO optical fiber T_{FOS}, but also by the lifetime T_1 of carriers on the upper energy level of the laser. At increase of DC component of the pumping current α_{0EN} over the threshold value, the setting time T_X decreases. At growth of the self-excitation reserve of OEO $\delta_{0J} = \alpha_{JN} - 1$, the OEO oscillations' setting time T_Y decreases. We can resume that the total setting time $T_X + T_Y$ of oscillations, from the one hand, decreases at the growth of DC component of the laser pumping current α_{EN}, and, on the other hand, it decreases at growth of the amplitude of AC component of the laser pumping current α_{JN}. We made the approximate estimation of the setting time of OEO oscillation. Now we can transfer to results of the accurate solution of the differential equation system (Eq. 5.35) with the help of the analog modeling.

5.3.3 *Dynamics of Transients in OEO DM*

Let us consider the transient process of the exit to the steady-state mode of the free generation of OEO DM at representation of the oscillator in Figs. 5.1a and Fig. 2.2. As it had been mentioned earlier, such a structure is described by the system of differential equations (Eq. 5.35). Here we consider the system of differential equations (Eq. 5.35) for the laser (or QWLD) enclosed by the positive feedback loop ("Feedback Chain" in the figure) formed by the delay line of FOS, the photodetector PD, the nonlinear amplifier A and the filter F.

On the base of OEO differential equations (Eq. 5.35), the analog model of OEO was constructed presented in Figs. 2.2 and 5.1a.

On the base of Eq. (5.35) and the mentioned analog model, the dependences of the population, the square of strength of optical emission and the AC component of the QWLD pumping current in transient at impact of stepwise pumping at the closed positive feedback loop in OEO. The time-functions of the square strength, the population, the pumping current, and phase portraits in the soft mode of RF oscillation setting in OEO with the direct modulation of the laser pumping current are presented in Fig. 5.3.

The one of difficulties at solution of Eq. (5.35) finding at the analog modeling is the determination of the nonlinearity of the RF nonlinear amplifier (A) in order to "compensate of the multiplicative QWLD nonlinearity."

At modeling of laser differential equations (Eq. 5.35), we use the following values of parameters (the same as in Chap. 3) for the mesa-strip laser with the thickness of the dielectric film $d = 1.2$ μm: $g_0 = 10^3$, $\tau_D = 7.2 \cdot 10^{-12}$ s, $I_{thr} = 12$ mA, $\varepsilon_{sh} = 0$. The values of parameters of QWLD are: the lifetime of carriers $T_1 = \tau_{n1} = 0.5 \cdot 10^{-9}$ s, the threshold level population difference is 10^{18} 1/cm^3, the lifetime of photons or the time constant of the optical resonator $T_{0F} = \tau_{ph} = 1.2 \cdot 10^{-12}$ s, the volume of the QWLD active zone is 10^{-11} cm^{-3}.

We investigated transient processes of oscillation setting in OEO without and with delay (Fig. 5.4) in the loop of positive feedback.

As the result of computer modeling, it is stated that the transient process of the exit to the OEO generation mode is accompanied by ripples. Plots are presented in Fig. 5.6. At large oscillation amplitude of the square strength, the strong nonlinear distortions are arisen, which are caused by the laser multiplicative nonlinearity.

The level of nonlinear distortions depends upon a choice the DC pumping current. The setting time of laser oscillations is 0.8 ns (or from 0 to 40 point in Fig. 5.3a–c). The setting time of OEO RF oscillations is on the time axis t of 40 ns (or from 50 to 100 points in Fig. 5.3e). The period of laser ripples in the transients equaled about 0.4 ns depends upon the pumping current level and is determined by the lifetime of carriers. The frequency of RF oscillation in the steady-state mode is close to the natural frequency RF filter (F) and was 4–10 GHz (the oscillation period is 0.25–0.1 ns) and depended on a choice of the natural frequency of the RF filter.

5.3.4 *General Remarks About the Limit Cycle Realization in the Closed OEO DM System of the Laser Emission*

The transient is realized in the case if the singular point is the stable knot, i.e., characteristic roots p_1 and p_2 are real and negative. In order to the singular point A (the focus) becomes unstable (i.e., characteristic roots p_1 and p_2 must be positive), it is necessary to intensify the positive feedback. At that, the unstable point A in enclosed by the stable limit cycle, which is shown in Fig. 5.4. This means that during

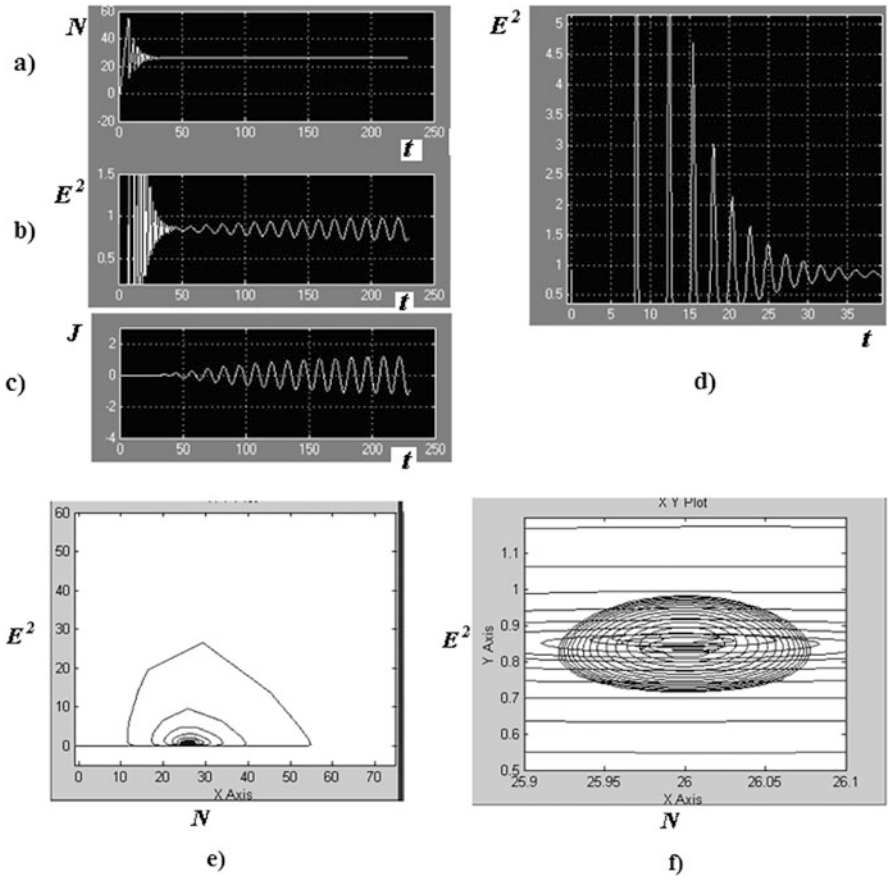

Fig. 5.3 The scenario of OEO excitation in the single-frequency mode at activation of pumping. The scenario of the transient process in OEO and in the laser. The constant pumping level $J_0 = 30$ mA. Activation of pumping occurs in the time moment $t = 0$. Time-functions of normalized values: (**a**) the population difference N (10^{18} 1/cm^3), (**b**) the normalized square of strength $(E)^2 = (E_{0L})^2$, (1.0 point = 1 mW), (**c**) AC component of pumping current, (**d**) the normalized square of strength $(E)^2 = (E_{0L})^2$, (1 point = 1 mW) at initial part [0,50], (**e**) the time diagram (the phase portrait) $(E)^2 = (E_{0L})^2$, N_0. (**f**) The time diagram (the phase portrait) $(E)^2 = (E_{0L})^2$, N_0. The transient process is presented with the exit to the limit cycle on the time diagram E_{0L}, N_0. The scale on the time axis t: 5 points = 0.1 ns. The setting time for the laser oscillations is 40 points (or 0.8 ns). The setting time of OEO RF oscillations is on the time axis t 50–250 points (or 40 ns)

laser emission, the strength is exposed to the periodic oscillation. It is important to note that in the presence in the upper half-plane of the single singular point, the laser self-excitation condition is satisfied and, hence, the excitation occurs in the soft manner. This conclusion can be extended to the case of the arbitrary odd number of nontrivial singular points. The generation is impossible if the isoclinic lines $F_1(N_L)$ and $F_2(E_L)$ are not intercepted. If the number of singular points is even (at presence of two singular intercepted points), the OEO self-excitation condition cannot be

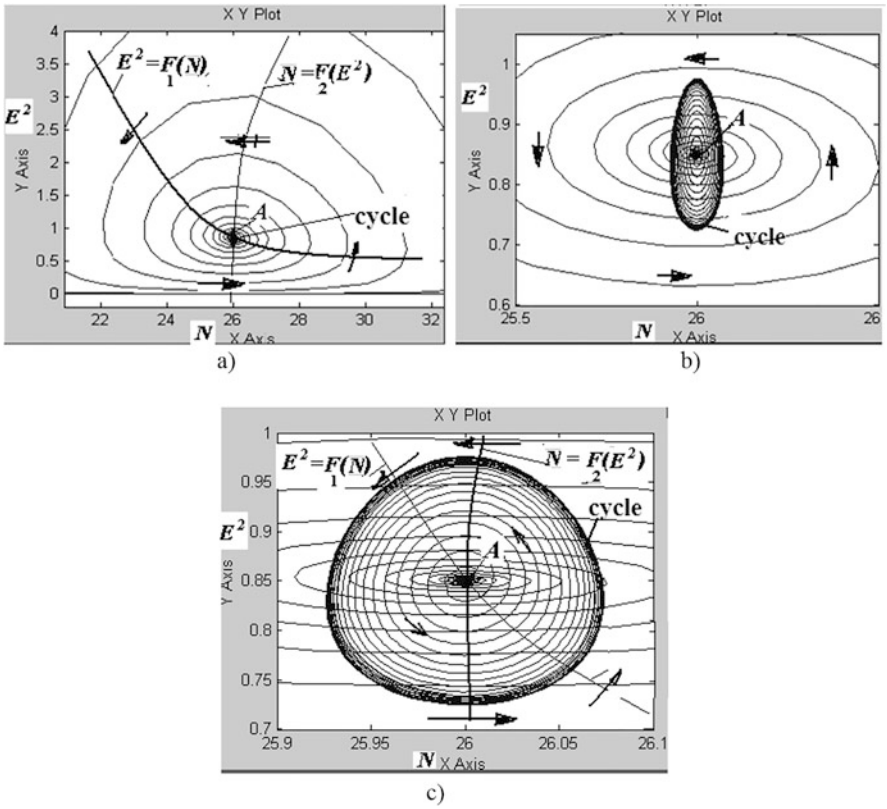

Fig. 5.4 Phase portraits in the "soft" mode of oscillation setting in OEO DM (**a**). The phase portrait of the normalized square strength $(E)^2 = (E_{0L})^2$ and the population difference N (**a**, **b**). Y-axis—the normalized square strength (or the intensity), X-axis—the population. The scale on the Y-axis is $1.0 = 1$ (V/m)^2. The scale on the X-axis is $1.0 = 1$ mW. N (1.0 point on the scale is 10^{18} 1/cm^3). (**c**) The enlarged image of the phase portrait is shown and the transient development with the exit to the limit cycle on the time diagram E_{0L}, N_0. The scale on the time axis t is 5 points = 0.1 ns

satisfied and the laser generation can be excited only in the "**rigid**" manner, which is initiated by the pulse from external source.

When the A point is unstable, the process of oscillation growth is developed in the oscillating system, which are restricted by the nonlinearity of the RF amplifier and there are conditions for the limit cycle existence for RF oscillations. The stability of this cycle is determined by the sign of the partial derivatives of right parts over the one variable at analysis of the characteristic equation obtained in Chap. 4. The limit cycle is stable if the appropriate expressions for coefficients are more than zero.

The phase plane of the oscillator with rigid excitation having the stable limit cycle is more complicate, at that, the number of singular points (interception point of isoclinic lines $F_1(N_L)$ and $F_2(E_L)$) is even and existence of lengthy generation of

OEO oscillations in the rigid more without the external oscillator, as a rule, is impossible. Oscillating OEO systems returns to the quiescent state.

The transient processes of oscillation setting in OEO DM without and with the retard in the positive feedback loop are depicted in Fig. 5.1. As the result of computer modeling, it is proved that the transient of the exit to the OEO generation mode is accompanies by ripples. At large oscillation amplitude, the strong nonlinear distortions occur, which are caused by the multiplicative nonlinearity of the laser described in Chap. 3. The level of nonlinear distortions depends upon a choice of the DC pumping current.

The mode of small amplitude of OEO oscillations (less than 1–10% of the maximal possible values) is performed at a choice DC bias current of small (on the level from 1.5 to 5.0) relative exceeding of the threshold pumping current of the laser. A choice of the nonlinearity type of the RF amplifier, the natural frequency of the RF filter, the delay value in RF FODL determine the character, and the transient duration of OEO oscillations. The limit cycle setting occurs in the soft mode, at a choice of the amplifier nonlinearity type taking into consideration the laser multiplicative nonlinearity.

Figure 5.5 show the modeling of differential equations of QWLD with the positive selective feedback. The transient processes of OEO oscillation setting without (a–c) and with the delay (d–f) in the positive feedback loop.

Plots in Fig. 5.5 show that at delay existence, after the strength and population setting, the oscillating process of the AC laser pumping current occurs with the time delay equaled to the delay in optical fiber. After that, the pumping oscillations, which increasing in the amplitude, modulate the laser population and strength.

We would like to make some conclusions that the OEO analysis is performed at representation of laser differential equations by semiclassical equations for the emission field strength and for the inversed population and the electrical pumping current. The positive feedback is included in the DE system with account of optical emission photodetection, of selectivity in radio frequency and the nonlinear amplification on the nonlinear amplifier. The new fact is that laser differential equations (which are adopted to call in mathematic as the Lotka–Volterra equation) for the strength (or for the intensity) of the optical field, the inversed population and the optical phase with the positive selective feedback with the retarded argument are finally reduced to the van-der-Pol differential equation for the electric pumping current at definite restrictions and conditions described earlier.

The analysis of solutions of the second-order differential equations shows that in such a system of OEO DM, the single-frequency and the double-frequency modes are possible in the radio frequency. The necessary condition of the stable single-frequency generation mode (in radio frequency) is more than the double excess of the RF circuit Q-factor of the laser relaxation oscillations, which is defined by the time constant of the electron relaxation in the laser active layer, by the laser optical amplification coefficient, and by the pumping excess over the threshold level. At that, for the single-frequency generation mode (in the radio frequency), the transmission is possible in the optical channel from the laser to the PD of two optical frequencies: one of the frequencies is the central optical frequency of the laser, while

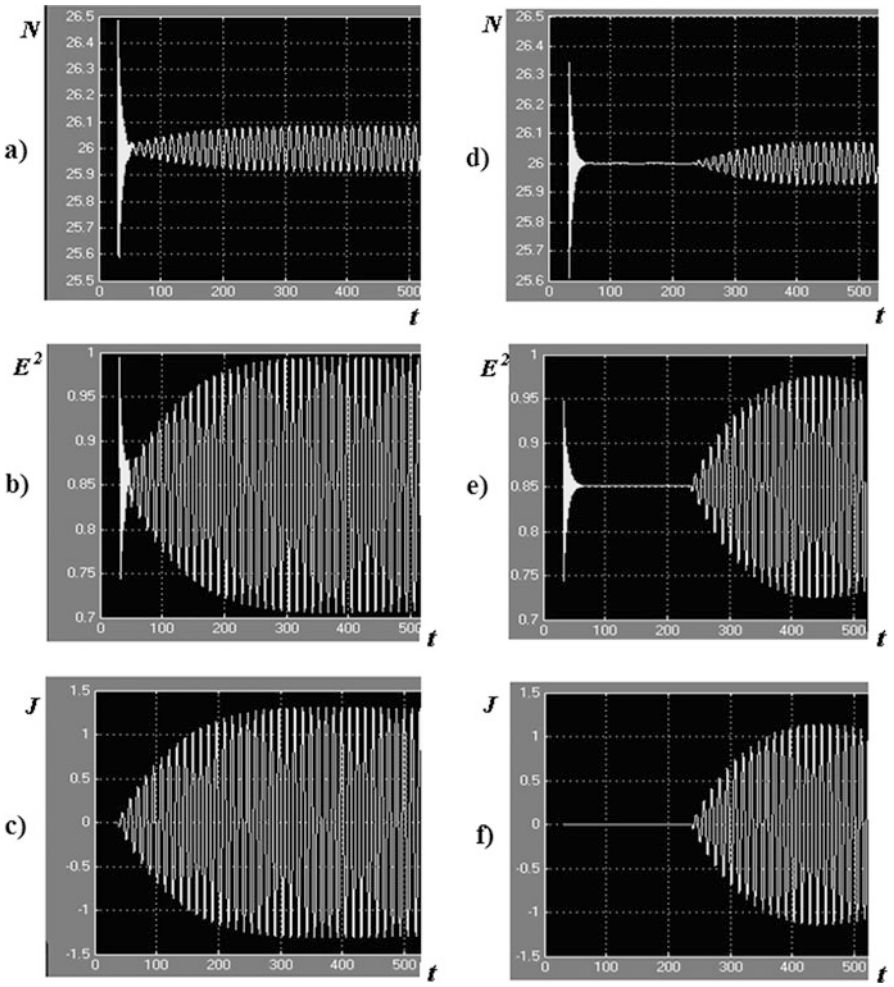

Fig. 5.5 Modeling of differential equations of QWLD with the positive selective feedback. The transient processes of OEO oscillation setting without and with the delay in the positive feedback loop. In abscissa axis—the normalized time, in ordinate axis—(**a**, **d**)—the inversed population; (**b**, **e**)—intensity; (**c**, **f**)—RF oscillations of OEO generation current (the electrical current of laser pumping

the second is the laser optical frequency shifted with regard to the central frequency by the OEO radio-frequency generation. After photodetection of these two optical frequencies, the RF oscillations can be extracted in the PD current. The phase of this RF oscillation depends on the phase difference of optical oscillations transmitted on the central frequency of laser generation and on the shifted optical frequency.

5.4 Fluctuation Differential Equations of OEO with the Langevinian Noise Sources

We described in detail in Sects. 5.1 and 5.2 the calculation procedure of the OEO DM and OEO MZ steady-state mode. Now we transfer to the fluctuation analysis of the oscillation amplitude and phase of OEO.

Under influence of noises of the laser active element, the deviations of amplitude and phase arise in OEO from the steady-state values. Before the start of the analysis, we describe the main positions of the fluctuation model of the laser.

5.4.1 Main Regulations of the Fluctuation Laser Model and Langevinian Noise Sources

The semiclassical laser theory considered in Chap. 3 leads to the deterministic motion equation for the field amplitude, and the problems concerning the spectral line width and fluctuations remain beyond the scope of this theory. Noises in differential equations can be taken into consideration by means of introduction of Langevinian noise sources, which is the procedure for which it is not easy to find the strict substantiation and the truth of which can be justified, to a great extent, by the coordination with other approaches. One of such approaches is the **quantum-field approach**, which is not used here, but it serves as the more consistent basis for the laser theory. It permits to answer of questions, which are not defined within the limits of the semiclassical theory, for instance, how much photons do exist at the threshold? Our task includes the investigation of OEO operation at large amplitudes of laser oscillation within the limits of semiclassical laser theory taking into account fluctuations.

The main regulations of the fluctuation model of the laser adopted at the OEO analysis can be formulated in the form of ten points, which are discussed below:

1. The random fluctuations of the oscillation phase of the laser optical emission are the main reason of laser spectral line widening.
2. The laser has the narrow spectral line and the high temperature stability.
3. Fluctuations of the laser field are caused by the spontaneous emission.
4. Owing to the relatively high average power, which falls on the PD area, and the large number of the random acts of spontaneous emission (according to the central limit theorem), the probability density has (in magnitude) the Gaussian or normal distribution law. The small value of phase fluctuations allows the linearization of the fluctuation equations. The equation for the field phase becomes similar to the equation for the random wandering under an impact of the Gaussian random Langevinian forces.
5. The distribution density of the phase increments of the laser emission has the Gaussian law.

6. Fluctuations of the laser intensities are negligible small because the laser pumping level is over the threshold.
7. The phase fluctuation model is described by the model of the Wiener random process, which is the limit case of the process of random wandering at aspiration of the number of steps for infinity.
8. The probability distribution density of the random quantity (the ψ_m phase) depends on time, has the normal Gaussian density with zero mean: $P(\psi_m) = \frac{1}{\sqrt{t\alpha}\sqrt{2\pi}} \exp\left(-\frac{\psi_m^2}{2\alpha t}\right)$, where t is time, α is the physical parameter, for example, for the laser the spectral line width (on the level 0.5).
9. The random process increments (i.e., increments of the phase difference during the time interval $(t,t + \tau)$ are stationary in time) and the probability distribution density $P(\Delta\psi_m)$ of the random quantity (the phase difference) does not depend on time, has the normal Gaussian density with zero mean $\Delta\psi_m = \psi_{m1}(t) - \psi_{m1}(t + \tau)$: $P(\Delta\psi_m) = \frac{1}{\sqrt{2\pi}\sigma_{\Delta\psi_m}} \exp(-\frac{\Delta\psi_m^2}{2\sigma^2_{\Delta\psi_m}})$, where $\sigma^2_{\Delta\psi_m}$ is the dispersion of the random phase difference $\Delta\psi_m = \psi_{m1}(t) - \psi_{m1}(t + \tau)$, which depends only upon the difference of the time moments τ.
10. For the dispersion of the random phase difference $\Delta\psi_m = \psi_{m1}(t) - \psi_{m1}(t + \tau)$, the true expression for the dispersion $\sigma^2_{\Delta\psi_m}$ is: $\sigma^2_{\Delta\psi_m} = \alpha t + \alpha(t + \tau) - 2\alpha t = \alpha|\tau|$, in which α is the constant width of the laser spectral line $\alpha = \Delta\nu_L = 1/T_c$, and T_c is the laser time of coherence (or the time constant).

Figure 5.2b, c shows the representation of the laser electromagnetic field strength in the complex space, i.e., in the phase space formed by the vector components with the module and the phase (the argument). From the point of view of the statistical analysis, this vector has fluctuations of the module (Fig. 5.2b) and the phase (Fig. 5.2c). Taking into consideration the *quantum description of the field*, the vector end can lay in any point of the phase space region, which has the minimal area $\pi\hbar/2$. This region of ambiguity can be a circle, which leads to symmetrical distribution of fluctuations.

5.4.2 *Symbolic Constitutive Differential Equations of the Laser with Fluctuations*

In this section, we analyze the symbolic fluctuation equations of the laser for the single-frequency generation mode with account of the differential equation for the population.

As in Chaps. 2 and 3, now we consider the single-frequency QWLD, which resonator allows performing of the traveling-wave mode (Fig. 2.2a). We note that formation and analysis of fluctuation equations of the laser with the resonator Fabry–Perot (the resonator of plane-parallel mirrors), in which the standing-wave mode in the cavity occurs.

In semiconductor and the fiber-optical lasers, the geometric length of the resonator is much more than the wavelength of the generated optical emission, and the oscillation frequency is close to the natural frequency of the optical resonator. We use the semiclassical representation of Maxwell equation for the double-level system in the dipole approximation.

For small perturbations, in Chap. 3, the system of three equations was investigated for the strength of the electromagnetic field $E_n(t) = E_L(t)$, for the polarization $P_n(t)$ of the QWLD active material and the population difference $N(t)$ between excited and non-excited levels of the laser active element. Taking into consideration the transformations made in Chap. 3, the system of differential equations (Eq. 5.35) for the single-frequency single-type mode, when the only main type of spatial oscillations is excited in the resonator, is added by the Langevinian noise sources ξ_E, ξ_P, ξ_N, which takes into account, relatively, the amplitude noise of the QWLD emission, the medium polarization noise, and the spontaneous noise of the active medium carriers. Then, the fluctuation system of differential equations for the laser can be written as:

$$\begin{cases} \dfrac{d^2E_n}{dt^2} + \dfrac{2}{T_{0F}}\dfrac{dE_n}{dt} + (2\pi\nu_{0n})^2 E_n = -\dfrac{1}{\varepsilon_n}\dfrac{d^2P_n}{dt^2} + \xi_E, \\ \dfrac{d^2P_n}{dt^2} + \dfrac{2}{T_2}\dfrac{dP_n}{dt} + (2\pi\nu_{12})^2 P_n = \dfrac{p_e^2}{h} N E_n + \xi_P, \\ \dfrac{dN}{dt} = \alpha_{N0} - \dfrac{N}{T_1} - \dfrac{1}{T_{1ind}} N E_n E_n^* + \xi_N, \end{cases} \tag{5.41}$$

where all variables of the DE system (Eq. 5.41) are indicated in the Table of Chap. 3 (besides the fluctuating variables ξ_E, ξ_P, ξ_N).

The analog model of QWLD with the Langevinian noise sources formed of the base of differential equation (Eq. 5.41) is presented in Fig. 5.6. Description of the main components of the analog model (Fig. 5.6) was done in Chap. 3. We remind that the laser model contains two closed loops, in one of which the strength oscillations E_n and the polarization oscillations P_n are circulated, while in the second, the population oscillations are circulated. The laser analog model reflects the functional connection of parameters of the laser model. This model gives the understanding how is the oscillation amplitude setting, how the time constants T_{0F}, T_2, T_1 and the frequency difference between ν_{0n} and ν_{12} influence on dynamic properties.

Now we consider the case of the solid-state QWLDs with the narrow spectral line (less than 50 MHz), which are used in OEO. Introduction into the analog model of the *fluctuations sources*—the population ξ_N, the EMF strength ξ_E, the polarization ξ_P simplifies understanding of these quantities on the self-oscillating system. Introduction of the fluctuation sources in the model in order to solve a problem about finding of power spectral densities (PSD) of the phase noise (PN) of the laser oscillations and PSD of PN in OEO.

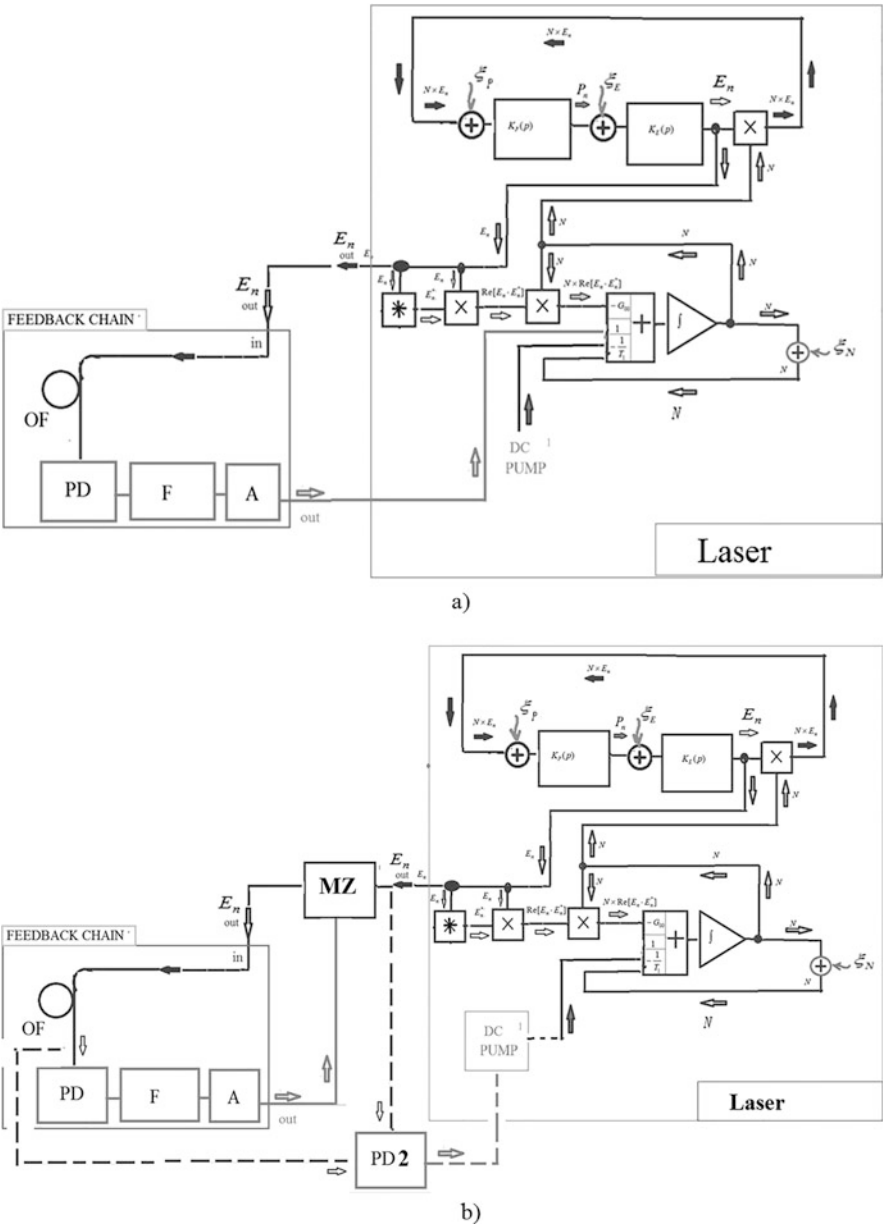

Fig. 5.6 The fluctuation analog models of OEO DM (**a**) and of OEO MZ (**b**) as QWLD enclosed by the positive feedback loop "Feedback Chain". The laser model is presented in the dipole approximation with the controlling population circuit. "Feedback Chain" consists of the optical fiber OF, the photodetector PD, the RF filter F, the amplifier A. Laser is QWLD, P is the polarizer, C the RF coupler. PD2 is the photodetector intended for determination of the power values in the MZ modulator input and/or in the output of the optical fiber

Let us transfer from Eq. (5.41) to *symbolic fluctuation equations*. For this, we use the Laplace transform: $d^2/dt^2 = p^2$ and $d/dt = p$. We note that at transfer from the operator record to the frequency record, we can replace the operator p by $j\omega = (j2\pi\nu - j2\pi\nu_{0n})$, where $\nu_{0n} = \nu_0$, ν is the QWLD generation frequency. Besides, we introduce the constant coefficients $A_{NE1} = 2/\varepsilon_n$ and $B_{NE1} = p_e^2/(2\pi h)$. The system of differential equations (Eq. 5.41) in the operator form represents the following system of symbolic fluctuation equations for the laser:

$$\begin{cases} \left[p^2 + \dfrac{1}{T_{0F}}p + (2\pi\nu_{0n})^2\right]E_n = -\dfrac{1}{\varepsilon_n}p^2P_n + \xi_E, \\ \left[p^2 + \dfrac{1}{T_2}p + (2\pi\nu_{12})^2P_n = \dfrac{p_e^2}{2\pi\hbar}NE_n + \xi_P, pN = \alpha_{N0} - \dfrac{1}{T_1}N - \dfrac{1}{T_{1ind}}NE_nE_n^* + \xi_n. \end{cases} \tag{5.42}$$

We consider the case when the resonator Q-factor of the laser essentially exceeds the Q-factor of the spectral emission line of the active element, i.e., the conditions $T_2 \ll T_1$, $T_2 \ll T_{0F}$ are fulfilled. We express P_n from the second equation of Eq. (5.42) $P_n = \frac{p_e^2}{2\pi\hbar}\frac{1}{p^2+(1/T_2)p+(2\pi\nu_{12})^2}NE_n$. We take into consideration that $N(t)$ is the slowly changing function compared to $E_n(t)$ and $P_n(t)$. Pumping α_{N0} in Eq. (5.42) can be expressed as $\alpha_{N0} = \alpha_{N00} \cdot J_{0L} + \alpha_{N01}i_{1L} = \alpha_{N00} \cdot J_{0L} + \alpha_{N01} \cdot J_{1L}$, where α_{N00} and α_{N01} are constants, $I_{0L} = J_{0L}$ is the DC component of the pumping current, $i_{1L} = J_{1L}$is the AC component of the pumping current. Now we have from Eq. (5.42) the system from two symbolic equations with fluctuations for QWLD:

$$\begin{cases} \left[p^2 + \dfrac{2}{T_{0F}}p + +(2\pi\nu_{0n})^2\right]\left[p^2 + \dfrac{2}{T_2}p + (2\pi\nu_{12})^2\right]E_n = \dfrac{2p_e^2}{2\pi\hbar\varepsilon_n}\omega^2p^2NE_n + \xi_{EP}, \\ pN = \alpha_{N00} \cdot J_{0L} + \alpha_{N01} \cdot J_{1L} - \dfrac{1}{T_1}N - \dfrac{1}{T_1}NE_n^2 + \xi_{NP}. \end{cases} \tag{5.43}$$

This system of fluctuation Eq. (5.43) is similar in mathematical notation to the equation system for the double-circuit RF oscillator with inertial auto-bias [1, 2] (or pumping) with noise sources ξ_{EP} and ξ_{NP}. The distinguish feature of Eq. (5.43) is the nonlinearity presence in the form of multiplication operation $N \cdot E_n$ or the multiplicative laser nonlinearity. The second fluctuation equation in Eq. (5.43) takes into account the carriers' noises, which are created by the laser spontaneous emission due to the spontaneous carrier transfer from the upper energy level to the lower in the double-level laser model in the dipole approximation.

5.4.3 Symbolic DEs of the Laser with Fluctuations in the Quasi-Stationary Small-Signal Mode

In the steady-state mode, for values $N = N_0$ and $E_n = E_{0n}$, at large excess (by 4–10 times) of the DC pumping component $\alpha_{N00} \cdot I_{0L}$ above the threshold value, the system (Eq. 5.74) can be reduced to the single differential equation of the fourth order, which simplifies the determination of PSD of the amplitude and phase noise. This can be done at small deviations of N and E_n from the appropriate steady-state values of N_0 and E_{0n}. At that, for population, in Chap. 3 the following expression was obtained:

$$N = \frac{1}{1 + T_1 \cdot j2\pi(\nu - \nu_0)} \cdot \frac{N_0}{1 + \frac{T_1 G_{00} E_{0n}^2}{1 + T_1 \cdot [\, j2\pi(\nu - \nu_0)]}}. \tag{5.44}$$

The expression (Eq. 5.44) shows that in the considered vicinity of the laser generation frequencies ν, which are shifted from the average generation frequency ν_0, the dependence of the inversed population is decreasing at $|\nu - \nu_0|$ growth. If to perform the analogy with RF circuits, then it reminds the transfer function of the low-pass filter.

Substituting Eq. (5.44) into Eq. (5.43) and approximating (Eq. 5.44) with the help of the cubic polynomials, as it is done in Chap. 3, we obtain the symbolic equation with the fluctuating noise sources for the laser:

$$\begin{aligned} &\left[p^2 + \frac{1}{T_{0F}} p + (2\pi\nu_{0F})^2\right]\left[p^2 + \frac{1}{T_2} p + (2\pi\nu_{12})^2\right] E_n \\ &= \alpha_{00} E_n - \beta_{00} E_n |E_n|^2 + \xi_N E_n \eta_{00} + \frac{\xi_P}{(2\pi\nu_{12})^2 Q_P} + \xi_E, \end{aligned} \tag{5.45}$$

where $Q_P = p^2 + (1/T_2)p + (2\pi\nu_{12})^2$, the coefficients α_{00} and β_{00} are: $\alpha_{00} = N_0 \frac{2p_e^2}{\varepsilon_0 \hbar} \eta_{00}$, $\beta_{00} = \frac{2p_e^2}{\varepsilon_0 \hbar} N_0 G_{0n} T_1 \eta_{00}$, and η_{00} is defined as $\eta_{00} = \frac{T_1 \exp(-j2\pi\nu_0 T_1)}{\sqrt{1 + (2\pi\nu_0 T_1)^2}}$.

As it follows from Eqs. (5.43) and (5.45), the intensity of the laser emission in the steady-state mode $|E_{0L}|^2$ is determined as: $|E_{0L}|^2 = \frac{\alpha_{00}}{\beta_{00}}\left(1 - \frac{1}{\alpha_{00}\beta_{00}}\right)$, in which the ratio of coefficients (α_{00}/β_{00}) is $(\alpha_{00}/\beta_{00}) = \frac{1}{G_{0n} T_1}$.

Equations (5.43) and (5.45) allow the calculation in the mentioned mode of the instantaneous values of the strength E_n, the oscillations' amplitude, frequency, and phase, and to take into account contributions of different physical quantities including the noisy impact and the spontaneous emission. The feature of these Eqs. (5.43) and (5.45) is that they are similar in the form to well-studied radio electronics fluctuation equations for the *double-circuit autonomous oscillator with the linear-cubic dependence* of the nonlinear inertial element upon the AC component of the voltage or current. But the coefficient included in Eqs. (5.74) and (5.76) are

expressed through the AC physical quantities of the laser: the population, the dipole moment, the lifetime on the upper operation level, the time constant of the laser optical filter, the Langevinian noise sources of the optical emission, population, and polarization.

The transfer from Eqs. (5.43) and (5.45) to the abbreviated equations and their linearization permits not only to determine in the steady-state mode the intensity of the laser emission, but to note down the abbreviated equations with fluctuations, from which we obtain the values for the power spectral density of phase and amplitude noises.

At analysis of Eqs. (5.43) and (5.45), we may make one more important conclusion: three last terms of the Langevinian sources in the right part of Eq. (5.45) determine the total noises of the ξ_{SN} impact accordion to the formula:

$$\xi_{SN} = \xi_N E_n \frac{T_1 \exp(-j2\pi\nu_0 T_1)}{\sqrt{1+(2\pi\nu_0 T_1)^2}} + \frac{\xi_P}{-(2\pi\nu_0)^2 + j(1/T_2)(2\pi\nu_0) + (2\pi\nu_{12})^2} + \xi_E. \tag{5.46}$$

We can neglect by the second and third terms included in the last expression (Eq. 5.46) at large pumping excess over the threshold value. Therefore, we can consider that the main fluctuation impact in the laser is the noise of the inversed population ξ_N. These noises depend upon the strength value E_n and the carrier lifetime T_1. The typical feature of fluctuations is the presence of inertia property, which is determined by the exponential function argument $-j2\pi\nu_0 T_1$.

We introduce the designation for short notation:

$$Q(p) = \left[p^2 + \frac{1}{T_{0F}}p + (2\pi\nu_{0F})^2\right]\left[p^2 + \frac{1}{T_2}p + (2\pi\nu_{12})^2\right]. \tag{5.47}$$

If to take into account the delay in the circular optical channel of the laser resonator by the T_L time, the expression for the symbolic equation (Eq. 5.45) takes the form of the symbolic equation with the inertial active element:

$$Q(p)E_n = \frac{S_{NE}(E_n)}{\sqrt{1+(2\pi\nu_0 T_1)^2}} \exp[-j2\pi\nu_0(T_1+T_L)] + \xi_{SN}, \tag{5.48}$$

where $S_{NE}(E_n) = [\alpha_{001}E_n - \beta_{001}E_n|E_n|^2]$, and new coefficients α_{001} and β_{001} are: $\alpha_{001} = N_0 \frac{2p_e^2}{\varepsilon_0 \hbar} T_1$, $\beta_{001} = \frac{2p_e^2}{\varepsilon_0 \hbar} N_0 G_{0n} T_1^2$. We note that in Eq. (5.48), the inertia property depends not only upon the delay time T_L of oscillations in the optical channel of the laser resonator, but it determines the carrier lifetime T_1 on the upper operation level.

In the analog model presented in Fig. 5.6, we see that the noise impact sources are included in the circular laser circuit with the help of adders. The obvious representation of the laser with Langevinian noise sources simplifies understanding of

contributions of the spontaneous emission, the amplitude noise, the medium polarization noises into formation of the power spectral density of phase noises.

Thus, we can conclude that we obtain for QWLD the fluctuation symbolic equation (Eq. 5.48) in the steady-state mode for values $N = N_0$ and $E_n = E_{0n}$ at large (by 4–10 times) excess of pumping $\alpha_{N00} \cdot J_{0L}$ over the threshold value. Deduced differential equation coincides in the form with the symbolic equation, which is usually used for calculation of the power spectral density of the amplitude and phase noises in traditional double-circuit RF oscillators with delay.

5.4.4 PSD of Amplitude and Phase Noise of the Laser

Let us perform the calculation of PSD of amplitude and phase noises of the laser at linearization of the fluctuation symbolic equation (Eq. 5.45). The total complex noisy component ξ_{SN} can be presented as a sum of the real ξ_{SNRe} and imaginary ξ_{SNIm} parts: $\xi_{SN} = \xi_{SNRe} + j\xi_{SNIm}$.

We use the standard approach for abbreviation of differential equations according to Evtianov method [1] for finding the PSD of amplitude and phase noises for the laser. We choose the own frequency of the laser optical resonator $2\pi\nu_{0F}$ as the reference frequency. Replacing p to $j2\pi f_{0e} + p_1$, combining terms in groups according to the smallness order, keeping only the first order of smallness terms, we obtain the expression for the abbreviated conductance in the first approximation in the left part of Eq. (5.48) [1]. Then, abbreviated equations for the slowly changing functions $Q_{Re}(p)$ and $Q_{Im}(p)$ at transfer to the operator p_1 will take the form $Q_{Re}(p) \xrightarrow{j2\pi\nu_0+p_1} Q_{FRe}(p_1)$, $Q_{Im}(p) \xrightarrow{j2\pi\nu_0+p_1} Q_{FIm}(p_1)$, where the arrow "$\xrightarrow{j2\pi f_{0e}+p_1}$" designates the representation of the controlling conductance in the abbreviated form.

Let us transfer to the frequency form of notation of expressions for $Q_{FRe}(p_1)$ and $Q_{FIm}(p_1)$. We replace the operator p_1 to the value of frequency offset F from the optical carrier $\nu_0 = \nu_{0L}$, where $F = 2\pi(\nu - \nu_0)$, ν is the current frequency of the analysis, and $\nu_0 = \nu_{0L}$ is the average frequency of the laser generation:

$$Q_{FRe}(F) = (1 + T_{0F}F)\cos[F(T_1 + T_L)]/(P_{0L}K_{0L}); \tag{5.49}$$

$$Q_{FIm}(F) = (1 + T_{0F}F)\sin[F(T_1 + T_L)]/(P_{0L}K_{0L}), \tag{5.50}$$

where P_{0L} is the laser power, K_{0L} is the transfer function on power in the optical channel of the resonator.

Further, to obtain the spectral representations of S_{SLRe} and S_{SLIm} for ξ_{SNRe} and ξ_{SNIm}, we use the Fourier transform and the Wiener–Khinchin theorem: $\xi_{SNRe} \xrightarrow{F\Re} S_{SNRe}$; $\xi_{SNIm} \xrightarrow{F\Re} S_{SNIm}$; where the designation "$\xrightarrow{F\Re}$" means the transfer from fluctuations in the time domain to spectral representations when using the Fourier transform and the Wiener–Khinchin theorem.

Now we perform the linearization of the function $S_{NE}(E_n)$ in the right part of Eq. (5.48) in the vicinity of above-mentioned steady-state values. We obtain for PSD of the amplitude $S_{ANL}(F)$ and phase $S_{PNL}(F)$ noises the following expressions:

$$S_{ANL}(F) = S_{mL} = \frac{(Q_{F\,Re} - S_{0E})^2 S_{SL\,Re} + (Q_{FIm})^4 S_{SLIm}}{\left[(Q_{F\,Re} - \sigma_{EL})(Q_{F\,Re} - S_{0E}) + (Q_{FIm})^2\right]^2}; \tag{5.51}$$

$$S_{PNL}(F) = S_{\varphi L} = \frac{(Q_{F\,Re} - \sigma_{EL})^2 S_{SLIm} + (Q_{FIm})^2 S_{SL\,Re}}{\left[(Q_{F\,Re} - \sigma_{EL})(Q_{F\,Re} - S_{0E}) + (Q_{FIm})^2\right]^2}; \tag{5.52}$$

where $S_{0E} \approx 1$ and σ_{EL} is 0.1–2.

In the general case, for the laser with delay in the optical feedback channel, the abbreviated representations are true:

$$(Q_{F\,Re})^2 = (1 + T_{0F}F)^2 \cos^2(FT_L)/(P_{0L}K_{0L}), \tag{5.53}$$

$$(Q_{FIm})^2 = (1 + T_{0F}F)^2 \sin^2(FT_L)/(P_{0L}K_{0L}). \tag{5.54}$$

We examine the case when values $\sin(FT_L) = 0$ and $\cos(FT_L) = 1$, then $Q_{FRe} = FT_{OF} + 1$; $Q_{FIm} = 0$. In this case, amplitude fluctuations are caused by the in-phase noise component only, while the phase fluctuations are caused by the quadrature component only:

$$\begin{cases} S_{ANL}(F) = S_{mL} = \dfrac{S_{SN\,Re}}{(Q_{F\,Re} - \sigma_{EL})^2}; \\ S_{PNL}(F) = S_{\varphi L} = \dfrac{S_{SNIm}}{(Q_{F\,Re} - S_{0E})^2}. \end{cases} \tag{5.55}$$

Substituting $Q_{FRe} = FT_{OF} + 1$; $Q_{FIm} = 0$; $S_{0E} = 1$ into Eq. (5.55), we obtain expressions for AN and PN noise of the laser:

$$\begin{cases} S_{ANL}(F) = S_{mL} = \dfrac{S_{SL\,Re}}{(FT_{OF} + 1 - \sigma_{EL})^2}; \\ S_{PNL}(F) = S_{\varphi L} = \dfrac{S_{SNIm}}{(FT_{OF} + 1 - S_{0E})^2} = \dfrac{S_{SLIm}}{(FT_{OF})^2}. \end{cases} \tag{5.56}$$

Transformation of spectra of relative noise amplitude strengths, as it follows from Eq. (5.56), occurs as in the single-chain RF RC-circuit with the time constant $T_{OF}/(1 - \sigma_{EL})$ and the transfer function on zero frequency $1/(1 - \sigma_{EL})$. The value of $1 - \sigma_{EL}$ is usually called the "limit cycle durability" in the nonlinear oscillation theory, and typical values in oscillators are usually 0.1–2. The case $1 - \sigma_{EL} = 0$ corresponds to the oscillation stability boundary. For considered case, when the

normalized values of $\sin(FT_L) = 0$ and $\cos(FT_L) = 1$, the value $S_{0E} = 1$, which in the considered case takes into account that after passing through the laser active element, the transformation slope of phase fluctuations is equal to 1. From the last expressions, it follows that the laser noises (similar to the noises of the RF autonomous oscillator) are determined by the time constant of the optical filter T_{OF} or the Q-factor of the optical resonator and by the oscillation power.

5.4.4.1 Laser PSD with Account of the Relaxation Resonance Peak

Deduced expressions (Eqs. 5.45 and 5.55) for laser PSDs not completely reflect of the important physical phenomenon in the laser—the presence of the relaxation resonance (or the photon-electron resonance) on the offset frequency from the carrier frequency and this offset frequency is equal: $\omega_{00L} = 2\pi f_{00L} = (2\pi/T_1) \times \sqrt{G_0(\alpha_{00L} - 1)}$, where T_1 is the carrier life, G_0 is the gain (saturation coefficient), $\alpha_{00L} = \alpha_{N00} \cdot J_{0L}$ is the DC component of pumping.

The transfer function K_{LD} of QWLD with the direct small-signal modulation, the module of the transfer function of the RF selective filter K_F and tvhe first harmonic of OEO DM RF oscillations, which have the average oscillation frequency about 10 GHz. As it is shown in Chap. 3, K_{LD} is determined by the formula: $K_{LD}(j\omega) = \frac{\omega_{00L}^2}{\left[\omega^2 - \omega_{00L}^2 - j\omega\alpha_{N00} \cdot J_{0L}\right]}$.

To take into consideration in the laser PSD of the relaxation resonance on ω_{00L}, we examine the symbolic differential equations (Eq. 5.46) of fourth order in the small-signal mode, which were presented in Sect. 5.2 for the e_L^2 variable. We remind that e_L^2 и has an essence of deviations from E_{00L}^2 of the intensity component E_{0L}^2 (or the strength square) of the laser optical emission, which operates in the steady-state point E_{00L}^2, and $E_{0L}^2 = E_{00L}^2 + e_L^2$. Adding Eq. (5.46), as in Eq. (5.45), by the total noise component ξ_{SN1}, we take $\alpha_{00L} = \alpha_P$ and obtain fluctuation equations of QWLD in the quasi-stationary small-signal mode with account of the relaxation resonance:

$$\left[p^2 + \frac{1}{T_{OF}}p + \omega_{0F}^2\right]\left[p^2 + \alpha_{00L}p + \omega_{00L}^2\right]e_L^2 = p^2 G_0^2 E_{0L}^2 N_{00} e_L^2 + \xi_{SN1}, \qquad (5.57)$$

where $\alpha_{00L} = \alpha_{N00} \cdot J_{0L}$.

We should note that in Eq. (5.57), the first multiplier $\left[p^2 + \alpha_{00L}p + \omega_{00L}^2\right]$ in the left part of the differential equation takes into account the DMping decrement (or losses) $\alpha_{00L} = \alpha_P$. It is equal to the DC component of pumping and has the natural resonance frequency of the relaxation resonance ω_{00L}. In other words, in this case, the DC component of pumping determines the resonance peak width. For such a case, abbreviates representations of the left part of the differential equation (Eq. 5.56) at $Q_{FIm} = 0$ for Q_{FRe} take the form: $(Q_{FRe})^2 = (1 + T_{0F}F)^2 [1 - T_1(F - F_{00L}) - G_0N_{00}]^2/(P_{0L}K_{0L})$, where $F_{00L} = 2\pi(f - f_{00L})$ (the relaxation resonance frequency f_{00L}).

Now we represent the approximated formulas for calculation of PSD of amplitude and phase noises of the laser at linearization of the fluctuation symbolic equation (Eq. 5.56). We use the same approach of PSD determination for AN and PN noises, as we applied for Eq. (5.45). As a result, we obtain for PSD of amplitude and phase noise the following expressions:

$$S_{\mathrm{AN}} = \frac{D_{01} S_{\mathrm{SL\,Re}}}{T_1^4 \left| F^2 - F_{00\mathrm{L}}^2 - jF[(1/T_{0\mathrm{F}}) + (1/T_1) - G_0 N_{00}] - \sigma_{\mathrm{EL}} \right|^2}, \tag{5.58}$$

$$S_{\mathrm{PN}} = \frac{D_{11} S_{\mathrm{SLIm}}}{|FT_1|^2} + \frac{D_{22} S_{\mathrm{SLIm}}}{T_1^4 \left| F^2 - F_{00\mathrm{L}}^2 - jF \cdot [(1/T_{0\mathrm{F}}) + (1/T_1) - G_0 N_{00}] \right|^2}, \tag{5.59}$$

where $F = 2\pi(\nu - \nu_0) = 2\pi(f - f_0)$ is the current frequency offset from the carrier frequency, D_{01}, D_{11}, and D_{22} are constant coefficients.

Formulas (Eqs. 5.58 and 5.59) show that the total AN and PN noises of the laser emission intensity depend upon $F_{00\mathrm{L}} = 2\pi(f - f_{00\mathrm{L}})$, parameters of the optical resonator $T_{0\mathrm{F}}$, the carrier lifetime T_1 on the upper operation level and the pumping level.

Theoretical functions are constructed using the formulas (Eqs. 5.58 and 5.59). At that, for calculation, we take the parameters of QWLD with narrowband optical resonator (the spectral line width is relatively 1 kHz (Fig. 5.13a) and 10 kHz on the Bragg cell base with $T_1 = 10^{-9}$ s, $T_2 = 10^{-12}$ s and the effective time constants of the optical resonator of $T_{\mathrm{OF}} = 10^{-4}$ s (Fig. 5.13a) and $T_{\mathrm{OF}} = 10^{-5}$ s). At optical frequency detuning from the carrier $F(\nu - \nu_0) = 10$ kHz, PSD of the QWLD phase noise is well approximated by the function $S_{\psi\mathrm{L}} = \beta_{\mathrm{sp}}/[10T_{\mathrm{OF}}(\nu - \nu_0)^2]$ (where β_{sp} is the constant characterizing the spontaneous noise of the laser) is $S_{\psi\mathrm{L}} = -120$ dBm/Hz and $S_{\psi\mathrm{L}} = -116$ dBm/Hz.

Now we can make the following conclusion: the total amplitude and phase noises of the laser emission intensity depend upon the power spectral densities of the carrier noise, the time constant of the optical resonator, the carrier lifetime on the upper energy level, and the pumping level. Further, we shall write the system of abbreviated equations of the laser amplitude and phase with fluctuations, which can be used for the noise analysis in OEO DM and OEO MZ.

5.4.5 *Abbreviated Equations for Amplitude and Phase with Fluctuations*

At analysis of OEO DM and OEO MZ with laser fluctuations, we can use two systems of differential abbreviated equations, which are presented below in the time domain for the laser single-state single-frequency mode. If it is necessary to take into consideration the population influence, for the slowly changing functions of the amplitude $E_{0\mathrm{L}}^2$, the phase $\varphi = \varphi_{10\mathrm{n}}$, the population N, we can use the system of three

abbreviated equations, which are obtained from the earlier-considered differential equations for the laser:

$$\begin{cases} \mathrm{d}E_{0\mathrm{L}}^2/\mathrm{d}t = G_0 E_{0\mathrm{L}}^2 N - E_{0\mathrm{L}}^2/T_{0\mathrm{F}} + \xi_{\mathrm{E1}}, \\ \mathrm{d}N/\mathrm{d}t = \alpha_{\mathrm{N00}} \cdot J_{0\mathrm{L}} + \alpha_{\mathrm{N01}} \cdot J_{\mathrm{L1}} - \dfrac{N_{0\mathrm{L}}}{T_1} - G_0 N E_{0\mathrm{L}}^2 + \xi_{\mathrm{N1}}, \\ \mathrm{d}\varphi_{10\mathrm{n}}/\mathrm{d}t = 2\pi\nu_{0\mathrm{P}} - 2\pi\nu_0 + \sigma_{0\mathrm{L}} + \rho_{0\mathrm{L}} E_{0\mathrm{L}}^2 + \xi_{\varphi 1}. \end{cases} \tag{5.60}$$

In Eq. (5.60), the first two equations are related with each other through parameters $E_{0\mathrm{L}}^2$ and N. The third equation for the slowly changing phase is dependent upon parameters $E_{0\mathrm{L}}^2$ and N, which are determined by the first two equations of Eq. (5.60) system. There are constant coefficients (σ_{n} and ρ_{n}) in the third equation, and the natural frequency of the laser optical resonator $\nu_{0\mathrm{P}}(N)$ depends upon the population $N = N_{0\mathrm{L}}$. The second system of abbreviated differential equations presented below is formed for the single-state single-frequency quasi-stationary mode of the laser and can be simplified by introduction of α_{n} and β_{n} parameters (for the nonlinear laser element) excluding the population difference N:

$$\begin{cases} \dfrac{\mathrm{d}E_{10\mathrm{n}}}{\mathrm{d}t} = \alpha_{\mathrm{N00}} \cdot J_{0\mathrm{L}} + \alpha_{\mathrm{N01}} \cdot J_{\mathrm{L1}} - \dfrac{1}{T_{0\mathrm{F}}} E_{10\mathrm{n}} - \beta_{\mathrm{n}} (E_{10\mathrm{n}})^2 + \xi_{\mathrm{EE}}, \\ \dfrac{\mathrm{d}\varphi_{10\mathrm{n}}}{\mathrm{d}t} = (2\pi\nu_{\mathrm{n}} - 2\pi\nu_{0\mathrm{n}}) + \sigma_{\mathrm{n}} + \rho_{\mathrm{n}} (E_{10\mathrm{n}})^2 + \xi_{\varphi\varphi}. \end{cases} \tag{5.61}$$

The system (Eq. 5.61) consists only of the two equations and represents the simplified notation of the Eq. (5.60) system. The first equation for the slowly changing amplitude $E_{\mathrm{n}10}$ consists of α_{n} and β_{n} parameters, which determine the nonlinear function of the laser nonlinear element. The second equation of Eq. (5.61) for the slowly changing phase of the laser oscillation field. In this system, we exclude the abbreviated equation for the population N, but, nevertheless, its influence is taken into account by coefficients α_{n} and β_{n}.

5.4.6 *Symbolic Fluctuation Equations of OEO*

To form the system of fluctuation differential equations for OEO DM (Fig. 5.6), we consider the oscillation of the laser strength E_{n} (Eq. 5.28) and the AC electrical component i_{L} (Eq. 5.29) with the amplitude of the first harmonic of the laser pumping current $J_{1\mathrm{L}}$: $E_{\mathrm{n}} = E_{10\mathrm{L}}\ \mathrm{Re}\ [\exp(2\pi\nu_0 t)]$, $i_{\mathrm{L}} = J_{10\mathrm{L}}\ \mathrm{Re}\ [\exp(2\pi f_0 t)]$, where ν_0 and f_0 are the average oscillation optical and RF frequencies.

We take as initial the system of differential equations (Eq. 5.43) for the square strength amplitude E_{n} of the electrical component of EMF with the amplitude of the first harmonic of $E_{10\mathrm{L}}$.

We take into consideration that in OEO DM, two oscillations $\alpha_{N0} = \alpha_{N00} \cdot J_{0L} + \alpha_{N01} K_{DL} E_n E_n^* = \alpha_{N00} + \alpha_{N01} K_{DL} |E_n|^2$ are added on the PD area.

Although E_n is, in the general case, $E_n = E_{0n} + E_{1n}$, here in the right part, the second term $\alpha_{N01} K_{DL} E_{1n} |E_{1n}|^2$ represents only the AC component of E_{1n}, since the DC component is filtered out by the "PD-A-F" circuit. The DC component of pumping independently affects the QWLD active substance, i.e., QWLD is supplied by the pumping current through the independent external circuit. Cutting down of algebraic transformations, under condition of the laser operation in the single-state single-frequency quasi-stationary mode (i.e., at average population level N_{02} above the threshold value), from the equation systems (Eqs. 5.42 and 5.43), we obtain for the "Laser" and for OEO DM the following system of symbolic equations with fluctuating noise sources at modulation by the AC pumping current i_{1L}:

Fluctuation differential equations for OEO DM:

$$\begin{cases} \left[p^2 + \frac{1}{T_{0F}} p + (2\pi\nu_{0F})^2\right]\left[p^2 + \frac{1}{T_2} p + (2\pi\nu_{12})^2\right] E_n = \alpha_{00} E_n + \alpha_{N01} J_{1L} E_n - \beta_{00} E_n |E_n|^2 + \xi_{ENP}, \\ \left[p^2 + (1/T_{eF}) p + (2\pi f_{0e})^2\right] J_{1L} = \cos[\Delta\phi_{OF}] \cdot |E_n|^2 \cdot \left(\frac{1}{T_{eF}}\right) \cdot K_{OF} K_{PD} S_{NY} p \exp(-p T_{FOS}) J_{1L}, \end{cases} \tag{5.62}$$

where $\alpha_{00} = N_{02} \frac{2p_e^2 (2\pi\nu)^2}{\varepsilon_0 h} - \frac{1}{T_{0F}}$; $\beta_{00} = p_e^4 N_{02} \frac{T_1 \exp(-j2\pi\nu_0 T_1)}{(2\pi\nu_{12})^2 h^2 \left[1 + (2\pi\nu_0 T_1)^2\right]^{1/2}}$. The noise component ξ_{ENP} is $\xi_{ENP} = \xi_N E_n \eta_{00} + \frac{\xi_P}{(2\pi\nu_{12})^2 Q_P} + \xi_E$, where $Q_P = (2\pi\nu_{12})^2 + (1/T_2)(2\pi\nu_{12}) + (2\pi\nu_{12})^2$ and $\eta_{00} = \frac{T_1 \exp(-j2\pi\nu_0 T_1)}{\sqrt{1 + (2\pi\nu_0 T_1)^2}}$.

Equation (5.62) permit to calculate PSD of the amplitude and phase noises for OEO DM, the instantaneous values of E_L, the amplitude, frequency and phase of oscillations as well as to take into account contributions of different physical quantities including the noisy impact ξ_{ENP} and the spontaneous emission of the carrier noise in the output emission of the laser as well as the current oscillations of the first harmonic of OEO DM.

The analog model of OEO DM is presented in Fig. 5.6a and is constructed according to the differential equations system (Eq. 5.62) as QWLD enclosed by the positive feedback loop "Feedback Chain."

The specific feature of equation (Eq. 5.62) is that they are similar in the form to well-studied equations in radio electronics for the double-circuit autonomous oscillator with linear-cubic function of the nonlinear inertial element of the AC voltage versus the current. But, coefficients included in Eq. (5.62) are expressed through the laser variable physical quantities: the population, the dipole moment, the lifetime on the upper operation level, the time constant of the laser optical filter, Langevinian noise sources ξ_{ENP} of the optical emission, the population, and polarization.

Equation (5.62) reflects the laser properties as the oscillating system in operation mode above the threshold at modulation of the AC pumping current i_{1L}. In the left part of Eq. (5.62) the operator "conductance" is presented. It is defined by the laser physical quantities: the transition frequency between the first and the second energy levels ν_{12}, the natural frequency of the optical filter included in the laser ν_{0F}, the time

constant of the active medium polarization T_2, and the time constant of the optical filter T_{0F}. Oscillations of E_n in Eq. (5.62) arise only at specific threshold value of pumping α_{N00}. In the right parts of Eq. (5.62), the $S_L = \alpha_{00}E_n - \beta_{00}E_n|E_n|^2$ expression is located, which defines the laser nonlinearity in the quasi-stationary mode.

We note that the equation system of OEO DM (Eq. 5.62) takes into consideration the *heterodyning* properties with the help of the multiplier $\cos[\Delta\phi_{OF}]$, at that, $\Delta\phi_{OF}$ is determined by the difference of the optical phases of the optical oscillations, which act on the PD after passage the optical filter. The contribution into the phase difference is made by not only the phase-frequency characteristic of the optical filter, but the phase-frequency characteristic of QWLD.

The specific peculiarity of OEO DM is the fact that the natural optical frequency of the optical filter depends on DC and AC components of pumping $\nu_{0F} = \nu_{0F}(\alpha_{N0})$ or $\nu_{0F} = \nu_{0F}(|E_n|^2)$. The DC pumping component J_{0L} in OEO DM does not depend on the state (ON-OFF) of the positive feedback loop. On the contrary, the AC pumping component of QWLD $i_{1L} = J_{1L}$ is defined by the closed loop of OEO DM, and the amplitude J_{10L} of the current i_{1L} and its radio frequency f_0 are the amplitude and frequency of the OEO DM output generation, which are determined by the module and the argument of the transfer function $K_{DL} = K_{FBN} = K_{BZ} = i_{1L}/|E_n|^2 = J_{1L}/|E_n|^2$ of the positive feedback loop: $|E_n|^2$ and $\Delta\phi_{OF}$. Therefore, in the closed loop in OEO DM, at $\cos[\Delta\phi_{OF}] = 1$ for QWLD $\alpha_{N0} = \alpha_{N00} \cdot J_{0L} + \alpha_{N01} \cdot i_L$ pumping, the expression is true: $\alpha_{N0} = \alpha_{N00}J_{0L} + \alpha_{N01}K_{DL}|E_n|^2$, where the DC pumping component $\alpha_{N00} = \alpha_{N0} \cdot J_{0L}$ defining as the product of the DC pumping current J_{0L} of QWLD by the constant coefficient α_{N00}, and $\alpha_{N01} \cdot i_L = \alpha_{N01} \cdot K_{DL} \cdot |E_n|^2$.

We must take into consideration that the laser optical frequency in OEO DM depends on the AC pumping current i_L. The AC pumping current modulates of the laser optical emission in its frequency.

At small amplitude modulation index, this tells on the accompanied frequency modulation of the QWLD strength optical oscillation, if the DE solution with the parametric dependence of the optical frequency leads to FM of oscillations and to formation of two harmonics on the left and on the right of the carrier frequency.

At direct modulation of QWLD by the pumping current, oscillations of the optical field are frequency modulated. We note that in Eq. (5.60), the natural optical frequency ν_{0P} of the laser resonator (or, which is the same, the frequency of the longitudinal generating mode of the laser resonator) depends on the inversed population N or $\nu_{0P}(N)$. Therefore, the optical frequency ν of the laser generation is dependable on the population N. At small deviations of the N population from the average value N_{0L}, the frequency deviations from the mean value ν_{0L} are equal $\nu - \nu_{0L} = C_\nu \cdot (N - N_{00L})$, where C_ν is the constant. Since the N population depends on pumping, as follows from Eq. (5.60), then at variation of the pumping current, N will change. In turn, the refraction index n_L of the laser active medium is determined by the inversed population of the active medium. At variation of the pumping current J with the frequency $f = f_0$ and the phase φ_{10L} as: $J = J_{0L} + J_{10L} \cdot \cos[(2\pi f_0 t - \varphi_{10L})]$, and the inversed population is modulated by the harmonic oscillations of the pumping current: $N = N_{0L} + N_{10L}\cos[(2\pi f_0 t - \varphi_{10LN})]$,

where N_{10L} is the amplitude of the modulated oscillations of N, φ_{10LN} is the oscillation phase; n_L also change. We take into account that at known n_L and the geometrical length L_{0L} of the optical resonator (for example, for the Fabry–Perot resonator) ν_{0P} is determined as: $\nu_{0P} = \frac{c}{2n_L L_{0L}}$, where c is the light speed in vacuum. The average optical frequency $\nu_0 = \nu_{0L}$ of the laser in the quasi-stationary mode is determined from Eq. (5.60) at $d\varphi/dt = 0$ as: $\nu_0 = \nu_{0P}(N) + \left[\sigma_{0L} + \rho_{0L}E_{0L}^2\right]/2\pi$.

Assuming that $\nu_0 - \nu_{0P} \gg \left[\sigma_{0L} + \rho_{0L}E_L^2\right]$, the laser generated optical frequency $\nu(t)$ will perform oscillations from its DC value $\nu_0 = \nu_{0L}$ at small AC component of the pumping current and also will be the periodic function: $\nu(t) = \nu_{0L} + \nu_{0P} \cdot \cos\left[(2\pi f_0 t - \varphi_{10LL})\right]$.

The spectrum of the field strength oscillations of the laser emission $E_L(t)$ represents oscillations, which are modulated in amplitude and in frequency. The field strength $E_L(t)$ for central ν_0 and two side harmonics $\nu_0 - f_0$ and $f_0 + \nu_0$ can be expressed as: $\nu_0 = \nu_{0P}(N) + \left[\sigma_{0L} + \rho_{0L}E_{0L}^2\right]/2\pi$.

The modulation of the QWLD optical frequency can be caused by not only the fast variation of the pumping current, but also by temperature variations of the refraction index of the active medium and, as the result of it, by heating/cooling of the QWLD active layer. The frequency deviation W (on level 0,7) at frequency modulation of the laser depends on the pumping current amplitude J_{10L} and the slope $\frac{d\nu}{dJ_{10L}}$ as: $W = J_{10L} \cdot \frac{d\nu}{dJ_{10L}}$. For example, for semiconductor "volumetric" injection lasers on the hetero-structures, $\frac{d\nu}{dJ_{10L}} = 10^{-3}$ THz/mA . Figure 5.7 shows the plot of the calculated optical spectra of the current modulating of the laser diode in OEO without fluctuations.

For modern cascade QWLD, the slope is $\frac{d\nu}{dJ_{10L}} = 10^{-6}$ THz/mA. The decrease approximately by 1000 times of the QWLD frequency deviation is caused firstly, by the factor of spatial restriction of optical emission (the transverse dimensions of the transition zone, in which the inversed population variations occur, are about 10 nm, the transverse dimensions of the optical channel, via which the emission propagates, are about the laser wavelength about 1000 nm); secondly, by utilization of more effective four-level pumping scheme (this is true for cascade QWLD with the number of quantum wells more than 3–4); thirdly, by decrease by more than the order of the threshold current and, accordingly, the amplitude of the AC pumping current.

If to examine the limit case of zero slopes $\frac{d\nu}{dJ_{10L}}$, then at analyzing of laser quantum-mechanical equations presented in Chap. 2, we can note that the variation of the constant field variation leads to widening and even to splitting of the quantum levels.

For the modulation amplitude of the laser current of 10 mA, the optical frequency bandwidth is $W = 10$ GHz. If this amplitude is 1 mA, the optical frequency bandwidth is $W = 1$ GHz. Thus, at growth of the laser modulation amplitude (or the modulation index), the frequency modulation band will increase.

Thus, we show that the complicate system (Eq. 5.64) from three equations is reduced in the quasi-stationary mode to relatively simple differential equations

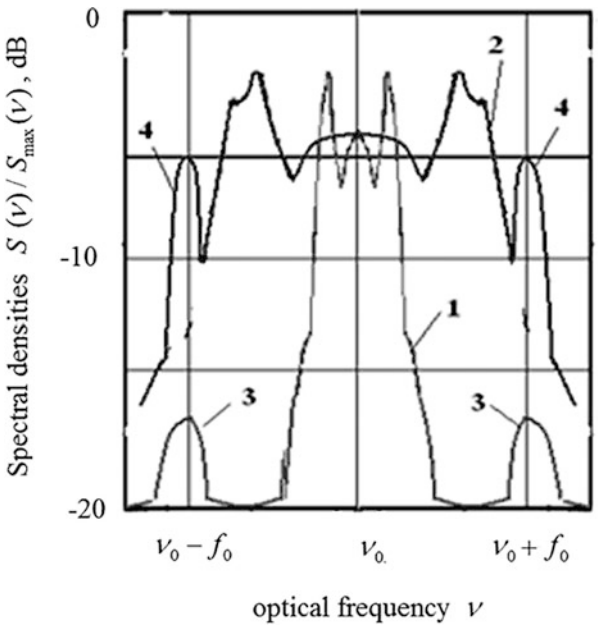

Fig. 5.7 The plot of the calculated optical spectra of the current modulating the laser diode in OEO without fluctuations. Laser optical emission spectra (curves 1 and 2) at various levels of the variable component of the pumping (curves are the harmonics of the subcarrier at a frequency of 10 GHz (curves 3.4). The differential equations (Eq. 4.104) are obtained by modeling the laser diode parameters with a carrier lifetime of 10^{-9} s, a threshold population difference of the threshold level of 10^{18} cm^{-3}, the photon lifetime of 10^{-12} s, and an LD core volume of 10^{-11} cm^{-3}. The amplitude of modulation of the pump current are 0.01 and 0.1 of the threshold pump current, respectively, curve 3 and curve 4.

(Eq. 5.62). This equation is similar to the equation for the double-circuit RF oscillator, which is repeatedly solved in the specific tasks of the oscillation theory. The specific property of this equation is the **inertial nonlinearity**, which is defined by the pumping circuit, and for lasers with the distributed pumping system with the third- and fourth-level of pumping, it is different. This is similar to the double-circuit RF oscillator equation, which was repeatedly solved in the specific problems of the oscillation tasks.

5.4.7 Differential Equations with Fluctuations and the Analog Model of OEO MZ

Before the writing of differential equation system for OEO MZ, we must explain some features of oscillation transformation in the optoelectronic structure of the "modulator of Mach–Zehnder—the coupler" (or MZ-C).

On to the PD optical input (or to light-sensitive area), the following delayed laser emission intensity falls, which represents a sum of AC and DC component:

$$(E_{12\mathrm{L}})^2 = (E_{01\mathrm{L}})^2\left(1+\gamma^2\right) + 0.5(E_{01\mathrm{L}})^2\gamma\cos\left[(\pi U_{0\mathrm{MZ}}/2U_{0\mathrm{MZ}\pi})\right.$$

$$\left.-(U_{10\mathrm{MZ}}/U_{0\mathrm{MZ}\pi})\cos\left(2\pi ft+\psi_{\mathrm{mMZ}}\right)\right]\}. \quad (5.63)$$

The AC component of the PD photocurrent is formed by the AC component of intensity. The amplified oscillations of the first harmonic, which passed the filter F, act in the input of RF amplifier. The transfer function on the first harmonic K_{F} of this filter can be defined as the RF circuit with the transformer coupling:

$$\frac{\mathrm{d}^2U_{10\mathrm{MZ}}}{\mathrm{d}t^2} + \frac{1}{T_{\mathrm{F}}}\frac{\mathrm{d}U_{10\mathrm{MZ}}}{\mathrm{d}t} + (2\pi f_{\mathrm{eF0}})^2U_{10\mathrm{MZ}} = \frac{\mathrm{d}S_{\mathrm{NY}}[U_{10\mathrm{MZ}}]}{\mathrm{d}t}. \quad (5.64)$$

Therefore, for the total intensity, we must differentiate in time of the variable $(E_{12\mathrm{L}})^2$:

$$(E_{12\mathrm{L}})^2 = 0.5(E_{01\mathrm{L}})^2\gamma\{\frac{(1+\gamma^2)}{2\gamma} + \cos\left[(\pi U_{0\mathrm{MZ}}/2U_{0\mathrm{MZ}\pi})\right.$$

$$\left.-(U_{10\mathrm{MZ}}/U_{0\mathrm{MZ}\pi})\cos\left(2\pi ft+\psi_{\mathrm{mMZ}}\right)\right]\} \quad (5.65)$$

of the voltage of the first harmonic: $U_{10\mathrm{MZ}} = [E_{12\mathrm{L}}(t-T_{\mathrm{FOS}})]^2K_{\mathrm{DL}}[1-(1+\gamma^2)/2]$.

Finally, we have for OEO MZ:

$$\begin{cases} \dfrac{\mathrm{d}^2E_{\mathrm{n}}}{\mathrm{d}t^2} + \dfrac{1}{T_{0\mathrm{F}}}\dfrac{\mathrm{d}E_{\mathrm{n}}}{\mathrm{d}t} + (2\pi\nu_{0\mathrm{F}})^2E_{\mathrm{n}} = -\dfrac{2\omega^2P_{\mathrm{n}}}{\varepsilon_{\mathrm{n}}} + \xi_{\mathrm{E}}; \\ \dfrac{\mathrm{d}^2P_{\mathrm{n}}}{\mathrm{d}t^2} + \dfrac{1}{T_2}\dfrac{\mathrm{d}P_{\mathrm{n}}}{\mathrm{d}t} + (2\pi\nu_{12})^2P_{\mathrm{n}} = \dfrac{p_{\mathrm{e}}^2}{h}NE_{\mathrm{n}} + \xi_{\mathrm{P}}; \\ \dfrac{\mathrm{d}N}{\mathrm{d}t} = \alpha_{\mathrm{N0}}J_{0\mathrm{N}} - \dfrac{N}{T_1} - \dfrac{1}{h}P_{\mathrm{n}}E_{\mathrm{n}} + \xi_{\mathrm{N}}; \\ \dfrac{\mathrm{d}^2U_{10\mathrm{MZ}}}{\mathrm{d}t^2} + \dfrac{1}{T_{\mathrm{n}}}\cdot\dfrac{\mathrm{d}U_{10\mathrm{MZ}}}{\mathrm{d}t} + (2\pi f_{\mathrm{eF0}})^2U_{10\mathrm{MZ}} = \dfrac{\mathrm{d}S_{\mathrm{NY}}[E_{\mathrm{n}},U_{10\mathrm{MZ}}]}{\mathrm{d}t} + \xi_{\mathrm{U}}. \end{cases} \quad (5.66)$$

The first three equations in the differential equation system of OEO MZ are independent with regard to the fourth, which can be introduced in the case of OEO DM for determination only of the amplitude of laser optical oscillations and PSD of amplitude and phase noises. In equations, the normalized laser power depends on the laser equation solution and is determined by the transfer function of the MZ modulator, which depends on the laser optical frequency closed to ν_{OF}.

The spectrum of RF oscillations of OEO is formed not only by noises, which have the electronic nature, but the phase fluctuations of laser optical emission, which have the *quantum nature* and are determined by the laser spontaneous emission. The spectral line width of RF oscillations is determined by parameters of two oscillating processes in the laser and on the whole in RF oscillator of OEO.

Figure 5.6b shows of the analog model of OEO MZ as QWLD enclosed by the positive feedback loop. The positive feedback on AC voltage component is formed by the circuit "the optical fiber, the photodetector PD, the RF filter F, RF amplifier A." The positive FB encloses the modulating light source (MLS). MLS is formed by the series-connected laser and the Mach–Zehnder modulator. The laser analog model is composed on the base of the fluctuation differential equations' system (Eq. 5.66).

In the structure of Fig. 5.6b, the adder and Langevinian noise sources are depicted. The dotted lines designate the possible additional circuit of FB on DC current (or voltage). The additional FB loop is intended for adjustment of the laser phase noise when using the frequency automatic control of the laser optical frequency. The optical laser oscillations pass to the PD and then act on the modulator after the optical fiber. The light interference on the PD2 area of two oscillations with the delay difference of some microseconds permits to extract the laser phase noise in the DC current of PD2, and to perform its adjustment in the block DC PUMP by means of DC laser pumping changing.

The common feature of analog models of OEO MZ (Fig. 5.6b) and OEO DM is that in them, the laser is the main energetic element and the main source of the phase noise caused by the spontaneous emission, which has the quantum character.

Analog models of OEO DM and OEO MZ are constructed on the unified principle: the enclosure by the positive FB of the modulating source of the coherent light (the laser). If in OEO DM, we use the internal (inside the optical resonator) or the direct laser modulation and the positive FB loop in OEO DM is constructed on AC component of the pumping current, then in OEO MZ, the modulation light source is the common "inseparable" unified modern construction of the "laser and the Mach–Zehnder modulator". The positive FB loop in OEO MZ is arranged on the AC voltage, and begins from the optical output of the optical modulator and finishes at the electric input of the MZ modulator.

The noticeable difference of the presented OEO MZ structure (Fig. 5.6b) from the analog model of OEO DM (Fig. 5.6b) is the fact that the laser itself in OEO MZ can be enclosed by the additional positive FB loop in DC component of the pumping current using the additional photodetector PD2, the systems of frequency automatic control or the phase-locked loop (PLL) system. We should note that in OEO DM structure (Fig. 5.6b), the implementation of the control system of the laser phase noise is possible with application of additional photodetector.

The main principal difference of the analog model of OEO MZ (Fig. 5.6b) from the analog model of OEO DM (Fig. 5.6a) is the potential possibility to use the extra-low-noise QWLDs in the OEO MZ structure. This follows from the fact that in the OEO MZ laser, as we see from the analog model in Fig. 5.6b, the carrier noise suppression can be realized directly in the internal closed loop (shown in the model) of the optical feedback or in the optical resonator. For this, we must not only reduce

the value of noise sources, but to increase the Q-factor of the optical resonator. The growth of the resonator Q-factor will significantly decrease of the laser modulation band in radio frequency. The excessive increase of the optical resonator Q-factor leads in OEO DM (Fig. 5.6a) to decrease of the oscillation amplitude. In OEO MZ, the external modulation is used. The optical modulation index does not depend upon the growth of the optical resonator Q-factor. The increase of optical resonator Q-factor will lead to improvement of the oscillation spectrum purity or to decrease of the laser phase noise. Another principal peculiarity, which can be deduced from the analysis of the presented analog model of OEO MZ (Fig. 5.6b) is the fact that carrier fluctuations' suppression can be performed in the feedback loop of population. The increase of the time constant of the carrier lifetime on the upper energy level T_1 also leads to significant decrease of the laser phase noise. In the OEO MZ structure, we have a possibility to use the high-coherent fiber-optical lasers with the large carrier lifetime of $T_1 = 0.1 - 100\,\mu s$. As we mentioned earlier, the compact modern OEO MZ uses the semiconductor QWLD with the spectral line width from 1 kHz to 10 MHz. The compact commercial samples of the semiconductor lasers appeared with the spectral line width of 10–500 Hz.

Let us transfer to simplification of the differential equation system (Eq. 5.66) with the aim to obtain the evident results for PSD of amplitude and phase noises for OEO MZ.

5.4.7.1 Differential Fluctuation Equations for OEO MZ

Let us demonstrate the deduction of PSD of the amplitude and phase noises for OEO MZ relying of the Evtianov–Kuleshov method. If we introduce in the equation system (Eq. 5.66) the operator $p = \mathrm{d}/\mathrm{d}t$ and take into consideration the total delay time $T_{\mathrm{FOS}} \approx T_{\mathrm{FOLD}}$ in the opened loop "MZ-C," introducing the transfer function of RF FODL $K_{\mathrm{FODL}} = K_{\mathrm{MZ}}K_{\mathrm{FOS}}K_{\mathrm{PD}}$, we shall obtain the system of symbolic equations with the fluctuating noise sources in the compact form for the laser and OEO:

$$\begin{cases} Q_0(p)E_{\mathrm{L}} = \alpha_{00}E_{\mathrm{L}} - \beta_{00}E_{\mathrm{L}}|E_{\mathrm{L}}|^2 + \xi_{\mathrm{SN}}, \\ i_{\mathrm{PD}} = 0.5\langle E_{\mathrm{L}}E^*_{\mathrm{L}\tau}\rangle\gamma\cos\left[\varphi_{0\mathrm{MZ}} + u_{\mathrm{MZ}}/U_{0\mathrm{MZ}\pi}\right]; \\ \left[p^2 + \dfrac{1}{T_{\mathrm{F}}}p + (2\pi f_{\mathrm{eF0}})^2\right]u_{\mathrm{MZ}} = \mathrm{K}_{\mathrm{MZ}}\mathrm{K}_{\mathrm{FOS}}pS_{\mathrm{A}}(i_{\mathrm{PD}})\exp\left[-pT_{\mathrm{FOLD}}\right] + \xi_{\mathrm{U}}. \end{cases} \tag{5.67}$$

The first equation in Eq. (5.67) is the fluctuation equation(Eq. 5.45) for the laser, which was examined earlier, and it has the operator term $Q_0(p) = Q_{0\mathrm{F}}Q_{0\mathrm{P}}$, where $Q_{0\mathrm{OF}} = \frac{p^2+(1/T_{0\mathrm{F}})p+(2\pi\nu_{0\mathrm{F}})^2}{(2\pi\nu_{0\mathrm{F}})^2}$ and $Q_{0\mathrm{P}} = \frac{p^2+(1/T_2)p+(2\pi\nu_{12})^2}{(2\pi\nu_{12})^2}$. The total noise component $\xi_{\mathrm{SN}} = \left(\xi_{\mathrm{N}}E_{\mathrm{n}}\eta_{00} + Q_{\mathrm{P}}^{-1}\xi_{\mathrm{P}} + \xi_{\mathrm{E}}\right)/(2\pi\nu_{0\mathrm{F}})^2(2\pi\nu_{12})^2$ is also determined for Eq. (5.45). Coefficients α_{00}, β_{00} included in the first equation of the system (Eq. 5.67) are defined earlier as in Eq. (5.45).

The first equation in Eq. (5.67) has a feature consisting in the fact that it reminds on the form of well-studied equations in the radio electronic double-circuit autonomous oscillator with the arc-wise cubic characteristic of the nonlinear inertial element of AC voltage as the function of the current. But, coefficients included in Eq. (5.67) are expressed through AC components of the laser physical quantities: the population, the dipole moment, the lifetime on the upper operation level, the time constant of the laser optical filter, Langevinian sources of the optical noise, the polarization.

The transfer from Eq. (5.67) to differential abbreviated equations permits not only to determinate of the laser power $|E_{0L}|^2$ in the steady-state mode as $|E_{0L}|^2 = \frac{\alpha_{00}}{\beta_{00}} \times \left(1 - \frac{1}{\alpha_{00}\beta_{00}}\right)$, but also to record abbreviated equations with fluctuations, from which we below obtain expressions for PSD of phase and amplitude noises. At that, the laser emission intensity is determined by expression $|E_{0L}|^2 = \frac{\alpha_{00}}{\beta_{00}}\left(1 - \frac{1}{\alpha_{00}\beta_{00}}\right)$. Thus, the coefficient (α_{00}/β_{00}) has the clear physical sense for lasers. The larger the amplitude of the output optical oscillation and the higher a ratio of time constant of the laser optical filter to the carrier lifetime on the upper operation level, then the higher a ratio of the relative excess of population and its level at excitation.

Taking into account the previous notation, the system of differential equations takes the simpler form:

$$\begin{cases} P_{0L} = (E_{01L})^2 = |E_n|^2 = \dfrac{\alpha_{00}}{\beta_{00}}\left(1 - \dfrac{1}{\alpha_{00}\beta_{00}}\right); \\ U = K_{MZ}K_{FOS}P_{0L}\{1 + \cos[(\pi U_{0MZ}/2U_{0MZ\pi}) + (U_{1MZ}/U_{0MZ\pi})]\}; \\ \left[p^2 + \dfrac{1}{T_F}p + (2\pi f_{eF0})^2\right]U = S_{NY}(pU)\exp[-pT_{FOLD}] + K_{MZ}K_{FOS}\psi_{mMZ}. \end{cases} \tag{5.68}$$

In order to deduce a formula for PSD of the noise, we widen the abbreviated representation $Q_0(p)$, which is designated in the real and imaginary parts: $Q(p) = Q_{Re}(p) + jQ_{Im}(p)$, where $Q_{FRe} = \frac{(1+FT_F)\cos(FT_L)}{P_{0L}|K_{0L}|}$ and $Q_{FIm} = \frac{(1+FT_{0F})\cos(FT_L)}{P_{0L}|K_{0L}|}$.

The delay in the resonator is T_L, $|K_{0L}|$ is the coefficient of the full losses of the optical power in the laser feedback loop. Now we present the total noise complex component by a sum of real and imaginary parts as: $\xi_{SN} = \xi_{SNRe} + j\xi_{SNIm}$.

Using the standard approach to the abbreviation of differential equations with the fluctuating sources, the Fourier transform, the Wiener–Khinchin theorem, we obtain the PSD of laser amplitude and phase noises. The real part ξ_{SNRe} has in the spectral representation the form S_{SLRe}, while the imaginary part ξ_{SNIm} has a form S_{SLIm}.

PSD equations obtained from Eq. (5.67) for the laser phase noise, which operates in the quasi-stationary mode (single-mode and single-frequency), have the following form:

$$S_{\mathrm{PL}} = \frac{(Q_{\mathrm{F\,Re}} - \sigma_{\mathrm{EL}})^2 S_{\mathrm{SLIm}} + (Q_{\mathrm{FIm}})^2 S_{\mathrm{SL\,Re}}}{\left\{(Q_{\mathrm{F\,Re}} - \sigma_{\mathrm{EL}})(Q_{\mathrm{F\,Re}} - S_{0\mathrm{E}}) + (Q_{\mathrm{FIm}})^2\right\}^2}; \tag{5.69}$$

where $S_{0\mathrm{E}} = 1$, σ_{EL} is the local slope of the nonlinear characteristic of the active medium of QWLD $\sigma_{\mathrm{EL}} = \alpha_{00} - \beta_{00}|E_{0\mathrm{L}}|^2$. If for Eq. (5.69) we consider the case when the imaginary part $Q_{\mathrm{FIm}} = 0$, $P_{0\mathrm{L}}K_{0\mathrm{L}} \approx 1$ and there is small delay, i.e., $\cos^2(FT_{\mathrm{L}}) \approx 1$, $\sin^2(FT_{\mathrm{L}}) \approx 0$, then the expression (Eq. 4.112) for PSD takes the classic form:

$$S_{\mathrm{PL}} = \frac{S_{\mathrm{SLIm}}}{(1 + T_{0\mathrm{F}}F - \alpha_{00} + \beta_{00}P_{0\mathrm{L}})^2} \approx \frac{S_{\mathrm{SLIm}}}{P_{0\mathrm{L}}(T_{0\mathrm{F}}F)^2}; \tag{5.70}$$

where $P_{0\mathrm{L}} = E_{0\mathrm{L}}^2$ is the power of the optical emission in the light-sensitive PD region.

The expression (Eq. 5.70) defines that the power increase and the time constant $T_{0\mathrm{F}}$ increase of the laser resonator (or the increase of the resonator Q-factor) leads to the decrease of the laser phase noise.

The expression (Eq. 5.70) for the laser PSD of the phase noise does not reflect the important property of the laser oscillation system: the presence of the relaxation resonance on the frequency $\nu_{00\mathrm{L}}$ with the offset from the carrier frequency $\nu_{0\mathrm{L}}$, i.e., at $F_{00\mathrm{L}} = 2\pi(\nu_{00\mathrm{L}} - \nu_{0\mathrm{L}})$. The "resonance peak" can be taken into consideration at the system (Eq. 5.66) linearization, taking into account the population equation. At that, the expression for PSD of the laser phase noise takes a form:

$$S_{\mathrm{PL}}/P_{0\mathrm{L}} \approx \frac{S_{\mathrm{SLIm}}}{(FT_{0\mathrm{F}})^2} + \frac{S_{\mathrm{LE}}D_{11}^2 + S_{\mathrm{LN}}D_{22}{}^2}{T_{0\mathrm{F}}^4\left\{\left(F^2 - F_{00\mathrm{L}}^2\right)^2 + [F(1/T_{0\mathrm{F}}) + (1/T_1)]^2\right\}}, \tag{5.71}$$

where $F_{00\mathrm{L}} = \frac{1}{T_1}\sqrt{(T_{0\mathrm{F}}/T_1)\alpha_{\mathrm{N}00} \cdot J_{0\mathrm{L}} - 1}$, $\alpha_{\mathrm{N}00} \cdot J_{0\mathrm{L}}$ is the excess of the DC pumping above its threshold value, D_{11} and D_{22} are constant coefficients, S_{LE} is PSD of the noise defining by the noisy component ξ_{E} of the strength $E_{\mathrm{n}} = E_{\mathrm{L}}$, S_{LN} is PSD of the noise defining by the noisy component ξ_{N} of carrier population N in the QWLD active material. Features of Eq. (5.71) derivation from the system (Eq. 5.66) are discussed in Chap. 6 (Sect. 6.6).

Figure 5.8 shows the plot of PSD of the laser phase noise (curve 1) calculated by the formula (Eq. 5.71) for $S_{\mathrm{SLIm}} \approx S_{\mathrm{LE}}D_{11}^2 + S_{\mathrm{LN}}D_{22}^2 \approx -10^5$ dB/Hz, $F_{00\mathrm{L}} \approx 14$ kHz, $T_{0\mathrm{F}} = 10^{-7}$ s.

From Eq. (5.67), with account of Eq. (5.68), for the nonlinear characteristic of the RF amplifier in the form of the cubic polynomial $i_{\mathrm{A}}(u) = \alpha_{\mathrm{e}0}u - \beta_{\mathrm{e}0}u^3$ (where u is the instantaneous voltage in the amplifier input and the average slope of this characteristic is $\sigma_{\mathrm{U}} = \alpha_{\mathrm{e}00} - (3/4)\beta_{\mathrm{e}00}P_{0\mathrm{G}}$), we can obtain the RF generation power of OEO $P_{0\mathrm{G}} = P_{0\mathrm{OEO}}$ for parameters of the laser and the delay line:

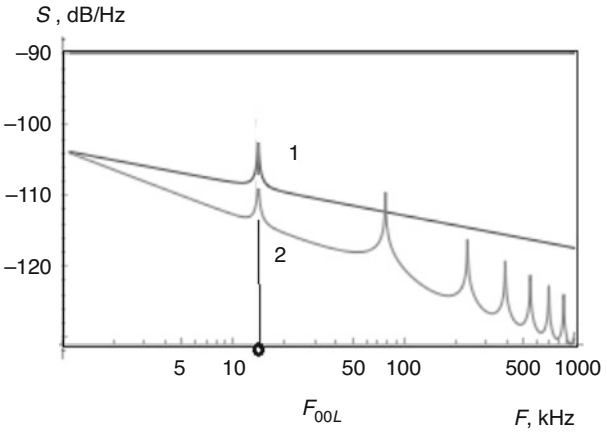

Fig. 5.8 PSD of the laser phase noise (curve 1) and PSD of the OEO MZ phase noise (curve 2)

$$P_{0G} = \frac{\alpha_{e00}}{\beta_{e00}}\left(1 - \frac{1}{P_{0L}|K_{FOLD}|\alpha_{e00}\beta_{e00}}\right)$$
$$\approx \frac{\alpha_{e00}}{\beta_{e00}}\left(1 - \frac{1}{2\frac{(N_{02}-N_{01})h}{N_{02}\varepsilon_n}\frac{T_{0F}}{T_1}|K_{FOLD}|\alpha_{e00}\beta_{e00}}\right). \quad (5.72)$$

Similarly to Eq. (5.69) for the laser PSD, from the general symbolic equation (Eq. 5.67), we obtain the equation for PSD $S_\Psi$for the OEO phase noise. The PSD S_Ψ reduced to the power P_{0G} of RF oscillation is determined by the following expression according to the Evtianov–Kuleshov method:

$$S = \frac{S_\Psi}{P_{0G}} = \frac{(Y_{a\,Re} - \sigma_U)^2 S_{ImFDNY} + Y_{aIm}^2 S_{Re\,FDNY}}{P_{0G}\left\{[Y_{a\,Re} - \sigma_U][Y_{a\,Re} - 1] + [Y_{aIm}]^2\right\}^2}, \quad (5.73)$$

where S_{ImFDNY}, S_{ReFDNY} are in-phase and quadrature components of fluctuations, which are determined by the mutual noises of the laser, the photodiode and the amplifier of the OEO closed loop; Y_{aRe}, Y_{aIm} are in-phase and quadrature components of OEO controlling conductance (abbreviated representations) ($Y_a = Y_{aRe} + jY_{aIm}$):

$$Y_{a\,Re} = y_M \frac{(1 + FT_F)\cos(FT_{FOLD})}{P_{0L}|K_{FODL}|} \approx y_M \frac{(1 + FT_F)\cos(FT_{FOS})}{P_{0L}|K_{FODL}|}, \quad (5.74)$$

$$Y_{aIm} = y_M \frac{(1 + FT_F)\sin(FT_{FOLD})}{P_{0L}|K_{FODL}|} \approx y_M \frac{(1 + FT_F)\sin(FT_{FOS})}{P_{0L}|K_{FODL}|}, \quad (5.75)$$

where the offset frequency $F = 2\pi(f - f_0)$ is difference of frequency of analysis f and frequency of OEO generation f_0; $|K_{FODL}|$ is the module of the transfer function of the

opened OEO loop, $T_{\mathrm{FODL}} \approx T_{\mathrm{FOS}}$ is the total oscillations delay time in the opened OEO loop including the delay in FOS, y_{M} is the normalized input electrical conductance of the MZ modulator.

If we consider the case for Eq. (5.73), when the imaginary part $Y_{\mathrm{aIm}} = 0$, $P_{0\mathrm{L}}|K_{\mathrm{FODL}}| \approx 1$ and there is the small delay, i.e., $\cos^2(FT_{\mathrm{L}}) \approx 1$. We recall, that here, we consider the case of generation of the first harmonic in the OEO MZ, and accordingly, the first harmonic of the voltage acts on the electrical input of MZ. Then the expression for PSD (Eq. 5.73) takes the classic form:

$$S = \frac{S_{\mathrm{PLIm}}}{\left(1 + T_{\mathrm{F}}F - \alpha_{\mathrm{e00}} + \beta_{\mathrm{e00}}P_{0\mathrm{G}}\right)^2} \approx \frac{S_{\mathrm{PLIm}}}{P_{0\mathrm{G}}\left(T_{\mathrm{F}}F\right)^2}. \tag{5.76}$$

Here we consider the case, where the laser's detected phase noise of the QWLD in the load resistor of the photodetector prevails over the intrinsic phase noise of the photodetector and the phase noise of the RF amplifier. We assume that the laser phase noise in the photocurrent predominates over fluctuations of the shot noise of PD and the noise of RF amplifier.

We substitute Eq. (5.70) in Eq. (5.76), then we obtain the simple formula for transformation of the phase noise fluctuations:

$$S \approx \frac{S_{\mathrm{PDPLIm}}}{P_{0\mathrm{G}}\left(T_{\mathrm{F}}F\right)^2} = \frac{P_{0\mathrm{L}}S_{\mathrm{PLIm}}}{P_{0\mathrm{G}}\left(T_{\mathrm{F}}F\right)^2} = \frac{\frac{P_{0\mathrm{L}}S_{\mathrm{SLIm}}}{P_{0\mathrm{L}}\left(T_{0\mathrm{F}}F\right)^2}}{P_{0\mathrm{G}}\left(T_{\mathrm{F}}F\right)^2} = \frac{S_{\mathrm{SLIm}}}{P_{0\mathrm{G}}\left(T_{0\mathrm{F}}F\right)^2\left(T_{\mathrm{F}}F\right)^2}. \tag{5.77}$$

From Eq. (5.77) we see that the laser phase noise decreases with the laser resonator Q-factor growth and the Q-factor of the RF filter F, but with the account of Eqs. (5.69) and (5.73), we have:

$$S \approx \frac{S_{\mathrm{PD}} \cdot E_{0\mathrm{L}}^2}{16\left(T_{0\mathrm{F}}F\right)^2\left(T_{\mathrm{F}}F\right)^2} S_{\mathrm{L}\psi 1}(F) + \frac{E_{0\mathrm{L}}^2\sigma_{\mathrm{EL}}^2}{P_{0\mathrm{G}}4\left(T_{0\mathrm{F}}F\right)^2\left(T_{\mathrm{F}}F\right)^2} S_{\mathrm{Lm}}(F). \tag{5.78}$$

Here, $S_{\mathrm{L}\psi 1}(F)$ is the laser PSD of the phase noise, $S_{\mathrm{Lm}}(F)$ is the laser PSD of the amplitude noise. From Eq. (5.78), the important conclusion follows that the power increase (both the laser and OEO in the limited case) does not lead to the OEO phase noise decrease (the first term). Such a growth essentially decreases the amplitude noise only (the second term).

We consider now the case of large delay, and we take into account the laser PSD as in Eq. (5.71). Let in Eq. (5.72) $S_{\mathrm{ImFDNY}} = S_{\mathrm{ReFDNY}} = N_{\mathrm{sp}}\hbar\nu$, where N_{sp} is the number of spontaneous photons obtained in PD, and Y_{aRe} and Y_{aIm} are defined as Eqs. (5.74) and (5.75). Then the PSD function of the OEO phase noise (Eq. 5.72) can be presented as:

$$S = \frac{S_\Psi}{P_{0G}} = \frac{K_{2\Gamma PN}^2 C_A h\nu N_{sp}}{P_{0G}}, \tag{5.79}$$

where C_A is the constant coefficient, $K_{2\Gamma PN}^2$ is the coefficient depending upon the delay time in the optical fiber and upon the laser optical power :

$$K_{2\Gamma PN}^2 = \frac{\sigma_U^{-2}}{\left[\frac{(1+FT_F)^2}{(P_{0L}|K_{BZ}|\sigma_U)^2} - 2\frac{(1+FT_F)\cos(FT_{FOS})}{P_{0L}|K_{FOLD}|\sigma_U} + 1\right]^2}. \tag{5.80}$$

From Eqs. (5.79) and (5.80), we see that the laser phase noise is suppressed with the growth of the geometric length of the optical fiber, with increase of the total transfer function in the OEO loop and the laser power, as well as by a choice of α_{e00} and β_{e00}. Supposing that $\sigma_U \approx 1$, we can present $K_{2\Gamma PN}^2$ in Eq. (5.80) as:

$$K_{2\Gamma PN}^2 \approx \frac{P_{0L}^4 |K_{FODL}|^4}{\left[(1+FT_F)^2 - 2P_{0L}|K_{FODL}|FT_F\cos(FT_{FOS}) + P_{0L}^2|K_{FODL}|^2\right]^2}. \tag{5.81}$$

Figure 5.9 contains the plots of the phase noise suppression factor $K_{2\Gamma PN}^2$ of Eq. (5.81).

The calculation of the compression coefficient K_2 according to Eq. (5.80) is presented in Fig. 5.9. We see that the growth of delay time from $T_{FOS} = T_{OF} = 1 \cdot 10^{-6}$ s to $T_{FOS} = T_{OF} = 3 \cdot 10^{-5}$ s leads to the decrease of the coefficient K_2 more than by 12 times in the bias range 1.20 kHz.

Figure 5.8 contains the plots of the phase noise (Eqs. 5.73, 5.79 and 5.80), which represent functions of OEO PSD of the phase noise taking into account small noises of the PD and the RF amplifier, at the laser phase noise for the frequency offset of 1 kHz, which is equal about −120 dB/Hz, at the laser power of 30 mW for the delay $T_{FOS} = 5 \cdot 10^{-6}$ s (the optical fiber length is about 100 m). We see that the first peak is determined by PSD of the laser phase noise, and the average phase noise suppression for the offset of 50 kHz is more than −10 dB/Hz.

It is shown that at given FOS length, the further decrease of the OEO phase noise is possible using the PLL system. Calculation results are well agreed with the experimental dependences of PSD of the OEO phase noise, which can be found in [3].

That is why, we find out that the analog model of OEO MZ, which is composed on the base of Eq. (5.66), gives a possibility to analyze the main features of OEO MZ. The calculation of PSD of amplitude and phase noises discovered the important role in formation of the OEO phase noise of intensity of the spontaneous laser emission.

In computation of the phase noise PSD, we use the approach based on the symbolic OEO equations and applied the method of abbreviated fluctuation equations by Evtianov–Kuleshov. In the next section, we shall use the approach for the

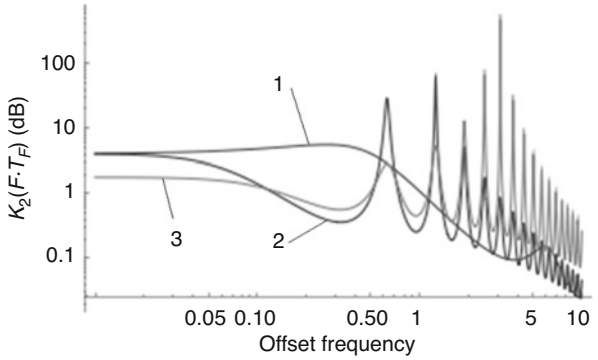

Fig. 5.9 The phase noise suppression factor $K_2 = K^2_{2\Gamma PN}$ (Eq. 5.80) versus the rated offset frequency $F \cdot T_F$ from OEO generation frequency f_0 at different delays in the optical fiber of delay time T_{FOS}/T_F and power of the laser optical emission P_{OL}, $|K_{FODL}| = |K_{BZ}|$ and $\sigma_U = 1$: $T_{OF}/T_F = 1$, $P_{0L}|K_{FODL}| = 2$ (curve 1); $T_{FOS}/T_F = 10$, $P_{0L}|K_{FODL}| = 2$ (curve 2); $T_{FOS}/T_F = 10$, $P_{0L}|K_{FODL}| = 4$ (3 curve)

OEO spectrum investigation and the noise analysis at OEO representation as the random quantities' *correlator*. Principles examined below are supplemented of our analysis fulfilled.

5.5 Correlator's Mathematical Model in OEO MZ

This section is devoted the analysis of OEO with Mach–Zehnder modulator at representation of the optoelectronic "laser—MZ modulator—PD" structure by the *correlator of two random quantities*. We calculate the oscillations spectrum taking into consideration the amplitude and phase fluctuations for the OEO MZ structure depicted in Fig. 5.10, which presents the heterodyning with a delay in OEO MZ, where the laser is the noise source.

Figure 5.10 shows the structure of OEO MZ earlier-examined (a) and pictures of the optical spectra (or spectral densities) (b, c) and RF spectra (or spectral densities) (d, e). The laser optical emission spectrum on the PD area (Fig. 5.10b) is shown without account of the optical filter action located in FOS, and Fig. 5.10c presents the account of the optical filter action, which suppresses the side harmonic on the frequency $\nu_0 - f_0$ or $\nu_{0L} - f_0$.

The normalized correlation function of the oscillation $E_L = E_L(t)$ in the MZ modulator output is the time-function, which unambiguously determines the frequency spectrum of the oscillation power. The laser EMF strength $E_L = E_L(t)$ and the strength $E_{L\tau} = E_L(t - \Delta t)$ delayed by the time $\Delta t = \tau$ are the random correlated quantities in the optical part of OEO. The random quantities are dependent. Now we study the autocorrelation function at passage of the laser emission through the MZ

modulator and its further photodetection with the purpose of the analysis of the correlation process of random quantities and the conditions of the phase noise suppression.

5.5.1 *Description of Mathematical Models of the Laser and the Mach–Zehnder Modulator at OEO Analysis as the Correlator Enclosed by the Positive FB*

The laser. At analysis, we assume that the laser is the high-coherent source of optical oscillations. In other words, the laser spectral line width is less than 100 MHz at the average generation frequency about 200 THz. We suppose that oscillations of the normalized strength of the electromagnetic field in the laser output are close to sinusoidal with the noisy phase component $\varphi_{\mathrm{Lm}}(t)$ and the normalized amplitude noises $m_{\mathrm{Lm}}(t)$: $E_{\mathrm{L}}(t) = [E_{0\mathrm{L}} + m_{\mathrm{Lm}}(t)] \cos [2\pi\nu_{0\mathrm{L}}t + \varphi_{0\mathrm{L}} + \varphi_{\mathrm{Lm}}(t)]$. Here $E_{\mathrm{L}}(t)$, $E_{0\mathrm{L}}$, $m_{\mathrm{Lm}}(t)$ are normalized dimensionless quantities of the instantaneous strength, the amplitude of EMF strength and the EMF amplitude noises, relatively. These quantities are normalized to the maximal value of the strength E_{Lmax},i.e.: $E_{0\mathrm{L}} = E_{0\mathrm{LL}}/E_{\mathrm{Lmax}}$, $E_{\mathrm{L}}(t) = E_{\mathrm{LL}}(t)/E_{\mathrm{Lmax}}$, and $m_{\mathrm{Lm}}(t) = m_{\mathrm{Lm}}(t)/E_{\mathrm{Lmax}}$, where $\nu_{0\mathrm{L}}$ is the average laser generation frequency, $\varphi_{0\mathrm{L}}$ is the initial constant phase shift, t is the current time. In the OEO, at fulfillment of the self-excitation conditions, in the RF section of this oscillator, the RF oscillations $u = u_{\mathrm{g}}(t)$ occur. At that, in the electrical input of the MZ modulator, from the output of the nonlinear amplifier through the coupler C, the radio-frequency signal passes during of the oscillation generation process, which instantaneous voltage is $u_{\mathrm{g}}(t) = [U_{10} + m_{\mathrm{em}}(t)] \cos [2\pi ft + \phi_{0\mathrm{e}} + \varphi_{\mathrm{em}}(t)]$, where $U_{01} = U_{01\mathrm{MZ}} = U_{01\mathrm{C}}$ is the oscillation amplitude of the first harmonic in the electric input of the MZ modulator or in the C output, f is the radio frequency of oscillations, $\phi_{0\mathrm{e}}$ is the constant phase shift, $\varphi_{\mathrm{em}}(t)$ are phase fluctuations, $m_{\mathrm{em}}(t)$ are amplitude fluctuations.

The Mach–Zehnder modulator in OEO. During the analysis in this section, we suppose that the voltage $u_{\mathrm{g}}(t)$ effect in the one of two optical MZ channels (Fig. 5.10) upon the refraction index of the electro-optical index (the lithium niobate), from which the optical channels of MZ modulator are made, which leads to the phase modulation of the optical oscillation. Combining of two optical emissions on the PD area, which passed the different optical channels of the MZ modulator, leads to intensity modulation of the laser emission. Delayed output emissions $E_{1\mathrm{L}}$ and $E_{2\mathrm{L}}$ of the first and second channels of the MZ modulator pass to the input of the photodetector PD. Let the fiber optical system be formed by the single lengthy optical fiber (OF) and the delay difference is determined as $\Delta T_{\mathrm{M}} = T_{2\mathrm{M}} - T_{1\mathrm{M}}$. In Fig. 5.10, the structure of OEO MZ with the delay in the optical path is presented. In this structure, we see the switch Sw. If this switch is closed, at fulfillment of self-oscillation conditions in the closed OEO MZ loop, the oscillation generation occurs. *When*

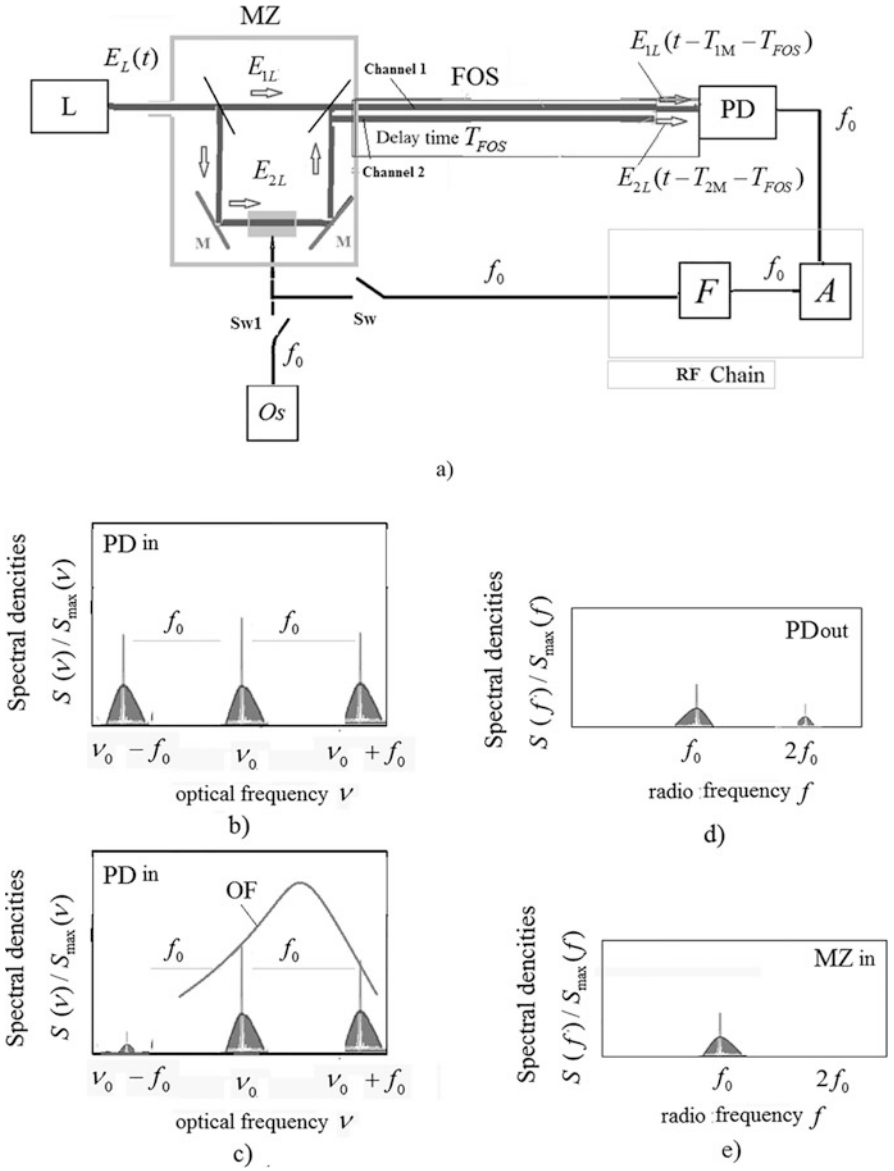

Fig. 5.10 The equivalent structure representing the heterodyning with a delay in OEO MZ (**a**), in which the laser (L) is the source of the phase noise. Optical oscillations pass through different optical channel of the Mach–Zehnder modulator, then they are delayed in the optical fiber by the PD time and pass through the switch Sw. Optical spectral densities of input optical filter (**b**), of the output optical filter (**c**); RF spectral densities at the PD output (**d**), in the MZ input (**e**)

this switch Sw is opened, the external RF generator must be connected to the electrical input of the MZ modulator to provide the optical emission modulation.

5.5.2 The OEO Model as the Correlator with the Positive Feedback

The structure for modeling of the statistical process in OEO with utilization of the traditional correlator of two random quantities is shown in Fig. 5.11. The correlator consists of a multiplier and the delay cell. Let us list the main features at theoretical analysis of fluctuations in OEO. There are:

- Investigation of the influence of strong enough optical oscillations with fluctuations upon the photodetector, which is the nonlinear element;
- The process of photodetection is represented as the process of multiplication (Figs. 5.10 and 5.11) of *optical oscillations* $E_{\mathrm{L}} = E_{\mathrm{L}}(t)$ and $E_{\mathrm{L}\tau} = E_{\mathrm{L}}(t - \Delta t)$;
- The system, in which there is the delay line and the multiplier, is adopted as the correlator of two random quantities;
- The electrical oscillation of the current in the PD load represents the convolution of two spectra of two optical oscillations S_{L} and S_{RFL}.

In OEO, the photodetector PD represents the correlator of two random quantities. The correlator is presented by the delay line and the multiplier "×", and the low-pass filter (LPF) is located. The Gaussian random process $\xi(t)$ with dispersion σ_ξ^2 acts in

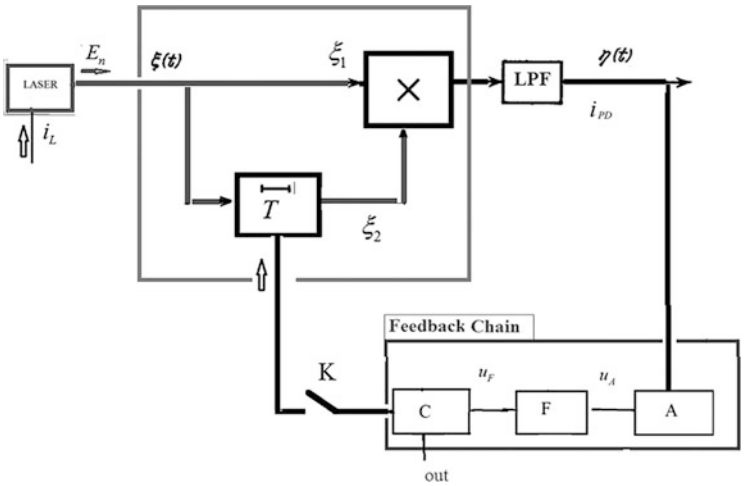

Fig. 5.11 The analog model of the statistical process in OEO MZ with utilization of the traditional correlator of two random quantities. The correlator consists of the multiplier "×" and the delay cell "*T*." OEO MZ representation as the correlator of two random quantities enclosed by the positive feedback. "LPF" is the low-pass filter included in the structure of photodetector PD

the input of the correlator, the low-pass filter (LPF) is connected to the output of the multiplier, the random process in the LPF output is $\eta(t)$. LPF performs the integration operation of the multiplication results of two random quantities.

At closing of the switch Sw, owing to oscillation excitation in the closed OEO, the process of the laser phase fluctuations occurs, which is caused by the carrier noise or by the spontaneous emission. In OEO, operations of multiplication and integration of LPF signals are performed by the photodetector.

5.5.3 *The Mach–Zehnder Correlator-Interferometer*

Let us examine the structure in Fig. 5.11 for modeling of the statistical process in OEO with utilization of the traditional correlator at opened switch Sw and *at absence of electrical oscillations in the electrical input* of the Mach–Zehnder modulation. At that, for determination of the laser emission spectrum, it is necessary to calculate of the autocorrelation function $R(t, t + \tau)$ of the laser random field [4]. ACF is determined by the coherent time T_c, which is inverse proportional to the laser spectral line width $\Delta\nu_L$:

$$R_L(t, t+\tau) = \int_{-\infty}^{\infty} E_L(t) E_L^*(t-\tau)\mathrm{d}t = E_{L0}^2 \exp\left(-\frac{\tau}{T_c}\right) \exp(\, j2\pi\nu_{0L}\tau), \quad (5.82)$$

where $\nu_L = \nu_{0L} = \nu_0$ is the current optical frequency of the laser, and $E_L(t) = E_{L0} \exp[j2\pi\nu_{0L}t + \psi_m(t)]$, while the conjugated and delayed by the time τ the quantity is $E_L^*(t-\tau) = E_{L0} \exp(-j2\pi\nu_{0L}t - j2\pi\nu_{0L}\tau - \psi_m(t-\tau))$.

The autocorrelation function $R_{00}(t, t-\tau)$ of the ***complex envelope*** of the laser random field strength is determined as $R_{L00}(t, t+\tau) = \langle E_{L0}(t) \cdot E_{L0}^*(t-\tau)\rangle = E_{L0}^2 \exp(-\Delta\nu_L \cdot \tau)$.

In order to calculate the required laser spectral density, we can use the Wiener–Khinchin formula:

$$\begin{aligned} S_L &= 4\int_0^{\infty} R_L(\tau)\cos(2\pi f\tau)\mathrm{d}\tau \\ &= 4\int_0^{\infty} E_L^2 \exp(-\Delta\nu_L\tau + j2\pi\nu\tau)\cos(2\pi f\tau)\mathrm{d}\tau. \end{aligned} \quad (5.83)$$

The laser emission spectrum is Lorentzian and can be written as:

$$S_L = \frac{1/(\Delta\nu_L)}{1 + [(\nu - \nu_{0L})/\Delta\nu_L]^2} = \frac{\Delta\nu_L}{\Delta\nu_L^2 + [(\nu - \nu_{0L})]^2}. \quad (5.84)$$

5.5.3.1 The Correlation Function of the Spectral Density of the Phase Noise and the QWLD Spectrum

At arbitrary analysis time, in order to ACF calculate at known laser phase fluctuations, we can use the following expression [3, 5], which can be written as:

$$R_{L00}(\tau) = K_{\varphi 12}(\tau) = \exp(-\Delta\nu_L\tau)\{\cos[(\nu-\nu_{0L})\tau] + [\Delta\nu_L/(\nu-\nu_{0L})]\sin[(\nu-\nu_{0L})\tau]\}. \quad (5.85)$$

The spectrum of the laser generation with account of fluctuations is determined as the Fourier transform of the expression (Eq. 5.83) and is written as:

$$S_1(f) = \exp(-2\pi\Delta\nu_L\tau_D)\delta(f) + \frac{\Delta\nu_L}{\Delta\nu_L^2 + [(f-f_0)]^2} \times \left\{1 - \exp(-2\pi\Delta\nu_L\tau_D)\cdot\left[\cos(2\pi f_0\tau_D) + \frac{\Delta\nu_L}{f_0}\sin(2\pi f_0\tau_D)\right]\right\}, \quad (5.86)$$

in which $\delta(f)$ is the Dirac delta-function, $\tau_D = \tau$ is the observation time or the time of analysis of the oscillation process of the laser generation, f the radio frequency of the analysis.

At small time of observation τ_D (less than 10^{-6} s), the QWLD spectrum shape (taking into account the smallness of quantities $\Delta\nu_L\tau_D$ and $f\tau_D$) is written as:

$$S_1(f) = \exp(-2\pi\Delta\nu_L\tau_D)\delta(f) + \frac{\Delta\nu_L}{\Delta\nu_L^2 + [(f-f_0)]^2} \times [1 - \exp(-2\pi\Delta\nu_L\tau_D)]\cdot \quad (5.87)$$

Figure 5.12 illustrates the calculated plots of the autocorrelation functions $K_{\varphi 12}$ (Eq. 5.85) as the function of the frequency offset $F = 2\pi(f - f_0)$ from the carrier frequency f_0 at different observation times $\tau_D = \tau$ for the laser with the half-width spectral line $\Delta\nu_L = 1$ kHz at different observation times $\tau = \tau_D = \Delta T_M$.

From plots in Fig. 5.12, we can make the conclusion that for the laser with the emission spectral line width $\Delta\nu_L = 1$ kHz, at observation times less than 10^{-5} s at offset $F/(2\pi) = f - f_0 = 10$ kHz, the laser ACF $R_{L00}(\tau, F) = K_{\varphi 12}(\tau, F)$ takes the values less than 0.909, which relates with the finite coherent time of the laser.

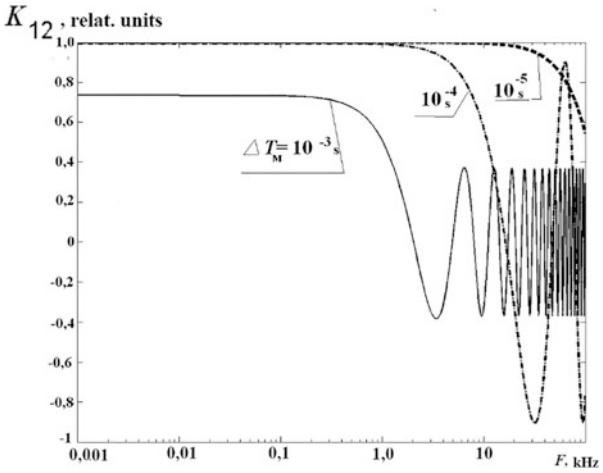

Fig. 5.12 Calculated plots of the autocorrelation function $K_{\varphi 12}$ (Eq. 4.132) as the function of the offset $F = f - f_0$ from the carrier frequency f_0 at different observation times $\tau = \tau_D = \Delta T_M = T_{2M} - T_{1M}$ for the laser with the half-width spectral line $\Delta\nu_L = 1$ kHz

5.5.4 *The Equivalent Circuit of OEO MZ as a Random Correlator*

Let us consider in detail the analog models of OEO MZ, which are shown in Figs. 5.10 and 5.11. Taking into account the mathematical calculations of Chap. 2, we compose the equivalent circuit for OEO MZ. In Chap. 2 of this book, at examination of the laser optical emission modulation in OEO MZ, we show that for simplicity of mathematical computations at finding of ACF and PSD, we can perform the approximation of the Bessel function and to transfer to the approximated formulas to determine the "MZ nonlinearity" in the quadratic and non-quadratic modes.

Figure 5.13 shows the structural diagrams of the equivalent circuit of OEO MZ as a random correlator**:** the general structure of OEO MZ (a); OEO MZ operates in quadrature mode with a phase difference in the MZ optical channels equal to "$\pi/2$" (b); OEO MZ operates in the quadrature mode with a phase difference in the MZ optical channels equal to "π" (c).

Thus, we transfer from the OEO model with the one multiplier (Fig. 5.13a) to the model with two multipliers (Fig. 5.13b, c). This transfer function was substantiated in Chap. 2 and is true not only for small (much lesser) voltage amplitudes, which influence the electrical input, but also comparable in the magnitude with the DC component of the bias voltage. Such representation of OEO MZ (with two multipliers) not only simplifies the mathematical analysis of the oscillating system, but also facilitates understanding of the process of fluctuation suppression.

We note that for the structure in Fig. 5.13c, in which OEO MZ operates in the "non-quadrature mode" with the phase difference in the MZ optical channels equal to "π," conditions of the soft self-excitation of the single-frequency generation of OEO MZ on the fundamental are possible only at the specially selected nonlinear

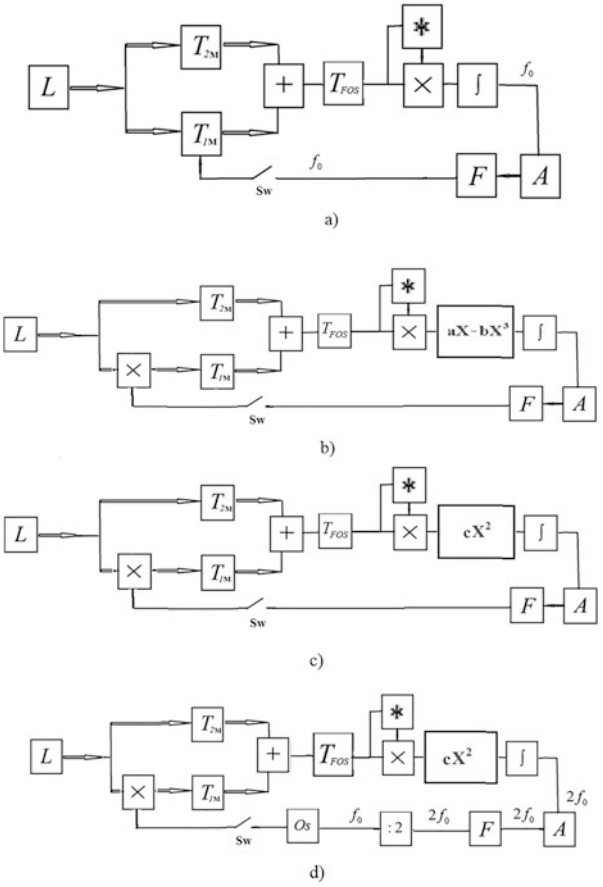

Fig. 5.13 The structural diagrams of the equivalent circuit of OEO MZ as a random correlator**:** general structure of OEO MZ (**a**); OEO MZ operates in the quadrature mode with a phase difference in the MZ optical channels equal to "π/2" (**b**); OEO MZ operates in the "non-quadrature mode" with a phase difference in the MZ optical channels equal to "π" (**c**); OEO MZ with additional RF oscillator "Os," in which input the electrical oscillations are applied from the frequency divider ":2" (**d**)

characteristic of the RF amplifier. In Chap. 2 of this book, we studied the self-excitation conditions of OEO MZ on the base of symbolic equations.

The nonlinear characteristic of the RF amplifier must, as minimum, compensate the quadratic nonlinearity "CX^2." The single-frequency mode of OEO MZ generation *on the first harmonic* f_0 in the case of the structure in Fig. 5.13c is not effective. The mode of the single-frequency generation in OEO MZ *on the second harmonic* $2f_0$ in the case of the structure in Fig. 5.13c is more effective. Excitation of OEO MZ *on the second harmonic* $2f_0$ better to perform in the rigid mode, using the additional RF oscillator "Os." In Figs. 5.13d and 5.14, relatively, we see the equivalent and functional diagrams with additional RF oscillator "Os," in the input of which the electrical oscillations are applied from the frequency divides ":2." This frequency divider converts the single-frequency oscillation of the *second harmonic* $2f_0$ into the single-frequency oscillation of the first harmonic f_0.

In Fig. 5.14b–d, we see plots of the optical spectrum of laser emission on the PD area (b), the RF spectrum of the electrical voltage on the PD load resistance (c), the

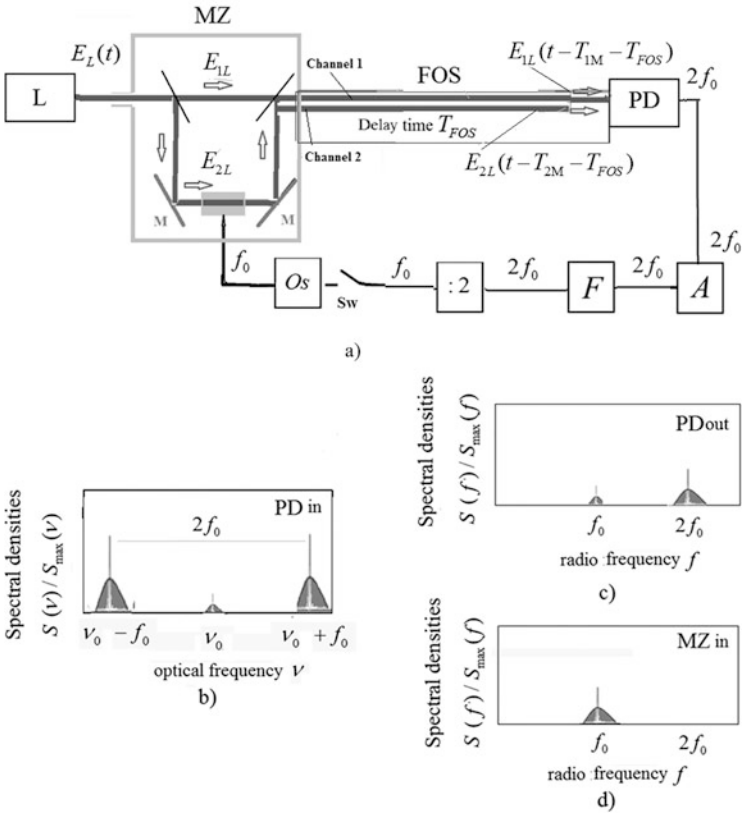

Fig. 5.14 The structure of OEO MZ with additional RF oscillator "Os," in the input of which the electrical oscillations are applied from the frequency divider ":2" (**a**). Plots of the spectral density of the laser emission on the PD area (**b**), the spectral densities of the electrical density on the PD load resistance (**c**), the spectral density of the electrical voltage in the input of MZ (**d**)

RF spectrum of the voltage in the MZ input (c). In the structure in Fig. 5.14a, at opened switch Sw, at impact in the electrical input of the voltage of the oscillator "Os" and at impact in the optical MZ input of laser emission with the strength $E_L(t)$, the interference on the PD area is observed of two emissions with different delays $E_{1L}(t - T_{1M} - T_{FOS})$ and $E_{2L}(t - T_{2M} - T_{FOS})$, which passed through MZ and the optical fiber FOS. The optical spectrum of oscillations is shown in Fig. 5.14b. At operation in the mode "π" ("non-quadrature," i.e., in the mode with the relative phase delay of optical oscillations in the first and second optical channels by "π"), in the optical spectrum (at interference of the PD area), we can extract the side harmonics with the frequencies $\nu_{0L} - f_0$ and $\nu_{0L} + f_0$ shifted from the central harmonic $\nu_{0L} = \nu_0$ by the RF frequency of MZ modulation oscillations f_0. In the PD load, the voltage spectrum is presented in Fig. 5.14c. In the "π" mode,

oscillations on the frequency $2f_0$ of the second harmonic dominate in the level over oscillations of the frequency f_0 of the first harmonic (Fig. 5.14c).

At that, oscillations are amplified by the RF amplifier, then pass to the input of RF filter, which has the natural frequency, which coincides approximately with $2f_0$. From the output of RF filter, oscillations pass to the RF frequency divider ":2." Then oscillations with frequency f_0 on the fundamental harmonic pass to the switch Sw.

When switch Sw is closed, these oscillations with the frequency f_0 pass to the electrical input of the oscillator "Os." At fulfillment of the locking conditions of the oscillator "Os," oscillations passed to the electrical input, and the "Os" synchronization takes place. Abbreviated equations for this structure will differ with regard to earlier-considered by the additional differential equation for the oscillator "Os." The solution of abbreviated equations for this structure of OEO MZ by traditional approach allows obtaining the locking band of the OEO MZ system with "Os," the amplitude and the frequency. The feature of this structure is the fact that in the electrical input of MZ oscillation with f_0 are applies, which multiply by 2. Thus, the opened OEO MZ system plays the role of the RF frequency multiplier.

Advantages of this structure of OEO MZ are described in Fig. 5.14, which can be called the structure with suppression of the central optical frequency, described earlier in Chap. 2, when we discussed the modulation methods of the laser emission. Here we should emphasize that the transition to the structure of OEO MZ with "Os" is substantiated only in the case when it is required to obtain the minimal level of PSD of the phase noise of RF oscillations.

Further, we consider in detail the mathematical analysis for the OEO MZ structure presented in Fig. 5.10.

5.5.5 *The Autocorrelation Function of MZ at the Opened Feedback Loop*

We consider the correlator diagram presented in Fig. 5.11a. Let the K switch be open and the electrical oscillation with the average frequency f_0, passes to the electric input of the MZ modulator. The spectrum of electrical harmonic oscillation represents the delta-function $\delta(f)$). At that, as in the previous case, *two optical oscillations* $E_L = E_L(t)$ and $E_{L\tau} = E_L(t - \Delta T_M)$, which are delayed with regard to each other by the time $\Delta T_M = \Delta T_{MZ}$, are added on the PD area. The autocorrelation function is $R_{MZ}(\tau) \approx \exp\left(-\frac{\Delta T_M}{T_c}\right) \cos(2\pi f_0 \tau)$ for the analysis time $\tau > \Delta T_{MZ}$.

Accordingly, the current spectrum S_{RFMZ} in the photodetector load at $\tau > \Delta T_{MZ}$ is determined by the formula: $S_{RFMZ} = \exp\left(-\frac{\Delta T_M}{T_c}\right) S_{0RFL} \frac{\Delta \nu_L}{\Delta \nu_L^2 + [(f - f_0)]^2}$, where F is the frequency offset from the average radio frequency f_0 of the voltage oscillations, which acts in the MZ electrical input.

Thus, at opened feedback loop, the spectrum S_{RFMZ} has the Lorentzian shape, is determined by the laser phase noise, and the maximal value of S_{RFMZ} is defined by

the ratio $\Delta T_M/T_c$. As a rule, $\Delta T_M/T_c$ is small, i.e., less than 0.001, and $\exp\left(-\frac{\Delta T_M}{T_c}\right) \approx 1$.

5.5.6 The Autocorrelation Function of the Strength Square of the MZ Field

Let us determine autocorrelation functions for the random photodetection process at the simultaneous effect on the optical and electrical inputs, relatively, of the laser optical emission $E_L(t)$ and the electrical oscillation $u_g(t)$. Let the electrical field of the optical carrier, which passes to the MZ optical input, be expressed as: $E_L(t) = E_{0L} \cos [2\pi\nu_0 t + \varphi_{0L} + \varphi_{Lm}(t)]$, where E_{0L} is the oscillation amplitude, ν_{0L} is the average laser generation frequency, φ_{0L} is the initial phase, $\varphi_{Lm}(t)$ is the noisy component or the random phase. The correlation function $R_{MZ}(\tau)$ is:

$$\begin{aligned} R_{MZE}(t,t-\tau) &= R_{MZ}(\tau) = \left\langle E_{12L}^2(t) \cdot \left[E_{12L}^2(t-\tau)\right]^* \right\rangle \\ &= \left\langle \left(\sqrt{E_{1L}^2+E_{2L}^2}\right)^2 \exp[\, j2\arg(E_{12L})] \cdot \left[\left(\sqrt{E_{1L}^2+E_{2L}^2}\right)^2\right] \exp\{-j2\arg[E_{12L}(t-\tau)]\} \right\rangle \\ &= \left\langle \left[E_{1L}^2(t)+E_{2L}^2(t)\right] \cdot \left[E_{1L}^2(t-\tau)+E_{2L}^2(t-\tau)\right]^* \right\rangle, \end{aligned} \tag{5.88}$$

where E_{1L}^2, E_{2L}^2 are the amplitude squares of the normalized strength of the laser emission in PD, which passed through the first and the second optical channels in MZ modulator (Figs. 5.10 and 5.11a).

We can show that ACF $R_{MZ}(\tau)$ for the observation time $|\tau| > |\Delta T_M|$ is determined by the expression

$$\begin{aligned} R\left[E_{12}^2(t,t+\tau)\right] = {} & E_{12L}^4 + E_{12L}^4 \cos\left(2\pi\nu_{0L}\Delta T_M\right] \exp\left(-\Delta\nu \cdot |\Delta T_M|\right) \\ & + E_{12L}^4 \cos\left[2 \cdot 2\pi\nu_{0L}\Delta T_M\right] \exp\left(-\Delta\nu_L \cdot 2|\Delta T_M|\right). \end{aligned} \tag{5.89}$$

The formula (Eq. 5.89) shows that ACF is determined by three terms: the first (E_{12L}^4) is the effect of DC component passing to the PD area, the second term is the result of influence of the oscillation on the optical frequency ν_0, while the third term is the result of the effect of the oscillation on the optical frequency $2\nu_0$. At influence in the MZ electrical input of the voltage $u_g(t) = U_{10} \cos [2\pi f_0 t + \phi_{0e} + \varphi_{em}(t)]$, where U_{10} is the voltage oscillation amplitude in the MZ electrical input, f_0 is the average laser generation frequency, ϕ_{0e} is the initial phase, and $\varphi_{em}(t)$ is the noisy phase component or the random phase.

ACF of MZ is determined by a sum of three components R_{MZ0}, R_{MZ1}, R_{MZ2}: $R_{MZ}(u,t,t+\tau) = R_{MZ0} + R_{MZ1} + R_{MZ2}$. At that, R_{MZ0} corresponds to the impact of

DC component of the optical emission intensity of the first harmonic with the average optical frequency of ν_0, and R_{MZ1}, R_{MZ2}, relatively, are ACF from the impact of the first (with radio frequency f_0) and the second (with $2f_0$) harmonics:

$$\begin{aligned} R_{MZ}(u,t,t+\tau) = \frac{E_{0L}^4}{4}\gamma^2\{ & \left[K_\gamma - \cos(\varphi_{0MZ})\cdot\left(1-\frac{x^2}{4}\right)\right]^2 \times \langle\cos(2\pi\nu_{0L}\tau+\beta_1-\beta_2)\rangle \\ & -\left[K_\gamma \sin(\varphi_{0MZ})\cdot\left(\frac{x}{2}-\frac{x^3}{16}\right)\right]^2 \times \langle\cos(2\pi\nu_{0L}\tau+2\pi f_0\tau+\beta_1-\beta_2)\rangle \\ & -\left[K_\gamma \cos(\varphi_{0MZ})\cdot\frac{x^2}{8}\right]^2 \times \langle\cos(2\pi\nu_{0L}\tau+2\cdot 2\pi f_0\tau+\beta_1-\beta_2)\rangle\}, \end{aligned} \tag{5.90}$$

where K_γ is the excitation coefficient of optical channels, φ_{0MZ} is the constant phase shift in MZ defining by the DC bias voltage $U_{0MZ\pi}$, $x = U_{1MZ}/U_{0MZ\pi}$, and $x \in [0; 1]$, U_{1MZ} is the amplitude of AC voltage harmonic passed to the MZ electrical input, $\beta_1 - \beta_2$ is the difference of the phase noise fluctuation values.

The important point in ACF determination of $u_g(t) = U_{10}\cos[2\pi ft + \phi_{0e} + \varphi_{em}(t)]$ is the determination of the average value $\langle\cos(2\pi\nu_{0L}\tau + 2\pi f_0\tau + \beta_1 - \beta_2)\rangle$, in which the difference $\beta_1 - \beta_2$ is the fluctuating term and values of β_1 and β_2 are relatively: $\beta_1 = \varphi_{Lm}(t - T_{1M}) - \varphi_{Lm}(t - T_{2M})$, $\beta_2 = \varphi_{Lm}(t - T_{1M} - \tau) - \varphi_{Lm}(t - T_{2M} - \tau)$.

In order to find the average difference of random quantities we use the formula:

$$\begin{aligned} & \cos(2\pi\nu_{0L}\tau+2\pi f_0\tau+\beta_1-\beta_2) \\ & = \langle\cos(2\pi\nu_{0L}\tau+2\pi f_0\tau)\cdot\cos(\beta_1-\beta_2)\rangle - \langle\sin(2\pi\nu_{0L}\tau+2\pi f_0\tau)\cdot\cos(\beta_1-\beta_2)\rangle \\ & = \langle\cos(\beta_1-\beta_2)\rangle\cos(2\pi\nu_{0L}\tau+2\pi f_0\tau) = \exp(-\Delta\nu_L|\Delta T_M|)\cos(2\pi\nu_{0L}\tau+2\pi f_0\tau). \end{aligned} \tag{5.91}$$

Taking Eq. (5.91) and last transformation into account, the expression for the product $\cos(2\pi\nu_{0L}\tau + \beta_1)\cdot\cos(2\pi\nu_{0L}\tau + \beta_2)$ can be written in the form:

$$\begin{aligned} \cos(2\pi\nu_{0L}\tau+\beta_1)\cdot\cos(2\pi\nu_{0L}\tau+\beta_2) &= \frac{1}{2}[\cos(\beta_1-\beta_2)+\cos(2\cdot 2\pi\nu_{0L}\tau+\beta_1+\beta_2)] \\ &= \frac{1}{2}[\cos(\beta_1-\beta_2)+\cos(\beta_1+\beta_2)\cos(2\cdot 2\pi\nu_{0L}\tau) - \sin(\beta_1+\beta_2)\sin(2\cdot 2\pi\nu_{0L}\tau)] \\ &= \frac{1}{2}[\cos(\beta_1-\beta_2)+\cos(\beta_1+\beta_2)\cos(2\cdot 2\pi\nu_{0L}\tau)]. \end{aligned} \tag{5.92}$$

With account of Eq. (5.92), $R_{MZ}(u, t, t + \tau)$ takes the different shape for the different observation time $|\tau| > |\Delta T_M|$ and $|\tau| \le |\Delta T_M|$:

$$R_{\mathrm{MZ}}(u,t,t+\tau) = \begin{cases} |\tau| > |\Delta T_{\mathrm{M}}| \rightarrow \frac{1}{2}\exp(-\Delta\nu_{\mathrm{L}}\cdot 2|\Delta T_{\mathrm{M}}|)[1+\cos(2\cdot 2\pi\nu_{\mathrm{L}}\tau)], \\ |\tau| \le |\Delta T_{\mathrm{M}}| \rightarrow \frac{1}{2}[\exp(-\Delta\nu_{\mathrm{L}}\cdot 2|\tau|)+\exp(-\Delta\nu_{\mathrm{L}}\cdot(4|\Delta T_{\mathrm{M}}|-2|\tau|))\cdot\cos(2\cdot 2\pi\nu_{\mathrm{L}}\tau)]. \end{cases} \tag{5.93}$$

ACF $R_{\mathrm{MZ}}(u, t, t + \tau)$ of the MZ field strength square is (taking Eq. (5.92) into consideration):

$$\begin{aligned} R_{\mathrm{MZ}}(u,t,t+\tau) &= R_{\mathrm{MZ0}} + R_{\mathrm{MZ1}} + R_{\mathrm{MZ2}} \\ &= \frac{E_{0\mathrm{L}}^4}{4}\gamma^2\{\left[K_\gamma - \cos(\varphi_{0\mathrm{MZ}})\cdot\left(1-\frac{x^2}{4}\right)\right]^2 \times \cos(2\pi\nu_{0\mathrm{L}}\tau)\exp(-\Delta\nu_{\mathrm{L}}\cdot 2|\Delta T_{\mathrm{M}}|) \\ &- \left[K_\gamma \sin(\varphi_{0\mathrm{MZ}})\cdot\left(\frac{x}{2}-\frac{x^3}{16}\right)\right]^2 \times \cos(2\pi\nu_{0\mathrm{L}}\tau + 2\pi f_0\tau)\exp(-\Delta\nu_{\mathrm{L}}\cdot 2|\Delta T_{\mathrm{M}}|) \\ &- \left[K_\gamma \cos(\varphi_{0\mathrm{MZ}})\cdot\frac{x^2}{8}\right]^2 \times \cos(2\pi\nu_{0\mathrm{L}}\tau + 2\cdot 2\pi f_0\tau)\exp(-\Delta\nu_{\mathrm{L}}\cdot 2|\Delta T_{\mathrm{M}}|). \end{aligned} \tag{5.94}$$

We would like to remind that here in Eq. (5.94), $\Delta\nu_{\mathrm{L}}$ is the spectral line width of the QWLD emission and it is defined approximately as $\Delta\nu_{\mathrm{L}} = \Delta\nu = \frac{1}{T_{\mathrm{c}}}$, where T_{c} is the QWLD coherence time.

Thus, we obtain the general expression (Eq. 5.94), with which help we can obtain the expression for PSD of OEO MZ.

5.5.7 *The Autocorrelation Function of the PD Load Voltage*

The impact on the MZ electrical input is described as: $u_{\mathrm{g}}(t) = [U_{10} + m_{\mathrm{em}}(t)]\cos[2\pi f_0 t + \phi_{0\mathrm{e}} + \varphi_{\mathrm{em}}(t)]$. In this case, the autocorrelation function $R_{\mathrm{MZ}}(\tau)$ at the analysis time $\tau > \Delta T_{\mathrm{M}}$ is $R_{\mathrm{MZU}}(t, t-\tau) = R_{\mathrm{MZ}}(\tau) = \langle U_{\mathrm{PD}}(t)\cdot[U_{\mathrm{PD}}(t-\tau)]\rangle$. In this case, the autocorrelation function is $R_{\mathrm{MZ}}(\tau) \approx \exp\left(-\frac{2\Delta T_{\mathrm{M}}}{T_{\mathrm{c}}}\right)\cos(2\pi\cdot f_0\tau)$ at the analysis time $\tau > \Delta T_{\mathrm{M}}$.

Accordingly, the current spectrum S_{RFMZ} in the photodetector load at $\tau > \Delta T_{\mathrm{M}}$ is determined by the formula: $S_{\mathrm{RFMZ}} = \exp\left(-\frac{2\Delta T_{\mathrm{M}}}{T_{\mathrm{c}}}\right)\cdot S_{0\mathrm{RFL}}\cdot\frac{\Delta\nu_{\mathrm{L}}}{\Delta\nu_{\mathrm{L}}^2+[(f-f_0)]^2}$.

Figure 5.15a, b show, relatively, the plots of the autocorrelation function $R_{\mathrm{MZ}}(\tau) \approx \exp\left(-\frac{2\Delta T_{\mathrm{M}}}{T_{\mathrm{c}}}\right)\cos(2\pi\cdot f_0\tau)$ and PSD of oscillation in the Mach–Zehnder modulator for three values of the ratio of delay time difference ΔT_{M} to the coherence time T_{c} at $\Delta T_{\mathrm{M}}/T_{\mathrm{c}} = 3; 4.5; 10$.

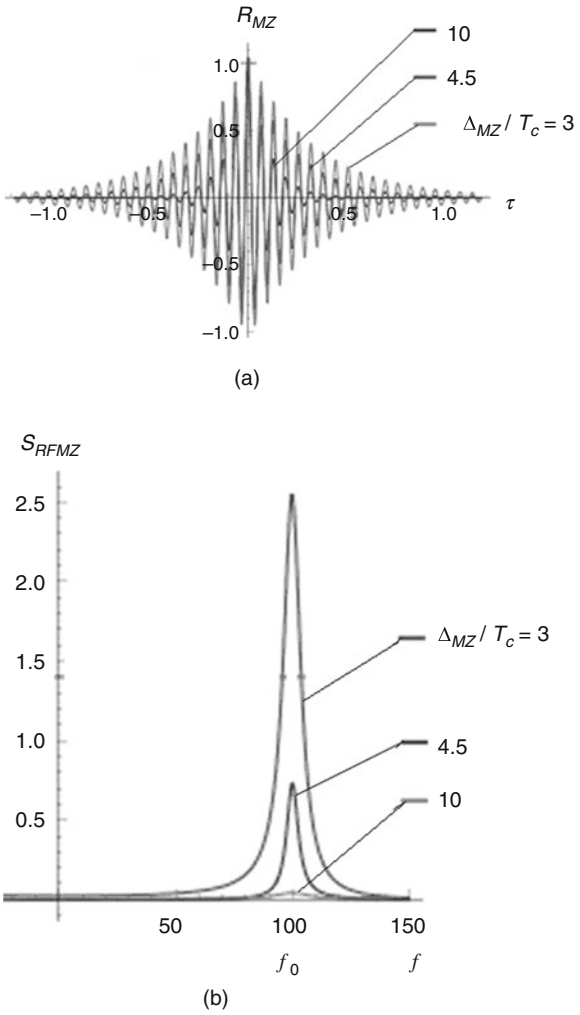

Fig. 5.15 Plots of the autocorrelation function $R_{MZ}(\tau)$ (**a**) and the spectrum S_{RFMZ} (at positive frequencies) of the optical oscillation (**b**) passed through the Mach–Zehnder modulator for three ratios of the delay time differences in MZ optical channels $\Delta T_M = \Delta T_{MZ}$ to the time constant of the laser coherence T_c for $\Delta T_M / T_c = 3; 4.5; 10$

In Fig. 5.16, we see plots of PSD of optical emission after passage through the MZ modulator in the quadrature and non-quadrature operation modes.

Presented plots in Fig. 5.16 allow the conclusions how are PSD of the laser emission changing, depending on the chosen mode, or at variation of φ_{0MZ} in the formula (Eq. 5.94). The level of PSD of DC component in the "π" mode decreases minimum by 20 dB. At the same time, the level of PSD of DC component in the "$\pi/2$" mode has significantly more level at offsets closed to the zero.

Now we can make a conclusion that representation of OEO MZ as the correlator of random quantities and consideration of the structure in different operation modes (quadrature and non-quadrature) gives a possibility to simplify the mathematical notation of the autocorrelation function $R_{MZ}(u, t, t + \tau)$ and in open loop of OEO

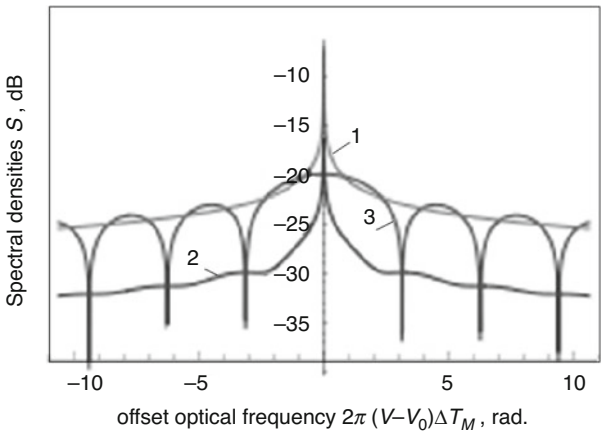

Fig. 5.16 Plots of the laser emission spectral densities before (plot 1) and after (plot 2) the passage of the MZ modulator. Spectral densities are shown in the "quadrature" ("$\pi/2$") mode (plot 2). Spectral densities are shown in the quadrature (cos) and the non-quadrature ("π") modes (plot 3). The plot of the laser spectral density (plot 1) at the input of MZ has the form of the Lorentz function

MZ. As the result, we obtain the relatively simple formula (Eq. 5.94) for $R_{MZ}(u, t, t + \tau)$, which reflects the sense of statistical processes in OEO MZ and explains the process of laser phase noise transformation into the phase RF noise of OEO. The autocorrelation function $R_{MZ}(u, t, t + \tau)$ is determined by three components: the DC component, which passes to the PD area after passage of MZ and the optical fiber R_{MZ0}, and also by AC components R_{MZ1} and R_{MZ2}, the values of which depend on φ_{0MZ} or the DC bias voltage on MZ.

Now we proceed to further examination of processes of statistical impact in OEO MZ.

5.5.8 *The Convolution Operation of Strength Squares of the Laser Field and the Radio-Frequency Oscillation in OEO MZ*

The convolution operation of two oscillation spectra, which are formed by the laser optical emission, takes the special place in OEO MZ correlator (Figs. 5.10 and 5.11) of random quantities. Let the electric field of the optical carrier, which passes to the MZ optical input, be expressed as $E_L(t) = E_{0L} \cos [2\pi\nu_{0L}t + \varphi_{0L} + \varphi_{Lm}(t)]$.

At the open switch Sw (Figs. 5.10 and 5.11), the voltage from the external oscillator (the generator is not shown in Figs. 5.10 and 5.11), which passes to the MZ electrical input, can be described as: $u_g(t) = [U_{10} + m_{em}(t)] \cos [2\pi f_0 t + \phi_{0e} + \varphi_{em}(t)]$.

Then, the electrical current oscillation in the PD load represents the product of ACF of the laser oscillation passed through the MZ modulator and ACF of $u_g(t)$ oscillations affected on the MZ electrical input: $R_{PD}(t, t - \tau) = R_L(\tau) \cdot R_{RFL}(\tau)$.

The electrical current oscillations in the PD load is then represented by the convolution of two spectra of two oscillations: optical S_L and radio frequency S_{RFL} : $S_{PDL} = S_L(f) * S_{RFL}(f)$, where $*$ is the symbol of the convolution operation. We remind that if, for instance, the stationary Gaussian noise with the probability density distribution, which is specified according to the normal law with the mathematical expectation m_ξ and the σ_ξ^2 dispersion, affects the non-inertial double-sided quadratic detector (Fig. 5.11a) with the characteristic $\eta(\xi) = T(\xi) = a \cdot \xi^2$, $a > 0$, then, in this case, the spectral density $S_\eta(f)$ of the random process $\eta(t) = \xi_1(t) \cdot \xi_2(t)$ (or $\eta(t) = \xi_L(t) \cdot \xi_{RFL}(t)$) is determined by the convolution formula: $S_\eta(f) = \frac{1}{2\pi}\int_{-\infty}^{\infty} S_1(\zeta) \cdot S_2(f - \zeta)d\zeta$. Figure 5.17 shows the correlator structure (Fig. 5.17a), plots of the spectral density $S_\eta(f)$ of the convolution of S_1 and S_2 oscillations passing on the PD with time constants b) and c). In the case b) for relatively S_1 and S_2 we have: $T_{c1} = 1$; $T_{c2} = 0.909$. For the case c), S_1 and S_2 relatively give: $T_{c1} = 2$; $T_{c2} = 1.5$.

From plots of the spectral density $S_\eta(f)$ of the convolution S_1 and S_2 presented in Fig. 5.17, it follows that the difference of time constants T_{c1} and T_{c2} in spectra of S_1 and S_2 more than by 10% leads to decrease of $S_\eta(f = 0)$ and to widening of the resulting spectrum $S_\eta(f)$. At closing of the K switch in OEO MZ (Fig. 5.11), we must analyze the correlation process of random quantities $\xi_L(t)$ and $\xi_{RFL}(t)$ for

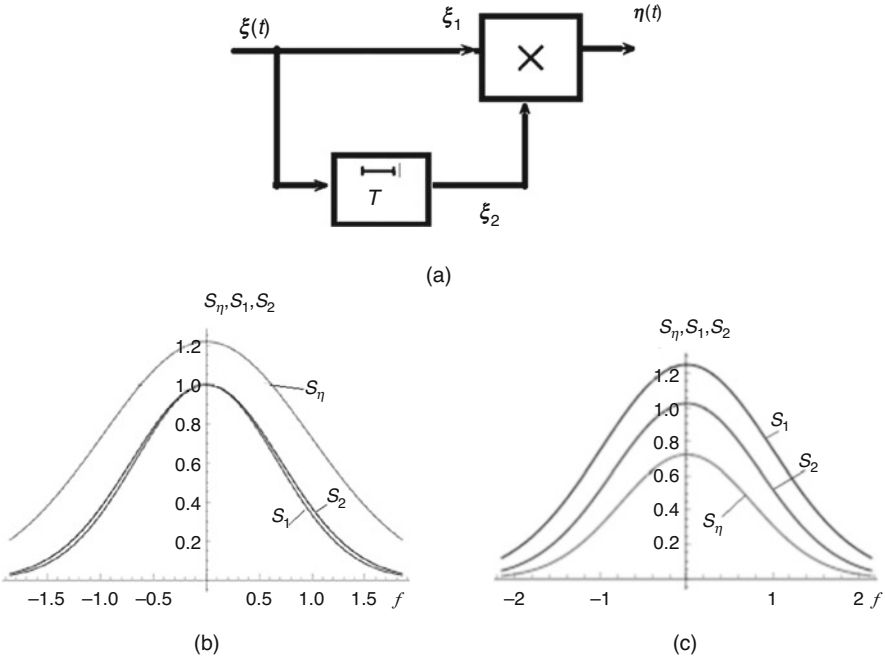

Fig. 5.17 The correlator structure (**a**), plots of the spectral density $S_\eta(f)$ of the convolution S_1 and S_2 of oscillations passing to PD with time constants (**b**, **c**). In the case (**b**) for S_1 and S_2, we have relatively $T_{c1} = 1$; $T_{c2} = 0.909$. For the case c), we obtain S_1 and S_2 relatively $T_{c1} = 2$; $T_{c2} = 1.5$

different cases, for example, for $T_{FOS}/T_c \ll 1$ and $T_{FOS}/T_c > 1$. It is clear that at $\Delta T_M/T_c \ll 1$, $\Delta T_{MZ} = \Delta T_M$, and (at small ratio of the delay time in the optical fiber to the coherence line in the laser) $T_{FOS}/T_c \ll 1$, we may expect the interaction of the completely correlated quantities in the multiplier. At $T_{FOS}/T_c > 1$ (and if this ratio is much more than 1), we can speak that the "correlation" process occurs of two mutually independent quantities, although random quantities are formed by the single noise source—the laser.

In the next section, we reduce the task of the correlator for two random quantities $\xi_1(t)$ and $\xi_2(t)$ in OEO MZ to the task of double-dimension distribution density finding of the probability of the Gaussian random process.

5.5.9 *The Power Spectral Density S_η in the Correlator Output in OEO*

The double-dimension probability distribution density of the Gaussian random stationary process $\xi(t)$ (Fig. 5.17a) with the zero mathematical expectation and with the σ_ξ^2 dispersion (we mean the normal distribution of the probability density of the random quantity) has the form:

$$p_1(\xi_1, \xi_2) = \frac{1}{2\pi\sigma_\xi^2 \cdot \sqrt{1 - \exp\left(-\frac{2\tau}{T_c}\right)}} \exp\left(-\frac{\xi_1^2 - 2\exp\left(-\frac{2\tau}{T_c}\right)\xi_1\xi_2 + \xi_2^2}{2\sigma_\xi^2 \cdot \left[1 - \exp\left(-\frac{2\tau}{T_c}\right)\right]}\right), \tag{5.95}$$

where ξ_1, ξ_2 are noisy impacts (Fig. 5.17a). It corresponds to *optical oscillation* $E_L = E_L(t)$ and $E_{L\tau} = E_L(t - \tau)$, which pass the MZ modulator to the PD area. We should note that if the stationary Gaussian random process $\xi(t)$ with the σ_ξ^2 dispersion, the zero mean acts in the correlator input, which consists of the delay line with difference of the delay time ΔT_M, the multiplier and the low-pass filter (Fig. 5.17a), then the autocorrelation function in the correlator output has a form: $R_\xi(\tau) = \sigma_\xi^2 \exp\left(-\frac{\tau}{T_c}\right) \cos(2\pi f_0 \tau)$, where τ is the analysis time, f_0 is the frequency. If to suppose that the low-pass filter lets pass only the low-frequency process components from the multiplier output, then the probability distribution density $p_2(\eta)$ of the $\eta(t)$ process in the correlator output is determined by the formula:

$$p_2(\eta) = \frac{1}{2\pi\sigma_\xi^2\sqrt{1 - \exp\left(-\frac{2T_{\text{FOS}}}{T_c}\right)}} \exp\left(-\frac{|\eta|}{2\sigma_\xi^2 \cdot \left[1 - \exp\left(-\frac{2T_{\text{FOS}}}{T_c}\right)\right]}\right). \quad (5.96)$$

From this formula for the probability distribution $p_2(\eta)$, the important conclusion follows that the *probability distribution of the random quantity* η (Figs. 5.10, 5.11, and 5.17) *depends not only upon the ratio of the oscillation amplitude and the noise dispersion of the random quantity (or upon the ratio signal-noise)* $|\eta|/\sigma_\xi^2$ *in the correlator input*, but upon the *laser coherence time* T_c *or the difference* $\left[1 - \exp\left(-\frac{2T_{\text{FOS}}}{T_c}\right)\right]$.

The distribution probability (Eq. 5.96) $p_2(\eta)$ determines the appropriate correlation function of the output process

$$R_\eta(\tau) = \int_{-oo}^{oo}\int_{-oo}^{oo} f(\eta)f(\eta_\tau)p_2(\eta)\mathrm{d}\eta\mathrm{d}\eta_\tau, \quad (5.97)$$

where $f(\eta)$ is the nonlinear characteristic of the photodetector, $\eta_\tau = \eta(t - \tau)$ of the $\eta(t)$ process in the correlator output. In order to calculate the required power spectral density S_η in the correlator output (Figs. 5.10, 5.11, and 5.17), we must use the Wiener–Khinchin formula: $S_\eta = 4\int_0^\infty R_\eta(\tau)\cos(2\pi f\tau)\mathrm{d}\tau$.

The deriving expression (Eq. 5.95) is also true for description of the statistical process of fluctuation suppression at interference of optical emission harmonics (Figs. 5.10 and 5.14). In this case, the random quantities ξ_1, ξ_2 are interpreted as harmonics' phase fluctuations of the emission passed to PD.

For example, in the open loop of OEO, to PD after the optical filter (which is located in FOS), two harmonics pass with frequencies ν_{0L} and $\nu_{0L} + f_0$, which strength is equal, relatively, to: $E_{10L}(t) = \sqrt{A_1}E_{0L}\cos[2\pi\nu_{0L}t + \varphi_{0L} + \varphi_{10Lm}(t)]$ and $E_{20L}(t) = \sqrt{A_2}E_{0L}\cos[2\pi(\nu_{0L} + f_0)t + \varphi_{0L} + \varphi_{20Lm}(t)]$, where coefficients A_1, A_2 are defined by the AFC of the optical filter and PD. Random quantities $\xi_1 = \varphi_{10Lm}$ and $\xi_2 = \varphi_{20Lm}$ here are dependable and are determined by the laser phase fluctuations $\xi_{0PN} = \varphi_{Lm}$. For them, owing to the phase fluctuation smallness and large values of the laser power E_{0L}^2, we can write: $\xi_1 = A_1E_{0L}^2 \cdot \xi_{0PN}$, $\xi_2 = A_2 \cdot E_{0L}^2 \cdot \xi_{0PN}$.

Then the expression (Eq. 5.96) can be written as:

$$p_1(\xi_1,\xi_2) = \frac{1}{2\pi\sigma_\xi^2 \cdot \sqrt{1 - \exp\left(-\frac{2\tau}{T_c}\right)}} \exp\left(-\frac{\xi_{0PN}^2E_{0L}^2\left[A_1 - 2\exp\left(-\frac{2\tau}{T_c}\right)\sqrt{A_1A_2} + A_2\right]}{2\sigma_\xi^2 \cdot \left[1 - \exp\left(-\frac{2\tau}{T_c}\right)\right]}\right). \quad (5.98)$$

Coefficients A_1 and A_2 corresponds to amplitudes of optical harmonics on the PD area. The level of the harmonic amplitudes is determined by AFC of FOS and AFC

of PD near the optical frequency, and by the difference between optical frequencies. The expression (Eq. 5.98) for $p_1(\xi_1, \xi_2)$ well demonstrates that at approximate equality of coefficients $A_1 \approx A_2$, $p_1(\xi_1, \xi_2)$ takes a form of the normal one-dimension distribution of the probability density ξ_{0PN}:

$$p_1(\xi_1, \xi_2) = \frac{1}{2\pi\sigma_\xi^2 \cdot \sqrt{1 - \exp\left(-\frac{2\tau}{T_c}\right)}} \exp\left(-\frac{2\xi_{0PN}^2 E_{0L}^2 A_1^2 \left[1 - \exp\left(-\frac{2\tau}{T_c}\right)\frac{A_2}{A_1}\right]}{2\sigma_\xi^2 \cdot \left[1 - \exp\left(-\frac{2\tau}{T_c}\right)\right]}\right). \tag{5.99}$$

We note in Eq. (5.99): the closer the ratio $\frac{A_2}{A_1}$ to 1, the closer $p_1(\xi_1, \xi_2)$ to 1, and the probability $p_1(\xi_{0PN})$ is defined by the multiplier $\exp\left(-\frac{2\tau}{T_c}\right)$. At that, $p_1(\xi_1, \xi_2)$ defines the probability density $p_2(\eta)$ of the statistical process in the correlator output (Fig. 5.11) or OEO MZ (Fig. 5.10a) at *opened loop* at $\tau > \Delta T_M$:

$$p_2(\eta) = \frac{1}{2\pi\sigma_\xi^2 \sqrt{\left[1 - \exp\left(-\frac{2\Delta T_M}{T_c}\right)\right]}} \exp\left(-\frac{|\eta|}{2\sigma_\xi^2 \cdot \left[1 - \exp\left(-\frac{2\Delta T_M}{T_c}\right)\right]}\right) \tag{5.100}$$

and for *closed loop* of OEO MZ at $\tau > T_{FOS}$:

$$p_2(\eta) = \frac{1}{2\pi\sigma_\xi^2 \cdot \sqrt{\left[1 - \exp\left(-\frac{2(\Delta T_M + T_{FOS})}{T_c}\right)\right]}} \exp\left(-\frac{|\eta|}{2\sigma_\xi^2 \cdot \left[1 - \exp\left(-\frac{2(\Delta T_M + T_{FOS})}{T_c}\right)\right]}\right). \tag{5.101}$$

In Fig. 5.18 we present plots of the distribution density $p_1(\xi_{0PN})$ (Eq. 5.99) in the multiplier input (a) and $p_{02}(\eta) = p_2(\eta) \cdot 2\pi\sigma_\xi^2 \cdot \sqrt{\left[1 - \exp\left(-\frac{2\Delta T_M}{T_c}\right)\right]}$ (Eq. 5.100) in the multiplier output of the double-channel correlator (b) (at opened and closed feedback loop) for different values of $2(\Delta T_M + T_{FOS})/T_c = 0.01, 0.1, 1$ at $A_1 \approx A_2$ and $\sigma_\xi^2 = 2$.

Figures 5.19 and 5.20 show plots of distribution density $p_{02}(\eta)$ in the multiplier input and $p_{02}(\eta) = p_2(\eta) \cdot 2\pi\sigma_\xi^2 \cdot \sqrt{\left[1 - \exp\left(-\frac{2\Delta T_M}{T_c}\right)\right]}$ (Eq. 5.100) in the multiplier output of the double-channel correlator at $A_1 \approx A_2$ for different values of $\sigma_\xi^2 = 2, 0.2, 0.02$ for values $2(\Delta T_M + T_{FOS})/T_c = 0.01$ (Fig. 5.19) and for values $2(\Delta T_M + T_{FOS})/T_c = 1$ (Fig. 5.20).

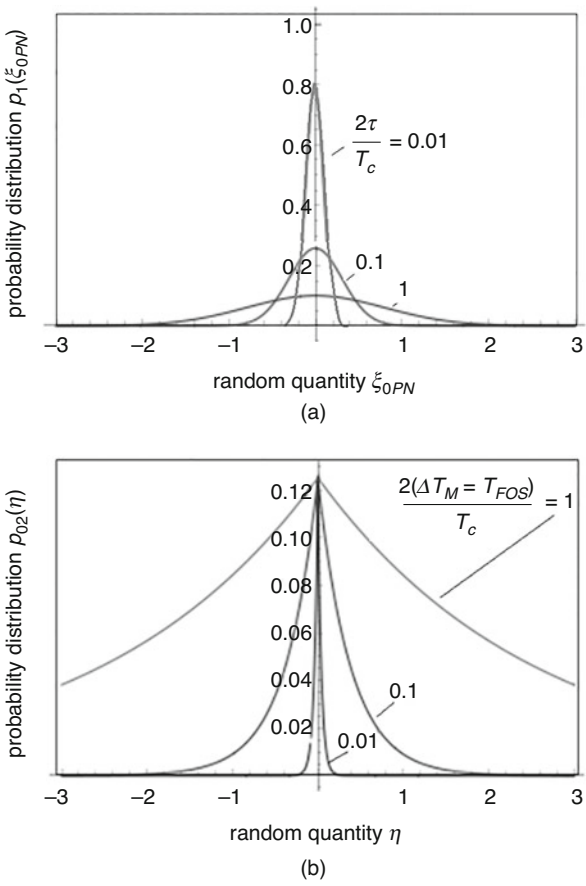

Fig. 5.18 The probability density $p_1(\xi_{0PN})$ (Eq. 5.99) in the multiplier input (**a**) and $p_{02}(\eta) = p_2(\eta) \cdot 2\pi\sigma_\xi^2 \cdot \sqrt{\left[1 - \exp\left(-\frac{2\Delta T_M}{T_c}\right)\right]}$ in the multiplier output of the double-channel correlator (**b**) (at opened and closed feedback loop) for different values $2(\Delta T_M + T_{FOS})/T_c = 0.01, 0.1, 1$ at $A_1 \approx A_2$ and $\sigma_\xi^2 = 2$

From analysis of expressions (Eqs. 5.98–5.101) and plots in Figs. 5.18, 5.19, and 5.20 depicted on these expressions, it follows that at closed ratio $\frac{A_2}{A_1}$ to 1, the probability in the input p_1 is closer to 1, and the probability p_1 is determined by the multiplier $\exp\left(-\frac{2\tau}{T_c}\right)$.

The probability distribution density of the correlator output process approaches to 1 at decrease of the ratio $2(\Delta T_M + T_{FOS})/T_c$ and at increase of the σ_ξ^2 dispersion of the phase noises. The statistical process of the fluctuations' suppression in OEO can be determined as the process of statistical summation of two optical harmonics on the PD area and in the PD load. Such process happens at opened feedback signal at connection of the external oscillator to MZ.

It is necessary to distinguish the statistical processes in the open feedback loop (i.e., at the connected external RF oscillator to the MZ modulator in Fig. 5.10) and in the closed feedback loop in OEO (the external RF oscillator is not connected). At that, on the PD area, there is the process of statistical averaging in time of the

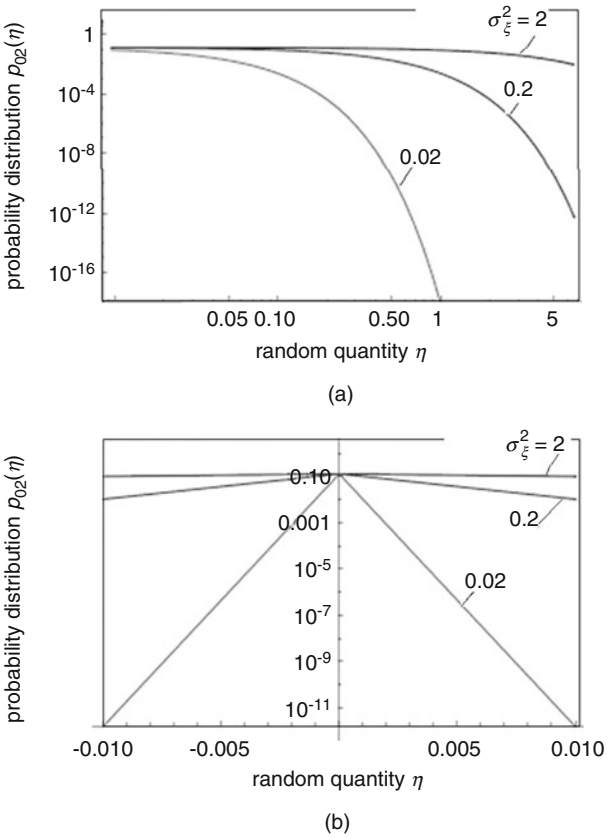

Fig. 5.19 The distribution density $p_{02}(\eta) = p_2(\eta) \cdot 2\pi\sigma_\xi^2 \cdot \sqrt{\left[1 - \exp\left(-\frac{2\Delta T_M}{T_c}\right)\right]}$ (Eq. 5.100) in the multiplier output of the double-channel correlator for values $2(\Delta T_M + T_{FOS})/T_c = 0.01$ at values $A_1 \approx A_2$ and $\sigma_\xi^2 = 2, 0.2, 0.02$. Plots are presented in the logarithm (**a**) and linear (**b**) scales

interference result of two optical harmonics, which are applied to the PD area: $E_{10L}(t) = \sqrt{A_1}E_{0L}\cos[2\pi\nu_{0L}t + \varphi_{0L} + \varphi_{10Lm}(t)]$ and $E_{20L}(t) = \sqrt{A_2}E_{0L}\cos[2\pi(\nu_{0L} + f_0)t + \varphi_{0L} + \varphi_{20Lm}(t)]$ with the amplitudes $\sqrt{A_1}E_{0L}$ and $\sqrt{A_2}E_{0L}$. As the result of the statistical averaging, the laser fluctuations in the PD photocurrent (in the PD load or in the correlator output) are suppressed. At open feedback loop, the difference of delay times in optical channels differs by ΔT_M. At open feedback loop, the effectiveness of suppression is determined by the ratio $2\Delta T_M/T_c$.

At closed feedback loop (Fig. 5.10) or in the autonomous OEO oscillator, in the statistical process of the phase fluctuation suppression, the delay time difference in optical channels is $\Delta T_M + T_{FOS}$. At closed feedback loop, the suppression effectiveness is determined by the ratio $2(\Delta T_M + T_{FOS})/T_c$.

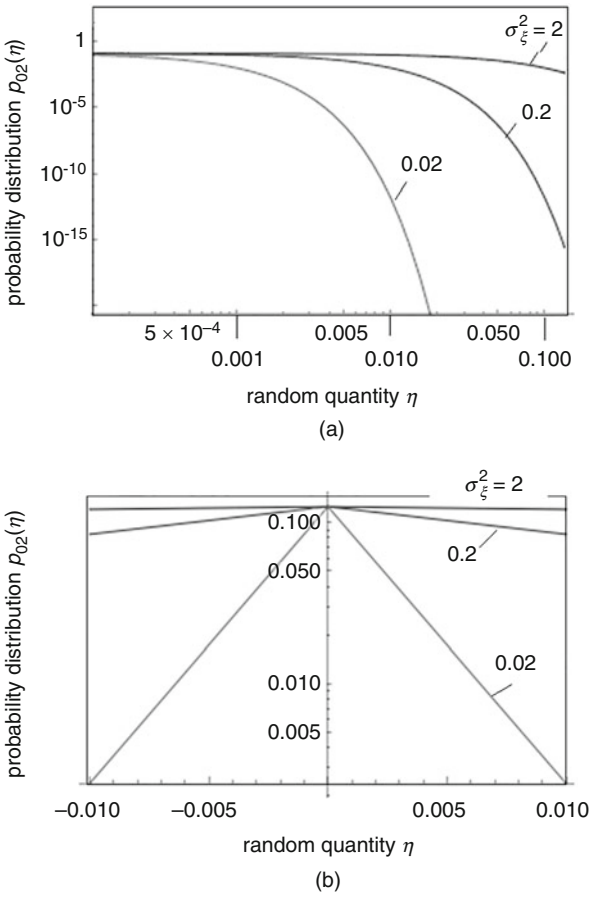

Fig. 5.20 The distribution density $p_1(\xi_{0PN})$ (Eq. 4.166) in the multiplier input (**a**) and $p_{02}(\eta) = p_2(\eta) \cdot 2\pi\sigma_\xi^2 \cdot \sqrt{\left[1 - \exp\left(-\frac{2\Delta T_M}{T_c}\right)\right]}$ in the multiplier output of the double-channel correlator (**b**) (at opened or closed feedback loop) for different values of $2(\Delta T_M + T_{FOS})/T_c = 1$ at different values of $\sigma_\xi^2 = 2, 0.2, 0.02$. Plots are presented in the logarithm (**a**) and linear (**b**) scales

5.5.10 *The Oscillation Spectrum at* Closed *Feedback Loop*

At the **closed** switch Sw, in the diagram shown Figs. 5.10 and 5.11, at fulfillment of OEO excitation conditions, the amplified electrical oscillation passes to the electrical input of the MZ modulator from the output of the photodetector. We would like to note that this oscillation is delayed by the time T_{FOS} with respect to the laser oscillation, which arrives to the photodetector. As shown in Chap. 6 of the present book, in this case, the radio-frequency spectrum in the PD output $S_{RFL}(F)$ is determined by the formula:

$$S_{\mathrm{RFL}}(F) = \frac{E_{0\mathrm{L}}^2}{2}\frac{U_{10\mathrm{MZ}}^2}{2}K_{2\Gamma\mathrm{PN}}^2 \cdot \frac{1/(\Delta\nu_{\mathrm{L}})}{1+[F/\Delta\nu_{\mathrm{L}}]^2} \cdot \left\{1 - \frac{A_2}{A_1}\exp\left(-\frac{2(\Delta T_{\mathrm{M}} + T_{\mathrm{FOS}})}{T_{\mathrm{c}}}\right)\right\}. \tag{5.102}$$

In the case of OEO, the N number is defined by the ratio $N \approx T_{\mathrm{c}}/T_{\mathrm{FOS}}$ of the laser coherence time and the delay time in the optical fiber. In further Chaps. 6 and 7, we shall show that the spectral density of radio-frequency OEO oscillations $S_{\mathrm{RFL}}(F)$ is determined by the formula:

$$S_{\mathrm{RFL}}(F) = \frac{E_{0\mathrm{L}}^4}{2}\frac{U_{10\mathrm{MZ}}^2}{2}\left\{\exp\left(-\frac{2(\Delta T_{\mathrm{M}} + T_{\mathrm{FOS}})}{T_{\mathrm{c}}}\right)\cdot\delta(F) + K_{2\Gamma\mathrm{PN}}^2\frac{1/(\Delta\nu_{\mathrm{L}})}{1+[F/\Delta\nu_{\mathrm{L}}]^2}\left[1 - \frac{A_2}{A_1}\exp\left(-\frac{2(\Delta T_{\mathrm{M}} + T_{\mathrm{FOS}})}{T_{\mathrm{c}}}\right)\right]\right\}, \tag{5.103}$$

where $\delta(F)$ is the delta-function, $K_2(F)$ is the coefficient of the noise suppression, which depends upon T_{FOS}, the laser optical power$E_{0\mathrm{L}}^2$, the transfer function of RF FODL$|K_{\mathrm{FODL}}|$, $U_{10\mathrm{MZ}}^2$ is the amplitude square of the AC voltage in the electrical input of MZ.

In formula (Eq. 5.103), $K_{2\Gamma\mathrm{PN}}^2$ is the noise suppression coefficient (Fig. 5.9), which depends upon T_{FOS}, the laser optical power $P_{0\mathrm{L}}$, the coefficient of nonlinearity σ_{U}, the time constant of the RF filter T_{F}, the transfer function of RF FODL $|K_{\mathrm{FODL}}|$, is determined as (Eq. 5.80).

Thus, at *closed feedback loop* in OEO MZ (circuit in Fig. 5.10), the spectrum in the photodetector output has the Lorentzian shape, is determined by the laser phase noises, and its maximal value depends upon the ratio $T_{\mathrm{FOS}}/T_{\mathrm{c}}$. At large lengths of the optical fiber (1 km and more), the ratio $T_{\mathrm{FOS}}/T_{\mathrm{c}}$ is not small and is $T_{\mathrm{FOS}}/T_{\mathrm{c}} \approx 1$ and more. The effectiveness of the noise suppression in OEO is determined not only by the fiber length, but also depends upon the ratio of the laser coherence time and the delay time in the optical in the optical fiber. At closed switch Sw, in the case of the steady-state mode setting in OEO, the effective statistical suppression occurs in the case if the laser coherence time T_{c} is comparable to the delay time in the optical fiber T_{FOS}, i.e., $T_{\mathrm{c}} \approx N \cdot T_{\mathrm{FOS}}$, where, for example, $N = 1 - 5$. In this case, the statistically correlated laser phase fluctuations will be suppressed. At small delays T_{FOS}, when $T_{\mathrm{c}} \gg T_{\mathrm{FOS}}$, the noise suppression does not occur, the correlator, as the device, does not perform its functions of the phase noise suppression. When $T_{\mathrm{c}} \ll T_{\mathrm{FOS}}$, the noise suppression is not also effective. In this case, the correlation coefficient is close to zero and the correlator effectiveness is low.

In experimental OEO investigations, the minimal level of the noise spectral density is achieved at utilization of the high-coherent lasers (with the spectral line width of 10–100 kHz) and with the geometrical lengths of optical fibers of 1–2 km, which provides the delay in the optical fiber of 10^{-5} s and more.

5.6 Conclusions

In this chapter, the analysis of OEO oscillating system is performed as the two oscillation sources with different frequencies—optical and radio. At that, OEO is enclosed by the positive feedback loop from the optical output to the electrical input. The positive selective feedback is provided by means of the photodiode, the radio-frequency filter, and the nonlinear RF amplifier. On the other hand, we can consider that the radio front-end is enclosed by the optoelectronic feedback including the laser, the optical fiber, and the photodetector.

The mathematical analysis of OEO is performed at laser (QWLD) representation by the differential semiclassical equations for the electromagnetic field strength (the optical emission) and kinetic equations for the emission intensity, the inversed population and the electrical pumping current. The positive feedback is included into the system of differential equations taking into consideration: the delay in the optical fiber, the photodetection of the optical emission, the extraction (selection) in radio frequency, the nonlinear amplification in the amplifier. The new results are that on the base of the laser differential equations, which are described by the Lotka–Volterra differential equations for the optical field intensity, the inversed population and the optical phase, we obtain the differential equations of OEO DM without and with fluctuations taking into account the positive selective feedback with the retarded argument.

We compose and discuss the analog models of OEO DM and OEO MZ without and with account of noises. The main principal difference of the OEO MZ analog model with regard to the OEO DM analog model is the potential possibility in OEO MZ to use the extra-low-noise QWLDs. This follows from the fact that in the laser model for OEO MZ, the carrier noise suppression can be arranged directly in the internal closed loop of the optical feedback or in the optical resonator. For this, we must not only decrease the value of noise sources, but to apply the high-Q optical resonator. The growth of the resonator Q-factor will significantly decrease the laser modulation bandwidth in radio frequency. The excessive increase of the optical resonator Q-factor leads in OEO DM to reduction of the oscillation amplitude. The external modulation is used in OEO MZ. The modulation index of the optical emission does not depend on the growth of the optical resonator Q-factor. The increase of this Q-factor will lead to the improvement of oscillation spectrum purity or to the decrease of the laser phase noise. Another principal feature, which follows from an analysis of the presented analog model of OEO MZ, is the fact that suppression of the carrier fluctuations can be provided in the feedback loop in population. The increase of the time constant or the carrier lifetime on the upper operation level T_1 also leads to significant decrease of the laser phase noise. In OEO MZ, it becomes possible to use the high-coherent fiber lasers with the large carrier lifetime of $T_1 = 1 - 100\,\mu s$. As we mentioned earlier, the modern compact OEO MZs use the semiconductor QWLDs with the spectral line width from 1 kHz to 10 NHz. The compact commercial samples of semiconductor lasers appear with the spectral line width 10–500 Hz.

An analysis of differential equation solutions shows that in OEO DM, the necessary condition of the stable single-frequency mode of the microwave generation is more than the double excess of the Q-factor of the radio-frequency filter with regard to the equivalent Q-factor of the optical filter in QWLD, which is determined by the electron relaxation time constant in the laser active layer, by the coefficient of the laser optical amplification and the pumping excess above the threshold value. As a result of studying of OEO DM solutions, we fulfilled an analysis of the local stability of the single-frequency oscillation mode on the base of the Rauth–Gurvitz method assuming the quadratic nonlinearity of the watt–ampere laser static characteristic. We proved that to achieve the "soft" mode of oscillation setting in OEO DM at the amplifier nonlinearity choice, we must take into account the multiplicative (close to quadratic) nonlinearity in the laser.

We performed the computer analog modeling of differential equations of OEO DM. We proved that at pumping switch-on, the transient of the exit to the single-frequency steady-state generation in OEO DM is accompanied by ripples. At large oscillation amplitude, the strong nonlinear distortions arise, which are caused by the nonlinear dependence of emission intensity on the QWLD pumping current. The level of nonlinear distortions depends on a choice of the bias DC current. The mode of small amplitudes in OEO (less than 1%...10% of the maximal value) is provided at the choice of the laser pumping DC current on the level from 1.5 to 5.0 relative excesses above its threshold value of the laser pumping current. A choice of the nonlinearity type of the RF amplifier, the natural frequency of the RF filter, the delay value in FOS determines the character and duration of the transient in OEO DM. The limit cycle in the phase space is stable and oscillation setting occurs in the soft mode at the choice of the nonlinearity type, taking into account the laser multiplicative nonlinearity.

The fluctuation differential equations obtained at the OEO analysis represent a system of four differential equations for the strength square, the population, the optical phase of QWLD emission, the electrical pumping current. At consideration of the small-signal mode on the base of fluctuation DE solutions for OEO DM, we obtain expressions for the amplitude, the generation frequency, PSD of amplitude and phase fluctuations.

We formed the fluctuation differential equations of OEO DM with Langevinian noise sources. The task of an analysis of fluctuation DE of OEO DM is to determine the connection of the noise influence of QWLD spontaneous emission on the RF phase noise of OEO. As the result of fluctuation DE solution in the small-signal mode, we obtained the analytical expressions for laser amplitude and phase noises, which are caused by the laser spontaneous emission. It stated that the one from important features of OEO DM is its high quality of oscillations (or the high SNR). This OEO DM is concerned to the microwave oscillation sources with the extra-low phase noise level (on the level -110 to -140 dB/Hz at frequency offset of 1–10 kHz from the nominal generation frequency of 10 GHz). We determine the main mechanisms of such a low phase noise in OEO DM.

The mechanism of natural QWLD noise suppression, which is caused by the spontaneous emission, is the base mechanism of decrease of the amplitude and phase

noise in OEO DM, owing to the positive selective (in radio frequency) feedback, which is formed by the fiber-optical system, the photodetector, the RF filter, and the amplifier. From obtained analytic expression, it follows that the decrease by the order and more of the amplitude noise of OEO DM follows at growth of the ratio of the feedback loop gain to the QWLD gain, which is determined as the ratio of the carriers' lifetime to the photon lifetime in the resonator. Owing to introduction of the positive feedback loop, the amplitude noise caused by QWLS spontaneous emission is reduced by the order or more. Another three important mechanisms of phase noise reduction of OEO DM are concerned, at first, to the coherent photo-self-heterodyning of two equal-in-amplitude but different in frequency optical components. In other words, in OEO DM, which operates in the mode of two optical oscillations, the statistical subtraction occurs of these two high-correlated optical components, each of which is modulated by the laser "phase" noise. Secondly, the phase noise suppression on OEO DM occurs owing to the mechanism of the optical delay in the optical fiber with the oscillation delay by 1–50 μs. Thirdly, the decrease of the phase noise in OEO DM is provided by a choice of the low-noise laser with small level of spontaneous emission and with small spectral line width of the optical generation of 1 MHz. Application of filtering of the laser DC pumping current and the temperature stabilization of the laser active layer are the other mechanisms of phase noise reduction in OEO DM.

As the result of OEO DM analysis, we can conclude that owing to the construction simplicity of QWLD, such OEOs in microwave and mm-wave ranges are forward-looking oscillators. The main restriction of the OEO DM phase noise improvement, i.e., QWLD DM, is the contradiction: to reduce the OEO phase noise we must achieve the phase noise of the laser, which can be done by the increase of the Q-factor of the oscillating optical system of the laser, the utilization of lasers with specific narrowband resonators. But, on the other hand, at growth of the equivalent time constant of the optical resonator, the laser modulation bandwidth decreases at modulation by microwave oscillations, the laser modulation coefficient decreases and, hence, the oscillation amplitude of OEO DM decreases. A choice of the spectral line width of the laser optical emission of 1–10 MHz (at pumping excess above the threshold value by 5–9 times) is optimal from the point of view of reduction of the ratio of the phase noise and the microwave OEO oscillation amplitude at the generation frequency of 10 GHz and at the laser optical frequency about 129 THz. This contradiction can be resolved at separation (complication the functional diagram) of the modulating emission source (the laser diode) into two devices—the separate laser, the high-coherent with the bandwidth of 0.01–1 MHz of the laser optical emission, and the electro-optical modulator itself (for instance, the Mach–Zehnder modulator). The next Chap. 6 is devoted to investigation of OEO MZ of such a type.

Representation of OEO MZ as the correlator of the random quantities and examination of the structure in different operation modes (quadrature and non-quadrature) gives a possibility to simplify the mathematical notation of the autocorrelation function $R_{\mathrm{MZ}}(u, t, t + \tau)$ in the opened feedback loop in OEO MZ. As the result, we obtain relatively simple formula (Eq. 5.94) for $R_{\mathrm{MZ}}(u, t,$

$t + \tau$), which reflects the sense of statistical processes in OEO MZ and explains the process of the laser phase noise transformation into the RF phase noise of OEO. The autocorrelation function $R_{MZ}(u, t, t + \tau)$ is determined by three components: the DC component, which passes to the PD area after passage of MZ and the optical fiber R_{MZ0}, and also by AC components R_{MZ1} and R_{MZ2}, which value depends on φ_{0MZ} or the DC bias voltage in MZ.

The presented analysis of OEO as the correlator of random quantities allows the conclusion that the *distribution probability of the random quantity η depends not only upon the ratio of the oscillation amplitude to the noise dispersion (or the SNR)* $|\eta|/\sigma_\xi^2$ *in the correlator input*, but *upon the laser coherence time* T_c *or the difference* $[1 - \exp(-2(\Delta T_M + T_{FOS})/T_c)]$. From the analysis of expressions (Eqs. 5.98–5.103) and plots in Figs. 5.10, 5.11, and 5.13 depicted on these expressions, it follows that at close ratio A_2/A_1 to 1, the probability p_1 in the input is closer to 1, and the probability p_1 is determined by the multiplier $\exp(-2\tau/T_c)$. The probability distribution density of the correlator output process approaches to 1 at decrease of the ratio $2(\Delta T_M + T_{FOS})/T_c$ and at decrease of the laser phase noise dispersion σ_ξ^2. The statistic process of fluctuation suppression in OEO can be defined as the process of statistical adding of two optical harmonics, which pass to the PD area. As the result of the statistical process and the process of photodetection, the laser phase noises are suppressed. Thus, at *closed feedback loop* in OEO MZ, the spectrum in the photodetector output has the Lorentzian shape, and it is determined by the laser phase noises, and its maximal value depends upon the ratio T_{FOS}/T_c.

References

1. I.V. Komarov, S.M. Smolskiy, *Fundamentals of Short-Range FM Radar* (Artech House, Norwood, 2003)
2. N. Yoshida, *Oscillation Theory Of Partial Differential Equations* (World Scientific Publishing, Singapore, 2008)
3. Alexander A. Bortsov and Sergey M. Smolskiy, Opto-Electronic Oscillator with Mach-Zender Modulator. Infocommunications Journal, Vol. XI, No 1, 45–53 (2019),DOI: 10.13140/RG.2.2.20992.69126
4. J.W. Goodman, *Speckle Phenomena in Optics: Theory and Applications* (Roberts and Company publishers, Englewood, 2006)
5. Alexander A. Bortsov, Yuri B. Il'in, Laser spectral line widening effect on RF phase and amplitude noises of an optoelectronic oscillator OEO. J. Radio Eng. (2), 21–31 (2010), DOI: 10.13140/RG.2.2.35665.07527

Chapter 6
Operation Analysis of Optoelectronic oscillator (OEO) with External Mach–Zehnder Modulator

This chapter is devoted to the analysis of the laser OEO with RF FODL considered as the system of two oscillators of the optical and RF ranges. We investigate in detail the problem of the generation spectrum formation of RF oscillations in OEO MZ taking into account the effect of laser optical emission parameters including of its spectral line width and the power.

The general task statement of OEO MZ investigation is discussed in Sect. 6.1. Section 6.2 describes the construction and the operation principle of OEO MZ.

The development principles of the mathematical model of OEO MZ and the components in the OEO MZ structure are discussed in Sect. 6.3. The Sect. 6.4 is devoted to characteristics and the transfer function of the MZ modulator in OEO MZ.

The differential fluctuation equations of OEO MZ are investigated in Sect. 6.5, and Sect. 6.6 is devoted to results of computer modeling of OEO MZ and description of the transients' investigations of oscillation formation in OEO MZ.

Problems of spectrum formation of OEO MZ are discussed in brief in Sect. 6.7.

The main results of this chapter are listed in Sect. 6.8.

6.1 The General Statement of the OEO MZ Investigation Task

OEO with RF FODL is the promising source of microwave and mm-wave oscillations. It can be used as the master oscillator in radio and optical radar complexes, as well as in systems of formation and processing of optical and RF precision signals, for instance, with the pulse duration of the pico-second order. OEO performed on the base of optical micro-resonators has small dimensions, a weight, and a cost. Experimental measurement results of the phase noises PSD of such an oscillator, which are −147 dB/Hz on the generation frequency of 10 GHz at the standard offset

A. A. Bortsov et al., *Laser Optoelectronic Oscillators*, Springer Series in Optical Sciences 232, https://doi.org/10.1007/978-3-030-45700-6_6

of 1 kHz, allow the conclusion that OEO is the secondary frequency standard and already now, it competes with the low-noise microwave oscillators with the dielectric resonators on the sapphire crystals on generation frequencies 8–70 GHz. At present, the methods of the phase stabilization of OEO oscillations are developed. At the same time, the problem of the laser (or the laser diode) optical emission influence, which is the base element of OEO, upon the spectral characteristics of OEO RF generation is not enough studied.

In this Section, we perform the analysis of OEO operation with the electro-optical Mach–Zehnder modulator with the purpose to obtain in this structure the extremely low RF phase noises. At first, we investigate the features of the structure and characteristics of the MZ modulator. We emphasize that in this section, OEO MZ is examined as the system of two different types of oscillators—the optical quantum oscillator (OQO) with the generation frequency about $\nu_0 = 200$ THz and the RF oscillator (RFO) with the generation frequency $f_0 = 4$–100 GHz. At that, OQO is the "pumping source" for RFO.

6.2 The Construction and Operation Principle of OEO MZ

OEO MZ consists of two self-oscillating systems—OQO or the laser (or the laser diode LD) and RFO (Fig. 6.1). The laser is the "pump" for RFO. RFO is formed by the series-closed into the feedback loop of the electro-optical MZ modulator, the fiber-optical system (FOS), the photodiode (PD), the nonlinear amplifier (NA), the RF narrowband filter (F), and the RF coupler (C) (see Fig. 6.1).

OEO MZ can be considered as the oscillator with the retarded feedback, in which the RF FODL of the RF signal is formed by the modulated light source (MLS) consisting of the laser and the modulator, FOS and PD. The modulated QWLD or the

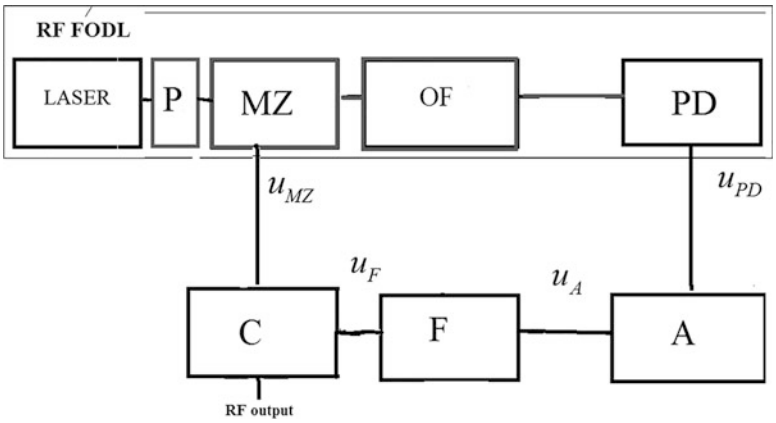

Fig. 6.1 OEO structures with the external Mach–Zehnder modulator with separation of MZ with voltages in the input and outputs of units. Designations are explained in the text

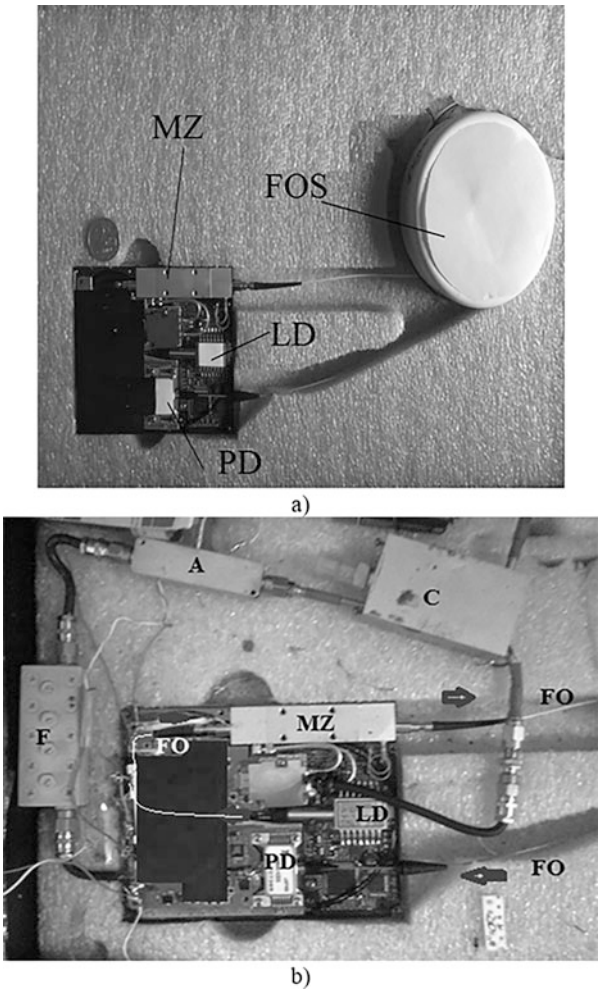

Fig. 6.2 The general view of the experimental models of the low-noise laser OEO of the microwave range (on the left there is the usual Russian coin). The mean generation frequency is 8–10 GHz: OEO with the direct modulation (**a**), the photo-picture of OEO with external MZ modulation (**b**)

laser with the external electro-optical modulator is, for example, the Mach–Zehnder modulator (Figs. 6.1 and 6.2).

The laser optical emission (the carrier) passes to the input of the optical modulator (MZ), in which the emission is modulated by the electrical signal $u = u_{\mathrm{RF}}(t)$. Then the optical emission passes to the photodetector (PD) input through the optical modulator and FOS. RF oscillations (the subcarrier) obtained in the PD output pass through the nonlinear amplifier (NA), the frequency-selective filter (F) and are directed in this loop system through the directional coupler (C) to the microwave input of the MZ modulator.

In the OEO system, when the self-excitation conditions are satisfied, in the RF part of such an oscillator, the RF oscillations arise $u = u_{\mathrm{RF}}(t)$. At that, to the RF input of MZ from the NA output through C, the RF signal is applied during the oscillation generation process and the instantaneous voltage of this signal is:

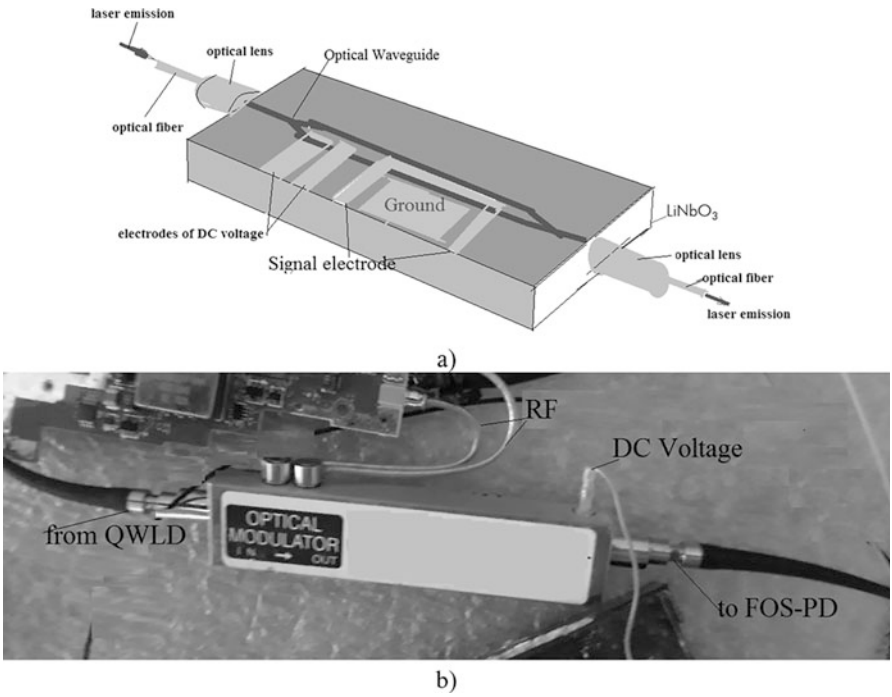

Fig. 6.3 The location scheme of the optical channels and electrodes in the electro-optical Mach–Zehnder modulator of the microwave range (**a**), the overall view of the electro-optical Mach–Zehnder modulator (**b**)

$$u_{\mathrm{RF}}(t) = U_0 \cos\left(2\pi f_0 t + \phi_{0\mathrm{e}}\right), \tag{6.1}$$

where $U_0 = U_{0\mathrm{M}} = U_{0\mathrm{F}}$ is the oscillation amplitude in the MZ modulator input or in the filter output, f_0 is the oscillation radio frequency, $\phi_{0\mathrm{e}}$ is the constant phase shift.

We should note that if the laser spectrum width $\Delta\nu_{\mathrm{L}}$ is much less than the radio frequency f_0 of the subcarrier $\Delta\nu_{\mathrm{L}} \ll f_0$, the modulated emission is formed in the modulator output in the small-signal mode. This optical emission represents the sum of three coherent components in the spectrum, which frequencies are, relatively, $\nu_1 = \nu_0 - f_0$, $\nu_2 = \nu_0$, $\nu_3 = \nu_0 + f_0$. Two of these optical frequencies ν_1 and ν_3 are separated from the central laser optical frequency ν_0 by the subcarrier frequency f_0.

In the further description, we examine OEO with the MZ modulator, in which the laser is the high-coherent source of the optical emission and $\Delta\nu_{\mathrm{L}} \ll f_0$, and the optical Mach–Zehnder modulator is the modulator in OEO.

The MZ modulator represents two strip optical waveguides connected in the input Y and in the output X by the optical directional couplers (DC) (Figs. 6.3, 6.4, and 6.5). The input Y-coupler executes the function of laser emission divider (splitter) (the electrical field strength E_{L}) in the two optical channels OC1 and OC2.

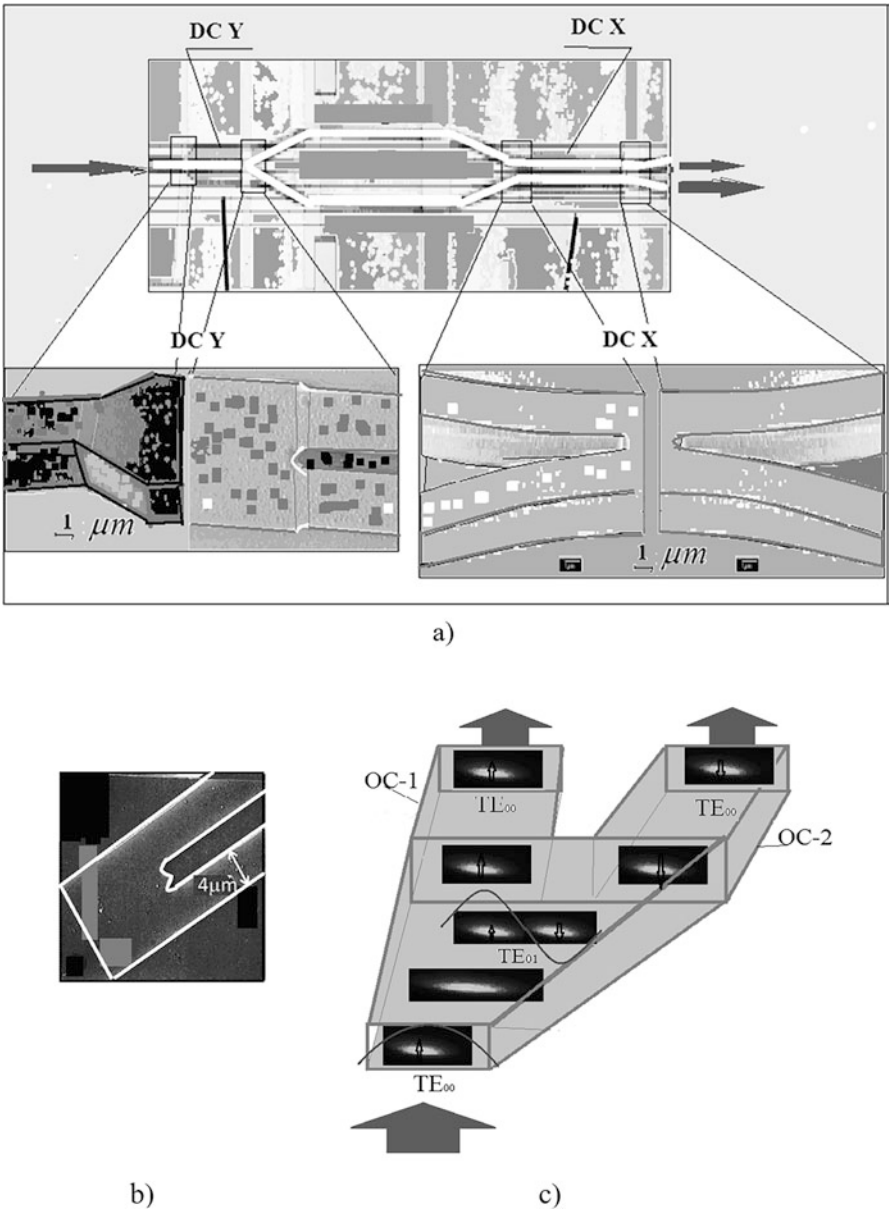

Fig. 6.4 The location scheme of the electro-optical Mach–Zehnder modulator of the microwave range with the optical channels and the directional optical coupler Y (DC Y) and X (DC X) types and their view in the longitudinal section (**a**). The view of the optical coupler Y (**b**). The location scheme of the optical Y-coupler of the laser emission (**c**)

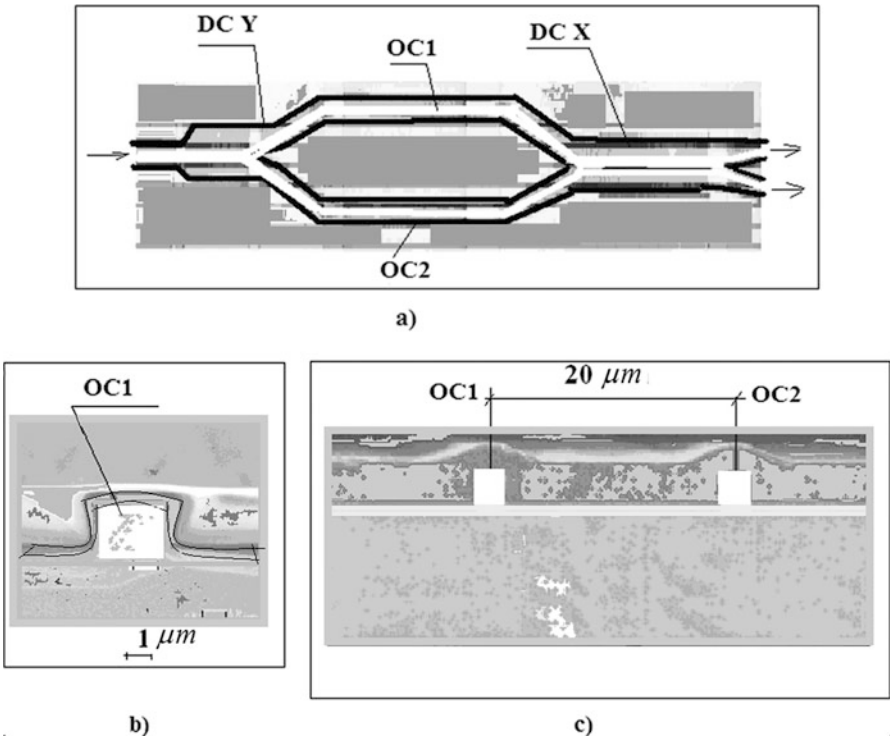

Fig. 6.5 The location scheme of the optical channels in the electro-optical Mach–Zehnder modulator of the microwave range (**a**) and their view in the transverse section (**b**), (**c**)

In OC2, the emission E_{2L} is modulated by the input RF signal of the voltage $u = u_{RF}(t)$ on the optical phase, and the time delay of the optical oscillation in the OC2 output with the regard to the MZ input is $T_{2M} = T_{2M}[u(t)]$. In the OC1 output, the time delay remains constant and equal to T_{1M}. Then, optical emissions from outputs of the first OC1 E_{1L} and the second OC2 E_{2L} optical channels, owing to the second output X-coupler, pass to the FOS input, in which they are delayed by the time T_{FOS} and then are applied to the photodetector PD.

6.2.1 *Influence of the Phase Noise PSD on the Irregularity of MZ Optical Channels and the Spatial Laser Coherence*

Presented photo-pictures (Fig. 6.6) of distribution variations of the optical emission intensities in the optical channels OC1 and OC2 in the MZ modulator of the microwave range are rather informative. From the analysis of intensity distribution,

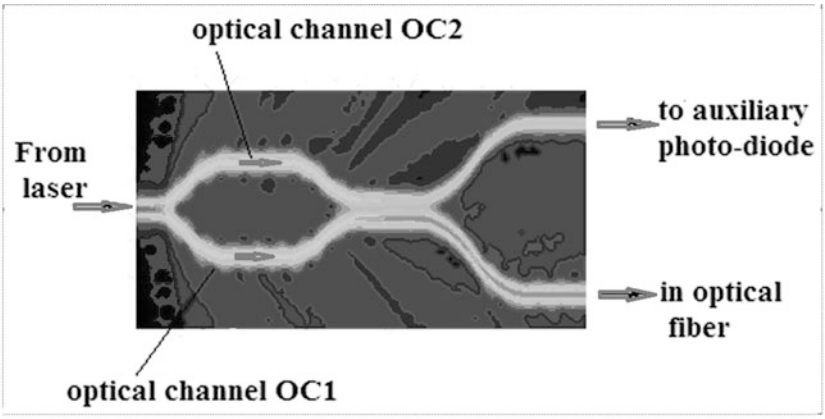

a)

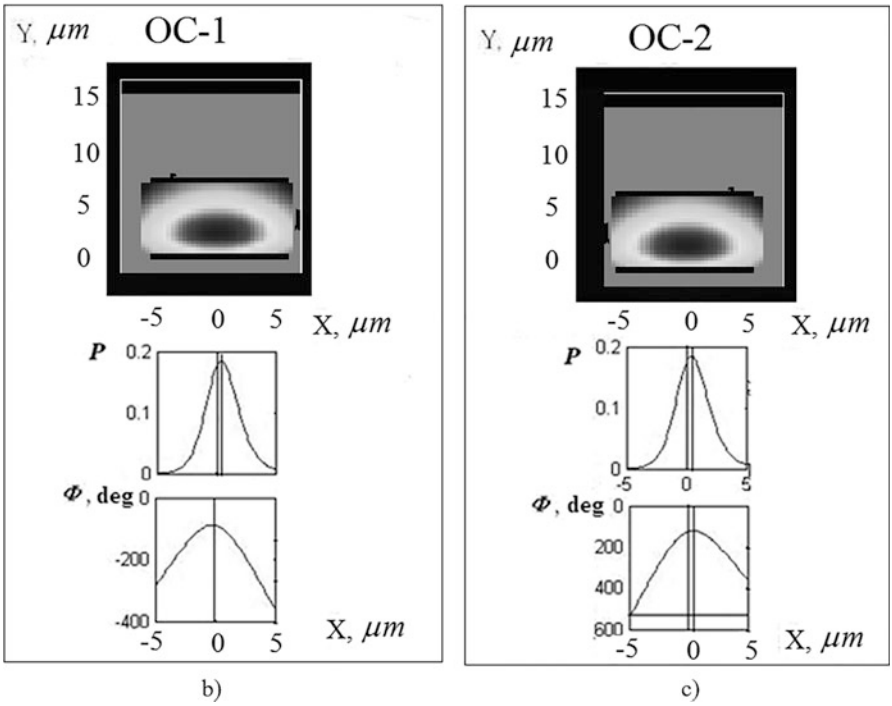

b) c)

Fig. 6.6 Distribution of the optical emission intensity with the wavelength of 1.55 μm in the optical channel OC1 and OC2 in the MZ modulator of the microwave range in the longitudinal section (**a**) and in the transverse section in the MZ output (**b**) and in the optical fiber output (**c**). The maximal light intensity passes in FOS from the MZ output, a part of emission with the minimal intensity passes to the auxiliary PD

a series of important conclusions follows: the optical MZ channels are nonuniform and nonideal, the emission in MZ strongly disperses on the media boundaries, the emission shape in the near zone in the MZ output is closed to an ellipse owing to the addition of coherent emissions, which are dispersed on channel boundaries. Taking into account the phase delays, we observe the minima zones in the form of dark circles located along the OC1 and OC2 channels with the period closed to the wavelength of emission.

In addition, we note that to compensate the laser phase fluctuations, we must fulfill the condition of equality with accuracy less than 0.1–0.001 from intensities in the outputs of the first and second channels in the transverse sections in the aperture. Otherwise, fluctuations' compensation is not fulfilled. We must take into consideration that detection of the optical emission occurs in the area of PD. The conditions of intensity equality in the transverse section with mentioned accuracies require the fulfillment of strict requirements to the material nonuniformity and to the drift of the geometrical sizes of channels in the modern MZ modulators.

Thus, the significant difference of heterodyning in the optical range from the similar operation of the radio-frequency range is the following. In the optical range, dimensions of the photodetection zone are commensurable with the laser wavelength. In the radio-frequency range, the geometrical dimensions of the detection zone of two electromagnetic oscillations at heterodyning can be simply performed as essentially less than the wavelength of radio oscillations, which participate in the process of its mixing. In this connection, the fluctuation compensation at heterodyning in the radio-frequency range is performed at equalization of the oscillation powers.

The above-mentioned can be illustrated by the fact that as the result of mixing on the PD area of the optical emissions, which passed the appropriate different optical MZ channels and having the power spectral densities $S_{1L}(F)$ and $S_{2L}(F)$ in the PD photo-current, we obtain: $S_{PD2}(F) = S_{1L}(F,R) + S_{2L}(F,R) - 2\left(\frac{A_2}{A_1}\right)K_{21}S_{12L}(F,R)$, where $S_{1L}(F)$, $S_{2L}(F)$ are PSD of optical phase fluctuations of emission, relatively, in optical channels OC1 and OC2, $S_{12L}(F,R)$ is mutual spectral density of PSD $S_{1L}(F)$, $S_{2L}(F)$; K_{21} is the autocorrelation function of the random process $K_{21} \approx \exp(-2\Delta\nu_L \cdot \Delta T_M) = \exp(-2\Delta T_M/T_c)$; $\Delta\nu_L \approx 1/T_c$ is the natural width of the spectral line of the reference generator (a laser) emission, T_c is the time of laser coherence, $S_{1L}(F)$, $S_{2L}(F)$ are PSD of the optical phase fluctuations, relatively, in the optical channels OC1 and OC2, $\Delta T_M = |T_{2M} - T_{1M}|$ is the delay difference in MZ channels and in FOS, A_2/A_1 is the ratio of quarter amplitude of optical harmonics: the $\sqrt{A_1}E_{0L}$ and $\sqrt{A_2}E_{0L}$ in the first harmonic and second harmonic, relatively. At that, on the PD area, there is the process of statistical averaging in time of the interference result of two optical harmonics ν_{0L} and $\nu_{0L} + f$, which are applied to the PD area: $E_{10L}(t) = \sqrt{A_1}E_{0L}\cos[2\pi\nu_{0L}t + \varphi_{0L} + \varphi_{10Lm}(t)]$ and $E_{20L}(t) = \sqrt{A_2}E_{0L}\cos[2\pi(\nu_{0L} + f_0)t + \varphi_{0L} + \varphi_{20Lm}(t)]$, with the amplitudes $\sqrt{A_1}E_{0L}$ and $\sqrt{A_2}E_{0L}$.

1. At large difference $\Delta T_M = |T_{2M} - T_{1M}|$, i.e., when this difference is much more (by 1000 and more times) than the time coherence of the laser T_c (and the oscillation period of the generator), the frequency discriminator plays the role of the converter of generator frequency into the phase fluctuations: $K_{21} = \exp(-\|T_{2M} - T_{1M}\|/T_c) \to 0$.
2. *But at small difference* $T_{2M} - T_{1M}$, *i.e., comparable* with the resonator time constant T_{OF} (and with the *oscillation period of the* generator)*, the frequency discriminator plays the role of the ideal suppressor of phase fluctuations:* $K_{21} = \exp(-|T_{2M} - T_{1M}|/T_{OF}) \to 1$. The suppression degree is defined by the channels equalization accuracy in the optical power or by the irregularity coefficient, which effects on the relative phase delays in the channel transverse section. In the optical range, the irregularity of the refraction index and micro-irregularities are deterministic from the point of view on the phase fluctuations' suppression quality.

We take into consideration that, firstly, the law of the emission intensity variation, which is passed from the laser to the MZ modulator input in the transverse section, is closed to the "Gaussian function," and phase delays of the coherent emission have the difference phase shift on the transverse section. Moreover, the law of the difference phase shift's variation in the transverse section is close to the parabolic one. Because of inaccuracies of manufacture of the optical waveguide MZ channels and the spatial variations of the material refraction index at applying in the input of the X-coupler, optical emissions are nonidentical in the intensity values in the transverse section and in phase shifts. Because of this, at adding with taking into account phase shifts in the MZ output, the intensity maximum is shifted. We note that the intensity of the spontaneous emission passing in the MZ input is by several ten times less than the coherent emission intensity (approximately, 10^{-3} to 10^{-4} for the modern quantum-well laser diodes). The intensity of the spontaneous emission passed to MZ input is uniformly distributed over the transverse section. Phase fluctuations of the optical emission are determined by the exactly spontaneous laser emission. Due to channel irregularities, the ratio in the transverse section of the spontaneous emission intensity to the coherent emission intensity in the input and in the output does not coincide. This leads to the imbalance of phase fluctuations' levels in channels OC1 and OC2. The level of the spontaneous emission in channels on the transverse section R remains almost unchanged, and the level of the optical emission intensity $P(R)$ in the transverse section of the optical emission channels (passed on the PD area) is changed due to irregularities.

Now we can conclude: at nonsymmetry of optical channels (due to irregularity of the permittivity) of 10^{-3}, we can achieve the integral value reduction of the phase noise in OEO MZ approximately by 40 times. The decrease of the permittivity irregularity value in MZ channels should lead to larger suppression of the phase noise.

As we see from Figs. 6.3, 6.4, and 6.6, the planar construction of modern microwave modulators with the bandwidth up to 15–20 GHz is the bright manifestation of engineering advantages in the field of microwave engineering and in

photonic at the end of twentieth century and in beginning of twenty-first century. For effectiveness increase of modern microwave modulators, the bias electrodes in them and the microwave electrodes are sprayed "from the top" of optical channels (Fig. 6.7), and the transverse distance between these channels is reduced to 20 μm. At that, the channel length is about 2000 μm, and the length of electrodes is about 1000 μm (Fig. 6.7). Electrodes which provide the constant bias, are sprayed directly near the *Y* directional coupler (Fig. 6.8). In some MZ modulator models, in order to increase the modulation effectiveness, the special "thin electron-holes *p-n* junction" is formed between the substrate and optical channel. In the simplified structure of the MZ modulator (Figs. 6.8, 6.10a), in the transverse section, the capacitance C_{pn} of the *p-n* junction is shown to be formed between optical channels OC1 and OC2 and the substrate, and the inter-electrode capacitance C_{cps} is formed between electrodes, which are connected to channels OC1 and OC2, and the resistor R_{pn}.

For operation of MZ modulator of the microwave range, the polarized emission of the high-coherent single-frequency laser is required. Quantum-well laser diodes with the polarizer are such a type of the emission sources.

Output emissions $E_{1\text{L}}$ and $E_{2\text{L}}$ of the first and second channels of the MZ modulator, in general case, may pass to the photodetector input through the different light guiders FOS1 and FOS2, and then the delay difference is: $\Delta T_{\text{M}} = T_{2\text{M}} - T_{1\text{M}} + T_{\text{FOS2}} - T_{\text{FOS1}}$.

Figure 6.8a, b show transverse sections of the MZ modulator for different variants of signal electrodes' location. The equivalent electrical circuit for connection of the RF signal and DC bias voltage for the AM 1550 modulator electrodes from JENOPTIK is presented in Fig. 6.8c.

In the case, when the FOS is formed by the single lengthy optical fiber, the delay difference is defined as: $\Delta T_{\text{M}} = T_{2\text{M}} - T_{1\text{M}}$.

It is necessary to emphasize that the fiber-optical delay line (RF FODL) in OEO MZ is the low-dispersed, i.e., the delay time in FOS is the function of the optical frequency: $T_{\text{FOS}} = T_{\text{FOS}}(\nu)$. OEO MZ represents the closed self-oscillating system with dissipation, in which structure the low-dispersed delay line is included. Specific MZ construction permits to provide not only the control of the MZ operation point, but to control of the optical powers in channels OC1 and OC2. Not only temporal laser coherence affects the MZ modulation effectiveness, but the spatial coherence as well.

6.3 Mathematical Model of OEO MZ

6.3.1 The Laser in OEO MZ

Below, for the analysis of the QWLD phase noises, we give the fluctuation equations for the laser deducted with the help of the semiclassical theory, which elements was demonstrated in Chap. 4. Dynamic character of laser noise characteristics can be

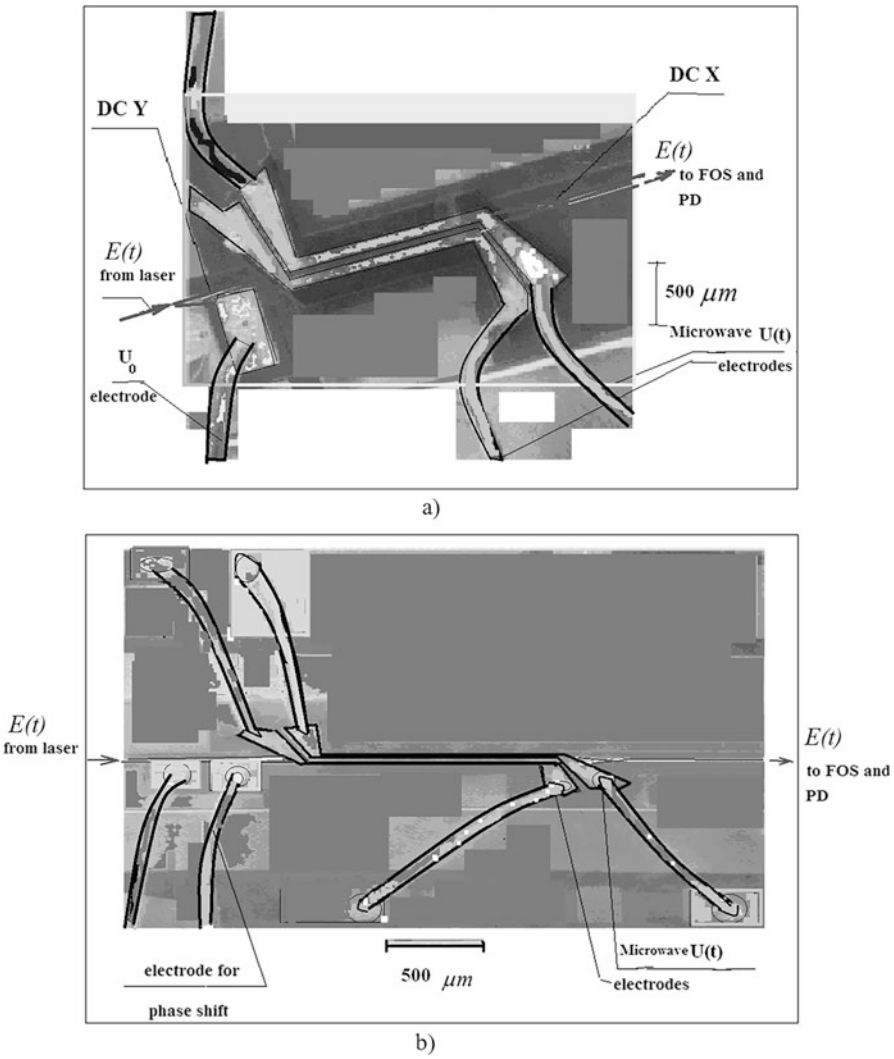

Fig. 6.7 Different types of the MZ modulator (**a**) and (**b**) with electrodes connecting to optical channels OC1 and OC2 in the electro-optical Mach–Zehnder modulator of the microwave range

described with the help of abbreviated equations for the electric field strength E_{L} and the laser optical phase φ:

$$\mathrm{d}E_{\mathrm{L}}/\mathrm{d}t = \left[\alpha_{0\mathrm{L}} - (2\pi\nu_{0\mathrm{P}}/Q_{0\mathrm{L}}) - \beta_{0\mathrm{n}}{E_{\mathrm{L}}}^2\right]E_{\mathrm{L}} - \xi_{\beta\mathrm{AN}}, \tag{6.2}$$

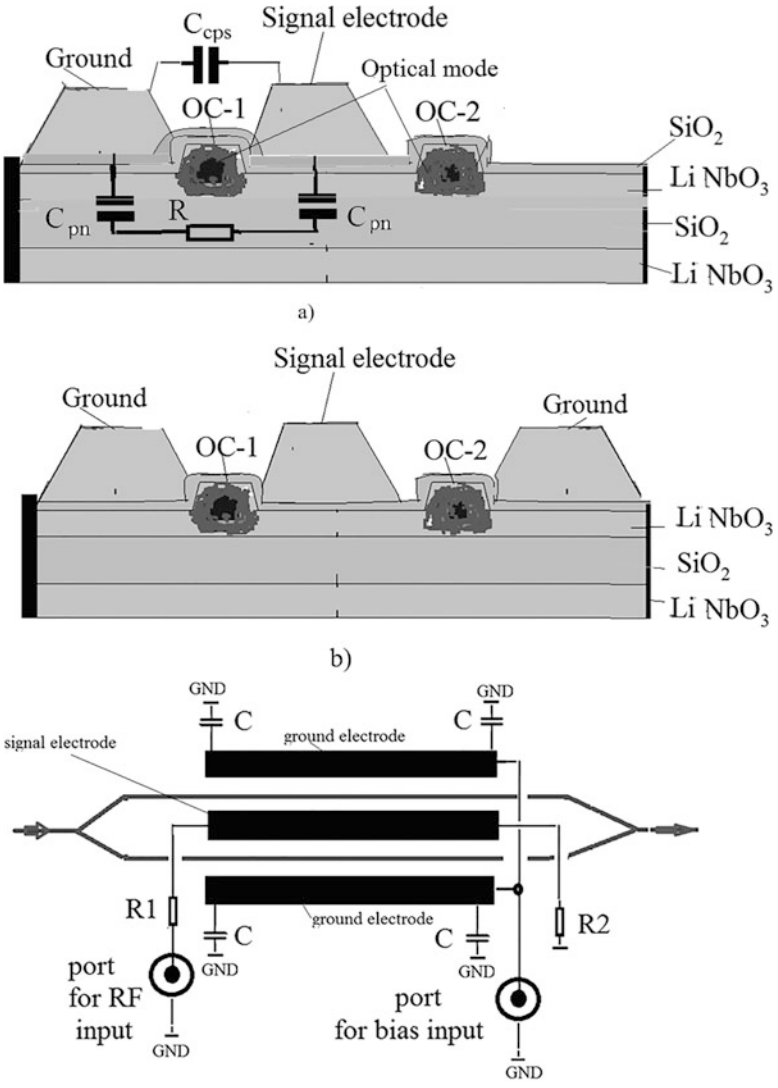

Fig. 6.8 The electrode location diagram, which are connected to optical channels OC1 and OC2 in the electro-optical Mach–Zehnder modulator of the microwave range: the circuit with the single electrode "Ground" (**a**); the circuit with double electrodes "Ground" (**b**). The circuit connection of the AM 1550 modulator electrodes from JENOPTIK $R_1 = 13\ \Omega$, $R_2 = 36\ \Omega$, $C = 100$ nF (**c**)

$$[2\pi\nu_0 - \Omega_L + d\varphi/dt] \cdot E_L = \left[\sigma_{0L}E_L - \rho_{0L}{E_L}^3\right] - \xi_{\beta PN}, \tag{6.3}$$

where α_{0L} is the optical gain of the laser active medium (pumping), ν_{0P} is the natural frequency of the laser resonator, Q_{0L} is the Q-factor of the laser resonator, β_{0n} is the constant coefficient (the saturation coefficient or the losses coefficient related with the spontaneous emission of the active medium), Ω_L is the angular optical frequency of the longitudinal generating mode of the laser resonator $\Omega_L = \pi c n_L (L_{0L})^{-1}$, n_L is the refraction index of the resonator material, L_{0L} is the geometrical length of the laser resonator, c is the light speed in vacuum, ε_0 is the permittivity, σ_{0L}, ρ_{0L} are constant coefficients, $\xi_{\beta AN}$, $\xi_{\beta PN}$ are the in-phase and quadrature components of Langevinian fluctuations (which spectral densities are equal relatively $S_{\beta AN}$ and $S_{\beta PN}$), which are determined by the field noises of active medium atoms in the laser resonator.

Taking into consideration that the photoreception is realized in the restricted band of optical frequencies at utilization in FOS, for example, of the narrowband optical filter, we may consider that the random process of the laser optical emission is stationary with the zero mean value. For such a process, spectral densities $S_{mL}(\nu)$ and $S_{\psi L}(\nu)$ of laser fluctuations $m_L(t)$, $\psi_m(t)$ are found at solution of abbreviated equations (6.2) and (6.3), taking into account the fluctuation Langevinian impacts $S_{\beta AN}$, $S_{\beta PN}$ and are defined by expressions: $S_{mL}(\nu) = \frac{S_{\beta AN} D_A}{T_{0L}^2 \cdot (\nu - \nu_0)^2 + B_L^2}$, spectral densities of phase $S_{\psi L}(\nu) = \frac{S_{\beta PN} D_F}{T_{0L}^2 \cdot (\nu - \nu_0)^2 E_0^2} = \frac{(\Delta\nu_{LP0})^2 S_{\beta PN} D_F}{(\nu - \nu_0)^2 E_0^2}$, where $B_L \approx \left[\sigma_{0L} - \rho_{0L} E_0^2\right]$. $\Delta\nu_{R0}$ is a half-width of the spectral line of the laser optical resonator $\Delta\nu_{LR0}$, which is inversely proportional to the laser resonator time constant T_{L0} : $\Delta\nu_{LR0} = 1/T_{0L}$, D_A, D_F are constant coefficients. The physical sense of $S_{mL}(\nu)$ and $S_{\psi L}(\nu)$ is clear: for the larger medium gain or pumping and for the higher laser resonator Q-factor and for lesser the spontaneous emission level, the amplitude noises and phase noises will be less at the fixed offset value from the carrier frequency. At the zero offset, AN is equal to the fixed value, and PN tends to infinity. The second approximate last formula in $S_{\psi L}(\nu)$ can be served for the fast qualitative estimation of the laser PN at known values for the spontaneous noise.

The similar expressions for laser spectral densities $S_{mL}(\nu)$, $S_{\psi L}(\nu)$ are obtained at consideration of the *quantum-mechanical equations* of van-der-Pol for the semiconductor laser [1] at account of spontaneous emission of the active medium. We should note that the spectral density of the laser phase fluctuations $S_{\psi L}(\nu)$, as for all other self-oscillating systems with dissipation, is inversely proportional to the normalized power $P_L = E_0^2$ and ${T_{L0}}^2$. The spectrum of the phase fluctuations $S_{\psi L}(\nu)$ forms the laser spectrum. In turn, the laser phase fluctuations are mainly determined by the value of the spontaneous emission.

One of OEO differences from the traditional oscillators is the fact that in the low-noise OEO, we must examine the optical channel of FOS as the spatial structure, in which the dispersion of the phase fluctuations is different in the transverse section. This is caused by the fact that, firstly, the emission phase fluctuations in the laser output in the transverse section are various. Secondly, the spatial optical channel of

RF FODL is nonuniform and nonideal. It contains the non-axis-symmetric planar optical waveguides, Y- and X-couplers of the MZ modulator, and the axis-symmetric fiber-optical light guide of FOS. We can take into consideration the dependence of the laser emission phase fluctuations in the transverse section, if we introduce the spatial parameter R.

We can show that the laser spectrum $S_{\psi L}(\nu) = S_{\psi L}(\nu, R)$ is the function of the spatial parameter R and the expression is true: $S_{\psi L}(\nu, R) \approx S_{\psi L}(\nu) \exp(\gamma_{L\psi} R)$, where $\gamma_{L\psi}$ is the spatial constant of the phase fluctuations of the laser output emission.

Now we explain the physical sense of the expression $S_{\psi L}(\nu, R) \approx S_{\psi L}(\nu) \exp(\gamma_{L\psi} R)$. In particular, we define the spatial parameter R as the radius (or the distance in the transverse section from the optical axis to the analysis point with the radius R). At that, the phase fluctuations of the laser emission in the transverse section increase at receding from the optical axis.

The plot presented in Fig. 5.12 shows that at the delay difference in MZ optical channels $\tau_D = \Delta T_M$ and less than 10^{-8} μs, the value is close to 1 with the accuracy to the third sign at the laser spectral width $\Delta\nu_L = 1$ kHz. This means that statistical random quantities of phase fluctuations of the laser emission are dependent in outputs of channels OC1 and OC2.

The linearly polarized optical emission E_L from the laser output passes to the modulator input. Then, the time-function of instantaneous field strength E_L on the central frequency ν_0 of QWLD generation taking into account of amplitude and phase laser fluctuations is determined by expression: $E_L = (E_{0L} + m_{lL}) \exp[j(2\pi\nu_0 t - \varphi_{0L} - \psi_m)]$, where $m_L = m_L(t, R)$, $\psi_m = \psi_m(t, R)$ are amplitude and phase field fluctuations E_L of the laser, which are defined by spectral densities, relatively, R is the index accounting the spatial dependence of the laser optical emission (for instance, the polarization dependence), $E_{0L} = E_{0L}(R)$ is the partial amplitude of the laser emission, $\varphi_{0L} = \varphi_{0L}(R)$ is the partial phase incursion of the laser emission.

The total output laser emission is defined as the result of integration on the PD area over all values of the spatial index R of the laser emission. *The spatial index R, which in the very simplest case is the distance or the radius from the optical axis to the specific point in the perpendicular section to the optical axis.* Laser emission has the spatial distribution $E_L(t, R)$ over the some section, which is in distant from QWLD output for some distance.

The physical sense of the integration over the R index is quite understandable: we perform integration over values of the field strength amplitudes taking into account the spatial distribution of the field amplitude.

6.4 Characteristics and the Transfer Function of the MZ Modulator in OEO

After passage of the optical emission through the modulator and FOS, on the PD area, two optical emissions will be added, which passed through the MZ modulator by the first E_{1L} and the second E_{2L} optical channels of the MZ modulator and FOS:

$$E_{1L} = k_{01}(E_{0L} + m_L)\exp\left[\, j2\pi\nu_0(t + T_{1M} + T_{FOS}) - j\varphi_{0L} - j\psi_{m1}\right], \tag{6.4}$$

$$E_{2L} = k_{02}(E_{0L} + m_L)\exp\left[\, j2\pi\nu_0(t + T_{2M} + T_{FOS}) - j\varphi_{0L} - j\psi_{m2}\right]. \tag{6.5}$$

Excitation coefficients k_{01}, k_{02} of the first and second modulator channels, in the general case, are relatively dependent upon the spatial index R and approximately are: $\gamma = k_{01}/k_{02}$.

Figure 6.9 shows the modulation characteristics of the MZ modulator.

Figure 6.10 shows the experimental functions of the optical power $P_O(U_{0MZ}/U_{0MZ\pi})$ (curves 1 and 2 in Fig. 6.10a), the RF power $P_{RF}(U_{0MZ}/U_{0MZ\pi})$ on the frequency $f = 10$ GHz (curves 3 in (a) versus the DC bias voltage U_{0MZ} (a)) and $P_O(\lambda)$ versus laser emission wavelength λ (Fig. 6.10b).

At the bias voltage $U_{0MZ} = U_{0MZMIN} = U_{0MZ\pi}$, the phase difference of optical oscillations propagating via the optical channels OC1 and OC2 is equal to π.

We would like to know that the difference between minimal values of $\Delta P_{OptRF} = P_O(U_{0MZ}/U_{0MZ\pi}) - P_{RF}(U_{0MZ}/U_{0MZ\pi}) \approx -20$ dB at $U_{0MZ}/U_{0MZ\pi} = 1$ in Fig. 6.10 (curve 1 and curve 3). The difference ΔP_{OptRF} between minimal values is the important characteristic of the modulator. This cannot confuse with the traditional characteristic, which is called the *modulator contrast* range. The contrast range is the difference ΔP_{Opt} : $\Delta P_{Opt} = P_{Omax} - P_{Omin}$ between maximal P_{Omax}, for example, at $P_{Omax} = P_O[(U_{0MZ}/U_{0MZ\pi}) = 0]$, and minimal values of P_{Omin}, for example, at $P_{Omin} = P_O[(U_{0MZ}/U_{0MZ\pi}) = 1]$ of the optimal power in the MZ modulator output for different DC voltage on MZ. The contrast range ΔP_{Opt} determines the maximal level of power of the side optical harmonics at RF modulation. ΔP_{OptRF} determines the final benefit as the result of statistical averaging over fluctuations. As we see from Fig. 6.10, ΔP_{OptRF} for the same type of the modulator (curves 1 and 2) is by 20 dB lesser than ΔP_{Opt}.

The plot $P_O(\lambda)$ versus the laser emission wavelength λ presented in Fig. 6.10b gives a possibility to determine the function of the $P_O(\lambda)$ minimum displace at variation of the DC bias voltage: 3 V/nm.

Figure 6.11a shows the power of RF oscillations $P_{RFPD}(P_{RFMZ})$ of "detected" optical emission in the PD load versus the microwave power P_{RFMZ} in the electrical input of MZ on the frequency $f = 10$ GHz.

Experimental functions $P_{RFPD}(P_{RFMZ})$ presented in Fig. 6.11a show that the ratio of PF power P_{RFPD} losses, which are applied to the electrical input of MZ in RF FODL (which is MZ-FOS-PD), to the oscillation power P_{RFPD} in the PD load is about -20 dB.

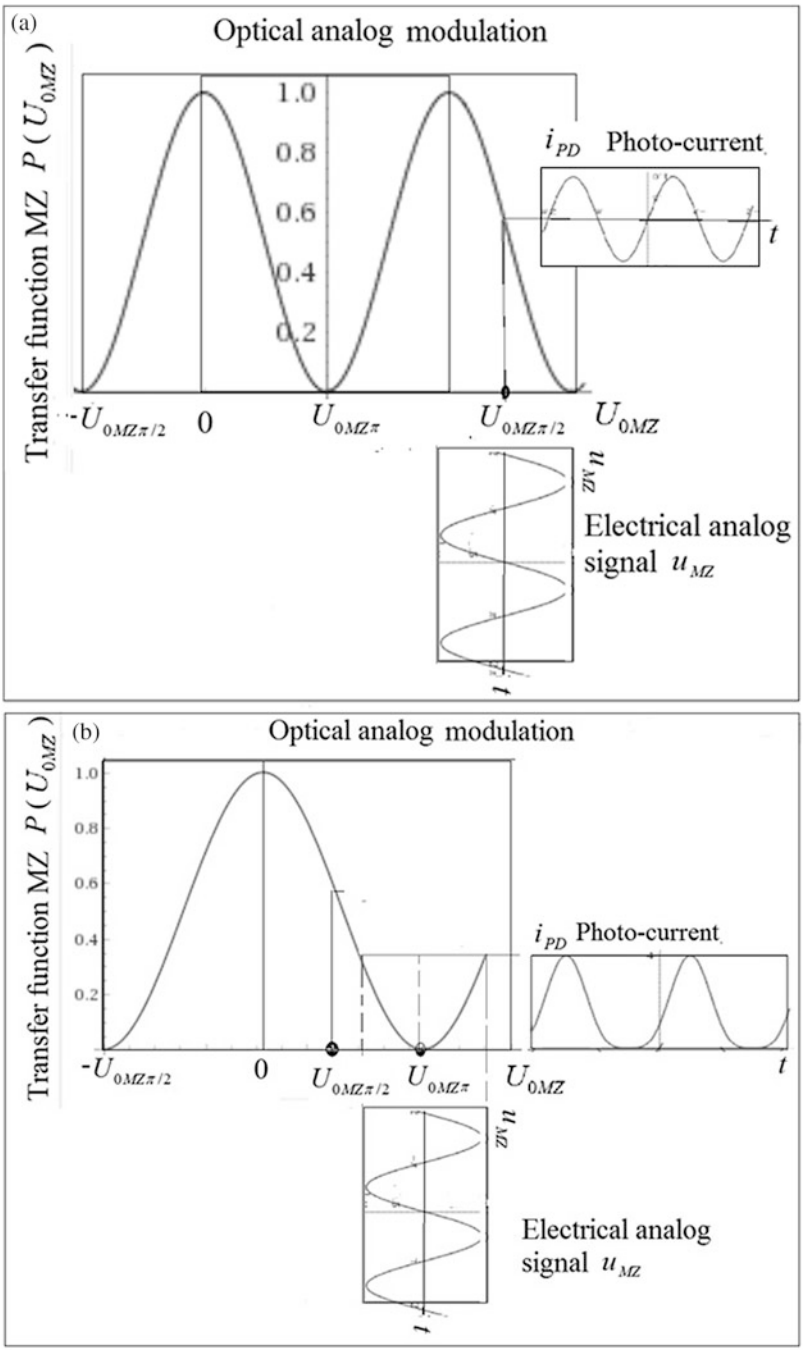

Fig. 6.9 The modulation characteristic of the MZ modulator: the function of the PD photo-current versus the phase difference variation of optical oscillations in the MZ channels at the operation point "$\pi/2$" (**a**). The transfer function $P(U_{0MZ})$ of the intensity modulator (or the analog modulator) in the operation point "π" (**b**)

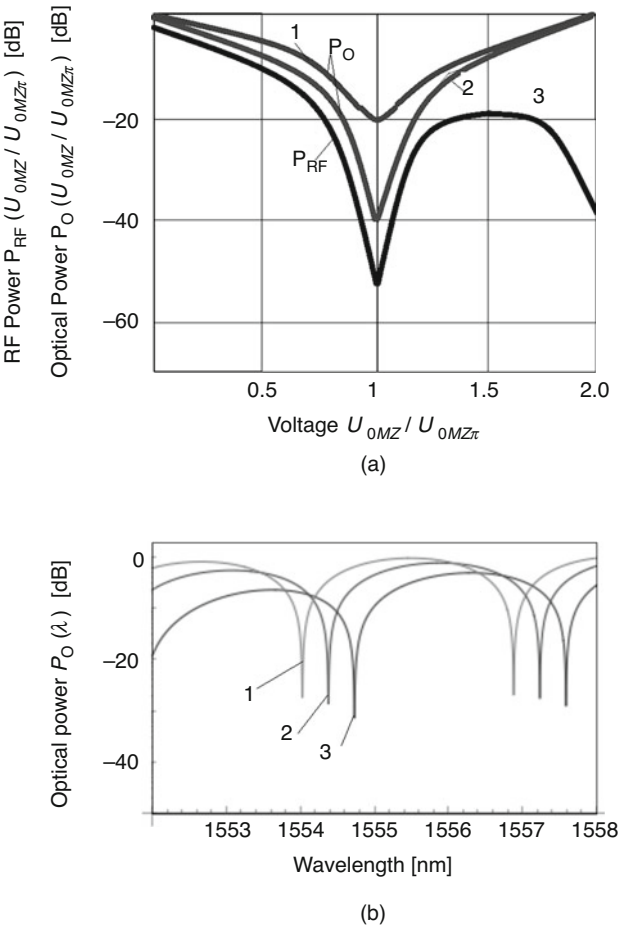

Fig. 6.10 Experimental functions of the optical power $P_O(U_{0MZ}/U_{0MZ\pi})$ (curves 1 and 2 in **a**), the RF power $P_{RF}(U_{0MZ}/U_{0MZ\pi})$ on the frequency $f = 10$ GHz (curves 3 in **a**) versus the DC bias voltage U_{0MZ} (**a**) and $P_O(\lambda)$ versus the laser emission wavelength λ (**b**). (**a**) for different MZ modulators: 1-st sample of MZ $U_{0MZ\pi} = 2$ V (curve 1), 2-тв sample of MZ $U_{0MZ\pi} = 5.5$ V (curve 2). The curve 3 corresponds to the first sample of MZ for $U_{0MZ\pi} = 2$ V. (**b**) corresponds to MZ with $U_{0MZ\pi} = 5.5$ V : $U_{0MZ} = 0$ V (curve 1), $U_{0MZ} = 3$ V (curve 2). Curve 3 for MZ for $U_{0MZ} = 6$ V

The time delay T_{1M} in the second modulator channel at application in the MZ modulator input of the harmonic signal $u_{RF}(t)$ is varied as: $T_{2M} = T_{20M} + u_{RF}(t)B_M$, where $T_{2M} = T_{2M}(U_{0MZ})$ is the delay of the optical signal in the second channel of the MZ modulator at application to MZ of the constant bias voltage $U_{0MZ} = U_{0M}$, and $B_M = dT_{2M}/(dU_{0MZ})$ is the conversion slope of the MZ modulator, relatively.

The increment of the optical phase $\Delta\varphi_{0M2}$ in the output of OC2 of MZ at application to electrodes of the second optical channel of the constant voltage U_{0M}

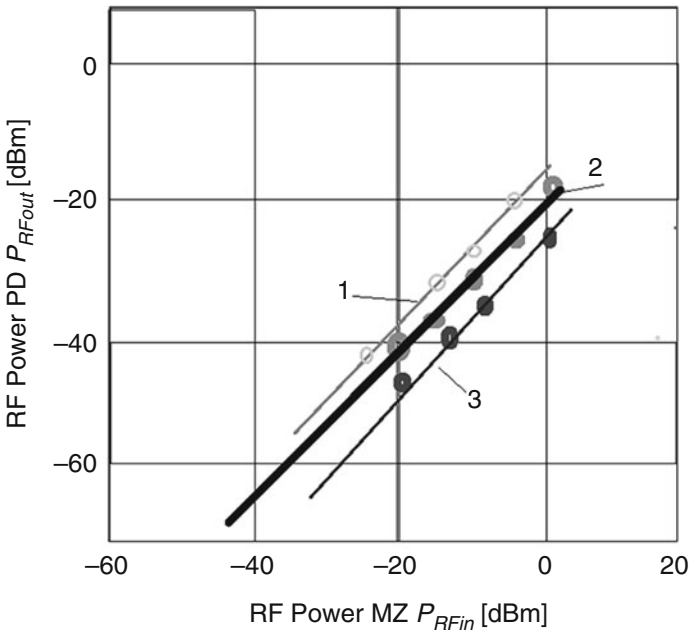

(a)

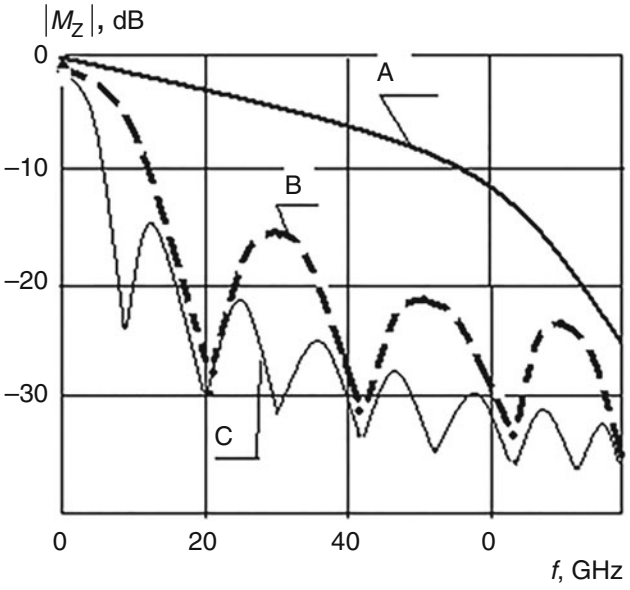

(b)

Fig. 6.11 (**a**) Dependence of the microwave power $P_{\mathrm{RFPD}}(P_{\mathrm{RFMZ}})$ of "detected" optical emission in the PD load versus the microwave power P_{RFMZ} in the electrical input of the MZ modulator on the frequency $f = 10$ GHz. The optical wavelength is $\lambda = 1550$ nm. The DC bias voltage in MZ is 1 V, $U_{0\mathrm{MZ}\pi} = 2$ V. Different lines in plots corresponds to different optical losses on matching on

is determined as: $\Delta\varphi_{0M2} = 2\pi\nu_0 B_M U_{0M} = 2\pi\nu_0 n_M^3 r_{33} L_M U_{0M}/(cd_M)$, where the effective length of the modulator electrodes $L_M = 0.02$ m, the distance between modulator electrodes is $d_M = 10$ μm, the coefficient $r_{33} = 30.8 \cdot 10^{-12}$ m/V, the effective refraction index of the material $n_M = 2.3$ and is several degrees at input voltages U_{0MZ} not more than 0.01 V. At that, the phase modulation index determining as $B_{UM} = 100\ \% \cdot \Delta\varphi_{0M2}/2\pi = 100\ \% \cdot \nu_0 U_{0MZ} B_M$ is several percents. We note that at large modulation signals, the expression for an argument $\arg E_{12L}$ should be presented by the nonlinear dependence through the Bessel functions.

The modulator effectiveness can be estimated by the coefficient η, which is defined as the ratio: $\eta = \frac{\Delta\varphi_{0M2}}{U_{0MZ}L} = \frac{2\pi\Delta n_{eff}}{\lambda U_{0M}}$. To determine the MZ effectiveness, we introduce the coefficient α_{ch} defining as a ratio of the phase shift increment and the optical losses $\Delta\alpha_{pt}L_M$ in MZ (or the ratio of the real part of the MZ refraction index to its imaginary part): $\alpha_{ch} = \frac{\Delta n_{ef\,Re}}{\Delta n_{efIm}} = \frac{2\Delta\varphi_{0M2}}{\Delta\alpha_{pt}L_M}$.

At small input modulation signal in MZ, we may use the linearization of the argument $\arg E_{12L}$ and to present the expression for the strength on the PD area $\mathbf{E}_{L12}$ as: $\mathbf{E}_{12L} = \mathbf{E}_{1L} + \mathbf{E}_{2L} = |\mathbf{E}_{12L}| \exp[j \arg(\mathbf{E}_{12L})]$, in which the module is $|\mathbf{E}_{12L}| = |\mathbf{M}_z \mathbf{E}_{0L}|$, where $\mathbf{M}_z$ is the module of the transfer function of the MZ modulator.

Using the fact that E_{0L}^2 is the normalized intensity in the MZ input, the coefficient $\gamma = k_{01}/k_{02}$ and $k_{01} \approx k_{02} \approx 0.5$, and the intensity module $|\mathbf{E}_{12L}|$in the MZ output is in Eqs. (3.30)−(3.34). In the small mode, at $\gamma \approx 1$, the following expression is obtained from Eq. (3.31) for the small argument deviations φ_1 and φ_2 from its average values of $\Delta(\Delta\varphi_{0M2}) = \arctan\left\{\frac{\sin\Delta\varphi_1 + \gamma\sin\Delta\varphi_2}{\cos\Delta\varphi_1 + \gamma\cos\Delta\varphi_2}\right\}$. And for the small argument deviations

$$\Delta(\Delta\varphi_{0M2}) \approx \frac{\Delta\varphi_1 + \gamma\Delta\varphi_2}{2 - \Delta\varphi_1{}^2 - \gamma\Delta\varphi_2{}^2} \approx \frac{\gamma\Delta\varphi_2}{2 - \gamma(\Delta\varphi_2)^2}. \tag{6.6}$$

From Eqs. (3.30) to (3.34), (6.6), the important conclusion follows that small variations of the irregularity coefficient γ of channel OC1 and OC2 excitation lead to variations of the difference phase shift $\Delta\varphi_{0M2}$. This means that for well operation, in OEO MZ should be satisfied the requirements to excitation uniformity of MZ optical channels. From this requirement, the demand to the spatial laser coherence follows and the demand to polarization of laser emission.

For the sake of simplicity, we may consider that in the small-signal mode $\arg\mathbf{E}_{12L} = [2\pi\nu_0(T_{2M} - T_{1M})]$. In the small-signal mode, the coefficient α_{ch} is defined as $\alpha_{ch} = 2E_{0L}^2 \frac{d\Delta\varphi_{02M}}{dE_{0L}^2}$. This means that at the output power maximum of the laser emission E_{0L}^2, there is the maximum of the α_{ch} parameter, while the power variations are minimal.

Fig. 6.11 (continued) (curve 1—1 dB, curve 2—5 dB, curve 3—10 dB). (**b**) The calculated functions of the MZ transfer function module $|M_{eZ}|$ in the small-signal mode Eqs. (6.8) and (6.9). The laser optical wavelength $\lambda = 1550$ nm($\nu_0 = 128$ THz). For curve (A) $\alpha_{1m} = 0.27$ dB/cm, $n_M = 2.4$, curve (B) $\alpha_{1m} = 0.41$ dB/cm, $n_M = 3.18$, (C) $\alpha_{1m} = 0.68$ dB/cm, $n_M = 4.24$

The voltage on the load resistance Z_{PD} of the photodetector is $u_{PD} = Z_{PD} \cdot i_{PD\Sigma}(R)$. The PD current $i_{PD\Sigma}(R)$ is a sum of all photo-currents $i_{PD}(R)$ with the index R. The photo-current $i_{PD}(R)$ is the result of multiplication of the emission strength E_{12L} by the complex-conjugated quantity E^*_{12L}. Therefore, for the PD current, the expression is true: $i_{PD\Sigma}(R) = \sum_R i_{PD}(R) = K_{PD} \cdot \sum_R \left[E_{12L}(R) \cdot E^*_{12L}(R)\right]$. The PD transfer function K_{PD} is defined by the expression $K_{PD} = |K_{PD}| \cdot \exp(-j2\pi f\tau_{PD})$, where $\tau_{PD}$is the time constant of PD.

6.4.1 The Total Transfer Function of the MZ Modulator

We must take into consideration the transfer function of RF electrodes. Expressions (3.30)−(3.34) for the MZ transfer functions are true when we neglect of losses and delay of the electrical microwave signal in the MZ system of electrodes. In the case, when we need to take into account the losses and delay of the electrical signals in the MZ electrode system, the expression for the MZ transfer function M_{eZ} can be written as:

$$M_{eZ} = \exp(-\alpha_{1m} l_{1m}) \frac{[\sin(\alpha_{1m} l_{1m}/2) + j \sin(\xi_1 \cdot l_{1m}/2)]}{[(\alpha_{1m} l_{1m}/2) + j(\xi_1 \cdot l_{1m}/2)]} \tag{6.7}$$

This expression is calculated with account of propagation of the direct and reflected electromagnetic waves, which propagates in the strip structure of the microwave MZ electrodes.

For the module of the MZ transfer function $|\mathbf{M}_{eZ}|$, the following expression is true:

$$|\mathbf{M}_{eZ}| = \exp(-\alpha_{1m} l_{1m}) \frac{\left[\sin^2(\alpha_{1m} l_{1m}/2) + \sin^2(2\pi f \cdot n_M \cdot l_{1m}/2c)\right]^{1/2}}{\left[(\alpha_{1m} l_{1m}/2)^2 + (2\pi f \cdot n_M \cdot l_{1m}/2c)^2\right]^{1/2}}. \tag{6.8}$$

For the argument of the MZ transfer function ($\arg\mathbf{M}_{eZ}$), the following expression is true:

$$\arg\mathbf{M}_{eZ} = \arctan\left[\frac{\sin(2\pi f \cdot n_M \cdot l_{1m}/2c)}{\sin(\alpha_{1m} l_{1m}/2)}\right] - \arctan\left[f \cdot \frac{(2\pi \cdot n_M/c)}{\alpha_{1m}}\right], \tag{6.9}$$

where α_{1m} is the microwave losses in electrodes, l_{1m} is the electrode length, $\xi_1 = (2\pi f \cdot n_M/c)$. Figure 6.11b shows the calculated dependences (6.8), (6.9) of the module of the MZ transfer function $\mathbf{M}_{eZ} = \mathbf{M}_{EZ}$ in the small-signal mode. At that, in Fig. 6.15 the plots correspond to different MZ parameters: (a) $\alpha_{1m} = 0.68$ dB/cm, $n_M = 4.24$; (b) $\alpha_{1m} = 0.41$, $n_M = 3.18$; (c) $\alpha_{1m} = 0.27$ dB/cm, $n_M = 2.4$.

The calculated dependences of the transfer function module shown in Fig. 6.15 are well agreed with the typical experimental characteristics for this class of MZ modulators, which have the modulation frequency band of 20–35 GHz (Fig. 2.11c in Chap. 2).

We calculated by Eq. (6.8) (a) and Eq. (6.9) (b) dependences of the module $|\mathbf{M}_{eZ}|$ and the argument $\arg\mathbf{M}_{eZ}$ of the MZ transfer function in the small-signal mode calculated accordingly by Eqs. (6.8) and (6.9) at for various geometrical length of electrodes $L_e = 1000, 3000, 5000$ μm and for various loss parameters for (a) $\alpha_{1m} = 0.27$ dB/cm, $n_M = 2.4$, (b) $\alpha_{1m} = 0.41$ dB/cm, $n_M = 3.18$, (c) $\alpha_{1m} = 0.68$ dB/cm, $n_M = 4.24$. $\alpha_{1m} = 0.27 - 0.68$ dB/cm.

From our calculation of the MZ transfer function and the analysis of the plots presented in Fig. 6.11b, we can make the following conclusion. The growth of the electrode lengths leads to the rejection character of the function of the module $|M_{eZ}|$ with clearly expressed minima of the transfer characteristic, which corresponds to adding of the out-of-phase direct wave and reflected wave from the end boundary of the strip, and the slope of function $\arg M_{eZ}$ versus the modulation frequency is determined by the losses α_{1m}.

6.4.2 *The Total MZ Transfer Function with Account of the Transfer Function of the Radio-Frequency Electrodes of MZ*

The MZ has the specific feature: its transfer function depends not only on the radio-frequency electrodes (their length, configuration, etc.) but upon the transfer function of the MZ optical system M_Z, which is determined by its differential structure.

In Fig. 3.14a, b (Chap. 3) we show the calculated functions of the module $|\mathbf{M}_Z|$ and the argument $\arg\mathbf{M}_Z$ versus the phase difference value in the optical channels OC1 and OC2: $2\pi\nu(T_{2M} - T_{1M})$ (ν is the laser optical frequency) of the MZ transfer function (a) for different values of the excitation coefficient $k_{01} = A = \alpha$ for $k_{02} = B = 1 - A$. These functions are calculated by formulas $\eta = \frac{\Delta\varphi_{0M2}}{U_{0MZ}L} = \frac{2\pi\Delta n_{eff}}{\lambda U_{0M}}$ and $\alpha_{ch} = \frac{\Delta n_{ef\,Re}}{\Delta n_{efIm}} = \frac{2\Delta\varphi_{0M2}}{\Delta\alpha_{pt}L_M}$. From the plots analysis shown in Fig. 2.14a, we can make a conclusion that the module $|\mathbf{M}_Z|$ and the argument $\arg\mathbf{M}_Z$ depend upon the excitation coefficient k_{01}. The total MZ transfer function (taking into consideration of the radio-frequency electrodes and the MZ differential structure) is determined with the accuracy to the constant coefficient at small-signal modulation: $\mathbf{M}_{ZZ} \approx \mathbf{M}_Z \cdot \mathbf{M}_{eZ}$.

The total transfer function of RF FODL defined as a ratio of the first harmonic voltage amplitude in the RF FODL output to the amplitude of the first harmonic voltage in the RF FODL input is determined as:

$$\begin{aligned}\mathbf{K}_{\mathrm{FODL}} &= P_{0\mathrm{L}} \cdot \mathbf{M}_{\mathrm{Z}} \cdot \mathbf{M}_{\mathrm{eZ}} \cdot \mathbf{K}_{\mathrm{FOS}} \cdot \mathbf{K}_{\mathrm{PD}}, \quad |\mathbf{K}_{\mathrm{DL}}| = |\mathbf{K}_{\mathrm{BZ}}| \\ &= |\mathbf{M}_{\mathrm{Z}}||\mathbf{M}_{\mathrm{eZ}}||\mathbf{K}_{\mathrm{FOS}}||\mathbf{K}_{\mathrm{PD}}|, \end{aligned} \tag{6.10}$$

$$\arg\mathbf{K}_{\mathrm{DL}} = \arg\mathbf{K}_{\mathrm{BZ}} = \arg\mathbf{M}_{\mathrm{Z}} + \arg\mathbf{M}_{\mathrm{eZ}} + \arg\mathbf{K}_{\mathrm{FOS}} + \arg\mathbf{K}_{\mathrm{PD}}, \tag{6.11}$$

where $P_{0\mathrm{L}}$ is the DC component of the laser power, S_{PD} is the slope of the watt–ampere characteristic of PD, K_{FOS} is the transfer function of the optical fiber with account of the matching elements. T_{MZ} is the coefficient of the voltage conversion into the light delay in the MZ optical channel or $T_{\mathrm{MZ}} = T_{\mathrm{M}} = \mathrm{d}\arg\mathbf{M}_{\mathrm{Z}}/\mathrm{d}U_{0\mathrm{MZ}}$.

Executed analysis of MZ in OEO and formulas obtained allow the transfer to the amplitude and frequency determination in the steady-state mode of the OEO MZ generation.

6.4.3 Abbreviated Equations of OEO MZ

With account of used designations, here we use the approach for deduction of abbreviated equations of the OEO oscillator, which is described in Chaps. 3 and 5. Here we shall consider all RF circuits (besides the RF filter) included into the RF part of OEO, as wideband circuits. At that, abbreviated differential equations of the OEO MZ for the slowly changed amplitude $U_{1\mathrm{L}} = U_{\mathrm{a}}$ and phase $\psi_{1\mathrm{L}} = \psi_{\mathrm{U}}$ of the first harmonic oscillations (in the output of OEO MZ) have the form:

$$\begin{cases} T_{1\mathrm{e}}\dfrac{\mathrm{d}U_{1\mathrm{L}}}{\mathrm{d}t} = U_{1\mathrm{L}} \cdot \mathrm{Re}\left(\mathbf{K}_{\mathrm{FOLD}}R_{\mathrm{con}}S_{\mathrm{NA0}}\right) - U_{1\mathrm{L}} \\ U_{1\mathrm{L}}T_{1\mathrm{e}}\dfrac{\mathrm{d}\psi_{1\mathrm{L}}}{\mathrm{d}t} = U_{1\mathrm{L}}2\pi(f_{\mathrm{res}} - f)T_{1\mathrm{e}} + U_{1\mathrm{L}}\mathrm{Im}(\mathbf{K}_{\mathrm{FOLD}}R_{\mathrm{con}}S_{\mathrm{NA0}}) \end{cases}, \tag{6.12}$$

where R_{con} is the control OEO resistance, S_{NA0} is the average slope of NA, $T_{\mathrm{F}} = T_{1\mathrm{e}}$ is the time constant of the RF filter, and f_{res} is its resonance frequency.

For the following nonlinear characteristic of the active element $i(u) = S_{01}u - S_{03}u^3$ and the average slope of this characteristic of AE in the NA $S_1(U) = S_{01} - (3/4)S_{03}U^2$, we search the solution of the differential equation. Then, from the first equation of the system (6.12), we have got the expression for the amplitude U of OEO MZ oscillations:

$$U = \sqrt{4S_{01}/3S_{03}} \cdot \left(1 - \frac{1}{S_{01}P_{0\mathrm{L}}R_{\mathrm{PD}}|M_{\mathrm{Z}}||M_{\mathrm{eZ}}||K_{\mathrm{FOS}}||K_{\mathrm{PD}}||K_{\mathrm{F}}|}\right)^{1/2}. \tag{6.13}$$

From abbreviated equation (6.12), we can obtain the equations of the phase and amplitude balance for the steady-state mode in the form:

$$\arctan\left\{\frac{\sin 2\pi\nu T_{2M}+\gamma_k \sin 2\pi\nu T_{1M}}{\cos 2\pi\nu T_{2M}+\gamma_k \cos 2\pi\nu T_{1M}}\right\}+\arctan(\omega T_{eM})$$
$$+\arctan(\omega T_{FOS})-\arctan(\omega T_F)=2\pi m, \tag{6.14}$$

where ν is the laser optical frequency, R_{PD} is the load resistance of PD, T_{eM} is the time constant defining by the MZ electrodes, T_{FOS} is the group light delay in the FOS, T_{1M}, T_{2M} are the group light delays in the MZ optical channels OC1 and OC2.

We calculated the frequency response of MZ transfer function module $|M_Z|$, of the RF filter $|K_F|$, and its products $|M_Z| \cdot |K_F|$. The graphical method of the frequency determination for OEO MZ is presented in Fig. 3.19 with the help of the solution of the balance equations for the phase and the amplitude for OEO MZ.

From Eq. (6.14), we obtain the equation for the radio frequency $f = f_{gen}$ in the steady-state mode in the form:

$$f_{gen} \cong \frac{m+f_F T_F}{T_F+\arg \mathbf{K}_{DL}/f_F}$$
$$=\frac{m+f_F T_F}{T_F+T_{eM}+T_{FOS}+\arctan\left\{\frac{\sin 2\pi\nu T_{2M}+\gamma_k \sin 2\pi\nu T_{1M}}{\cos 2\pi\nu T_{2M}+\gamma_k \cos 2\pi\nu T_{1M}}\right\}/f_F}. \tag{6.15}$$

From Eq. (6.15), one of the most important features of OEO follows: *there is the dependence of the radio frequency f versus the optical frequency ν of the laser generation.* As it follows from the right part of the second equation (6.12), the multiplier $\mathrm{Im}\mathbf{K}_{DL}$(the imaginary part of the transfer function of the circuit "FOS-NA") depends upon the laser optical frequency. This dependence is caused by the effect of the optical frequency upon the phase incursion in different MZ optical channels. From the Eq. (6.15), assuming that transfer functions of the optical channels $k_{01} = A = \alpha$ and $k_{02} = B = 1 - A$ are approximately equal to 0.5, i.e., the coefficient $\gamma_k = \gamma = k_{01}/k_{02} \approx 1$, we obtain the formula for radio-frequency deviation $\Delta f = \Delta f_{gen}$ of the OEO generation from its mean value at deviation of the laser optical frequency $\Delta\nu$ in the form:

$$\Delta f_{gen} \cong \frac{m+f_F T_F}{\frac{T_{2M}+T_{1M}}{2}+\frac{T_{2M}-T_{1M}}{2}(1-\gamma_k)\frac{\Delta\nu}{f_F}+T_{eMZ}+T_{FOS}+T_F}, \tag{6.16}$$

where T_{FOS} is the delay in the optical fiber. From Eq. (6.16) it follows that deviations of the radio frequency Δf are determined by also deviations of the laser optical generation $\Delta\nu$, and by the delay difference in optical channels $T_{2M} - T_{1M}$. Deviations Δf_{gen} are determined by the ratio of optical frequency deviations $\Delta\nu$ to the average OEO generation frequency: $\Delta\nu/f_{RF}$. Deviations Δf_{gen} are less for lesser difference of the excitation coefficients of optical channels k_{01} and k_{02} (or the coefficient of excitation irregularity of MZ optical channels is close to 1: $\gamma_k \approx 1$)

and for larger time constant T_F of the RF filter and for the larger delay time in FOS T_{FOS}.

If the following inequality is satisfied: $T_{FOS} > T_{eMZ} + T_F + \frac{T_{2M}+T_{1M}}{2} + \frac{T_{2M}-T_{1M}}{2}(1-\gamma)\frac{\Delta\nu}{f_{RF}}$, then the influence of the quasi-static parameter variations of the OEO MZ optical part can be estimated by the formula for the relative deviations from the steady-state values $\Delta\Delta\nu$ and $\Delta\Delta(1-\gamma)$: $\frac{\Delta f_{gen}}{f_{gen}} = \left[\frac{\Delta\nu}{f_{RF}} \cdot \frac{T_{2M}-T_{1M}}{2}(1-\gamma) + \frac{\Delta(1-\gamma)}{(1-\gamma)}\frac{\Delta\nu}{f_F}\right] \cdot \frac{T_{eMZ}+T_F}{T_{FOS}}$.

We would like to note the specific case if different optical emissions transmitted in the different MZ optical channels OC1 and OC2 after MZ are not connected. In other words, optical oscillations with different delays propagate through different optical fibers of the similar or different length. In such a case, the quantity $\frac{T_{2M}-T_{1M}}{2} \cdot (1-\gamma)$ becomes significantly important. For instance, at $\frac{T_{2M}-T_{1M}}{2} \cdot (1-\gamma) = 10^{-9} - 10^{-7}$ μs, deviations of the laser optical frequency $\Delta\nu$, even at account of the stabilizing effect of the long optical fiber with the delay T_{FOS}, for example, 1 μs, should be taking into consideration.

6.4.4 *Fluctuations of the Photodetector Photo-Current in OEO MZ*

Now we find the voltage fluctuations in the PD load, which are caused by amplitude $m_L(t)$ and phase $\Delta\psi_L(t)$ fluctuations of the electromagnetic field strength E_{12L}, considering that these fluctuations are small compared to its mean values and neglecting the harmonics of the noise currents. We may prove using expressions (6.2) and (6.3) for laser fluctuations with spectral densities of amplitude $S_{mL}(\nu)$ and phase $S_{\psi L}(\nu)$, relatively, that fluctuations μ_n of PD $i_{PD\Sigma}$ are determined by the detected amplitude $m_L(t)$ and the difference phase fluctuations $\Delta\psi_L = \psi_{m2} - \psi_{m1}$ and by AN-PN fluctuations of the electrical component strength of the laser electromagnetic field and it can be written in the complex form as:

$$\mu_n = \mu_{AN} + \mu_{PN\text{-}AN} + j\mu_{PN}, \tag{6.17}$$

where μ_{AN}, $\mu_{PN\ -\ AN}$, μ_{PM} are fluctuation of PD current caused, relatively, by the amplitude (AN) $m_L(t)$, AN-PN conversion, and phase (PN) $\Delta\psi_L(t)$. Values of these fluctuations of output PD current *are results of heterodyning* and depend upon the oscillation amplitude U_{10MZ}, for them the following expressions are true:

$$\mu_{AN} = m_L^2 U_{10MZ}\cos(2\pi f_0 t), \quad \mu_{PN} = 2(\Delta\psi_L)^2 U_{10MZ}\cos(2\pi f_0 t). \tag{6.18}$$

$$\mu_{\text{PN-AN}} = 2(\Delta\psi_{\text{L}})^2 \sin\left[2\pi\nu_0(T_{1\text{M}} - T_{2\text{M}}) + \pi(U_{0\text{MZ}}/U_{\pi 0\text{MZ}})\right] \cdot U_{10\text{MZ}} \cos(2\pi f_0 t), \tag{6.19}$$

Thus, as the result of heterodyning, the spectrum of fluctuations of the PD output current is obtained by the "transfer" of the optical noise spectrum from the *laser* (or QWLD) generation frequency ν_0 to the OEO radio-frequency generation f_0. To Eqs. (6.18) and (6.19), we must add the noise current in the photodetector load, which obtained from the detected noise of the DC of the laser emission.

6.4.5 Power Spectral Density of the Detected Laser Fluctuations

The PSD $S_\mu(\omega)$ of the detected laser fluctuations of each type of μ_{AN}, $\mu_{\text{AN - PN}}$, μ_{PN} voltages in the PD load is determined as the result of the Fourier transform of its correlation functions.

For the amplitude noises, which are usually much less than the conversion AN-PN noises, the power spectral density of the in-phase $S_{\mu\text{Re}} = S_{\text{LRe}}(\omega)$ and the quadrature $S_{\mu\text{Im}}(\omega) = S_{\text{LIm}}(\omega)$ components of the current fluctuations is described, relatively, by the following relations:

$$S_{\text{L Re}}(\omega) = G_{12} \cdot \left(S_{\mu\text{AN}} + S_{\mu\text{AN-PN}}\right) = G_{12} S_{\mu\text{AN}} + \frac{S_{\beta\text{PN}} D_{\text{FA}} U_{0\text{MZ}}^2 \sin\left[2\pi\nu_0(T_{1\text{M}} - T_{2\text{M}})\right] \cdot G_{12}}{(\omega - \omega_0)^2 T_{0\text{L}}^2 \cdot 0.25 \cdot B_{\text{L}}^2}, \tag{6.20}$$

$$S_{\text{LIm}}(\omega) \approx \frac{4 S_{\beta\text{PN}} D_{\text{PN}} U_{10\text{MZ}}^2 G_{12}}{(\omega - \omega_0)^2 T_{0\text{L}}^2 P_{0\text{L}}}, \tag{6.21}$$

where G_{12} is the coefficient of the phase fluctuation suppression of the laser optical emission at the expense of correlation of the random phase of laser emission in the system "MZ–optical fiber—photodetector."

At the *closed feedback loop* of OEO MZ, G_{12} is: $G_{12} = 1 - (A_1/A_2) \cdot \exp(-2\Delta T_{\text{FOS}} \cdot \Delta\nu_{\text{L}})$, while at the *opened feedback loop* of OEO MZ, G_{12} is: $G_{12} = 1 - (A_1/A_2) \cdot \exp(-2\Delta T_{\text{M}} \cdot \Delta\nu_{\text{L}})$, where the coefficient $A_1/A_2 \approx 1$, $\Delta\nu_{\text{L}}$ is the laser spectral line width $\Delta\nu_{\text{L}} = 1/T_{\text{c}}$, T_{c} is the laser coherence time.

We cannot create the ideal case$A_1/A_2 \approx 1$ and really, the suppression coefficient is $G_{12} \approx 10^{-1} - 10^{-3}$.

Taking into consideration the transfer function of the nonlinear amplifier and the pass-band filter of the microwave range, the expression for the instantaneous value of the $u_{\text{PD}} =$ Re $\boldsymbol{U}_{\text{PD}} \exp(-j2\pi f_0 t)$ voltage on the load impedance Z_{PD} of PD or the NA input voltage can be written as:

$$u_{\mathrm{PD}} = E_{0\mathrm{L}}^2 K_{0\mathrm{FOLD}} \operatorname{Re} \boldsymbol{U}_{10\mathrm{MZ}} \exp\left(j2\pi f_0 t + T_{\mathrm{FOS}} + T_{1\mathrm{M}}\right) + E_{0\mathrm{L}}^2 K_{0\mathrm{FOLD}} Z_{\mathrm{PD}} \mu_{\mathrm{n}}, \tag{6.22}$$

where transfer functions of RF FODL $K_{0\mathrm{FODL}}$ is defined as:

$$K_{0\mathrm{FODL}} = |\mathbf{K}_{\mathrm{FODL}}(f = f_{0\mathrm{e}})| = P_{0\mathrm{L}} |\mathbf{M}_{\mathrm{Z}}||\mathbf{M}_{\mathrm{eZ}}||\mathbf{K}_{\mathrm{PD}}||\mathbf{K}_{\mathrm{F}}|. \tag{6.23}$$

Further, we consider the nonlinear RF amplifier as the noninertial device (since NA is implemented on the ultra-wideband transistors with the bandwidth more than 20 GHz), and having based on considerations of Chap. 3, we present NA by the single bipolar transistor stage with the volt-ampere function $i_{\mathrm{C}} = \alpha u_{\mathrm{B}} - \beta u_{\mathrm{B}}^3$, where i_{C} is the collector current, u_{B} is the base voltage. The transfer slope can be defined as $S_{\mathrm{NA}} = i_{\mathrm{C}}/u_{\mathrm{B}} = \alpha - (3/4)\beta u_{\mathrm{B}}^2$; the average slope on the first harmonic can be defined as $S_{\mathrm{NA1}} = I_{\mathrm{C}}/U_{\mathrm{B}} = \alpha - (3/4)\beta U_{\mathrm{B}}^2$.

Then, for the instantaneous output voltage of NA, we can write the expression:

$$u_{\mathrm{NA}} = S_{\mathrm{NA}}\left[E_{0\mathrm{L}}^2 K_{0\mathrm{FOLD}} u_{\mathrm{PD}}(t - T_{\mathrm{FOS}})\right] + S_{\mathrm{NA}} E_{0\mathrm{L}}^2 K_{0\mathrm{FOLD}} \mu_{\mathrm{n}}. \tag{6.24}$$

In the closed OEO MZ system, the narrowband high-Q RF filter is intended for filtering of the one type of oscillation from the variety of possible oscillations. The transfer function (on the microwave current) of the RF filter can be defined as

$$\mathbf{K}_{\mathrm{F}} = \frac{(j\omega)\cdot(1/T_{\mathrm{eF}})}{1 + (1/T_{\mathrm{eF}})\cdot(j\omega) + (2\pi f_{0\mathrm{e}})^2 (j\omega)^2}, \tag{6.25}$$

where $\omega = 2\pi f$, δ_{e} is the loss in the filter: $\delta_{\mathrm{e}} = 1/T_{\mathrm{eF}} = f_{0\mathrm{e}}/f_{0\mathrm{e}} T_{\mathrm{eF}} = f_{0\mathrm{e}}/Q_{\mathrm{eF}}$, T_{eF} is the filter time constant, Q_{eF} is the filter Q-filter, $f_{0\mathrm{e}}$ is the filter natural frequency. The "abbreviated" transfer function of the RF filter on the frequency f is defined as: $\mathbf{K}_{\mathrm{F}} = |K_{\mathrm{F}}| \cdot \exp\left[-2j\pi(f - f_{\mathrm{F0}})T_{\mathrm{EF}}\right]$, where $|K_{\mathrm{F}}| = 1/\left[1 + (2\pi)^2 (f - f_{\mathrm{F0}})^2 T_{\mathrm{EF}}^2\right]^{1/2}$ is the module of this transfer function, and $T_{\mathrm{eF}} = T_{\mathrm{EF}} = T_{\mathrm{F}}$ and $f_{0\mathrm{e}} = f_{\mathrm{F0}}$ is the time constant and the resonance frequency of the RF filter, relatively.

Taking into consideration that the PD output voltage and the input voltage of NA has own noises μ_{PD} and μ_{NA}, relatively, with in-phase $S_{\mathrm{PDRe}}(\omega)$ and $S_{\mathrm{NARe}}(\omega)$ and quadrature $S_{\mathrm{PDIm}}(\omega)$ and $S_{\mathrm{NAIm}}(\omega)$ PSD of the fluctuation components, then for the sum $S_{\mu\mathrm{Im}}(\omega)$ and $S_{\mu\mathrm{Re}}(\omega)$ of these fluctuations and the detected laser PSD fluctuations of PD for the *opened* loop (the circuit switch in Fig. 5.10, where the coupler is located) of OEO MZ, we can write for $S_{\mu\mathrm{Im}}(\omega)$ and $S_{\mu\mathrm{Re}}(\omega)$:

$$S_{\mu\mathrm{Im}}(\omega) = K_{\mathrm{PD}}^2 \cdot G_{12} \cdot S_{\mathrm{LIm}}(\omega) + S_{\mathrm{PDIm}}(\omega) + S_{\mathrm{NAIm}}(\omega), \tag{6.26}$$

$$S_{\mu\,\mathrm{Re}}(\omega) = K_{\mathrm{PD}}^2 G_{12} \cdot \left[S_{\mu\mathrm{AN}}(\omega) + S_{\mu\mathrm{AN\text{-}PN}}(\omega)\right] + S_{\mathrm{PD\,Re}}(\omega) + S_{\mathrm{NA\,Re}}(\omega), \tag{6.27}$$

where the quadrature $S_{\mathrm{LIm}}(\omega)$ and in-phase $S_{\mathrm{LRe}}(\omega)$ PSD are equal, relatively Eqs. (6.20) and (6.21).

Expressions (6.26) and (6.27) give a possibility to compute PSD of amplitude and phase noises in OEO MZ.

6.5 Differential Fluctuation Equations of OEO MZ

Using expressions (6.20)–(6.27), according to the standard approach, the differential equation is obtained for the instantaneous voltage u (in the OEO MZ output) for the closed loop of OEO MZ, which contains RF FODL and the Mach–Zehnder optical modulator taking into account the detected fluctuations of the optical carrier [2, 3]. At that, the differential equation for the instantaneous voltage $u(t)$ of OEO MZ is written as:

$$\frac{\mathrm{d}^2u}{\mathrm{d}t^2}+\frac{1}{T_{\mathrm{F}}}\frac{\mathrm{d}u}{\mathrm{d}t}+(2\pi f_{\mathrm{F0}})^2u=\frac{\mathrm{d}S_{\mathrm{NA}}[P_{0\mathrm{L}}K_{0\mathrm{FODL}}\cdot u(t-T_{\mathrm{FOLD}})]}{\mathrm{d}t}+\Psi_{\mathrm{n}}, \qquad (6.28)$$

where Ψ_{n} is the noise component of the PD voltage formed by the fluctuations of amplitude and phase of the QWLD optical carrier, at that, $\Psi_{\mathrm{n}}=S_{\mathrm{NA}}K_{0\mathrm{FODL}}\mu_{\mathrm{n}}$. The equivalent circuit of examined here OEO with account of noises $\Psi_{\mathrm{n}}=u_{\mathrm{N}}(t)$ is presented in Fig. 6.12. The noise component Ψ_{n} is added with the RF voltage of PD. The differential equation (6.28) obtained by authors is used for the analysis of PSD of the phase noise and for formation of OEO MZ spectrum taking into account the noises effect in the transients, and analysis results are presented below in the section of computer modeling.

The differential equation (6.28) with fluctuations permits to transfer to abbreviated differential equations of OEO for fluctuations of amplitude $m_{\mathrm{L}}(t)$ and phase $\psi_{\mathrm{m}}(t)$ of oscillations with the help of the standard operation of averaging over the fast motions. The solution of these abbreviated differential equations allows searching of necessary required analytical dependences for PSD of the amplitude S_{mOEO} and phase $S_{\Psi\mathrm{OEO}}$ fluctuations of the RF oscillations in OEO MZ.

Now we obtain expressions for the PSD of phase noises of RF oscillations in OEO. For this, we examine the abbreviated differential fluctuation equations of OEO MZ (Fig. 6.12a).

The differential equation (6.28) for the instantaneous voltage u in the OEO output does not permit a possibility to connect the appropriate input and output currents in the closed OEO system for each "block" of NA, F, RF FODL. This can be done at formation of symbolic abbreviated differential equations with fluctuations for OEO MZ and at introduction of symbolic (operator) normalized control conductance $Y_{\mathrm{con}}(p)$. The form of equations completely coincides with the same equations for the transistor oscillator [2, 3].

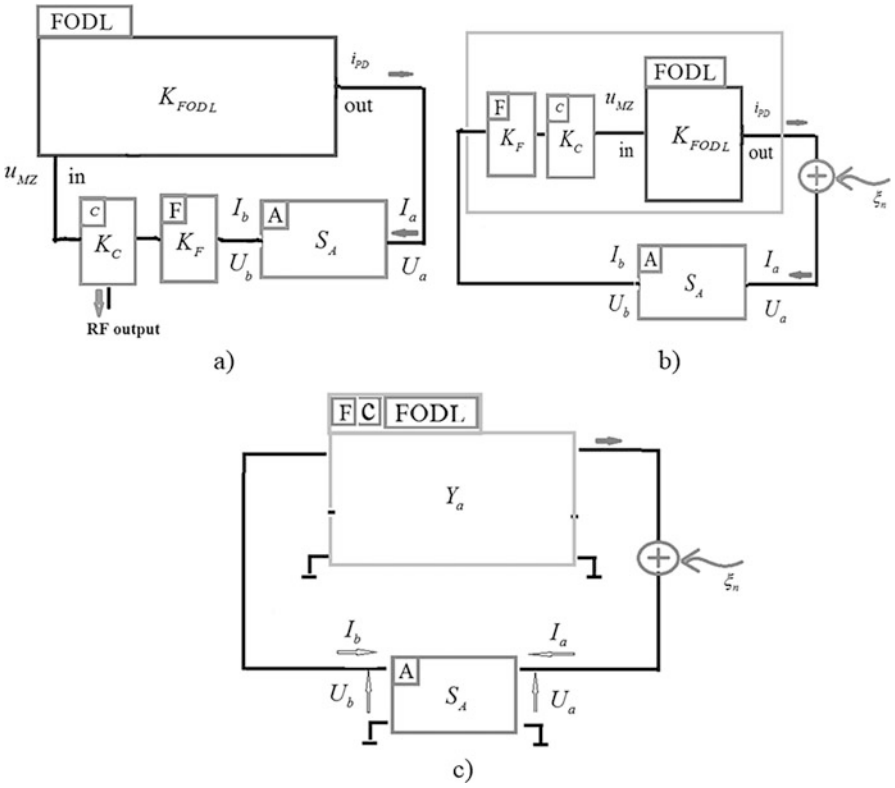

Fig. 6.12 Structures of OEO MZ with different extraction of included components: (**a**) OEO MZ with extracted optoelectronic part "MZ-FOS-PD" into the block RF FODL; (**b**) representation of OEO MZ with the noise source as the nonlinear RF amplifier spanned by the positive feedback, consisting of series-connected blocks of the RF filter, RF coupler and RF FODL; (**c**) representation of OEO MZ with the noise source as the nonlinear amplifier covered by the positive feedback or the block "F-C-RF FODL" with the complex conductance Y_a and the noise voltage $\xi_n = \xi_{YYn}$

6.5.1 *Symbolic Differential Equations of OEO MZ with Fluctuations*

The symbolic differential equations of OEO MZ (Fig. 6.12a) with fluctuations have discussed in Chap. 5, where the system (5.67) was obtained:

$$\begin{cases} Q_0(p)E_{\mathrm{L}} = \alpha_{00}E_{\mathrm{L}} - \beta_{00}E_{\mathrm{L}}|E_{\mathrm{L}}|^2 + \xi_{\mathrm{SN}} \\ i_{\mathrm{PD}} = 0.5\langle E_{\mathrm{L}}E^*_{\mathrm{L}\tau}\rangle\gamma\cos\left[\varphi_{0\mathrm{MZ}} + u_{\mathrm{MZ}}/U_{0\mathrm{MZ}\pi}\right] \\ \left[p^2 + \dfrac{1}{T_{\mathrm{F}}}p + (2\pi f_{\mathrm{eF0}})^2\right]u_{\mathrm{MZ}} = (|K_{\mathrm{FODL}}|/S_{\mathrm{PD}})pS_{\mathrm{A}}(i_{\mathrm{PD}})\exp\left[-pT_{\mathrm{FOLD}}\right] + \xi_{\mathrm{U}} \end{cases} \tag{6.29}$$

This equation system reflects the connection of OEO MZ circuit parameters, which is shown in Fig. 6.12a. The first equation of the system determines the connection of the oscillating characteristics $Q_0(p)$, the laser parameters with fluctuations ξ_{SN}. The second equation defines the instantaneous value of the AC current in the PD load.

Here $T_{FODL} = T_{FOS}$ is the delay in FOS, u_{MZ} is the instantaneous voltage (AC) in the MZ electrical input, φ_{0MZ} is the constant phase incursion in MZ, $U_{0MZ\pi}$ is the constant bias voltage in MZ, $\left\langle E_L E^*_{L\tau} \right\rangle$ is the average from the product of delayed and non-delayed field oscillations for account of the noise after the optical emission passage through MZ, γ is the coefficient of the excitation irregularity of optical channels in MZ. If to recalculate of the laser noises ξ_{SN} in the input of the RF amplifier and to take into consideration that ξ_n is the noise taking into account the detected noises of the laser ξ_{SN} and noises of the RF parts ξ_U, then the symbolic differential equation (6.46) will take the form:

$$\left[p^2 + \frac{1}{T_F}p + (2\pi f_{eF0})^2\right] u_{MZ} = (|K_{FODL}|/S_{PD})pS_A\left(|E_{0L}|^2, i_{PD}\right)$$

$$\exp\left[-pT_{FOS}\right] + \xi_n. \tag{6.30}$$

Below, we shall give the deduction of these formulas for PSD of the amplitude noise and the phase noise according to the Evtianov–Kuleshov approach.

6.5.2 *Abbreviated Differential Equations of OEO MZ with Fluctuations*

Let us consider the circuit in Fig. 6.12a–c with complex slowly changing oscillation amplitude U_a.

In order to obtain the abbreviated equations of OEO MZ with the single optical fiber, we write differential equations for OEO in operator form (3.63):

$$\left[p^2 + (1/T_{EF})p + (2\pi f_{0e})^2\right] u_{MZ} = (1/T_{EF})K_{0FODL}pi_A(u_{PD})$$

$$\exp\left(-j2\pi f_{0e}T_{FOS}\right) + \xi_n \tag{6.31}$$

in which the instantaneous voltage on the load resistance R_{PD} of PD is $u_{PD} = R_{PD} \cdot i_{PD}$, and the instantaneous PD current i_{PD} is $i_{PD} = 0.5(E_{0L})^2 K_{0FOS.\,MZ} \cos\left[\pi(U_{0MZ} - u_{MZ})/2U_{0MZ\pi}\right]$, where $(E_{0L})^2 = P_{0L}$ is the power of laser emission, U_{0MZ} is the DC bias voltage of the MZ modulator, $K_{0FOS.\,MZ}$ is the RF FODL transfer function on the frequency f_{0e}.

We write the following abbreviated equation of the first approximation:

$$\left(\frac{1}{Q_{\mathrm{EF}}}+2p_1\right)\exp\left[j\Phi_1\right]\cdot U_{10\mathrm{MZ}}=\frac{K_{0\mathrm{FODL}}}{Q_{\mathrm{EF}}}\{I_{1\mathrm{ACOS}}\cos\left[2\pi f_{0\mathrm{e}}T_{\mathrm{FOS}}\right] +jI_{1\mathrm{ASIN}}\sin\left[2\pi f_{0\mathrm{e}}T_{\mathrm{FOS}}\right]\}\exp\left[j\Phi_1\right]+\xi_{\mathrm{Yn}} \tag{6.32}$$

Now we can write:

$$\frac{T_{\mathrm{EF}}\exp\left(j2\pi f_{0\mathrm{e}}T_{\mathrm{FOS}}\right)}{K_{0\mathrm{FOLD}}}\left[p^2+(1/T_{\mathrm{EF}})p+(2\pi f_{0\mathrm{e}})^2\right]u_{\mathrm{MZ}} =pi_{\mathrm{A}}(u_{\mathrm{PD}})+T_{\mathrm{EF}}K_{0\mathrm{FOLD}}\exp\left(j2\pi f_{0\mathrm{e}}T_{\mathrm{FOS}}\right)\xi_{\mathrm{n}}, \tag{6.33}$$

where $K_{0\mathrm{FODL}}=K_{\mathrm{FODL}}(f=f_{0\mathrm{e}})=P_{0\mathrm{L}}|M_{\mathrm{Z}}||K_{\mathrm{PD}}||K_{\mathrm{F}}|$, $\xi_{\mathrm{YYn}}=T_{\mathrm{EF}}K_{0\mathrm{FODL}}\exp(j2\pi f_{0\mathrm{e}}T_{\mathrm{FOS}})\xi_{\mathrm{n}}$.

6.5.3 Noise Currents in the NA Input and Output

Since the bandwidth of the feedback circuit is narrow, in current spectra and at equations analysis we may take into account only the first harmonics by writing the currents in the form:

- for the voltage in the NA input: $u_{\mathrm{PD}}=u_{\mathrm{a}}=\ \mathrm{Re}\,\boldsymbol{U}_{\mathrm{a}}\exp(-j2\pi f_0t)$,
- for the current in the NA input: $i_{\mathrm{PD}}=i_{\mathrm{a}}=\ \mathrm{Re}\,\boldsymbol{I}_{\mathrm{a}}\exp(-j2\pi f_0t)$,
- for the current in the NA output: $i_{\mathrm{F}}=i_{\mathrm{B}}=\ \mathrm{Re}\,\boldsymbol{I}_{\mathrm{b}}\exp(-j2\pi f_0t)$,

where slowly changing amplitude $\boldsymbol{U}_{\mathrm{a}}=U_{\mathrm{a}}\exp(j2\pi\Delta ft+\varphi_{\mathrm{u}})$, slowly changing amplitude $\boldsymbol{I}_{\mathrm{a}}=\boldsymbol{I}_{\mathrm{a0}}(U_{\mathrm{a}})\exp(j2\pi\Delta ft+\varphi_{\mathrm{u}})$, and slowly changing amplitude $\boldsymbol{I}_{\mathrm{b}}=\boldsymbol{I}_{\mathrm{b0}}(U_{\mathrm{a}})\exp(j2\pi\Delta ft+\varphi_{\mathrm{u}})$.

At that, functions $\boldsymbol{I}_{\mathrm{a0}}(U_{\mathrm{a}})$ and $\boldsymbol{I}_{\mathrm{b0}}(U_{\mathrm{a}})$ are obtained at the harmonic analysis of the active element currents. Owing to slow changing of $U_{\mathrm{a}}(t)$, currents $\boldsymbol{I}_{\mathrm{a0}}(U_{\mathrm{a}})$ and $\boldsymbol{I}_{\mathrm{b0}}(U_{\mathrm{a}})$ are also slowly changing functions.

For the noise current for OEO MZ circuit (Fig. 6.12), we use the following representations:

- for the noise current in the NA input (or the PD output): $i_{\mathrm{nPD}}=i_{\mathrm{NA}}=\ \mathrm{Re}\,\boldsymbol{I}_{\mathrm{na}}\exp(-j2\pi f_0t)$,
- for the noise current in in the filter input): $i_{\mathrm{nF}}=i_{\mathrm{nB}}=\ \mathrm{Re}\,\boldsymbol{I}_{\mathrm{nb}}\exp(-j2\pi f_0t)$, for the noise current in the NA input $\boldsymbol{I}_{\mathrm{na}}=(I_{\mathrm{anCOS}}+jI_{\mathrm{anASIN}})\exp(-j2\pi\Delta ft+\varphi_{\mathrm{U}})$, for the noise current in the NA output $\boldsymbol{I}_{\mathrm{nb}}=(I_{\mathrm{bnCOS}}+jI_{\mathrm{bnASIN}})\exp(-j2\pi\Delta ft+\varphi_{\mathrm{U}})$, where $\Delta f=f-f_0$ is the amendment to the oscillation frequency, φ_{u} is the slowly changing phase.

We now transform the abbreviated equation (6.33) of OEO MZ taking into account the mentioned notes to the form, in which we shall introduce of the "abbreviated" conductance.

For the circuit in Fig. 6.12 for the complex slowly changing oscillation voltage $\boldsymbol{U_a}$ in the nonlinear amplifier input (taking into account of detected laser noises), the abbreviated differential equations for OEO MZ can be written as:

$$\frac{\exp\left[\,j(2\pi f - 2\pi f_{\mathrm{eF0}})T_{\mathrm{FODL}}\right][1 + T_{\mathrm{EF}}(2\pi f - 2\pi f_{\mathrm{eF0}})p_1]}{K_{0\mathrm{FODL}}} \cdot U_{10\mathrm{MZ}} = (1/S_{\mathrm{PD}})S_{\mathrm{A}}(I_{\mathrm{PD}}) + \xi_{\mathrm{YYn}}, \tag{6.34}$$

where $\xi_{\mathrm{YYn}} = T_{\mathrm{EF}}K_{0\mathrm{FODL}} \exp\,(j2\pi f_{0\mathrm{e}}T_{\mathrm{FOS}})\xi_{\mathrm{n}}$. Now we introduce the symbolic (operator) "abbreviated" controlling conductance Y_{a} and represent it in the form of the sum of its real Y_{aRe} and imaginary parts Y_{aIm} : $Y_{\mathrm{a}}(p) = Y_{\mathrm{aRe}}(p) + jY_{\mathrm{aIm}}(p)$,

$$Y_{\mathrm{a}} = \frac{\exp\left[\,j(2\pi f - 2\pi f_{\mathrm{eF0}})T_{\mathrm{FODL}}\right][1 + T_{\mathrm{EF}}(2\pi f - 2\pi f_{\mathrm{eF0}})p_1]}{K_{0\mathrm{FODL}}} = Y_{\mathrm{a\,Re}} + jY_{\mathrm{aIm}}. \tag{6.35}$$

Now we introduce the designation of the frequency offset from the carrier $F = (2\pi f - 2\pi f_{\mathrm{eF0}})$. In the case of using of the solitary single-mode optical fiber as the RF filter of the single oscillating circuit with the natural frequency ω_0 with the time constant of the filter T_{F} in the RF FODL (with total effective delay $T_{\mathrm{FOS}} = T_{\mathrm{BZ}}$), the following expressions are true for the real Y_{aRe} and the imaginary Y_{aIm} parts and Y_{00}:

$$Y_{\mathrm{a\,Re}} = \frac{y_{\mathrm{M}}[1 + FT_{\mathrm{EF}}]\cos\left[FT_{\mathrm{FODL}}\right]}{P_{0\mathrm{L}}|M_{\mathrm{Z}}||K_{\mathrm{PD}}||K_{\mathrm{F}}|},$$

$$Y_{\mathrm{aIm}} = \frac{y_{\mathrm{M}}[1 + FT_{\mathrm{EF}}]\sin\left[FT_{\mathrm{FODL}}\right]}{P_{0\mathrm{L}}|M_{\mathrm{Z}}||K_{\mathrm{PD}}||K_{\mathrm{F}}|}, \quad Y_{00} = \frac{y_{\mathrm{M}}[1 + FT_{\mathrm{EF}}]}{|M_{\mathrm{Z}}||K_{\mathrm{PD}}||K_{\mathrm{F}}|}. \tag{6.36}$$

In Eqs. (6.31) and (6.36), the module of the RF FODL transfer function $|K_{\mathrm{FODL}}| = |K_{\mathrm{BZ}}| = P_{0\mathrm{L}}|M_{\mathrm{Z}}||K_{\mathrm{PD}}||K_{\mathrm{F}}|$ and $|M_{\mathrm{Z}}|$ is the transfer function in amplitude of the voltage of first harmonic in the MZ electrical input, which was defined earlier, and the module of which is $|M_{\mathrm{Z}}| = k_{01} \cdot |M_{\mathrm{ZE}}| \cdot \{1 - \cos\,[2\pi\nu_0(T_{2\mathrm{M}} - T_{1\mathrm{M}})]\}$, $P_{0\mathrm{L}}$is the laser power in the MZ optical input, $|K_{\mathrm{PD}}|$ is the module of the transfer function, which has the sense of the transform slope of the optical modulated power of the laser emission into the first harmonic current of the PD load, $|K_{\mathrm{F}}|$ is the module of the transfer function of the RF filter (which is defined as a ratio of the voltage amplitude of the first harmonic in the output to the same value in the input of the RF filter). Other designations in Eq. (6.31) have the following sense: y_{M} is the input conductance of the circuit "the RF filter—the coupler—RF FODL," which is equal to the input conductance of the RF filter.

The total delay of oscillations in RF FODL T_{FODL} is $T_{\text{FODL}} = T_{\text{MZ}} + T_{\text{FOS}} + T_{\text{PD}}$, where T_{MZ}, T_{PD}, T_{FOS} are, relatively, oscillation delays in MZ, PD, and in optical fiber.

We introduce the symbolic coefficient K_{a} of the current influence in the input I_{a} of the active element upon the voltage in the input $\boldsymbol{U}_a$ of this active element.

If to substitute expressions (for the structure in Fig. 6.12) and to take into account the steady-state equation, then we obtain the complex fluctuation abbreviated equation for OEO MZ:

$$Y_{\text{a}}(p)\boldsymbol{U}_{\text{a}} = \boldsymbol{I}_{\text{b}}(U_{\text{a}}) - K_{\text{a}}\boldsymbol{I}_{\text{a}} + \boldsymbol{I}_{\text{nb}} + \xi_{\text{YYn}}. \tag{6.37}$$

6.5.4 Fluctuation Deviations of Amplitudes and Phase

Here we designate the relative fluctuation deviations (6.37) of the amplitude $\boldsymbol{U}_a$ and the phase φ_{U} from the own steady-state values as: $U_{\text{a}} = U_{\text{a0}} \cdot (1 + m_{\text{U}})$ and $\varphi_{\text{U}} = \varphi_{0\text{U}} + \psi_{\text{U}}$, where m_{U} are fluctuations of the amplitude U_{a}, ψ_{U} are phase fluctuations from its mean values, φ_0 is the initial constant phase shift. The complex amplitude $\boldsymbol{U}_{\text{a}}$ can be presented in the form:

$$\boldsymbol{U}_{\text{a}} = U_{\text{a0}}(1 + m_{\text{U}}) \exp(\ j2\pi\Delta ft + j\varphi_{0\text{U}} + j\psi_{\text{U}}). \tag{6.38}$$

To simplify equations deduction, taking into account the smallness of deviations ψ_{U}, the following relation is true for small observation time: $\exp(j\psi_{\text{U}}) = 1 + j\psi_{\text{U}}$. Then, the complex amplitude is: $\boldsymbol{U}_{\text{a}} = U_{\text{a0}}(1 + m_{\text{U}} + j\psi_{\text{U}})$. The slowly changing amplitude of the first harmonic $\boldsymbol{U}_{\text{a}} = U_{\text{a0}}(1 + m_{\text{U}}) \exp(j2\pi\Delta ft + j\varphi_{0\text{U}} + j\psi_{\text{U}})$ can be written with account of fluctuations in the form: $\boldsymbol{U}_{\text{a}} = U_{\text{a0}}(1 + m_{\text{U}} + j\psi_{\text{U}}) \exp(j2\pi\Delta ft + j\varphi_{0\text{U}})$. Having linearized functions in the vicinity of steady-state values U_a and φ_{U}, we obtain expressions:

$$\begin{aligned} \boldsymbol{I}_{\text{a}} &= \boldsymbol{I}_{\text{a0}}(U_{\text{a}}) \exp(\ j2\pi\Delta ft + \varphi_{\text{u}}) \\ &= \boldsymbol{I}_{\text{a0}}[U_{\text{a0}}(1 + m_{\text{U}} + j\psi_{\text{U}}) \exp(\ j2\pi\Delta ft + \varphi_{\text{u}})] \cdot \exp(\ j2\pi\Delta ft + \varphi_{\text{u}}) \end{aligned}. \tag{6.39}$$

For record simplification, we introduce the relative local slope of the oscillating characteristic or coefficients σ_{aU}, $\sigma_{\text{bU}} = \sigma_{\text{U}}$, which can be defined as $\sigma_{\text{aU}} = \frac{\mathrm{d}I_{\text{a}}/\mathrm{d}U_{\text{a}}}{I_{\text{a}}/U_{\text{a}}}$, $\sigma_{\text{bU}} = \sigma_{\text{U}} = \frac{\mathrm{d}I_{\text{b}}/\mathrm{d}U_{\text{a}}}{I_{\text{b}}/U_{\text{a}}}$. The coefficient σ_{U} has a sense of a ratio of the relative local slope of the AE oscillating characteristic $\mathrm{d}I_{\text{b}}/\mathrm{d}U_{\text{a}}$ reduced to the ratio $I_{\text{b1}}/U_{\text{a1}}$, which is constructed taking into account the noninertial property of NA. In economics, to explain of the profit growth at variation of the price, we can introduce the concept of the function elasticity. The coefficient σ_{U} has the similar sense. It shows how fast the function $I_{\text{a}}(U_{\text{a}})$ decreases or increases in the steady-state mode point. Taking into consideration the last notation for $\boldsymbol{I}_{\text{a}}$, we can write: $\boldsymbol{I}_{\text{a}} = I_{\text{a0}}(1 + \sigma_{\text{aU}}m_{\text{U}} + j\psi_{\text{U}})$.

Similarly, we have for the current $\boldsymbol{I}_{\mathrm{b}}$ in the NA output:

$$\begin{aligned}\boldsymbol{I}_{\mathrm{b}} &= \boldsymbol{I}_{\mathrm{b0}}(U_{\mathrm{a}})\exp(\ j2\pi\Delta ft+\varphi_{\mathrm{u}})\\ &= \boldsymbol{I}_{\mathrm{b0}}[U_{\mathrm{a0}}\cdot(1+m_{\mathrm{U}}+j\psi_{\mathrm{U}})\exp(\ j2\pi\Delta ft+\varphi_{\mathrm{u}})]\cdot\exp(\ j2\pi\Delta ft+\varphi_{\mathrm{u}})\end{aligned}. \tag{6.40}$$

With account of the last notation for $\boldsymbol{I}_{\mathrm{b}}$, we can write: $\boldsymbol{I}_{\mathrm{b}} = \boldsymbol{I}_{\mathrm{b0}}(1+\sigma_{\mathrm{U}}\cdot m_{\mathrm{U}}+j\psi_{\mathrm{U}})$. Now we substitute expressions after linearization into the abbreviated fluctuation equation and take into consideration the steady-state equation, then we write the complex fluctuation equation in the form:

$$Y_{\mathrm{a}}(p+j\Delta f)U_{\mathrm{a}}(m_{\mathrm{U}}+j\psi_{\mathrm{U}}) = \boldsymbol{I}_{0\mathrm{b}}(\sigma_{\mathrm{U}}\cdot m_{\mathrm{U}}+j\psi_{\mathrm{U}})$$

$$-K_{\mathrm{a}}\boldsymbol{I}_{0\mathrm{a}}(\sigma_{\mathrm{aU}}m_{\mathrm{U}}+j\psi_{\mathrm{U}})+\boldsymbol{I}_{\mathrm{nb}}. \tag{6.41}$$

The expression for the noise current $\boldsymbol{I}_{\mathrm{nb}}$ with account that $\boldsymbol{I}_{\mathrm{na}} = (I_{\mathrm{anCOS}} + jI_{\mathrm{anASIN}})\exp(-j2\pi\Delta ft + \varphi_{\mathrm{U}})$, $\boldsymbol{I}_{\mathrm{nb}} = (I_{\mathrm{bnCOS}} + jI_{\mathrm{bnASIN}})\exp(-j2\pi\Delta ft + \varphi_{\mathrm{U}})$ can be written as:

$$\boldsymbol{I}_{\mathrm{nb}} = (I_{\mathrm{bnCOS}}+jI_{\mathrm{bnASIN}}) - K_a\cdot(I_{\mathrm{anCOS}}+jI_{\mathrm{anASIN}})+\boldsymbol{I}_{\mathrm{nb}}+\xi_{\mathrm{YYn}}. \tag{6.42}$$

The expression (6.42) for the abbreviated fluctuation equation is complicate to obtain of analytical functions. For simplicity in the future, we shall be limited by a case, when we can neglect by the effect of the input voltage upon the input current. In other words, the complex (in the general case) coefficient K_{a} can be equated to zero.

6.5.5 *The Coefficient of the Local Slope* $\boldsymbol{\sigma_U}$

Values of the coefficient σ_{U} can be accepted for the single-stage nonlinear amplifiers constructed, for instance, in the common emitter circuit, from 0.1 to 0.99. The coefficient σ_{U} is related to the coefficient of the limit circle strength of OEO as $S_\sigma = 1-\sigma_{\mathrm{U}}$. The value $S_\sigma = 0$ or $\sigma_{\mathrm{U}} = 1$ corresponds to the stability boundary of the oscillator on the inertia-less AE and with the single oscillating circuit at absence of the retarded feedback or the delay line. Then, in the steady-state point, the coefficient $\sigma_{\mathrm{U}} < 0$. If there is the delay in the feedback loop, then the value of the coefficient σ_{U} may take both negative and positive values. The domain of permissible values of the coefficient σ_{U} is necessary defined from the oscillation stability condition in the steady-state mode. The OEO stability condition in the steady-state point, as it follows from the differential equation (6.29), in the case of OEO with the RF filter with the single circuit and with FOS formed by the single optical fiber, is determined as: $\sigma_{\mathrm{U}}\cdot\ \cos[fT_{\mathrm{FODL}}] < 0$. Coefficient σ_{U} can be also expressed through the AE average slope in the first harmonic, which can be determined as the ratio of AE characteristic slope to the amplitude of the first harmonic voltage.

6.5.6 Symbolic Expressions for Fluctuations

From Eq. (6.32), we obtain the equation for fluctuations of amplitudes and phases. For this, we can express $\boldsymbol{U}_a$ through $\boldsymbol{I}_{b0}$ using the connection: $\boldsymbol{U}_a = \boldsymbol{I}_{b0} \cdot \frac{1}{Y_{a0}(\ j\Delta f)}$, where at $p = 0$ we used the equality $Y_a(p + j\Delta f) = Y_{a0}(j\Delta f)$. Let us present of the normalized symbolic conductance $Y_{Na}(p) = Y_a(p + j\Delta f)/Y_{a0}(j\Delta f)$. Then

$$\frac{Y(p + j\Delta f)}{Y(\ j\Delta f)} \cdot (m_U + j\psi_U) = \sigma_U \cdot m_U + j\psi_U + \mu_{a\,Re} + j\mu_{aIm}. \tag{6.43}$$

Now we can present of the *normalized* conductance in the form: $Y_{Na} = \frac{Y(p+j\Delta f)}{Y(\ j\Delta f)} = Y_{Na\,Re} + jY_{NaIm}$. We substitute this expression Y_{Na} in Eq. (6.43) and equating the real and imaginary parts from the right and left sides, we have:

$$Y_{Na} \cdot (m_U + j\psi_U) = \sigma_U \cdot m_U + j\psi_U + \mu_{a\,Re} + j\mu_{aIm}. \tag{6.44}$$

We would like to note that for fluctuating components, the following relation is true: $pm_U = m_U - \psi_U$. Then, the symbolic equations for the *real* and *imaginary* parts of the fluctuating quantities will take the form:

$$Y_{Na\,Re}(p) \cdot m_U - Y_{NaIm}(p) \cdot \psi_U = \sigma_U \cdot m_U + \mu_{a\,Re}, \tag{6.45}$$

$$Y_{NaIm}(p) \cdot m_U + Y_{Na\,Re}(p) \cdot \psi_U = \psi_U + \mu_{aIm}. \tag{6.46}$$

Converting to the matrix view, according to the Kramer rule, we find determinants, and the following expressions can be found for m_U and ψ_U:

$$m_U = \frac{\mu_{a\,Re} \cdot (Y_{a\,Re} - 1) + \mu_{aIm} \cdot Y_{aIm}}{[Y_{a\,Re}(p) - \sigma_U] \cdot [Y_{a\,Re}(p) - 1] + [Y_{aIm}(p)]^2}, \tag{6.47}$$

$$\psi_U = \frac{(Y_{a\,Re} - \sigma_U) \cdot \mu_{aIm} - Y_{aIm} \cdot \mu_{a\,Re}}{[Y_{a\,Re}(p) - \sigma_U] \cdot [Y_{a\,Re}(p) - 1] + [Y_{aIm}(p)]^2}. \tag{6.48}$$

In the general case for OEO, PSD of fluctuations of the amplitude S_{mOEO} and the phase $S_{\Psi OEO}$ have the complicate analytical form and each of them are defined by the in-phase $S_{\mu Re}(\omega)$ and the quadrature $S_{\mu Im}(\omega)$ components.

The influence of the OEO power and the natural bandwidth of the laser spectral line upon the noise properties shows approximately the following expressions for S_{mAG} and $S_{\Psi AG}$:

$$S_{\mathrm{mOEO}}(\omega)=\frac{S_{\mathrm{a\mu\,Re}}\cdot\left(Y_{\mathrm{a\,Re}}-1\right)^2+S_{\mathrm{a\mu Im}}\cdot\left[Y_{\mathrm{aIm}}\right]^2+2\left(Y_{\mathrm{a\,Re}}-1\right)Y_{\mathrm{aIm}}\,\mathrm{Re}\left[S_{\mathrm{a\mu ReIm}}\right]}{\left\{Y_{\mathrm{a\,Re}}-\sigma_{\mathrm{U}}\right]\cdot\left[Y_{\mathrm{a\,Re}}-1\right]+\left[Y_{\mathrm{aIm}}\right]^2\}^2},\tag{6.49}$$

$$S_{\Psi\mathrm{OEO}}(\omega)=\frac{\left(Y_{\mathrm{a\,Re}}-\sigma_{\mathrm{U}}\right)^2\cdot S_{\mathrm{a\mu Im}}+Y_{\mathrm{a\mu Im}}^2\cdot S_{\mathrm{a\mu\,Re}}-2\left(Y_{\mathrm{a\,Re}}-\sigma_{\mathrm{U}}\right)\cdot Y_{\mathrm{aIm}}\,\mathrm{Re}\left[S_{\mathrm{a\mu ReIm}}\right]}{\left\{\left[Y_{\mathrm{a\,Re}}-\sigma_{\mathrm{U}}\right]\cdot\left[Y_{\mathrm{a\,Re}}-1\right]+\left[Y_{\mathrm{aIm}}\right]^2\right\}^2},\tag{6.50}$$

where $S_{\mathrm{a\mu Re}}$ is PSD of mutual fluctuations of the amplitude $S_{\mathrm{a\mu\,Re}}=4\int_0^\infty\mu_{\mathrm{a\,Re}}(t)\mu_{\mathrm{a\,Re}}(t-\tau)\cos(2\pi f\tau)\mathrm{d}\tau$, $S_{\mathrm{a\mu Im}}$ is PSD of mutual fluctuations of the phase $S_{\mathrm{a\mu Im}}=4\int_0^\infty\mu_{\mathrm{aIm}}(t)\mu_{\mathrm{aIm}}(t-\tau)\cos(2\pi f\tau)\mathrm{d}\tau$, PSD of mutual fluctuations the amplitude and the phase $S_{\mathrm{a\mu ReIm}}=4\int_0^\infty\mu_{a\,\mathrm{Re}}(t)\mu_{a\mathrm{Im}}(t-\tau)\cos(2\pi f\tau)\mathrm{d}\tau$. Expressions (6.49) and (6.50) have a close form to the similar expressions in for the transistor oscillators [3] and OEO MZ [1, 4]. But, the sense of the symbolic conductance and the in-phase $S_{\mu\mathrm{Re}}(\omega)$ and the quadrature $S_{\mu\mathrm{Im}}(\omega)$ components is different.

6.5.7 *An Analysis of Formulas for PSD of Amplitude and Phase Noises*

The quadrature $S_{\mathrm{LIm}}(\omega)$ and the in-phase $S_{\mathrm{LRe}}(\omega)$. PSD included in Eqs. (6.49) and (6.50) are determined by the earlier obtained expressions (6.26), (6.27) and (6.20), (6.21). As we see from Eqs. (6.26) and (6.27), the quadrature $S_{\mathrm{LIm}}(\omega)$ and the in-phase $S_{\mathrm{LRe}}(\omega)$ PSD are not equal in the general case. Here we consider the specific case to obtain the evident, relatively simple formulas for PSD of the amplitude and phase noises. We assume that $S_{\mathrm{LIm}}(\omega)\approx S_{\mathrm{LRe}}(\omega)\approx S_{\mathrm{a\mu ReIm}}(\omega)$. Let us examine the case when $G_{12}=1-(A_1/A_2)\cdot\exp(-T_{\mathrm{FOS}}/T_{\mathrm{c}})\approx 1$ and $\sin[2\pi\nu_0(T_{2\mathrm{M}}-T_{1\mathrm{M}})]=1$. Such an equality $2\pi\nu_0(T_{2\mathrm{M}}-T_{1\mathrm{M}})=\pi m$ is possible in the quadrature operation mode of MZ and at that, $\sin[2\pi\nu_0(T_{2\mathrm{M}}-T_{1\mathrm{M}})]=1$, i.e., $2\pi\nu_0(T_{2\mathrm{M}}-T_{1\mathrm{M}})=m\pi/2$, and then $S_{\mu\mathrm{AM}}\approx S_{\mu\mathrm{AM\,-\,PM}}$, at condition fulfillment that the laser coherence time T_{c} is much more than the delay time $T_{\mathrm{FODL}}=T_{\mathrm{FOS}}$ in RF FODL, i.e., $G_{12}=1-\exp(-T_{\mathrm{FOS}}/T_{\mathrm{c}})\approx 1$. For this case, when $S_{\mathrm{LIm}}(\omega)\approx S_{\mathrm{LRe}}(\omega)$, expressions $\boldsymbol{U}_{\mathrm{a}}=U_{\mathrm{a}0}(1+m_{\mathrm{U}})\exp(j2\pi\Delta ft+j\varphi_{0\mathrm{U}}+j\psi_{\mathrm{U}})$, $\exp(j\psi_{\mathrm{U}})=1+j\psi_{\mathrm{U}}$ are written in the following form:

$$S_{\mathrm{mOEO}}(F)=S_{\mathrm{a\mu\,Re}}\cdot\left[\frac{Y_{\mathrm{a\,Re}}-1+Y_{\mathrm{aIm}}}{\left[Y_{\mathrm{a\,Re}}-\sigma_{\mathrm{U}}\right]\cdot\left[Y_{\mathrm{a\,Re}}-1\right]+\left[Y_{\mathrm{aIm}}\right]^2}\right]^2,\tag{6.51}$$

$$S_{\Psi OEO}(F) = S_{a\mu Im} \cdot \left[\frac{Y_{a\,Re} - \sigma_U - Y_{aIm}}{[Y_{a\,Re} - \sigma_U] \cdot [Y_{a\,Re} - 1] + [Y_{aIm}]^2} \right]^2. \tag{6.52}$$

When we use the single oscillating circuit with the natural frequency ω_0, the filter time constant T_F as the RF filter and we use in RF FODL (with the total effective delay T_{FODL}) of the solitary single-mode optical fiber, the following expressions are true for the real $Y_{a\,Re} = \frac{y_M[1+FT_{EF}]\cos[FT_{FOS}]}{P_{0L}|M_Z||K_{PD}||K_F|}$ and the imaginary $Y_{aIm} = \frac{y_M[1+FT_{EF}]\sin[FT_{FOS}]}{P_{0L}|M_Z||K_{PD}||K_F|}$ parts, taking into account $F = \omega - \omega_0 = 2\pi f - 2\pi f_0$. We introduce the designation $Y_{00} = \frac{y_M[1+FT_{EF}]}{|M_Z||K_{PD}||K_F|}$. After substitution Y_{aRe} and Y_{aIm} (determined in Eq. (6.36)), using Y_{00} (6.36), the expressions (6.51) and (6.52), we can write the expression for $S_{mOEO}(\omega)$, $S_{\Psi OEO}(F)$ is:

$$S_{mOEO}(\omega) = S_{\mu\,Re} \cdot K^2_{\Gamma AN}, \quad S_{\Psi OEO}(\omega) = S_{\mu Im} \cdot K^2_{\Gamma PN}, \tag{6.53}$$

where coefficients $K^2_{\Gamma AN}$ and $K^2_{\Gamma PN}$ are:

$$K^2_{\Gamma AN} = \frac{\left\{ \frac{\gamma}{P_{0L}} \left[\sqrt{2} \sin\left(FT_{FOS} + \pi/4\right) \right] - 1 \right\}^2}{\left\{ \left[\frac{Y_{00}}{P_{0L}} \right]^2 - \frac{Y_{00}}{P_{0L}} \cdot (1 + \sigma_U) \cos\left[FT_{FOS}\right] + \sigma_U \right\}^2}, \tag{6.54}$$

$$K^2_{\Gamma PN} = \frac{\left\{ \frac{\gamma}{P_{0L}} \sqrt{2} \sin\left(\pi/4 - FT_{FOS}\right) - \sigma_U \right\}^2}{\left\{ \left[\frac{Y_{00}}{P_{0L}} \right]^2 - \frac{Y_{00}}{P_{0L}} \cdot (1 + \sigma_U) \cos\left[FT_{FOS}\right] + \sigma_U \right\}^2}. \tag{6.55}$$

We used for Eqs. (6.54) and (6.55) the trigonometric formula for the sum: $\cos[FT_{FOS}] + \sin[FT_{FOS}] = \sqrt{2}\sin(\pi/4 + FT_{FOS})$, and the trigonometric formula for difference: $\cos[FT_{FOS}] - \sin[FT_{FOS}] = \sqrt{2}\sin(\pi/4 - FT_{FOS})$.

Figures 6.13, 6.14, 6.15, and 6.16 show the plots constructed on the expressions (6.54) and (6.55) of the suppression coefficients of the amplitude $K^2_{\Gamma AN}(F)$ and the phase $K^2_{\Gamma PN}(F)$ noise in OEO MZ for various values of σ_U and $\frac{P_{0L}}{Y_{00}}$.

Plots of suppression coefficients of the amplitude $K^2_{\Gamma AN}(\sigma_U)$ and the phase $K^2_{\Gamma PN}(\sigma_U)$ noise of OEO MZ are presented in Fig. 6.17 depicted by expressions (6.54) and (6.55) for different σ_U at the normalized offset $F = 3$.

Plots depicted in Figs. 6.13, 6.14, 6.15, 6.16, and 6.17 by expressions (6.54) and (6.55) allows the following conclusions. Suppression coefficients of the amplitude and the phase noises are completely determined of PSD of the amplitude and phase noises on OEO MZ.

At growth of the module of the local slope coefficient σ_U up to 10, we can suppress the amplitude noises by more than 100 times in the normalized offset region $F > 2$. At that, the phase noises are suppressed insignificantly by the value not

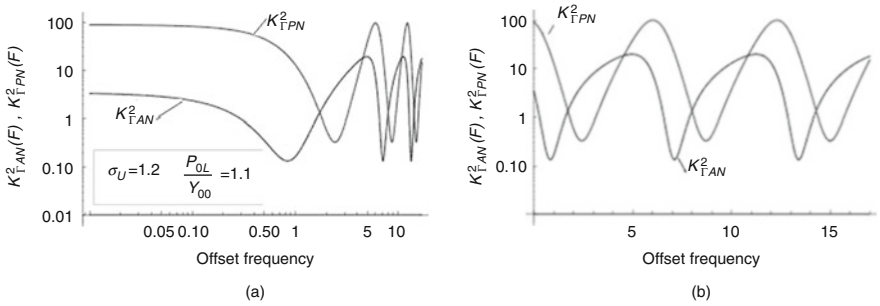

Fig. 6.13 Suppression coefficients for the amplitude $K^2_{\Gamma AN}(F)$ and the phase $K^2_{\Gamma PN}(F)$ noise in OEO MZ at $P_{0L}/Y_{00} = 1.1$ for $\sigma_U = 1.2$ depicted on expressions (6.54) and (6.55). On the abscissa axis the logarithmic scale (**a**); on the abscissa axis the linear scale (**b**)

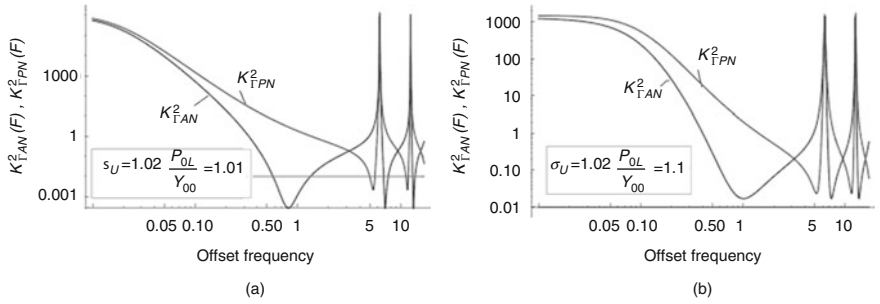

Fig. 6.14 Suppression coefficients of the amplitude $K^2_{\Gamma AN}(F)$ and the phase $K^2_{\Gamma PN}(F)$ noise in OEO MZ at $\sigma_U = 1.02$ and $P_{0L}/Y_{00} = 1.01$ (**a**); $\sigma_U = 1.02$ and $P_{0L}/Y_{00} = 1.1$ for (**b**) depicted on expressions (6.54) and (6.55). The abscissa axis has the logarithmic scale (**a**). The abscissa axis has the linear scale (**b**)

more than 5–10 times. The extreme suppression of the phase noises is achieved at small values of σ_U and for P_{0L}/Y_{00} values closed to the stability boundary in the steady-state mode, for example, $\sigma_U = 1.02$ and $P_{0L}/Y_{00} = 1.01$, or closed the generation mode with small excess over the threshold value. The increase of the laser power and the ratio P_{0L}/Y_{00} does not improve the picture of phase noise suppression in OEO MZ, but at that, the threshold level of OEO generation undoubtedly decreases.

PSD of the phase noise is much more than PSD of the amplitude noise or $S_{a\mu Re} \cdot (Y_{aRe} - 1)^2 \ll S_{a\mu Im} \cdot [Y_{aIm}]^2$.

Further, we examine the mode when the in-phase component $S_{a\mu Re}$ is much more than the quadrature $S_{a\mu Im}$. In other words, the level of detected laser noises in the PD load (PSD of the phase noise) is much more than PSD of the amplitude noise. In this case, we can simplify Eqs. (6.49) and (6.50): $S_{a\mu Re} \cdot (Y_{aRe} - 1)^2 \ll S_{a\mu Im} \cdot [Y_{aIm}]^2$.

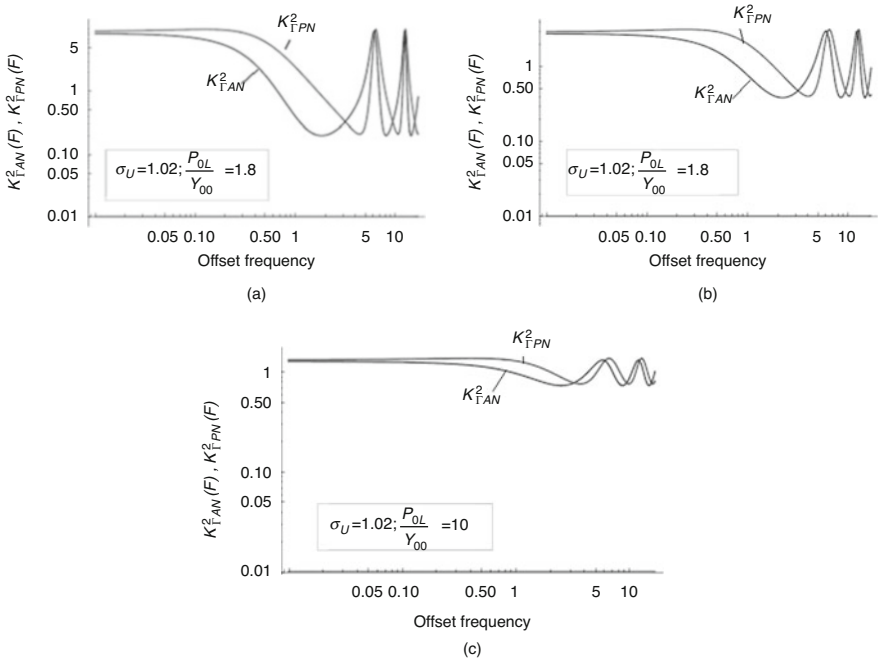

Fig. 6.15 Suppression coefficient of the amplitude $K^2_{\Gamma AN}(F)$ and the phase $K^2_{\Gamma PN}(F)$ noise depicted by expressions (6.54) and (6.55) in OEO MZ at $\sigma_U = 1.02$ and $P_{0L}/Y_{00} = 1.8$ (**a**); $\sigma_U = 1.02$ and $P_{0L}/Y_{00} = 1.1$ for (**b**), $\sigma_U = 1.02$ and $P_{0L}/Y_{00} = 10$ for (**c**)

Here we consider only the action of the laser noises assuming that detected laser noises significantly exceed the own PD noises and reduced to the NA input. For simplicity, we suppose that $D_{PN} = D_{AN}$.

Fulfillment of mentioned conditions is possible in the case of the non-quadrature mode, when $\sin[2\pi\nu_0(T_{1M} - T_{2M}) + \pi U_{0MZ}/U_{\pi MZ}] \approx 0$ or $2\pi\nu_0(T_{1M} - T_{2M}) + \pi U_{0MZ}/U_{\pi MZ} = \pi m$. Then, the second term in Eq. (6.27) becomes neglibly small. i.e., $S_{\mu AN\ -\ PN} \approx 0$ and $S_{\mu\psi 1PN}(F) > S_{\mu AN}(F)$. In these assumptions, expressions (6.49) and (6.50) for $S_{mOEO}(F)$ and $S_{\Psi OEO}(F)$ take the form:

$$S_{mOEO}(F) = \frac{[Y_{aIm}]^2 S_{a\mu Im}}{\left\{[Y_{a\,Re} - \sigma_U][Y_{a\,Re} - 1] + [Y_{aIm}]^2\right\}^2},$$

$$S_{\Psi OEO}(F) = \frac{(Y_{a\,Re} - \sigma_U)^2 S_{a\mu Im}}{\left\{[Y_{a\,Re} - \sigma_U][Y_{a\,Re} - 1] + [Y_{aIm}]^2\right\}^2}. \tag{6.56}$$

Then expressions (6.36) and (6.55) for (6.62), (6.63) can be written as follows: $S_{mOEO} = S_{a\mu\,Re} K^2_{\Gamma AN}$, $S_{\Psi OEO} = S_{a\mu Im} K^2_{\Gamma PN}$, where coefficients $K^2_{\Gamma AN}(F)$ and $K^2_{\Gamma PN}(F)$ have the form:

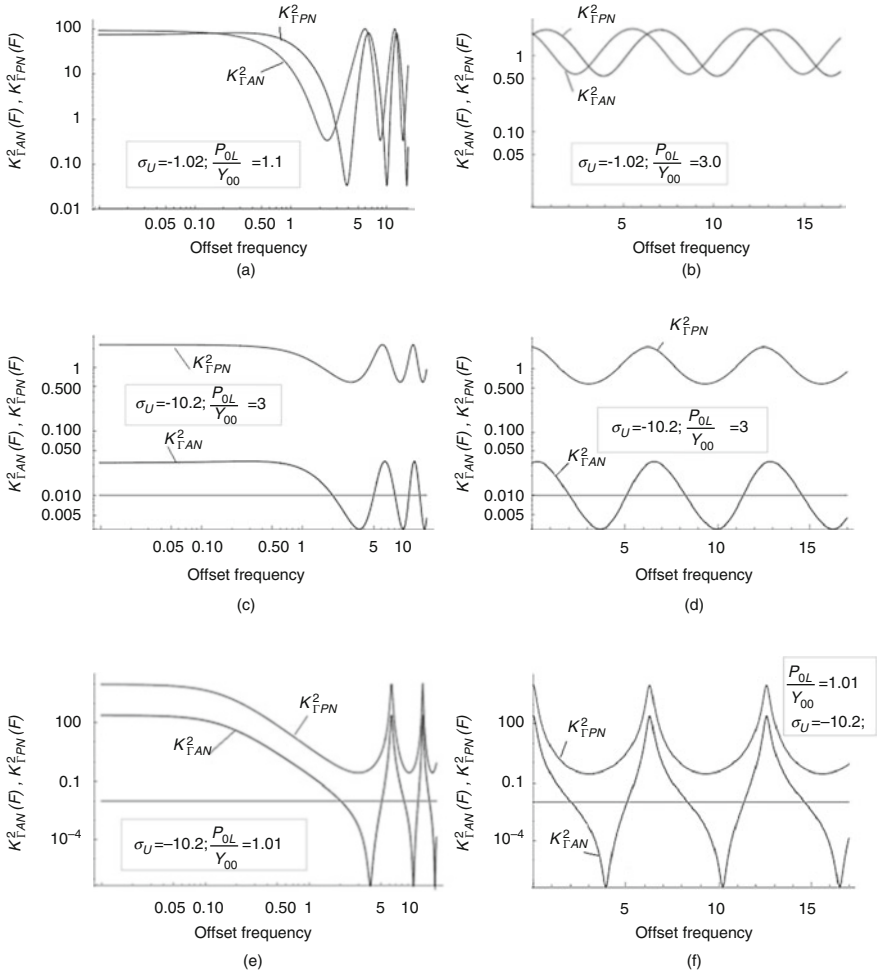

Fig. 6.16 Suppression coefficients of the amplitude $K^2_{\Gamma AN}(F)$ and the phase $K^2_{\Gamma PN}(F)$ noise depicted by expressions (6.54) and (6.55) in OEO MZ at $\sigma_U = -1.2$ and $P_{0L}/Y_{00} = 1.1$ (**a**); $\sigma_U = -1.02$ and $P_{0L}/Y_{00} = 3.0$ for (**b**); $\sigma_U = -1.02$ and $P_{0L}/Y_{00} = 3.0$ for (**c**, **d**); $\sigma_U = -10.2$ and $P_{0L}/Y_{00} = 1.01$ for (**e**, **f**). On the abscissa axis the logarithmic scale (**a**, **c**, **e**); on the abscissa axis the linear scale (**b**, **d**, **f**)

$$K^2_{\Gamma AN}(F) = \frac{\left[\frac{\gamma}{P_{0L}} \sin\left(FT_{FOS}\right)\right]^2}{\left\{\left[\frac{Y_{00}}{P_{0L}}\right]^2 - \frac{Y_{00}}{P_{0L}} \cdot (1+\sigma_U)\cos\left[FT_{FOS}\right] + \sigma_U\right\}^2}, \tag{6.57}$$

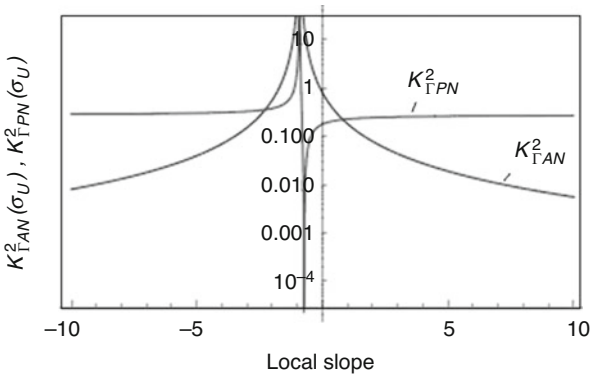

Fig. 6.17 Suppression coefficient of the amplitude $K^2_{\Gamma AN}(F)$ and the phase $K^2_{\Gamma PN}(F)$ noise depicted by expressions (6.54) and (6.55) in OEO MZ at different σ_U at the normalized offset $F = 3$

$$K^2_{\Gamma PN}(F) = \frac{\left[\frac{\gamma}{P_{0L}}\cos\left(FT_{FOS}\right) - \sigma_U\right]^2}{\left\{\left[\frac{Y_{00}}{P_{0L}}\right]^2 - \frac{Y_{00}}{P_{0L}}\cdot(1+\sigma_U)\cos\left[FT_{FOS}\right] + \sigma_U\right\}^2}. \tag{6.58}$$

Figures 6.18 and 6.19 show the plots depicted by expressions (6.57) and (6.58) of suppression coefficients of the amplitude $K^2_{\Gamma AN}(F)$ and the phase $K^2_{\Gamma PN}(F)$ noise in OEO MZ for different values of σ_U and P_{0L}/Y_{00}.

From analysis of plots in Figs. 6.18 and 6.19 for suppression coefficients of the amplitude and phase noises in OEO MZ, we can conclude that at fulfillment of the condition $S_{a\mu Re}\cdot(Y_{aRe}-1)^2 \ll S_{a\mu Im}\cdot[Y_{aIm}]^2$, the maximal suppression of PSD of phase noises occurs at small values of σ_U and P_{0L}/Y_{00} (Fig. 6.19), which are close to the stability boundary of the OEO MZ generation mode. At that, we observe the significant level of peak values at multiple offsets $FT_{FOS} = 2\pi m$, where m is the integer number. The power increase (or the normalized value of P_{0L}/Y_{00}) in this case leads to reduction of phase noise suppression (Fig. 6.19).

6.5.8 *The Function of the Suppression Coefficient of PSD of the Phase Noise in OEO MZ Versus the Laser Power*

The function of PSD of the phase noise of the laser power P_{0L} is defined by Eq. (6.55). The specific feature of OEO MZ is the fact that the coefficient of the local slope σ_U also depends on P_{0L}. The formula for interconnection of σ_U of P_{0L} at approximation of NA nonlinear characteristic by the cubic polynomial is: $\sigma_U = 1 - \frac{S_{03}}{S_{01}}U^2_{10MZ} = \frac{1}{3}\left(1 - \frac{4Y_{00}}{P_{0L}}\frac{1}{S_{01}}\right)$. Such function σ_U is defined by the square amplitude U^2_{10MZ} with expression obtained from the abbreviated equation of OEO MZ in the Chap. 3 (Eq. 3.59) at fulfillment of self-excitation conditions and the

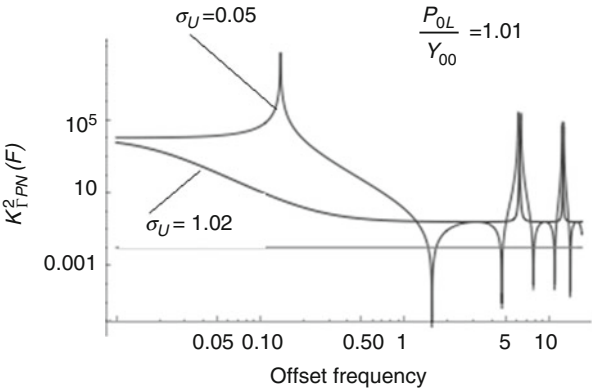

Fig. 6.18 Suppression coefficient of the phase noise in OEO MZ at $P_{0L}/Y_{00} = 1.01$ for $\sigma_U = 1.02$ and $\sigma_U = 0.05$

generation conditions in the steady-state mode: $U_{10MZ} = \sqrt{4S_{01}/3S_{03}} \cdot \left(1 - \frac{1}{S_{01}P_{0L} \cdot R_{PD}|K_{FODL}|}\right)^{1/2}$, where $|K_{FODL}|$ is the module of the RF FODL transfer function $R_{PD}|K_{FODL}| = 1/Y_{00}$.

Since in the general formula (6.52) for PSD of the phase noise, the value of the laser quadratic component $S_{\mu Im}$ depends on U^2_{0MZ} (or on the power of RF oscillations $P_{OEO} = U^2_{0MZ}/(2R_{MZ})$, where R_{MZ} is the input resistance of MZ): $S_{\mu Im} = \frac{4S_{\beta FM}D_{FM} \cdot U^2_{0MZ}}{(\omega-\omega_0)^2 T^2_{0L} \cdot P_{0L}}$, we can present: $U^2_{10MZ} = (2R_{PD})P_{OEO} = (2R_{PD})P_G = \frac{4S_{01}}{3S_{03}} \cdot \left(1 - \frac{Y_{00}}{S_{01}P_{0L}}\right)$. Then, the complete expression for PSD of the phase noise in OEO MZ (6.52) can be written taking into account:

$$S_{\Psi OEO} = \frac{S_{\mu Im}}{F^2 T^2_{0L}} \frac{16D_{PN}S_{01}}{3S_{03}} K^2_{\Gamma PN} \frac{1}{P_{0L}} \left(1 - \frac{Y_{00}}{S_{01}P_{0L}}\right). \tag{6.59}$$

We note that the oscillation power of OEO MZ P_{OEO} versus P_{0L} is determined as:

$$P_{OEO} = P_G = \frac{2S_{01}}{3R_{PD}S_{03}} \cdot \left(1 - \frac{Y_{00}}{S_{01}P_{0L}}\right). \tag{6.60}$$

Finally, taking into consideration Eq. (6.59), we can write for $S_{\Psi OEO}$:

$$S_{\Psi OEO} = K^2_{\Gamma PN} \frac{8D_{PN}S_{\mu Im}}{F^2 T^2_{0L}} \frac{P_{OEO}}{P_{0L}}. \tag{6.61}$$

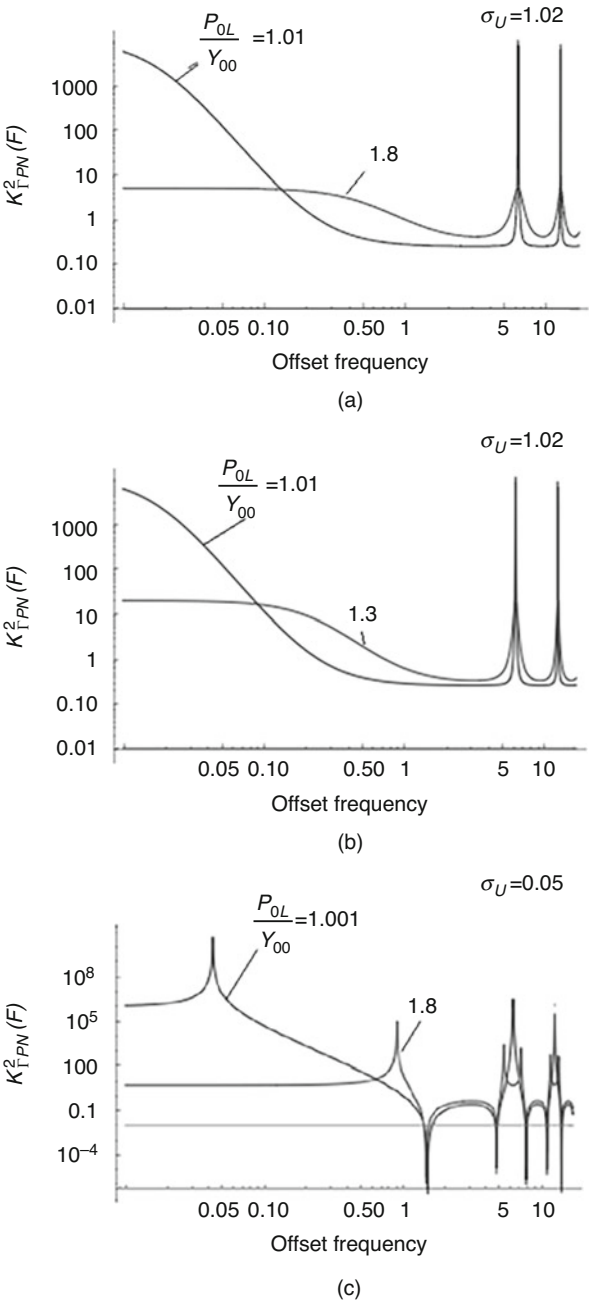

Fig. 6.19 Dependences of suppression coefficients of the phase noise $K^2_{\text{TFM}}(F)$ in OEO MZ at $P_{0\text{L}}/Y_{00} = 1.01$ and 1.8 for $\sigma_{\text{U}} = 1.02$ (**a**); at $P_{0\text{L}}/Y_{00} = 1.01$ and 1.3 for $\sigma_{\text{U}} = 1.02$ (**b**); at $P_{0\text{L}}/Y_{00} = 1.001$ and 1.8 for $\sigma_{\text{U}} = 0.05$ (**c**)

6.5.9 The Formula for PSD of the Phase Noise in OEO MZ

Let us rewrite Eq. (6.61) by dividing of the right and left parts by P_{OEO} and then we shall have the final formula in the form:

$$\frac{S_{\Psi\text{OEO}}}{P_{\text{OEO}}} = K_{\Gamma\text{FN}}^2 \frac{8D_{\text{PN}}S_{\mu\text{Im}}}{F^2T_{0\text{L}}^2}\frac{1}{P_{0\text{L}}}. \tag{6.62}$$

The formula (6.62) is the basis for engineering calculations of the ratio of PSD of the phase noise to the power of RF oscillations of OEO MZ. Figure 6.20a, b show suppression coefficients of the phase noise in $\frac{K_{\Gamma\text{PN}}^2}{P_{0\text{L}}}$ and present the functions of the coefficient $\sigma_{\text{U}}(P_{0\text{L}})$ versus the laser power $P_{0\text{L}}$ at $\sigma_{\text{U}} < 0$ (c) and $\sigma_{\text{U}} > 0$ (d).

It is necessary to note that σ_{U} can take both positive and negative values, which is defined by the OEO stability in the steady-state point: $\sigma_{\text{U}} \cdot \cos(FT_{\text{FOS}}) < 0$. At $\cos(FT_{\text{BLZ}}) > 0$, the condition $\sigma_{\text{U}} < 0$ should be fulfilled and vice versa: at $\cos[FT_{\text{FOS}}] < 0$, the condition $\sigma_{\text{U}} > 0$ should be fulfilled. Substituting $\sigma_{\text{U}} = \frac{1}{3} \times \left(1 - \frac{4Y_{00}}{P_{0\text{L}}}\frac{1}{S_{01}}\right)$ into the formulas (6.57) and (6.58), we obtain two various formulas for $\cos[FT_{\text{FOS}}]$ and σ_{U} : 1 (1) for $\cos[FT_{\text{FOS}}] > 0$, $\sigma_{\text{U}} < 0$, $\sigma_{\text{U}} = +\frac{1}{3} - \frac{1}{3}\frac{Y_{00}}{P_{0\text{L}}}\frac{4S_{03}}{S_{01}} < 0$; and (2) for $\cos[FT_{\text{FOS}}] < 0$, $\sigma_{\text{U}} > 0$, $\sigma_{\text{U}} = -\frac{1}{3} + \frac{1}{3}\frac{Y_{00}}{P_{0\text{L}}}\frac{4S_{03}}{S_{01}} > 0$. We note that in Fig. 6.20a, b, the presented functions correspond to values $P_{0\text{L}}/Y_{00} < 1$ below of the OEO generation threshold, and relatively to $P_{0\text{L}}/Y_{00} > 1$ above this threshold. The formula (6.62) contains the quadrature component of the laser PSD $S_{\mu\text{Im}}$, the laser time constant $T_{0\text{L}}$ (equal approximately to laser coherence time T_{c}), the square of the suppression coefficient $K_{\Gamma\text{PN}}^2$, which is defined by the expression (6.55) for $\cos[FT_{\text{FOS}}] < 0$, $\sigma_{\text{U}} > 0$, $\sigma_{\text{U}} = -\frac{1}{3} + \frac{1}{3}\frac{Y_{00}}{P_{0\text{L}}}\frac{4S_{03}}{S_{01}} > 0$, including the offset F, the delay time T_{FOS} in the optical fiber, parameters of the oscillating system of OEO MZ: Y_{00}, S_{01}, S_{03} and the laser power $P_{0\text{L}}$. $K_{\Gamma\text{PN}}^2$ insignificantly depends on the laser power. With laser power P_{0L} growth, variations of $K_{\Gamma\text{PN}}^2$ are tenth parts of unit, which is caused with the increase of RF oscillations power $P_{\text{OEO}} = P_{\text{G}} = U_{10\text{MZ}}^2/(2R_{\text{PD}})$ (increase is proportional to the noise). The total decrease of $S_{\Psi\text{OEO}}/P_{\text{OEO}}$ with $P_{0\text{L}}$ growth is more than ten times, at growth of the laser power is related not to OEO oscillating system parameters, but directly with the quadrature components of the laser PSD $S_{\mu\text{Im}}$.

Figure 6.21 show the plots of suppression coefficients of the phase noise in OEO MZ $K_{\Gamma\text{PN}}^2$, $\frac{K_{\Gamma\text{PN}}^2}{P_{0\text{L}}}$, the power of OEO RF oscillations P_{OEO} depending on the laser power in the linear (a) and logarithm (b) scales in the abscissa axis.

Formulas (6.54) and (6.55) for calculation of suppression coefficients of PSD of the amplitude and phase noises permit to calculate $K_{\Gamma\text{PN}}^2(F)$ not only in the steady-state generation mode in OEO MZ, but in the case, when self-excitation conditions are not satisfied as well. We computed by the formula (6.55) the function $K_{\Gamma\text{PN}}^2(F)$, which is presented at $\sigma_{\text{U}} = 1.02$ below excitation threshold of OEO MZ, which

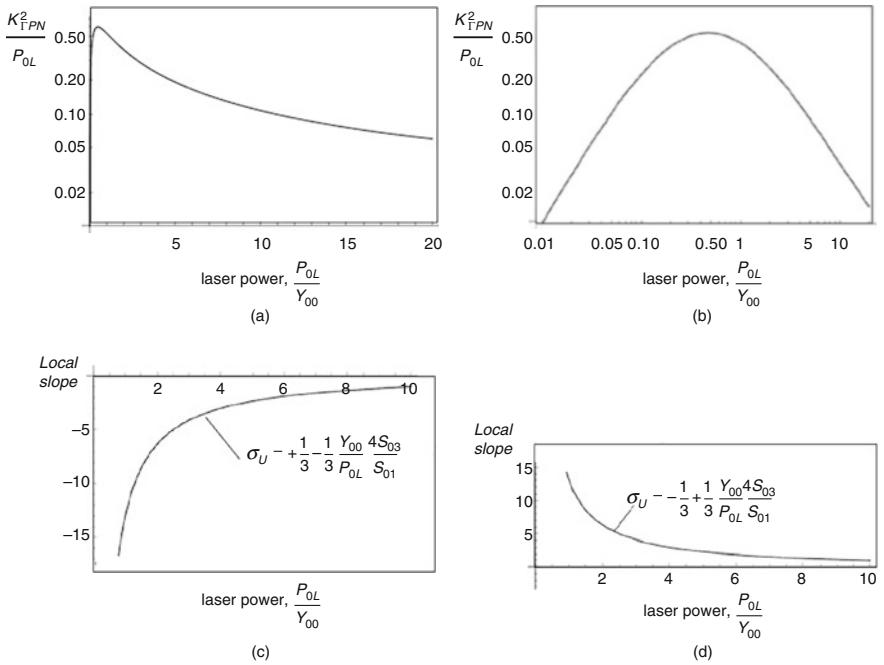

Fig. 6.20 Plots of suppression coefficient of the phase noise in OEO MZ of the laser power at $\frac{S_{03}}{S_{01}} = 10$ for $\sigma_U = +\frac{1}{3} - \frac{1}{3}\frac{Y_{00}}{P_{0L}}\frac{4S_{03}}{S_{01}} < 0$ (**a**) and for $\sigma_U = -\frac{1}{3} + \frac{1}{3}\frac{Y_{00}}{P_{0L}}\frac{4S_{03}}{S_{01}} > 0$ (**b**). Plots of the coefficient σ_U versus the laser power P_{0L} for $\sigma_U < 0$ (**c**) and $\sigma_U > 0$ (**d**)

corresponds to the value $Y_{00}/P_{0L} = 0.4$. From the analysis of our computation, it follows that $K^2_{\Gamma PN}(F)$ takes the values, which are essentially less than 1 in the wide range of offsets. We may conclude that it is necessary to perform the noise analysis of OEO in the regenerative mode including the synchronization mode of OEO MZ by the external RF oscillator. At that, the RF FODL output can be connected to one of the electrical input of the external oscillator so as to realize its self-synchronization through RF FODL.

6.5.9.1 Peaks in PSD of Phase Noises in OEO MZ

The presence of resonance peaks in PSD of the phase noise, which correspond to the adjacent types of RF oscillations, which are not generated, is the sharp problem. One of the solutions of this problem is an application in OEO MZ of differential and combined RF FODL, which has AFC of the rejection type. The total transfer function of the combined RF FODL with several optical fibers of different length can be calculated as:

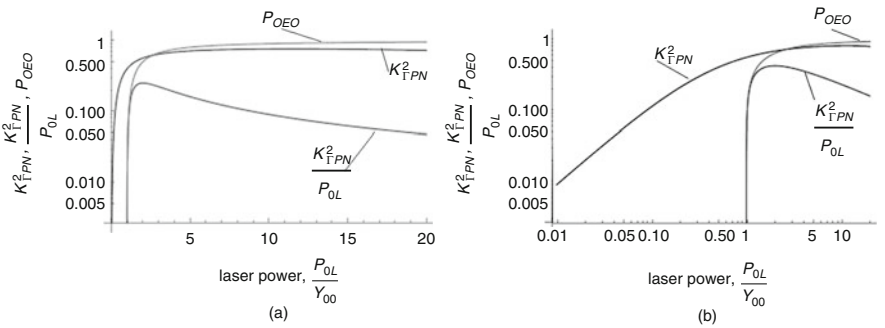

Fig. 6.21 Plots of suppression coefficients of the phase noises in $K^2_{\Gamma FM}$, $K^2_{\Gamma PN}/P_{0L}$, the power of OEO RF P_{OEO} depending on the laser power P_{0I}/Y_{00} in the linear (**a**) and logarithm (**b**) scales in abscissa axis at $S_{03}/S_{01} = 10$ and at $\sigma_U = +\frac{1}{3} - \frac{1}{3}\frac{Y_{00}}{P_{0L}}\frac{4S_{03}}{S_{01}} < 0$

$$K_{\text{FODL}} = AK_{\text{A}} \exp\left[-j2\pi f(T_{\text{FOS}} + T_{1\text{FOS}})\right]$$
$$+BK_{\text{B}} \exp\left[-j2\pi f(T_{\text{FOS}} + T_{2\text{FOS}})\right] + CK_{\text{C}} \exp\left[-j2\pi f(T_{\text{FOS}} + T_{3\text{FOS}})\right.$$
$$+\cdots + NK_{\text{N}} \exp\left[-j2\pi f(T_{\text{FOS}} + T_{N\text{FOS}})\right], \tag{6.63}$$

where $T_{\text{FOS}} + T_{1\text{FOS}}$, $T_{\text{FOS}} + T_{2\text{FOS}}$, $T_{\text{FOS}} + T_{3\text{FOS}}$, $T_{\text{FOS}} + T_{N\text{FOS}}$ are the light delays, relatively, in first, second, third, and Nth optical channels. $A \cdot K_{\text{A}}$, $B \cdot K_{\text{B}}$, $C \cdot K_{\text{C}}$, ... are products of the excitation coefficients of optical fibers by the modules of their transfer functions, relatively, of optical fibers 1, 2, 3, 4, ..., N.

6.5.10 *Utilization of Differential and Combined FOS to Suppress the Resonance*

Differences in delays between the "adjacent" channels of optical channels should satisfy the condition $F(T_{2\text{FOS}} - T_{1\text{FOS}}) = \frac{1}{N}$. Minima of K_{FODL} modules should correspond to the frequency values, which are not included into the generation of OEO MZ. Figure 6.22 shows AFC of differential and combined RF FODL with two, three, and four optical fibers of different geometrical length, which are used in OEO for suppression of the adjacent (from the fundamental harmonic) types of oscillations, which are not attracted into generation.

From Fig. 6.22, we see that at differential RF FODL with two optical fibers, the first minimum of AFC satisfies to the condition $F(T_{2FOS} - T_{1FOS}) = 1/2$, further, the position of adjacent next minimum is defined as $F(T_{2\text{FOS}} - T_{1\text{FOS}}) = \frac{1}{2} + 1$.

The deeper suppression of the spurious noise harmonics can be achieved at application of RF FODL consisting of three and more fibers with different length (Fig. 6.22). We should note that the growth of optical channel number with utilization of Y-couplers leads to the increase of total losses in RF FODL and to decrease of its transfer function $|K_{\text{FODL}}|$ and therefore it restricts its usage.

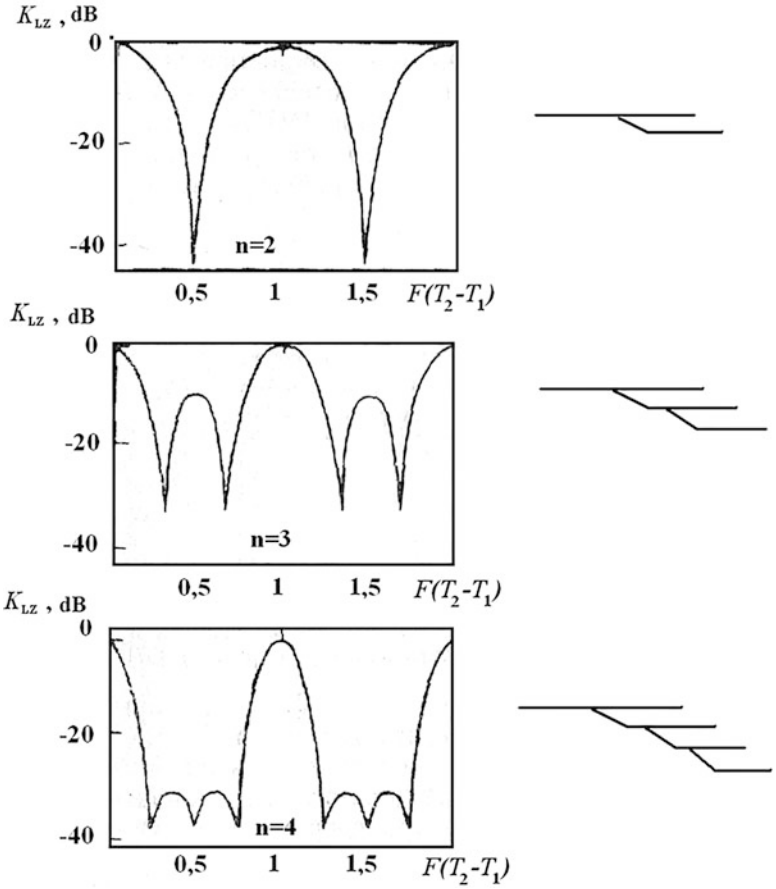

Fig. 6.22 Calculated AFC of the differential and combined RF FODL with two, three, and four FOS of different geometrical length, which are used in OEO for suppression of adjacent types of oscillations, which are not attracted to generation. Here $K_{LZ} = |K_{FODL}|$, $F(T_2 - T_1) = F(T_{2FOS} - T_{1FOS})$

6.5.11 *PSD of the Phase Noise in OEO MZ with RF FODL and MZ Modulator Taking into Account the laser, PD and NA Noises*

In this section, we derive the formula for PSD of the phase noise in OEO MZ taking into consideration of the detected laser noises, the PD output noises and the input NA noises. For this, we examine expressions (6.50), (6.52), (6.26), (6.27) and (6.56) taking into account PSD of PD and NA.

The circuit of OEO MZ with account of RF noise sources is presented in Fig. 6.23a: the detected QWLD noise (1), the own noise of PD (2), noises in the

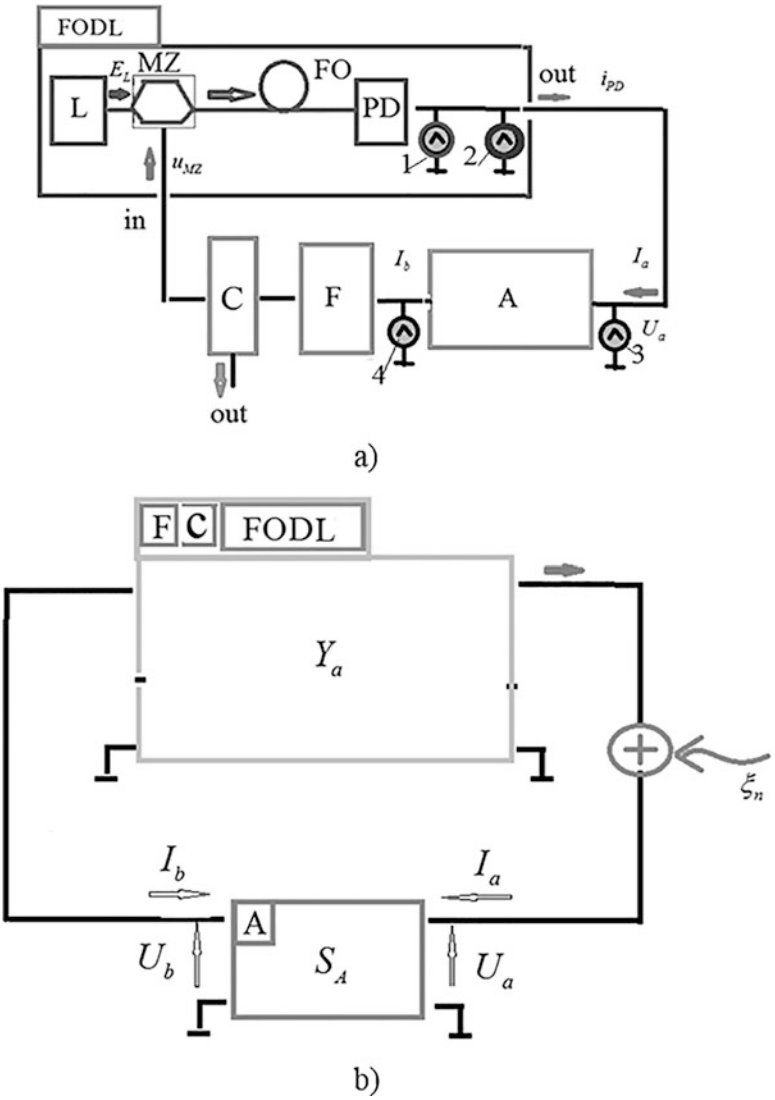

Fig. 6.23 The structure of OEO MZ taking into account the laser, PD, and NA noise source. (**a**) The structure of OEO MZ with sources of RF noise: the detected QWLD noise (1), the own noise of PD (2), noises in the input and output of RF amplifier (3, 4). (**b**) The structure of OEO MZ as the RF amplifier with nonlinear characteristics S_A, which is covered by the block of the positive feedback with the conductance Y_a. The source of the RF noise are shown: four noise sources presented in (**b**) are reduced to the one equivalent noise source ξ_n

input and output of RF amplifier (3, 4). Figure 6.23b shows the OEO MZ with the single equivalent noise source ξ_n.

In the general case, for OEO MZ, the PSD curve of phase fluctuations $S_{\Psi AG}$ has the complicate analytical shape, which is determined by the in-phase $S_{\mu Re}(\omega)$ and the quadrature $S_{\mu Im}(\omega)$ components:

$$\frac{S_{\Psi A\Gamma}}{P_G} = \frac{(Y_{aRe} - \sigma_U)^2 \cdot S_{ImPDNA} + Y_{aIm}{}^2 \cdot S_{RePDNA} - 2(Y_{aRe} - \sigma_U) \cdot Y_{aIm}{}^2 S_{ImRePDNA}}{P_G \left\{ [Y_{aRe} - \sigma_U] \cdot [Y_{aRe} - 1] + [Y_{aIm}]^2 \right\}^2}, \tag{6.64}$$

where P_G is the microwave power of the fundamental harmonic of OEO MZ, $S_{ImPDNA} = G_{12} K_{PD}^2 P_G \cdot S_{ImL} + S_{ImPD} + S_{ImNA}$, $S_{ReFDNY} = G_{12} P_G K_{PD}^2 S_{ReL} + S_{ReFD} + S_{ReNA}$ are the quadrature and in-phase components of laser total noises.

We can assume that PD and NA have, for example:

$$S_L \approx S_{ImL} \approx S_{ReL} = \frac{S_{\beta PN}}{P_{0L} F^2 T_{0L}^2}, \tag{6.65}$$

where $G_{12} = 1 - (A_1/A_2) \cdot \exp(-T_{FOS}/T_c) = 1 - K_{\Psi 12}$, $K_{\Psi 12} = (A_1/A_2) \cdot \exp(-T_{FOS}/T_c)$ is the correlation coefficient defining by MZ and approximately equal to 1 with accuracy 0.9–0.999 depending on the geometrical length of the optical fiber, K_{PD}^2 is the coefficient, which takes into account the spectrum transformations at passing through MZ and at photodetection of PSD of the laser emission in the MZ input and the RF oscillation PSD in the PD load.

With purpose of the simple expressions, we assume that in-phase and quadrature components of the own noises of PD is approximately the same: $S_{RePD} \approx S_{ImPD} = 2eI_{0PD}R_{PD} = 2eS_{0PD} \cdot P_{0L}R_{PD}$, where the electron charge $e = 1.6 \cdot 10^{-19} Q$, I_{0PD} is DC component of the PD photo-current, which is $I_{0PD} = S_{0PD} \cdot P_{0L}$, where S_{0PD} is the static slope of the watt–ampere PD characteristic, R_{PD} is the load resistance of PD in DC.

We suppose that own noises of the ultra-wideband low-noise noninertial RF NA are determined only by "thermal" noises (i.e., we do not take into consideration flicker-noises etc.). For calculation simplicity, we assume that in-phase and quadrature components of PSD of "thermal" noises in the NA input are equal [3]: $S_{ReNY} = S_{ImNY} = D_Y kT$, where D_Y is the noise-factor of NA, $k = 1.38 \cdot 10^{-23}$ J/K is the Boltzmann constant, T is the absolute temperature in Kelvin degrees.

Then, at substitution $S_{RePD} \approx S_{ImPD}$ and $S_{ReNY} = S_{ImNY}$, the expression (6.64) is written as:

$$\frac{S_{\Psi OEO}}{P_G} = \frac{\left(G_{12}K_{PD}^2 \frac{S_{\beta PN}P_G}{P_{0L}F^2T_{0L}^2} + 2eI_{0PD}R_{PD} + D_Y kT\right)}{P_G} K_{\Gamma PN}^2, \tag{6.66}$$

where the coefficient $K_{\Gamma PN}^2$ corresponds to Eq. (6.58). Also, we used in Eq. (6.36) for Y_{aRe}, Y_{aIm} and Y_{00}, the abome-introduced formulas. Supposing that OEO MZ operates at small exceeds above the generation threshold (with small excitation reserve) and $\frac{Y_{00}}{P_{0L}} = \frac{y_M[1+FT_{EF}]}{P_{0L}|K_{FODL}|} \approx 1$. Then the expression (6.66) is:

$$\frac{S_{\Psi OEO}}{P_G} = K_{\Gamma PN}^2 \left[\frac{G_{12} \cdot K_{PD}^2 S_{\beta PN}P_G}{P_G P_{0L}F^2T_{0L}^2} + \frac{2eS_{0PD} \cdot P_{0L}R_{PD}}{P_G} + \frac{D_Y kT}{P_G}\right]. \tag{6.67}$$

We use for an analysis the expression (6.67) and for the OEO power Eq. (6.60): $P_G = P_{OEO} = \frac{2S_{01}}{3R_{PD}S_{03}} \cdot \left(1 - \frac{Y_{00}}{S_{01}P_{0L}}\right)$, and $I_{0PD} = S_{0PD} \cdot P_{0L}$.

If we take into consideration that the Q-factor of oscillating system is equal to $Q_L = \nu_{0L}T_{0L}$, where $\nu_{0L} = \nu_0$ is the optical generation frequency of the laser, $T_{0L} \approx T_c$, T_{0L} is the time constant of the laser oscillating system, the RF oscillation power in OEO (at cubic NA nonlinearity)

Using the earlier-considered function P_G of P_{0L} determining as Eq. (6.60), then the expression (6.67) is simplified as:

$$\frac{S_{\Psi OEO}}{P_G} = K_{\Gamma PN}^2 \cdot K_{PD}^2 \frac{G_{12}S_{\beta PN}}{P_{0L}F^2T_{0L}^2} + \frac{K_{\Gamma PN}^2}{\frac{2S_{01}}{3R_{PD}S_{03}} \cdot \left(1 - \frac{Y_{00}}{S_{01}P_{0L}}\right)} \cdot \left[\frac{2eS_{0PD} \cdot R_{PD}}{1} P_{0L} + \frac{D_Y kT}{1}\right], \tag{6.68}$$

The expression (6.68) shows that the increase of the laser optical power P_{0L} leads to the decrease of the first term (related to the laser noise) and the third term (related to the RF amplifier noise) in Eq. (6.68). The second term related to PD noise increases at the P_{0L} growth. Such ambiguous noise variation at growth of the laser optical power—the second source of the optical energy in OEO—is one of the specific properties of OEO, if we can consider the electrical power source as the first energy source.

The expression (6.68) gives a possibility to understand that the power density of the phase noise in OEO MZ (at microwave modulation in the one of MZ optical channels and at taking into account of only the thermal noise of NA and the shot noise of PD) is determined by three components: the laser phase noise due to its spontaneous emission (the first term in Eq. (6.68)), the shot phase noise of PD (the second term in Eq. (6.68)) and the thermal noise (third term). Suppression coefficients $K_{\Gamma PN}^2 \cdot K_{PD}^2$ (6.74) and $K_{\Gamma PN}^2$ (6.68) for "laser" and RF noises have the similar structures and the same denominators. The key difference of the "laser" $K_{\Gamma PN}^2 \cdot K_{PD}^2$ from the RF $K_{\Gamma PN}^2$ is the presence in the numerator of K_Γ of the additional

suppressing coefficient G_{12}, the physical sense of which is opened by the mechanism of "statistical" noise suppression at self-heterodyning in the Mach–Zehnder interferometer. The coefficient $G_{12} = 1 - (A_1/A_2) \cdot \exp(-T_{FOS}/T_c)$ is lesser for the higher time and spatial coherence of the laser and for lesser the difference of two MZ optical channels in the difference of refraction indices of the core and the envelope and in overall sizes of channels. The growth of the laser power, as we see from Eq. (6.68), leads to the decrease of PSD of the phase noise in OEO MZ not only due to the reduction of coefficients $K^2_{\Gamma PN} \cdot K^2_{PD}$, $K^2_{\Gamma PN}$, but is determined by the third term in expression (6.68). The delay growth T_{FOS} in RF FODL with the single optical fiber at increase of the geometrical FOS length in OEO MZ leads to reduction of PSD of the phase noise, but as we see from Eq. (6.68), this reduction is defined by the term in the denominator equaled to $(1 + \sigma_U) \cos[FT_{FOS}]$ and therefore, this decrease is restricted and is, as a rule, not more than 8–11 dB/Hz.

PSD of the phase noise in OEO MZ significantly decreases at utilization of the so-called "two-arms" or the mutual microwave modulation of refraction index in two optical channels of MZ modulator.

6.5.12 Modulations of Two Channels in MZ

We can significantly reduce of PSD of the phase noise in OEO MZ by using at optical phase modulation in both optical channels of the MZ interferometer. At that, the relative phase shift in radio frequency between channel electrodes is 90–180°.

Figure 6.24a shows the structure of OEO MZ with the external PD at modulation of MZ in both optical channels. Besides the modulation circuit in both channels of the single MZ modulator, at present, we can use commercially available modulators, in which the modulation methods in different optical channels are used, which are included in different MZ.

Let us consider the calculation features of PSD of the phase noise in this case, taking into account the noises of the laser, PD and NA. In PD area, the components passed the MZ modulator through the first $E_{1L} = E_{1L}(R)$ and the second $E_{2L} = E_{2L}(R)$ optical channels of MZ and FOS, have a form (Fig. 6.24a):

$$E_{1L} = k_{01}(E_{0L} + m_{SL}) \operatorname{Re}\{\exp[j2\pi\nu_0(t + T_{M1} + T_{FOS}) - j\varphi_{10L} - j\psi_{sm1}]\}, \tag{6.69}$$

$$E_{2L} = k_{02}(E_{0L} + m_{SL}) \exp[j2\pi\nu_0(t + T_{M2} + T_{FOS}) - j\varphi_{20L} - j\psi_{Sm2}], \tag{6.70}$$

where m_{SL} are fluctuations of the electrical component strength amplitude of EMF, ψ_{sm1} and ψ_{Sm2} are fluctuations of the optical phase of the electrical component strength in the output of first and second optical channels of FOS, k_{01} and k_{02} is the excitation coefficients of the optical channel OC1 and OC2 in the MZ modulator. At RF modulation, as shown in Chap. 5, in OEO MZ after the optical filter (which is

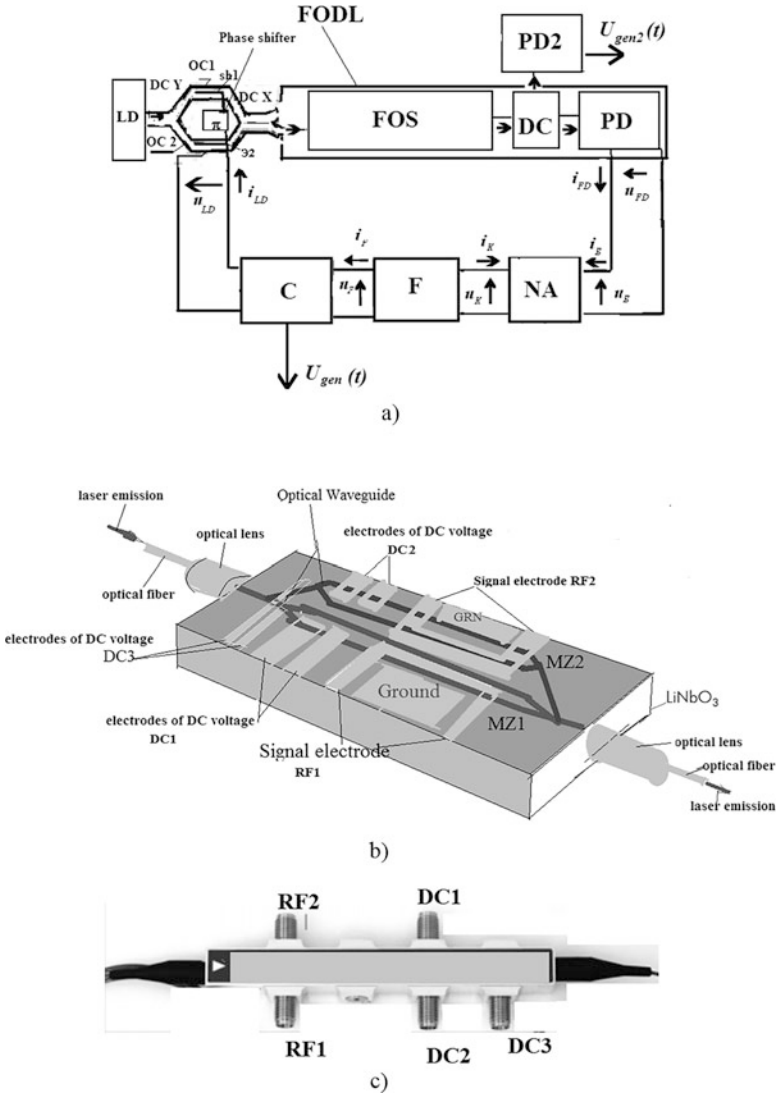

Fig. 6.24 Structure of OEO MZ with external PD at MZ modulation in both optical channels with the relative phase shift of the microwave oscillation with regard to the phase of RF oscillations in the second channel (**a**). Schematic diagram of the amplitude double modulator MXIQ-LN-40 from iXBlue Photonics Company. In this diagram are included: two sets of RF electrodes RF1 and RF2, electrodes of the DC bias DC1 and DC2, and electrodes of DC bias DC3, which regulate the phase difference between emissions in two modulators MZ1 and MZ2 (**b**). The double MZ modulator from EOspace Company (**c**)

located in FOS in Figs. 2.4 and 4.10), two optical harmonics pass on the photodetector area with frequencies ν_{0L} and $\nu_{0L} + f_0$, which strengths are equal, relatively, to:

- First harmonic $E_{10L}(t) = \sqrt{A_1}E_{0L}\cos[2\pi\nu_{0L}t + \varphi_{0L} + \varphi_{10Lm}(t)]$,
- Second harmonic$E_{20L}(t) = \sqrt{A_2}E_{0L}\cos[2\pi(\nu_{0L} + f_0)t + \varphi_{0L} + \varphi_{20Lm}(t)]$.

Here A_1 andA_2, as introduced in Chaps. 2 and 5, show the level of optical harmonic amplitudes.

In modern MZ modulators (for example, showed in Fig. 6.8b, c) the mutual modulation of both channels OC1 and OC2 is used. This is possible owing to existence of the differential phase delay $\varphi_{20L} - \varphi_{10L} = \pi$ of optical oscillations E_{1L} and E_{2L}, which propagate in different optical channels OC1 and OC2. Linearly polarized spatial oscillations in inputs of different optical channels OC1 and OC2 have the phase shift of 180° (Fig. 6.4c).

A modulation in MZ showing in Fig. 6.24b is another type of effective modulation. Two modulators MZ1 and MZ2 (Fig. 6.24b) are located on the single substrate. Powers of optical emissions E_{1MZL}, E_{2MZL}, which pass in MZ1 and MZ2, are proportional, relatively, to coefficients k_{0MZ1} and k_{0MZ2} : $k_{01} = P_{MZ1}/P_{0L}$ and $k_{02} = P_{MZ2}/P_{0L}$, where P_{MZ1} and P_{MZ2} are the optical powers in the modulator MZ1 and MZ2. P_{0L} is the total optical power in the input before splitting. Optical emissions modulated in MZ1 and MZ2 modulators pass to the photodetector area. Statistical averaging at photodetection (Chap. 5) leads to the phase noise decrease of RF oscillations at level equalization of optical power in MZ1 and MZ2 modulators.

MZ1 and MZ2 are mounted on the single substrate and are excited from the single laser. Figure 6.24b shows the schematic diagram of the amplitude double modulator MXIQ-LN-40 of iXBlue Photonics Company. Two sets of RF electrodes RF1 and RF2 are included in this diagrams, electrodes of the DC bias DC1 and DC2, and electrodes of DC bias DC3, which regulate the phase difference between emissions in two modulators MZ1 and MZ2. Figure 5.24c shows the double MZ modulator from EOspace Company.

Let us examine the diagram in Fig. 6.24a and we show which benefit in RF oscillations' phase noise we can obtain in OEO at the double-channel modulation. We remind, as shown in Chap. 5, the statistical averaging of phase fluctuations of detected laser noises leads to suppression of phase fluctuations of OEO RF oscillations.

Phase fluctuations $\psi_{sm1}$and ψ_{Sm2} in Eqs. (6.69) and (6.70) are defined not only by the laser phase noise but the amplified (in NA and NA1) phase noises of PD (PD or PD2) and amplified thermal RF noises (in NA). As the result of photodetection by the external PD2 located outside OEO MZ, we obtain for PSD of the phase noise in the photo-current of PD2 for OC1 and OC2, relatively from Eqs. (6.67) and (6.68), two following equations:

$$S_{1\mathrm{L}}(F) \approx \frac{S_{1\Psi\mathrm{OEO}}}{P_{\mathrm{G}}} = K_{\Gamma\mathrm{PN}}^2 \left\{ \frac{G_{12} \cdot K_{\mathrm{PD}}^2 S_{1\beta\mathrm{PN}}}{P_{0\mathrm{L}} F^2 T_{0\mathrm{L}}^2} + \frac{P_{0\mathrm{L}}}{P_{\mathrm{G}}} \cdot \left[\frac{2eS_{0\mathrm{PD}} \cdot R_{\mathrm{PD}}}{1} + \frac{D_{\Upsilon} kT}{P_{0\mathrm{L}}} \right] \right\}, \tag{6.71}$$

$$S_{2\mathrm{L}}(F) \approx \frac{S_{2\Psi\mathrm{OEO}}}{P_{\mathrm{G}}} = K_{\Gamma\mathrm{PN}}^2 \left\{ \frac{G_{12} K_{\mathrm{PD}}^2 S_{2\beta\mathrm{PN}}}{P_{0\mathrm{L}} F^2 T_{0\mathrm{L}}^2} + \frac{P_{0\mathrm{L}}}{P_{\mathrm{G}}} \cdot \left[\frac{2eS_{0\mathrm{PD}} \cdot R_{\mathrm{PD}}}{1} + \frac{D_{\Upsilon} kT}{P_{0\mathrm{L}}} \right] \right\}. \tag{6.72}$$

We note that in result of PSD adding $S_{1\mathrm{L}}(F)$ and $S_{2\mathrm{L}}(F)$ in the photo-current of PD2, we obtain:

$$S_{\mathrm{PD2}}(F) = S_{1\mathrm{L}}(F) + S_{2\mathrm{L}}(F) - 2(k_{01}/k_{02}) K_{21} S_{1\mathrm{L}}(F) * S_{2\mathrm{L}}(F), \tag{6.73}$$

where "$*$" is the convolution operation, K_{21} is the correlation function $K_{21} = \exp(-2\Delta\nu_{\mathrm{L}} \cdot \Delta T_{\mathrm{M}} - 2\Delta\nu_{\mathrm{L}} \cdot \Delta T_{\mathrm{FOS}})$ of the random process, $\Delta\nu_{\mathrm{L}}$ is the natural width of the spectral line of the laser emission, ΔT_{M} is the difference of delays in MZ and FOS channels, γ_k is the irregularity coefficient of optical channel excitation $\gamma_k = k_{01}/k_{02}$, k_{01} and k_{02} is the excitation coefficients of optical channel OC1 and OC2 in the MZ modulator: $k_{01} = P_{1\mathrm{L}}/P_{0\mathrm{L}}$ and $k_{02} = P_{2\mathrm{L}}/P_{0\mathrm{L}}$; $P_{1\mathrm{L}}$ and $P_{2\mathrm{L}}$ is the optical power in the optical channel OC1 and OC2 modulator MZ.

From expression (6.73), the important conclusion follows that at equalization in the optical power in OC1 and OC2, the following relation is fulfilled: $S_{1\mathrm{L}}(F) \approx S_{2\mathrm{L}}(F)$. At small $\Delta\nu_{\mathrm{L}} \cdot \Delta T_{\mathrm{M}} \to 0$, $\Delta T_{\mathrm{M}} \ll \Delta T_{\mathrm{FOS}}$ and $\gamma_k = k_{01}/k_{02}$ close to 1, we may use the expression:

$$S_{\mathrm{PD2}}(F) = S_{1\mathrm{L}}(F)[1 - (k_{01}/k_{02}) \cdot \exp(-2\Delta\nu_{\mathrm{L}} \cdot \Delta T_{\mathrm{M}} - 2\Delta\nu_{\mathrm{L}} \cdot T_{\mathrm{FOS}})]. \tag{6.74}$$

Then this expression can be written as:

$$S_{\mathrm{PD2}}(F) = G_{22} K_{\Gamma\mathrm{PN}}^2 \cdot \left\{ \frac{G_{12} K_{\mathrm{PD}}^2 S_{2\beta\mathrm{PN}}}{P_{0\mathrm{L}} F^2 T_{0\mathrm{L}}^2} + \frac{P_{0\mathrm{L}}}{P_{\mathrm{G}}} \cdot \left[\frac{2eS_{0\mathrm{PD}} \cdot R_{\mathrm{PD}}}{1} + \frac{D_{\Upsilon} kT}{P_{0\mathrm{L}}} \right] \right\} K_{\mathrm{PD}}^2, \tag{6.75}$$

where $G_{22} = [1 - (k_{01}/k_{02}) \cdot \exp(-2\Delta\nu_{\mathrm{L}} \cdot \Delta T_{\mathrm{M}} - 2\Delta\nu_{\mathrm{L}} \cdot T_{\mathrm{FOS}})]$, $G_{12} = [1 - (A_1/A_2) \cdot \exp(-2\Delta\nu_{\mathrm{L}} \cdot \Delta T_{\mathrm{M}} - 2\Delta\nu_{\mathrm{L}} \cdot T_{\mathrm{FOS}})]$. Thus, during simplification: $\frac{K_{\mathrm{PD}}^2 S_{2\beta\mathrm{PN}}}{P_{0\mathrm{L}} F^2 T_{0\mathrm{L}}^2} \gg \frac{P_{0\mathrm{L}}}{P_{\mathrm{G}}} \cdot \left[\frac{2eS_{0\mathrm{PD}} \cdot R_{\mathrm{PD}}}{1} + \frac{D_{\Upsilon} kT}{P_{0\mathrm{L}}} \right]$, we obtain the following expression:

$$S_{\mathrm{PD2}}(F)=\frac{\left[1-\left(\frac{k}{k_{02}}\right)\cdot\exp(-\Delta\nu_{\mathrm{L}}\cdot T_{\mathrm{FOS}})\right]\left[1-\left(\frac{A_1}{A_2}\right)\cdot\exp(-\Delta\nu_{\mathrm{L}}\cdot T_{\mathrm{FOS}})\right]K^2_{\Gamma\mathrm{PN}}\cdot K^4_{\mathrm{PD}}S_{2\beta\mathrm{PN}}}{P_{0\mathrm{L}}F^2T^2_{0\mathrm{L}}},\tag{6.76}$$

From Eq. (6.76), it follows that at RF modulation in both optical channels, PSD of RF phase noise is determined not only by the suppression coefficient $K^2_{\Gamma\mathrm{PN}}$ (6.55), which depends on the geometrical length of the optical fiber or on the delay time T_{FOS}, the laser spectral line $\Delta\nu_{\mathrm{L}}$ or its coherence time T_{c}, but upon the excitation irregularity of optical harmonics $\left(\frac{A_1}{A_2}\right)$ and the excitation irregularity of optical channels $\left(\frac{k_{01}}{k_{02}}\right)$. At double-channel modulation in MZ, the new multiplier appears in expression for PSD (6.76), which additionally effects on the reduction of the phase noise PSD.

Now we take into account in Eq. (6.76) that $\Delta\nu_{\mathrm{L}}=1/T_{\mathrm{c}}$ and $T_{\mathrm{FOS}}\gg\Delta T_{\mathrm{M}}$. We write the new formula for $K^2_{\Gamma\mathrm{PN2}}(T_{\mathrm{FOS}})=\left[1-\left(\frac{k_{01}}{k_{02}}\right)\cdot\exp\left(-\Delta\nu_{\mathrm{L}}\cdot T_{\mathrm{FOS}}\right)\right]\times\left[1-\left(\frac{A_1}{A_2}\right)\cdot\exp\left(-T_{\mathrm{FOS}}/T_{\mathrm{c}}\right)\right]K^2_{\Gamma\mathrm{PN}}$, in the formula (6.76) $S_{\mathrm{PD2}}(F)=K^2_{\Gamma\mathrm{PN2}}\frac{K^4_{\mathrm{PD}}S_{2\beta\mathrm{PN}}}{P_{0\mathrm{L}}F^2T^2_{0\mathrm{L}}}$:

$$K^2_{\Gamma\mathrm{PN2}}=\frac{G_{12}G_{22}\left\{\frac{\sqrt{2}\sin(\pi/4-FT_{\mathrm{FOS}})Y_{00}}{P_{0\mathrm{L}}}-\sigma_{\mathrm{U}}\right\}^2}{\left\{\left[\frac{Y_{00}}{P_{0\mathrm{L}}}\right]^2-\frac{Y_{00}}{P_{0\mathrm{L}}}\cdot(1+\sigma_{\mathrm{U}})\cos\left[FT_{\mathrm{FOS}}\right]+\sigma_{\mathrm{U}}\right\}^2}.\tag{6.77}$$

Figure 6.25 shows functions of the suppression coefficients of the phase noise $K^2_{\Gamma\mathrm{PN2}}(T_{\mathrm{FOS}})$ in OEO MZ at $\frac{P_{0\mathrm{L}}}{Y_{00}}=1.01$ and 1.8 for $\sigma_{\mathrm{U}}=1.02$ (a) for $\frac{P_{0\mathrm{L}}}{Y_{00}}=1.01$ and 1.3 for $\sigma_{\mathrm{U}}=1.02$ (b); for $\frac{P_{0\mathrm{L}}}{Y_{00}}=1.001$ and 1.8 for $\sigma_{\mathrm{U}}=0.05$ (c) at$G_{22}=1$, $G_{12}=\left[1-\exp\left(-\frac{FT_{\mathrm{FOS}}}{FT_{\mathrm{c}}}\right)\right]$, $FT_{\mathrm{c}}=10$ and $\gamma_{\mathrm{k}}=1$.

In Figs. 6.25 and 6.26, we see functions of the suppression coefficients of the phase noise in OEO MZ $K^2_{\Gamma\mathrm{FM}}(FT_{\mathrm{FOS}})$ and $G_{12}\cdot K^2_{\Gamma\mathrm{FM}}(FT_{\mathrm{FOS}})$ calculated with the help of the formula (6.77) at $P_{0\mathrm{L}}/Y_{00}=1.01$ for $\sigma_{\mathrm{U}}=1.02$ and for Fig. 6.26 $\sigma_{\mathrm{U}}=10.0$.

Plots presented in Figs. 6.25 and 6.26 and calculated by the formula (6.77), well demonstrate the *important property of the OEO MZ system: the decrease of the phase noise is possible owing to the growth of the laser coherence time and the increase of the optical fiber length.* From Eq. (6.77) it follows that the *increase of the optical fiber length or* T_{FOS} *time constant leads to the growth of the laser coherence time* T_{c}. For instance, at given laser coherence $T_{\mathrm{c}}=10/F$ (which corresponds to the offset $F=10$ kHz or to $T_{\mathrm{c}}=10^{-3}$s in the ideal case of $\gamma_k=k_{01}/k_{02}=1$, i.e., at equal excitation of MZ both optical channels), the value $FT_{\mathrm{FOS}}=2.5$ becomes optimal from the point of view of the decrease of the OEO phase noise (Fig. 6.25a) or $T_{\mathrm{FOS}}=2.5/F=2.5\cdot10^{-4}$ s, which corresponds to the optical fiber length of 50,000 m. At growth of σ_{U} to 10, the function $G_{12}\cdot K^2_{\Gamma\mathrm{FM}}(FT_{\mathrm{FOS}})$ has the first

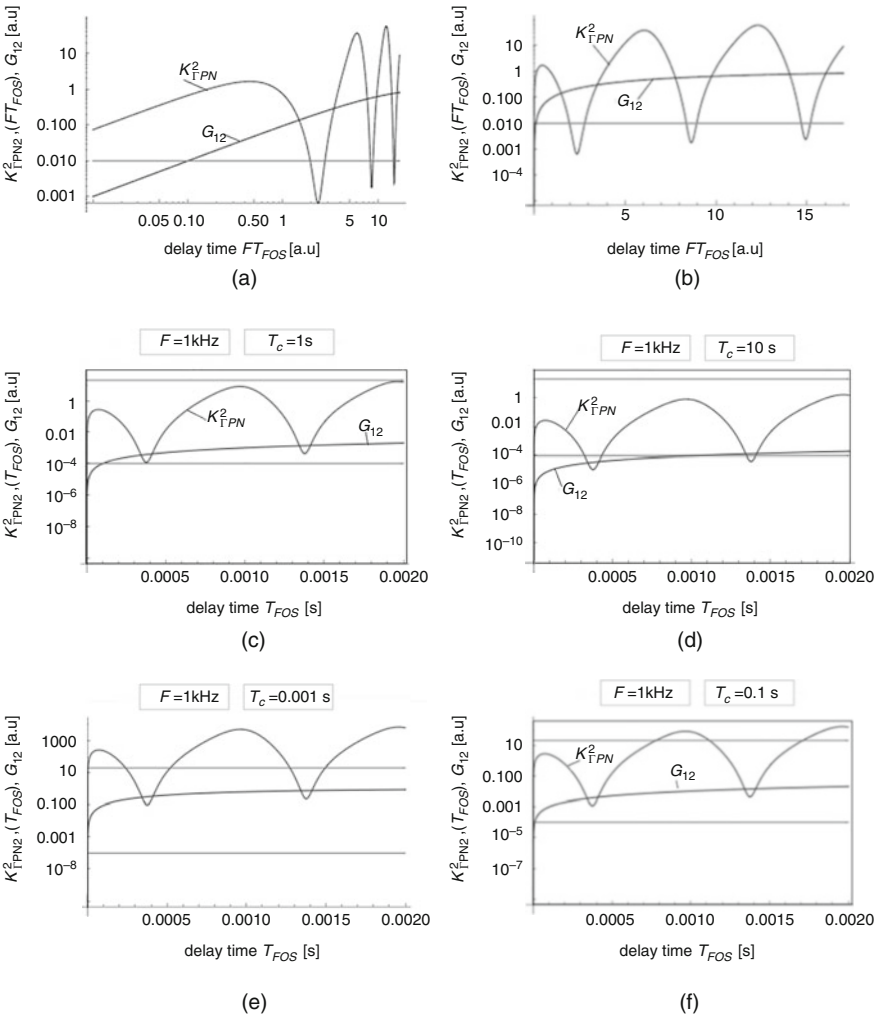

Fig. 6.25 Functions of the suppression coefficients of the phase noise $K^2_{\Gamma PN2}(T_{FOS})$ (6.77) and G_{12}in OEO MZ at $P_{0L}/Y_{00} = 1.01$ and 1.8 for $\sigma_U = 1.02$ at $G_{12} = \{1 - \gamma_k \cdot \exp[-FT_{FOS}/(FT_c)]\}$ at $FT_c = 10$ and $\gamma_k = k_{01}/k_{02} = 1$; on abscissa axis the logarithm scale (**a**), the linear scale (**b**), $K^2_{\Gamma PN2}(T_{FOS})$ at $F = 1$ kHz, $T_c = 1$ s (**c**), $K^2_{\Gamma PN2}(T_{FOS})$ at $F = 1$ kHz, $T_c = 10$ s (**d**). $K^2_{\Gamma PN2}(T_{FOS})$ at $F = 1$ kHz, $T_c = 0.1$ s (**e**)

minimum "shifts to the right along the abscissa axis" to $FT_{FOS} = 3$, and the value of the first minimum is two-orders lesser than at $\sigma_U = 1.02$.

Plots $K^2_{\Gamma PN2}(T_{FOS})$ presented in Fig. 6.25c–f at $F = 1$ kHz and $T_c = 0.001 - 10$ s well show that the phase noise suppression by 10–1000 times at the delay, for example, $T_{FOS} = 3.5 \cdot 10^{-4}$ s (the optical fiber length is 70,000 m) is possible at offsets $F = 1$ kHz at laser coherence times more than $T_c = 10^{-3}$ s. We more than

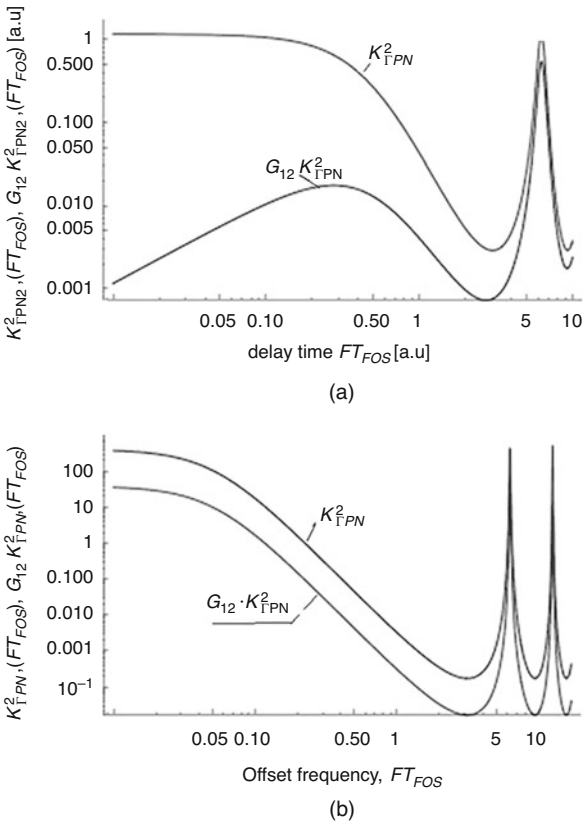

Fig. 6.26 Functions of the suppression coefficient of the phase noise in OEO MZ $K^2_{\Gamma PN}(FT_{FOS})$ and $G_{12}K^2_{\Gamma PN}(FT_{FOS})$ at $P_{0L}/Y_{00} = 1.01$ for $\sigma_U = 10.0$; for $T_c = 10$; at $G_{12} = \{1 - \exp[-FT_{FOS}/(FT_c)]\}$. $K^2_{\Gamma PN}(FT_{FOS})$ is calculated on the formula (6.77) (**a**). Functions of the suppression coefficient square $K^2_{\Gamma FM}(FT_{FOS})$ of the phase noise in OEO MZ and $G_{12} \cdot K^2_{\Gamma FM}(FT_{FOS})$ at $P_{0L}/Y_{00} = 1.01$ for $\sigma_U = 1.0$ at $T_c = 10T_{FOS}$ for $G_{12} = \{1 - \exp[-T_{FOS}/(T_c)]\}$. Function were calculated by the formula (6.77) (**b**)

once mentioned in Chaps. 3–6 that the phase noise suppression only owing to the increase of the geometrical length of FOS is not the solution of the problem of the phase noise reduction at offsets $F = 1$ kHz. The other more effective methods of the phase noise suppression are: the statistical averaging at photodetection of the optical harmonics, the equalization in power excitation in the MZ optical channels, the application of the high-coherent in time and in space QWLD with the spectral line width of 10 kHz and less.

6.5.13 *The Approximate Formula for the Coefficient* $K^2_{\Gamma PN}$

In this section, we analyze the main part of the expression (6.58) for $K^2_{\Gamma PN}$ for utilization in engineering calculations. Assuming that OEO MZ operates and small exceeds above the excitation threshold (with the small excitation reserve) and at $\frac{Y_{00}}{P_{0L}} = \frac{y_M[1+FT_{EF}]}{P_{0L}|K_{FOLD}|} \approx 1$, for expression (6.58) for $K^2_{\Gamma PN}$ the following transformations are true:

$$K^2_{\Gamma PN} = \frac{[\cos(FT_{FOS}) - 1 + 1 - \sigma_U]^2}{\{1 - (1+\sigma_U)\cos[FT_{FOS}] + \sigma_U\}^2}$$
$$= \frac{4\sin^4(FT_{FOS}/2) - 2\sin^2(FT_{FOS}/2)(1-\sigma_U)}{\{1 - (1+\sigma_U)\cos[FT_{FOS}] + \sigma_U\}^2} + \frac{[1-\sigma_U]^2}{\{1 - (1+\sigma_U)\cos[FT_{FOS}] + \sigma_U\}^2} \quad (6.78)$$

In the last expression, we extract the second term and introduce the designation $K^2_{2\Gamma PN} = \frac{[1-\sigma_U]^2}{\{1-(1+\sigma_U)\cos[FT_{FOS}]+\sigma_U\}^2}$.

The approximate coefficient $K^2_{2\Gamma PN}$ can be used only for rough engineering estimates of PSD of the OEO phase noise. It correctly reflects the oscillating character of PSD, but it does not give the exact limit values. In engineering calculations, the suppression coefficient $K^2_{\Gamma PN}$ can be calculated at $\sigma_U = 1.0$ with utilization of the simplified formula:

$$K^2_{2\Gamma PN} = \left[\frac{1-\sigma_U}{\sigma_U{}^2\left\{\frac{1}{\sigma_U{}^2} - 2\frac{\cos[FT_{FOS}]}{\sigma_U} + 1\right\}}\right]^2. \quad (6.79)$$

If the term $\frac{\gamma_M[1+FT_F]}{P_{0L}|K_{LZ}|} \approx 1$, for the coefficient K_{PN} the following expression is true: $K^2_{2\Gamma PN} = \left[\frac{0.1}{0.81\{2.23-2.22\cos[FT_{FOS}]\}}\right]^2 \approx \left[\frac{0.1}{1.81\cdot\{1-0.995\cdot\cos[FT_{FOS}]\}}\right]^2$. Figure 6.26b shows functions of the suppression coefficient square $K^2_{\Gamma FM}(FT_{FOS})$ of the phase noise in OEO MZ, and Fig. 6.26b shows the suppression coefficient $K_{\Gamma FM}(FT_{FOS})$ of the phase noise in OEO MZ calculated on the expression (6.79).

From analysis of curves presented in Fig. 6.26b, we may make a conclusion that using the approximated formula for $K^2_{2\Gamma FM}(FT_{FOS})$ (6.79) for calculation of the suppression coefficient of the phase noise $K^2_{\Gamma FM}(FT_{FOS})$, we must take into consideration that minimal values of $K^2_{2\Gamma FM}(FT_{FOS})$ differ by the one order than at utilization of more exact formula for $K^2_{\Gamma FM}(FT_{FOS})$ (6.77).

The MZ modulator made on the base of Fig. 6.24 provides the effective suppression of the laser, PD and NA phase noises owing to the optical phase modulation in both channels OC1 and OC2 and the effect caused by the self-heterodyning, which is described in Chap. 3. We also note that effective suppression of the phase noise in OEO will occur in the case if the noises are absent caused by the DC component of optical emission.

6.5.14 Natural Line Width and PSD of the Phase Noise of OEO MZ

If laser phase noises dominate above the phase noises of PD and NA, we obtain that for $\sigma_U \approx 1$, at the laser power growth $P_{0L} = E_{0L}^2$, PSD of the phase noise in OEO $S_{PD2}(F)$aspires to the value (6.76):

$$S_{PD2}(F) = G_{12}G_{22}\left\{K_{\Gamma PN}^2 \cdot K_{PD}^2 \frac{S_{2\beta PN}}{P_{0L}F^2T_{0L}^2}\right\}K_{PD}^2. \tag{6.80}$$

Taking into consideration the mentioned assumptions, we obtain that for the coefficient (6.80) at small offsets from the carrier, the following assumptions are true: $\sin[2\pi\nu_0(T_{1M} - T_{2M})] = 1$, $Y_{00}/P_{0L} \approx 1$, $P_{0L}|K_{LZ}| \approx 1$. Then, the PSD function of the OEO phase noise (5.79) can be presented as: $\frac{S_\psi}{P_{0G}} = \frac{K_{2\Gamma PN}^2 C_A h\nu N_{sp}}{P_{0G}}$, where C_A is the constant coefficient, $K_{2\Gamma PN}^2$ is the coefficient depending upon the delay time in the optical fiber and upon the laser optical power.

At small offsets ($FT\text{FOS} < 1$) (or within the limits of the laser line width), we obtain PSD of the OEO phase noise $S_{\Psi AG}(F) = \frac{G_{12}G_{22}K_{PD}^4}{[1+FT_{FOS}]^2} \cdot \frac{C_A h\nu N_{sp}}{P_{0L}F^2T_{0L}^2}$, which is equal: $S_{\Psi AG}(F) \approx G_{12}G_{22}K_{PD}^4 \frac{C_A h\nu N_{sp}}{P_{0L}F^2T_{0L}^2}$. We consider that PSD of the phase noise in OEO MZ has a form of the Lorentz function, then we obtain the formula:

$$\Delta f_{gen} = \frac{S_{\Psi AG}\left(F = \Delta f_{gen}\right) \cdot D_Y}{4(T_{EF} + T_{FOS})^2} \tag{6.81}$$

or $S_{\Psi AG}\left(F = \Delta f_{gen}\right) = \frac{4(T_{EF}+T_{FOS})^2 \Delta f_{gen}}{D_Y}$. We consider that PSD of the phase noise S_L of QWLD has the form of the Lorentz function, then we obtain the formula: $\Delta\nu = \frac{S_L(F=\Delta\nu)}{4T_{0L}^2}$ or we can write: $S_L(F = \Delta\nu) = 4T_{0L}^2\Delta\nu$. From Eqs. (6.80) and (6.81), it follows that at small offsets F from the nominal generation frequency, the level of PSD of the phase noise becomes lower at decrease of the laser emission bandwidth $\Delta\nu_L$, as well as at reduction of the laser generation frequency, the difference in delay times ΔT_M in the MZ optical channels and the level of the laser spontaneous emission S_β and the amplification factor of NA D_{PN}. PSD of the phase noise decreases at growth of the delay time in RF FODL or in FOS.

Taking into account that the OEO MZ line width $\Delta f_{gen} = \Delta f_{0.5}$ is related to PSD of the phase noise for the natural line width $\Delta f_{gen} = \Delta f_{0.5}$, we have (taking into account Eqs. (6.80) and (6.81)) the *fundamental* dependence on the natural laser line width $\Delta\nu_L$ in the form:

$$\Delta f_{\text{gen}} = \frac{S_{\Psi\text{AG}}\left(F = \Delta f_{\text{gen}}\right) \cdot D_{\text{Y}}}{4T_{0\text{L}}^2} = G_{22}G_{12}K_{\Gamma\text{PN}}^2 \cdot K_{\text{PD}}^4 \cdot D_{\text{Y}} \frac{\Delta\nu}{T_{0\text{L}}^2 P_{0\text{L}} \Delta f_{\text{gen}}{}^2} \quad (6.82)$$

or for $T_{0\text{L}}^2 F^2 \approx 1$:

$$\begin{aligned} \Delta f_{\text{gen}} &= G_{12}G_{22} \frac{\left\{\left[\sqrt{2}\sin\left(\pi/4 - FT_{\text{FOS}}\right)\right] - \sigma_{\text{U}}\right\}^2}{\left\{1 - (1+\sigma_{\text{U}})\cos\left[FT_{\text{FOS}}\right] + \sigma_{\text{U}}\right\}^2} \cdot K_{\text{PD}}^4 \cdot D_{\text{Y}} \frac{\Delta\nu}{P_{0\text{L}}} \\ &\approx G_{12}G_{22} \frac{\left\{1 - \sigma_{\text{U}}\right\}^2}{\left\{1 - (1+\sigma_{\text{U}})\cos\left[\Delta\nu T_{\text{FOS}}\right] + \sigma_{\text{U}}\right\}^2} \cdot K_{\text{PD}}^4 \cdot D_{\text{Y}} \frac{\Delta\nu}{P_{0\text{L}}} \end{aligned}. \quad (6.83)$$

The first limit case. From Eqs. (6.83), it follows that at given $\Delta\nu_{\text{L}}$, a choice of ΔT_{M} and T_{FOS} strongly affects onto the radio frequency natural spectral width of OEO. Let us examine the *first limit case* for expression (6.83) for $G_{12}G_{22} = [1 - \gamma_k \exp(-\Delta\nu_{\text{L}} \cdot \Delta T_{\text{M}})] \approx 1$ (i.e., when optical phases of the coherent laser emission at arrival to PD are completely non-correlated (independent of each other) with the correlation coefficient, which is essentially less than 1. In this case, the correlation coefficient $K_{\Psi 12} \to 0$. This, for instance, is true at utilization in OEO of differential RF FODL with two optical fibers, at the time delay in FOS $T_{\text{FOS}} = 10^{-9}$ s (the geometrical FOS length is close to 1 m), but the MZ delay difference is equal to $\Delta T_{\text{M}} = 10^{-4}$ s (which corresponds to the FOS geometric length of 20 km), the natural width of the laser spectral line is equal to $\Delta\nu_{\text{L}} \approx 10$ kHz, i.e., the product $\Delta T_{\text{M}} \cdot \Delta\nu_{\text{L}} = 1$, we from formula (6.83) obtain that

$$\Delta f_{\text{gen}} = 2G_{22}G_{12}K_{\Gamma\text{PN}}^2 \cdot K_{\text{PD}}^4 \frac{\Delta\nu_{\text{L}}}{D_{\text{Y}}} \approx \frac{2G_{22}G_{12}K_{\text{PD}}^4}{P_{0\text{L}}|K_{\text{FOLD}}|D_{\text{Y}}} \Delta\nu_{\text{L}}. \quad (6.84)$$

Taking into account the last formula for the RF generation spectral line width, we obtain the formula:

$$\begin{aligned} \Delta f_{\text{gen}} = \Delta f_{0.5} &\approx G_{12}G_{22} \frac{\left\{1 - \sigma_{\text{U}}\right\}^2}{\left\{1 - (1+\sigma_{\text{U}})\cos\left[\Delta\nu T_{\text{FOS}}\right] + \sigma_{\text{U}}\right\}^2} \cdot K_{\text{PD}}^4 \cdot D_{\text{Y}} \frac{\Delta\nu}{P_{0\text{L}}} \\ &\approx G_{12}G_{22} \frac{\Delta\nu_L}{P_{0\text{L}}|K_{\text{FOLD}}|\left[1 + \Delta\nu_{\text{L}} T_{\text{FOS}}\right]^2} \end{aligned}. \quad (6.85)$$

The connection of the laser emission spectral line width $\Delta\nu_{\text{L}}$ with the RF generation bandwidth Δf_{gen} can be defined from Eqs. (6.85) by the approximated expression (at $G_{12}G_{22} \approx 1$):

$$\Delta\nu_{\text{L}} \approx \Delta f_{0.5} \cdot P_{0\text{L}}|K_{\text{FODL}}| \cdot 4, \quad (6.86)$$

where we remind that $P_{0L}|K_{FODL}|$ is the dimensionless quantity and it defines by the product of the laser power P_{0L} by the transfer function $|K_{FODL}|$ on the amplitude of the first voltage harmonic in the MZ electrical input.

In this case, at the choice of $(\Delta T_M \cdot \Delta\nu_L) \to 1$ with the help of OEO MZ, we make the measurement of the laser spectral line width $\Delta\nu_L \approx [\Delta f_{0.5}]/4$. For lasers with the generation line width less than 10 kHz, such measurements are very relevant and very important, because the measurement technique of modern commercially available optical spectrometers (for example, from Hitachi company) is restricted by the limit values 0.1 nm (which corresponds the laser bandwidth). The property of OEO MZ to transform of the laser phase fluctuations in the above-mentioned case into phase fluctuations of OEO RF signal can be used for measurement of the laser spectral line width with small values of $\Delta\nu_L$.

The second limit case. Let us examine the *second limit case*, when the product $(\Delta T_M \cdot \Delta\nu_L) \to 0$. For example, at the laser spectral line width lesser or equal to $\Delta\nu_L \approx 10$ kHz and for long lengths of FOS (more than 1000 m). In this case, we obtain that the correlation function is determined by spatial parameters of the MZ modulator $K_{\Psi 12} \to G_R$ and it defines by the spatial coefficient. For instance, at $G_{22}G_{12} = 0.999$, $T_{FOS} = 10 \cdot 10^{-6}$ s, $\Delta\nu_L T_{FOS} = 10^{-1}$, $\Delta T_M = 10^{-12}$ s, $S_\beta \cdot D_{FM} = 10^{-12}$ and from Eqs. (6.85), it follows:

$$\Delta f_{0.5} \approx 10^{-4} \cdot \Delta\nu_L. \tag{6.87}$$

In this case, at frequency offset with regard to the nominal generation frequency equaled to $F = \Omega = 2\pi(f - f_0) = 2\pi \cdot 4 \cdot 10^{-2} \cdot \Delta\nu_L$, PSD of the phase noise in OEO MZ is $S_{\Psi AG}(F) \approx -120$ dB/Hz, and at the offset F equaled to the laser bandwidth $F = \Omega = 2\pi(f - f_0) = 2\pi\Delta\nu_L$ in $G_{12}G_{22} = 0.01$, $P_{0L} = 0.1$ W, $F = 10^4$ Hz, $T_{FOS} = 10^{-4}$ s (the fiber-optical length is 20,000 m) at $FT_{FOS} = 1$, $K^2_{\Gamma PN} \cdot K^4_{PD} = 0.01$.

$$S_{\Psi AG} \approx G_{12}G_{22}K^2_{\Gamma PN} \cdot K^4_{PD} \frac{S_\beta D_{PN}}{P^2_{0L}\left[(FT_F)^2 + (FT_{FOS})^2\right]} = G_{12}G_{22}K^2_{\Gamma PN} \cdot K^4_{PD} \frac{10^{-12}}{P^2_{0L}F^2 \cdot T^2_{FOS}}.$$
$$= 10^{-4}\frac{10^{-12}}{0.01} \approx 10^{-14}\ \text{dB/Hz} \tag{6.88}$$

The last quantity is the record quantity of PSD of the phase noise on the modern stage of engineering developments of high-stable microwave oscillators. At that, the last expression shows that the potential reduction of the OEO MZ spectral line width with regard to the laser line occurs owing to heterodyne coherent photo-receiving with the phase modulation on the optical phase and to the high Q-factor of oscillating system. The last approximate expression reflects the features of OEO MZ as the system of two oscillators: the laser (quantum generator of the pumping) and RF oscillator.

Noises in such a system are mainly determined by the laser phase fluctuations, which, in turn, mainly depends upon the spontaneous emission and they define the generation line width of OEO MZ only in above-mentioned case of definite relations between the system parameters of OEO MZ, such as the natural laser emission line bandwidth $\Delta\nu_{\mathrm{L}}$, the laser generation frequency ν_0, difference in delay time in the MZ optical channels ΔT_{M}, the level of spontaneous laser emission S_β and the NA amplification factor D_{FM}.

6.5.15 Approximate Expression for the Suppression Coefficient and PSD in OEO MZ

Neglecting in expressions by the effect of the σ_{U} coefficient and taking into account that the coefficient $K_{\mathrm{FODL}} = P_{\mathrm{L0}}|K_{\mathrm{MZ}}||K_{\mathrm{FOS}}||K_{\mathrm{PD}}||K_{\mathrm{F}}|$, where $|K_{\mathrm{MZ}}|$, $|K_{\mathrm{FOS}}|$, $|K_{\mathrm{PD}}|$, $|K_{\mathrm{F}}|$ are relatively, modules of coefficients of the MZ modulator, FOS, RF filter, we obtain the expression for PSD in the form:

$$S(F) = K^2_{\Gamma\mathrm{PN}}[S_{\mathrm{L}}(F) + S_{\mathrm{PD}}(F) + S_{\mathrm{NA}}(F)], \tag{6.89}$$

where $K^2_{\Gamma\mathrm{PN}} \approx K^2_{2\Gamma\mathrm{PN}} = \frac{1}{\left[1-2K_{\mathrm{FOLD}}\cos\left(FT_{\mathrm{FOS}}\right)+\left(K_{\mathrm{FOLD}}\right)^2\right]^2}$, $S_{\mathrm{L}}(F)$, $S_{\mathrm{PD}}(F)$, $S_{\mathrm{NA}}(F)$ are components of the poser spectral density of phase noises, relatively, of detected laser noises in PD output, the PD shot noise, and the NA thermal noise. The component of detected laser noises $S_{\mathrm{L}}(F)$ in the PD output current is defined by the expression: $S_{\mathrm{L}} = B\Delta\nu\frac{D_{\mathrm{OA}}}{4F^2}K_{\mathrm{FOLD}}U^2_{10\mathrm{M}}$, where D_{OA} is the noise-factor of the optical amplifier, $\Delta\nu$ is the spectral line width (on level 0.5) of the laser optical emission, $U_{10\mathrm{M}}$ is the voltage of the first harmonic of RF oscillations in the MZ modulator input, B is the constant coefficient depending on the laser type:

$$\frac{S_{\Psi\mathrm{OEO}}}{P_{\mathrm{G}}} = K^2_{2\Gamma\mathrm{PN}}K^2_{\mathrm{PD}} \cdot \left\{K^2_{\mathrm{PD}}\frac{S_{\beta\mathrm{PN}}}{P_{0\mathrm{L}}F^2T^2_{0\mathrm{L}}} + \frac{K^2_{\Gamma\mathrm{PN}}}{\frac{2S_{01}}{3R_{\mathrm{PD}}S_{03}}\cdot\left(1-\frac{Y_{00}}{S_{01}P_{0\mathrm{L}}}\right)}\cdot\left[\frac{2eS_{0\mathrm{PD}}\cdot R_{\mathrm{PD}}}{1}P_{0\mathrm{L}} + \frac{D_{\mathrm{Y}}kT}{1}\right]\right\}. \tag{6.90}$$

From expression (6.90), we see that under condition of small PD noises, the reduction of PSD of the phase noise $S(F)$ can be achieved due to the growth of the delay time in RF FODL, the laser power P_{OL} and the decrease of the width square $\Delta\nu$ of the laser spectral line. Neglecting by the first and second terms in Eq. (6.90) at the frequency offset $F = \Delta\nu$, we obtain the value $S(F) \approx K^2_{2\Gamma\mathrm{PN}}BK_{\mathrm{FOLD}}D_{\mathrm{OA}}/4$. For instance, at $F = \Delta\nu = 1$ kHz, $D_{\mathrm{OA}} = 40$, $K_{\mathrm{FODL}} = 1$ $K_2 = K^2_{2\Gamma\mathrm{PN}} = 10^{-2}$, for

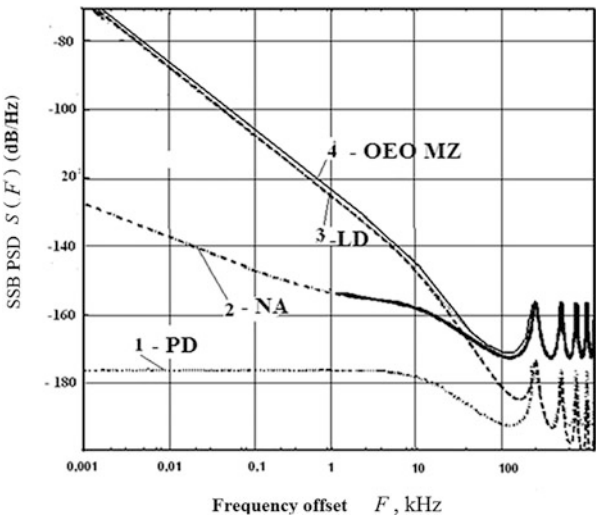

Fig. 6.27 Calculated functions of the power spectral density of the phase noise $S(F)$ of RF oscillations in OEO MZ with the nondispersive RF FODL and the high-coherent laser as functions of frequency offset F from the nominal frequency of the subcarrier 10.0 GHz at spectral line width of the laser optical emission $\Delta\nu = 100$ kHz. The plots of PSD of the phase noise of: 1—PD, 2—NA, 3—the laser, 4—OEO MZ are presented

obtaining $S(F) = -120$ dB/Hz, the value B must be $B = 10^{-10}$, which takes place in the fiber lasers and the semiconductor lasers with the specific resonators.

The calculated functions of the relative power spectral density of the phase noise of RF oscillations of OEO MZ $S(F)$ versus the frequency offset by F from the mean generation frequency 10 GHz are presented in Fig. 6.27.

In Fig. 6.27, the presented plots correspond to PSD of the phase noise of OEO MZ $S(F)$: curve 1—of PD $K^2_{2\Gamma PN} S_{PD}(F)$, curve 2—of NA $K^2_{2\Gamma PN} S_{NA}(F)$, curve 3—of QWLD $K^2_{2\Gamma PN} S_L(F)$, curve 4—of OEO MZ calculated by Eqs. (6.89) and (6.90) for the following OEO parameters: $\Delta\nu = 10.0$ kHz; $P_{OL} = 20$ mW; $D_{NA} = 100$; $D_{OA} = 40$; $\eta_1 = 1$; $K_{OMZ} = 0.5$; $K_{FODL} = 1$; $T_{FOS} = 1$ μs (the FOS length is 200 m); $K_{FODL} = 1.1$, the optical frequency of QWLD $\nu_0 = 1.29 \cdot 10^{14}$ Hz.

On the base of formulas (6.77) and (6.90) obtained in the present section, we calculated the power spectral density of the phase noise of OEO MZ RF oscillations $S(F)$ as a function of the ratio of the laser optical power to its threshold value and the dependences of the normalized first harmonic amplitude in OEO MZ and the RF FODL transfer function versus this ratio. The module of the slope of $S(\sigma_U)$ increases at offset decrease and is $\Delta S/\Delta\sigma_U = 2$ dB/Hz. The function of the power spectral density S of the phase noise in OEO MZ $S(\sigma_U)$ versus the nonlinearity coefficient $\sigma_U = \sigma$ was calculated by Eqs. (6.77) and (6.90). At that, the generation frequency is 10 GHz, the mean width of the laser emission spectral line $\Delta\nu = 10$ kHz.

Figure 6.28a shows the function of the SSB power spectral density of the phase noise in OEO MZ $S(T_{FOS})$ versus the delay time T_{FOS} in the optical fiber for different values of offsets F from the generation frequency of 10 GHz. At that, the generation frequency of OEO MZ is equal to 10 GHz, the width of the laser emission spectral line is $\Delta\nu = 10$ kHz.

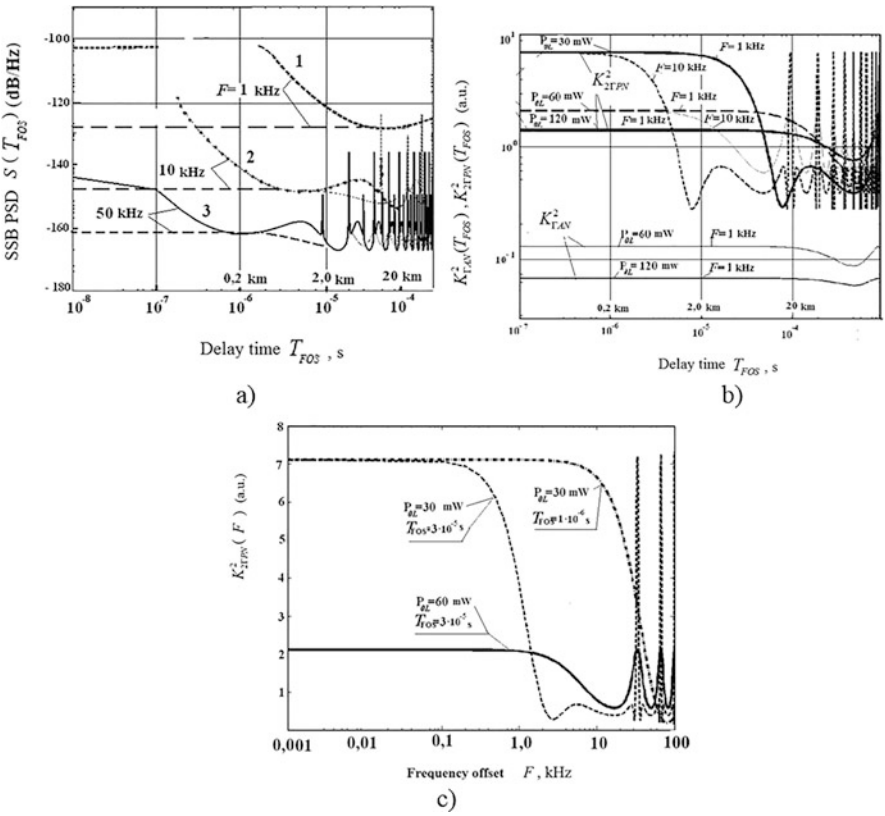

Fig. 6.28 (**a**) Functions of the SSB power spectral density (SSB PSD) of the phase noise in OEO MZ $S(T_{\mathrm{FOS}})$ versus the delay time T_{FOS} in FOS for different values of offsets F of the generation frequency 10 GHz. The width of the laser emission spectral line is $\Delta\nu = 10$ kHz. Different curves in plots correspond to different offsets F from the generation frequency 10 GHz. Curve 1 $F = 1$ kHz, curve 2 $F = 10$ kHz, curve 3 $F = 100$ kHz. (**b**) Functions of suppression coefficients of the phase noises $K^2_{2\Gamma\mathrm{PN}} = KFN$ and the amplitude noises $K^2_{\Gamma\mathrm{AN}} = KAN$ in OEO MZ with the single optical fiber in RF FODL versus the delay in FOS T_{FOS} at different frequency offsets by F (from the generation frequency of OEO MZ $f_0 = 10$ GHz) and for different power P_{OL} of the QWLD optical emission. (**c**) The coefficient $KFN(F)$ as a function of the offset F (from the generation frequency of OEO MZ $f_0 = 10$ GHz) at different values of delay in FOS T_{FOS} and the power P_{OL} of the QWLD optical emission

Functions presented in Fig. 6.28b of suppression coefficients $K^2_{2\Gamma\mathrm{PN}} = KFN$ and $K^2_{\Gamma\mathrm{AN}} = KAN$ allow the conclusion that suppression (owing to optimization of the laser and RF FODL parameters) of the phase noise is approximately by ten times more than PSD of the phase noise in OEO MZ on the offset from the carrier of 1 kHz at the geometrical length of the optical fiber of 8–20 km at the laser power of 30 mW. At offset from the carrier of 10 kHz, at tenfold suppression of the phase noise, requirements to the geometrical length of the optical fiber are reduced and is 2–5 km at the laser power of 30 mW.

Figure 6.28c shows the transfer function of the closed loop OEO MZ $KFN(F)$ versus the offset F (from the generation frequency f_0 of OEO MZ) at different delay values T_{FOS} in FOS and the power P_{OL} of the QWLD optical emission.

The functions of the suppression coefficients $K^2_{2\Gamma\text{PN}} = KFN$ presented in Fig. 6.28b, c permit to estimate the suppression degree of PSD of the phase noise in OEO. The tenfold suppression of PSD of the phase noise can be realized in OEO MZ in the offset region at the delay in FOS $T_{\text{FOS}} = 3 \cdot 10^{-5}$ s and the power of QWLD optical emission of $P_{\text{OL}} = 30$ mW.

From the analysis of Figs. 6.27 and 6.28, it follows that achievement of small values of the power spectral density of the phase noise of RF oscillations in OEO MZ on the offset frequency F = 1 kHz less than $S(F) = -120$ dB/Hz is provided by the significant growth of laser power $P_{0\text{L}}$ (for example, more than 20 mW), by the reduction of the laser line bandwidth $\Delta\nu$ (for instance, less than 10 kHz) and by increase of the delay time T_{FOS} of optical oscillations in the FOS (or the geometrical length of FOS till several kilometers).

6.6 Analog Modeling of OEO MZ

In previous section of this chapter, we investigated of OEO MZ on the linear models, which allowed to study of OEO MZ at presence of the complicate fluctuation impact. But, this linear model does not take into consideration in full measure the nonlinear properties of systems. The question is raised about investigation performing on the base of the analog modeling of OEO MZ structure with utilization of specific software packets with the aim, on the one hand, of checking of results obtained by the other approaches, and on the other hand, to execute investigations being beyond application areas of these methods. Such investigations are, for example, studying of transients in OEO MZ, and are also an examination of FOS dispersion influence on the oscillation spectrum in OEO MZ, on PSD of the phase and amplitude noise taking into consideration the laser fluctuations in the OEO structure. At that, the analog model allowed laser spectrum formation, which is close to the Lorentz form on the frequency function.

In view of above-told, the goal of the next part of Chap. 6 is to provide the analog modeling of OEO MZ with the help of specific mathematical packet, to obtain the time-functions of PSD and transients in OEO MZ at its switching-on basing on the analog model in Fig. 6.29a.

6.6.1 Description of the Analog Model

We construct the model of OEO MZ and solve the problem on input noise impacts. The model is based on imitation of the real functioning of the system. The laser

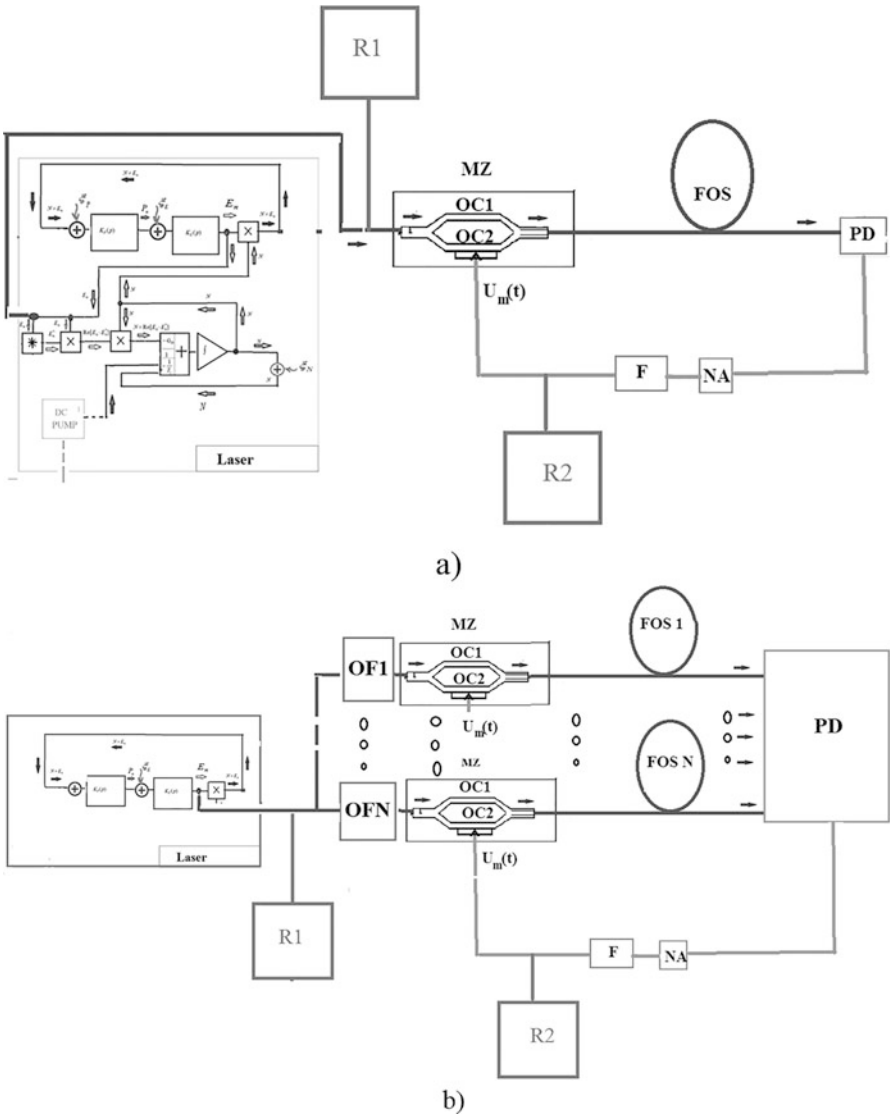

Fig. 6.29 (**a**) The structure of the analog model of OEO MZ with registering blocks R1 and R2. (**b**) The structure of the analog model of OEO MZ for studying of influence of the material refraction index dispersion of the optical fiber. R1 and R2 are registering blocks. R1 is the measuring system of PSD of the phase noise of the laser. R2 is the measuring system of PSD of the phase noise of the laser and OEO MZ

generation frequency and the OEO MZ frequency differs by 10,000 times. At modeling of the phase noises, we use the Leeson phase noise model [5] and the approach to the noise synthesis using the Langevinian equations. We assume that the optical fiber in OEO MZ is excited by the laser, which PSD of the phase noise is close to the Lorentzian curve, and the laser emission spectral line is equal to $\Delta\nu_{\mathrm{L}} = \Delta\nu$ and is for different modeling conditions of 1 kHz, 10 kHz, 10 MHz, 100 MHz, 1 GHz, 10 GHz, 30 GHz, 100 GHz, the average generation frequency of the laser is $\nu_{\mathrm{L}} = \nu_0 = \nu$ and is 128 THz.

The laser included in the OEO MZ structure is formed by enclosed into the loop of the optical nonlinear amplifier (OA), the narrowband optical filter, and RF FODL. The laser is modeled in the operational mathematical system with the help of standard blocks (integrators, multipliers, adders, filtering blocks, amplifying blocks, nonlinear blocks, etc.), which models the instantaneous values of the strength oscillations of the laser optical oscillations $E(t)$ of the nonlinear differential equation of the type 1: the differential equation (5.60).

The closed loop of OEO MZ (the RF oscillator) is modeled with the help of the standard blocks (integrators, multipliers, adders, filtering blocks, nonlinearity blocks, etc.) for RF oscillations of OEO $u(t)$ (instantaneous values), which models the differential nonlinear equation of the type 2: the differential equation (6.28).

In the differential equation (6.28), $E_{0\mathrm{L}}^2$ is the normalized laser output, $E_{0\mathrm{P}}$ is the strength of the electrical field of the laser pumping, S_{ONA}, S_{NA} are AE nonlinear functions, relatively, of the optical amplifier and the RF amplifier in OEO MZ, K_{OA} is the transfer function of the optical amplifier in the laser, K_{FODL} is the RF FODL transfer function, $\nu_{\mathrm{OF}}, f_{\mathrm{F0}}$ are natural frequency of the lased optical resonator and the RF filter, relatively, T_{OL} and T_{FOS} are delay time in the laser and in RF oscillator, relatively, T_{OF}, $T_{\mathrm{F}} = T_{\mathrm{EF}}$ are time constants of the laser optical resonator and the RF filter, relatively. The "Langevinian" noise sources ξ_{n}, ψ_{n} of the field strength in the laser and the electrical oscillation voltage in OEO MZ are modeled by the standard blocks of the white noise with a possibility to change the noise level within the limits for 10^{-15} to 10^{-1}. MZ is modeled by the parallel-connected delay lines. At that, the delay time of the single delay line is changed at variation of the modulating signal. PD is modeled by the multiplication block.

The time scale is chosen taking into account that the laser oscillation frequency would be by 1000–10,000 times more than the frequency of RF oscillations of OEO, and the oscillation period in OEO is about 0.01–0.1 s. During modeling, the laser's generation line width is varied (with the help of the level variation of the "white noise" block) and the dispersion slope of FOS is $\tau_{\mathrm{D}} = -10^{-1} \cdots + 10^{-1}$ 1/GHz.

6.6.2 *Analog Modeling of the Process Formation of the Oscillation Spectrum in OEO MZ in Transients*

An analysis of computer modeling results of Eqs. (5.60) and (6.28) shows that at utilization in RF FODL of low-dispersed light guides with the dispersion of FOS less than 10 ps/(n·m·km) and the high-coherent lasers with the generation line width $\Delta\nu$ less than 10 MHz, the increase of PSD of the phase noise in OEO MZ at growth of this width of the laser spectral line is mainly related to the conversion of phase noises into the amplitude noises in the MZ modulator.

The most intensive effect of the laser line width $\Delta\nu$ in OEO MZ is demonstrated at utilization of the high-dispersed optical fibers with the slope $\tau_D = dT/d\nu = 10^{-2}$ 1/GHz, which corresponds to FOS dispersion of 50 ns/(nm·km) and the low-coherent lasers with the line width $\Delta\nu_L = \Delta\nu$ and more than 30 GHz.

One of the results of computer modeling is presented in Fig. 6.32 in the form of functions of PSD of the phase noise in OEO MZ for different values of the laser generation line width, of the FOS dispersion: curve 1 in the Fig. 6.32 is the laser line width $\Delta\nu = 10$ MHz, the dispersion slope is equal to zero; curve 2 is the width 10 GHz, the dispersion slope $\tau_D = dT/d\nu = 10^{-2}$ 1/GHz (which corresponds to the FOS dispersion of 50 ns/(nm·km); curve 3 is the width 50 GHz, $\tau_D = dT/d\nu = 10^{-2}$ 1/GHz. The average generation frequency of OEO MZ is 10 GHz. The delay time in FOS is $T_{FOS}(\nu_0) = 100$ μs, which corresponds to the geometrical length of FOS of $L = 20$ km.

Figure 6.30 shows the one result of computer modeling. Here we see the scenario of the spectrum formation of OEO MZ taking into consideration the laser phase noise.

The scenario of spectrum formation of OEO MZ with the account of the laser phase noises is shown in Fig. 6.31. Time-functions are normalized along the time axis to the period of RF oscillations t/T_0, where T_0 is the period of RF oscillations of OEO MZ.

6.6.3 *Influence of the Material's Refraction Index Dispersion of the Optical Fiber upon PSD of the Phase Noise in OEO MZ*

On the base of the analog model of OEO MZ (Fig. 6.29b), the investigation is performed for the influence of dispersion of the refraction index upon spectrum formation in OEO MZ.

Historically, the analysis of dispersion influence of the refraction index of the AE material upon the laser generation spectrum was performed at examination of semiconductor lasers in the middle of 1960s [6–9]. With the development of fiber-optical communication lines, the problems of dispersion influence of the optical fiber upon the limit possibilities of the carrying capacity of the single-mode and multi-

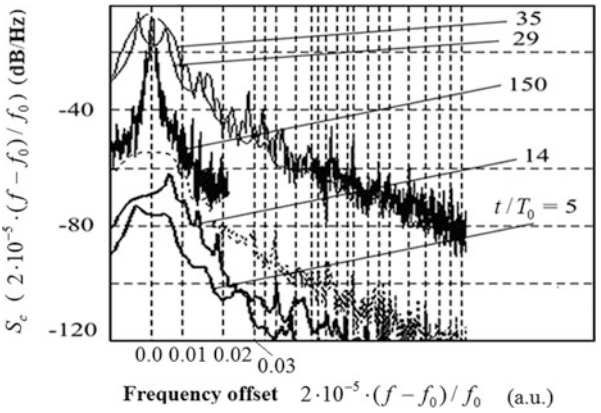

Fig. 6.30 The scenario of the spectrum formation of OEO MZ taking into consideration of the laser phase noise for different time (in the normalized time to the period of RF oscillation $t_0 = t/T_0$, where T_0 is the period of RF oscillations of OEO MZ)

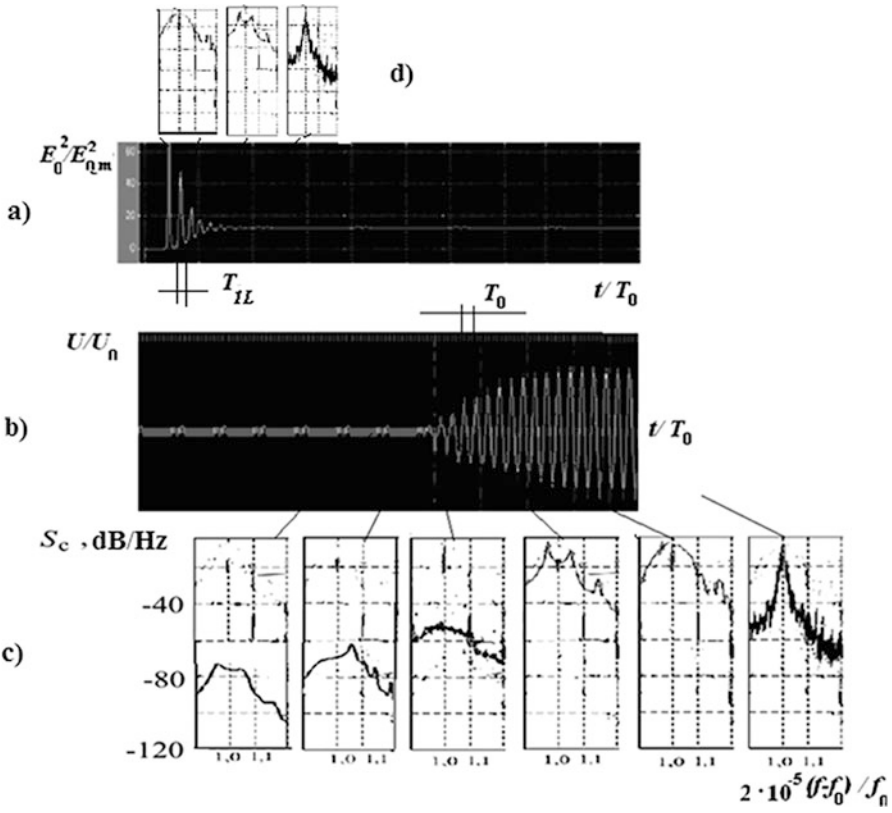

Fig. 6.31 The scenario of spectrum formation of OEO MZ taking into account the laser phase noises. Time-functions are normalized along the time axis to the time-period of RF oscillations t/T_0, T_0 is the period of RF oscillation in OEO MZ

mode (with the stepped and the gradient profile of the refraction index) become relevant at information transmission.

In our investigation of the effect of refraction index variations versus the optical frequency, we assume that the optical fiber in OEO MZ is dispersive, i.e., the delay time in FOS is the function of the optical frequency $T_{\mathrm{FOS}}(\nu)$.

In the vicinity of the central optical frequency $\nu_{\mathrm{L}} = \nu_0 = \nu$ of the laser emission, the function of delay of the optical frequency $T_{\mathrm{FOS}}(\nu)$ at $\Delta\nu_{\mathrm{L}} \ll f_0$ is linear and can be presented by the function:

$$T_{\mathrm{FOS}}(\nu) = T_{\mathrm{FOS}}(\nu_0) + (\nu - \nu_0)\tau_{\mathrm{D}}, \tag{6.91}$$

where τ_{D} is the retarding slope is determined by material and waveguide dispersion of the optical fiber and for modern optical fibers is $\tau_{\mathrm{D}} = \mathrm{d}T/\mathrm{d}\nu = 10^{-7}$ 1/GHz. Modern specially developed optical fibers for the dispersion correction have the positive and negative dispersion with $\tau_{\mathrm{D}} = -10^{-1} \cdots + 10^{-1}$ 1/GHz.

Taking into consideration the nonlinear variation of the refraction index, the function of the refraction index versus the optical frequency can be approximated by expanding this function into the Taylor series restricting in this expansion

by the first and second derivatives:

$$N_{\mathrm{FOS}}(\nu) = N_{\mathrm{FOS}}(\nu_0) + (\nu - \nu_0)\frac{\mathrm{d}N_{\mathrm{FOS}}}{\mathrm{d}\nu} + (\nu - \nu_0)^2\frac{\mathrm{d}^2N_{\mathrm{FOS}}}{\mathrm{d}\nu^2}. \tag{6.92}$$

In our research of the analog model of OEO MZ, we studied how does the width of the spectral line of the laser emission influence on the spectrum of RF oscillations in OEO MZ. We studied the functions of PSD of the phase noise at variation of the FOS refraction index from the laser optical frequency.

In computer investigations we have implemented the values of $T_{\mathrm{FOS}}(\nu)$ from 1 ns to 100 μs, and $\tau_{\mathrm{D}} = -10^{-1} \cdots + 10^{-1}$ 1/GHz. In OEO MZ with the dispersive delay line, the increase of the width $\Delta\nu$ (Fig. 6.32) by more than 10 GHz led at modeling to the growth of PSD of the phase noise by four orders. At that, in the OEO MZ spectrum, on offset frequencies by 0.1–1 kHz from the nominal frequency of 10 GHz, there are adjacent oscillation types, which do not "provide the generation mode" (which alteration is defined by the delay time in the optical fiber) and the spectrum has the comb structure—the periodic dependence upon the frequency offset from the nominal generation frequency.

We can conclude that at *increase* of the laser line width $\Delta\nu$, the difference between adjacent own types of oscillations of OEO MZ, which is indicated in the plot as DF (Fig. 6.32) decreases and depends on the delay time in FOS $T_{\mathrm{FOS}}(\nu)$ on the laser average frequency ν_0 and on the product of the dispersion slope τ_{D} by the laser emission bandwidth

$$\Delta\nu_{\mathrm{L}} = \Delta\nu : DF = (1 - \Delta\nu_{\mathrm{L}} \cdot \tau_{\mathrm{D}})/T_{\mathrm{FOS}}(\nu_0). \tag{6.93}$$

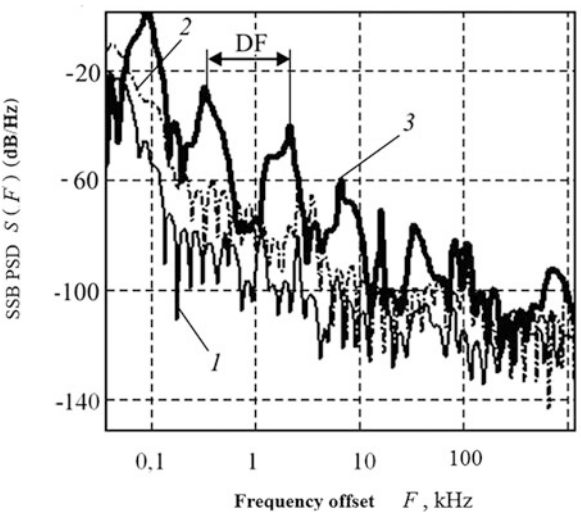

Fig. 6.32 Calculated functions of PSD of the phase noise $S(f)$ in OEO MZ with the high-dispersive FOS in RF FODL with the low-coherent laser versus the frequency offset by F from the nominal operation frequency. The curves on the graph corresponds 1—$\Delta\nu_L = 10$ GHz, 2—$\Delta\nu_L = 1$ GHz, 3—$\Delta\nu_L = 0.1$ GHz

Expansion of the laser spectral line width (Fig. 6.32) leads to significant growth of PSD level of the phase noise of OEO due to FOS dispersion. This is true even for small laser emission spectral line compared to RF generation in OEO MZ. Owing to FOS dispersion, the PSD spectrum of the phase noise has the remarkable feature: the comb structure—the periodic dependence of the offset F from the nominal RF frequency of oscillations. The period of this dependence is proportional to the product of the dispersion time by laser emission bandwidth. Such the physical property of PSD of the phase noise in OEO MZ is similar to the spectrum property of laser diodes with high-dispersive active media [6–9], we obtain:

$$N_{FOS}(\nu) = N_{FOS}(\nu_0) + (\nu - \nu_0)\frac{dN_{FOS}}{d\nu} + (\nu - \nu_0)^2\frac{d^2N_{FOS}}{d\nu^2}. \tag{6.94}$$

If $dN_{FOS}/d\nu \neq 0$ and constant and $d^2N_{FOS}/d\nu^2 = 0$, the spectrum of oscillation types in OEO remains equidistant. The dispersion effect on the mode spectrum in the second order must be taken into consideration, if the first and the second derivatives of the function of the optical frequency are not equal to zero, i.e., $dN_{FOS}/d\nu \neq 0$ and $d^2N_{FOS}/d\nu^2 \neq 0$. At that, the equidistant property is disturbed or intervals between adjacent spectrum oscillation types decreases.

We are speaking here about the single-frequency mode, but there are types of oscillations, which cannot begin to generation, but they are present in the spectrum. The value of the second derivative on the optical frequency $d^2N_{FOS}/d\nu^2$ of the FOS refraction index may serve as the equidistant measure. At that, the expression for the interval between the adjacent oscillation type can be written as $S_L(f)$:

$$\Delta f_{\text{oag}}(v) = \Delta f_{0\text{oag}}(v_0)\left[1 - (v - v_0)^2 \mathrm{d}^2 N_{\text{FOS}}/\mathrm{d}v^2\right], \tag{6.95}$$

where $\Delta f_{0\text{oag}}(v_0)$ is the value of the interval between the adjacent oscillation types at laser optical frequency equaled to the average generation frequency.

6.6.4 *Comparison of the "Comb Character" Effect in OEO MZ Spectrum at Strong FOS Dispersion with the Optical Spectrum in Semiconductor Lasers*

The similar comb character of the spectrum was discovered at investigation of semiconductor lasers at low temperatures in the beginning of 1960s and was described in [6–9]. During investigation of semiconductor lasers, the experimental determination of the continuously generating laser on the GaAs at temperature of 80 K with the resonator length 520 μm gave the interval value between frequencies of the adjacent longitudinal modes of 57 GHz, the average "group index" of the laser material refraction was 5.04 and non-equidistant measure was 84 MHz [7, 9].

The group velocity and the appropriate refraction index of the material are included into the expression for the "inter-mode interval" or the interval between the adjacent oscillation types.

Computer modeling of OEO MZ at account of FOS dispersion gave a possibility to conclude that dispersions of the standard low-dispersive single-mode FOS, which are used in the fiber-optical communication lines, have not the serious effect on PSD of the phase noise at laser line width less than 10 MHz due to its smallness (less than $\tau_{\text{D}} = \mathrm{d}T/\mathrm{d}v = 10^{-7}$ 1/GHz). When using the high-dispersive FOS with large $S_{\text{L}}(f)$, $\tau_{\text{D}} = \mathrm{d}T/\mathrm{d}v = 10^{-4}$ 1/GHz and (or) the low-coherent laser with the line width more than 1000 MHz, in the generation spectral line of OEO, ripples are observed at growth of the offset frequency.

6.7 Formation of the OEO MZ Oscillation Spectrum

6.7.1 *PSD of the Phase Noise in OEO MZ as the Convolution of Spectra of the Laser Optical Oscillations and RF Oscillations*

We should note that the autocorrelation function in Eq. (5.88) depends on the observation time τ.

To PD, after the optical filter (which is located in FOS in Figs. 2.4 and 5.14), harmonics pass with frequencies $\nu_{0\text{L}}$ and $\nu_{0\text{L}} + f_0$, which strength is equal, relatively, to harmonic

$$E_{10L}(t) = \sqrt{A_1}E_{0L}\cos\left[2\pi\nu_{0L}t + \varphi_{0L} + \varphi_{10Lm}(t)\right], \tag{6.96}$$

$$E_{20L}(t) = \sqrt{A_2}E_{0L}\cos\left[2\pi(\nu_{0L} + f_0)t + \varphi_{0L} + \varphi_{20Lm}(t)\right], \tag{6.97}$$

where coefficients A_1, A_2 are defined by the AFC of the optical filter and PD.

Taking into consideration Eqs. (5.90), (6.96), and (6.97), PSD in the PD area (without account of electrical oscillation influence in the MZ electrical input) can be calculated by the approximate formula:

$$\begin{aligned} S_\eta(f) &= 4\int_0^\infty R_{\eta L}(\tau)\cos(2\pi f\tau)d\tau \\ &= \exp\left(-\frac{2\Delta T_M}{T_c}\right)\delta(f) + S_L(f)\left[1 - \frac{A_1}{A_2}\exp\left(-\frac{2\Delta T_M}{T_c}\right)\right], \end{aligned} \tag{6.98}$$

where $\delta(f)$ is the delta-function, coefficients A_1, A_2 are defined by the AFC of the optical filter and PD, $S_L(f)$ is laser PSD, which is determined at utilization of Eq. (3.8) by the expression: $S_L(f) = \frac{1/(\Delta\nu_L)}{1+[f/\Delta\nu_L]^2} = \frac{T_c}{1+(2\pi T_c f)^2}$.

If we take at calculation the small offsets from the optical carrier $\Delta T_M \cdot 2\pi f \ll 1$, then we can write Eq. (6.98) in the form:

$$\begin{aligned} S_\eta(f) = &\exp\left(-\frac{4\Delta T_M}{T_c}\right)\delta(f) + \frac{T_c}{1+(2\pi T_c f)^2} \\ &\cdot\left[1 - \frac{A_1}{A_2}\exp\left(-\frac{2\Delta T_M}{T_c}\right)\right]. \end{aligned} \tag{6.99}$$

From Eq. (6.99), it follows that with the growth of the ratio $\frac{\Delta T_M}{T_c}$, the first term, which defines the oscillation amplitude of the regular component (5.102), decreases and the second term increases and aspires to $S_L(f)$.

Further, the convolution of $S_\eta(f)$ and $S_V(f)$ is:

$$\begin{aligned} &S_{\eta V}(f) = S_\eta(f) * S_V(f) \\ &= \frac{U_e^2}{2}\frac{E_{0L}^4}{2}\exp\left(-\frac{2\tau}{T_c}\right)\cdot\delta(f) + \left[1 - \frac{A_1}{A_2}\exp\left(-\frac{2\tau}{T_c}\right)\right]\cdot\frac{U_e^2}{2}\frac{E_{0L}^4}{2}S_L(f) * S_G(f), \end{aligned} \tag{6.100}$$

where "$*$" is convolution, and

$$S_L(f) * S_G(f) = \frac{T_c}{1+(T_c f)^2} * \frac{T_{gen}}{1+(T_{gen} f)^2}. \tag{6.101}$$

From this, the conclusion follows that $S_{\eta V}(f)$ for the optimal matching, the equality $T_c \approx T_1$ is necessary and sufficient. We remind that the coherence time is

defined in many respects by the lifetime T_1 of carriers on the upper laser operation level $T_c \approx T_1$.

6.7.2 *Oscillations Spectrum in the OEO* Closed *Feedback Loop*

The analog model of the statistical processes in OEO MZ with the utilization of the traditional correlator of two random quantities is shown in Figs. 5.10, 5.11, and 5.13 (Chap. 5).

At closeness of the feedback loop (switch Sw1 is closed, switch Sw2 is opened in Fig. 5.13b), at fulfillment of self-excitation conditions in OEO, the convolution of $S_\eta(f)$ and $S_V(f)$ is:

$$S_{OEO\eta V}(f) = S_\eta(f) * S_{OEO}(f)$$
$$= \frac{V_e^2}{2}\frac{E_{0L}^4}{2}\exp\left(-\frac{2\tau}{T_c}\right)\cdot\delta(f) + \left[1 - \frac{A_1}{A_2}\exp\left(-\frac{2\tau}{T_c}\right)\right]\cdot\frac{V_e^2}{2}\frac{E_{0L}^4}{2}S_L(f) * S_{OEO}(f). \quad (6.102)$$

In the formula (6.102), $K_L(F)$ is the noisse suppression coefficient, which depends on T_{FOS}, the laser optical power P_{0L}, σ_U is the nonlinearity coefficient of NA AE, T_F is the time constant of the RF filter. The transfer function of RF FODL | K_{FODL}| is determined by the expression:

$$S_{OEO}(F) = S_{0AN,OEO}K_{\Gamma AN}^2 + S_{0PN,OEO}K_{\Gamma PN}^2, \quad (6.103)$$

where $K_{\Gamma AN}^2$, $K_{\Gamma PN}^2$ are in Eqs. (6.57) and (6.58), relatively, or for $K_{\Gamma PN}^2$ we have Eq. (6.79).

In the next section, we analyze, which influence is affected by PSD of the laser phase noise upon PSD of the OEO RF phase noise.

6.7.3 *Influence of the Photon–Electron Resonance of QWLD on PSD of the Phase Noise*

Let us consider the influence of the photon–electron laser resonance on the shape of PSD of the phase noise. The problem of the fight against resonance peaks, which are determined by the laser and the optical fiber, at development of the low-noise OEO is the one of the important problem. The thing is that resonance peaks, which contain in the laser spectra (or PSD of the laser phase noise), are manifested in PSD of OEO MZ. In QWLD and the fiber-optical lasers, the natural frequency of this resonance

mainly depends on the time of photon being in the laser resonator and is determined by the time constant T_1 of the optical resonator or the resonator length. The frequency of the photon–electron resonance for different types of lasers takes a value from 1 kHz to 10 GHz. In modern low-noise QWLD used with the external microwave modulator, the system of frequency automatic control is used with application of optical discriminators, for example, on the Bragg cell with the cell step of 100 nm and the length up to 1 cm, with which help the phase noises decrease more than by 1000 times and is −110 to −100 dB/Hz at the offset of 1 kHz from the carrier.

The phenomenon of the photon–electron resonance in lasers and its influence on the PSD formation in the laser and OEO was discussed by us in Chaps. 4 and 5, where we form and discuss the differential equations for OEO taking into consideration the differential equation for the inversed population. The physical sense of this phenomenon is defined by the process of the energy pumping in the laser. The own resonance frequency is defined by the finite lifetime of carriers T_1 on the upper energy level and by the lifetime of photons T_{OF} in the optical resonator. The natural resonance frequency can be found with the help of the formula: $\omega_{00L} = 2\pi f_{00L} = (2\pi/T_1)\sqrt{G_0(\alpha_{00L} - 1)}$, where T_1 is the carrier life, G_0 is the gain (saturation coefficient), α_{00L} is the DC component of pumping. The electron–photon resonance in the laser, which natural frequency is defined by the square root from the product of the laser gain and the pumping exceed over the threshold value. The small-signal transfer function of the laser, which is defined as the ratio of the AC amplitude of the optical emission power to the AC amplitude of the input electrical pumping current, is determined by the formula: $K_{LD}(j\omega) = \frac{\omega_{00L}^2}{\left[\omega^2 - \omega_{00L}^2 - j\omega\alpha_{00L}\right]}$.

At utilization of fluctuation differential equations of the laser in Chap. 5, we obtained PSD of the amplitude and phase noises for QWLD. As a result, we obtain for PSD of amplitude and phase noise the following expressions (5.58) and (5.59) (Chap. 5):

$$S_{L\,Re} = \frac{T_1^{-4} D_{01} S_{SL\,Re}}{\left|F^2 - F_{00L}^2 - jF[(1/T_{0F}) + (1/T_1) - G_0 N_{00}] - \sigma_{EL}\right|^2}, \tag{6.104}$$

$$S_{LIm} = \frac{D_{11} S_{SLIm}}{|FT_1|^2} + \frac{T_1^{-4} D_{22} S_{SLIm}}{\left|F^2 - F_{00L}^2 - jF[(1/T_{0F}) + (1/T_1) - G_0 N_{00}]\right|^2}, \tag{6.105}$$

where F is the current frequency offset from the carrier frequency, D_{01}, D_{11}, and $D_{22}$are constant coefficients. Formulas (5.58) and (5.59) show that the total AM and PM noises of the laser emission intensity depend upon $F_{00L} = 2\pi(f - f_{00L})$, parameters of the optical resonator T_{0F}, the carrier lifetime T_1 on the upper operation level and the pumping level.

Values of S_{SLRe} and S_{SLIm} are:

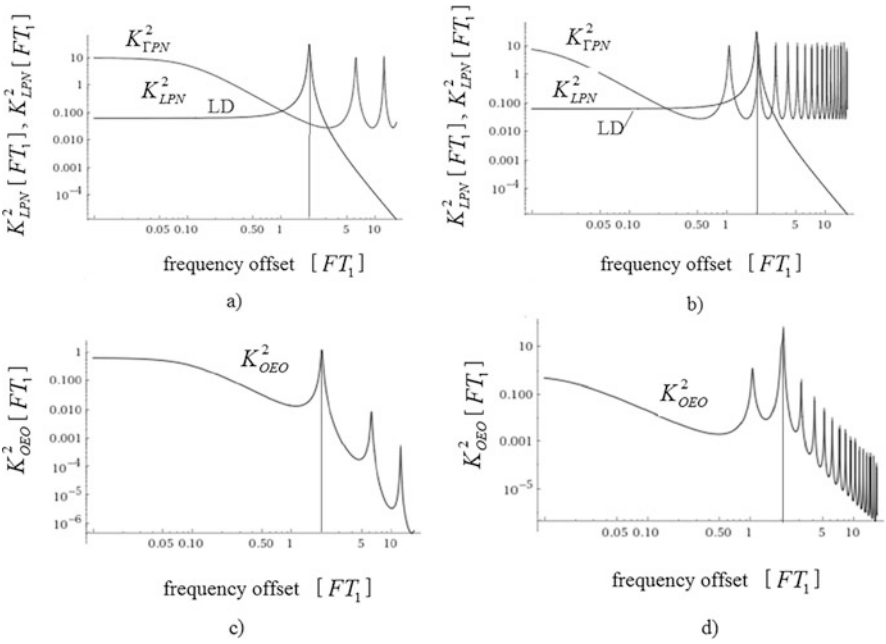

Fig. 6.33 The laser transfer function, which defines of its PSD of the amplitude noise, the noise suppression coefficient of RF oscillations in OEO for different levels of the relative laser phase noise (RIN-1 and RIN-2). (**a**) $FT_{\mathrm{FOS}} = 7$, (**b**) $FT_{\mathrm{FOS}} = 1$, (**c**) $FT_{\mathrm{FOS}} = 7$, (**d**) $FT_{\mathrm{FOS}} = 2$. Calculations are executed using (6.79) and (6.107) for $K^2_{\Gamma\mathrm{PN}}$ and K^2_{LPN}. The frequency of the laser natural relaxation resonance is equal to $F_{00\mathrm{L}} = 2/T_1$

$$K^2_{\mathrm{LAN}} = \frac{T_1^{-4} D_{01}}{\left|F^2 - F^2_{00\mathrm{L}} - jF[(1/T_{0\mathrm{F}}) + (1/T_1) - G_0 N_{00}] - \sigma_{\mathrm{EL}}\right|^2}, \tag{6.106}$$

$$K^2_{\mathrm{LPN}} = \frac{D_{11}}{|FT_1|^2} + \frac{T_1^{-4} D_{22}}{\left|F^2 - F^2_{00\mathrm{L}} - jF[(1/T_{0\mathrm{F}}) + (1/T_1) - G_0 N_{00}]\right|^2}. \tag{6.107}$$

Then the PSD of amplitude and phase noise$S_{\mathrm{L\,Re}} = K^2_{\mathrm{LAN}} S_{\mathrm{SL\,Re}}$, $S_{\mathrm{LIm}} = K^2_{\mathrm{LPN}} S_{\mathrm{SLIm}}$.

The PSD function of the OEO phase noise Eq. (5.79) can be presented as:

$$S = \frac{K^2_{\Gamma\mathrm{PN}} C_{\mathrm{A}} h\nu N_{\mathrm{sp}}}{P_{0\mathrm{G}}}, \tag{6.108}$$

where C_{A} is the constant coefficient, $K^2_{\Gamma\mathrm{PN}}$ (6.79) is the coefficient depending upon the delay time in the optical fiber and upon the laser optical power.

Figures 6.33 and 6.34 show the plots of the transfer function of the laser K^2_{LPN}, which are determined of its PSD of the amplitude noise, the noise suppression

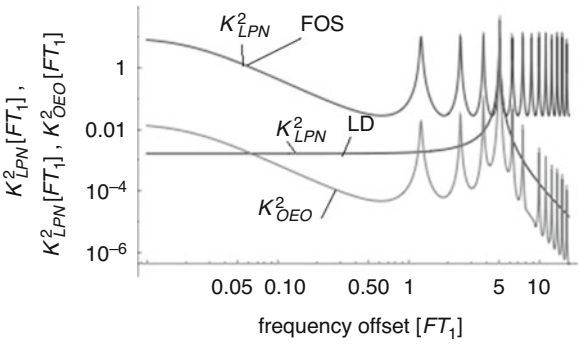

Fig. 6.34 The power spectral density of the phase noise of RF oscillations of OEO for different levels of the relative laser phase noise (RIN-1 and RIN-2)

coefficient of RF oscillations in OEO for different levels of the relative laser phase noise (RIN-1 and RIN-2).

For calculation the K^2_{OEO} plots presented in Figs. 6.33 and 6.34, we use the expression: $K^2_{\text{OEO}} = K^2_{\text{LPN}} \cdot K^2_{\Gamma\text{PN}}$, in which we use, relatively, the expression (6.79) for $K^2_{\Gamma\text{PN}}$, and (6.107) for K^2_{LPN}. Calculations are performed for the dimensionless offset FT_1 from the carrier, and in Eq. (6.105), we neglect by the first term for simplicity.

The frequency of the laser natural relaxation resonance is $F_{00\text{L}} = 2/T_1$.

On the presented plot in Fig. 6.34 we obviously see that with the growth of FT_{FOS} and at coincidence of resonance peaks in $K^2_{\Gamma\text{PN}}(F)$ and $K^2_{\text{LPN}}(F)$, for example, for $F_{00\text{L}}T_1 = FT_{\text{FOS}} = 2$, the peak level in K^2_{OEO} sharply grows.

For examination of laser resonance influence on PSD of OEO, which is formed by the photon–electron resonance, authors calculated PSD of the phase noise, taking into consideration PSD of the phase noises of the laser. PSD of the phase noises of the laser were calculated on the base of formulas obtained in Chaps. 5 and 6 at solution of the differential equation system with fluctuations.

At calculations, we take OEO with RF FODL, which consists of three optical fibers of different length, which are connected in the inputs by the couplers. This permitted (at correct choice of geometrical length difference of FOS included in RF FODL) to suppress the own resonances determined be the delay time on RF FODL. The calculation results of PSD of the phase noise of RF oscillation in OEO MZ for different variants of QWLD ("RIN-1" and "RIN-2") with different levels of the phase noise. The natural frequency of the photon–electron resonance of QWLD "RIN-1" was equal 10,000 kHz, and relatively, for QWLD "RIN-2" was equal to 20 kHz.

At calculations, we used expressions for laser PSD taking into account the photon–electron resonance of QWLD obtained in Chap. 5 for different values of the laser resonator Q-factor. The differential RF FODL consists of three optical fibers of different length $L = 6$ km, 6.2 km, 6.5 km. Optical fibers were connected in their inputs and outputs by the directional couplers of Y-type. The calculation is performed on the base of analytical expressions for PSD of the phase noise, which

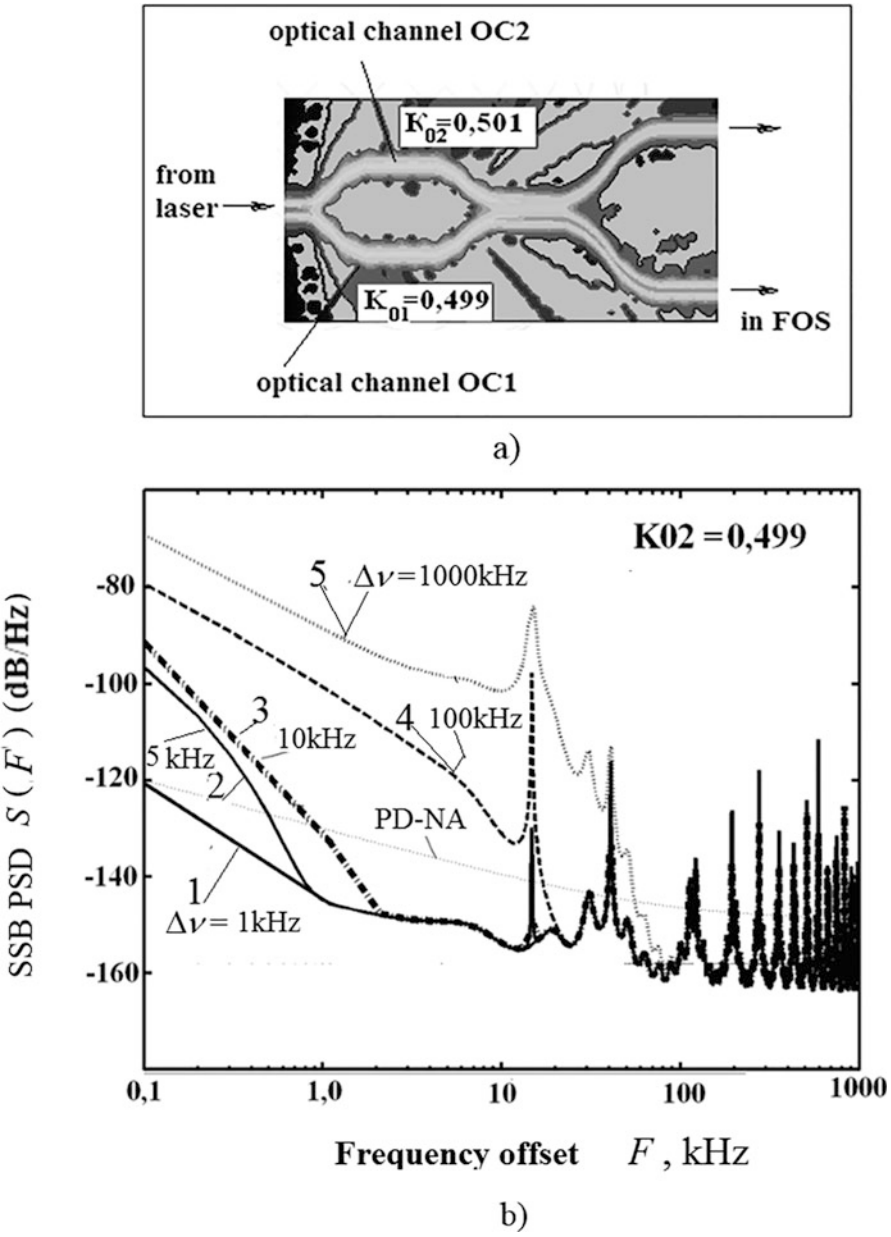

Fig. 6.35 Calculated functions of PSD of the phase noise of RA oscillations in OEO $S(F)$ versus the spectral line width of the high-coherent laser. Plots of $\Delta\nu = 1$ kHz (curve 1), 5 kHz (curve 2), 10 kHz (curve 3), 100 kHz (curve 4), and 1000 kHz (curve 5) (the observation time is 1 ms). The excitation coefficient of the optical channel OC2 is $K_{02} = 0.499$. The optical fiber length is $L = 6$ km, the generation frequency is 10 GHz

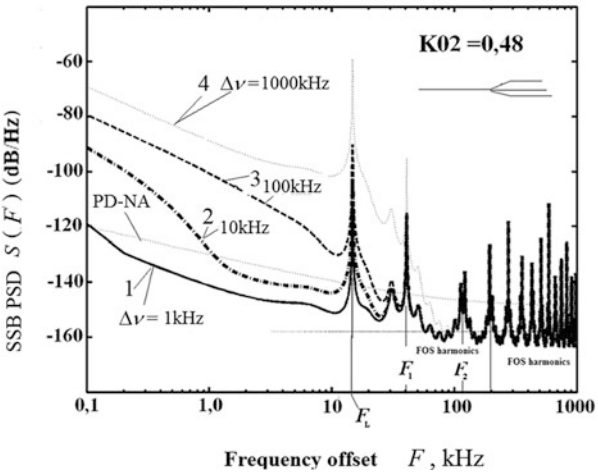

Fig. 6.36 Calculated PSD of the phase noise of RF oscillations in OEO MZ $S(f)$ for different values of the laser spectral line width. The width of the laser spectral line of the high-coherent laser is $\Delta\nu = 1$ kHz (curve 1), 10 kHz (curve 2), 100 kHz (curve 3) and 1000 kHz (curve 4) (the observation time is 1 ms). The curve PD-Y corresponds to the own PSD of the phase noise of PD. The optical fiber length is $L = 6$ km, the generation frequency is 10 GHz. FOS consists of three optical fibers of different lengths connected by the Y-couplers. Owing to utilization of the composite FOS from three optical fibers of different lengths, we can decrease the level of spurious harmonic components

are obtained in this chapter taking into account the optical power in the MZ optical channels.

We note that phase noises exceeds the amplitude noises by 10–25 dB/Hz, and the natural value of the resonance peak increases by almost the order with the growth of values of the pumping current exceed from three to seven.

Figures 6.35 and 6.36 show the calculated functions of PSD of the phase noise of RF oscillations in OEO MZ $S(F)$ versus the offset F from the carrier. At that, the width of the spectral line of the high-coherent laser is $\Delta\nu = 10$ kHz, 1 kHz, 5 kHz, 100 kHz, and 1000 kHz (the observation time is 1 ms). The optical fiber length is $L = 6$ km, the generation frequency is 10 GHz. The excitation coefficient of the optical channel OC2 is $K_{02} = 0.499$.

From plots presented in Figs. 6.35 and 6.36, we can conclude that the variation of laser spectral line width from 1 to 1000 kHz leads to increase of PSD of the phase noise at frequency offsets by 1–10 kHz more than by 30 dB/Hz. It is specially necessary to note the increase of PSD of the phase noise on the frequency offsets, which corresponds to the frequency of the photon–electron resonance F_1 (in Fig. 6.36).

The functions presented in Fig. 6.36 well explain the complicated picture of PSD of the phase noise added by the electron–photon resonance of QWLD. In experimental samples of OEO MZ, we see the clearly expressed resonance peak on the frequency offset from the RF carrier of 10 GHz. First of all, the position of the

resonance peak is determined by the chosen laser type as well as by constant pumping current. So, lasers with the width of the emission spectral line from 10 to 1000 kHz have the resonance peak, which is defined by the own frequency of the photon–electron resonance on the appropriate offset frequencies.

6.7.4 Limit Values of PSD of the Phase Noise

Now we examine the limit values of PSD of the phase noise and the natural generation line of OEO MZ taking into account the spontaneous emission of QWLD and the transverse spatial irregularity of the MZ optical channels. Utilization in OEO MZ of QWLD is kindly reported on the OEO overall sizes. The limit OEO values of the natural generation line are defined, as it follows from deduced expressions in this chapter, by the value of $S_{\beta FN}$: the quadrature component of the laser spontaneous emission. We know that the integral index of spontaneous emission in the laser mode (coefficient of spontaneous emission) for semiconductor lasers with the hetero-structure (not QWLD) can change in wide limits from 10^{-1} to 10^{-5} depending on sizes of the active region and the laser resonator.

Spontaneous laser emission plays the principal role in such phenomena as natural widening of single-frequency generation line, formation of the ultra-luminescence spectrum, as well as in generation dynamics at instantaneous switching-on of generation development. At least, in semiconductor laser, if the one of resonator dimensions is commensurable or smaller of the wavelength. In addition, the values of amplification (absorption) are high enough in order to the approximation of the uniform plane waves would be unacceptable. In this situation, the finding of the emission part into the laser mode from the separate active dipole within the limits of conventional approach, which is used for other types of lasers, is not adequate enough for semiconductor lasers, on which, as we know, the attention was attracted in publications.

Besides, QWLD has low values of the output level of spontaneous emission in the generated laser mode. PSD of the output spontaneous emission level S_β depends on the carrier lifetime on the upper level, on the generation level, on the emission polarization, etc.

Let us take for QWLD the integral index of spontaneous emission (the ratio of the gain of stimulated emission and spontaneous emission) into the laser mode equaled $\beta = 10^{-3}$, at the width of the spectral line of spontaneous emission of $\Delta\nu = 10^{10}$ Hz (we cannot confuse of this characteristic with the width of the laser spectral line, which is equal 1–10 kHz for the best samples). Then PSD of the QWLD phase noise at offset 1 kHz is $S_\beta \approx \beta/\Delta\nu = 10^{-12}$ [−120 dB/Hz]. At accepted values of QWLD parameters and taking into account that relative deviations of material refraction index of MZ modulator (in the transverse section, at distance between the optical channels not more than 60 μm, $G_{22} = \Delta\varepsilon/\varepsilon = 10^{-3}$), at the optical fiber length of 2–5 km, PSD of the phase noise in OEO MZ at offset 1 kHz from the generated frequency 10 GHz is equal $S_{\Psi AG}(F = 10^3\ \ 1/s) \approx 10^{-12} - 10^{-17}$[1/Hz].

We examined how the choice of RF FODL component parameters (included in OEO MZ) affects the operation. We found out that for providing of minimal level of PSD of the phase noise (−120 dB/Hz at offset 1–10 kHz from the microwave carrier), it is necessary to use the high-coherent lasers with the spectral line width of 1–50 kHz with geometrical FOS length of 2–20 km. To suppress peaks of oscillation types, which are not generated, we can use differential and combined delay lines with two or three optical fibers of different length.

The further level reduction of PSD of the phase noise is possible at utilization of PLL system in OEO MZ, as in the case of traditional RF oscillators. We shall consider in detail the features of PLL system application in OEO in the next chapter. Below we present results of numerical calculation of PSD of OEO MZ with the PLL system.

The power spectral density of the phase noise of RF oscillations in OEO MZ is presented in Chap. 7.

6.8 Conclusions

The OEO MZ analysis is performed as the system of two oscillators of the optical and RF ranges, the differential equations with fluctuations are obtained and analyzed. The analytical functions for the power spectral densities of amplitude and phase fluctuations of RF subcarrier (generated by OEO) are obtained. It is proved that the power spectral density of phase noises in OEO MZ is determined by phase fluctuations of the laser optical emission. The value of PSD of phase noises in OEO MZ is proportional to the natural width of the laser spectral line, and inversely proportional to the equivalent (taking into consideration the optical fiber an RF FODL) Q-factor of the OEO oscillating system and inversely proportional of the laser power.

Noises in OEO MZ are mainly defined by the laser phase fluctuations, which, in turn, depend upon the spontaneous emission. The decrease of OEO phase noises can be provided by a choice of the high-coherent sources of optical emission with the relatively high power of optical emission (20–40 mW). The other methods of PSD decrease of phase noises in OEO MZ are: the growth of delay time of the optical carrier in FOS optical fibers, the control of MZ operation point and application of combined modulators (which use the more than two parallel optical channels), MZ with increased dynamic range (on the value of a ratio of optical phase increments at variation of the control voltage).

It is stated than at utilization of standard low-dispersive optical fibers in MZ, the dispersion of fibers has no serious influence on PSD of the phase noises at widths of the laser line less than 10 MHz. At application of the high-dispersive optical fibers (with the dispersion level 50 ns/nm km) or the low-coherent laser (with the line width more than 1000 MHz), ripples on the offset frequency are observed, which period is determined by dispersion on FOS and by the natural width of the laser generation line, in the spectral line of OEO MZ generation. Fulfilled computer

modeling and experimental investigation of OEO MZ samples on the operation frequencies 8–10 GHz show the well-comparison of calculated and experimental static dependences of amplitude and frequency of OEO MZ taking into account the stabilization effect at large pumping currents of QWLD and FOS lengths of 1–5 km.

In this chapter, we proved that OEO MZ can be used as the measuring system of the width of the laser spectral line. Performed analysis shows that the RF spectrum is determined by detected phase noises of laser optical emission. The value of PSD of the phase noise is proportional to the square of the natural width of laser optical emission spectral line. It is shown that in OEO MZ the various variants of the PLL system structure are possible with laser control basing on the reference RF oscillator and with RF oscillator control basing on the reference laser. We prove that the PLL system in OEO MZ significantly decreases requirements to the spectral line width of the laser generation and to the length of the optical fiber. At introduction of PLL loop in OEO MZ, the essential (more than by 15 dB/Hz) decrease of PSD level of phases noises on the generation frequencies 8–10 GHz. The theoretical and experimental studying of the low-noise laser generator (OEO MZ) with the PLL system is performed. We considered theoretical problems of oscillation generation with low level of phase noises in the system of OEO MZ with PLL as a function of the laser spectral line width.

It is shown that OEO MZ with PLL system is the RF oscillator with the ultralow level of PSD of the phase noise. The value of single-side PSD of the phase noise may achieve $-120 \div -150$ dB/Hz at frequency offsets 1–10 kHz from the nominal generation frequency 10 GHz when using the high-coherent lasers with the line width 1–10 kHz. Development and analysis of the theoretical model of OEO MZ revealed that the power spectral density of the phase noise of microwave oscillations is determined by the laser phase noise and by the line width of the laser optical emission, by the laser power, by delay in the optical fiber. The decrease of PSD of the phase noise by more than 10 dB/Hz is provided by equalization of the optical power in MZ channels.

As the result of investigations, the conclusion is derived that to provide the PSD level of the OEO phase noise less than -130 dB/Hz on frequency 10 GHz at offset of 1 kHz, the spectral line width of optical emission of commercially available lasers (at the output power not less than 10 mW) should be less than 1–10 kHz.

The different types of low-noise oscillators are developed and experimentally implemented with RF FODL with the stabilized electrical circuits of laser diode's bias current, or the bias voltage of the operation point of the electro-optical modulator and the bias current of the photodiode.

The optoelectronic oscillators were developed for centimeter wave range on the base of QWLD, stabilized by RF FODL and by self-heterodyning, provide the phase noise at the room temperature with the offset 1 kHz from the carrier at the following level:

– Approximately -120 dB/Hz in the simplest variants with lasers with the optical emission line width of 1 MHz and at application of optical fibers with delay

2–10 μs,—approximately −130 dB/Hz at QWLD utilization with the optical line width of 3 kHz at application of optical fibers with delay 10–50 μs,

– Approximately −150 to −160 dB/Hz at QWLD utilization with the optical line width less than 5 kHz at application of optical fibers with delay 10–50 μs at complex optimization of OEO MZ and utilization of PLL system.

Presented scientific results, conclusions and recommendations permit to think about the discovering of the new direction in the field of the compact precision sources of microwave and mm-wave oscillations.

References

1. Alexander A. Bortsov and Sergey M. Smolskiy, Opto-Electronic Oscillator with Mach-Zender Modulator. Infocommunications Journal, Vol. XI, No 1, 45–53 (2019), DOI: 10.13140/RG.2.2.20992.69126
2. I.V. Komarov, S.M. Smolskiy, *Fundamentals of short-range FM radar* (Norwood, Artech House, 2003)
3. V. Zhalud, V.N. Kuleshov, *Noise in Semiconductor Devices. Under Edition of A.K. Naryshkin* (Sovetskoe Radio, 416 p. (in Russian), Moscow, 1977)
4. Alexander A. Bortsov, Yuri B. Il'in, Laser spectral line widening effect on RF phase and amplitude noises of an optoelectronic oscillator OEO. J. Radio Eng. (2), 21–31 (2010), DOI: 10.13140/RG.2.2.35665.07527
5. D.B. Leeson, A simple model of feed back oscillator noise spectrum. Proc. IEEE **54**, 329–330 (1966)
6. V.D. Kurnosov, V.I. Magalyas, A.A. Pleshkov, L.A. Rivlin, V.G. Trukhan, V.V. Svetkov, Self-modulation of semiconductor injection laser. Pis'ma Zh. Eksp. Teor. Fiz. **4**(11), 449 (1966)
7. L.A. Rivlin, *Dynamics of Semiconductor Laser Emission [in Russian]* (Sovetskoe Radio, Moscow, 1976)
8. J.E. Ripper, T.L. Paoli, J.C. Dyment, Characteristics of bistable CW GaAs junction lasers operating above the delay-transition temperature. IEEE J. Quantum Electron. **6**(6), 300–304 (1970)
9. C.A. Brackett, Second-order dispersion in oscillating GaAs junction lasers. IEEE J. Quantum Electron. **QE-8**(2), 66–69. 27.279 (1972)

Chapter 7
Optoelectronic oscillator (OEO) as the Time and Spatial Correlator of Random Variables with Differential Delay Line

This chapter is devoted to the analysis of OEO as the time and spatial correlator of random variables. In Sect. 7.1, we describe the general issues of this OEO operation mode. The model of the nonsymmetric dielectric waveguide structure with the laser and the optical waveguide is discussed in Sect. 7.2. The analysis of OEO DM on the base of abbreviated differential equations is executed in Sect. 7.3 together with the issues of frequency control in OEO DM by the laser pumping current. The diagrams of frequency control in OEO DM with differential RF FODL are described in Sect. 7.4. Section 7.5 is devoted to problems of parametric and long-term frequency instability in OEO with RF FODL. Fluctuation equations for PSD of amplitude and phase noises in OEO DM are discussed in Sect. 7.6. Section 7.7 is devoted to an analysis of frequency and phase control systems in OEO.

7.1 OEO as the Time and Spatial Correlator of Random Variables

Before the discussion of characteristics of the electromagnetic field in the nonsymmetrical waveguide channel of the MZ modulator, we make some conclusions of the analysis of PSD of the phase noise in OEO, which are obtained in Chaps. 3–6. We formulate the main mechanisms which causes the phase noise suppression in the oscillating system of OEO (Fig. 7.1), and discuss the influence of time and spatial coherence of QWLD emission upon PSD of the phase noise in OEO MZ.

We single out several **main mechanisms of the phase noise suppression** in OEO owing to:

- The fiber-optical *delay line with the geometrical length more than 1000 m* (the suppression coefficient due to the length $K^2_{1\Gamma}(F)$ was analyzed in Chap. 6).

A. A. Bortsov et al., *Laser Optoelectronic Oscillators*, Springer Series in Optical Sciences 232, https://doi.org/10.1007/978-3-030-45700-6_7

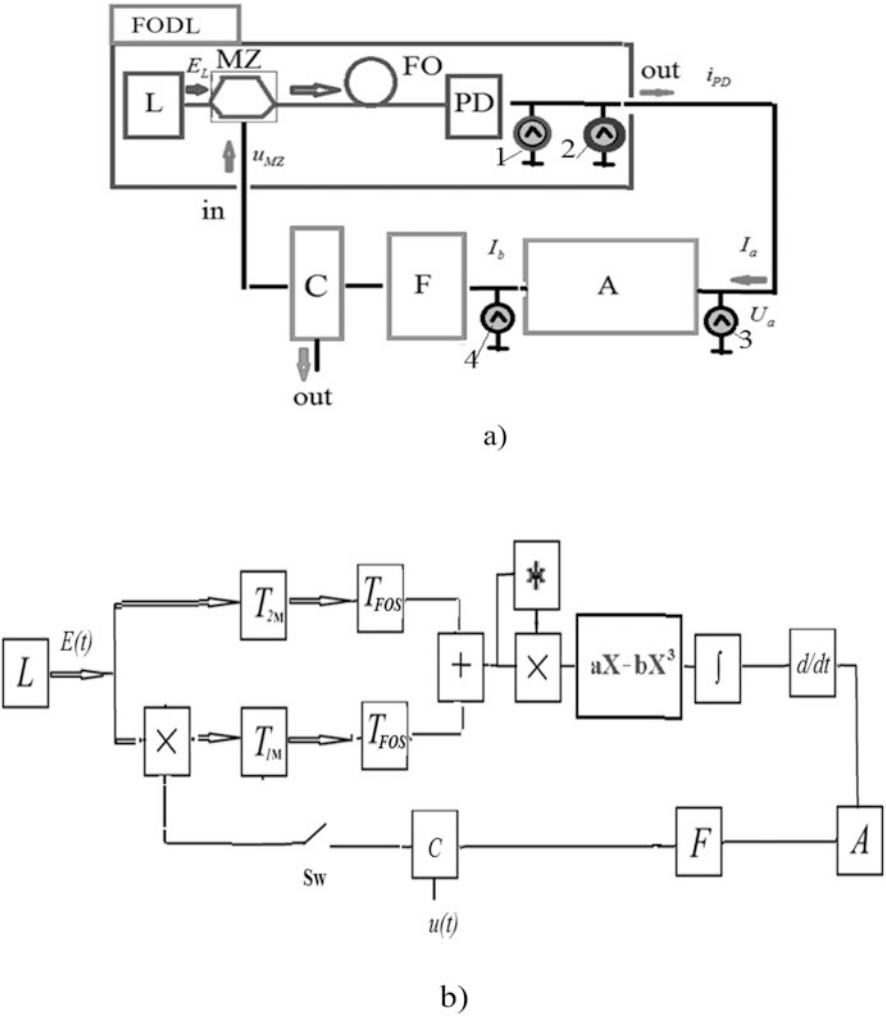

Fig. 7.1 The structure of OEO MZ with sources of RF noise: the detected QWLD noise (1), the own noise of PD (2), noises in the input and output of RF amplifier (3, 4) (**a**). The analog model of the statistical process in OEO MZ with utilization of the random variable correlator (**b**). The correlator consists of multipliers "×," the delay cell "*T*," the adder "+," the integrator, the differential device, the RF amplifier "A," the RF filter "F," the coupler "C" (**b**)

- The utilization in OEO of *QWLD with ultralow phase noises* (accordingly, PSD of QWLD is equal to $S_{\text{PNL}}(F)$).
- The *suppression of DC component of the laser emission*, which passes on the photodetector, and hence, the suppression coefficient is equal to $K^2_{2\Gamma}$.
- The *statistical correlation of noises at combining of the side optical harmonics* on the photodetector (accordingly, the suppression coefficient is equal to $K^2_{3\Gamma}$).

Two last mechanisms are discussed in Chap. 3 at analysis of modulation systems of the laser emission in OEO.

We would like to add that in OEO MZ with the frequency division, for instance, by 2 (Fig. 5.14), the benefit in phase noise suppression is achieved owing to not only by the emission suppression on the central optical carrier ν_0, but by execution of the square root operation. As we know [1], at radio frequency division by the integer number l, PSD of the phase noise $S_{\mathrm{RFPN}}(F)$ decreases as $S_{\mathrm{RFPN}}(F)/l^2$.

Figure 7.1a shows the structure of OEO MZ with noise sources. Taking into consideration the fluctuation theory described in Chap. 6, we note that in the OEO MZ structure (Fig. 7.1), the noise sources are:

- The phase noise of the laser optical oscillations (not shown in the structure).
- The detected laser noise (shown in Fig. 7.1) in the PD load.
- The noise of the photodetector (shown in Fig. 7.1).
- The noise in the input and output of the RF amplifier (shown in Fig. 7.1 by black circles).

In the closed OEO oscillating system, the noise conversion occurs together with the spectrum convolution of the detected laser phase noise $S_{\mathrm{LPN}}(F)$ with the spectrum of the total electronic noise $S_{\mathrm{EPN}}(F)$.

Figure 7.1b shows the analog model of statistical processes in OEO MZ with utilization of the random variables correlator. The correlator structure is described earlier in Chaps. 3, 5, and 6. It consists of the multiplier "×," two optical channels with different delays, and the delay cell defining by the delay in the optical fiber.

For PSD of the phase noise in OEO $S_{\mathrm{OEOPN}}(F)$, the following formula is true:

$$S_{\mathrm{OEOPN}}(F) = K^2_{1\Gamma}(F)K^2_{2\Gamma}(F)K^2_{3\Gamma}(F)\{S_{\mathrm{PNL}}(F) * S_{\mathrm{PNE}}(F)\}. \tag{7.1}$$

It is necessary to note that the process of spectra convolution of the detected laser phase noise $S_{\mathrm{LPN}}(F)$ with the spectrum of the total RF noise $S_{\mathrm{PNE}}(F)$ has the new character from the point of view of the oscillation theory and the statistical communication theory. We know that the spectrum of the RF noise $S_{\mathrm{EPN}}(F)$, to an accuracy of constants $C_{1\mathrm{E}}$ and $C_{2\mathrm{E}}$, are well described by the formula:

$$S_{\mathrm{EPN}}(F) \approx \left(\frac{C_{1\mathrm{E}}}{F^2} + \frac{C_{2\mathrm{E}}}{F^3}\right). \tag{7.2}$$

The convolution of the detected laser phase noise $S_{\mathrm{LPN}}(F)$, which form can be characterized by the Lorentzian curve, with the spectrum of the RF noise $S_{\mathrm{EPN}}(F)$ (Eq. 7.2) gives the new form different from the Lorentzian curve of the form (Eq. 7.2).

The joint factor of own RF noise $S_{\mathrm{PNE}}(F)$ suppression in OEO varies and takes the values $K^2_{1\Gamma}(F)K^2_{2\Gamma}(F)K^2_{3\Gamma}(F) = 0.1 - 0.001$.

Let us discuss the influence of the coherence and the width of the laser spectral line on the PSD of the phase noise in OEO.

7.1.1 The Influence of the Coherence and the Width of the Laser Spectral Line on the PSD of the Phase Noise in OEO

We again address to consideration of the structure in Fig. 7.1.

The result E_{12L} of adding of two optical oscillations E_{1L} and E_{2L} with different delays is determined by the sum in Fig. 7.1: $E_{12L} = E_{1L} + E_{2L} = \sqrt{E_{1L}^2 + E_{2L}^2}\exp[j\arg(E_{12L})]$.

The field strengths of two oscillations on PD passed through the MZ modulator on the first and second optical channels are equal relatively:

$$E_{1L}(t) = |E_{1L}|\mathrm{Re}\{\exp[j2\pi\nu\cdot(t - T_{FOS} - T_{1M}) + j\varphi_{0L1}]\exp[+j\psi_{m1}(t - T_{FOS} - T_{1M})]\};$$
$$E_{2L}(t) = |E_{2L}|\mathrm{Re}\{\exp[j2\pi\nu\cdot(t - T_{FOS} - T_{2M}) + j\varphi_{0L2}]\exp[+j\psi_{m2}(t - T_{FOS} - T_{2M})]\}.$$

If we assume that the delay difference in the MZ optical channels is equal to $\Delta T_M = T_{1M} - T_{2M}$ for the resulting ACF E_{12L} on the PD area at impact on the MZ optical input of the laser optical emission, we must distinguish the observation times $-2\Delta T_M < |\tau| < 2\Delta T_M$ and $|\tau| > \Delta T_M$ at calculation and at integration over τ.

So, for $|\tau| > \Delta T_M$, the ACF of the strength E_{12L} is determined by the expression: $R_{\eta L}(\tau) = \exp\left(-\frac{2\Delta T_M}{T_c}\right)\cos(2\pi\nu\tau)$. At $-2\Delta T_M < |\tau| < 2\Delta T_M$, the ACF E_{12L} is determined by the expression:

$$R_{\eta L}(\tau) = \exp\left(-\frac{2\tau}{T_c}\right)\cos(2\pi\nu\tau). \tag{7.3}$$

We attract our attention to the fact that at open switch Sw, the structure in Fig. 7.1b represents the correlator structure with the difference or differential delay ΔT_M.

7.1.1.1 The Open Sw

Figure 7.2 shows the model of the single-dimension optical circuit (L is the laser, PD is the photodetector) with the difference delay ΔT_M (a), the visual representation of integration of the laser ACF $R_{\eta L}(\tau)$ (b), the visual representation of integration and adding of the laser ACF $R_{\eta L}(\tau)$ with delayed laser ACF $R_{\eta L}(\tau - \Delta T_M)$ for in-phase (c) and out-or-phase (d).

We emphasize that at open Sw (Fig. 7.1), the correlation function of the process in the output of the adding device with delay lines with the difference in delays $\Delta T_M = T_{1M} - T_{2M}$ can be obtained, as in the structure of the classical adder with two delay lines [2, 3], in the form:

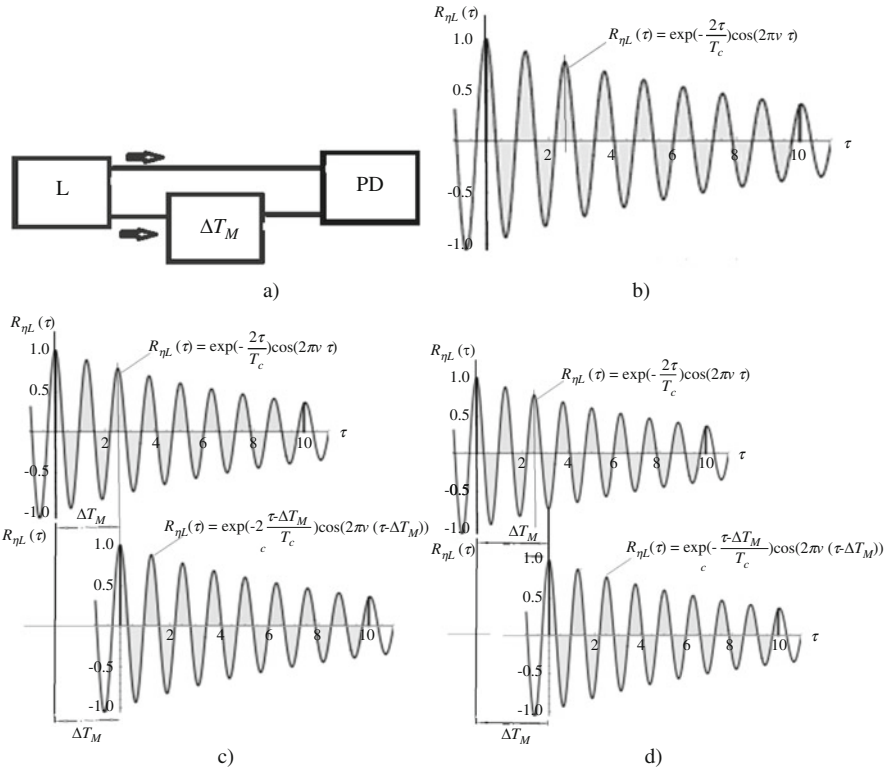

Fig. 7.2 The model of the single-dimension optical structure (L is the laser, PD is the photodetector) with the difference delay ΔT_{M} (**a**), the visual representation of the laser ACF integration $R_{\eta \mathrm{L}}(\tau)$ (**b**), the visual representation of the integration and adding of the laser ACF $R_{\eta \mathrm{L}}(\tau)$ with the delayed Laser ACF $R_{\eta \mathrm{L}}(\tau - \Delta T_{\mathrm{M}})$ in-phase (**c**) and out-of-phase (**d**)

$$R_{\eta \mathrm{PD}}(\tau) = 2R_{\xi \mathrm{L}}(\tau) + R_{\xi \mathrm{L}}(\tau - \Delta T_{\mathrm{M}}) + R_{\xi \mathrm{L}}(\tau + \Delta T_{\mathrm{M}}), \tag{7.4}$$

where $R_{\eta \mathrm{PD}}(\tau)$ is the correlation function of the stationary random process in the PD input (or in the MZ output) $R_{\xi \mathrm{L}}(\tau) = \exp\left(-\frac{2\tau}{T_{\mathrm{c}}}\right)\cos(2\pi\nu\tau)$, where T_{c} is the laser coherence time. Integration of the adding (or subtracting) the result of mutually delayed ACFs (Eq. 7.4) determines the energy spectrum or PSD:

$$S_{\eta \mathrm{PD}}(f) = \int_{-\infty}^{\infty} R_{\eta \mathrm{PD}}(\tau)\cos(2\pi f\tau)\mathrm{d}\tau. \tag{7.5}$$

From Fig. 7.2, we see that at adding in out-of-phase (d), the PSD level in the PD input will be minimal and is equal to zero. Hence, noises introduced by the DC component will be minimal in the PD load. At in-phase adding (Fig. 7.2c), the

spectrum in the PD input will have the maximal value. Accordingly, noises introduced by the DC component will be maximal in the PD load.

Since the problem of noises caused by the DC component had discussed in Chap. 3, here we pay attention to the circumstance that due to the spatial nonuniformity (in transverse section) of MZ waveguide optical channels, in order to achieve of DC suppression to values, for example, less than 10^{-5} is technically the difficult enough task. This is caused by the fact that the laser wavelength is close to the overall dimensions of the waveguide, and the nonuniformity of optical channels in MZ causes the significant phase deviations of the wave in the transverse section during its propagation. It is easy to make sure that PSD in the PD input and the suppression degree of DC component will also depend on the excitation coefficients of optical channels A and B.

Figure 7.3 presents the model of the differential delay line in OEO, which is formed by optical channels of the MZ modulator and the optical fiber at optical oscillations adding in-phase (a) and out-of-phase (or at subtraction) (b). The interference pattern (3D and the contour plot) in the far zone (on PD area) of two delayed optical oscillations in the transverse section on the screen of the PD area are shown in Fig. 7.3c, d: at modulator operation in the quadrature mode (or at relative phase difference of 90°) (c) and in the non-quadrature mode (or at the relative phase difference of 180°) (d).

Let us illustrate the influence of excitation coefficients A and B of the first and second MZ optical channels upon PSD $S_{\eta\mathrm{PD}}(f)$ for structures in Fig. 7.3a, b. Now we write ACF in the PD input as the formula (taking into account A and B):

$$\begin{aligned} R_{\eta\mathrm{PD}}(\tau) &= A \cdot R_{\xi\mathrm{L}}(\tau - T_{1\mathrm{M}} - T_{\mathrm{FOS}}) + B \cdot R_{\xi\mathrm{L}}(\tau - T_{2\mathrm{M}} - T_{\mathrm{FOS}}) \\ &+ A \cdot R_{\xi\mathrm{L}}(\tau + T_{1\mathrm{M}} + T_{\mathrm{FOS}}) + B \cdot R_{\xi\mathrm{L}}(\tau + T_{2\mathrm{M}} + T_{\mathrm{FOS}}). \end{aligned} \tag{7.6}$$

PSD $S_{\eta\mathrm{PD}}(F)$ can be found by integrating of $R_{\eta\mathrm{PD}}(\tau)$ as:

$$\begin{aligned} S_{\eta\mathrm{PD}}(F) &= 4A \int_0^\infty \exp\left(-2\frac{\tau - T_{1\mathrm{M}} - T_{\mathrm{FOS}}}{T_{\mathrm{c}}}\right) \cos\left[2\pi\nu(\tau - T_{1\mathrm{M}} - T_{\mathrm{FOS}})\right] \cos(2\pi f\tau)\mathrm{d}\tau \\ &+ 4B \int_0^\infty \exp\left(-2\frac{\tau - T_{2\mathrm{M}} - T_{\mathrm{FOS}}}{T_{\mathrm{c}}}\right) \cos\left[2\pi(\nu - T_{2\mathrm{M}} - T_{\mathrm{FOS}})\right] \cos(2\pi f\tau)\mathrm{d}\tau. \end{aligned} \tag{7.7}$$

For short, in Eq. (7.7), we took into consideration only two first components in Eq. (7.6). In the formula (7.7), the excitation coefficients A and B affect to formation of PSD of the phase noise. It is well seen in Fig. 7.4b, where the calculated PSD $S_{\eta\mathrm{PD}}(F)$ are presented for different phase delays of oscillations.

Figure 7.4 shows the module $|K_{\mathrm{DFODL}}(2\pi\nu\Delta T_{\mathrm{M}})|$ and the argument Arg $[K_{\mathrm{DFODL}}(2\pi\nu\Delta T_{\mathrm{M}})]$) of the differential delay line of MZ optical channels

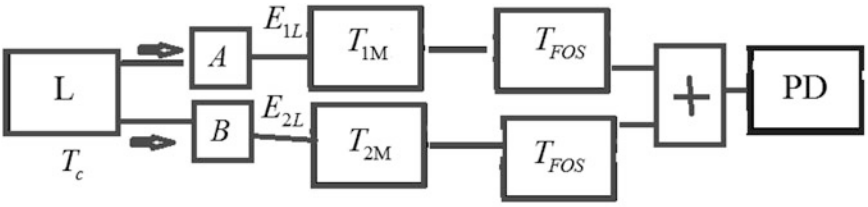

a)

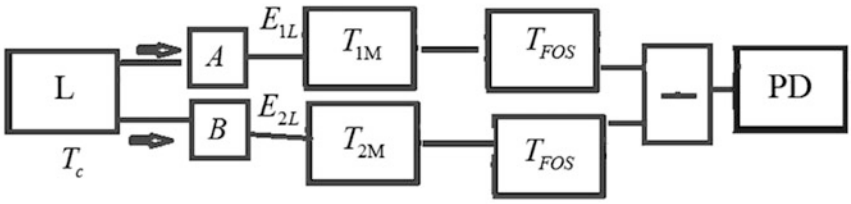

b)

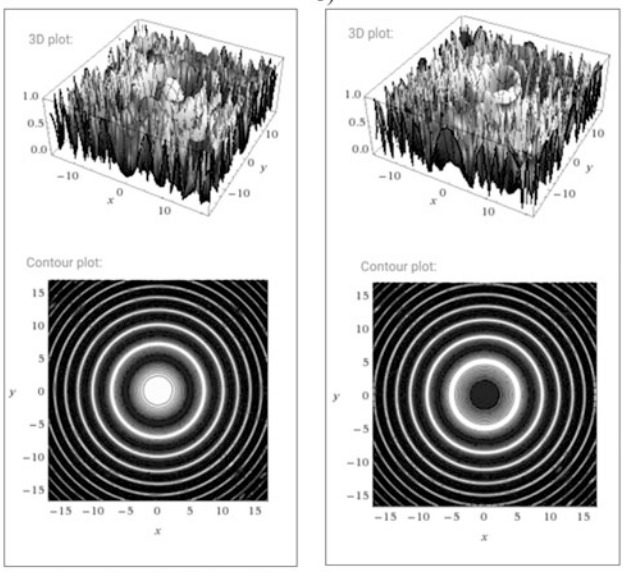

c) d)

Fig. 7.3 The model in differential delay line in OEO formed by MZ optical channels and the optical fiber at adding in-phase of optical oscillations (**a**) and out-of-phase (subtraction) (**b**). Interference pattern in the far zone of two delayed emissions in the transverse section on the screen or the PD area: at modulator operation in the quadrature mode (**c**) and the non-quadrature mode (**d**)

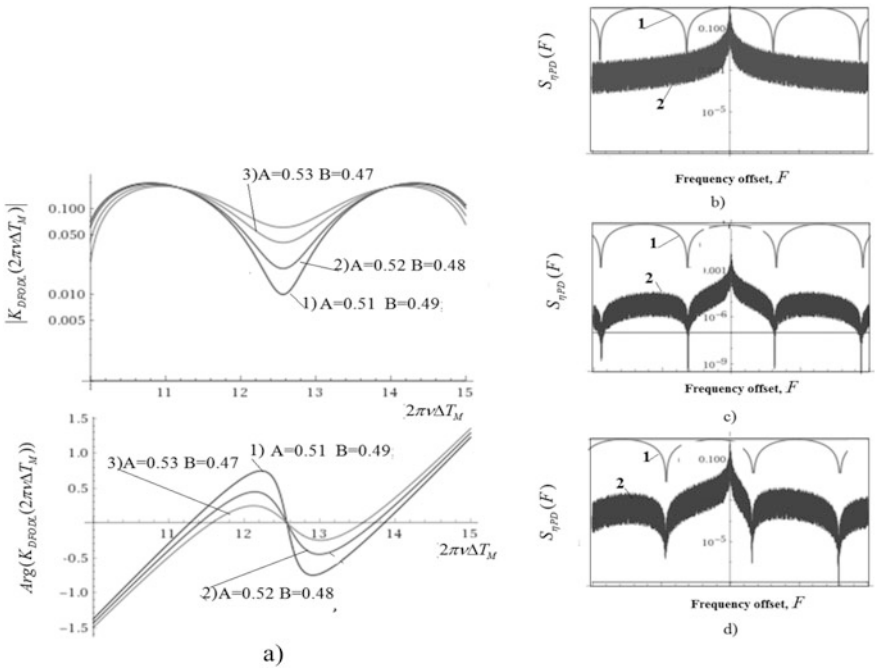

Fig. 7.4 The module $|K_{\mathrm{DFODL}}(2\pi\nu\Delta T_{\mathrm{M}})|$ and the argument $\mathrm{Arg}[K_{\mathrm{DFODL}}(2\pi\nu\Delta T_{\mathrm{M}})]$ of the differential delay line of MZ optical channels (Fig. 7.3) with different excitation coefficients A and B: (1) $A = 0.51$, $B = 0.49$; (2) $A = 0.52$, $B = 0.48$; (3) $A = 0.53$, $B = 0.47$ (**a**). The laser spectrum in the MZ input (**b**) and passed through MZ (**c**, **d**). The module of the MZ transfer function at different phase shifts between oscillations in MZ optical channels (**b–d**)

(Fig. 7.3) with different excitation coefficients A and B: (1) $A = 0.51$, $B = 0.49$; (2) $A = 0.52$, $B = 0.48$; (3) $A = 0.53$, $B = 0.47$. In Fig. 7.4b, we see the laser spectrum (curves 2) $S_{\eta\mathrm{PD}}(F)$ in the MZ input (1b) and the MZ output (2b, 3b). The MZ transfer function (curve 1) at different phase shifts between oscillations in MZ optical channels (Fig. 7.4b–d).

The analytical PSD form (Eq. 7.7) with account of coefficients is enough complicate; calculations are performed with the help of the standard integrals of the type: $\int \exp\left(-\frac{x-a}{b}\right)\cos(wx - wa)\mathrm{d}x = \frac{-be^{(a-x)/b}\{bw\sin[w(a-x)]+\cos[w(a-x)]\}}{b^2w^2+1} + \mathrm{const}$. From plots in Fig. 7.4b–d, we see that at phase difference in MZ channels close to 180° (d), the detected laser PSD $S_{\eta\mathrm{PD}}(F)$ decreases by several ten times and becomes congruent with internal phase noises determined by the phase noise of the RF amplifier and PD. Such a decrease of the detected PSD gives a possibility to provide the RF noises suppression owing to the above-described mechanisms of suppression determined by Eq. (7.1).

7.2 The Model of the Dielectric Waveguide Structure of the Laser and the Optical Channel

One of the main differences of modulators of the optical range from the RF modulators is the adequacy of the optical wavelength with the transverse dimensions of optical channels. We can often forget about this difference and represent the ideal model of the optical device without speaking about spatial distribution of the optical field. The numerical modeling of MZ optical channels with account of spatial channel dimensions shows that the wave propagating through the optical channel cannot be considered as the plane wave. In the transverse section, not only the intensity or the power of emission varies nonuniformly, but the optical phase as well. At that, variations of the optical phase achieves from 100° to 300° depending on the type of the optical channel, its length and irregularity.

Further, we consider the spatial model of the waveguide structure of the laser and the optical channel.

Deriving of the formulas for amplitude and phase calculation of RF oscillations in OEO MZ from the abbreviated equations (Fig. 7.1a) is performed in Chaps. 3 and 5. In these formulas, there are the module and the argument of the MZ transfer function. At variation of the module and the argument of the MZ transfer function, the amplitude and the frequency of MZ will oscillate. To take into consideration the influence on the module and the MZ transfer function of the symmetry disturbances in the transverse section, we form and analyze the model of the dielectric waveguide structure of the laser and the optical channel of the MZ modulator.

Figure 7.5a, b shows the structure of OEO MZ on the base of *Y*- and *X*-optical couplers with the spatial filter SF (a), the structure of OEO MZ with dividing optical plates (mirrors) and the spatial filter ("M" is the lens).

The one of the aims of investigations in this section is studying of the effect of the optical channel asymmetry upon the amplitude square and the phase shift in the transverse section in the MZ output. The asymmetry in the waveguide optical channels, as shown below, exposes the essential influence on the distribution of the amplitude and the phase of oscillations not only in the transverse section of the separated channel OC-1 or OC-2. The waveguide asymmetry is the reason of the asymmetric distribution of the amplitude square (or intensity) after summation of the output emissions in the near and far zone on the photodetector area. The presence of the waveguide channel asymmetry in MZ is the one of reasons of the nonzero level of DC of the optical emission on the PD.

Figure 7.5c–f shows the spatial pictures of the amplitude square of the electromagnetic field in the transverse section in the output of the MZ modulator, after summation of two optical oscillations passed via OC-1 and OC-2 optical channels of MZ (Fig. 7.5a, b). In Fig. 7.5c, we see results of the structural equation modeling and patterns of the contour lines of the amplitude square of the electromagnetic field in the transverse section in the output of the MZ modulator in the case of the *full symmetry* of waveguide channels, and in Fig. 7.5d–f we see similar results of the structural equation modeling and patterns of contour lines in the case of the *asymmetry* of waveguide channels. So, Fig. 7.5d–f show that due to asymmetry of

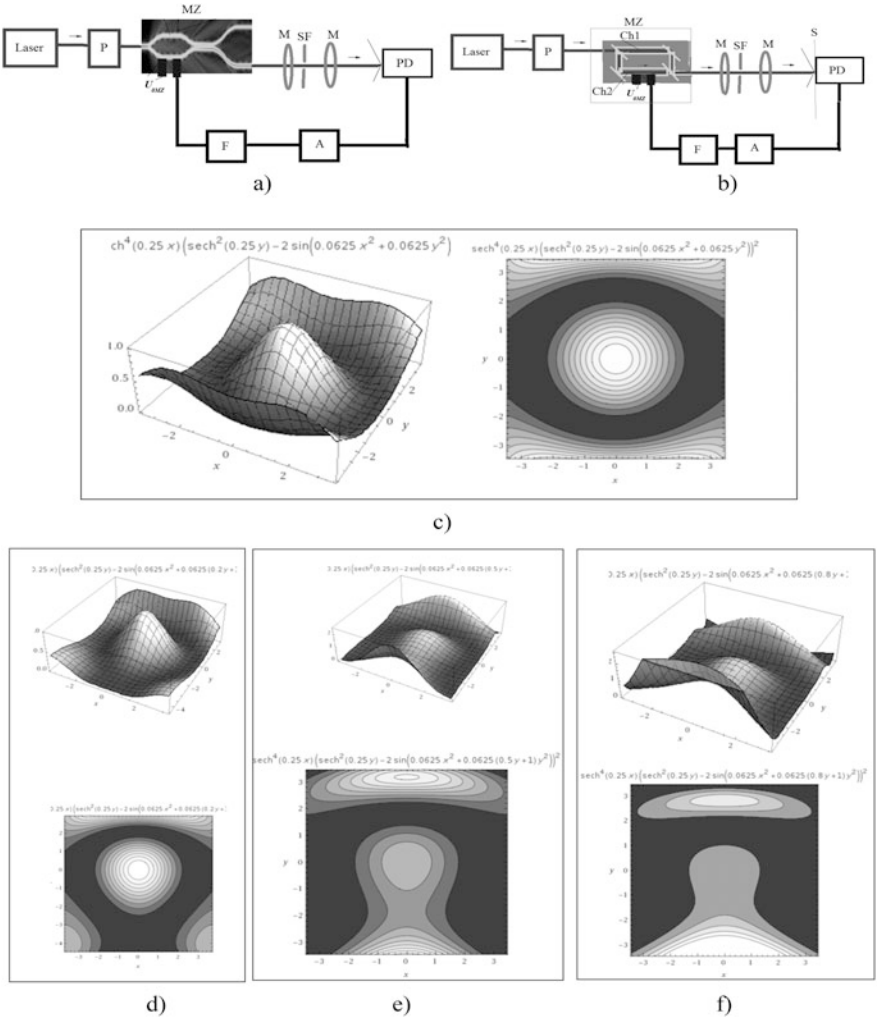

Fig. 7.5 The structure of OEO MZ on the base of Y- and X-optical couplers with the spatial filter SF (**a**), the structure of OEO MZ with dividing optical plates (mirrors) and the spatial filter SF (**b**). "M" is the lens. In (**c**–**f**) we see the spatial patterns of the amplitude squares of the electromagnetic field in the transverse section in the output of the MZ modulator after summation of two optical oscillations passed through OC-1 and OC-2 optical channels of MZ (**a**, **b**)

waveguide channels, the field pattern in the MZ output becomes asymmetric with redistribution of the field intensity from the main maximum to the side maxima.

Now we consider the injection strip laser (Fig. 7.6). The strip contact occupies the limited part and is equal l_1, approximately from 5 to 20 wavelengths of the laser emission. Mirrors are formed by the sheared facet ways of the crystal.

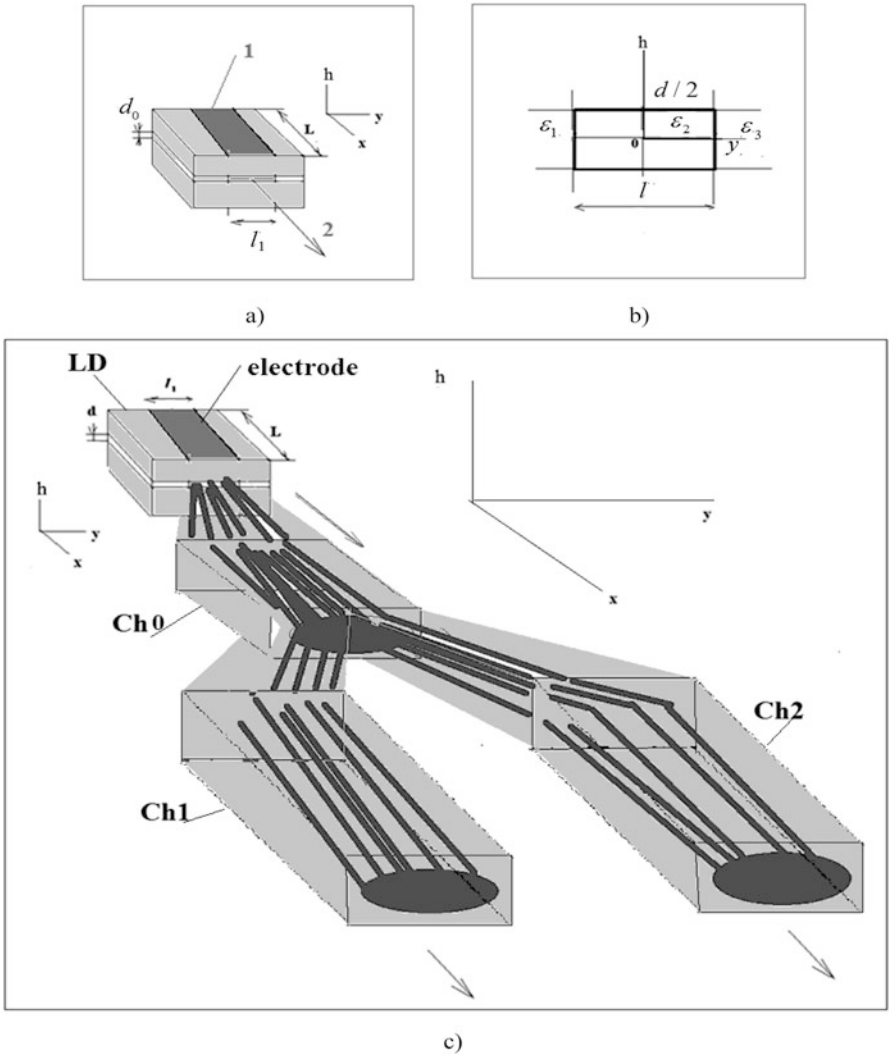

Fig. 7.6 The planar strip laser (**a**), the transverse laser section and the model of the waveguide (**b**). The electrode is the strip contact, d_0 is the thickness of the active layer (junction), L is the laser resonator length between mirrors, l_1 is the strip width, and l is the parameter of the layer width. The model of excitation of optical waveguide channel from the laser diode with optical channels Ch0, Ch1, Ch2 (**c**)

For calculation of the amplitude and phase profile on the laser front mirror (or the waveguide front), we make use by the wave equation solution, taking into account that the complex permittivity $\varepsilon(x, y)$ inside the resonator has the following form in the transverse section:

- Along the h axis:

$$\varepsilon(h) = \begin{cases} \varepsilon_1, h < -d_0/2 \\ \varepsilon_2, \ -d_0/2 < h < d/2\,, \\ \varepsilon_3, h > d_0/2 \end{cases} \tag{7.8}$$

The variation of the permittivity $\varepsilon(h, y)$ along the y axis can be specified in the form of the so-called "Epstein layer." Such a model describes at best the laser field in the near and far zones for injection lasers, if the emission beam has the "non-Gaussian" shape.

In the general case, the type of permittivity dependence is asymmetrical with respect to the x axis. The dielectric permittivity "from the left" and "from the right" is equal: $\varepsilon_1 = \varepsilon_3$ (Fig. 7.6b). The deviation from the constant value for the **symmetric distribution** of the dielectric permittivity $\varepsilon_{20} = \varepsilon_2(y = 0)$:

- Along the y axis:

$$\varepsilon(y) = \begin{cases} 0, y < -d/2 \\ \varepsilon_2(y) = \varepsilon_{20} + \dfrac{4(\varepsilon_{20} - \varepsilon_1)\exp(y/l)}{[1 + \exp(y/l)]^2}, \ -d/2 < h < d/2\,. \\ 0, y > d/2 \end{cases} \tag{7.9}$$

Approximations (Eq. 7.9) in the form of symmetrical distribution do not describe the nonsymmetric distribution of the permittivity $\varepsilon(y)$, which takes place in waveguide without the passive side restriction, when the light is emitted in the form of the non-Gaussian beam. QWLD in OEO is the so-called Lambertian source of the laser emission, which is caused by the laser optical resonator, which is formed by the plane-parallel mirrors.

7.2.1 Asymmetrical Distribution of the Permittivity

For description of *asymmetrical distribution* of the relative variation of the permittivity $\Delta\varepsilon(y) = \varepsilon_2(y) - \varepsilon_{20}(0)$, where $\varepsilon_2(y)$ is the function of the absolute value of the permittivity versus the coordinate y, $\varepsilon_{20}(0)$ are permittivity values for $y = 0$, where for the Epstein layer model for direction along the y axis the following approximation is specified:

$$\varepsilon_2(y) = \varepsilon_{20} + (\varepsilon_3 - \varepsilon_1)\frac{\exp(y/l)}{1 + \exp(y/l)} + 2(2\varepsilon_{20} - \varepsilon_1 - \varepsilon_3) \times \frac{\exp(y/l)}{[1 + \exp(y/l)]^2}, \tag{7.10}$$

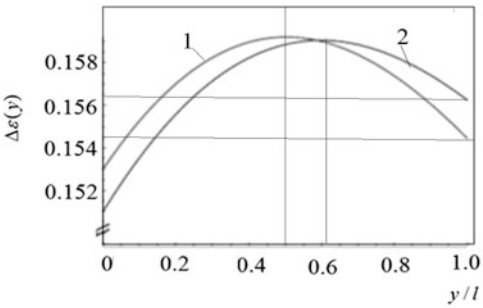

Fig. 7.7 The permittivity of the optical waveguide $\Delta\varepsilon(y) = \varepsilon_2(y) - \varepsilon_{20}(0)$ of the nonsymmetric type at $(\varepsilon_3 - \varepsilon_1) = 0.101, 2$ $(2\varepsilon_{20} - \varepsilon_1 - \varepsilon_3) = 0.41$ (curve 1); $(\varepsilon_3 - \varepsilon_1) = 0.111{,}2$ $(2\varepsilon_{20} - \varepsilon_1 - \varepsilon_3) = 0.382$ (curve 2), Functions are calculated by Eq. (7.10)

where l is the waveguide width (Fig. 7.6), $\varepsilon_{20} = \varepsilon_2(y = 0)$. Modes in the three-dimension structure with the two-dimension profile can be divided into modes of two types, namely, of the E_x type (with $E_y = 0$) and the E_y type (with $E_h = 0$).

The expression (Eq. 7.10) for nonsymmetrical distribution at $(\varepsilon_3 - \varepsilon_1) = 0$ transfers into the expression for the symmetrical distribution (Eq. 7.9).

Figure 7.7 presents plots depicted on Eq. (7.10), the permittivity of the optical waveguide $\Delta\varepsilon(y) = \varepsilon_2(y) - \varepsilon_{20}(0)$ of the nonsymmetric type for plots is:

1. At $(\varepsilon_3 - \varepsilon_1) = 0.101$, $2(2\varepsilon_{20} - \varepsilon_1 - \varepsilon_3) = 0.41$ (curve 1),
2. At $(\varepsilon_3 - \varepsilon_1) = 0.111$, $2(2\varepsilon_{20} - \varepsilon_1 - \varepsilon_3) = 0.382$ (curve 2).

If to find the solution in the form:

$$E_{x0}(h, y, z = x, t) = E_{x0}(h, y) \exp(-jqx - j2\pi\nu t), \tag{7.11}$$

with the complex propagation constant q, the wave equation for modes E_x will have the form:

$$\frac{\partial^2 E_h}{\partial h^2} + \frac{\partial^2 E_h}{\partial y^2} + \frac{\partial^2 E_h}{\partial z^2} + \left[k_0^2 \varepsilon(h, y) - q^2\right] E_h = 0, \tag{7.12}$$

where we rename the generally accepted coordinate along the emission propagation axis as $z = x$ (for utilization of generally accepted designations in the Euler function), $k_0 = 2\pi\nu_0/c$.

The equation for modes E_y is more complicate, since it contains the term depending on grad ln $\varepsilon(y)$. Therefore, we must be limited in consideration by modes E_x, for which the analytical solution can be presented. We can consider that in planar strip lasers, configurations of E_h and E_y along the y axis are identical.

Equation (7.12) is solved by the variables separation. The value q is mainly determined by the waveguide parameters along the x axis. Then assuming that

$$E_h(h, y) = E_{\mathrm{H}h}(h) \cdot E_{\mathrm{Y}h}(y), \tag{7.13}$$

we obtain [4]:

$$\frac{\partial^2 E_{\mathrm{H}h}}{\partial h^2} + \left[\varepsilon(h) + p^2 - q^2\right] E_{\mathrm{H}h} = 0, \tag{7.14}$$

$$\frac{\partial^2 E_{\mathrm{Y}h}}{\partial y^2} + \left[k_0^2 \Gamma_0 \varepsilon(h, y) - p^2\right] E_{\mathrm{Y}h} = 0, \tag{7.15}$$

where p is the complex constant of the variables separation, which plays the role of the wave propagation constant along the y axis, q is the wave propagation constant along the $z = x$ axis, Γ_0 is the coefficient of the optical restriction (for simplicity we assume that it is 0.5). Multiplying Eq. (7.14) by $[E_{\mathrm{H}h}(h)]^2$ and integrating over h, we obtain the equation (7.15). For the optical waveguide along the h axis (or for the laser in perpendicular direction to the plane of the p-n junction (along the h axis)), the solutions of the equation (7.14) has the form:

$$E_{\mathrm{H}h}(h) = \begin{cases} 0.5 \cdot B_0 \cdot \exp(rh), h < -d_0/2 \\ 0.5 \cdot \cos(qh + \varphi), -d_0/2 < h < d_0/2, \\ 0.5 \cdot A_0 \cdot \exp(-\gamma h), h > d_0/2 \end{cases} \tag{7.16}$$

Parameters r,γ, and coefficients A_0 and B_0 are determined from the condition of the function $E_{\mathrm{H}h}(h)$ continuity on boundaries. Further, for simplicity, we designate $E_{\mathrm{Y}h} = E_{\mathrm{Y}}$.

For the direction parallel to the plane of the p-n junction (for the optical waveguide along the y axis), we write the equation (7.15) as:

$$\frac{1}{k_0^2 \Gamma_0} \cdot \frac{\partial^2 E_{\mathrm{Y}}}{\partial y^2} + \varepsilon(y) E_{\mathrm{Y}} = \frac{p^2}{k_0^2 \Gamma_0} E_{\mathrm{Y}}. \tag{7.17}$$

Then, for the main mode in the nonsymmetrical waveguide [5, 6], we have the distribution in the strength of the EMF obtained from the solution of the waveguide equation. The **solution** for the main mode $E_{\mathrm{Y}0}(y)$ can be written as:

$$E_{\mathrm{Y}0}(y) = E_{00} \cdot \frac{\exp(a_0 y/l)}{[\mathrm{ch}(y/l)]^{S_0}} P_0^{S_0 - a_0, S_0 + a_0}[-\mathrm{th}(y/l)], \tag{7.18}$$

where E_{00} is the normalized constant. Here there is the Jakobi polynomial of the zero order: $P_0^{S_0 - a_0, S_0 + a_0}[-\mathrm{th}(y/2l)] = 1$, the asymmetry parameter is

$$a_0 = \frac{(2\pi\nu)^2 \frac{l}{c^2} \Gamma_0}{S_0} (\varepsilon_3 - \varepsilon_1). \tag{7.19}$$

It is necessary to be especially attentive when choosing of the S_0 parameter, which is complex in the general:

$$S_0 = S_{01} + jS_{02} \tag{7.20}$$

and is determined from the relation:

$$S_0 = 0.5\left[-1 \pm \sqrt{1 + 8(2\pi\nu)^2 \frac{l^2}{c^2}\Gamma_0(2\varepsilon_2 - \varepsilon_1 - \varepsilon_3)}\right]. \tag{7.21}$$

In this formula, the sign "+" corresponds to the case $\varepsilon_2 \geq$ Re ε_1, $\varepsilon_2 \geq$ Re ε_3, when the waveguide properties are caused by the real part of the permittivity, the sign "−" corresponds to the case, when the real part corresponds to the anti-waveguide effect and the waveguide properties of the structure are supported owing to the amplification, i.e., due to the contribution of the imaginary part of ε_2 (Im$\varepsilon_2 < 0$).

7.2.2 The Field in the Near Zone for the Main Mode

The field in the near zone for the fundamental zone is given by the expression:

$$E_{Y0}(y) = E_0(y)\exp\left[j\Phi(y)\right], \tag{7.22}$$

where $E_0(y)$ is the amplitude, $\Phi(y)$ is the phase of the EMF strength. At that, for the main mode in the ***symmetric*** case ($\varepsilon_3 = \varepsilon_1$ and therefore $a_0 = 0$), we obtain formulas as:

$$E_0(y) = \frac{E_{00}}{[\mathrm{ch}(y/l)]^{S_{01}}} = \frac{E_{00}}{[0.5\exp(y/l) + 0.5\exp(-y/l)]^{S_{01}}}, \tag{7.23}$$

$$\Phi(y) = S_{02}\ln[\mathrm{ch}(y/l)] = S_{02}\ln\{[0.5\exp(y/l) + 0.5\exp(-y/l)]\}, \tag{7.24}$$

where $E_{00} = E_0(y = 0)$, the function of the hyperbolic cosine is equal to:

$$\mathrm{ch}(y/2l) = 0.5\cdot[\exp(y/2l) + \exp(-y/2l)]. \tag{7.25}$$

Figure 7.8 shows the function of the amplitude $E_0(y)$ (Eq. 7.23) and the phase $\Phi(y)$ (Eq. 7.24) in the near zone. From Fig. 7.8, we see that the variation of the phase $\Phi(y)$ in the near zone varies by almost two radians from its maximal value in the center for the symmetric waveguide.

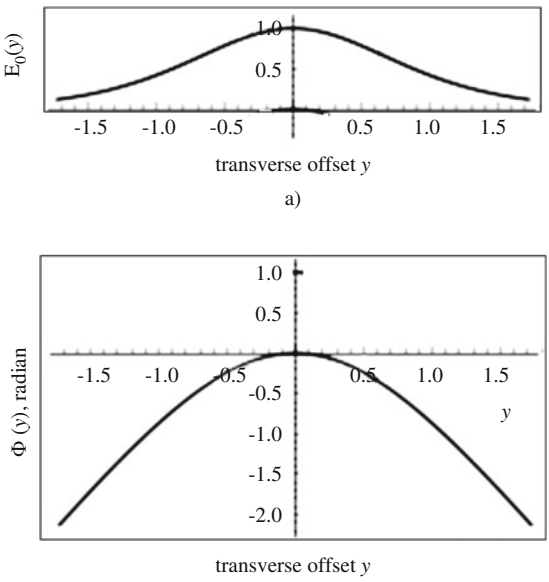

Fig. 7.8 Functions of the amplitude $E_0(y)$ (**a**) and the phase $\Phi(y)$ (**b**) of the field strength in the *near zone* versus the transverse offset y for $S_0 = S_{01} + jS_{02}$ at $S_{01} = 2$, $S_{02} = 2$

7.2.3 The Model of the Nonsymmetric Waveguide

For the strength for the main field mode, for **nonsymmetric** waveguide ($\varepsilon_3 \neq \varepsilon_1$ and therefore $a_0 \neq 0$), we obtain the following formula:

$$E_{Y0}(y) = \frac{E_{00} \exp(a_0 y/l)}{[\mathrm{ch}(y/l)]^{S_{01}+jS_{02}}}. \tag{7.26}$$

The expression (Eq. 7.26) we normalize on E_{00} and take the logarithm, taking into account Eq. (7.27), and as a result, we have:

$$\ln[E_{Y0}(y)/E_{00}] = \left\{ \left[(a_0 y/l) - S_{01} \ln[\mathrm{ch}(y/l)]^2 + \{S_{02} \ln[\mathrm{ch}(y/l)]\}^2 \right] \right\}^{1/2} \times \exp\left(j \arctan \frac{S_{02} \ln[\mathrm{ch}(y/l)]}{[(a_0 y/l) - S_{01} \ln[\mathrm{ch}(y/l)]}. \right. \tag{7.27}$$

Thus, the expression (Eq. 7.27) can be presented as:

$$\ln(E_{Y0}/E_{00}) = E_{LN00}(y) \cdot \exp[\, j\Phi_{LN}(y)], \tag{7.28}$$

Here in Eq. (7.28) we use the expression for the normalized amplitude mentioned in Eq. (7.28):

$$E_{\mathrm{LN00}}(y) = \left\{(a_0 y/l) - S_{01}\ln\left[\mathrm{ch}(y/l)\right]^2 + \left\{S_{02}\ln\left[\mathrm{ch}(y/l)\right]\right\}^2\right\}^{1/2} \tag{7.29}$$

and the phase mentioned in Eq. (7.28):

$$\Phi_{\mathrm{LN}}(y) = \arctan\frac{S_{02}\ln\left[\mathrm{ch}(y/l))\right]}{(a_0 y/l) - S_{01}\ln\left[\mathrm{ch}(y/l)\right]}. \tag{7.30}$$

The field in the far zone (at distance, which essentially exceeds the laser wavelength) for the main mode is:

$$E_{\mathrm{YL0}}(\theta) = \int_{-\mathrm{oo}}^{+\mathrm{oo}} E_{\mathrm{Y0}}(y)\exp\left(-jk_0 y\sin\theta\right)\mathrm{dy}. \tag{7.31}$$

The field in the far zone for the main mode is determined by the formula:

$$E_{\mathrm{YL0}} = E_{\mathrm{YL00}}\cdot\Gamma\left(\frac{S_{01}+jS_{02}-a_0}{2}+jk_0 l\sin\theta\right) \cdot\Gamma\left(\frac{S_{01}+jS_{02}+a_0}{2}-jk_0 l\sin\theta\right), \tag{7.32}$$

where $\Gamma(x + jy)$ is the Euler gamma-function.

The distribution of the field **intensity** is, accordingly, determined by formulas:

- In the near zone (when the module of the longitudinal coordinate $|x|$ is approximately equal to the width l of the emission source $|x| \approx l$):

$$I_{\mathrm{Y0}}(y) = |E_{\mathrm{Y0}}(y)|^2, \tag{7.33}$$

- In the far zone (or at $|x| \gg l$):

$$I_{\mathrm{Y0}}(y) = \cos\theta\cdot|E_{\mathrm{YL0}}(y)|^2. \tag{7.34}$$

The Euler gamma-functions $\Gamma(x + jy)$ has the symmetric distribution [7].

The Euler function $\Gamma(x + jy)$ at decreasing (at $x < 0$) monotonically increases; at $x > 0$ this function has clearly expressed resonant spatial maxima (in the far zone at $|x| \gg l$). Center of maxima are located on the optical axis at the zero transverse offset $y = 0$. In our case, the offset for x corresponds to the longitudinal offset along the optical axis from the emission source.

In Fig. 7.9, we see the square module $|E_{\mathrm{YL0}}(x)|^2$ and the argument $\mathrm{Arg}[E_{\mathrm{YL0}}(x)]$ of the EMF strength for the function (Eq. 7.32).

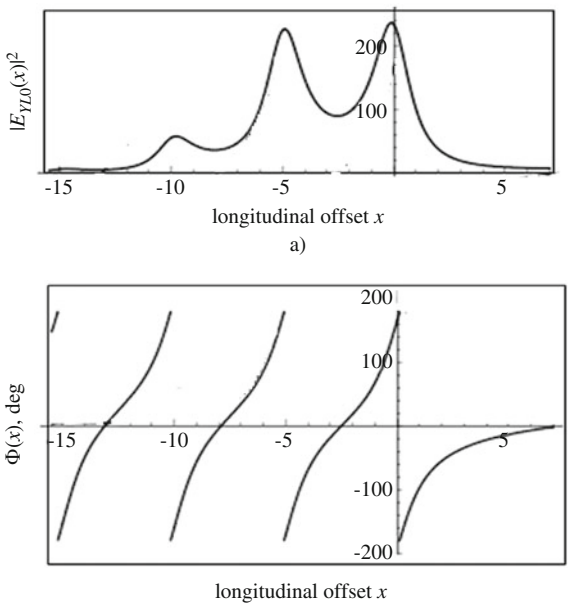

Fig. 7.9 Dependences upon the longitudinal offset x for the symmetric case ($a_0 = 0$) in the far zone of the module $|E_{YL0}(x)|^2$ and the argument $\mathrm{Arg}[E_{YL0}(0.2x)]$ of the function (Eq. 7.32) at $\sin\theta = 0$, $a_0 = 0$, $S_{01} = 0.4$, $S_{02} = 0.4$

Alternation of maxima and minima (Fig. 7.9) at the longitudinal offset on x in the far zone from the emission source emphasizes the fact of adding of optical oscillations with different phase shifts. This result of the spatial interference field pattern is true for the source, which has the finite dimensions of the emitting area. The special attention we would like to attract to the dependence of the phase upon the longitudinal offset.

7.2.4 *Plots of the Symmetric Distribution of the Field in the Far Zone*

Let us examine the plots in Figs. 7.10 and 7.11 of the symmetric distribution at $a_0 = 0$ of the module $|E_{YL0}(x)|^2$ and the argument $\mathrm{Arg}[E_{YL0}(0.2x)]$ of the function (Eq. 7.36) in the far zone.

The region of values S_{01}, S_{02}, when practically all laser emission in the far zone is concentrated in the single of double lobes of the directional pattern, has a special interest in Fig. 7.10. The lobe position varies with S_{02} variation. The plots of the phase variations $\Phi_{YL0}(y)$ of the optical emission are presented with the special practical interest for OEO. Phase deviations from the "central value" are at $S_{01} = -0.8$, $S_{02} = 0.4$ about 10°, while in the case of double-lobe mode at $S_{01} = 0.2$, $S_{02} = -1$, the phase deviation is more than 150°. At values $S_{01} = 0$,

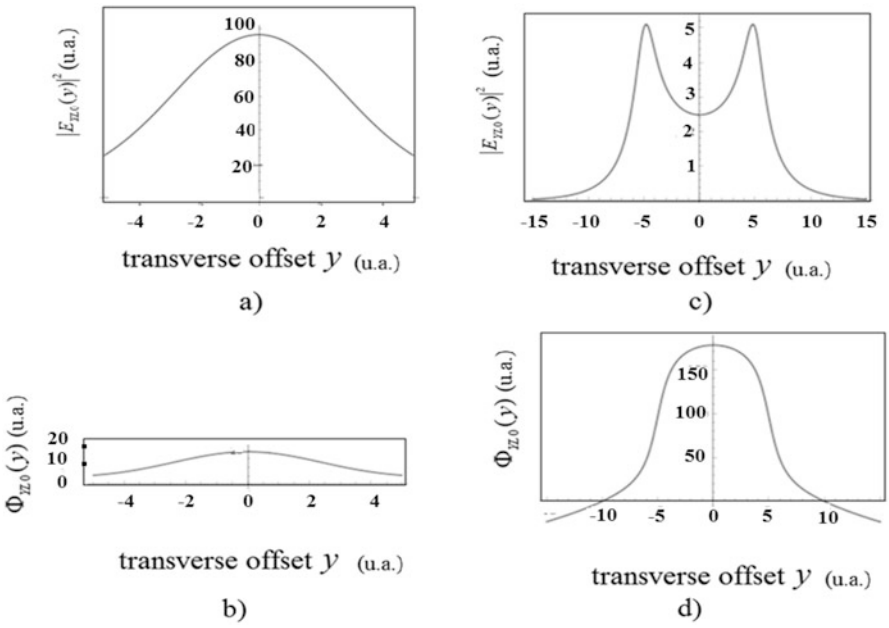

Fig. 7.10 Functions of the module $|E_{YL0}(y)|^2$ and the argument $\Phi_{YL0}(y) = \mathrm{Arg}[E_{YL0}(y)]$ for the *symmetric* case ($a_0 = 0$) in the far zone of the function (Eq. 7.32) at $y = k_0 l \sin\theta$ for (**a**, **b**): $S_{01} = -0.8$, $S_{02} = 0.4$, $a_0 = 0$; for (**c**, **d**): $S_{01} = 0.2$, $S_{02} = -1$, $a_0 = 0$

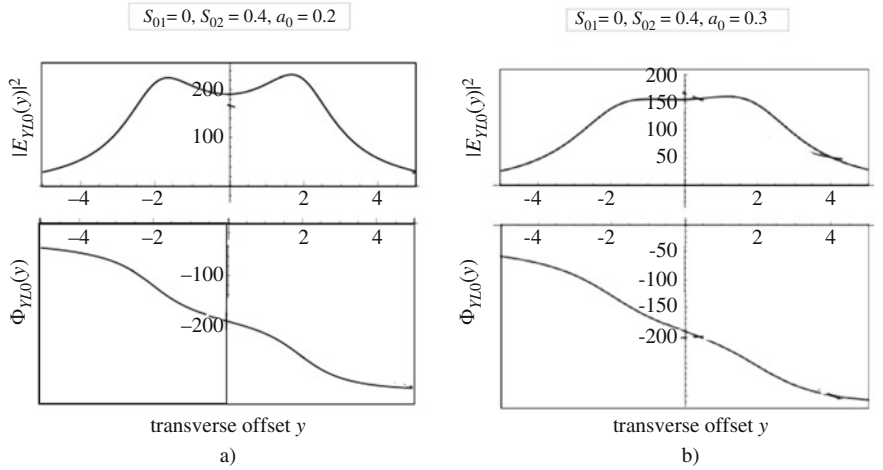

Fig. 7.11 Functions of the module $|E_{YL0}(y)|^2$and the phase $\Phi_{YL0}(y) = \mathrm{Arg}[E_{YL0}(y)]$ of the function (Eq. 7.32) in the far zone at nonsymmetrical distribution ($a_0 \neq 0$) versus the transverse offset $y = k_0 l \sin\theta$ at (**a**) $S_{01} = 0$, $S_{02} = 0.4$, $a_0 = 0.2$, (**b**) $S_{01} = 0$, $S_{02} = 0.4$, $a_0 = 0.3$

$S_{02} = 0.4$, $a_0 = 0$, the double-lobe character of the directional pattern becomes more expressed.

7.2.5 *Plots of the Nonsymmetric Distribution of the Field in the Far Zone*

The case of the nonsymmetric distribution of the permittivity has the specific interest for practical application. Figure 7.11 shows the functions of the module $|E_{YL0}(y)|^2$ and the phase $\Phi_{YL0}(y) = \text{Arg}[E_{YL0}(y)]$ of the function (Eq. 7.32) in the far zone at nonsymmetric distribution ($a_0 \neq 0$) at the transverse offset $y = k_0 l \sin\theta$.

We should note (Figs. 7.12 and 7.13) that deviations of the symmetry parameter a_0 of waveguide channels $a_0 = 0.2$, $a_0 = 0.3$ from the zero values leads not only to deviations of the module $|E_{YL0}(y)|^2$ maximum from the axis of $y = k_0 l \sin\theta = 0$, but to the significant deviations of the phase $\Phi_{YL0}(y) = \text{Arg}[E_{YL0}(y)]$. At that, the phase difference between minimal and maximal values varies from 60° to 120°, relatively, at $a_0 = 0.2$ and $a_0 = 0.3$.

7.2.6 *3D Plots of Symmetrical and Nonsymmetrical Field Distribution in the Far Zone*

Functions at symmetrical ($a_0 = 0$) distribution of the module $|E_{YL0}(x, y)|^2$ for the double-lobe laser directional pattern in the far zone are presented in Fig. 7.13. We see 3D picture (plots (a–c)), which are calculated from Eq. (7.32) at transverse offset $y = k_0 l \sin\theta$ for parameters $S_{01} = 0.2 \cdot x$, $S_{02} = -0.2$. For the symmetric case $a_0 = 0$, the pictures are presented in Fig. 7.16a, b for different scales. Figure 7.16c shows 3D picture for the nonsymmetrical case for parameters $S_{01} = 0.2 \cdot x$, $S_{02} = -0.2$.

Figure 7.13 shows possibilities of fields modeling for the complex physical phenomena in lasers and coupled waveguides. We use the developed theoretical model of the emission source with the finite dimensions of the emission area. The case of the laser double-lobe pattern is examined. In the region of values at $x = 5$, the beginning of the first maximum formation is observed, while in the region of values $x = -10$, the second maximum is observed and at $x = -15$: the small third maximum. If the symmetry parameter is not equal to zero, in the plot of the contour lines (Fig. 7.13e), the asymmetric turn of the pedestal by the angle of 30° is observed.

The functions of $|E_{YL0}(x, y)|^2$ (a) and $\Phi_{YL0}(y) = \text{Arg}[E_{YL0}(y)]$ (b) in 3D depiction calculated, and their contour lines of the function (Eq. 7.32) calculated for the **nonsymmetric** waveguide at dependence of asymmetry parameters from x or $a_0 = 0.2 \cdot x$ at $S_{01} = 0.4$, $S_{02} = 0.4$, $|E_{YL00}|^2 = 0.0001$.

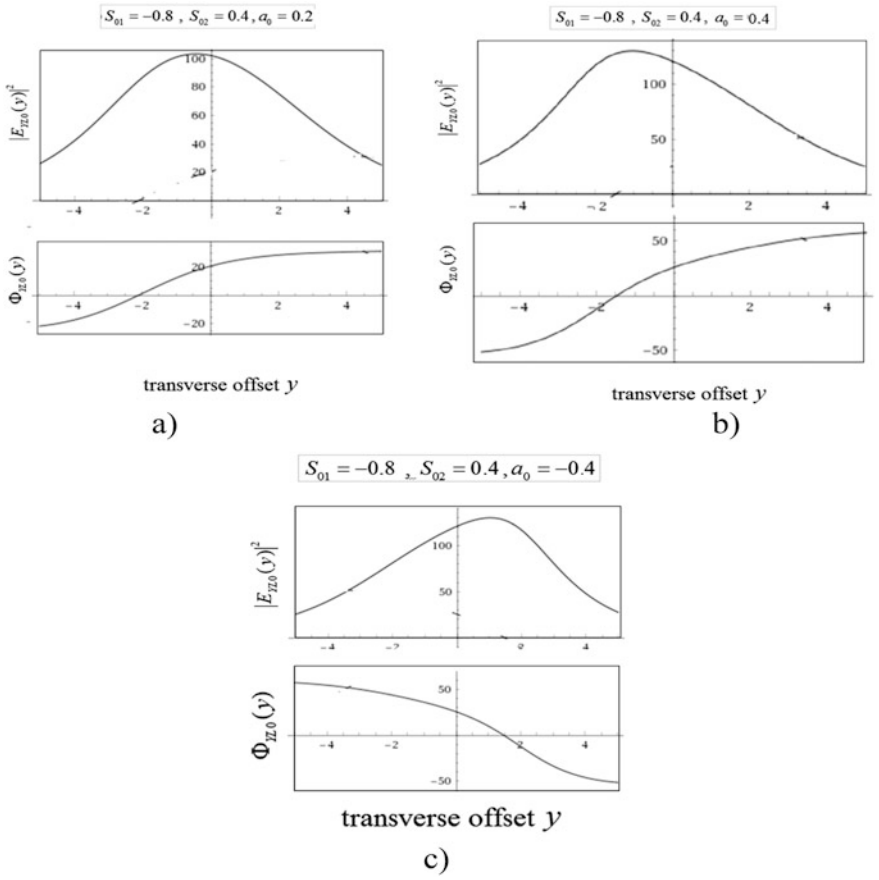

Fig. 7.12 Functions of the module $|E_{YL0}(y)|^2$ and the phase $\Phi_{YL0}(y) = \text{Arg}[E_{YL0}(y)]$ of the function (Eq. 7.32) in the far zone at nonsymmetrical distribution ($a_0 \neq 0$) versus the transverse offset $y = k_0 l \sin\theta$ at (**a**) $S_{01} = -0.8$, $S_{02} = 0.4$, $a_0 = 0.2$, (**b**) $S_{01} = -0.8$, $S_{02} = 0.4$, $a_0 = 0.4$, (**c**) $S_{01} = -0.8$, $S_{02} = 0.4$, $a_0 = -0.4$

In the case of the nonsymmetrical waveguide for dependence of the nonsymmetry parameter on x (Fig. 7.14), as $a_0 = 0.2 \cdot x$, two main maxima turn to the angle of 45°. In Fig. 7.14b, in plots of 3D patterns for $\Phi_{YL0}(y) = \text{Arg}[E_{YL0}(y)]$, we see the regions of decrease and increase of the phase, as well as the regions of the phase function breaks in the region of the local maxima. The complicate character of lines with formation of resonance regions is determined by adding conditions of the optical oscillations in the far zone from the source with the finite dimensions of the emission area.

The above-described theory of passive and active waveguides with account of the nonsymmetry of optical channels allows development of the mathematical instrument for modeling of waveguides in modulators and in differential delay lines, which are used in OEO OEO MZ and OEO DM.

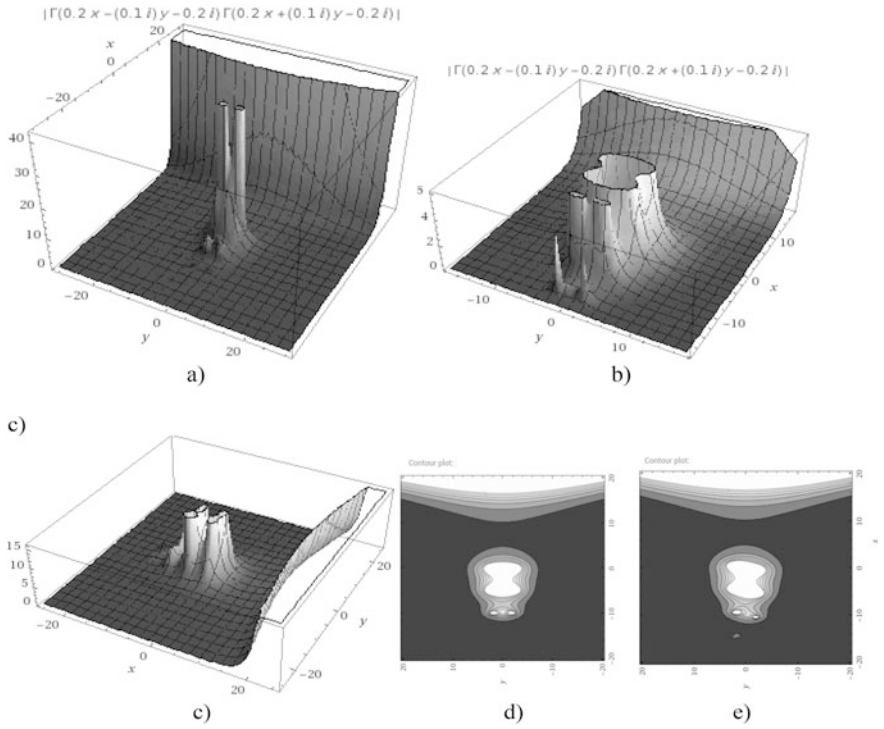

Fig. 7.13 Functions in the far zone at **symmetric** $a_0 = 0$ and **nonsymmetric** $a_0 = 0.2$ distribution of the module $|E_{YL0}(x, y)|^2$ (3D plots (**a**–**c**)) on the expression (Eq. 7.32) versus the transverse section $y = k_0 l \sin\theta$. In (**d**) and (**e**), plots of the contour lines are presented, which are depicted on Eq. (7.32) $|E_{YL0}(x, y)|^2$ for symmetric case at parameters $S_{01} = 0.4 \cdot x$, $S_{02} = -0.4$, $a_0 = 0$ (**d**) and nonsymmetric case for $S_{01} = 0.4 \cdot x$, $S_{02} = 0.4$, $a_0 = 0.2$ (**e**). Depiction is performed for parameters $S_{01} = 0.4 \cdot x$, $S_{02} = -0.4$, $a_0 = 0$ (**a**) and (**b**) for different scales. For nonsymmetric case $S_{01} = 0.4 \cdot x$, $S_{02} = 0.4$, $a_0 = 0.2$ (**c**) and (**e**)

7.2.7 *The Model of Nonsymmetrical Waveguides in MZ Optical Channels*

The above-considered theoretical model is used for mathematical modeling of fields in passive nonsymmetrical waveguides. The permittivity is specified by the expression (Eq. 7.9), and the geometrical dimensions in the waveguide transverse section are shown in Fig. 7.6b, c. For calculation of the field in the waveguide transverse section in the near field, we used the expression (Eq. 7.32). Two nonsymmetrical optical waveguides Ch1 and Ch2 were excited in the input by the source with finite dimensions.

In waveguides Ch1 and Ch2, relatively, two oscillations propagated, which correspond to expression (Eq. 7.2) and had the following spatial coordinates: $E_{1L}(t, h, y, x) = |E_{1L}(h, y, x)| \cos[2\pi\nu \cdot t + \varphi_{0L1}(h, y, x)]$; and with phase shift $\pi/2$

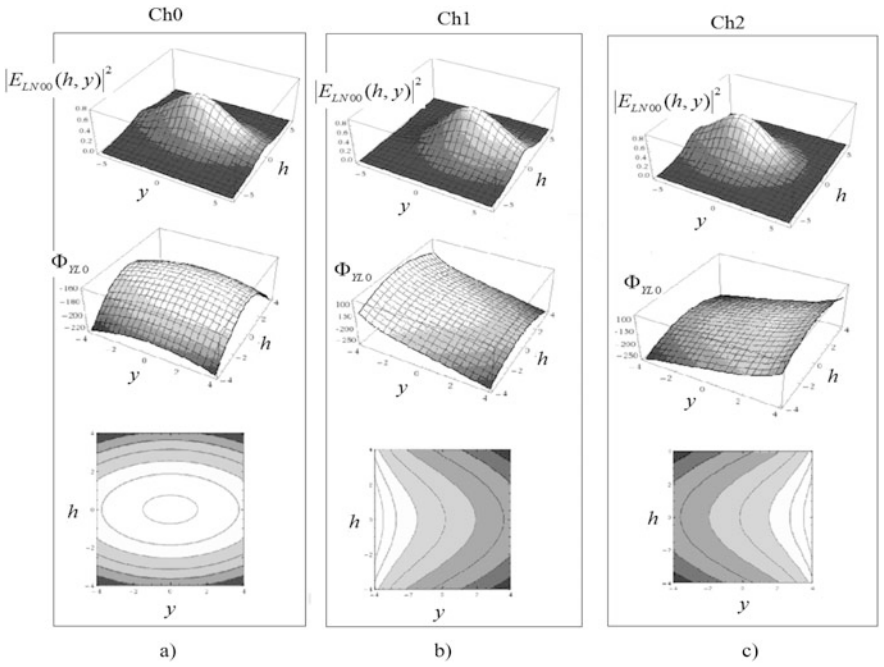

Fig. 7.14 Functions $|E_{\mathrm{LN00}}(h,y)|^2$, $\Phi_{\mathrm{YL0}} = \mathrm{Arg}[E_{\mathrm{LN00}}(h,y)]$ and contour lines for the phase Φ_{YL0} calculated by expressions (Eqs. 7.26–7.30) for **symmetric** waveguide Ch0 (**a**), **nonsymmetric** waveguides of the first Ch1 (**b**) and the second Ch2 (**c**) MZ optical channels excited in the input by the symmetric source with finite dimensions or the symmetric waveguide of the optical channel Ch0 (**a**). The excitement circuit of Ch0, Ch1, Ch2 is presented in Fig. 7.6

$E_{2\mathrm{L}}(t,h,y,x) = |E_{2\mathrm{L}}(h,y,x)|\cos[2\pi\nu \cdot t + \varphi_{0\mathrm{L}2}(h,y,x) + \pi/2]$. The symmetry parameter a_0 of the single waveguide, in which the oscillation $E_{1\mathrm{L}}(t,h,y,x)$ propagates, was $a_0 > 0$, while the second waveguide, in which oscillation $E_{2\mathrm{L}}(t,h,y,x)$ propagates, was $a_0 < 0$. Figure 7.14 shows the functions of the module $|E_{\mathrm{LN00}}(h,y)|^2$ (a) and the argument $\Phi_{\mathrm{YL0}}(y) = \mathrm{Arg}[E_{\mathrm{LN00}}(h,y)]$ calculated from expressions (Eqs. 7.26–7.30) for **nonsymmetrical** waveguides of the first and second optical channels excited in the input by symmetrical source with finite dimensions (the waveguide Ch0).

It is necessary to note that 3D plots and contour lines presented in Fig. 7.14 are well agreed with plots presented in Fig. 7.15. We see that deviations of the symmetry parameter a_0 of waveguide channels $a_0 = 0.2y$, $a_0 = -0.2y$ from the zero value leads not only to deviations of the module $|E_{\mathrm{YL0}}(y)|^2$ maximum from the $y = 0$ axis for $a_0 = 0.2y$ to the right from optical axis ($y = 0$), and for $a_0 = -0.2y$ to the left from the left from the optical axis ($y = 0$).

In 3D plots for the phase $\Phi_{\mathrm{YL0}}(y) = \mathrm{Arg}[E_{\mathrm{LN00}}(x,y)]$, we can see the significant phase deviation in the y coordinate. The phase difference between minimal and maximal values is up to 120°. In different optical channels Ch1 and Ch2, the negative and positive slope takes place in the y coordinate.

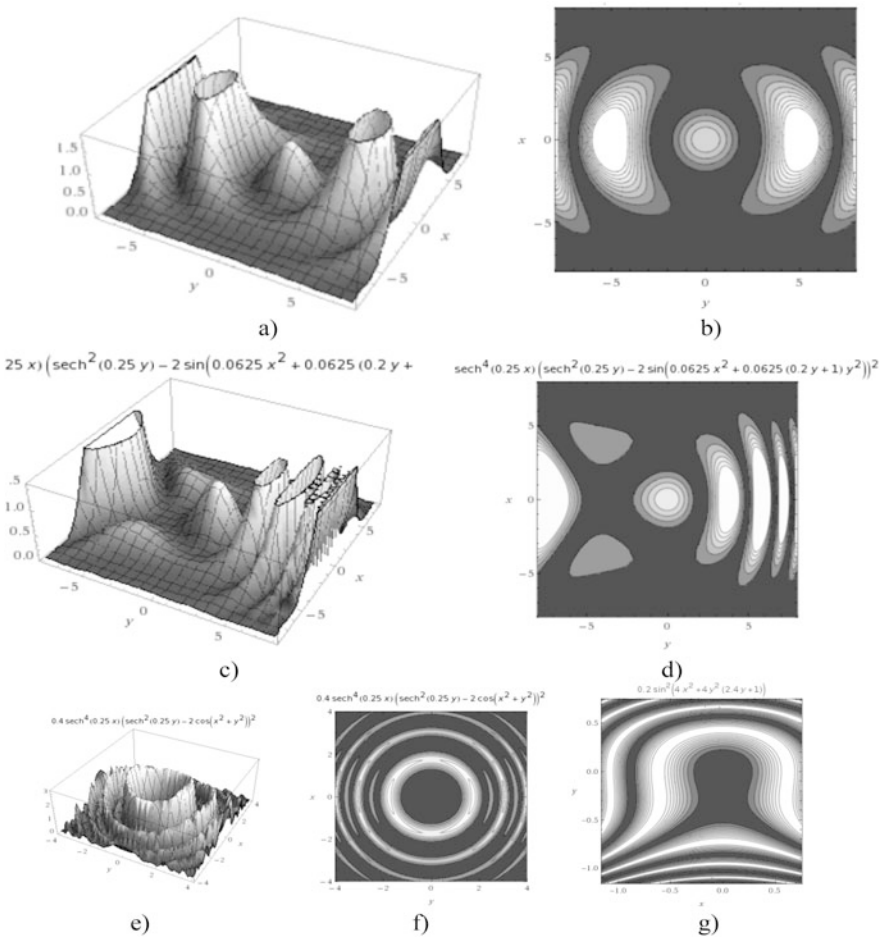

Fig. 7.15 Functions of the module $|E_{SLN00}(h,y)|^2$(**a**, **c**, **e**) and contour lines calculated from Eqs. (7.26–7.30) for **symmetric** (**a**, **b**) and **nonsymmetric** waveguides (**c**, **d**) of the first and second optical channels Ch1, Ch2 (**a**–**d**), which correspond to oscillation $E_{1L}(t,h,y,x)$ and $E_{2L}(t,h,y,x)$ adding in the in-phase or the quadrature modes. Figures (**e**, **f**, **g**) correspond to oscillations adding in out-of-phase or in the "non-quadrature" mode

Variation of phase function Φ_{YL0} due to the optical channels nonsymmetry leads at oscillations adding $E_{1L}(t,h,y,x)$ and $E_{2L}(t,h,y,x)$ in the near and far zones in the optical channel output to the symmetry disturbance and to formation of additional local maxima and minima.

The oscillations adding result depends upon phase distributions $\Phi_{1L}(h,y)$ and $\Phi_{2L}(h,y)$ and amplitude distributions $\mathbf{E}_{1L}(h,y) = E_{1L}(h,y)\ \exp\ [j\Phi_{1L}(h,y)]$ and $\mathbf{E}_{2L}(h,y) = E_{2L}(h,y)\ \exp\ [j\Phi_{2L}(h,y)]$ of values in the transverse section and is determined by expressions: $|E_{SLN00}(h,y)|^2 = \left|\mathbf{E}_{1L}^2(h,y) + \mathbf{E}_{2L}^2(h,y)\right|^2$.

One of pictures of the oscillations $E_{1L}(t, h, y, x)$ and $E_{2L}(t, h, y, x)$ adding result in the far zone is presented in Fig. 7.15. Here functions of the module $|E_{SLN00}(h, y)|^2$ and the contour lines calculated from Eqs. (7.26–7.30) are presented for **symmetric** waveguides (Fig. 7.15 a, b) and **nonsymmetric** waveguides (Fig. 7.15 c, d) of the first and second optical channels Ch1, Ch2.

From Fig. 7.15 we see that the symmetry disturbance in the optical channels Ch1, Ch2 leads to the main maximum offset (Fig. 7.15c, d); the side components from the right side from the main maximum increase by several times. At oscillations $E_{1L}(t, h, y, x)$ and $E_{2L}(t, h, y, x)$ adding in out-of-phase or in "non-quadrature" mode (Fig. 7.15e–g) for the case of nonsymmetric adding (Fig. 7.15g), the interference rings undergo the strong distortions with the nonuniform intensity redistribution over the perimeter of interference rings.

7.2.8 *OEO as the Correlator with Utilization of Spatial Filtering*

The structure of OEO MZ presented in Fig. 7.5 contains the spatial filter SF, which is intended for suppression improvement of the DC component of the optical carrier. Application of spatial filters in OEO for improvement of the oscillations' quality is the promising direction in OEO investigations. In this case, we use methods of adaptive optics, Fourier transforms, and the spatial correlation analysis.

The OEO MZ structure presented in Fig. 7.5 can be considered as the coherent optical processor [8] or as the spatial correlator with utilization of spatial filtering. In OEO, we can perform the convolution operations not only in optical and RF ranges, but the spectra convolution operation over spatial frequencies. As the spatial filters, we can use the miniature circular and sector spatial filters, which are well studied in publications on the Fourier optics.

In the perspective, we may think about researches on a suppression of the DC component of laser emission in OEO, on equalization of the optical phase in the transverse section, on correction of the image symmetry on the PD area with utilization of the nanotechnology innovations. On the one hand, the further investigations are required for new methods of spatial filtering of QWLD emission in OEO MZ (Fig. 7.5) for improvement of PSD of the phase noise. On the other hand, OEO is used as a device for the spatial correlation analysis of objects with application of matched filtering at the RF exact indication.

7.3 OEO DM Analysis on the Base of Abbreviated Differential Equations

7.3.1 Structures of OEO DM and Features of OEO Operation with the Direct LD Modulation with Coherent Optical Self-Heterodyning

Let us examine OEO with the direct amplitude modulation of the laser diode. Let the laser be the high-coherent source of stimulated optical emission, i.e., the spectral line width of laser emission $\Delta\nu_L$ is much less than the nominal (reference) operation frequency f_0 of the microwave subcarrier: $\Delta\nu_L \ll f_0$. We assume that the pumping current of the laser diode $J_{1L}(t)$, besides the DC bias I_{0L} of the operating point on the static watt–ampere modulation characteristic of QWLD, has the additive harmonic RF component $J_{1L}(t) = J_{10L} \cos(2\pi ft + \varphi_0)$ with the frequency f, the initial phase φ_0 and the relatively small amplitude $J_{10L} < J_{0L} - J_{thr}$, where J_{thr} is the threshold LD pumping current, the exceed of which leads to the QWLD soft excitation and settling of the steady-state generation mode of quasi-harmonic stimulated laser emission in the near infra-red (IR) range. In the laser output, in such a small-signal mode of optical modulation, the stimulated weakly modulated emission is formed. This optical emission represents (in the amplitude spectrum) the sum of three harmonic optical carriers, which frequencies are relatively, $\nu_1 = \nu_0 - f_0$, $\nu_2 = \nu_0$, $\nu_3 = \nu_0 - f_0$.

Two of these optical frequencies ν_1 and ν_2 are separated from the central laser optical frequency ν_0 by the subcarrier frequency f_0. Now we consider the different functional structures of OEO with direct modulation of LD emission (Fig. 7.16).

In the structure in Fig. 7.16, the following elements (closed in the loop) are included: the laser diode; FOS, for example, on the base of the single-mode low-dispersive optical fiber; the photodetector, for instance, *p-i-n*–photodiode; the nonlinear wideband low-noise amplifier (NA); the narrowband RF filter (F), for example, on the base of the solid-state dielectric resonator and the directional coupler C.

7.3.2 Quantum-Well Laser Diode in OEO DM

Appearance in the market of the ultra-wideband mesa-strip quantum-well laser diodes, which have the modulation frequency band of RF signal up to 12 GHz, opens the great perspectives for their application not only in systems for information transmission, but for development of the new class of devices: stabilized in the radio-frequency oscillators with the fiber-optical delay line operating in the microwave range, as well as for development of phased fiber-optical lines for the microwave subcarrier transmission.

For creation of such devices, in which the information about the phase of the transmitting sine radio signal in the microwave range plays the important and

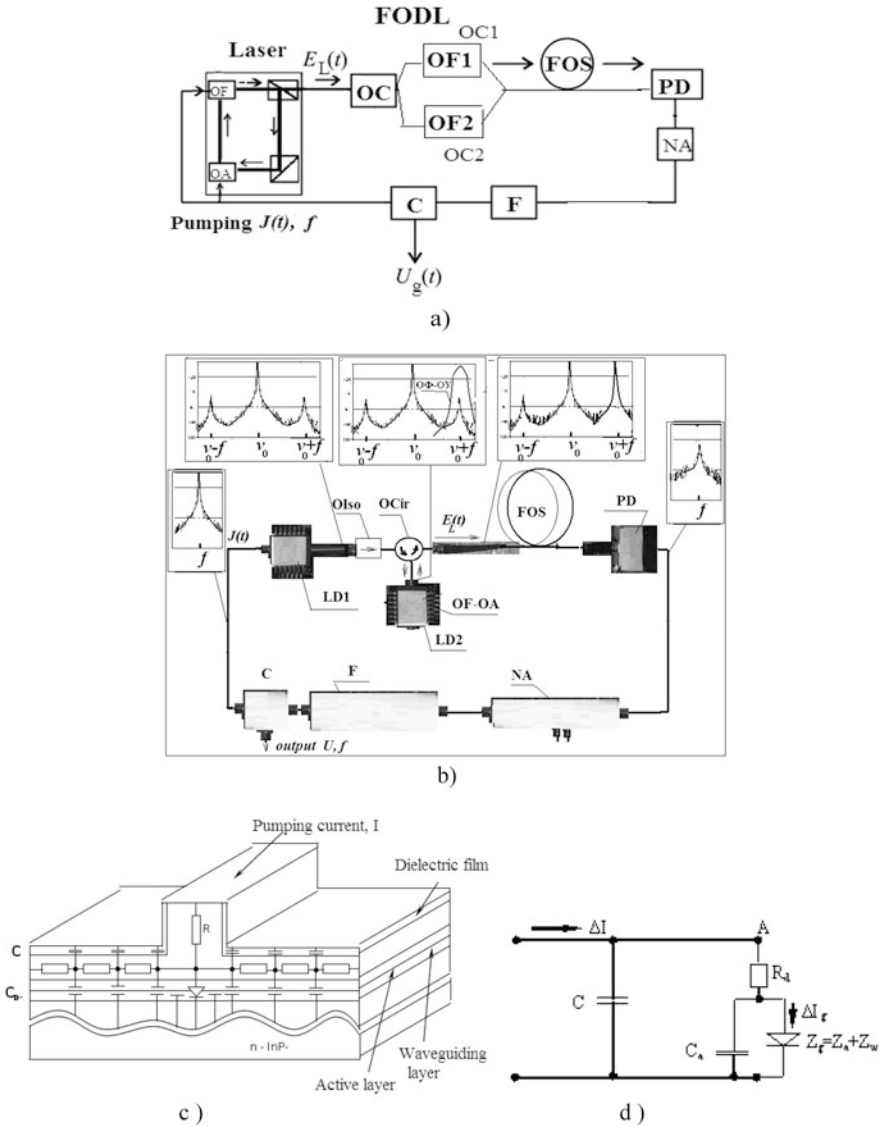

Fig. 7.16 The structural diagram of OEO DM (**a**) with the direct modulation of the laser diode with suppression by the optical filter OF1 of the one from optical carriers $\nu_1 = \nu_0 - f_0$, $\nu_2 = \nu_0$, $\nu_3 = \nu_0 - f_0$. (**b**) The structure of OEO DM with realization of suppression of the one from optical frequencies by the optical filter OF-OA (б). ОУ is the laser optical amplifier, OF1, OF2 are optical filters with different own frequencies, which are equal relatively to the laser generation frequency $\nu_2 = \nu_0$ and the frequency $\nu_3 = \nu_0 - f_0$, FOS is the fiber-optical system, PD is the photodetector, NA is the RF nonlinear amplifier, F is the RF filter, OC is the optical coupler, OIso is the optical isolator, OCir is the optical circulator. In (**b**) the spectra of optical emission in FOIS are presented and spectra of RF generation in the output of PD and in the input of LD1. The optical filter OF-OA (**b**) is implemented on the base of commercial laser diode. The structural diagram of QWLD (**c**) and equivalent circuit of external parametric circuits (**d**). In the circuit (**d**) the laser diode with the complex impedance Z_g is shown

determining significance, it is necessary to investigate the phase-frequency and amplitude-frequency characteristics of the laser diode, as well as functions of the slope deviations of the LD phase characteristic (at fixed radio frequencies) versus the variations of the DC pumping current I_0.

In this section, we give calculations and experimental measurements of the watt–ampere characteristic, of optical spectra at different pumping levels, of AFC and PFC characteristics of the RF modulation of the mesa-strip LD operating in the single-frequency and multi-frequency optical modes.

QWLD may be attributed to the class of injection semiconductor laser light sources. These modern optoelectronic devices for generation of the laser optical emission can be constructed on the base of traditional structure of the laser including the active optical element, optical mirrors and the RF pumping. In modern fast-acting semiconductor lasers, the semiconductor material (active medium) is the active optical element, and as mirrors, the output faces of the active element are used.

Besides laser diodes with the wide contact, the strip laser structures are used. Compared to the laser diodes with the wide contact, the strip diodes have the following advantages: (1) they have the low value of the threshold current owing to small area of the active strip; (2) they have improved condition for heat sink; (3) they have small dimensions of the emitting region on the resonator mirror; (4) they have the simple structure of modes (oscillation types), i.e., the small number of transverse modes in the resonator (the parallel spatial generation modes are excluded).

In the fast-acting laser diodes, the strip width is 2–5 μm. Such LDs are called mesa-strip laser diodes. At present, to increase the modulation frequency band in microwaves, the **quantum-well mesa-strip** laser diode is used. We describe below its main features and properties. It is known that in laser optical spectra on the base of semiconductors, which have several ultrathin layers with thickness 5–50 nm, the effect of quantization of energy states is demonstrated. Due to dependence of this effect upon the layer thickness, this LD can be attributed to the quantum-dimension laser diodes. At layer thickness comparable with the de Broglie wavelength, the electron manifests its quantum properties. In radio-physical language, we may speak that, at that, the oscillating system is formed for carriers, and as a result, in the amplification loop of the laser structure, the clearly expressed sharp "peaks" appear, which correspond to resonances.

Observation and creation of the quantum-dimension effect in injection lasers becomes possible after assimilation of the hetero-structure technology with the uniform thickness of the active layer of 5–50 nm. Carriers (electrons) in the active layer are captured from the wide-zone regions into the quantum well. At small layer thickness, electrons stop to have time for relaxation into the deepest levels before their recombination with holes. This leads to the growth of the gain slope of the active layer, and hence, to the decrease of threshold pumping (by 5–20 times), to the growth of pumping power density in the active region and to the increase of the power of output emission (by 10–20 times), to improvement of emission polarization characteristics, to reduction of the spontaneous emission (by 10–100 times), and to reduction of the phase noise level. In laser diodes, to create quantum wells, the

InGaAlAs/InP structure is used, and at that, the LD emission wavelength is 1.3 μm. Such laser diodes with thin structures are called quantum-well laser diodes (QWLD).

At present, QWLD investigations are intensively executed, and their radio-frequency modulation band becomes permanently widened. The maximal modulation frequency f_m of QWLD is determined by expression: $f_m = (1/T_1)\sqrt{E_0^2 G_{0p}/(1+\varepsilon_0 E_0^2)}$, where $E_0^2 = S_p$ is the normalized emission power, S_p is the internal photon density in the QWLD active region, $G_{0p} \approx T_1/T_{OF}$ is the slope of the optical amplification coefficient of the active layer, ε_0 is the coefficient characterizing the gain nonlinearity, $T_1 = \tau_e$ is the lifetime of electrons, $T_{OF} = \tau_p$ is the lifetime of photons in the optical resonator. It follows from this expression that the growth of the photon density in the active layer and the gain slope leads to the increase of the maximal modulation frequency. This can be achieved, for example, at large exceeds of pumping above the threshold value. In modern QWLD, the pumping (bias) current is 6–9 times more than the threshold pumping value.

The second mechanism of increase of the QWLD modulation frequency band is the reduction of the optical amplification dependence upon temperature owing to the temperature stabilization and by means of introduction of the thermal-compensating selective optical filter in the QWLD structure. At negative slope of the "resonance peak" dependence of such optical filter upon temperature, for the positive room temperature, for example, −0.15 nm/°C leads to the growth of the optical QWLD wavelength approximately by the same value but with the opposite sign +0.15 nm/°C, taking into account the QWLD temperature increase, we can achieve the significant thermal compensation and the increase of the output power to 30 mW at the pumping current of 80 mA and at the QWLD slope increase of the watt–ampere characteristic to 0.4 W/A. At that, the modulation frequency range of QWLD is 14 GHz at 25 °C and 12 GHz at 85 °C, relatively.

The author of [9] informs about the creation of QWLD on the base of InGaAsP/InP with the output power introduced into the optical fiber at about 7 mW and the modulation frequency band about 40 GHz. At that, in the synchronization mode of QWLD longitudinal modes, the duration of the emission pulse is 2.8 ps with the low level of the "jitter" equals to 73 fs.

Let us consider the QWLD operation. The structural diagram of QWLD and its physical operation principle is explained in Fig. 7.16. This Fig. 7.16a shows the QWLD structural diagram, which has got the largest distribution at present. This diagram explains the operation principle of QWLD on the base of so-called "model 3N". The equivalent electrical scheme of QWLD is shown at the same Fig. 7.16b. The main "spurious" laser elements are shown in [10–12]: C_f is the capacitance formed by the dielectric film, C_{pn} is the barrier capacitance of the laser p-n junction, which is formed owing to the fact that p- and n-emitters are alloyed, and the active medium and wave-guiding layers are non-alloyed.

Let us perform the AFC and PFC analysis of QWLD and their functions upon the DC pumping current. We also note that the QWLD watt–ampere characteristic, the optical spectrum of generation at various pumping currents, the power spectral

density of the phase noise of QWLD output emission, the directional pattern of output emission can be attributed to the main characteristics of QWLD besides AFC and PSD.

7.3.3 QWLD Differential Equations and the Transfer Function

To determine the analytical connection of the QWLD bias current with the OEO generation frequency, we derive expressions for the QWLD transfer function on the base of its velocity equations. In [9–12] shows the structural diagram and the QWLD equivalent circuit without account of the electron–photon resonance. At deriving of transfer functions, we must take into consideration that usually in order to create the restrictions of the optical field along the active region, the under-etching to the wave-guiding layer thickness of the *p*-emitter should be 0.1–0.15 μm; the resistance of the remained layer achieves several hundreds Ω. In this case, we can consider that capacitances C_f and $C_{p\text{-}n}$ are connected in series and the charge-discharge of the capacitance $C = C_f C_{p\text{-}n}/(C_f + C_{p\text{-}n})$ will be provided through the series-connected resistances R_d and Z_d. The value of R_d is determined by the resistance of *p*- and *n*-ohmic contacts, by the thickness of the *p*-emitter over the active region and the substrate resistance, by the resistance Z_d: the parallel-connected capacitance C_a and the impedance of the laser diode Z_g. The value of C_a is the part of the barrier capacitance of the *p-n* junction of the laser's pumping region. The impedance of the laser diode is complex, i.e., it consists of the real and reactive parts.

In order to derive the transfer function expressions of the laser diode and its types of AFC and PFC, we can usually use the various models. We here use the "model 3N." The system of velocity (kinetic or balance) equations for this model [10–12] can be written as follows:

$$\begin{cases} \dfrac{dn_3}{dt} = D\dfrac{d^2 n_3}{dz^2} - R_3(n_3), \dfrac{dn_2}{dt} = \dfrac{I_{n2}}{eV_a} - \dfrac{I_{net}}{eV_a} - R_2(n_2), \dfrac{dn_1}{dt} = \dfrac{I_{net}}{eV_a} - R_1(n_1) - \Gamma_a \upsilon_{gr} G E_0^2, \\ \dfrac{dE_0^2}{dt} = \Gamma_a \upsilon_{gr} G E_0^2 - \dfrac{E_0^2}{\tau_{ph}}, \end{cases} \tag{7.35}$$

where $E_0^2 = S_p$ is the photon density in the resonator, E_0^2 is the normalized emission power (the normalized amplitude of the electromagnetic field strength of QWLD optical oscillations); G is the gain; Γ_a is the coefficient of the optical field restriction; v_{gr} is the group light speed; D is the coefficient of the ambipolar diffusion; n_1, n_2, n_3 are carrier density; $R_1 = n_1/\tau_{n1}$, $R_2 = n_2/\tau_{n2}$, $R_3 = n_3/\tau_{n3}$ are recombination speeds; τ_{n1}, τ_{n2}, τ_{n3} the carrier lifetimes in the active region in the wave-guiding layer above the active region and in wave-guiding layers; I_{net} is the pumping current (bias current

of QWLD); V_a the volume of the active region; e is the electron charge, $T_{OF} = \tau_p$ is the photon lifetime in the QWLD resonator.

We note that differential kinetic (balance) QWLD equations (Eq. 7.35) couple by the cause-and-effect relationship of the inversed population or the carrier density n_1, n_2, n_3 with the photon flow S_p (Eq. 7.35). At deriving, we use the small-signal approximation for AC components of the pumping currents, of the carrier densities, of the photon density. Therefore, we use for an analysis at small-signal approximation of the following linearization of the gain in the vicinity of the point with the values $n_1 = n_{10}$, $S_p = S_0$:

$$\begin{aligned} G(n_1, S_p) &= G(n_{10}, S_0) + \frac{\partial G}{\partial n_1}\Big|_0 \cdot \Delta n_1 + \frac{\partial G}{\partial S}\Big|_0 \cdot \Delta S \\ &= g_0 + G_n \cdot \Delta n_1 + G_S \cdot \Delta S \end{aligned} \tag{7.36}$$

In Eq. (7.36) $G_n = \frac{\partial G^{(1)}}{\partial n_1}\Big|_0$; $G_S = \frac{\partial G}{\partial S}\Big|_0 = -\frac{G_0 \varepsilon_{sh}}{1+\varepsilon_{sh} S_0}$; where g_0 is the differential gain at $n_1 = n_{10}$, $S_p = S_0$; ε_{sh} is the gain nonlinearity defined by the spectral "burnout" of carriers; the symbol "$|_0$" designates that the partial derivative is taken in the point with the coordinates $n_1 = n_{10}$, $S_p = S_0$; in calculations for $G^{(1)}(n_1)$ we use the linear approximation of the gain maximum: $G^{(1)}(n_1) = g_0(n_1 - n_0)$.

The pumping current $I_{net}(n_2, n_1) = I_{net}(n_{20}, n_{10}) + \frac{\partial I_{net}}{\partial n_1}\Big|_0 \cdot \Delta n_1 + \frac{\partial I_{net}}{\partial n_2}\Big|_0 \cdot \Delta n_2$ in Eq. (7.35), which is determined by the carriers' capture and rejected from the quantum well, is defined by the formula: $I_{net}(n_2, n_1) = eV_a\left(\frac{n_{20}}{\tau_{c0}} - \frac{n_{10}}{\tau_{e0}} + \frac{\Delta n_2}{\tau_c} - \frac{\Delta n_1}{\tau_e}\right)$, where τ_{c0}, τ_{e0}, τ_c, τ_e are local time constant of the carrier capture and reject for DC current and the AC signal.

Now we obtain the QWLD transfer function and PFC and AFC from the velocity equations (Eq. 7.36). At that, we assume that QWLD operates in the single-frequency optical generation mode (exactly for this case these equations are true).

In the structure of the small-single direct modulation of the laser emission, the pumping (bias) current can be presented in the form: $I = I_0 + I_1 \cdot \exp(j\omega t)$, where I_0 and I_1 are DC and AC components of the pumping current, and ω is the radio frequency of the pumping current. Similarly, the photon flow density in the resonator can be presented as: $S = S_0 + S_1 \cdot \exp(j\omega t)$, where S_0, S_1 are DC and AC components of the photon flow density in the QWLD resonator. The complex laser transfer function for the linearized system of the velocity equations is defined as the ratio: $K_{LD}(j\omega) = [S_1(j\omega)/S_1(0)]/[I_1(j\omega)/I_1(0)]$.

The expression for the complex transfer function of the mesa-strip quantum-well laser diode, which operates in the single-frequency mode for the small radio signal of modulation in its input, can be simplified for modulation frequencies in the range from 1 to 12 GHz. At that, we can present in the form of the parallel-connected total capacitance C_L and the active differential resistance R_d of the complex impedance, which takes into consideration the constructive parameters of the "laser chip" (the film thickness, the barrier capacitance, etc.). The differential resistance R_d is

determined by *p*- and *n*-ohmic contacts, by the thickness of the *p*-emitter above the active region and the substrate resistance.

The total capacitance C_L value is determined by the series-connected barrier capacitance of the junction C_{pn} and the capacitance C_d formed by the dielectric film with the thickness *d*, i.e.: $C_L = C_{pn}C_d/(C_{pn} + C_d)$.

The complex transfer function of QWLD $K_{LD}(j\omega)$ at such restrictions is written as:

$$K_{LD}(j\omega) = \frac{\omega_{0L}^2}{(1 + j\omega C_L R_d)(1 + j\omega\tau_{ce})\left[\left(\omega_0^2 - \omega^2\right) + j\omega\mu\right)]}, \tag{7.37}$$

where $\tau_{ce} = r_D\tau_c + \tau_e$; $R_\tau = \frac{\tau_c}{\tau_e}$; $r_D = \frac{L_w}{L_a}$; $\varepsilon_{ce} = \frac{Rr_D\Gamma_a U_{gr} g_0 \tau_{ce}}{(1+R_\tau r_D)^2}$; $\tau_D = \frac{(L_w - L_a)^2}{8D_a}$; L_a is the total thickness of quantum wells; the damping decrement of QWLD is $\mu = \frac{1}{(1+R_\tau r_D)\tau_{n1}} + \omega_0^2\left[\tau_{ph} + \frac{(\varepsilon_{sh}+\varepsilon_{ce})(1+Rr_D)}{\Gamma_a U_{gr} g_0}\right]$; L_w is the thickness of the laser wave-guiding layer; $P_{L0} = S_{1L} \cdot (J_{0L} - J_{0Lth})$ is the DC component of the photon flow density in the resonator; Γ_a is the coefficient of the optical field limitation; V_{gr} is the group light speed; D_a is the coefficient of ambipolar diffusion; τ_c, τ_e are the local lifetime of capture and rejection of carriers for the AC signal, ε_{sh} is the nonlinear gain; g_0 is the gain of the active layer; τ_{ph} is the photon lifetime in the resonator; S_{1L} is the proportionality coefficient defining the dependence of the photon flow density (in laser optical resonator) versus the DC pumping current in QWLD; J_{0L}, J_{0Lth} are the DC components of the QWLD pumping current and its threshold value, relatively; τ_{n1} is the carrier lifetime in the active area.

In Eq. (7.37), the first multiplier in the denominator reflects the QWLD constructive parameters, which is determined by the thickness of the dielectric film, by the barrier capacitance, etc. The second multiplier reflects the inertial properties of QWLD owing to time constant of carriers according to the "model 3N". The third multiplier reflects the own inertial properties of QWLD describing by differential equations (Eq. 7.35).

Executing the standard operation of finding of the argument and the module of the complex transfer function from the expression (Eq. 7.37), we obtain the functions of PFC and AFC of QWLD versus the pumping current. Plots of these functions are shown in Fig. 7.17c, d. Figure 7.17 shows the experimentally measured AFC and PFC of QWLD from "DILAZ" company, which are measured by authors according to the standard method. Experimentally measured curves of this QWLD output emission are presented in Fig. 7.17a, b.

Functions of the emission power (measured experimentally) versus the DC pumping current of QWLD are presented in Fig. 7.17a. Measured by authors, the QWLD spectra allow conclusion that the function of the wavelength of the QWLD central mode at growth of the DC pumping current monotonically increases (Fig. 7.17b). Accordingly, with the growth of the pumping current, the optical frequency of the central mode of laser emission decreases as: $\nu = \nu_0[1 - S_\nu(I_0/I_{th} - 1)]$, where S_ν is the function slope, ν_0 is the frequency of the central mode at

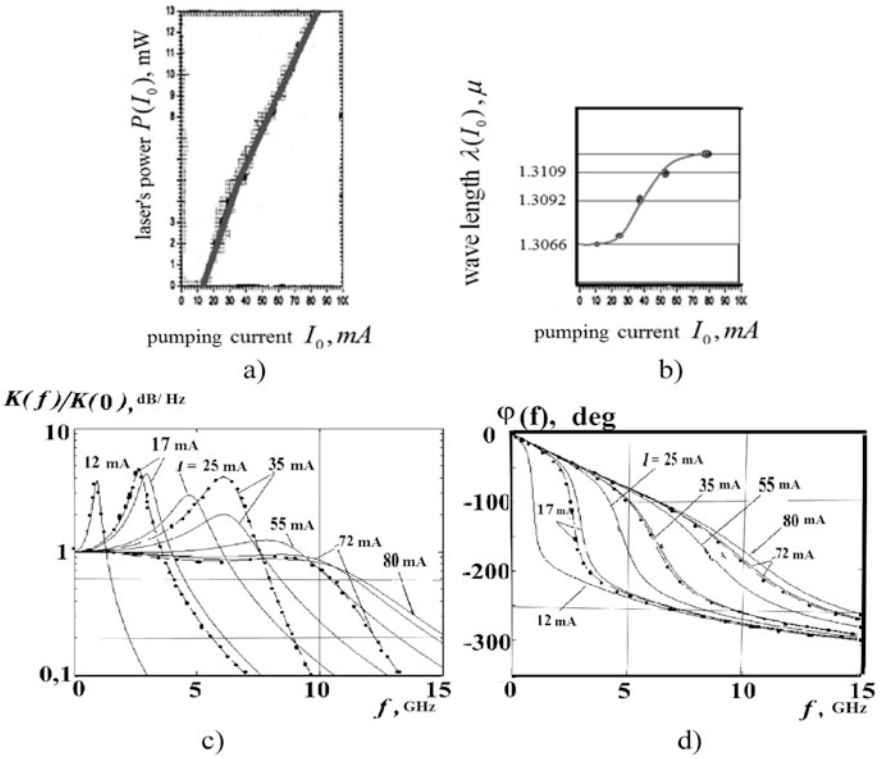

Fig. 7.17 The watt–ampere characteristic of QWLD (**a**). The function of the wavelength of QWLD emission versus the pumping current (**b**). Calculated (solid curves) and experimental (dotted curves) AFC (**c**) and PFC (**d**) of the mesa-strip QWLD for various bias (pumping) currents. The threshold pumping current of QWLD is 12 mA

threshold pumping. At that, the slope of the wavelength function of the central mode equaled "on the threshold" to 13,002 μm versus the DC pumping current of QWLD is 0.086 μm/mA or 0.086 mm/mA, which corresponds to the function slope of the QWLD versus the DC current of pumping $S_v = 0.75$ THz/(50 mA) = 0.015 THz/mA. The maximal relative deviations of the optical frequency in the current range 20–70 mA are 0.75 THz/229 THz = 0.0032.

At calculation of AFC and PFC of the laser, we used the following values of parameters in Eq. (7.41), which are the same as in [10, 12] for the mesa-strip QWLD with the thickness of the dielectric film of $d = 1.2$ μm and with the number of quantum wells equaled to five: $g_0 = 10^3$, $R_d = 5\ \Omega$, $C_L = 4 \times 10^{-12}$ F, $\Gamma_a = 0.043$, $r_D = 10.6$; $R_\tau = 0.05$, $\tau_{ph} = T_{OF} = 1.2 \times 10^{-12}$ s, $\tau_D = 7.2 \times 10^{-12}$ s; $I_{thr} = 12$ mA, $\varepsilon_{sh} = 0$, $\tau_{n1} = T_1 = 0.5 \times 10^{-9}$ s.

Figure 7.17c, d shows AFC and PFC of the mesa-strip QWLD calculated from Eq. (7.37) for different pumping currents from 15 to 85 mA at the value of the threshold pumping current of 12 mA and 13 mA, relatively. We see that at small

pumping currents, the phase-frequency characteristic has a large slope in the frequency region corresponding to the clearly expressed resonance peaks in AFC with the natural frequency ω_0 in the frequency range from 1 to 5 GHz.

Depending on AFC, the "resonance peak" is caused by the phenomenon of the "electron–photon" resonance, which is demonstrated in injection semiconductor lasers in the region of the microwave modulation. The "electron–photon" resonance arises at equality of the pumping oscillation period and the own relaxation time of excited particles in QWLD. The resonance frequency of QWLD modulation f_{res} depends on the pumping exceed above the threshold value, on the electron lifetime τ_e and the photon lifetime τ_p in the resonator and determined by the expression: $f_{\text{res}} = (1/\tau_e)\sqrt{(\tau_e/\tau_p)(I_0/I_{\text{th}} - 1)}$.

In the region of the large pumping currents from 50 to 80 mA, the phase-frequency characteristic $\varphi(\omega)$ approaches to linear and is described by the expression to accuracy to the constant φ_0: $\varphi(\omega) = 2\pi\, fR_{\text{LD}}C_{\text{LD}} + \text{Arg}[K_{\text{LD}}(j\omega)]$.

For demonstration of phase offsets on the fixed radio frequency, the functions of the phase differences for different small offsets of the constant pumping current are calculated. An analysis shows that the pumping current influence on the PFC slope in the whole frequency region is different. At small exceeds of the pumping current (1.2–2.0) at variation of the pumping current of 1 mA, the maximal slope of PFC is 30–70°/mA at fixed radio frequency in the range 1.0–5.0 GHz. At large pumping currents, the maximal PFC slope is 1–5°/mA at fixed frequency in the range 5.0–10.0 GHz.

From these calculated data, we can conclude that at providing of stabilization of the constant QWLD pumping current is not worse than 10^{-4} (which corresponds to absolute current offsets of 7.5×10^{-3} mA at the pumping current of 75 mA), the absolute variations of time constant of QWLD under investigation, owing to DC pumping current variations, are about 2×10^{-3} ps/mA at modulation in the radio-frequency range of 8–12 GHz.

Thus, obtained calculated and experimental values of PFC and QWLD time constant (or the PFC values on the modulation frequency f_{mod} dividing by the value of the given frequency) $T_{\text{LD}} = \varphi_{\text{LD}}/(2\pi f_{\text{mod}})$ variations give the possibility to perform measurements of the light time delays (with utilization of these types of QWLDs as the modulated light source) in fiber-optical systems and in light-guiding fibers with the help of oscillator methods [13, 14] not worse than 2×10^{-3} ps, which is equivalent, for instance, to registration of geometrical lengthening of the optical fiber on the level 0.2 μm. Therefore, such QWLD is expedient to use in the high-sensitive oscillator fiber-optical sensors as well as in oscillators with RF FODL for generation of the high-stable harmonic radio signal.

On the other hand, at transmission of the harmonic microwave radio signal, for example, in lines by the phased active arrays (PAA), the absolute phase offsets on the frequency of 10 GHz, due to the instability of the QWLD DC pumping current, are 0.72×10^{-2} degrees. The application of these types of QWLDs in PAA is also promising.

Unfortunately, the single-frequency model restricts possibilities in investigation of phase offsets and QWLD time constant offsets at the multi-frequency optical generation. Therefore, we examine the calculation features of the laser diode's transfer function for the multi-frequency mathematical model.

We can note that the group phase incursion in RF FODL: "QWLD—single-mode optical fiber with the length 1.5 m—the photodetector" is 7.5 ns (taking into account the 1.5-m segment of the single-mode FOS). Experimentally measured AFC and PFC obtained in Fig. 7.17 have well qualitative and quantitative agreement with theoretical ones. The discrepancy of calculated and experimental resonance peaks and amplitudes up to 2–4 dB can be attributed to limitations of the velocity equation model, which, in general case, do not take into consideration the temperature variations of the operating substance and the energy exchange between the optical modes participating in the generation, as well as the situation when we do not take into account the own small temperature variations of the active region and the pumping current.

On the basis of the calculation and experimental studying of AFC and PFC of mesa-strip QWLD, we can make the conclusion that appearance (together with the fundamental mode) of other optical modes at large pumping currents (the emission multi-frequency properties) does not qualitatively distort of AFC and PFC in the frequency band from 5 to 12 GHz.

Small non-monotonies in AFC and PFC on the level 1–2 dB and 2–4°, are, relatively, manifested in the existence region of sharp resonance peaks from 1 to 5 GHz. Observing in the experiment, non-monotonies in AFC on the level 1–3 dB in the frequency band of 5–12 GHz are related to matching elements of the microwave paths.

On the base of calculations and experimental investigations of the operation and characteristic features of AFC and PFC of QWLD, we can make the following conclusions:

1. The influence of the pumping current upon the slope of PFC is different in the whole frequency band. At small exceeds of the pumping current (1.2–2.0), at pumping current variation of 1 mA, the maximal PFC slope is 30–70°/mA at fixed radio frequency in the range 1–5 GHz. At large pumping currents, the maximal PFC slope is 1–5°/mA at the fixed frequency in the range 5–10 GHz. Experimental measurements of PFC qualitatively and quantitatively coincide with the calculated values obtained on the base of velocity equations.
2. Appearance (together with the fundamental mode) of other optical modes at large pumping currents (the emission multi-frequency property) does not qualitatively distort of AFC and PFC in the frequency band from 5 to 12 GHz. Small non-monotonies in AFC and PFC are manifested in the existence region of sharp resonance peaks from 1 to 5 GHz.

In Fig. 7.18, AFC (a) and PFC (b) of QWLD transfer function are shown for different pumping currents in the generation mode at various ratios of the pumping current to the threshold current. Designation SE is concerned to AFC and PFC of the transfer function owing to spontaneous emission (the luminescence) and it is shown

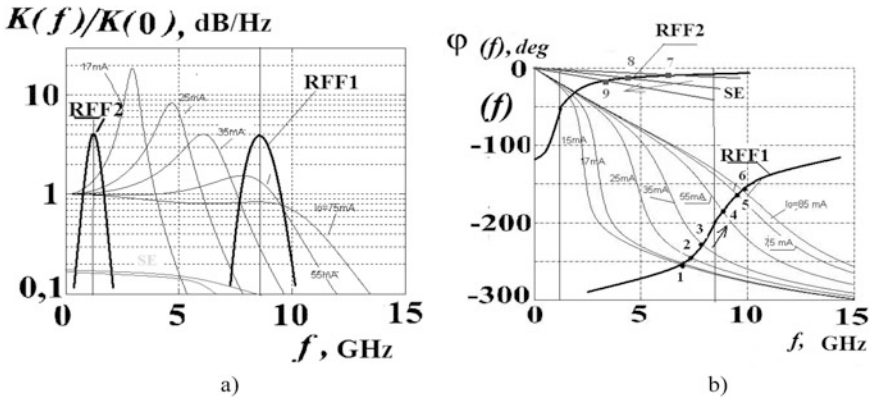

Fig. 7.18 Calculated AFC (**a**) and PFC (**b**) of the mesa-strip QWLD for different pumping currents. The threshold pumping current is 12 mA. RFF1, RFF2 are modules and "inverted" arguments of different (used in Figs. 2.1 and 2.2 in Chap. 2) RF filters with various own frequencies, SE is the module and argument of the transfer function owing to spontaneous emission

for different pumping current without the fixation to the exact values only for understanding of physical processes. Values and the slope of PFC decrease with the growth of the pumping current. The ratio of the module of the QWLD transfer function owing to the coherent stimulated emission to the module of the transfer function owing to spontaneous emission is 10^{-2} to 10^{-3} for different QWLDs. With the pumping current growth, the PFC value and the slope due to the luminescence increase for different frequency values. Designations RFF1 and RFF2 is concerned to the inverted PFC of RF filters, which are tuned in different frequencies.

7.3.4 Frequency and Amplitude Control in OEO with QWLD

Now we consider structures of OEO with QWLD presented in Fig. 7.16a, which differential equations had analyzed in Chap. 5. From the differential equation (Eq. 5.64) or from the solution of equations of amplitude and phase balance with account of AFC and PFC of QWLD for the structure in Fig. 7.16a presented in Fig. 7.18, we obtain expressions for the amplitude and the frequency of oscillations in OEO with QWLD in the steady-state mode:

$$f_{\mathrm{OEO}} \cong \frac{m + f_{\mathrm{eF}} \cdot T_{\mathrm{eF}}}{T_{\mathrm{PD}} + T_{\mathrm{A}} + T_{\mathrm{FOS}} + T_{\mathrm{eF}} + \arg K_{\mathrm{LD}}/(2\pi f_{\mathrm{eF}})}, \tag{7.38}$$

where T_{eF} is the effective delay time in the opened OEO, T_{PD}, T_{NA} are time constants of PD and NA, T_{FOS} is the delay in FOS, $\arg K_{\mathrm{LD}}$ is the argument of the QWLD transfer function, f_{eF} is the natural frequency of the RF filter.

For nonlinear AE characteristic $i(u) = S_{01}u - S_{03}u^3$ and for the average slope of this characteristic $S_1(U) = S_{01} - (3/4)S_{03}U^2$, the solution of differential equation (Eq. 3.50) in the steady-state mode gives the expression for the amplitude in the steady-state mode:

$$U = \sqrt{4S_{01}/3S_{03}} \cdot \left(1 - \frac{1}{S_{01}R_{11} \cdot |K_{\text{FODL}}|}\right)^{1/2}, \tag{7.39}$$

where R_{11} is the constant coefficient, which takes into account the losses in RF FODL elements. Now we take into consideration that the transfer function of RF FODL $|K_{\text{FODL}}| = |K_{\text{LD}}||K_{\text{FOS}}||K_{\text{PD}}||K_{\text{F}}|$ depends on the laser transfer function $|K_{\text{LD}}|$, where $|K_{\text{LD}}| = P_{0\text{LD}} \cdot S_{\text{LD}}$: the product of the RF variable component power and the transfer slope. The laser power $P_{0\text{LD}} = S_{\text{LD}} \cdot (\alpha_{0\text{l}} - 1)$ is determined by the exceed level $\alpha_{0\text{l}} = J_{0\text{L}}/J_{0\text{Lth}}$ of the pumping current $J_{0\text{L}}$ above the threshold value $J_{0\text{Lth}}$, $\text{Arg}K_{\text{LD}}/(2\pi f_{\text{eF}}) \approx -T_1\sqrt{(\alpha_{0\text{l}} - 1)}$, where T_1 is lifetime of carriers in QWLD. Then the last expression (transfer function, relatively, of PD $|K_{\text{PD}}|$ and the RF filter $|K_{\text{F}}|$) for the amplitude and phase of oscillations is determined as:

$$U = \sqrt{4S_{01}/3S_{03}} \cdot \left(1 - \frac{1}{S_{01}R_{11} \cdot S_{\text{LD}} \cdot (\alpha_{0\text{l}} - 1)|K_{\text{FOS}}||K_{\text{PD}}||K_{\text{F}}|}\right)^{1/2}, \tag{7.40}$$

$$f_{\text{gen}} \cong \frac{m + f_{\text{eF}} \cdot T_{\text{F}}}{T_{\text{FD}} + T_{\text{NA}} + T_{\text{FOS}} + T_{\text{eF}} + T_1\sqrt{(\alpha_{0\text{l}} - 1)}}. \tag{7.41}$$

From these expressions, the conclusion follows that the amplitude of OEO oscillations in the steady-state mode increases at the growth of the pumping current $J_{0\text{l}}$ exceed $\alpha_{0\text{l}} = J_{0\text{L}}/J_{0\text{Lthr}}$ above its threshold value $J_{0\text{lthr}}$.

At that, at fulfillment of OEO RF generation conditions, the expression must be satisfied for the QWLD pumping $\alpha_{0\text{l}}$: $(\alpha_{0\text{l}} - 1) > 1/(S_{01}R_{11} \cdot S_{\text{LD}} \cdot |K_{\text{FOS}}||K_{\text{FD}}||K_{\text{F}}|)$.

From Eq. (7.41), it follows that with the growth of the pumping current, oscillations' frequency of OEO with QWLD increases due to the increase of the natural frequency of the electron–photon resonance in QWLD.

Figure 8.13c (in Chap. 8) shows experimental function of OEO of the microwave range versus the pumping current $J_{0\text{l}} = I$. At small lengths of the optical fiber, the function of the amplitude and the frequency of OEO generation are well approximated by expressions (Eqs. 7.40 and 7.41).

At increase of the geometrical length of the optical fiber more than by 70 m, the frequency jumps (Fig. 8.13c in Chap. 8) are manifested, which are caused by fulfillment of the single-frequency generation conditions for the adjacent oscillation types of RF generation.

At small pumping currents, the slope of oscillation frequency variations versus the pumping current is 0.3 MHz/mA. At large pumping currents in QWLD (5–8), the slope of the oscillation frequency function versus the pumping current is 0.003 MHz/mA.

7.3.5 *The Effect of the Polarity Change of the Argument Slope of the QWLD Transfer Function*

The above-described theory is true under a condition that the spontaneous laser emission, which applied to PD and modulated by the pumping current, is extremely small, and the OEO generation due to spontaneous emission does not happen because of the nonfulfillment of the amplitude balance conditions.

If the spontaneous emission power is sufficient in order to satisfy the conditions for oscillations excitation (at high gain of NA), then OEO generation is possible owing to the laser spontaneous emission. In this case, the law of oscillation frequency variations at the growth of the pumping current has the opposite character, i.e., with the pumping increase, the frequency decreases.

Experimental functions of the OEO oscillation frequency $f(I_{\text{pump}})$ of the pumping current I_{pump} are presented in Fig. 7.19 for OEO, in which the Russian laser diode ILPN-204 is used (the optical matching system for emission in the form of the "micro-lens" contains in its construction). At that, functions $f(I_{\text{pump}})$ have the non-monotonic variation for the polarity change of the slope: at growth of the pumping current from zero to the threshold values, the function monotonically decrease, while at the pumping current increase above the threshold value—they monotonically increase. In contrast to the previous case, the presence of the matching system in the laser diode allows obtaining of the OEO generation for pumping currents, which are less than the threshold value.

The main reason for such a behavior of the generation frequency functions is the various dominating mechanisms of the influence on the effective delay time in RF

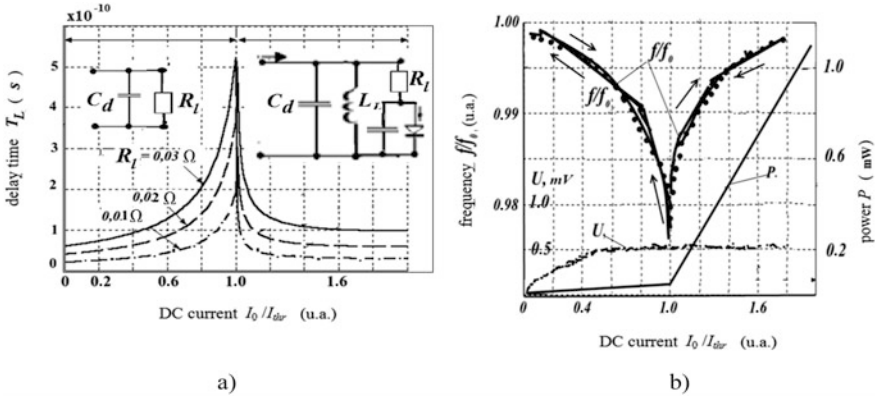

Fig. 7.19 Variation of the delay time of RF oscillations at passage of the system "LD–PD" versus the DC pumping component I_0/I_{thr} (I_0 is the pumping DC current. I_{thr} is the threshold pumping current) for different values of the losses resistance $R_l = 0.01\ \Omega$; $0.02\ \Omega$; $0.03\ \Omega$ (**a**). Experimental function of the relative frequency f/f_0, the amplitude of the generated voltage U of OEO with RF FODL and the output power P versus the pumping current (**b**). LD is the ILPN-204 type. The average generation frequency f_0 is 30 MHz

FODL at variation of the LD time constant for pumping current, which are higher and lower than the threshold value. At increase of the pumping current in the region of values, which are less than the threshold value, the time constant of LD increases due to the growth of the barrier capacitance. In this current range, the LD optical emission represents the spontaneous emission of photons. At that, the equivalent circuit of the laser diode for pumping currents, which are less than the threshold values, can be represented as the parallel-connected barrier capacitance C_b and the loss resistance R_{loss}, and the time constant of LD (or the delay of the harmonic signal in LD) is determined as $T_{LD} = R_{loss}C_b$, where $C_b = C_{b0} \exp(\gamma_{str} I_{pump}/I_{thr})$, C_{b0} is the value of the barrier capacitance at the zero pumping current, γ_{str} is the real coefficient defining by the geometry and the structure of the laser diode.

In the range of pumping current values, which are lower than the threshold value, the LD operation is similar to the light emitting diode (LED). In the range of pumping current values, which are higher than the threshold value, the optical emission represents the laser generation. The influence on the time constant T_{LD} of the barrier capacitance of the junction becomes insignificant. The speed of the carrier concentration achievement on the upper level to the threshold value, which is directly connected with the level of the pumping exceed above the threshold value, is the main factor, which determines of the LD time constant. Owing to the growth of the carrier concentration speed, the delay in phase decreases of the harmonic signal in LD. The delay time of the signal phase or the LD time constant is determined by the approximated expression $T_{LD} = \tau_e \exp[-(I_{pump}/I_{thr} - 1)]$, where τ_e is the lifetime of electrons (carriers).

At current values equaled to the threshold value, the frequency function $f(I_{pump})$ has the minimum. The hysteresis character of this function at increase and decrease of the pumping current is explained by the thermodynamic processes of heating of cooling of the LD active region at small variations of the environment temperature.

The measured in experiments average slopes S_f of the function $f(I_{pump})$ (at equal offsets $|I_{pump} - I_{thr}|$ versus the threshold value I_{thr}), in regions of the current variations above and below of the threshold value, are approximately equal for OEO with RF FODL and LD: $S_f = \Delta f/\Delta I_{pump} = 15$ kHz/mA.

The phenomenon of the polarity change of the slope of LD time constant and the slope S_f of the function $f(I_{pump})$ for OEO with LD, which was for the first time experimentally discovered and explained by authors by means of the theoretical analysis for LD, gives a possibility to correctly select the operating pumping currents of LD in OEO and the modulation signal amplitude, as well as to optimize the construction of the LD modulator, of matching optical device with the optical fiber and of the thermal stabilizing block.

7.3.6 Modern QWLDs and Their Characteristics

The QWLD construction, which analysis was presented in [9] on the base of InGaAsP/InP with the output power about 7 mW introduced into the optical fiber

Table 7.1 Characteristics of the modern narrowband QWLD (the width of the spectral line is 1–3 kHz)

Parameter	Value	Units
Temperature	22.0	°C
Pumping current	80	mA
Maximal pumping current	95	mA
Threshold pumping current	5.0	mA
Generated wavelength of QWLD	1549.303	nm
ITU channel	35	–
Channel offset	−17	10^{-6}
Output power of QWLD generation	11.0	mW
Suppression norm for side harmonics	43	dB
The norm of "polarization purity"	>26	dB

at the modulation frequency band about 40 GHz. The structure of such QWLD includes three series-connected sections: "the block of phasing"—formation of QWLD optical emission, "the block of optical lattice"—the discriminator on the base of the narrowband optical filter made on the Bragg lattice, "the amplification"—the block of QWLD optical emission amplification. The AFC of the ultra-wideband QWLD with the modulation band of 40 GHz is presented in [9] shows the watt–ampere characteristic and the emission spectrum of the ultra-wideband QWLD with the modulation band of 40 GHz [9].

The frequency of the photon–electron resonance is determined by the lifetime of carriers (photons) on the upper level and by the exceed of pumping above the threshold level. The frequency of the photon–photon resonance in QWLD is defined by the frequency of the external optical filter of QWLD located outside the main resonator and tuned to the optical frequency equaled to the generated central frequency $\nu = 30$ GHz.

The attention of manufacturers is increased to development of the narrowband QWLD [15–19] with extremely low permissible phase noises. In [15–19], the construction (a) and the overall view of the package (b) of the narrowband modern QWLD are shown. Such QWLD is commercially available. The price of such QWLD is about $3000–$5000 per one piece. The spectral line width of optical emission on the wavelength of 1.55 μm is 1–3 kHz. PSD of the phase noise for the offset of 1 kHz from carrier is −110 to −115 dBm/Hz, which is the record value for the compact commercial QWLD.

Experimental values of PSD of the QWLD phase noise at different offsets from the optical carrier frequency, which corresponds to the generated wavelength of 1.55 μm (a), the watt–ampere QWLD characteristic (b) and the emission spectrum of QWLD (c) are shown in [15–19]. The emission spectrum is measured with the help of the spectrum analyzer "Anritcy" with resolution in wavelength of 0.01 nm.

Characteristics of the narrowbands QWLD are presented in Table 7.1. At maximal output power of 11 mW, the QWLD has the low threshold pumping current, the transform slope of the pumping current into the optical emission power is $S_{\mathrm{LDI}} = \mathrm{d}P/\mathrm{d}I = 2\,\mathrm{mW/mA}$, the transform slope of the electrical power into the optical emission power is $S_{\mathrm{LDP}} = \mathrm{d}P/\mathrm{d}P_{\mathrm{bx}} = 1\,\mathrm{mW/mW}$, the efficiency of such

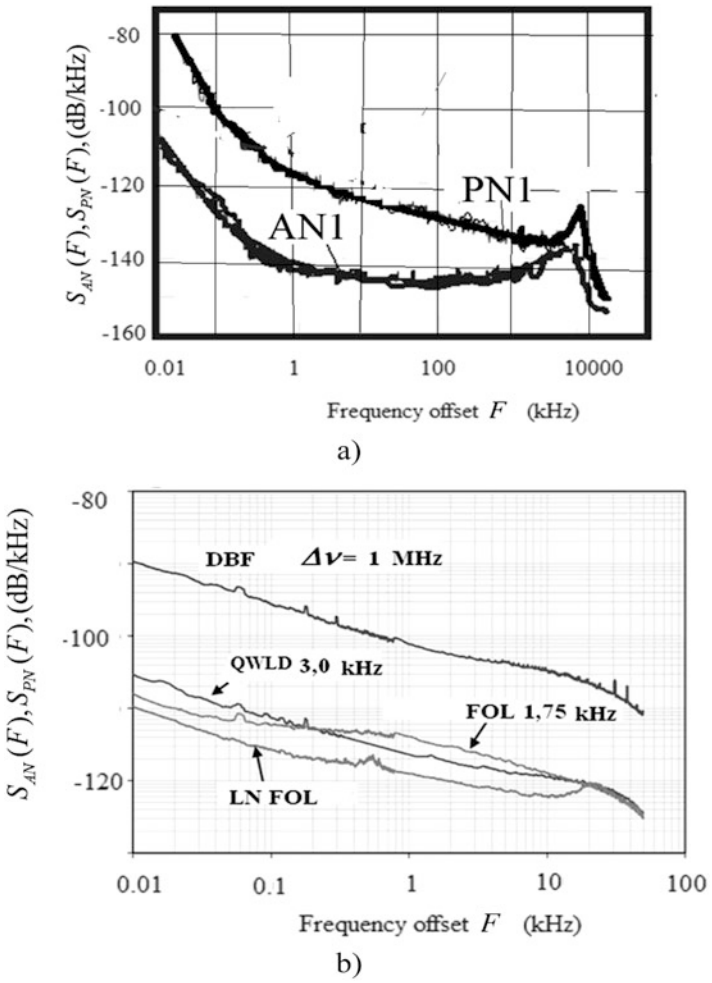

Fig. 7.20 (**a**) Experimental values of PSD of the amplitude (AN1) and the phase noise (PN1) of for different modern lasers QWLD with Bragg diffraction lattice; (**b**) Experimental values of PSD of the phase noise of for different modern lasers QWLD DBF, QWLD, FOL, LN FOL. DBF is the laser diode with the resonator with the Bragg diffraction lattice, FOL is the DBR fiber-optical laser, LN FOL is the low-noise FOL

QWLD is $\eta = P/P_{\text{bx}} = 50\%$ (b) and the power spectrum of QWLD optical emission (c) with the bandwidth of the spectral line of the optical emission (on the half-width) is 3.0 kHz.

For comparison with other narrowband lasers, Fig. 7.20a, b shows the typical experimental values of PSD of the amplitude noise and the phase noise of optical emission of the narrowband QWLD, which characteristics are presented in [15–19] and in Table 7.1, and PSD of the phase noise of other lasers: DBF, QWLD, FOL, LN FOL (experimental functions of PSD of the phase noise versus the offset from the

carrier). In Fig. 7.20 the following designation are introduced: DBF is the laser diode with the Bragg resonator, FOL is the fiber-optical laser, LN FOL is the low-noise fiber-optical laser with different half-widths of the optical emission spectrum.

Now we can make the following conclusions from this comparison. On the one hand, we have the commercially available QWLD with low PSD of the phase noise and the high output power of emission (more than 10 mW), which can play the role of modulated and non-modulated narrowband sources in the low-noise OEO. On the other hand, experimental dependences of PSD of the phase noise of QWLD presented in Fig. 7.20, cannot be modeled by the presented in previous part of this chapter kinetic differential equations for QWLD (Eq. 7.46) because the important parameter—the optical phase of the laser emission is not included in these equations. For analysis of PSD of the phase noise and the influence on the PSD of phase noises in RF range, we must present the form and analyze of the semiclassical differential equations of QWLD, in which the phase of optical emission is included. This is done in Sect. 7.6 of this book.

7.3.7 *Brief Conclusions*

Thus, as the result of theoretical investigation of the laser diode performed in this part of this chapter, we can make the following conclusions:

On the base of velocity equations for the mesa-strip QWLD, the analysis is performed of its electro-optical and electrical characteristics in the microwave range (1–12 GHz), and the QWLD transfer functions are also obtained for the first time, and their PFC and AFC for different pumping currents. On the base of calculation of AFC and PFC of QWLD, we see that the influence on the PFC slope of the pumping current is various in the whole frequency range:

- At small exceeds of the pumping current (1.2–2.0) at variations of the pumping current of 1 mA, the maximal slope of PFC is 30–70°/mA (0.6–1.3 rad/mA or 1–2 ps/mA) on the fixed radio frequency in the range 1–5 GHz.
- At large exceeds of the pumping current above the threshold value (5–8), the maximal slope of PFC is 1–5°/mA on the fixed frequency in the range 5–10 GHz. Experimentally measurements of PFC qualitatively and quantitatively coincide with calculated values obtained on the base of velocity equations.

Revealed functions of QWLD AFC and PFC give us the possibility to estimate the range of possible detuning of the OEO generation frequency (at the single-frequency generation mode of OEO) in the microwave range at variation of the pumping current, and also to estimate the function slope of the generation frequency versus the pumping current in the microwave range. At that, the relative range of detuning of OEO frequency in the microwave range (8–12 GHz) at small exceeds of the pumping current above the threshold value (1.5–3) is (20–60) (ps/T_{FOS}).

The relative range of detuning in OEO in the microwave range (8–12 GHz) at large exceeds above the threshold values (5–8) is about (2–6) ps/T_{FOS}. For example,

the frequency detuning range equals to 2(10^{-3} to 10^{-4}), relatively, at FOS length of 6 m and 60 m. This range depends on the ratio of the delay time of the microwave signal envelope in QWLD to the delay time of the microwave signal in FOS.

The slope of OEO generation frequency function versus the pumping current in the microwave values (8–12 GHz) at small exceeds of the pumping current above the threshold value (1.5–3) is about (10–30) ps/(ma·T_{FOS}), while at large exceeds (5–8), it is about (1–3) ps/(ma·T_{FOS}).

On the base of the analysis of OEO generation frequency upon the pumping current at utilization of QWLD in the microwave range and the laser diode in RF range, we proved theoretically a possibility to control the generation frequency by the DC pumping current of the laser diode. The perspective of QWLD application as the modulated light source in stabilized tuned OEO with RF FODL in microwave and mm-wave ranges is also proved.

7.4 Frequency Control in OEO with RF FODL with Two Optical Fibers

7.4.1 The Structure of OEO DM with RF FODL with Two Optical Fibers

For the combined FOSs, which are formed by two optical fibers of different length, the expression for the controlled resistance of OEO with the differential RF FODL (Fig. 7.21) can be written as:

$$\mathbf{K}_{\mathrm{FODL}}(j\omega) = \mathbf{R}(j\omega) = \dot{\mathbf{D}}(j\omega) \times \exp\left[-\alpha_n(L_0 + L_1)\right] \frac{A\exp\left[-j\omega(T_{0\mathrm{FOS}} + T_{1\mathrm{FOS}})\right] + B\exp\left[-j\omega(T_{0\mathrm{FOS}} + T_{2\mathrm{FOS}})\right]}{1 + j(\omega - \omega_{\mathrm{F}})T_{\mathrm{F}}}, \tag{7.42}$$

where A and B are excitation coefficients of FOS1 and FOS2, relatively, and they are equal: $A = P_1/(P_1 + P_2)$, $B = P_2/(P_1 + P_2)$; P_1, P_2 are introduced absolute values of the light power in FOS1 and FOS2, relatively; L_0, L_1, L_2 are geometric lengths of fiber FOS0, FOS1, FOS2, relatively; $T_{0\mathrm{FOS}}$, $T_{1\mathrm{FOS}}$, $T_{2\mathrm{FOS}}$ are delay times of the optical signal in FOS0, FOS1, FOS2, relatively, are equal: $T_{0\mathrm{FOS}} = L_0 \cdot N(\nu)/c$, $T_{1\mathrm{FOS}} = L_1 \cdot N(\nu)/c$, $T_{2\mathrm{FOS}} = L_2 \cdot N(\nu)/c$, where c is the light speed in the free space, v is the optical frequency, $N(\nu)$ is the refraction index of the light-guiding thread, $\dot{D}(j\omega)$ is the complex coefficient, which is determined by QWLD and PD parameters.

Under following conditions:

- Noninertial AE in NA
- Linearity of the modulated light source (LD), PD, and FOS

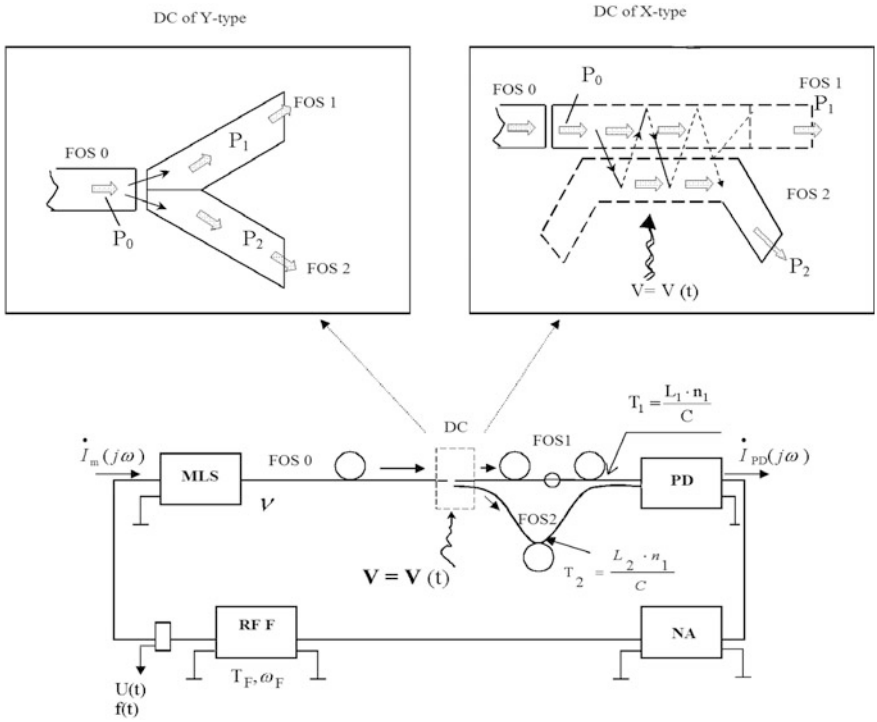

Fig. 7.21 The functional structure of OEO with the differential RF FODL and directional couplers of Y and X-types

- Propagation in the separate light guiders FOS0, FOS1 and FOS2 of the single linear-polarized light wave, optical frequency of which is equal to ν_L
- Application of the usual oscillating circuit as the filter

the differential equations with delay are given as:

$$T_F \frac{dU(t)}{dt} = R[AS_1 U(t-t_1)\cos(\Phi_1) + BS_2 U(t-t_2)\cos(\Phi_2)] - U(t), \quad (7.43)$$

$$T_F U(t)\frac{d\Psi(t)}{dt} = R[-AS_1 U(t-t_1)\sin(\Phi_1) + BS_2 U(t-t_2)\sin(\Phi_2)] + (\omega_F - \omega_0)T_F U(t), \quad (7.44)$$

Here Φ_1, Φ_2 are current phase incursions, $\Phi_1 = \tau \cdot (\omega_{eF} - \omega_0) - \Psi(t) + \Psi(t - t_1)$, $\Phi_2 = \tau \cdot (\omega_F - \omega_0) - \Psi(t) + \Psi(t - t_2)$, $t_1 = [(T_{1FOS} + T_{2FOS})/2] - (T_{1FOS} - T_{2FOS})/2$, $t_2 = [(T_{1FOS} + T_{2FOS})/2] + (T_1 - T_2)/2$, $\tau = (T_{1FOS} - T_{2FOS})/2$, $S_1 = S[U(t + t_1)]$, ω_{eF}, T_{eF} are the natural frequency and time constant of the RF circuit (the filter), relatively; $S_2 = S[U(t - t_2)]$; $T = (T_{1FOS} + T_{2FOS})/2$, ω_0 is the reference frequency of oscillations; R is the module of the controlled resistance on the frequency closed

to ω_F, which is equal: $R = K_M K_{NA} K_F/(G_1 G_2)$; G_1, G_2 are the input resistance of QWLD and the output resistance of PD, relatively; K_M, K_{NA}, K_F are modules of the transfer functions of modulated light source, the RF nonlinear amplifier and modulator, and the filter, relatively; S is the average slope of VAC of AE of NA, $S = g_1 U - (3/4) g_2 U^2$, where g_1, g_2 are constant coefficients.

The important thing is that in these differential equations (Eqs. 7.43 and 7.44), the optical frequency of QWLD v_L of the modulated light source is taken into consideration. This defines the main differences of OEO with RF FODL from traditional oscillators. This account is performed in the coefficient of the refraction index of the material $N(v_L)$ of the light-guiding thread, which depends on the optical frequency v_L.

The account in differential equations (Eq. 7.53) of the optical frequency v_L allows obtaining of solutions for the amplitude, the phase and the radio frequency f_{gen} of oscillations, on the one hand, at introduction in FOS of the various tuned filters, selectors, and other elements. On the other hand, the account of $v_L(t)$ allows determination of the fast variations of the OEO radio frequency if the optical frequency of the modulated light source depends on time, for instance, by the sine law.

Differential equations with delay (Eqs. 7.43 and 7.44) can be applied for FOS, which contains the only one optical fiber. At absence of the light guiders FOS0 and FOS2 in the structure in Fig. 7.21, i.e., at the only one FOS, and at presence in Eqs. (7.43) and (7.44) of two different light delays T_1 and T_2, Eqs. (7.43) and (7.44) take into consideration the presence in the one single-mode optical fiber of two propagating light waves, which are different in polarization and have different optical frequencies.

Equations (7.43) and (7.44) allow obtaining of solutions for the oscillations frequency and the amplitude at presence of *quasi-static* varying (i.e., by the small varying in time impact at time-variations much less than the period of OEO oscillations) in time of excitation coefficients A and B. If these coefficient vary in time, i.e., $A = A(t)$, $B = B(t)$, we can provide the quasi-static frequency modulation of OEO with RF FODL.

The frequency control in OEO is performed, on the one hand, with the help of tuned directional couplers of Y- and X-types containing electro-optical or acoustical-optical cells, piezo-elements etc., and on the other hand, by retuning of the laser optical frequency. From Eqs. (7.43) and (7.44), it follows that the presence of the own modulation of the optical frequency of the modulated light source leads to the frequency modulation of the generated RF signal. The structure of OEO with differential RF FODL on the base of two or several FOSs can contain the fiber-optical couplers of Y- and/or X-types. As shown in Chap. 5, AFC and PFC of these RF FODL on the base of the optical couplers of Y- and X-types have the qualitative differences. At utilization in OEO of directional couplers of the Y-type, coefficients A and B can be mutually dependent and connected by the relation $B = 1 - A$.

In accordance with Chap. 5, at application of the single-mode directional couplers of X-type in OEO with RF FODL, excitation coefficients A and B will be periodic and dependable on the coefficient of optical coupling C_{C0}:

$$A = \cos^2(C_{C0} \cdot Z), \quad B = \sin^2(C_{C0} \cdot Z), \tag{7.45}$$

where $C_{C0} = C_1(1 + C_2\nu)$.

Differential equations with delay (Eqs. 7.43 and 7.44) are convenient for the analysis of OEO with RF FODL in the small-signal mode, because they give information about the amplitude, the frequency, and the phase of generated oscillations during its settling. This equation gives a possibility to find the differential equations of OEO with RF FODL on the base of the single optical fiber:

$$\begin{cases} T_F \dfrac{dU(t)}{dt} = D \cdot [AS_1 U(t - t_1)\cos(\Phi_1)] - U(t), \\ T_F U(t) \dfrac{d\Psi}{dt} = D \cdot [AS_1 U(t - t_1)\sin(\Phi_1)] + (\omega_F - \omega_0) T_F U(t). \end{cases} \tag{7.46}$$

Taking into consideration that the phase delay in RF FODL is defined by the argument of the RF FODL transfer function ($\arg K_{DL}$) and D and R are constant coefficients, which take in account the losses in QWLD and PD, differential equations (Eq. 7.46) can be converted into abbreviated equations, which are similar in the mathematical form to traditional oscillators (at small lengths of FOS in RF FODL and at fulfillment of conditions $\cos(\Phi_1) = 1$ and $\sin(\Phi_1)$):

$$\begin{cases} T_F \dfrac{dU(t)}{dt} = R \cdot [|K_{DL}| S_1(U) U(t)] - U(t), \\ T_F \dfrac{d\Psi}{dt} = R \cdot [\arg K_{DL} + (\omega_F - \omega_0) T_F]. \end{cases} \tag{7.47}$$

From Eq. (7.47), we obtain expressions for the oscillations amplitude and the frequency in the steady-state mode. We note that for the inertial active element in NA (i.e., when $S_\perp(U) \neq 0$ in the $S(U) = S_{II}(U) + jS_\perp(U)$), OEO is non-isochronous and the frequency in the steady-state mode (i.e., at $dU(t)/dt = 0$ and $d\Psi(t)/dt = 0$) depends on the oscillation amplitude:

$$\omega_{gen} \cong \frac{2\pi m + \omega_F T_F}{T_F + \arg K_{DL}/\omega_F} + R \frac{S_\perp(U)}{T_F + \arg K_{DL}/\omega_F} = \omega_{o,gen} + R \frac{S_\perp(U)}{T_{eff}}, \tag{7.48}$$

where ω_0 is the generation frequency determined by the first term in Eq. (7.48), T_{eff} is the effective delay time in the open OEO loop: $T_{eff} = T_F + \arg K_{DL}/\omega_F$.

For instance, for nonlinear AE characteristic $i(u) = S_{01}u - S_{03}u^3$ and for the average (on the first harmonic) slope of this characteristic $S_1(U) = S_{01} - (3/4)S_{03}U^2$, the solutions of the differential equations at the steady-state mode give the approximate expression (under condition that the generation frequency is close to the natural frequency of the RF filter) for the amplitude in the steady state: $U = \sqrt{4S_{01}/3S_{03}} \cdot \sqrt{1 - 1/[S_{01}R_{11} \cdot |K_{DL}|]}$, where R_{11} is the constant coefficient, which takes into account the losses in RF FODL elements. For example, for RF FODL formed by two optical fibers of different lengths, the approximate expression

(under condition the generation frequency is close to the fundamental frequency of the RF filter) for the amplitude at the steady-state mode:

$$U = \sqrt{\frac{4S_{01}}{3S_{03}}} \cdot \sqrt{1 - \frac{\sqrt{1 + T_{\text{EF}}^2(\omega - \omega_{\text{EF}})^2}}{R_{11}S_{01}K_{\text{L}}\sqrt{A^2 + B^2 + 2BA\cos\omega\,(T_{1\text{FOS}} - T_{2\text{FOS}})}}}. \quad (7.49)$$

Before the analysis of the frequency control in OEO with the differential RF FODL, we start the examination of transients.

7.4.2 The Analysis of Transients in OEO with Differential RF FODL

At development of OEO with the combined RF FODL, the developer must understand the general dynamic picture of oscillations formation: how the transient processes of the frequency, the amplitude, and the phase are developed after the moment of power supply switching-on, as well as at variations of excitation coefficients of optical channels.

In [13, 20], on the base of abbreviated differential equations for OEO with the combined RF FODL (Eqs. 7.43 and 7.44), the dependences of settling of the frequency, the amplitude and the phase of the OEO generation signal at variation of influence parameters—excitation parameters of combined RF FODL channels. At that, the combined RF FODL is formed by two parallel light guiders FOS1 and FOS2 of different length.

The system of mentioned equations can be solved with the help of operational mathematical system MatLab with utilization of the Euler method of the second order.

The pulse of initial conditions is specified in the segment $[-t_n, 0]$. The amplitude of the initial condition is U_{init} and the frequency is f_{init}.The analysis of calculated functions for the amplitude and the frequency shows that for the stable operation of OEO with combined RF FODL, it is necessary to satisfy the condition: $T_{\text{EF}} > T_{2\text{FOS}} - T_{1\text{FOS}}$, where T_{EF} is the time constant of the RF filter, $T_2 = T_{2\text{FOS}}$, $T_1 = T_{1\text{FOS}}$ are delays in light guiders FOS1 and FOS2, relatively.

We consider the single-frequency generation mode of OEO with combined RF FODL at variation of the excitation coefficient A of the FOS1 light guide. At that, the excitation coefficient of the FOS2 light guide is equal to $B = 1 - A$ for different values of the excitation reserve δ (or S_{del}). The character of functions $f(t)$ and $U(t)$, while the oscillation settling time T_{sett} significantly depends upon the excitation reserve δ.

The excitation reserve δ is defined as: $\delta = [\alpha_{\text{NA}} - \alpha_{\text{NA, thr}}]/\alpha_{\text{NA, thr}}$, where α_{NA} is the slope of the nonlinear function of the nonlinear amplifier current in OEO output

versus the input voltage $i = \alpha_{NA}u$, $\alpha_{NA,\ thr}$ is the minimal slope of the current nonlinear function, at which the excitation of OEO oscillations occurs.

The offset is defined as: $\theta = 2\pi(T_{2FOS} - T_{1FOS})(f_{EF} - f_0)$. Here f_{EF} is the natural frequency of the RF filter, f_0 is the mean (or reference) frequency of OEO generation. The settling time T_{sett} of the oscillation amplitude and the frequency for OEO with differential RF FODL is about: $T_{sett} > (4 - 10)(AT_{1FOS} + BT_{2FOS})$.

On the base of Eqs. (7.43) and (7.44), the analysis of the effect on the character of transients for the laser optical frequency at its fast variations. As the result of this investigation, the conclusion is made that fast modulations of QWLD optical frequency lead to the modulation of the amplitude and the phase of RF oscillations. At spasmodic variations of the QWLD optical frequency, the oscillations' settling time of OEO with differential combined RF FODL depends on the excitation coefficients A and B of FOS1 and FOS2 light guides, on natural frequency of OEO filter. At that, it is found out that the character of oscillations settling is similar to the dynamics of oscillations settling at modulation of the natural frequency of the RF filter.

The dynamics of transients in OEO with RF FODL has the interesting feature at variation of the excitation coefficient A of the FOS1 light guide.

Figure 7.22a–c show the plots of the frequency f and the amplitude U settling of the generation signal for the excitation coefficient $A = 0.4$; 0.5; 0.6; 0.7; 0.8, at that, $B = 1 - A$ for different values of the excitation reserve $\delta = 0.5$ (Fig. 7.22a, b), $\delta = 1.15$ (Fig. 7.22c). As we see, dynamics of transient is complicate and manifold.

At the value of the excitation coefficients of the light-guiding channels A and $B = 1 - A$ for $A = 0$; 0.13; 0.23; 0.33, the process of oscillation formation has the character of the interrupted generation. With the growth of the excitation coefficient A of the first channel, the oscillation amplitude of the interrupted generation increases and at $A = 0.43$; 0.49 it has the stable character. At $A = 0.509$; 0.529; 0.555, which corresponds to the minimum in AFC of combined RF FODL, the oscillation character again becomes unstable. At further increase of $A = 0.595$; 0.605, oscillations have the stable character, and the process from the interrupted generation becomes the continuous wave and the amplitude after $(4 - 5) \cdot (T_{2FOS} + T_{1FOS})/2$ "comes out" to the steady-state level. Variations of excitation coefficients A and B lead to change of the transient character, to variation of oscillation settling time and to the oscillation disruption

From Fig. 7.22b, we see that at values of the excitation coefficient 0.2; 0.3, OEO does not come out into the steady-state generation mode, which is explained by nonfulfillment of the phase balance condition at these values.

The oscillation settling time T_{sett} decreases with the growth of the excitation reserve δ and may be $T_{sett} = (4 - 15)(T_{1FOS} + T_{2FOS})/2$, where T_1, T_2 are the delays of the signal in FOS1 and FOS2, relatively.

The value of the modulation frequency Ω, at which the inertial properties are strongly manifested in OEO with the combined RF FODL, which are comparable with the inverse mean delay in FOS, i.e.: $\Omega > 1/[T_{0FOS} + (T_{1FOS} + T_{2FOS})/2]$.

The main determining factors, which affect the process of oscillation formation, are: (1) the value of excitation reserve $\delta = S_{del}$; (2) the ratio of delay time difference

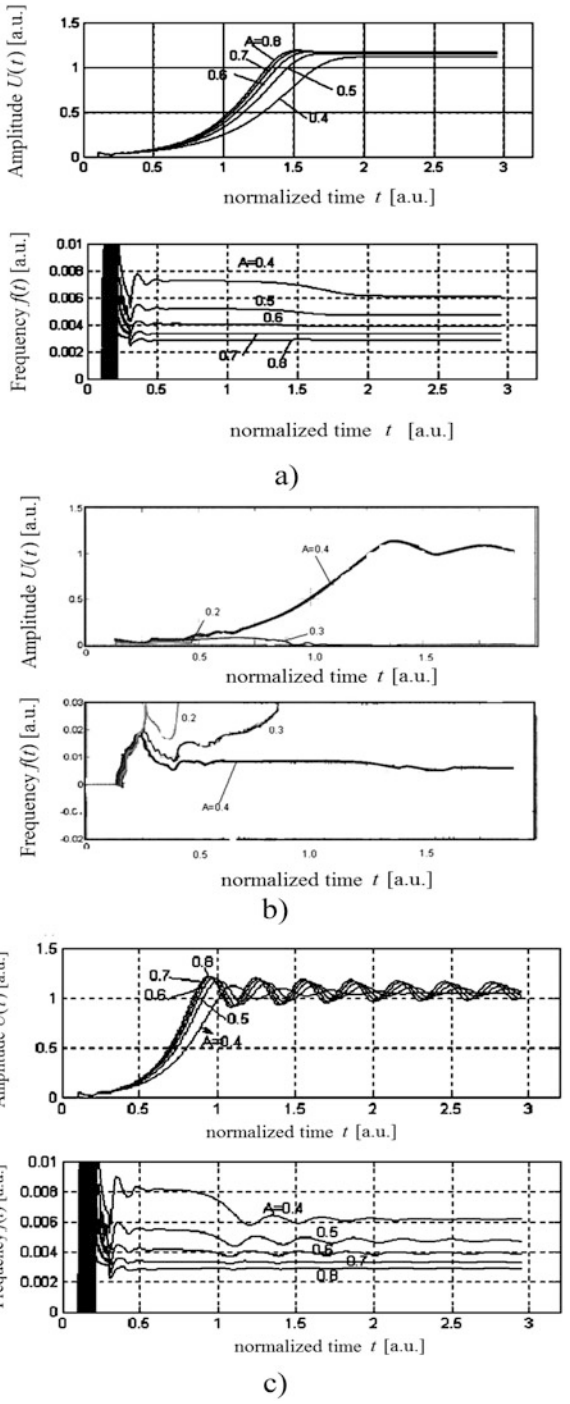

Fig. 7.22 Transients of the normalized amplitude $U(t)$ and the normalized frequency $f(t) = \dot{\Psi}(t)$ of OEO with combined RF FODL generation. The normalized time t is dimensionless and normalized to the variable $T_{EF} = [(T_{1FOS} + T_{2FOS})/20]$. The offset $\theta = 0.03$ at $A = 0.4; 0.5; 0.6; 0.7; 0.8$. (**a**) The excitation reserve $\delta = 0.5$ at the excitation coefficient of light guides is $A = 0.2; 0.3; 0.4; B = 1 - A$. (**b**) The excitation reserve $\delta = 0.5$ at $A = 0.4; 0.5; 0.6; 0.7; 0.8$. (**c**) The excitation reserve $\delta = 1.15$

in light guides (channels) to the time constant of the RF filter: $(T_{2FOS} - T_{1FOS})/T_F$, and (3) the excitation coefficients of FOS1 and FOS2: A and $B = 1 - A$.

7.4.3 *The Analysis of the Generation Frequency Control in OEO with the Differential RF FODL in the Steady State*

Dependences of the signal frequency and the amplitude versus FOS parameters in steady state can be obtained from the phase and amplitude balance equations in Chap. 3. We assume that transfer functions for QWLD, FOS, PD, RF F, and NA together with the nonlinear characteristic of AE in NA are known.

On the base of Eqs. (7.53) and (7.54), taking into consideration the performed analysis, we obtain the approximated expressions for the frequency and the amplitude of the signal generated by OEO with the combined RF FODL and examine the functions for the frequency and the amplitude of the generated signal by the solution of the phase and amplitude balance equations.

Let us consider the steady-state equations of OEO with combined RF FODL, which is constructed on the base of the differential FOS from two light guides of different length (Fig. 7.33). From Eqs. (7.53) and (7.54), the conditions of the amplitude and phase balance for OEO with the combined RF FODL follow.

The following expressions for the amplitude and phase balance, which are obtained from Eqs. (7.53) and (7.54) for OEO with differential combined RF FODL, is:

$$\begin{cases} U = \sqrt{\dfrac{4S_{01}}{3 \cdot S_{03}}} \cdot \sqrt{1 - \dfrac{\sqrt{1 + T_{EF}^2(\omega - \omega_{EF})^2}}{R_{11}S_{01}K_L\sqrt{A^2 + B^2 - 2BA\cos\omega(T_1 - T_2)}}}, \\ -\arctan\dfrac{A\sin(\omega T_1) + B\sin(\omega T_2)}{A\cos(\omega T_1) + B\cos(\omega T_2)} - \arctan[(\omega - \omega)T_{EF}] - \arctan(\omega T_L) = 2\pi n \end{cases} \tag{7.50}$$

In Fig. 7.23a, we see the plot of the function of the generated amplitude versus the frequency (resonance characteristics) in OEO with the differential RF FODL for different excitation coefficients $A = \alpha$ at $B = 1 - A$ for optical fibers of RF FODL. Figure 7.23b shows plots of functions of the amplitude $U(A)/U_{max}$ and relative variations of the OEO generation frequency: $\Delta f/f_{gen}(A = 0.5) = f_{gen}(A) - f_{gen}(A = 0.5)/f_{gen}(A = 0.5)$ (see Fig. 7.23b, c) at different types of variations of excitation coefficients $A = \alpha$, $B = \beta$ of optical fibers of RF FODL. In Fig. 7.23b, c, we see curves 1, which correspond to mutual variations of the excitation coefficients $A = \alpha$, $B = \beta = 1 - A$, and curves 2, which correspond to nonmutual variations of the

excitation coefficients at variation of $A = \alpha$, while the coefficient $B = \beta = \text{const}$ remains unchanged.

Presented in Fig. 7.23 plots give us the possibility to select correctly the generation mode, tuning ranges, to estimate the linearity of adjusting functions of OEO with the differential RF FODL. These calculated functions are true and interesting for us at utilization in OEO of devices for variations of excitation coefficients $A = \alpha$, $B = \beta$ on the base of electro-optical controlling elements (Fig. 7.24) or the modern MZ modulators on $LiNbO_3$.

Let us introduce, as in Eqs. (7.53) and (7.54), the following designations for the difference between the delay time in light guides and for average delays in FOS: $T_{1\text{FOS}} = \frac{T_{2\text{FOS}}+T_{1\text{FOS}}}{2} - \frac{T_{2\text{FOS}}-T_{1\text{FOS}}}{2}$, $T_{2\text{FOS}} = \frac{T_{2\text{FOS}}+T_{1\text{FOS}}}{2} + \frac{T_{2\text{FOS}}-T_{1\text{FOS}}}{2}$.

Now we obtain equations for the frequency and the amplitude of the OEO generation signal. At $A = B$ (i.e., at equal light power passed in channels), the phase balance equation (7.50) can be transformed.

The approximate expression for the OEO generated frequency $\omega = \omega_{\text{gen}} = 2\pi f_{\text{gen}}$ can be derived from Eq. (7.50) and presented as: $\omega_{\text{gen}} \cong (2\pi m + \omega_{\text{F}} T_{\text{F}})/[0.5T_{1\text{FOS}} + 0.5T_{2\text{FOS}} + T_{\text{L}} + T_{\text{F}}]$.

At the value $A \approx B$ of approximately (but not exactly) equal of excitation coefficients, we can derive the formula $\omega_{\text{gen}} \cong 2\pi m + \omega_{\text{F}} T_{\text{F}}]/[AT_{1\text{FOS}} + BT_{2\text{FOS}} + T_{\text{L}} + T_{\text{F}}]$ for calculation of the OEO generation frequency.

The expression for the generation frequency at non-exact equal excitation coefficients has a form:

$$\omega_{\text{gen}} \cong \frac{2\pi m + \omega_{\text{F}} T_{\text{F}}}{\frac{T_{2\text{FOS}}+T_{1\text{FOS}}}{2}(A+B) + \frac{T_{2\text{FOS}}-T_{1\text{FOS}}}{2}(B-A) + T_{\text{L}} + T_{\text{F}}}. \tag{7.51}$$

Thus, we obtain the approximate expression (Eq. 7.51) for the generation frequency of OEO with the differential RF FODL on the base of two fibers of different length. The generation frequency of OEO with RF FODL depends on the difference of light powers in outputs of FOS1 and FOS2 channels, relatively.

As the result of numerical solution of phase and amplitude balance equations of OEO with combined differential FOS, which AFC has the "rejection" character, we reveal relationships for interconnection of the OEO generated frequency with parameters of FOS, the RF filter, and NA. The relative range of OEO retuned frequencies (at minimal variations of the signal amplitude) is about 0.01–0.15 from the average OEO frequency and depends on values of the time constant of the RF filter, the difference of delay time in light guides of different lengths FOS1 and FOS2, the natural filter frequency, and the gain of NA. At that, the choice of the natural frequency of the RF filter and the ratio of time constant of RF filter to the difference of delay time in FOS1 and FOS2 influences on the slope of the OEO frequency at control from the FOS parameter—the excitation coefficient of the A light guide.

At utilization of OEO with the differential RF FODL as the retuned source of RF oscillations or as the functional transducer of physical quantities, we must know the

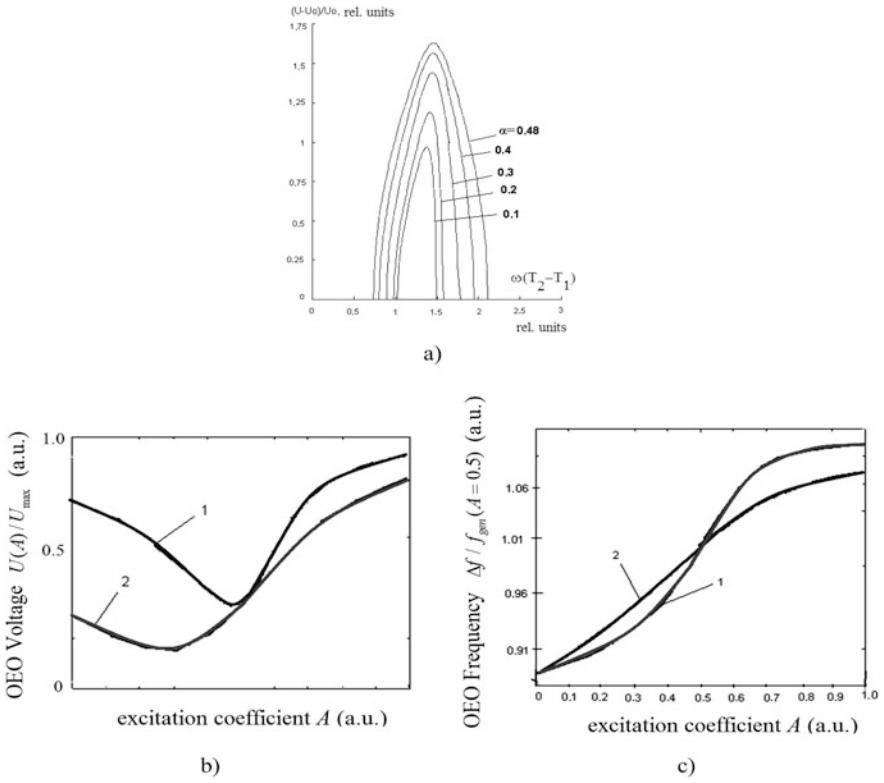

Fig. 7.23 Dependence of the signal amplitude versus the current frequency of OEO with differential RF FODL for different $A = \alpha$ at $\omega_{\text{gen}} = \frac{0.95 \cdot 7\pi}{8(T_{2\text{FOS}} - T_{1\text{FOS}})}$, $R_{\text{con}} S_{0\text{NE}} = 6$, $T_{\text{EF}} = (T_{1\text{FOS}} - T_{2\text{FOS}}) \cdot 5$ (**a**). The function of relative amplitude $U(A)/U_{\max}$ (**b**) and frequency $\Delta f / f_{\text{gen}}(A = 0.5) = \frac{\left[f_{\text{gen}}(A) - f_{\text{gen}}(A=0.5) \right]}{f_{\text{gen}}(A=0.5)}$ (**c**) of OEO versus the excitation coefficient $A = \alpha$ for different reciprocal and nonreciprocal variations of $B = \beta$. For the function 1 the condition $\beta = 1 - \alpha$ is true, while for the function 2 $\beta = 0.5$

transducer slope: $S_{f_{\text{gen}}} = \Delta f_{\text{gen}} / \Delta\alpha$, where Δf_{gen}, $\Delta\alpha$ are small increments of the generation frequency f_{gen} and $\alpha = A$. At that, the transducer characteristic is close to linear one at $\alpha = A \approx 0.5$, $S_{f_{\text{gen}}} = 0.5$ (Fig. 7.23c).

Due to "rejection" character of AFC of the differential RF FODL on the base of two light guides of different length, the maximal range of OEO frequency is achieved at the definite gain of NA. The higher the offset of the RF filter natural frequency from the rejection frequency (the frequency, at which AFC of RF FODL takes the minimal value), the higher the value of the NA gain. For example, at mentioned offset (0.7–0.8) from the rejection frequency, the NA gain must be from 4 to 8.

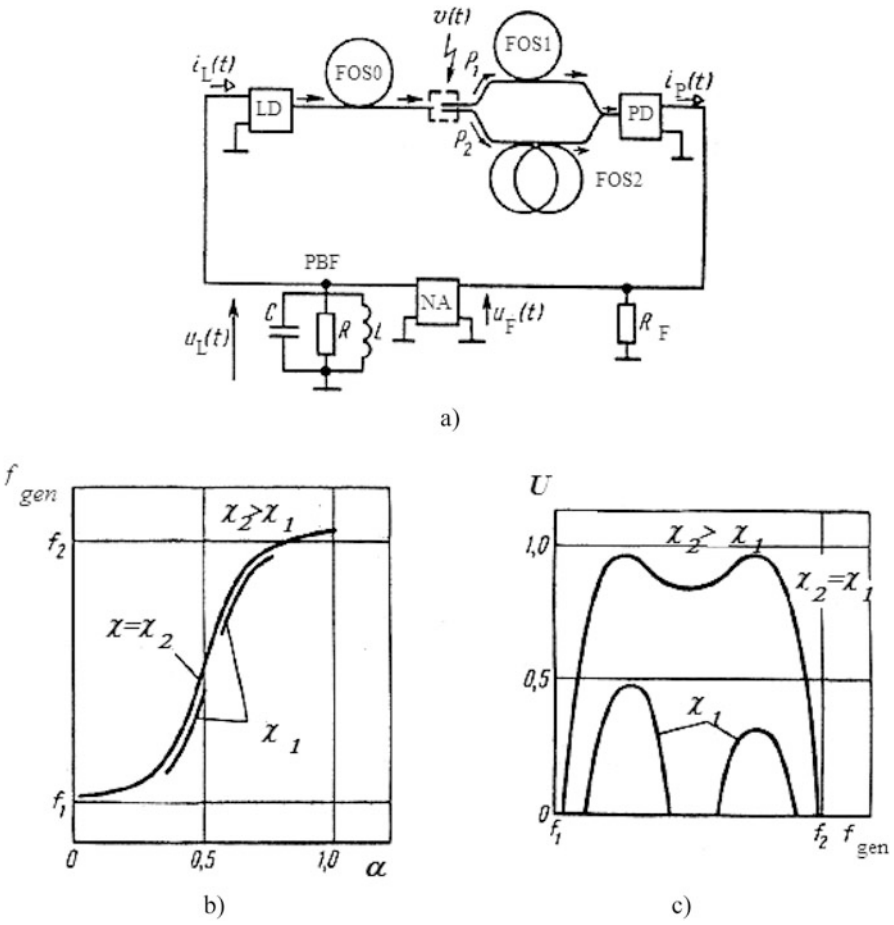

Fig. 7.24 The functional structure with the frequency control of OEO with differential RF FODL with the directional coupler of Y-type (**a**). Calculated frequency (**b**) and amplitude (**c**) functions of OEO with differential RF FODL with the directional coupler of Y-type

7.4.4 The Frequency Control of OEO with the Differential RF FODL

As shown in Chaps. 2 and 3 of this book, OEO is the promising low-noise source of microwave and mm-wave oscillations. At the same time, for practical utilization of OEO, we must, on the one hand, develop and investigate for the steady state of the optoelectronic methods of frequency control, which are nontraditional for RF oscillators, while, on the other hand, we must analyze the long-term frequency instability of OEO. The analysis of methods of the frequency control and the problem of the long-term frequency instability are tightly connected, because they are related with

the basing functions of the frequency versus the OEO parameters. Since the OEO differs from the traditional RF oscillators by the optoelectronic RF FODL, therefore, here we pay the main attention to determination of functions of the frequency and the amplitude versus optical parameters of the optical fiber and optical couplers: geometrical dimensions, the refraction index of the material, the temperature constants.

OEO can have in the RF FODL structure the optical fiber in two or several fibers, which are connected in inputs and outputs by optical couplers. The one of methods to increase the control range of retuning in frequency is the transfer from the single optical fibers in RF FODL to structures on the base of two optical fibers of different length, which are connected in the input with the help of X or Y directional couplers. Such RF FODLs are called differential. In this chapter, together with the OEO frequency control, we examine the important problem of the long-term frequency instability in OEO with RF FODL on the base of lengthy quartz optical fibers. We show that the utilization of differential RF FODL improves the long-term OEO frequency instability. Investigations of the frequency retuning in OEO with the differential RF FODL developed on the base of X- and Y-couplers is relevant also because in OEO with external modulation, the Mach–Zehnder modulator is used, which has two light guides (optical channels) of the different length, which are connected by X and Y directional couplers.

7.4.5 The Frequency Control of OEO with the Differential RF FODL on the Base of the Directional Y-Coupler

In this section, we describe the structures with control of OEO with the differential RF FODL on the base of single-mode and small-mode optical fibers, and also we consider the features of the frequency and amplitude calculations taking into account the complicate directional couplers of the Y-type.

Let us examine the system of the OEO frequency control (Fig. 7.24a) in which the following units (series-connected in the loop) are included: MLS—the laser diode LD, the differential RF FODL formed by light guides FOS0, and the light guides of different length FOS1 and FOS2, the photodiode (PD), the RF nonlinear amplifier (NA), the RF PBF. At that, light guides FOS0, FOS1 and FOS2 are connected as shown in Fig. 7.38 with the help of the optical directional coupler of Y-type.

The directional coupler of Y-type can be formed with the help of the single-mode or the small-mode optical fiber, and it can be created by attachment of FOS0, FOS1, and FOS2 with the gap between light guides. The gap between light guiders is filled by an air or the optical material. Earlier, we showed that varying of the excitation coefficients of FOS1 and FOS2, we can effectively control by the delay time in such a RF FODL, and, hence, by the generated frequency of OEO.

We can show the location of optical channels and directional optical channels of Y and X-types and their view in the longitudinal section in MZ. The MZ modulator made on the base of differential RF FODL represents two strip optical waveguides of

different length, which are connected in the input by Y- and in the output by X-optical directional couplers. The input Y-coupler executes the function of a divider of the laser emission with the electrical field strength E_L into two channels OC1 and OC2. The X-coupler located in the output serves for gathering and directing of optical emission, which comes out from the channels OC1 and OC2 to the optical channel located after the X-coupler and further directing of this emission to the photodetector.

Let us describe the results of analysis of the radio-frequency control for OEO with the differential RF FODL formed by single-mode light guides and connected as shown in Fig. 7.24a. Authors consider and analyze the transfer function of such a differential RF FODL $\mathbf{K}_{TR}(j\omega)$ for the control of excitation coefficients of FOS1 and FOS2. The expression for the transfer function of such a RF FODL can be presented as: $K(j\omega) = \alpha(r)K_1(j\omega) + \beta(r)K_2(j\omega)$, where $\alpha(r)$, $\beta(r)$ are coefficients of excitation relatively of FOS1 and FOS2, $\mathbf{K}_1(j\omega) = \exp[-\alpha_{01}(n/c)(T_{0FOS} + T_{1FOS}) - j\omega(T_{0FOS} + T_{1FOS})]$, $\mathbf{K}_2(j\omega) = \exp[-\alpha_{01}(n/c)(T_{0FOS} + T_{2FOS}) - j\omega(T_{0FOS} + T_{2FOS})]$, n is the refraction index of the material of the light-guiding threat of FOS0, FOS1, and FOS2, c is the light speed, α_{01}, α_{02} are specific light losses in FOS1 and FOS2, relatively.

The normalized transfer function of differential RF FODL is $|\mathbf{K}_{NTR}(j\omega)| = |\mathbf{K}_{TR}(j\omega)|/[S_{LD}S_{PD}\mu \exp(-\gamma_0 L_0)]$, where S_{LD} is the slope of the watt–ampere characteristic of the laser diode, S_{PD} is the slope of the volt–ampere characteristics of PD, μ are optical losses on the FOS matching. The phase-frequency characteristics of RF FODL $\varphi(\omega)$ are obtained in assumption of the light losses absence in FOS1 and FOS2, when $\gamma_1 L_1 = \gamma_2 L_2 \approx 0$ and $\mu = 1$.

At variation of the excitation coefficient of the FOS1 light guide $\alpha = A$ from 0 to 1, AFC of the differential RF FODL deforms and has the comb character with clearly expressed minima at $\omega(T_{2FOS} - T_{1FOS}) = \pi + 2\pi m$; $m = 1, 2, \ldots$; the PFC of differential RF FODL for values $\alpha \approx 0.5$ is characterized by the presence of periodically repeated sharp portions, which are degenerated into jumps by π at $\alpha = 0.5$.

In the region of $\omega(T_{2FOS} - T_{1FOS}) < \pi/2$, PFC is close to the linear function. It should be noted that in the limit cases ($\alpha = 0$ and $\alpha = 1$), PFC of the differential RF FODL represents the straight lines $\varphi = \omega T_{1FOS}$ and $\varphi = \omega T_{2FOS}$.

The adjusting curves of the frequency retuning in OEO with the differential RF FODL are shown in Fig. 7.24b, c. Taking into consideration of obtained transfer functions of the differential RF FODL, the solution of OEO abbreviated equations gives a possibility to obtain of frequency and amplitude functions versus the external impact and to find the regions of stable stationary generation of OEO with the differential RF FODL.

The comb character of $|K_{NTR}(j\omega)|$ of differential RF FODL applies features on the generation mode at impact indication in such types of devices. Figure 7.24b, c shows the plots of $f_{gen}(\alpha)$ and $U(f_{gen})$ at varying α depicted for different values of the small-signal gain in the open loop χ. The growth of χ leads to the qualitative variation of the function $U(f_{gen})$, and at small χ_1, the zone generation is observed.

In the general case, curves of frequency retuning in OEO with the differential RF FODL are nonlinear functions of the $\alpha = A$ parameter, and for $\alpha \approx 0.5$, neglecting by the small oscillator non-isochronity, the frequency of OEO with differential RF FODL is:

$$f_{\text{gen}} = \frac{\omega_{\text{gen}}}{2\pi} \approx \frac{2\pi m + \omega_{\text{F}} T_{\text{F}}}{2\pi(T_{\text{F}} + T_{0\text{FOS}} + AT_{1\text{FOS}} + BT_{2\text{FOS}})}, \tag{7.52}$$

where T_{F} is the time constant of the RF PBF, $m = 1, 2, \ldots$ Obtained functions show a series of features of the f_{gen} behavior of the oscillator under investigation, which are important for development of the fiber-optical sensors. The frequency retuning, as we see from Eq. (7.52), is possible owing to variations not only lengths of FOS0, FOS1 and FOS2, but owing to variations of excitation coefficients $A = P_1/(P_1 + P_2)$ or $B = P_2/(P_1 + P_2)$ (see Fig. 7.25). This circumstance is especially attractive since modulation methods of such parameters as α and β are well developed in the technique of amplitude fiber-optical sensors owing to impacts $v_{\text{imp}}(t)$ controlling by the sensor element. The such type of the frequency modulation in OEO (Fig. 7.25a) is accompanied by the relatively small spurious amplitude modulation, because due to the direct mutual coupling of the light powers P_1 and P_2, which are excited in FOS1 and FOS2, the total power $P = P_1 + P_2$ remains almost constant at Δx variation.

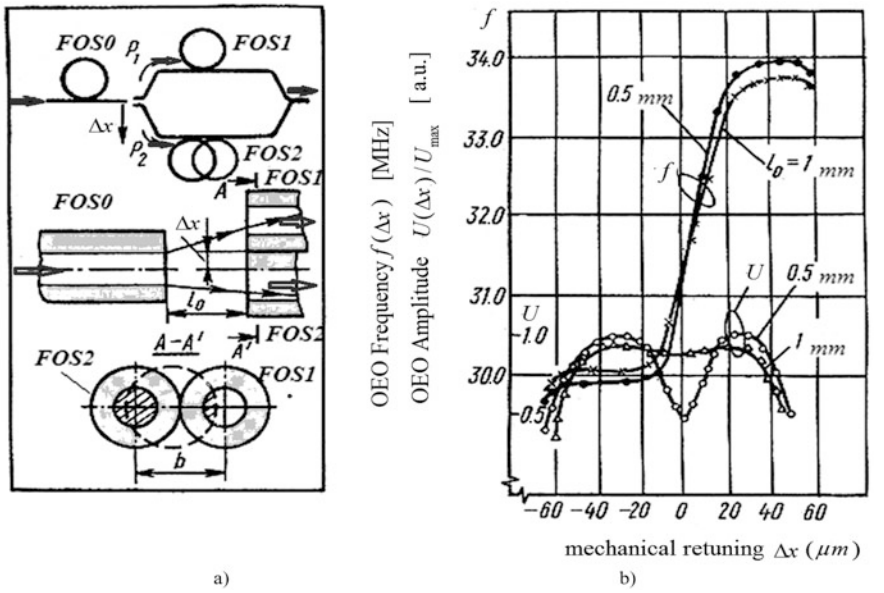

Fig. 7.25 The control system of OEO with the differential RF FODL and the directional coupler of Y-type in the breakage (**a**), and calculated and experimental functions of frequency $f(\Delta x)$ and amplitude $U(\Delta x)$ of oscillations at mechanical retuning Δx (**b**)

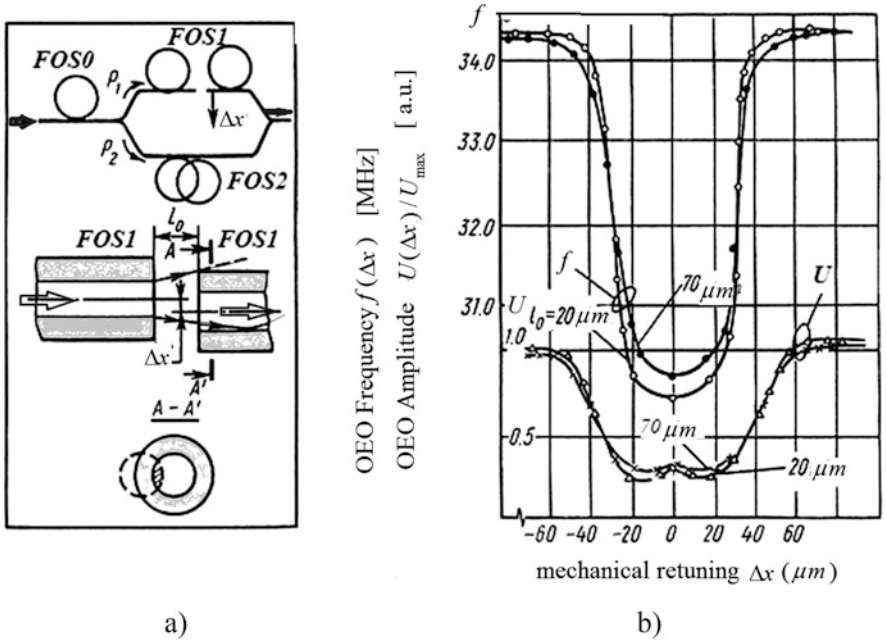

Fig. 7.26 The method of the frequency control of OEO with the differential RF FODL with the directional coupler of Y-type (**a**) and functions of oscillation frequency and amplitude (**b**) at mechanical retuning in FOS breakage

At increase of χ, the accompanied parasite amplitude modulation of the generation signal decreases. When OEO with differential RF FODL is used as the retuning source of RF oscillations, and also as the functional transducer of physical quantities, we must take into consideration that the maximal slope of transformation $S_{f_{gen}} = \Delta f_{gen}/\Delta\alpha = \Delta f_{gen}/\Delta x$, takes place at α closed to 0.5 (Fig. 7.24b), where Δf_{gen}, $\Delta\alpha$ are small increments. At that, the transformation characteristic is close to linear.

Another method of frequency modulation of OEO under consideration, at which attachment and alignment of faces is provided noticeably simpler, consists in the creation of losses of optical emission only in the single light guides FOS1 of FOS2 at misalignment of faces in the break place of one of them (Fig. 7.26). At such a method, the accompanied spurious amplitude modulation is manifested greatly than for the method in Fig. 7.25, since the mutual coupling of P_1 and P_2 is absent.

7.4.6 *The Frequency Control in OEO with the Differential RF FODL with the Directional Coupler of* X*-Type*

To study of the frequency control in OEO with differential RF FODL, we consider the structure of OEO with RF FODL with the directional coupler with X-type (Fig. 7.27). The directional coupler of X-type is concerned to optical retarding

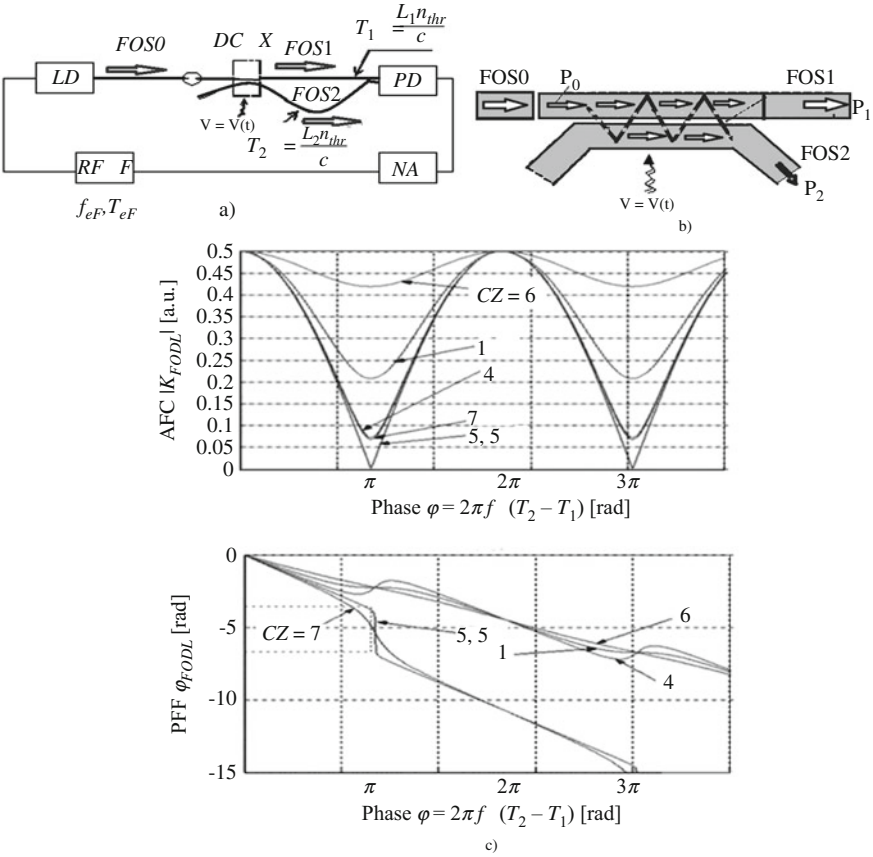

Fig. 7.27 (**a**) The system of the generation frequency control in OEO with the help of the directional optical coupler of X-type. Parameters RF FODL in OEO: delay times in FOS1 $T_{1FOS} = L_1 n_{thr}/c$ and in FOS2 $T_{2FOS} = L_2 n_{thr}/c$, the natural frequency of the RF filter is f_{eF}, the time constant of RF filter is T_{eF}. (**b**) The structure of the directional optical coupler of X-type. (**c**) AFC of $|K_{FODL}|$ and PFF $\varphi_{FODL} = 2\pi f(T_{2FOS} - T_{1FOS})$ of the differential combined RF FODL with the directional coupler of X-type for the single-mode optical fiber with different coefficients of OF: $CZ = 1; 4; 5; 5.5; 7$

systems with distributed optical coupling. The optical coupling between light guides in this coupler occurs on the definite segment, which is much more than the optical emission wavelength 1.55 μm of QWLD, but at that, the length of the coupling segment is much less than the geometrical length of FOS. As the rule, the length of the coupling segment between optical channels is 0.5–3 mm.

We note that thanks to the distributed optical coupling on the optical segment of small length, the directional optical coupler of X-type represents not only the division element of the optical power between different channels. The optical coupler of X-type represents the optical filter with the "comb" dependence of the module of the transfer function on RF and optical frequency. The readjustment of

such a filter is possible at variation of the refraction index on the boundary of channels.

Retuning of parameters of the directional coupler of X-type, we can change the excitation coefficients of the different length light guides, which form the differential RF FODL, and hence, to effectively control by the generation frequency of OEO through the delay in FOS.

Figure 7.27a shows the OEO structure with the directional fiber-optical coupler of X-type, while Fig. 7.27b shows the structure of the directional coupler of X-type.

This method of frequency control $f = f(\xi)$ versus the control parameter ξ in OEO differs from the control method in OEO on the base of the directional coupler of Y-type. Owing to the connection of optical powers P_1 and P_2 in FOS1 and FOS2, relatively, in the fiber-optical directional X-coupler, the light flows with powers P_1 and P_2 are mutually related with each other. Owing to this, the function of generation frequency in OEO $f(\xi)$ due to the mechanism of mutual optical coupling $P_{1,\,2} \sim \cos^2(\xi)$ becomes periodic on ξ, i.e., $f \sim \cos^2(\xi)$. At that, the power P in the output of the directional coupler in FOS1 varies according the law $P_{1,\,2} \sim \cos^2(\xi)$, and the frequency in OEO with differential RF FODL also varies according the law $f \sim \cos^2(\xi)$. The control types examined in previous sections are quasi-linear methods for frequency control: $f = f(\xi) \approx a\xi + b$, where a and b are constant coefficients.

The generation frequency of OEO with RF FODL at small variations of arguments of the arctangent functions can be determined as

$$f_{\text{gen}} = \frac{m + T_{\text{gen}}}{\frac{T_{1\text{FOS}} + T_{2\text{FOS}}}{2} + \frac{T_{1\text{FOS}} - T_{2\text{FOS}}}{2} \cos\left(2C_{\text{coupl}}Z\right)}. \tag{7.53}$$

AFC and PFC of differential RF FODL for different coefficients of the optical coupling are presented in Fig. 7.27c. Functions of AFC are calculated for the following values of the light-guiding parameters: $L_1 = 9.3$ m, $T_{1\text{FOS}} = 4.7 \times 10^{-8}$ s, $A = 0.5$, $B = 1 - A$, $L_2 = 13.3$ m, $T_{2\text{FOS}} = 6.7 \times 10^{-8}$ s, $T = (T_{1\text{FOS}} + T_{2\text{FOS}})/2 = 5.7 \times 10^{-8}$ s. As shown in Fig. 7.27a, b AFC and PFC of the differential RF FODL with the coupler of X-type differ from the similar AFC and PFC with the coupler of Y-type. Its main feature is the periodic dependence on the product of the optical coupling coefficient by the length of the boundary segment ($C_{\text{coupl}}Z$) at the fixed frequency of the module and the argument of the transfer function of the differential RF FODL.

From derived functions for the generation frequency of OEO with the coupler of X-type, it follows that at linear law of variation of the optical coupling coefficients C_{coupl} in the coupler of X-type, the law of generation frequency variation is periodic, which period is determined by the product of $C_{\text{coupl}}Z$.

The dependence of the optical coupling coefficient on the optical frequency v is determined by the expression: $C_{\text{coupl}} = C_0(1 + C_1 v)$, in which C_0 and C_1 are real coefficients depending on refraction indices of the light guide material, the boundary medium and geometrical dimensions. This linear function is the approximation for

the relative narrow range of optical frequencies. For the wide range of optical frequencies for the coupler of X-type, this function may be non-monotonic.

The promising approach for the frequency control in OEO with differential RF FODL is the variation of the optical coupling coefficient C_{coupl} due to the variation of the optical frequency ν of MLS, since this coefficient is proportional to the optical frequency (Fig. 7.28). Methods of the optical frequency variation in traditional quantum generators are well developed. It can be provided, for instance, in the

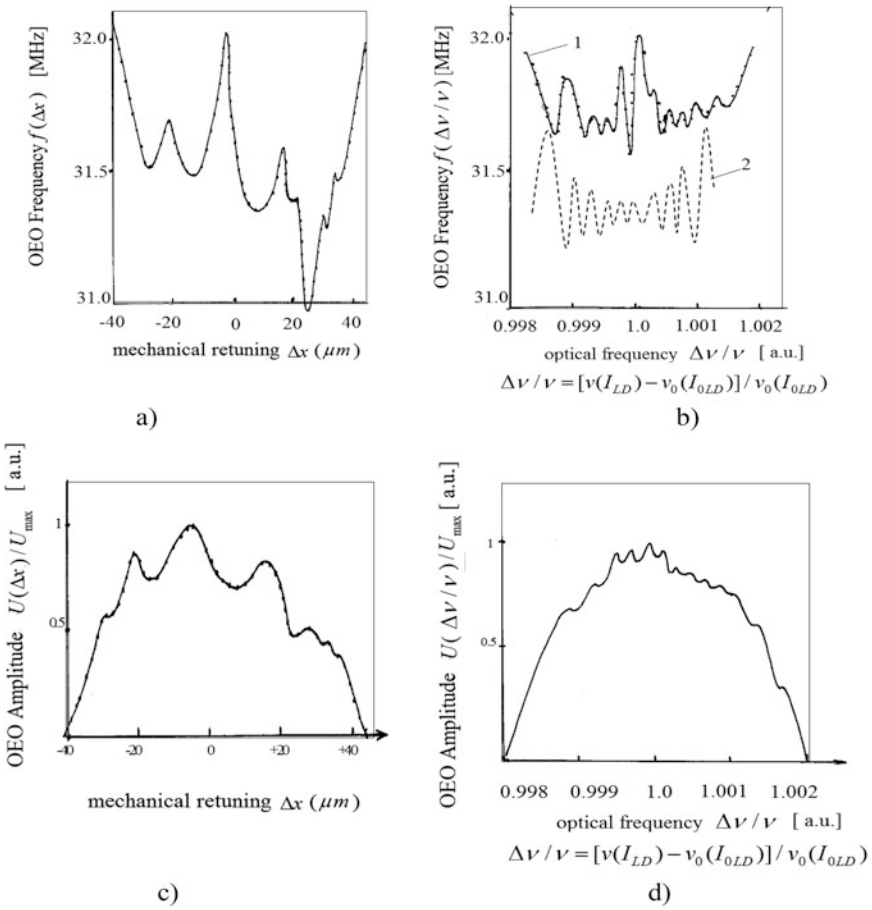

Fig. 7.28 Experimental (solid lines) and theoretical (dotted curve 2) functions of the frequency $f(\Delta x)$ (**a**), $f(\Delta\nu/\nu)$ (**b**) and the amplitude $U(\Delta x)/U_{max}$ (**c**), $U(\Delta\nu/\nu)/U_{max}$ (**d**) of OEO with the differential RF FODL with the directional coupler of the X-type at relative displace of FOS0 Δx with respect to the input face of FOS1 and at relative variations of the laser optical frequency $\Delta\nu/\nu = [\nu(I_{LD}) - \nu_0(I_{0LD})]/\nu_0(I_{0LD})$ by variation of the DC pumping current I_{LD} with regard to the average value of I_{0LD}. The optical fiber lengths in the differential RF FODL are: FOS0 $L_0 = 2$ m, FOS1 $L_1 = 1.5$ m, FOS2 $L_2 = 8$ m, the distance between the output face of FOS0 and the input face of FOS1 is $d = 20$ μm. The relative frequency instability in OEO during the experiment is $\Delta f/f = 10^{-5}$, $I_{0LD} = 50$ mA, $\nu_0 = 352$ THz (the laser wavelength is $\lambda_0 = 0.85$ μm)

laser diode by means of variation of the pumping current; in the solid-state lasers with optical pumping—by means of variation of the central frequency of the external or internal narrowband optical filter.

Figure 7.28 shows experimental (solid lines) and theoretical (dotted line) functions of the frequency $f(\Delta x)$ (a), $f(\Delta\nu/\nu)$ (b) and the amplitude $U(\Delta x)/U_{\max}$ (c), $U(\Delta\nu/\nu)/U_{\max}$ (d) for OEO with the differential RF FODL with the directional coupler of the X-type.

Experimental and theoretical investigations of OEO with differential RF FODL with the directional coupler of the X-type reveals the oscillating character of its frequency and amplitude functions (Fig. 7.28). These experimental functions are well agreed with the developed mathematical model and the analytical functions. We should note such important property of OEO that the slope of the frequency variations $f(\Delta x)$ (Fig. 7.28a) is $S_f = \Delta f/\Delta x = 0.015$ kHz/μm, the slope of frequency variations of the laser optical frequency $f(\Delta\nu/\nu)$ (Fig. 7.28b) is $S_f = \Delta f/(\Delta\nu/\nu) = 0.05$ kHz/(1 relative unit).

Another peculiarity of OEO with the combined differential RF FODL with the coupler of X-type is the variation of RF frequency of OEO at variation of the QWLD optical frequency. Because the transformation slope of the optical frequency at different choice of the optical frequency of QWLD is different owing to the "cosine" function of the optical frequency (Eq. 7.53), the slope of radio frequency retuning at variation of the optical frequency is different at the different choice of the central frequency of QWLD generation. This described property of OEO with the coupler of X-type, which plays the role here of the optical frequency discriminator, which is recommended to use in OEO systems for registration of the laser emission spectrum as well as in systems of the secretive (masking) optical control of the radio frequency of the remote oscillator in OEO with RF FODL.

Thus, in OEO with RF FODL with couplers of Y and X types, we can choose several approaches for the control of the generation frequency. The control owing to variation of excitation coefficients of optical channels or the FOS of different geometrical length, by means of variations of the refraction index of the optical material in couplers and due to variations of the laser optical frequency.

7.5 Parametric Frequency Instability of OEO with RF FODL at Temperature Impact of the Single Optical Fiber

The parametric frequency instability of OEO with respect of temperature at large delays in the optical fiber (more than 0.5 μs, the geometrical length of FOS is 100 m) is mainly determined be temperature variations of the optical fiber parameters.

7.5.1 The Heating Process of Optical Fiber, Which Is in Non-tensioned State for Free Thread Setting

Let us consider the temperature impact on the single optical fiber with the free thread setting in the coil or winding in the reel. The heating process of the optical fiber, which is in the non-tensioned state with the free thread setting, is described by thermodynamic system equations at examination of the nonuniform cylindrical body with the geometrical length L. Figure 7.29 shows the transverse (a) and longitudinal (b) sections of the optical fiber segment in the free state. We see in Fig. 7.29 of the quartz light-guiding thread, the quartz reflecting envelope and the polymer protective envelope, relatively, with diameters a_{thr}, $a_{\text{prot, env}}$, a_{polym}. For further analysis, we introduce the weight coefficients $a_{\text{q. thr}}$ and $a_{\text{q. env}}$, which are defined by the ratio of volumes, which are occupied by the quartz thread plus the quartz envelope, to the volume occupies by the polymer envelope of the optical fiber. At that, the weight coefficients are determined by equations: $a_{\text{q.thr}} = (a_{\text{q.thr0}})^2/(a_{\text{pol}})^2$ and $a_{\text{q. env}} = (a_{\text{pol}} - a_{\text{q. thr0}})^2/(a_{\text{pol}})$.

At the quasi-static variation of the optical fiber, we assume that the temperature distribution over its volume is uniform and we neglect by the influence of microbends arising in the optical fiber surface at temperature impact. Then, increments of refraction indices of the thread n_{thr} and the envelope n_{env} and of the geometrical length L of the optical fiber as the response on the temperature impact can be written as: $n_{\text{thr}} = n_{\text{thr0}}\left(1 + \frac{\mathrm{d}n_{\text{thr}}}{\mathrm{d}T_{\text{OF}}}\right)T_{\text{OF}}$, $n_{\text{env0}}\left(1 + \frac{\mathrm{d}n_{\text{env}}}{\mathrm{d}T^0_{\text{OF}}}\right)T^0_{\text{OF}}$, $L = L_0\left(1 + \frac{\mathrm{d}L}{\mathrm{d}T^0_{\text{OF}}}\right)T^0_{\text{OF}}$, $\frac{\mathrm{d}L}{\mathrm{d}T^0_{\text{OF}}} = a_{\text{thr}}\frac{1}{L_0}\frac{\mathrm{d}L_{\text{pol}}}{\mathrm{d}T^0_{\text{OF}}}$, where L_0, n_{thr0}, n_{env0} are initial values of the optical fiber lengths, the thread refraction and envelope indices, relatively, at zero temperature, T^0_{OF} is temperature of the optical fiber in degrees centigrade, $\frac{1}{L_0}\frac{\mathrm{d}L}{\mathrm{d}T^0_{\text{OF}}}$ is the temperature constant or relative linear variations of the optical fiber, $\frac{\mathrm{d}n_{\text{thr}}}{\mathrm{d}T^0_{\text{OF}}}$ and $\frac{\mathrm{d}n_{\text{env}}}{\mathrm{d}T^0_{\text{OF}}}$ are temperature constants (or slopes) of refraction indices of the thread and envelope, relatively. For the quartz optical fiber without the special boron and germanium dopes, its relative values are $\frac{1}{n_{\text{thr}}}\frac{\mathrm{d}n_{\text{thr}}}{\mathrm{d}T^0_{\text{OF}}} = 10^{-5}$, $\frac{1}{n_{\text{env}}}\frac{\mathrm{d}n_{\text{env}}}{\mathrm{d}T^0_{\text{OF}}} = 10^{-5}$. We note that for the optical fiber from the fused quartz, which is produced without special dopes, temperature constants of the refraction indices of the thread and the envelope are less by an order than the crystalline quartz. By means of an introduction of special dopes from germanium

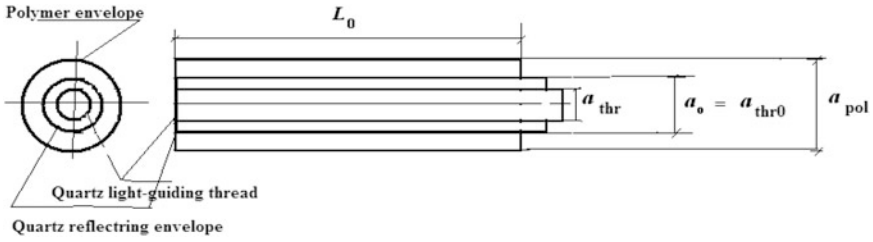

Fig. 7.29 Transverse and longitudinal sections of the optical fiber

and boron, we can achieve the temperature constants of refraction indices of the quartz thread up to values $\frac{1}{n_{\text{thr}}}\frac{\mathrm{d}n_{\text{thr}}}{\mathrm{d}T^0_{\text{OF}}} = 10^{-6}$, temperature constants of linear variations $\frac{\mathrm{d}L_{\text{thr}}}{\mathrm{d}T_{\text{OF}}}$ (spreading), of geometrical lengths of the quartz thread $\frac{1}{L_0}\frac{\mathrm{d}L_{\text{thr}}}{\mathrm{d}T^0_{\text{OF}}} = 10^{-6}$ to 10^{-7} of the geometrical length of the envelope, and the linear variations $\frac{\mathrm{d}L_{\text{pol}}}{\mathrm{d}T^0_{\text{OF}}}$ (spreading) of the polymer envelope is $\mathrm{d}L_{\text{pol}}/\left(L_0\mathrm{d}T^0_{\text{OF}}\right) = 10^{-3}$ to 10^{-4}.

The expression for the generated frequency in OEO with the single optical fiber at the temperature impact on the single OF in RF FODL is determined by the expression obtained for the OEO structure from the solution on the phase balance equations (Eqs. 7.41 and 7.42) presented in:

$$f = \frac{m + f_{\text{F}}T_{\text{FOS}}}{T_{\text{FOS}} + T_{\text{F}} + T_{\text{FD}} + T_{\text{LD}} + T_{\text{NA}}}, \tag{7.54}$$

where $m = 1, 2, 3\ldots$, T_{FOS} is the delay time in the optical fiber, T_{F} is the time constant of the RF filter, T_{FD} the time constant of the photodetector, T_{LD} the QWLD time constant, $T_{\text{NA}}$is the time constant of the RF nonlinear amplifier, f_{F} is the natural frequency of the RF filter in OEO.

Taking into account that at the temperature impact on OEO with RF FODL, the delay in the optical fiber equaled to $T_{\text{FOS}} = \frac{Ln_{\text{thr}}}{c}$ greatly exceeds the delay in the RF part of OEO. In other words, the condition is satisfied that the delay time in the optical fiber T_{FOS} is greatly more than the sum of delays in other elements $T_{\text{F}} + T_{\text{PD}} + T_{\text{LD}} + T_{\text{NA}}$ and deviations of the delay time in the optical fiber (owing to the temperature impact) from its average value ΔT_{FOS} is much more than the total deviation in all components OEO $\Delta T_{\text{F}} + \Delta T_{\text{PD}} + \Delta T_{\text{LD}} + \Delta T_{\text{NA}}$.

Under these conditions, $\Delta f/f = -(\Delta T_{\text{FOS}}/T_{\text{FOS}}) \cdot \left(\Delta T^0_{\text{OF}}/T^0_{\text{OF}}\right)$ is the relative variation of the OEO frequency. To calculate the function of the OEO frequency versus temperature, we can use the formula: $f = f_0 - \Delta f\left(T^0_{\text{OF}}\right) = f_0\left[1 - \left(\Delta T_{\text{FOS}}/T_{\text{FOS}}\right)\left(\Delta T^0_{\text{OF}}/T^0_{\text{OF}}\right)\right]$.

Taking into consideration the relative variations of the delay in the optical fiber, variations of the OEO frequency at temperature variations in the temperature range from 15 to 150 °C are well described by the following expressions, in which we use the weight coefficients: the relative variations of the delay $\frac{\Delta T_{\text{FOS}}}{T_{\text{FOS}}} = \left(\frac{1}{n_{\text{thr}}}\frac{\mathrm{d}n_{\text{thr}}}{\mathrm{d}T^0_{\text{OF}}} + \frac{a_{\text{thr}}}{L}\frac{\mathrm{d}L_{\text{thr}}}{\mathrm{d}T^0_{\text{OF}}} + \frac{a_{\text{pol}}}{L}\frac{\mathrm{d}L_{\text{pol}}}{\mathrm{d}T^0_{\text{OF}}}\right)\frac{\Delta T^0_{\text{OF}}}{T^0_{\text{OF}}}$; and the relative variations of the frequency $\frac{\Delta f}{f} = \left(\frac{1}{n_{\text{thr}}}\frac{\mathrm{d}n_{\text{thr}}}{\mathrm{d}T^0_{\text{OF}}} + \frac{a_{\text{thr}}}{L}\frac{\mathrm{d}L_{\text{thr}}}{\mathrm{d}T^0_{\text{OF}}} + \frac{a_{\text{pol}}}{L}\frac{\mathrm{d}L_{\text{pol}}}{\mathrm{d}T^0_{\text{OF}}}\right)\frac{\Delta T^0_{\text{OF}}}{T^0_{\text{OF}}}$.

Substituting in this expression the specific values of temperature coefficients, we obtain: $\Delta f/f = \left(10^{-5} + a_{\text{thr}} \cdot 10^{-7} + a_{\text{pol}} \cdot 10^{-4}\right)\left(\Delta T^0_{\text{OF}}/T^0_{\text{OF}}\right)$. From above-mentioned expressions, we see that the refraction index of the thread determines the main tendency in frequency functions of OEO. With the optical fiber temperature growth from 15 to 150 °C, the OEO generation frequency decreases according the law closed to the linear function. The linearity of this function is mainly determined by the ratio of diameters of the quartz envelope and the polymer envelope of the

single optical fiber. If the thickness of the protective polymer envelope is commensurable with the thickness of the quartz envelope, then, at that, the thickness of the protective polymer envelope determines the effective extension of the optical fiber.

If the relatively small segments of the optical fiber, for instance, 50–150 m in length, are used in OEO, then it is recommended to take into consideration the time constant of the high-Q filter T_F, which natural frequency is equal to f_F.

The relative frequency offsets in OEO with the single single-mode optical fiber, which are excited by single-frequency optical emission with the linear polarization, determined by the temperature coefficient of the refraction index of the light-guiding thread α_{0T} and can be determined by the expression $\Delta f/f_0 \approx \alpha_{0T} \cdot \left(T^0_{OF} - T^0_{0OF}\right)/T^0_{0OF}$, in which T^0_{OF}, T^0_{0OF} is the current and average values of the optical fiber temperature in RF FODL, relatively. We note, once more, that the temperature coefficient of variations of the refraction index for the pure quartz glass is $\alpha_{0T} = 1.5 \times 10^{-6}\,K^{-1}$, while the temperature coefficient for the quartz glass with different compensating dopes of boron and germanium at different concentrations is $\alpha_{0T} = 1.0 \times 10^{-5}\,K^{-1}$ [21].

The coefficient of the linear thermal extension of different types of the silicate glasses is from $5 \times 10^{-7}\,K^{-1}$ to $120 \times 10^{-7}\,K^{-1}$ in the interval 15–100 °C.

At stabilization of the relative variations of the optical fiber temperature, for example, to values 10^{-1} to 10^{-3} in OEO with the single optical fiber, the expected frequency instability in OEO is: $\Delta f/f_0 \approx 10^{-6}$ to 10^{-9}.

The last expressions for $\Delta f/f_0$ permit to assert that for OEO with the lengthy optical fiber (more than 1000 m), at changing of the environment temperature in the large operating range within −40 to +60 °C, at utilization of thermal compensation methods (i.e., at temperature adjustment of the optical fiber), we can realize the relative frequency variations in OEO not worse than $\Delta f/f_0 \sim 10^{-6} \div 10^{-7}$. The modern level of the temperature stabilization in limited volumes from 1 to 50 cm^3 allows the provision of the control and stabilization of temperature on the level of one micro-degree centigrade, i.e., to the level of relative temperature variations at 2 °C to the levels 10^{-3} to 10^{-6}. Therefore, in OEO with the single optical fiber, the achievable level of the long-term frequency instability is less than 10^{-8} to 10^{-9}.

7.5.2 *Prospects of the Ultrasmall RF FODL Development Less than 1 cm^3 and with the Delay 5–50 μs/km*

From the thermodynamic analysis for the solid uniform body being under the temperature impact, we know that the best thermal stabilization (i.e., the conservation of the constant body temperature with specified accuracy in its whole volume) at uniform heating of the optical fiber material in the closed thermal-isolated volume can be achieved better and faster for the lesser useful volume of the solid uniform body (or optical fiber in our case). Under the useful volume of the optical fiber, we understand the volume of the quarts material of the light-guiding thread and the envelope, which participate in the transmission process or the propagation process of

the light emission from the laser to the photodetector. The useful volume of the single optical fiber in OEO with RF FODL is less than 1 cm^3 per 1 km of the fiber-optical thread with the total delay in RF FODL of 5 μs/km. For instance, for the single-mode optical fiber with 1 km-length and the thread diameter of 7–10 μm, the quarts envelope of 21 μm, the total diameter of 33 μm, the useful volume is about 1 cm^3. In the limit case, we have for the single-mode optical fiber with 1 km-length with the thread diameter of 2 μm, with the quartz envelope diameter 9 μm, the total optical fiber diameter of 11 μm, the useful volume is about 0.1 cm^3 with the total delay in RF FODL of 5 μm/km with transmission via RF FODL of microwave oscillations with the frequency of 10 GHz.

At development of the ultrasmall in the volume of RF FODL of 1 cm^3 and less, the main technological problem is the increasing optical losses, which are formed at splicing owing to the small radii of the optical fiber bending during splicing. So, for optical fiber thread packing at 1 km-length, approximately 10,000–50,000 turns are required at the average turn length of 18–30 mm with the bending radii about 3–5 mm.

The rough calculation at the bending radius of 10 mm, at losses of 0.0002 dB/1bend at number of such bends of 10,000 pieces allows obtaining the losses value on 2 dB-level per 1 km of the optical fiber, which satisfies to the practical application of RF FODL.

At manufacture of the ultrasmall RF FODL in volume, the rolling process is specially important for the lengthy thread of the optical fibers produced with old traditional technologies of the vapor-phase deposition with utilization of the plasma torches at small curvature radii less than 15 mm. Figure 2.13d, e shows the plot of the optical loss function of the traditional optical fibers and the photo-crystal (or perforated) fibers versus the value of the bending radius for different fibers [22].

The transverse sections of the fiber with the one-dimension circular structure (the Braggian fiber) (d) and the photon-crystal fiber with auxiliary holes around the thread (e) are presented in Fig. 2.13d, e together with the example of the transmission function versus the wavelength in the Braggian fiber.

At present, in Russia and in many countries, the whole series of new types of optical fibers exists, which allow the bend practically under any angles and at that, have the insignificant losses in the bending. These are so-called photon-crystal fibers (PCF) having in addition the whole series of other remarkable properties.

Modern technologies of the quartz optical fiber manufacture with the nitrogen doping with manufacture of the variety of high-accuracy envelopes give a possibility to produce of optical fibers with low losses at limit bending radii less than 5 mm. In perspective, at utilization of patented by authors high-accuracy technology of optical fiber manufacture with application of the half-finished product heating with the help of the plasma pillar created by the microwave oscillators, we can produce the optical fibers with ultralow optical losses at small bending radii less than 5 mm. This patented technology and the small useful volume of the optical fiber in OEO with RF FODL give us the right to state that the limit volume of RF FODL with the single lengthy optical fiber is 0.1 cm^3/1 km of the optical fiber at delay 5 μs/km.

7.5.3 Parametric and Long-Term Frequency Instability of OEO with the Differential RF FODL

One of the methods for decrease of relative temperature offsets of the OEO frequency is the application of the differential RF FODL. At that, the main stabilization principle at temperature changing is utilization of segments of significant (more than by an order) decrease of the PFC slope from the temperature variations of the combined differential RF FODL on the base of two or several optical fibers of different length. At that, for specified OEO frequency, we can select, for example, two optical fiber of the different length in such a manner that total PFC of RF FODL has in definite portions of low slope of temperature variations, and the module of the transfer function in this chosen segment varies insignificantly (less than by 10–50%). In turn, temperature of the thermostat for the optical fiber, for instance, 25 °C must be kept constant and adjusts at external variations of the temperature.

The influence of small quasi-static variations of OEO with RF FODL parameters, on the base of two optical fibers of different lengths FOS1 and FOS2 (excitation coefficients of these FOS1 and FOS2 are, relatively, A and B), taking into account that delay time in FOS is much more than the time constant of the RF filter upon its frequency, at small OEO non-isochronity and at condition that the equality $B = 1 - A$ is not fulfilled (i.e., the sum of coefficients is $A + B \neq 1$), is described by the following expression derived from the phase balance equation:

$$\frac{\Delta f}{f} = \frac{(A+B)\Delta f_{\mathrm{F}}}{f_{\mathrm{F}}}\frac{\Delta T_{\mathrm{FOS}}}{T_{\mathrm{FOS}}} - \frac{(A+B)\Delta T_{\mathrm{FOS}}}{T_{\mathrm{FOS}}} + (A-B)\cdot\frac{T_{\mathrm{FOS2}} - T_{\mathrm{FOS1}}}{2T_{\mathrm{FOS}}} \cdot\frac{\Delta T_{\mathrm{FOS2}} - \Delta T_{\mathrm{FOS1}}}{T_{\mathrm{FOS2}} - T_{\mathrm{FOS1}}}, \tag{7.55}$$

in which $\Delta f_{\mathrm{F}}/f_{\mathrm{F}}$ is the relative offsets of the natural frequency of the RF filter due to the temperature action, $T_{\mathrm{FOS}} = (T_{\mathrm{FOS2}} + T_{\mathrm{FOS1}})/2$ is the average delay in the differential FOS, $\Delta T_{\mathrm{FOS}}/T_{\mathrm{FOS}}$ is the relative offset of average delay in RF FODL on the base of two optical fibers of the different length due to temperature, $(\Delta T_{2\mathrm{FOS}} - \Delta T_{1\mathrm{FOS}})/(T_{2\mathrm{FOS}} - T_{1\mathrm{FOS}}) = \Delta\tau_1/\tau_1$ are relative offsets of the differential delay in FOS $\tau_1 = T_{1\mathrm{FOS}} - T_{2\mathrm{FOS}}$ owing to temperature, where T_1, T_2 are delay times in FOS1 and FOS2, relatively.

From Eq. (7.55) it follows that small temperature offsets of average delay in RF FODL on the base of two optical fibers of different lengths are compensated by the correct choice of excitation coefficients A and B. From Eq. (7.55) we also see that the second term, which is responsible for reduction of the generation frequency of OEO with RF FODL, is negative at the temperature growth, while the third term responsible for the relative variations of the differential delay.

The following condition of the temperature compensation in OEO with differential RF FODL can be derived from Eq. (7.55):

$$(A+B)\frac{\Delta T_{\mathrm{FOS}}}{T_{\mathrm{FOS}}} = (A-B)\frac{T_{2\mathrm{FOS}}-T_{1\mathrm{FOS}}}{2T_{\mathrm{FOS}}}\frac{\Delta T_{2\mathrm{FOS}}-\Delta T_{1\mathrm{FOS}}}{T_{2\mathrm{FOS}}-T_{1\mathrm{FOS}}}. \tag{7.56}$$

From Eq. (7.56), the condition of temperature compensation is $\frac{A-B}{A+B} \approx \frac{2T_{\mathrm{FOS}}}{T_{\mathrm{FOS2}}-T_{\mathrm{FOS1}}}$. The analysis of parametric dependence upon temperature variations in Eq. (7.55) permit to conclude that in OEO with the differential RF FODL, it is possible to obtain the high indices of long-term frequency dependence owing to the presence in FOS at least two optical fibers of different length.

7.5.4 *The Phase-Generator Measuring Method of Differential Delays of the Optical Fiber at Its Temperature Change*

The functional structure of the phase-generator OEO is shown in Fig. 7.30. It contains OEO with RF FODL and additionally the photodiode FD1 connected to it through the optical mode selector (OMS) and the light guide FOS1. OEO is formed by series-connected in the loop by the laser diode (LD) (of MLS), the optical mixer (OM), FOS0, the optical selector (OS), the photodiode PD2, the nonlinear amplifier (NA), the RF filter (RFF) and the coupler (C). In this structure, the measuring devices: the phase-meter ("$\Delta\varphi$"), the frequency-meter ("f") and the voltmeter ("U") are included. At that, the phase-meter measures the phase difference of RF oscillations, which pass from the photodiodes PD1 and PD2. The frequency-meter and the voltmeter measure the frequency and the amplitude of RF oscillations of OEO, relatively. The main principle consists in utilization of phase measurements (phase difference $\Delta\varphi$) of differential delays of optical emissions in the output of FOS0 together with measurements of the frequency and the amplitude.

The phase-generator method developed and patented by authors [23] is used for the complex investigation of quartz optical fibers for temperature variation within the limits 0–150 °C. On the base of this approach, the sensors and functional transducers

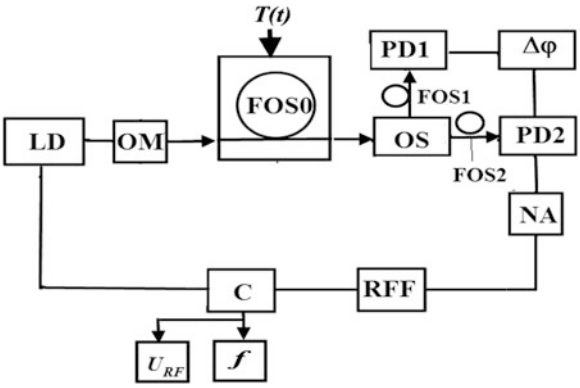

Fig. 7.30 The OEO structure with application of the patented "phase-generator" method of phase difference measurement. (Patent belongs to authors [23])

of physical quantities (temperature, pressure, electrical voltage, mechanical tensions) are developed as well, and investigations of spatial directional patterns of light sources (lasers, laser diodes, light-emitting diodes) are performed.

The phase-generator method can be used not only for measurement of differential delays of different groups of light guide modes in multi-mode and small-modes optical fibers, but also for studying of spatial, polarization, disperse, and nonlinear characteristics of the single-mode optical fibers. With the help of this method, we can examine the spatial and time coherence of optical emission sources, to study the "speckle" interference picture in the output of optical fiber, to measure characteristics of spatial optical filters.

At development of this method, the analytical functions of parameters of the RF oscillation phase difference $\Delta\varphi = \varphi_2(R_2) - \varphi_1(R_1)$ are determined versus parameters of the fiber-optical section of OEO with RF FODL. At that, $\varphi_2(R_2)$ and $\varphi_1(R_1)$ are phases of RF oscillations in the outputs of PD1 and PD2, relatively, and R_1, R_2 are generalized characteristic parameters of optical emission groups applied, relatively, to the light-sensitive areas of PD1 and PD2.

For the optical selector OS, which extracts the light guide modes, the parameter R is determined, for example, for the optical fiber, which has the step-like profile of the refraction index as the ratio $R = (\Theta/\Theta_0)^2$, where Θ_0 is the maximal angle (numerical aperture) of the light emission propagation in the output of the optical fiber FOS0 with respect to the optical fiber axis, Θ is the angle of the light emission propagation of the degenerated group of modes in the FOS0 output with respect to the optical fiber FOS0 axis.

At calculation of the phase difference $\Delta\varphi = \varphi_2(R_2) - \varphi_1(R_1)$, the values of R_1, ΔR_1 and ΔR_2 are constants during the variation process of the R_2 quantity under condition that $R_2 \leq 1 - \Delta R_2$. At increase of $R_2 \geq 1 - \Delta R_2$ value, the quantity $R_2 = 1 - \Delta R_2$, because the selecting area will come out of the aperture of the FOS0 light emission.

Figure 7.31 shows the experimental dependences of the generation frequency (a) and the phase differences $\Delta\varphi = \varphi_2(R_2) - \varphi_1(R_1)$ (b) of OEO corresponding to the structure in Fig. 7.30 at temperature variations of the optical fiber in the air thermostat. At that, the multimode optical fiber has no the polymer envelope and has the geometrical length of 100 m, the relative ratio of the refraction index of the thread and the envelope is 0.01, the thread diameter is 50 μm.

On the base of presented experimental plots in Fig. 7.31, we can make the following conclusions: the temperature frequency instability of OEO is the same as quartz instability, i.e., it defines by the refraction index of the quartz light-guiding thread, which for the optical fiber from the melted quartz (with doping) is 10^{-5} 1/°C.

Deviations from the linear law for the frequency function are connected with the phenomenon of modes coupling and redistribution of optical emission between the light-guiding thread and its quartz envelope. These periodic deviations from the linear function are more noticeable in phase functions shown in Fig. 7.31b.

It is obtained from these functions that the slope of temperature variations of the mode coupling coefficient of the single fiber with the length 100 m is 10^{-3} to 10^{-2}/degree.

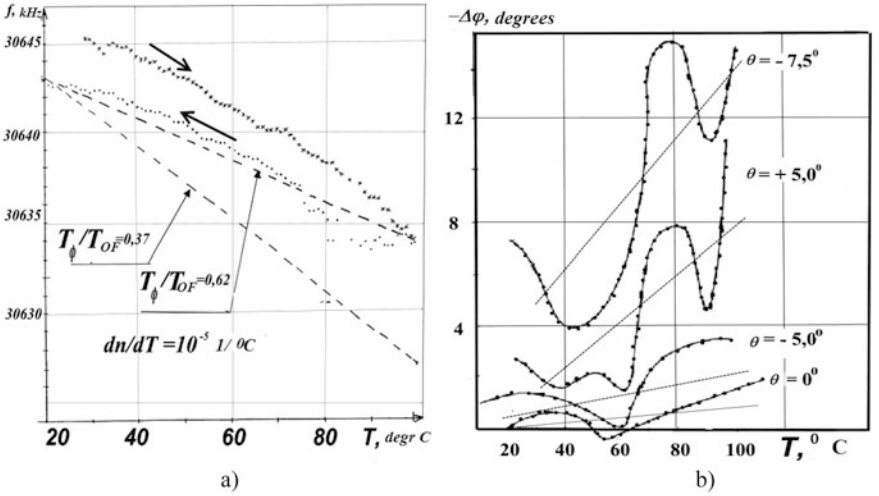

Fig. 7.31 Experimental functions of the frequency (**a**) and phase differences (**b**) of OEO at temperature variation in the air thermostat; the light guide with the length of 100 m is without the polymer envelope. Figure (**b**) shows the dependence of the phase difference for different positions of the optical selector: 0°, −5°, +5°, −7.5° with regard to the optical axis of the optical fiber in its output

At utilization in RF FODL of the special single-mode optical fiber with the length 4.6 km, the OEO frequency instability of 10^{-6}/degree is obtained in the experiment on the OEO frequency 8.2 GHz. The accuracy of the temperature measurement is 0.1 °C, and the accuracy of the frequency measurement is 10^{-6}.

The hysteresis character of the temperature frequency functions (Fig. 7.31) is concerned to the original result of theoretical and experimental investigations, which can be explained not only by the variation of the light guide refraction index, but by the temperature volumetric extensions of the double protective polymer envelope. The decrease of weight coefficients till the values of 10^{-2} is possible if to decrease the thickness of the polymer envelope till 1–2 μm (or not to form of the polymer envelope of FOS at the technological cycle of the FOS manufacture). In this case, the temperature frequency instability in OEO is as in usual quartz systems, i.e., it is determined by the refraction index of the quartz light-guiding thread: 10^{-5} to 10^{-6}. The temperature stabilization of FOS till the values $\Delta T_{OF}/T_{OF} = 10^{-3}$ leads to the OEO frequency instability $\Delta f/f = 10^{-8}$.

On the base of the analysis of theoretical experimental results of this phenomenon, authors developed and patented the structure of temperature-compensated OEO (Fig. 7.32) [24]. We recommend providing the decrease of the OEO temperature instability using the thermal compensation methods of the FOS0 optical fiber. By selection of weight coefficients a_{thr} and a_{pol} of the quartz thread and the envelope, we achieve the decrease of the temperature coefficient of the refraction index of the FOS thread till the values $\Delta n_{OF}/(n_{OF}\Delta T_{OF}) = 10^{-6}$ to 10^{-7}, for instance, during the

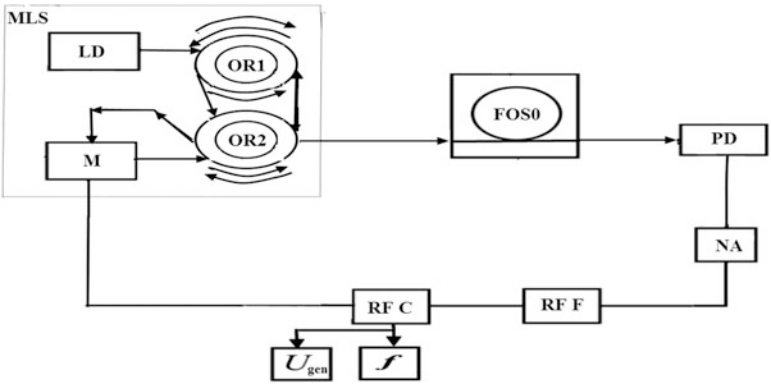

Fig. 7.32 The structure of the temperature-compensated OEO. OR1, OR2 are optical resonators, M is the electro-optical modulator (Patent belongs to authors [24])

process of FOS manufacture owing to doping in the quartz thread of boron and germanium elements and their oxides and by selection of mutually compensating dopes in the thread and FOS envelope.

The variant of the temperature compensation is the utilization in OEO of differential RF FODL. One of methods of compensation of OEO frequency offsets due to temperature is the application of the control systems with external stable quartz oscillators or the quantum-frequency standards on cesium vapors.

Figure 7.33 shows the dependences of the OEO generation frequency at variations of OF temperature: (a) OF without the polymer envelope (see d); (b) OF with the polymer (length is 300 m) (see e); (c) the OF cable with the double polymer envelope (see f).

The analysis of frequency-temperature functions (Fig. 7.31) gives a possibility to conclude that the presence of the OF polymer envelope leads to the hysteresis character of functions. These original results in measurement of the frequency-temperature functions allow the correct selection and optimization of RF FODL construction for OEO, which are exposed by the temperature impact.

7.5.5 Brief Conclusions

The analysis of the frequency control in OEO with differential RF FODL on the base of two optical fibers of different lengths connected by their inputs by directional couplers of Y- or X-type is performed, and the long-term frequency instability in OEO is studied. The following conclusions are made.

The utilization of selection on the optical frequency in FOS with DC of Y-type for the frequency control is possible at presence of the additional optical frequency spatial selector, for instance, of the optical dispersive crystal mounted in the break

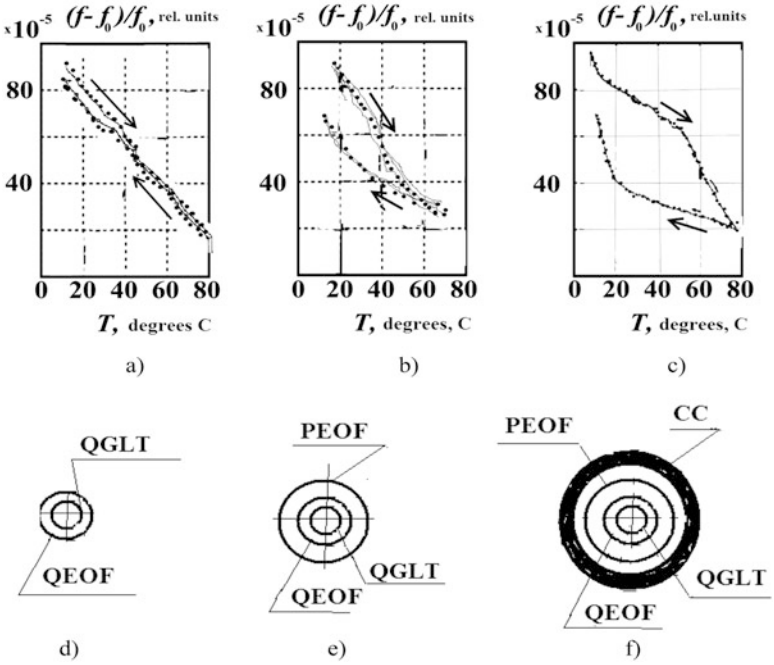

Fig. 7.33 The dependences of OEO generation frequency at variations of OF temperature: (**a**) OF without the polymer envelope (see **d**); (**b**) OF with the polymer (length is 300 m) (see **e**); (**c**) OF cable with the double polymer envelope (see **f**). PEOF is the polymer envelope of the optical fiber, OF is the optical fiber, CC is the cable covering, QGLT is the light-guiding thread from the quartz glass, QEOF is the quartz envelope of OF

between OFs. At that, the slope of the radio-frequency control is 10^{-4} to 10^{-7} Hz/nm and essentially depends on the selector choice.

At the linear law of the optical coupling coefficient C_{coup} variation in the directional coupler of X-type, the law of OEO generation frequency variation at the differential RF FODL is periodic, which period is determined by the product $C_{\text{coup}}Z$. In turn, the coefficient of optical coupling depends upon the optical frequency ν_{L} of QWLD in MLS and determines by the expression $C_{\text{coup}} = C_0(1 + C_1\nu_{\text{L}})$, in which C_0 and C_1 are real coefficients depending on the refraction index of the material of the light guider, the boundary medium and their geometrical sizes. Thus, we show that the one of features of OEO is the connection of the QWLD optical frequency with the radio frequency in OEO.

The fulfilled theoretical and experimental analysis of the OEO frequency control systems on the base of directional optical couplers of Y- and X-types shows that the retuning frequency range is from 1 till 20%, and the slope of the generation frequency control versus the FOS bias is from 10 Hz/μm till 10 kHz/μm, the nonlinear distortion coefficient in Frequency functions is less than 2%.

As the investigation results of frequency and amplitude oscillations functions in OEO at variations of FOS parameters, we obtain the new earlier unknown mechanisms of frequency control in OEO:

- The linear at using of DC of Y-type and variations of excitations coefficients in the single optical channel.
- The quasi-linear at using of DC of Y-type and variations of excitation coefficients in two optical channels.
- The periodic at using of DC of X-type by means of longitudinal optical coupling.

Considered methods of OEO frequency control are new and not-studied in publications and they expand the application areas of OEO. New devices, which use in its base the described methods of OEO frequency control, are protected by Russian patents.

We show that the OEO long-term frequency instability with utilization of "specific" optical fibers can achieve 10^{-8}. To provide the high-stability generation, we can use relatively low-Q tuned RF filter (which is nonexpensive) and the stable RF FODL with the large delay time (10–25 μs), for example, on the base of the single light guide. At that, the benefit in frequency stability is determined by the ratio of the signal delay in the optical part of OEO with RF FODL to the time constant of the RF part.

This benefit is 20–300. There is a possibility to improve the indices of RF high-stable low-noise microwave oscillators, which operate at room temperatures on the principle of frequency pulling by the high-Q external resonators owing to the structure of OEO with RF FODL. This approach does not resort of the complicate and expensive methods of PLL systems in the microwave range. The decrease of weight coefficients till values 10^{-2} by reduction of the thickness of the protective polymer envelope to 1–2 μm (or without formation of the polymer envelope of the optical fiber at the technological cycle of the OF manufacture) provides that the OEO temperature frequency instability is as in any quartz systems (10^{-5}), i.e., it is determined by the refraction index of the quartz light-guiding thread. The temperature stabilization of the optical fiber to values $\Delta T_{\text{OF}}/T_{\text{OF}} = 10^{-3}$ leads the OEO instability $\Delta f/f = 10^{-8}$. It recommended to provide the decrease of OEO temperature instability using methods of the temperature compensation of the optical fiber by the choice of weight coefficients a_{thr} and a_{pol} of the quartz thread and the polymer envelope, relatively. This provides the decrease of the temperature coefficient of the thread refraction index to values $\Delta n_{\text{OF}}/\left(n_{\text{OF}}\Delta T^{0}_{\text{OF}}\right) = 10^{-6}$ to 10^{-7}, for example, during the process of the optical fiber manufacture owing to addition into the quartz thread of boron and germanium dopes and their oxides, by selection of mutually compensating dopes into the thread and the envelope of the optical fiber. The utilization in OEO of differential RF FODL on the base of two or several optical fibers of the different length is the variant of the temperature compensation.

In previous sections of this chapter, we show that at utilization in OEO of optical fibers produced according to authors recommendations for the new technology [25] for manufacturing of the optical fibers with complicate micro-structural thread and the envelope with application of the high-accuracy method for regulation of plasma

pillars in the manufacture process for OF containing the nitrogen. This method gives a possibility to manufacture the ultrasmall (less than 1 cm^3 in volume) RF FODL with the effective delay of 5–50 μs for the microwave oscillations for the frequency of 10 GHz at optical losses in OF not more than 2–5 dB at the OF total length 1–10 km.

7.6 Power Spectrum Density of Amplitude and Phase Noise in OEO DM

7.6.1 Fluctuation Equations of OEO DM

Differential equations of slowly changing normalized square of the strength E_{0L}^2, the population N_{0L} and the phase φ for QWLD (for the double-level model) in the single-frequency optical emission at absence of the positive feedback in OEO DM with account of the Langevinian laser noises can be written as Eq. (5.100), where $\xi_{\beta AN} = \xi_{E1}$, $\xi_{\beta PN} = \xi_{N1}$ are in-phase and quadrature components of Langevinian fluctuations of the laser field strength (which PSDs are equal, relatively, $S_{\beta AN}$, $S_{\beta PN}$), which are determined by the noise of spontaneous emission and depend on lifetime of excited particles on the metastable level of the active medium in the laser resonator, ξ_{LN} is the component of Langevinian fluctuations of the inversed population.

Taking into consideration the photoreception in the restricted band of optical frequencies at utilization in the laser, for example, of the narrowband optical filter (OF in Fig. 6.1), the random process of laser optical emission can be considered as the stationary process with the zero mean value. For instance, PSD $S_{\beta PN}$ is determined by spontaneous emission in the laser mode and is equal to $S_{\beta PN} = P_{sp}/\Delta\nu_{P0}$, where P_{sp} is the power of the spontaneous emission in the laser mode, $\Delta\nu_{P0}$ is the half-width of the resonance curve (or AFC) of the laser optical resonator, ν_{0P} is the natural frequency of the optical resonator.

The natural frequency of the optical resonator depends upon N_{0L}: $\nu_{0P} = \nu_{0P}(N_{0L})$. Introducing the constant C_N, we obtain the function $f_{00P} = \nu_{00P} - \nu$ at small deviations from the average frequency ν_{00P}, which corresponds to the population value $N_{0L} = N_{00L}$, and we present the optical frequency as $\nu_{0P} = \nu_{0P}(N_{0L}) = \nu_{00P} \cdot C_N$. Here $C_N = (\nu_{00P} - \nu_{0P})/(N_{00L} - N_{0L})$.

7.6.2 The Open Feedback Loop Expression for the Laser PSD

For this process, at opened feedback loop in OEO structure (there is loop closing in one place in OEO), where the coupler is located in Fig. 7.20, the spectral densities $S_{mL}(\nu) = S_{\beta AN} D_A / \left[(\nu - \nu_0)^2 + B_L^2\right]$, and $S_{\psi L}(\nu) = S_{\beta PN} \cdot D_F / \left[T_{OF}^2 \cdot (\nu - \nu_0)^2 P_L\right]$

of fluctuations of the amplitude and the phase, which excite the laser fluctuations $m_L(t)$, $\psi_m(t)$, can be obtained at solution of abbreviated equations (Eqs. 5.60 and 5.61) with account the fluctuation Langevinian impacts $S_{\beta AN}$, $S_{\beta PN}$, where $(\nu - \nu_0)$ is the offset from the central optical generation frequency of QWLD, $B_L = [\alpha_{0L} - (2\pi\nu_{0P}/Q_{0L})] - \beta_0 \cdot [1 + 3E_0^2]$, ν_{0P} is the natural frequency of the optical resonator, Q_{0L} is the resonator Q-factor, $\Delta\nu_{LP0}$ is the half-width of the resonance curve (or AFC) of the laser optical resonator, which is inverse proportional to the time constant $T_{OF} = T_{L0}$ of the laser resonator: $\Delta\nu_{LP0} = 1/T_{OF}$, D_A, D_F are the constant coefficients, α_{0L} the amplification (pumping), β_0 is the constant coefficient. We note that PSD of laser phase fluctuations $S_{\psi L}(\nu)$, as for all self-oscillating system with dissipation, is inverse proportional to the normalized power of optical oscillations: $P_L = E_0^2$ and T_{L0}^2.

7.6.3 The Power of Spontaneous Emission and PSD of Laser (or QWLD) Spontaneous Emission

Taking into account that the power of the LD spontaneous emission is $P_{sp} = \beta_{sp} \cdot P_L$, then we have: $S_{\beta PN} = \beta_{sp} P_L/\Delta\nu_{P0}$. The value of β_{sp} for modern QWLD is $\beta_{sp} = 10^{-3}$ to 10^{-4}. Beginning from the physical sense, β_{sp} is determined roughly (with account of the amendment in several orders) from the classic differential equations of Einstein for the laser, as the ratio $\beta_{sp} \approx A_{21}/B_{21}$, where B_{21}, A_{21} are the Einstein coefficients for stimulated and spontaneous emission, relatively. We can consider with well enough approximation for QWLD that $\beta_{sp} = T_2/T_1$, where T_2 is the time constant of polarization (or time of the longitudinal relaxation), T_1 is the life time of carriers (or time of the transverse relaxation). Then, $S_{\psi L}(\nu)$ can be written as $S_{\psi L}(\nu) = \Delta\nu_{LP0}\beta_{sp}D_F/(\nu - \nu_0)^2$ or $S_{\psi L}(\nu) = \beta_{sp}D_F/[T_{0P}(\nu - \nu_0)^2]$.

7.6.4 Estimation of Phase Noises of QWLD

According to obtained expression (if we assume that $\beta_{sp} = T_2/T_1$), we obtain: $S_{\psi L}(\nu) = T_2 D_F/[T_1 T_{P0}(\nu - \nu_0)^2]$ for laser PSD, we can make the rough estimation of PSD of phase noises.

1. ***QWLD with the traditional Fabry–Perot optical resonator***
   For example, at values $D_F = 0.1$, $T_2 = 10^{-12}$ s, for QWLD parameters: the lifetime of carriers (electrons in semiconductor QWLD) $T_1 = \tau_{n1} = 10^{-9}$ s, the lifetime of photons in the optical resonator $T_{0P} = T_{OF} = \tau_{ph} = 10^{-12}$ s, at the offset in the optical frequency from the carrier $(\nu - \nu_0) = 1$ MHz we obtain: PSD of the phase noise of QWLD is $S_{\psi L} = 1/[10T_1 \cdot (\nu - \nu_0)^2] = 10^{-7}$ dBm/Hz.
2. In ***QWLD with the narrowband optical resonator on the base of the Bragg cell***, at offset in the optical frequency from the carrier $(\nu - \nu_0) = 1$ MHz for the

following time constants $T_{0P} = \tau_{ph} = 10^{-6}$ s, $T_1 = \tau_{n1} = 10^{-9}$ s, $T_2 = 10^{-12}$ s, we obtain: PSD of the phase noise of QWLD is $S_{\psi L} = \beta_{sp}/[10T_{0P}(\nu - \nu_0)^2] = 10^{-10}$ dBm/Hz.

Thus, we obtain formulas $S_{\psi L}(\nu) = \beta_{sp}D_F/[T_{0P}(\nu - \nu_0)^2]$ for the rough estimation of PSD of the phase noise, which are correct enough compared with the experimental data for QWLD phase noises, which are presented in Sect. 7.3. These formulas are obtained at assumption that laser phase fluctuations are defined by the spontaneous emission.

The spectral line width of QWLD. Let us suppose that the spectral line is Lorentzian, then the width of QWLD spectral line is found as $\Delta\nu_L = S_{\beta PN}(F = 0)D_F/(T_{P0})^2$. In engineering calculations of the QWLD phase noise, we can use one from presented formulas $\Delta\nu_L = \beta_{sp}P_L D_F/[\Delta\nu_{P0} \cdot (T_{P0})^2]$ or $\Delta\nu_L = P_{sp}D_F/[\Delta\nu_{P0} \cdot (T_{P0})^2]$.

Fluctuations in the photodetector output. Now we obtain the current fluctuations in the PD output caused by amplitude $m_L(t)$ and phase $\Delta\psi_L(t)$ fluctuations of optical emission E_{12L}, considering that the own PD noises are small and neglecting by harmonics of the noisy currents.

Spectral densities of laser-detected fluctuations $S_{\mu AN}$, $S_{\mu AN-PN}(\omega)$, $S_{\mu\psi 1PN}(\omega)$ in the PD output; μ_{AN}, μ_{AN-PN}, μ_{PN}, relatively, are determined as the Fourier transform of their correlation functions; μ_{AN} is the amplitude noise of QWLD, μ_{AN-PN} is the conversional amplitude-phase noise of QWLD, μ_{PN} is the phase noise of QWLD; $\mu_n = \mu_{AN} + \mu_{AN-PN} + j\mu_{PN}$.

Account of noises in NA and RF filter outputs in OEO DM. The expression for the instantaneous signal value u_{FD} on the PD output (or in the NA input) can be written as:

$$u_{PD} = \mathbf{K_{PD}R_{PD}K_{FOS}} \cdot e_L + \left(E_{0L}^2 + e_{0L}\right) \cdot \mathbf{K_{PD}R_{PD}K_{FOS}}\mu_n + \mathbf{R_{PD}}\mu_{PD}, \quad (7.57)$$

where $\mathbf{K_{BLZ} = K_{FOS}}$ is the transfer function of FOS (optical fiber or fiber-optical system), $\mathbf{K_{PD}}$ is the transfer function of PD (optical part), $\mathbf{R_{PD}}$ is the transfer function of PD (RF part), μ_{PD} is the own noise of PD, e_L is the AC component of the intensity of laser optical emission of the first harmonic (RF oscillations), $e_L = e_{0L} \cdot \exp[j2\pi f_0 t)]$, e_{0L} is the amplitude of the AC component of the intensity.

Assuming for simplicity that NA of RF signal is non-inertial, the average slope S_{NA} of the static volt–ampere characteristic of the active element can be determined as $S_{NA} = -g_{11} + (3/4)g_{22}U_{01}^2$, where g_{11}, g_{22} are constant coefficients.

Then the expression for the instantaneous voltage value u_{NA} in the NA output (or in the RFF input) can be written (taking into account the NA own noises μ_{NA} recalculated to its input) as: $u_{NA} = S_{NA} \cdot E_{0L}^2 K_{BLZ}u_{PD}(t - T_{FOS}) + S_{NA01}E_{0L}^2 K_{BLZ}\mu_n + S_{NA01}(\mu_{PD} + \mu_{NA})$

The transfer function of the passband RF filter is defined as $\mathbf{K}_F = |K_F| \cdot \exp[-2j\pi(f - f_{F0})T_{eF}]$, where the module is $|K_F| = 1/\left[1 + (2\pi)^2(f - f_{F0})^2 T_{eF}^2\right]$, T_F and f_{F0} are the time constant and the resonance frequency of RF filter, relatively.

7.6.5 *Fluctuation Differential Equations of OEO DM at Closed Positive Feedback Loop*

At closed loop of the OEO positive feedback, the laser pumping current (taking into account of noises) can be written as the instantaneous laser current values J_{1L} (the first harmonic) or in the output of the RF filter with account the NA noises μ_{NA} recalculated to its input. Then the input complex impedance of the laser diode Z_L is:

$$\begin{aligned} J_{1L} &= (1/Z_L)\mathbf{K}_F\{S_{NA}[|K_{FOS}||K_{PD}|e_L(t - T_{FOS})] \\ &+\mathbf{K}_F \cdot S_{NA} \cdot \left(E_{0L}^2 + e_{0L}\right)|K_{FOS}||K_{PD}|\mu_n + \mathbf{K}_F S_{NA} \cdot (\mu_{PD} + \mu_{NA})\}. \end{aligned} \tag{7.58}$$

Here S_{NA} is the RF amplifier's slope in the first harmonic of RF oscillations. The photodetector and the nonlinear amplifier have own noises μ_{PD} and μ_{NA} with PSD of in-phase $S_{PDRe}(\omega)$ and $S_{NARe}(\omega)$ and quadrature $S_{PDIm}(\omega)$ and $S_{NAIm}(\omega)$ components of these noises, relatively. Then, the single-side PSD of the noise in the PD output in the closed loop of OEO is defined by the expression: $S_{\mu Im}(\omega) = K_{PD}^2[1 - K_{\Psi 12}]S_{\psi F}(\omega) + S_{PD\,Re}(\omega) + S_{PDIm}(\omega)$. $\mathbf{K}_F = (j\omega)(1/T_{1eF})/[(j\omega)^2 + (1/T_{1eF})(j\omega) + (2\pi f_{0e})^2]$ is the transfer function the RF filter.

The equation system (Eq. 5.100) must be added by the equation, which connects the AC component of the pumping current J_{1L} and the AC component of the intensity of laser optical emission e_L of the first harmonic (RF oscillations) by the expression:

$$J_{1L} = e_L\mathbf{K}_{DL} = e_L\frac{(j\omega)(1/T_{1eF})K_{DL0}}{(j\omega)^2 + (1/T_{1eF})(j\omega) + (2\pi f_{0e})^2)}\exp(-j\omega T_{DL}). \tag{7.59}$$

where $\mathbf{K} = K_{DL0}\exp(-j\omega T_{DL})$ e $K_{DL0} = |K_{PD}||K_{FOS}|R_{PD}\cos(\Phi_L)$, Φ_L is the phase difference between oscillations of optical harmonic on PD.

Then, Eqs. (5.60) and (7.59) are written as the system of equations.

With the account of made designations and assuming that delay time in FOS is small: $T_{DL} \approx 0$, $T_{1e} = T_{1eF} = T_{eF} = T_F$, we introduce designations for the real and imaginary parts of the transfer function as, relatively, $\mathrm{Re}K_{DL}R_{NA}S_{NA0}$ and $\mathrm{Im}K_{DL}R_{NA}S_{NA0}$, which is formed by FOS, PD, and NA. Omitting transformations for differential equations (Eqs. 5.60 and 7.59), we obtain abbreviated differential equations for the amplitude of AC component of the QWLD pumping current of the first harmonic J_{1L} and its phase $\psi_{1L} = \psi_J$. In this case, oscillations of the first harmonic at its output have the forms:

$$\begin{cases} T_{\mathrm{eF}}\dfrac{\mathrm{d}J_{1\mathrm{L}}}{\mathrm{d}t} = J_{1\mathrm{L}}\,\mathrm{Re}\,K_{\mathrm{BZ}}R_{\mathrm{NA}}S_{\mathrm{NA0}} - J_{1\mathrm{L}} + \mu_{\mathrm{a\,Re}}, \\ J_{1\mathrm{L}}T_{\mathrm{eF}}\dfrac{\mathrm{d}\psi_{1\mathrm{L}}}{\mathrm{d}t} = J_{1\mathrm{L}}2\pi(f_{\mathrm{res}} - f)T_{\mathrm{eF}} + J_{1\mathrm{L}}\mathrm{Im}K_{\mathrm{BZ}}R_{\mathrm{NA}}S_{\mathrm{NA0}} + \mu_{\mathrm{aIm}}, \end{cases} \tag{7.60}$$

where μ_{aRe} is in-phase and μ_{aIm} is quadrature components of the noise.

Let us examine the small-signal modulation mode of the laser in OEO and at that, $E_{0\mathrm{L}}^2 = E_{00\mathrm{L}}^2 + e_{\mathrm{l}}$, $N_{0\mathrm{L}} = N_{00\mathrm{L}} + n_{\mathrm{l}}$, $\varphi = \varphi_{00\mathrm{L}} + \varphi_{\mathrm{L}}$, $J_{1\mathrm{L}} = J_{00\mathrm{L}} + \alpha_{00\mathrm{l}}$, where $E_{00\mathrm{L}}^2$, $N_{00\mathrm{L}}$, $\varphi_{00\mathrm{L}}$ are steady-state solutions of the differential equations, and e_{l}, n_{l}, φ_{L}, $\alpha_{00\mathrm{l}}$ are small deviations from the steady-state values, relatively, for AC components $E_{00\mathrm{L}}$, $N_{00\mathrm{L}}$, $\varphi_{00\mathrm{L}}$, $J_{1\mathrm{L}}$ (i.e., the inequalities $E_{00\mathrm{L}} \gg e_{\mathrm{l}}$, $N_{00\mathrm{L}} \gg n_{\mathrm{l}}$, $\varphi_{00\mathrm{L}} \gg \varphi_{\mathrm{L}}$, $J_{1\mathrm{L}} \gg \alpha_{00\mathrm{l}}$ are fulfilled). Now we consider the features of OEO DM operation under conditions of existence of the positive selective feedback and the fulfillment of the limit cycle stability condition.

At first, we make normalization of differential equations (Eqs. 7.59 and 7.60). We introduce the normalized time $\tau = t/T_{1\mathrm{L}}$ and suppose that $G = G_0T_{1\mathrm{L}}$. Using the Laplace transform, we pass to the parameter $\mathrm{d}/\mathrm{d}t = p; j2\pi(f - f_0) = j(\omega - \omega_0)$, where ω_0 is the generated frequency of OEO DM close to the frequency of the RF filter. Now we investigate Eqs. (7.59) and (7.60) under conditions of the quasi-static mode in the steady-state point: $E_{00\mathrm{L}}^2$, $N_{00\mathrm{L}}$, $\varphi_{00\mathrm{L}}$. We neglect by the second order and designates the *small deviations* of the field strength amplitude e_{l}, the amplitude noises m_ξ, the noise component of the pumping current $\alpha_{00\mathrm{l}}$, the population noises n_ξ for the population n_{l}, for the optical phase φ_{L} the noises of the laser optical phase φ_ξ.

Now we obtain the system of symbolic equations for the small deviation of the amplitude e_{l}, the population n_{l}, the phase φ_{L}, the amplitude of the pumping current $\alpha_{00\mathrm{l}}$ of OEO DM with fluctuation Langevinian components for the amplitude of the laser optical oscillations ξ_{Le}, for carriers in the laser active medium $\xi_{\mathrm{Ln}}^{\mathrm{c}}$, for the phase of the optical oscillations $\xi_{\mathrm{L}\varphi}^{\mathrm{c}}$:

$$\begin{cases} -(\alpha_{00\mathrm{l}} - 1)n_\xi + pm_\xi - p\varphi_\xi = \xi_{\mathrm{Le}}, \\ (p + \alpha_{00\mathrm{l}})n_\xi - (\mathrm{Re}\,K_{\mathrm{S}} - G)m_\xi - p\varphi_\xi = \xi_{\mathrm{Ln}}^{\mathrm{c}}, \\ 2\pi f_{00\mathrm{P}}C_{\mathrm{N}}T_{1\mathrm{L}}n_\xi - (T_{1\mathrm{L}}\rho_{0\mathrm{L}} + \mathrm{Im}K_{\mathrm{S}})m_\xi + p\varphi_\xi + \varphi_\xi - \varphi_\xi(\mathrm{Re}\,K_{\mathrm{S}} - G) = \xi_{\mathrm{L}\varphi}^{\mathrm{c}}. \end{cases} \tag{7.61}$$

In the equation system (Eq. 7.61), for fluctuation parameters in the third equation, the term $2\pi f_{00\mathrm{P}}C_{\mathrm{N}}T_{1\mathrm{L}}n_\xi$ defines the contribution in PSD of OEO amplitude and phase noises from carrier population n_ξ in the laser active medium; the term $(T_{1\mathrm{L}}\rho_{0\mathrm{L}} + \ \mathrm{Im}\ K_{\mathrm{S}}) \cdot m_\xi$—the contribution of laser amplitude noises m_ξ; the term $[p\varphi_\xi + \varphi_\xi - \varphi_\xi \cdot (\mathrm{Re}K_{\mathrm{S}} - G)]$—the contribution of laser phase noises φ_ξ. We remind here that C_{N} is constant, $f_{00\mathrm{P}} = \nu_{00\mathrm{P}} - \nu$, where $\nu_{0\mathrm{P}}$ is the natural frequency of the optical resonator, $T_{1\mathrm{L}} = T_1$ is the lifetime of carriers.

Let us obtain also the system of symbolic equations of OEO DM for small deviations of the pumping current amplitude $\alpha_{00\mathrm{l}}$, the phase of RF oscillations $\psi_{\mathrm{L}1}$, the noise components of noisy in-phase μ_{aRe}, and quadrature μ_{aIm} components:

$$\begin{cases} T_{\text{eF}} p\alpha_{001} = J_{1\text{L}} \operatorname{Re} K_{\text{BZ}} R_{\text{NA}} S_{\text{NA0}} - \alpha_{001} + \mu_{\text{a Re}}, \\ \alpha_{001} T_{\text{eF}} p\psi_{\text{L1}} = \alpha_{001} 2\pi(f_{\text{res}} - f) T_{1\text{e}} + \alpha_{001} \text{Im} K_{\text{BZ}} R_{\text{NA}} S_{\text{NA0}} + \mu_{\text{aIm}}. \end{cases} \tag{7.62}$$

Systems of symbolic equations (Eqs. 7.61 and 7.62) with fluctuation components are basing systems. Small AC components of the pumping current are included in the first, second, fourth, and fifth equations. Phases φ_ξ of QWLD optical emission and phases of RF oscillations of OEO DM are interconnected in the general case and determined by relationships from equations of the phase balance for QWLD and OEO DM, relatively.

At that, the beat mode can exist, in which we can neglect by the phase connection in the optical section and the RF section of OEO DM. In this case, QWLD included in the OEO structure and spanned by the positive feedback loop, generates on the optical frequency, and OEO DM generates on the radio frequency.

In the synchronization mode, we cannot neglect by the phase connection. At that, the frequency of RF oscillations of OEO DM is determined from the general equation for the phase balance at fulfillment of self-excitation of OEO DM, which were considered earlier in this book.

7.6.6 *Noises of OEO DM*

Let us consider the generation mode of OEO DM for the ***closed feedback loop***. In this situation, for the system of symbolic equations (Eqs. 7.61 and 7.62) with fluctuation components, we examine the beats mode and make the assumption that we can neglect by the dependence of the φ_ξ phase of QWLD optical emission and the ψ_{L1} phase of RF oscillation of OEO DM. Then, taking into consideration that in the second equation of Eq. (7.61), we make an account of the positive selective feedback with the transfer function $\mathbf{K}_{\text{S}} = \mathbf{K}_{\text{DL}} = \mathbf{K}_{\text{FOS}} \cdot \mathbf{K}_{\text{PD}} R_{\text{NA}} S_{\text{NA0}}$, we obtain the noise components of the population n_ξ, the intensity $m_{\text{e}\xi}$ and the φ_ξ phase in the form $n_\xi = \Delta_1/\Delta$, $m_{\text{e}\xi} = \Delta_2/\Delta$, $\varphi_\xi = \Delta_3/\Delta$, where determinants are obtained according to the Cramer method solving the system of first three equations.

At neglect of the influence upon the phase of strength amplitude variations of optical emission, introducing the frequency of the photon–electron resonance of QWLD $\omega_{00\text{L}}^2 = (\alpha_{001} - 1)G$, we obtain for fluctuations:

$$m_{\text{L}} = \Delta_2/\Delta = \frac{\left(\xi_{\text{Ln}} + \xi_{\text{L}\varphi 1}\right)\left[(2\alpha_{001} - 1) + j\omega\right]}{(T_{1\text{L}})^2\left(\omega^2 - \omega_{00\text{L}}^2[1 - (\operatorname{Re} K_{\text{S}}/G)] - j\omega\alpha_{001}\right)}, \tag{7.63}$$

$$\varphi_\xi = \Delta_3/\Delta = \frac{\xi_{\text{L}\varphi}}{(j\omega T_{1\text{L}})} + \frac{\xi_{\text{L}\varphi} 2\omega_{00\text{L}}^2 (1 - \text{Im} K_{\text{S}}/G)}{(T_{1\text{L}})^2\left[\omega^2 - \omega_{00\text{L}}^2(1 - \operatorname{Re} K_{\text{S}}/G) - j\omega\alpha_{001}\right]}. \tag{7.64}$$

We make the important conclusions from last obtained expressions (Eqs. 7.63 and 7.64). At introduction of feedback (by the coefficient $K_{\text{S}} = \operatorname{Re} K_{\text{DL}} R_{\text{NA}} S_{\text{NA0}} =$

$K_{\mathrm{FOS}} \cdot K_{\mathrm{PD}} R_{\mathrm{NA}} S_{\mathrm{NA0}}$), $\mathrm{Re}K_{\mathrm{S}} = K_{\mathrm{FOS}} K_{\mathrm{PD}} R_{\mathrm{NA}} S_{\mathrm{NA0}} \cos(FT_{\mathrm{FOS}})$, $\mathrm{Im}K_{\mathrm{S}} = K_{\mathrm{FOS}} K_{\mathrm{PD}} R_{\mathrm{NA}} S_{\mathrm{NA0}} \sin(FT_{\mathrm{FOS}})$, the amplitude and phase noises of QWLD optical oscillations and of RF oscillations in OEO DM essentially decrease. The phase noises of OEO DM at small frequency offsets from the carrier are determined by the quadrature component of the laser spontaneous noise $\xi_{\mathrm{L}\varphi}/(j\omega)$. At offset frequencies close to the frequency of the photon–electron resonance $\omega^2 = \omega_{00\mathrm{L}}^2 \cdot (1 - K_{\mathrm{S}}/G)$, the value of the phase noise is inversely proportional to the laser damping decrement $\alpha_{00\mathrm{l}}$. Taking into account that the transfer function $K_{\mathrm{S}} = \mathrm{Re}\, K_{\mathrm{DL}} R_{\mathrm{NA}} S_{\mathrm{NA0}} = K_{\mathrm{FOS}} \cdot K_{\mathrm{PD}} R_{\mathrm{NA}} S_{\mathrm{NA0}}$ contains the optical fiber with (in potential) the retarded time T_{BZ}, then, the laser phase noise and the RF phase noise of OEO decrease with account of the stabilization effect on the long delay line. Amplitude noises are defined by the carrier noise of QWLD and by the noise of the optical phase.

Now we examine the structure of OEO DM at ***open feedback loop***, i.e., at zero transfer function of feedback $K_{\mathrm{S}} = 0$. Neglecting of small emission frequency modulation and of the influence of amplitude variations of the laser emission intensity upon the phase, we take into consideration that $K_{\mathrm{S}} = 0$ and the determinants for differential equations are:

$$\frac{\Delta}{j\omega} = \omega^2 - (\alpha_{00\mathrm{l}} - 1)G - j\omega\alpha_{00\mathrm{l}} = \omega^2 - \omega_{00\mathrm{L}}^2 - j\omega\alpha_{00\mathrm{l}}, \tag{7.65}$$

$$\begin{aligned}\frac{\Delta_2}{j\omega T_{1\mathrm{L}}} =& \{(\alpha_{00\mathrm{l}} - 1)\left(\xi_{\mathrm{Ln}} + \xi_{\mathrm{L}\varphi 1}\right) + \xi_{\mathrm{Le}}[(j\omega + \alpha_{00\mathrm{l}}) + 2\pi\nu_{00}C_{\mathrm{N}}T_{1\mathrm{L}}] \\ &+ (j\omega + \alpha_{00\mathrm{l}})\xi_{\mathrm{L}\varphi 1} + \xi_{\mathrm{Ln}} 2\pi\nu_{00\mathrm{P}} C_{\mathrm{N}} T_{1\mathrm{L}}\},\end{aligned} \tag{7.66}$$

$$\begin{aligned}\Delta_3 = (\alpha_{00\mathrm{l}} - 1)G\xi_{\mathrm{L}\varphi} + j\omega\xi_{\mathrm{L}\varphi}(j\omega + \alpha_{00\mathrm{l}}) &= \xi_{\mathrm{L}\varphi}\left[\omega_{00\mathrm{L}}^2 + j\omega(j\omega + \alpha_{00\mathrm{l}})\right] \\ &= \xi_{\mathrm{L}\varphi}\left[\omega_{00\mathrm{L}}^2 - \omega^2 + j\omega\alpha_{00\mathrm{l}}\right)].\end{aligned} \tag{7.67}$$

We note that expressions for determinants of fluctuation equations of OEO DM (Eq. 7.61), (Eq. 7.62) have the more complicate set of terms than expressions for determinants of fluctuation equations for OEO MZ. Then, in the case of the opened feedback loop, expressions for amplitude and phase fluctuations are:

$$m_{\mathrm{L}} = \frac{\Delta_2}{\Delta} = \frac{\left(\xi_{\mathrm{Ln}} + \xi_{\mathrm{L}\varphi 1}\right)[(2\alpha_{00\mathrm{l}} - 1) + j\omega]}{(T_{1\mathrm{L}})^2\left(\omega^2 - \omega_{00\mathrm{L}}^2 - j\omega\alpha_{00\mathrm{l}}\right)}, \tag{7.68}$$

$$\begin{aligned}\varphi_{\xi} = \frac{\Delta_3}{\Delta} &= \frac{\xi_{\mathrm{L}\varphi}}{j\omega(T_{1\mathrm{L}})} + \frac{\xi_{\mathrm{L}\varphi} 2\omega_{oo\mathrm{L}}^2}{(T_{1\mathrm{L}})^2\left(\omega^2 - \omega_{00\mathrm{L}}^2 - j\omega\alpha_{00\mathrm{l}}\right)} \\ &= \frac{\xi_{\mathrm{L}\varphi}}{j\omega(T_{1\mathrm{L}})}\left[1 + \frac{1}{T_{1\mathrm{L}}} K_{\mathrm{LD}}(j\omega)\right],\end{aligned} \tag{7.69}$$

Here for the QWLD transfer function $K_{\mathrm{LD}}(j\omega) = \omega_{00\mathrm{L}}^2/\left(\omega^2 - \omega_{00\mathrm{L}}^2 - j\omega\alpha_{00\mathrm{L}}\right)$ on AC component of the pumping current is proportional to the EMF strength square determined in Chap. 4.

We make important conclusions from obtained expressions. The laser phase noises φ_ξ can be treated as noises caused by the quadrature component of its spontaneous emission $\xi_{s\varphi}$,multiplied by the common transfer function $[\xi_{L\varphi}/(j\omega T_{1L})] \cdot [1 + K_{LD}(j\omega)]$.

If the frequency is equal to the photon–electron resonance frequency of QWLD: $\omega^2 = \omega_{00L}^2$, then the QWLD phase noise is inversely proportional to the laser damping decrement (which is proportional to the pumping exceeding above the threshold value) and equals: $\varphi_\xi \approx \xi_{L\varphi}/\alpha_{00l}$.

PSD of amplitude and phase noises of OEO DM with QWLD *at closed and open* feedback loop. Here we obtain expressions for PSD of amplitude and phase noises of the laser without account of frequency modulation of the optical emission at *opened* feedback loop in OEO. For this case, we obtain PSD for QWLD in the form:

1. **Closed feedback loop in OEO**

$$S_{AN} = S_m = \frac{(\alpha_{00l} - 1)^2 S_{LN1} + S_{LE1}(j\omega + \alpha_{00l})^2}{(T_{1L})^4 \left|\omega^2 - \omega_{00L}^2[1 - (\mathrm{Re}\, K_S/G)] - j\omega\alpha_{00l}\right|^2}, \tag{7.70}$$

$$S_{PN} = S_\varphi = \frac{S_{\varphi\xi}}{\left|j\omega T_{1L}\right|^2} + \frac{S_{LE}{D_{11}}^2 + S_{LN}{D_{22}}^2}{(T_{1L})^4 \left|\omega^2 - \omega_{00L}^2[1 - (\mathrm{Re}\, K_S/G)] - j\omega\alpha_{00l}\right|^2}. \tag{7.71}$$

2. **Open feedback loop $K_s = 0$**

$$S_{AN} = S_m = \frac{(\alpha_{00l} - 1)^2 S_{LN} + S_{LE}(j\omega + \alpha_{00l})^2}{(T_{1L})^4 \left|\omega^2 - \omega_{00L}^2 - j\omega\alpha_{00l}\right|^2}, \tag{7.72}$$

$$S_{PN} = S_\varphi = \frac{S_{\varphi\xi}}{\left|j\omega T_{1L}\right|^2} + \frac{S_{LE}{D_{11}}^2 + S_{LN}{D_{22}}^2}{(T_{1L})^4 \left|\omega^2 - \omega_{00L}^2 - j\omega\alpha_{00l}\right|^2}; \tag{7.73}$$

where $D_{11} = T_{1L}\rho_{0L}\alpha_{00l} - (K_S - G)2\pi f_{00P}C_N T_{1L} + j\omega T_{1L}\rho_{0L}$, ω is the angular generated radio frequency, $D_{22} = (\alpha_{00l} - 1)T_{1L}\rho_{0L} - j\omega\pi f_{00P}C_N T_{1L}$, ν is the laser optical generated frequency, Q_{pL} the loaded Q-factor of the laser resonator, $S_{\varphi\xi} = S_{L\varphi} +$ Im $(K_{BCFDNY}S_{Le} + K_{NY}S_{FD} + S_{NY})$, α_0 is the exceed of DC current of QWLD pumping above the threshold value, $S_{LN} = S_{Ln} +$ Re $(K_{BCFDNY}S_{Le} + K_{NY}S_{FD} + S_{NY})$ K_{LZ0} is the transfer function of the delay line without account of the laser transfer function, S_{100} is the gain of the nonlinear amplifier.

Thus, we obtain expressions for calculation of PSD of amplitude and phase noises of the laser not taking into account the frequency modulation of the laser emission at closed and opened feedback loop in OEO.

Figure 7.34 shows the calculated functions (Eqs. 7.70–7.73) of phase and amplitude noises of QWLD versus the F offset in frequency from the reference (or nominal) frequency of the subcarrier of 10 GHz in the opened feedback loop in

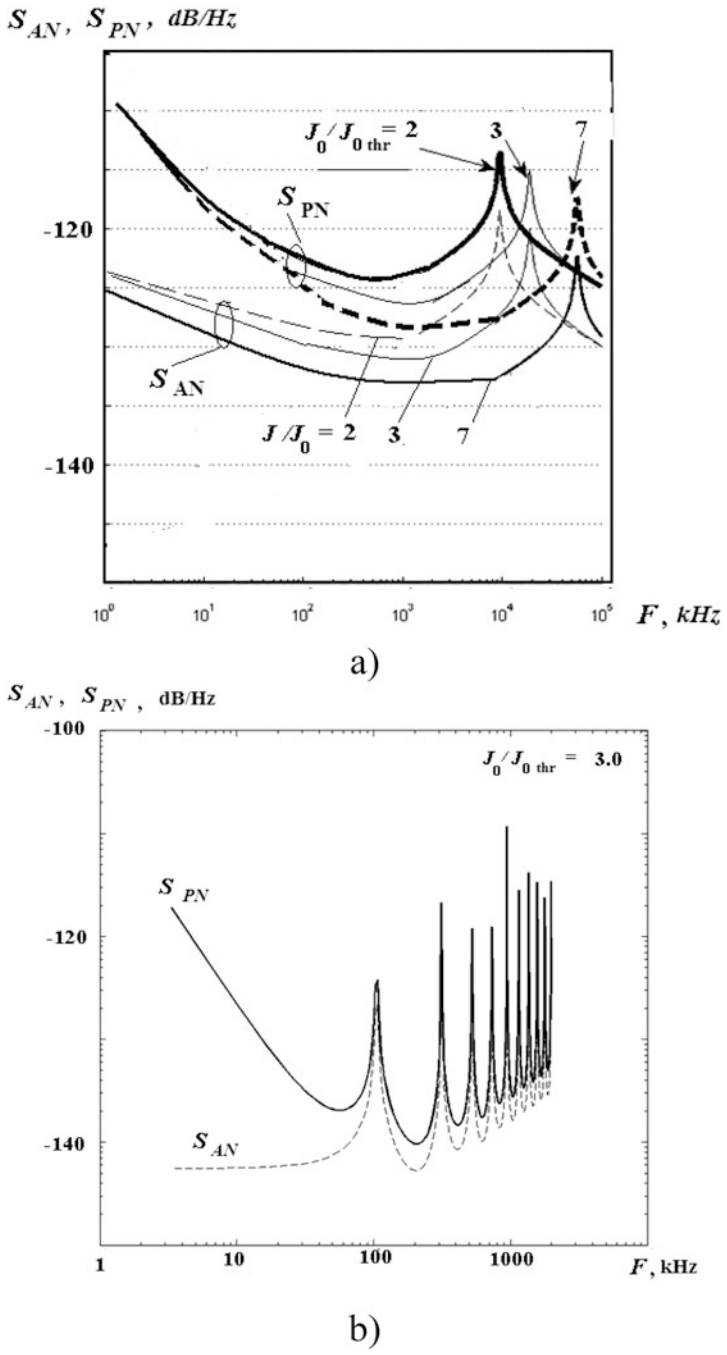

Fig. 7.34 (**a**) Calculated functions (Eqs. 7.72 and 7.73) of phase and amplitude noises of QWLD versus the F offset in frequency from the reference/nominal value of the subcarrier frequency of 10 GHz in the closed feedback loop in OEO at different exceeds of the pumping currents above the threshold value with account of carriers noise. (**b**) Calculated functions (Eqs. 7.70 and 7.71) of

OEO at different exceeds of the pumping current above the threshold value with account of carrier noises.

We note that the laser phase noise (Fig. 7.34a) increases almost by the order with the growth of exceeds of the pumping current above the threshold value by 3–7 times, which confirms the obtained theoretical results.

The calculated dependences (Eqs. 7.70 and 7.71) of phase and amplitude noises in the *closed* oscillating system of OEO DM with QWLD are presented in Fig. 7.34b versus the offset F in frequency from the subcarrier in the OEO single-frequency mode in the coherent photodetection mode.

Figure 7.35 shows the calculated functions (Eqs. 7.70–7.73) of the OEO phase noises versus offsets at different exceeds of the pumping current J/J_0 in the oscillating system of OEO with QWLD at DM in the single-frequency mode at coherent photodetection.

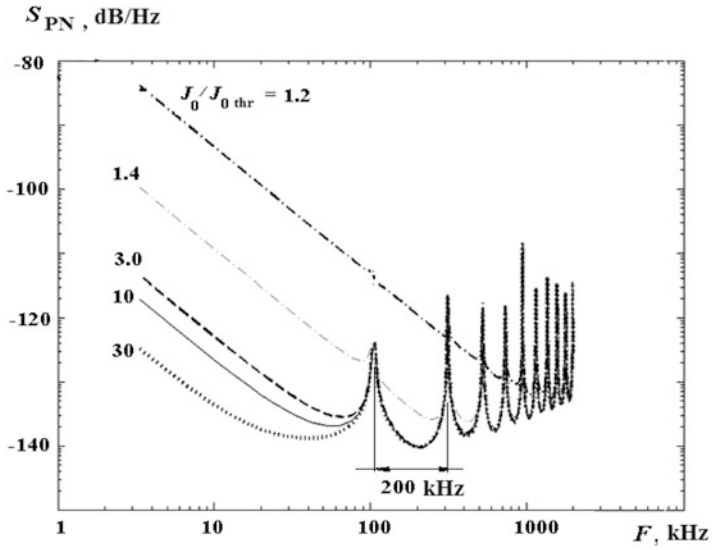

Fig. 7.35 Calculated functions (Eqs. 7.70–7.73) of phase noises of OEO at different exceeds of the pumping current J/J_0 in OEO with QWLD at DM in the single-frequency mode at coherent detection. The OF length is 1000 m, the delay is 5 μs, the emission power is 20 mW at the pumping current exceed of 10 above the threshold value

Fig. 7.34 (continued) phase and amplitude noises in closed oscillating system of OEO DM with QWLD versus the offset F in frequency from the subcarrier in the single-frequency OEO mode in the coherent photodetection mode. The length of the optical fiber is 1000 m, the delay in time in OF is 5 μs, the emission power at exceed of the pumping current above the threshold value $J_0/J_{0thr} = 3$

From the analysis of plots in Figs. 7.34b and 7.35, we can deduce some remarkable conclusions: PSD of phase noises in OEO exceed the amplitude noises by 10–25 dB/Hz on the frequency offset of 10 kHz, with pumping current growth, PSD of the phase noise significantly decreases, namely, at frequency offset from the RF carrier of 10 kHz, PSD is by 35–40 dB/Hz less, which is caused, on the one hand, by the decrease of laser PSD by 25 dB/Hz, but on the other hand, by the decrease of PSD of the OEO phase noise by 10–15 dB/Hz owing to the growth of the Q-factor of RF FODL with the optical fiber of the length 1000 m with the total delay of 5 μs.

Comparison of PSD of the phase noise in OEO DM (Figs. 7.34b and 7.35) and OEO MZ (Figs. 6.27b and 6.34) permit to make the important conclusion. The main difference of OEO DM from OEO MZ is a choice of a laser or the low-noise source of the coherent emission. For OEO DM, the bandwidth of the laser (or QWLD) RF modulation must be approximately equal to the OEO operation RF generation. The bandwidth of the laser RF modulation is approximately equal to the natural frequency of the relaxation photon–electron resonance. Phase noises of a laser are smaller for narrow bands of the RF modulation.

In OEO MZ, in which the external modulation is used, the laser can have the bandwidth of the RF modulation, which is several hundred times less than the operation frequency of generation. So, for example, at the operation frequency of 10 GHz, in OEO DM, the laser with the bandwidth of the RF modulation of 12 GHz must be used. In OEO MZ, at the operation frequency of 10 GHz, the laser with the extremely narrow RF modulation bandwidth is chosen, as a rule, 0.1–10 MHz. Such lasers, as it shown in Chaps. 2, 3, 4 and 7 of this book, has the ultralow natural phase noises (about −100 dB/Hz at the 10 kHz-offset from the carrier). Of course, the utilization of lasers with the ultralow phase noises in OEO MZ is more effective, from the point of view of the oscillator low RF phase noise obtaining.

But, application in OEO of the statistical averaging schemes with extraction of two optical harmonic (as shown in Chaps. 3–7 and experimentally confirmed, for instance, in [26]), makes OEO DM (which is 3–5 times cheaper than OEO MZ) as the promising source of the RF oscillations with the ultralow noises in microwave and mm-wave ranges.

7.7 Systems of Frequency and Phase Automatic Control in OEO

In this section, we give the description and the conception of systems of frequency and phase automatic control with the fiber-optical delay line for application in radio systems and devices for stable oscillations formation including OEO.

7.7.1 Systems of Frequency and Phase Automatic Control with RF FODL for OEO

Systems of frequency (FLL) and phase (PLL) automatic control systems are widely used in radio engineering for solution of the oscillator frequency stabilization problems, for synthesis of the discrete variety of stable frequencies, for extraction of signal informational parameters from its mixture with the noise, in manifold devices for radio signal formation and oscillation control including OEO. Development of technology of RF FODL manufacture with reference (etalon) characteristics makes perspective the creation of the specific class FLL and PLL systems, operation of which is based on the utilization of elements of precision delay.

The great delay time τ achieved in modern RF FODL at the wide passband B, i.e., at the product $B \cdot \tau \approx 10^6$, gives a possibility to develop the FLL and PLL systems with new useful, often unique, properties. On the other hand, investigating variations of FLL and PLL modes happening at variation of RF FODL parameters, we can use the obtained regulations for measurement of the signal delay value in RF FODL.

Figure 7.36a depicts the FLL structure, in which the role of the frequency discriminator (FD) is played by RF FODL and by the phase detector together. The error signal $e = e(t)$ from the FD output, through the control circuit (CC), under action of the signal $g = g(t)$, regulates the frequency of the controlled OEO in such a manner that in the vicinity of any nominal frequencies of RF FODL: $\omega_{\text{nom},\,n} = 2\pi n/\tau$, where τ is the delay time of RF FODL; $n = 1, 2, 3,\ldots$ As the result, the initial instability of the OEO natural frequency significantly decreases. Since RF FODL can provide significant delay in rather wide frequency band, we can realize in microwave range the great variety of stable frequencies with rather small discrete step: $\Delta\omega_{\text{nom}} = \omega_{\text{nom},\,(n+1)} - \omega_{\text{nom},\,n} = 2\pi/\tau$.

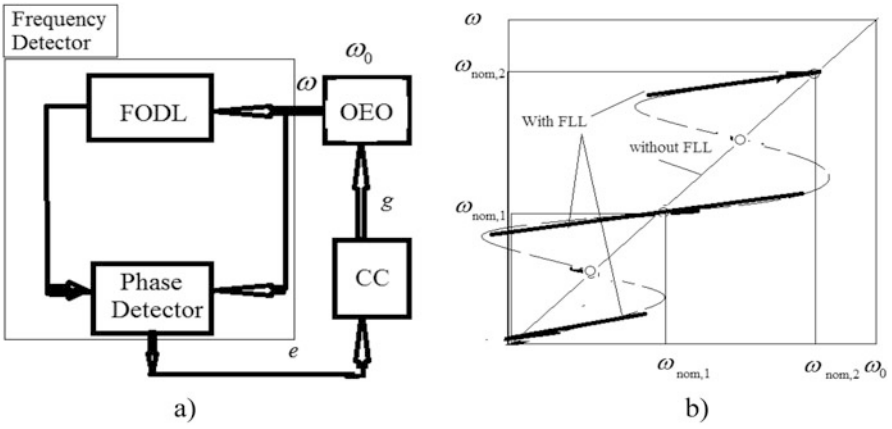

Fig. 7.36 Stabilization of discrete variety of frequencies in the system of frequency automatic control with RF FODL: (**a**) the structure, (**b**) frequency regulation curves

Properties and modes of FLL with the frequency detector on RF FODL are described by the symbolic equation ($p = \mathrm{d}/\mathrm{d}t$) for the current frequency of the controlled OEO:

$$\omega + \Omega \cdot K(p) \cdot F(p\tau) = \omega_0. \tag{7.74}$$

Here the function $F = F\left[\frac{1-\exp(-\tau p)}{\tau p}\tau\omega_{\mathrm{k}}\right]$ and we take into consideration not only inertness of the control circuit with the operator transfer function $K(p)$, but the total signal delay in RF FODL in the form of the operator of the ideal delay $\exp(-pt)$, including in the argument of the 2π-periodic characteristic $F(\varphi)$,where $\varphi(\omega)$—is the current phase incursion of the radio signal in RF FODL.

With the help Eq. (7.74), in Fig. 7.36b, the regulation characteristic of the FLL system is shown, i.e., the function of the stabilized frequency versus the variation of the natural frequency of autonomous OEO.

With the help of Eq. (6.126), we can obtain the expression describing the stabilization action of FLL with the frequency detector on RF FODL in the vicinity of any nominal frequency:$\omega - \omega_{\mathrm{nom},\,n} = (\omega_0 - \omega_{\mathrm{nom},\,n})/[1 + \Omega \cdot \tau \cdot K(0) \cdot F'(\varphi_0)]$.

We see that the regulation coefficient of the system $A = \Omega\tau K(0)F'(\varphi_0)$ containing of the largest correcting offset Ω, the transfer function of the control circuit on DC $K(0)$ and the slope $F'(\varphi_0)$ of the frequency detector characteristic, increases with the growth of the signal delay τ in RF FODL.

With the help of FLL system (of the PLL system) with RF FODL, we can solve not only the problem of frequency stabilization, but also the problem of tracking for unknown frequency $\omega_{\mathrm{ext}}(t)$ of the external signal, if to add the mixer to the initial structure, as shown in Fig. 7.37a. In such a system, the current frequency of the external signal displaced on the value of any RF FODL plays the role of the nominal frequency $\omega_{\mathrm{nom},\,n}(t) = \omega_{\mathrm{ext}}(t) + 2\pi n/\tau$.

To exclude the ambiguity at the choice of necessary value of operation frequency, it is enough to use the limiter in the output of the phase detector. The solid line in regulation characteristics presented in Fig. 7.37b depicts the action of such a limiter. The stability of nominal frequencies can be estimated with the help of obvious relationship:

$$\frac{\Delta\omega_{\mathrm{nom},n}}{\omega_{\mathrm{nom},n}} = \frac{\omega_{\mathrm{ext}}}{\omega_{\mathrm{nom},n}}\left|\frac{\Delta\omega_{\mathrm{ext}}}{\omega_{\mathrm{ext}}}\right| + \frac{2\pi n}{\tau\omega_{\mathrm{nom},n}}\left|\frac{\Delta\tau}{\tau}\right|. \tag{7.75}$$

The value of the frequency instability of the external signal can be made small using quartz oscillators or quantum generator: $\frac{\Delta\omega_{\mathrm{ext}}}{\omega_{\mathrm{ext}}} \le 1 \times 10^{-9}$. The relative temperature instability of delay in RF FODL is about 10^{-5} 1/°C and less for thermal-compensated optical fibers.

The phase difference in the output of the phase detector in PLL system (Fig. 7.37c) is: $\Delta\varphi_{\mathrm{OEO}}(t) = \varphi_{\mathrm{OEO}}(t - T_{\mathrm{FODL}}) - \varphi_{\mathrm{OEO}}(t)$. The control signal from the output of the control circuit $g(t)$ is applied to OEO.

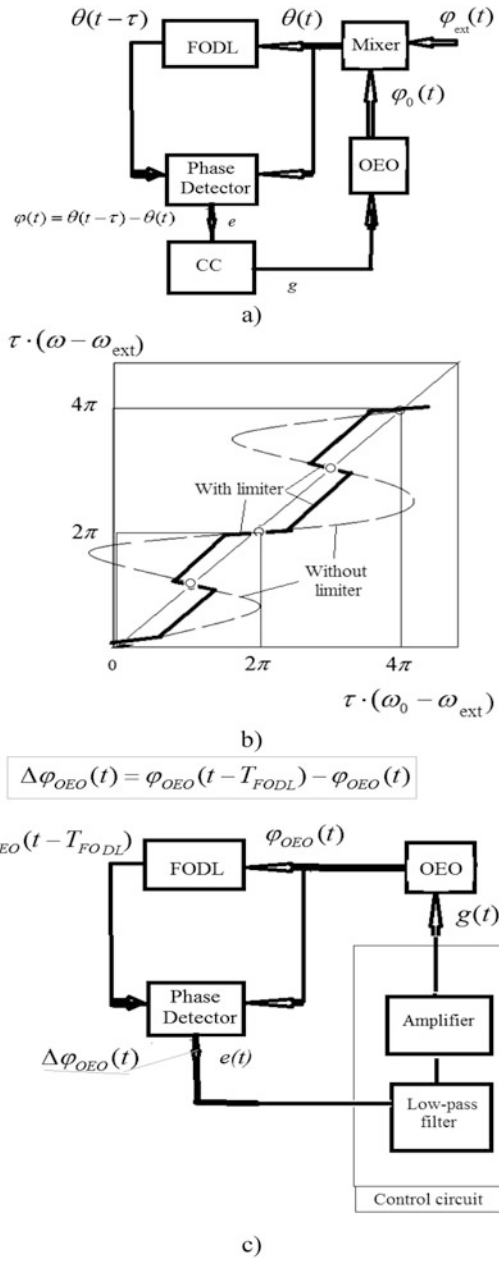

Fig. 7.37 The tracking system on the base of frequency (**a**) and phase (**c**) automatic control system with RF FODL. Regulation curves (**b**)

Authors have got the patent on the method of the phase automatic control system with utilization of the differential RF FODL with two optical fibers of the differential geometrical length. The structure of OEO with such the PLL system is presented in Fig. 7.38.

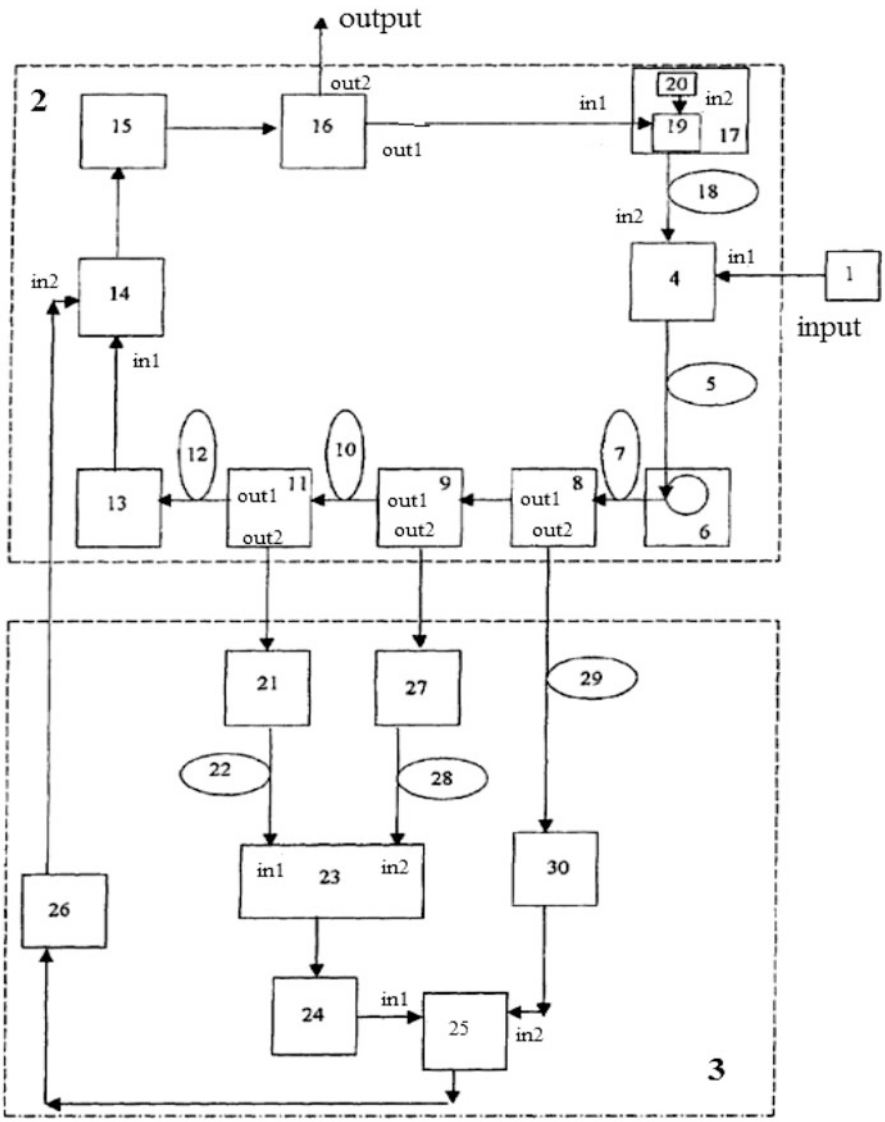

Fig. 7.38 The PLL system for OEO. Here we use the following designations: 20—a laser, 19—a modulator, 14—the phase-shifter, 13—the photodetector, 15—an amplifier and the RF filter, 16—a coupler, 22, 28, 29—optical fibers of the PLL system, 23—the photodetector, 30—the second photodetector and the second amplifier, 24—the third amplifier, 25—the phase detector, 8, 9, 11—optical couplers, 7, 10, 12—optical fibers, 4—the second modulator, 5, 6, 7, 8, 9, 10, 11, 12—optical fibers, 1—the external RF oscillator, 2—OEO, 3—the PLL system, 26—an amplifier. (Patent belonging to authors [27])

The PLL system may be successfully applied in OEO [28] for decrease of the phase noise of OEO. At that, we show that the PLL system in OEO can reduce phase noises by 7–15 dB/Hz in the offset range from the carrier frequency of 1–10 kHz. The presence of PLL in OEO, at other advantages, gives a possibility to decrease by 2–3 times the geometrical length of the optical fiber for the narrowband laser source.

In Fig. 7.38 [29, patent (2006)], the closed feedback loop of OEO is formed by blocks: 20 (a laser), 19 (a modulator), 14 (a phase-shifter), 13 (a photodetector), 15 (an amplifier and the RF filter), 16 (a coupler). To the block 3 (PLL system) the optical oscillation are applied from blocks 8, 9, 10, which are included into the OEO structure. Optical oscillations pass to photodetectors 23 and 30. Then signals are amplified and pass to the phase detector 25. In the output of 25, the electrical voltage acts (error signal), which is proportional to the level of the phase noise. This error signal is amplified and passes to the second input of the phase-shifter 14.

The error signal extracted by 25 is proportional to the OEO phase noise. When it passes on the phase-shifter 14, the regulation of the OEO phase noise level occurs. The distinctive feature of the PLL system of OEO, which is presented in Fig. 7.38, is the suppression of RF carrier of OEO oscillations by blocks 21, 22, 23, 27, 28. Owing to suppression of the RF carrier, the effectiveness of the PLL system operation increases.

We note that utilization of FLL and PLL systems in the radio electronic equipment including OEO gives advantages at application of RF FODL. At that, requirement to the laser phase noise are reduced, we can decrease of the geometrical length of the delay line.

7.7.2 PLL Systems in OEO

Figure 7.39a, b shows the structures of PLL systems in OEO:

- At utilization of the electrical output of OEO, from which voltages (or RF oscillation) passes to the RF FODL input and to the input of the phase detector (Fig. 7.39a).
- At utilization on the optical output of OEO, from which the optical oscillation passes to the input of the optical fiber FOS1 and to the input of the phase detector (Fig. 7.39b).

For utilization of the PLL system in OEO we can use the electronic phase detector (for example, using diodes as the nonlinear elements) with RF FODL (Fig. 7.39a). In this case, electrical oscillations are applied to both inputs. We can use another circuit of the phase detector shown in Fig. 7.39b on the base of the photodetector in the input of which the optical emission is applied via two optical channels of the different geometrical length.

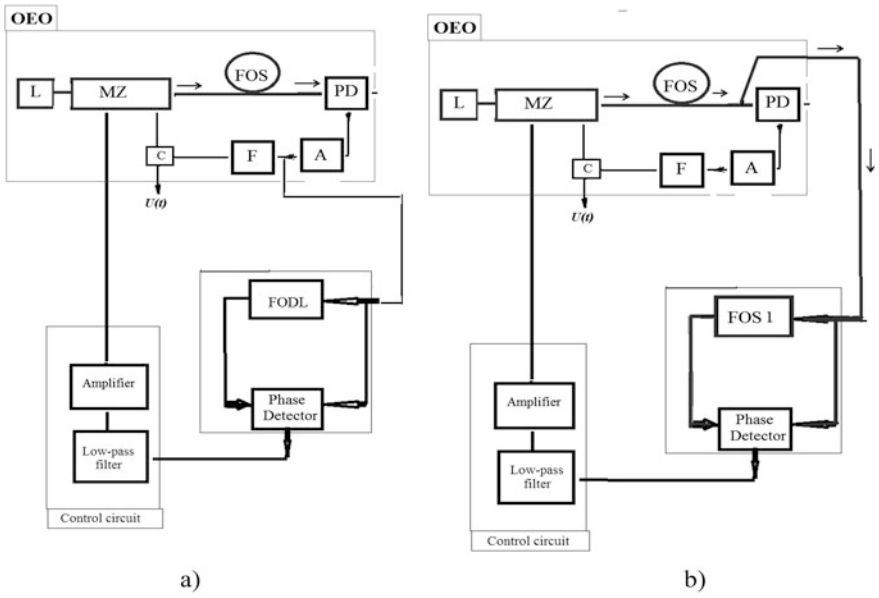

Fig. 7.39 Structures of PLL systems in OEO: (**a**) at utilization of the electrical output of OEO, from which voltages or RF oscillations pass in the input of RF FODL and in the phase detector; (**b**) at utilization of the optical output in OEO, from which the optical oscillation passes to the input of the optical fiber FOS1 and to the input of the phase detector

We consider characteristics of the main blocks forming the block diagram of OEO with PLL system (Fig. 7.39a). Electrical oscillations from the PD load are amplified and pass to the input of the phase detector. Oscillations are exposed to the delay in RF FODL and pass to its output. Delayed and non-delayed oscillations pass to the input of the phase detector. The output voltage of the phase detector is proportional to the "error signal" or to phase noises of OEO. The voltage from the output of the phase detector passes to the input of LPF and then is amplified. The amplifier output voltage passes through the adder to the electrical input of DC bias voltage of the MZ modulator. Variation of DC bias voltage of MZ leads to variation of the phase delay of the optical oscillation in the one of MZ optical channels.

We remind that the amplitude of the oscillation strength in this optical channel is E_{1L}. Thus, changing the phase of E_{1L}, the regulation of phase noise of RF oscillations in OEO is provided. Thus, phase noises of OEO decrease at the correct choice of parameters.

The introduced phase noises of RF FODL, which contains in its structure of the laser, the electro-optical modulator, the optical fiber and photodetector, are concerned to the one disadvantage of the structure in Fig. 7.39a. Introduced phase noises can be reduced if to transfer to the structure, in which the second photodetector is used as the phase detector, and the delayed and non-delayed optical oscillations pass from the output of FOS (Fig. 7.39b) to this photodetector. Another

alternative structure of automatic control of frequency and phase in OEO is the structure discussed in Sect. 7.7.1 with suppression of the RF subcarrier (Fig. 7.38).

For calculation of the relative PSD of the phase noise of OEO RF oscillations with the operating PLL system, we deduce the main mathematical relations. We consider the structure in Fig. 7.39a.

Let it be the field strength of the laser emission in the first optical channel of MZ defined as: $E_{1L} = E_{0L} \exp [j2\pi\nu(t) - j\varphi_{0L} - j\psi_{m1}(t)]$, where the optical frequency $\nu(t) = \nu_0 + \Delta\nu(t)$, ν_0 is the average laser frequency, $\Delta\nu(t)$ is the variation of the optical frequency from its average value, φ_{0L} is the constant phase incursion, $\psi_{m1}(t)$ is the phase variation of the laser optical emission due to the noise of spontaneous emission.

Electrical oscillations are applied to the electrical input of the phase detector (Fig. 7.39a) from the output of the amplifier in the OEO structure in the steady-state mode, and the instantaneous voltage of these oscillations is: $u_M(t) = U_{M0} \cos [2\pi f_{gen}(t)t + \varphi_{0etal} + \Delta\varphi_{m,\ etal}(t)]$, where U_{M0} is the amplitude of OEO generation in the steady-state mode, $\Delta\varphi_{m,\ etal}(t)$ is the etalon phase variation due to the noisy impact.

We assume that the voltage $u_M(t) = U_{M0} \cos [2\pi f_{gen}(t)t + \varphi_{0etal} + \Delta\varphi_{m,\ etal}(t)]$ is close to harmonic and we write $u_M(t) = U_{M0} \cos [\varphi_{m,\ etal}(t)]$.

We suppose that this voltage $u_M(t) = u_{gen}(t)$ is produced by the equivalent *radio-frequency generator* and assume that the field strength in the first optical channel of the MZ modulator is close to harmonic: $E_{1L} = E_{0L} \cdot \cos [2\pi t\nu(t) + \varphi_{0L} + \varphi_{opt}(t)] = E_{0L} \cdot \cos [\varphi_{opt}(t)]$.

We give to the current phases of laser oscillations $\psi_{Lm1}(t)$ and of the RF generator $\varphi_{m,\ eff}(t)$ variations $\Delta\psi_L(t)$ and $\Delta\varphi_{gen}(t)$ with respect to the uniformly increasing etalon phase of RF generator for the generality of examination.

For the phase $\varphi_{opt}(t)$ of oscillations of the *laser* field strength we can write: $\varphi_{opt}(t) = 2\pi\nu_{0opt} \cdot t + 2\pi f_{gen}t + \Delta\varphi_{opt}(t)$. For the phase $\varphi_{m,\ etal}(t)$ *RF generator* oscillations, we have: $\varphi_{m,\ etal}(t) = 2\pi f_{gen}t + \Delta\varphi_{gen}(t)$. From formulas $\varphi_{opt}(t) = 2\pi\nu_{0opt} \cdot t + 2\pi f_{gen}t + \Delta\varphi_{opt}(t)$ and $\varphi_{m,\ etal}(t) = 2\pi f_{gen}t + \Delta\varphi_{gen}(t)$, it follows that at detection of the *RF generator* phase $\Delta\varphi_{gen}(t)$ with the help of the traditional electronic phase detector with RF FODL or with the help of the phase detector made of the structure with FOS1 (Fig. 7.39b). The phase control in the first optical channel $\Delta\varphi_{opt}(t, U_{0M})$ is performed by means of variation of the DC bias voltage U_{0MZ} of the MZ modulator. In other words, there is the process of phase control of RF oscillations in OEO, and hence, the process of phase noises suppression of OEO RF oscillation occurs.

Let us describe briefly the features of the phase detection in PLL system of OEO made according to Fig. 7.39b.

7.7.3 The Phased Detector on the Base of FOS1

In the structure composition, FOS1 and the phase detector are included. The photodetector, on the light-sensitive area of which the emissions pass from the different optical fibers (as shown in Fig. 7.39b), is used as the phase detector.

Let us assume that the field strength $E_{FOS1}(t)$ in the first optical channel in the FOS1 input is close to harmonic: $E_{FOS1}(t) = E_{0FOS1} \cos [2\pi t\nu(t) + \varphi_{0L} + \varphi_{FOS1opt}(t)]$, or $E_{FOS1}(t) = E_{0FOS1} \cos [\varphi_{FOS1opt}(t)]$, or the voltage in the output of this photodetector (or the phase detector) (Fig. 7.39b), in linear approximation (in small index of the optical modulation in the output of the optical discriminator), the following expression is true: $U_{PD} = R_{PD}K_{PD}|E_{0FOS1}|^2 \sin [2\pi\nu_0 T_{FOS1}] \sin (2\pi f_0 t + \varphi_{0etal} + \Delta\varphi_{PD})$, where K_{PD} is the slope of the photodetector equaled to the ratio of the current to the applied to the PD area of normalized emission power $P_{opt} = |E_{0FOS1}|^2$, R_{PD} is the load resistance of the photodetector. We designate the voltage U_{0PD} as: $U_{0PD} = R_{PD}K_{PD}|E_{0FOS1}|^2$. For the low-frequency component of the voltage $u_{PDLF}(t) = U_{0PD} \sin [2\pi\nu_0(T_{1M} - T_{2M})] \sin (\Delta\varphi_{PD})$ in the photodetector output (or the phase detector) the following expression is true: $u_{PDLF}(t) = U_{0PDLF} \sin (\Delta\varphi_{PD})$. We note that the low-frequency voltage $u_{PDLF}(t)$ in the photodetector (or the phase detector) depends on the power of the laser optical emission on the PD area.

The maximal low-frequency voltage $U_{0FDLF} = U_{0PD} \cdot \sin (2\pi\nu_0 T_{FOS1})$ in the PD output, at $\sin(\Delta\varphi_{PD}) = 1$. The phase difference in the output of the photodetector (or the phase detector) under investigation is: $\Delta\varphi_{PD}(t) = \Delta\varphi_{opt}(t) - \Delta\varphi_{gen}(t)$. We see that the characteristic of the phase detector of the structure under examination (see Fig. 7.39b) has the sine form, and its slope depends on the delay time T_{FOS1}.

7.7.4 PLL System of the Laser

One of the features of the automatic control in OEO is a possibility to use the control of not only OEO, but the laser as well. By means of the laser phase of the frequency control, we can significantly decrease the laser phase noise by several ten times.

As we show in Chap. 2 of this book (Figs. 2.7–2.10), to decrease the laser phase noise, we can apply for extraction of the laser phase noise the high-Q discriminators on the base of diffraction lattices with the period less than 100 nm (in Fig. 2.9), the disk optical resonators, etc.

Methods and mathematical computations for the frequency and phase control systems for the laser optical frequency are the same as earlier-considered for the RF oscillator. The double-channel fiber-optical system with two optical fibers of different lengths, which is presented simplistically in [20], can be concerned to the one of types of the optical discriminator.

Now we obtain the function $\Delta\nu_{con}(e_{con})$ of the correcting offset $\Delta\nu_{con}(t)$ of the laser optical emission frequency versus the control voltage e_{con}. In modern compact laser systems of QWLD type, the electronic control of the optical frequency is used.

As the controlling devices for the optical frequency, we can use the voltage-controlled optical filters, Fabry–Perot cells, etc. The control of the optical frequency of the laser diode is provided by changing of the DC bias current.

In the general case, the modulation characteristic is nonlinear; nevertheless, it can be approximated as the straight line with the slope: $S_{\text{con}} = \frac{\text{d}\nu}{\text{d}e_{\text{con}}}$. Then, the frequency detuning $\Delta\nu(t)$ of the laser optical emission versus the control voltage: $\Delta\nu_{\text{con}}(e_{\text{con}}) = \nu_0 - S_{\text{con}}e_{\text{con}}$.

In the general case, for the automatic frequency control in OEO with utilization of the external reference oscillator (Fig. 7.37a), we write expressions for the spectral densities of the output phase fluctuations as: $S_{\text{out}}(f) = |K_{\text{AC}}(f)|^2 S_{\text{in}}(f) + |K_{\text{FC}}(f)|^2 S_{\xi n,\,\text{gen}}(f)$, where $S_{\text{in}}(f)$ is the spectral density of phase fluctuations of the signal in the system input (or from controlled oscillator in OEO), $S_{\xi n,\,\text{gen}}(f)$ is the spectral density of the phase fluctuations of the reference generator. We designate the module squares of the transfer functions of LPF included in the control chain (Fig. 7.36a), relatively, $|K_{\text{AC}}(f)|^2$ for controlling oscillation in the input of the automatic control system, $|K_{\text{FC}}(f)|^2$ for the reference oscillation of the oscillation of the reference oscillator. In the structure in Fig. 7.37a the external oscillator plays a role of the reference source of oscillation, and OEO plays a role of the controlling oscillation source.

The control circuit included into the section of automatic control between the phase detector and the frequency controller represents the low-pass filter, which is used for interference suppression distorting the reference signal of the RF generator. As PLF, we consider the simplest RC integration filter.

In this case, at utilization of the integration chain in LPF of the RC-filter type, the appropriate equations are: $L_{\text{AC}}(f) = |K_{\text{AC}}(f)|^2 = \Omega_0^2/[(\Omega_0 - T_{\text{RC}}4\pi^2 f^2)^2 + 4\pi^2 f^2]$, $L_{\text{FC}}(f) = |K_{\text{FC}}(f)|^2 = [(T_{\text{RC}}4\pi^2 f^2)^2 + 4\pi^2 f^2]/[(\Omega_0 - T_{\text{RC}}4\pi^2 f^2)^2 + 4\pi^2 f^2]$, where T_{RC} is the time constant of the circuit, $\Omega_0 = E_{\text{F}}S_{\text{con}}$ the system parameter characterizing its locking range. For this system, the $\Omega_0 = E_{\text{F}}S_{\text{con}}$ parameter is determined as: $\Omega_0 = R_{\text{PD}}K_{\text{PD}}|E_{0\text{FOS1}}|^2 \sin(2\pi\nu_0 T_{\text{FOS1}})S_{\text{con}}$.

At regulation of OEO radio frequency (structure in Fig. 7.39): $S_{\text{conRF}} = \text{d}f/\text{d}e_{\text{con2}}$. At adjustment of the laser optical frequency: $S_{\text{con, opt}} = \text{d}\nu/\text{d}e_{\text{con}}$. The Ω_0 differs from the locking range by a multiplier equaled to the characteristic slope of the phase detector in the operation point. Using functions $L_{\text{AC}}(f)$ and $L_{\text{FC}}(f)$, therefore, we write expression for the spectral densities of the output phase fluctuations:

$$S_{\text{out}}(f) = L_{\text{AC}}(f)S_{\text{in}}(f) + L_{\text{FC}}(f)S_{\xi\text{n,gen}}(f), \tag{7.76}$$

where $S_{\text{in}}(f)$ is the spectral density of phase fluctuations of the signal in the system input of or the controlling generator, $S_{\xi\text{n},\,\text{gen}}(f)$ is the spectral density of the phase fluctuations of the reference generator.

Depending on the level of phase noises of elements, the various variants of the structure of PLL system for frequency control are possible in OEO.

In one of variants, the **laser can be the controlling** element, and RF generator is the reference one. At that, the expression (Eq. 7.76) can be written in the form:

$$S_{\text{out}}(F) = L_{\text{AC}}(F)K_{2\Gamma\text{PN}}^2 S_{\text{L}}(F) + L_{\text{FC}}(F)K_{2\Gamma\text{PN}}^2[S_{\text{conRF}}(F) + S_{\text{PD}}(F)]. \quad (7.77)$$

In another variant, the laser can be the reference source, and the **RF generator is the controlling element**. At that, the expression Eq. (7.76) is written as:

$$S_{\text{out}}(F) = L_{\text{AC}}(F)K_{2\Gamma\text{PN}}^2[S_{\text{conRF}}(F) + S_{\text{PD}}(F)] + K_{2\Gamma\text{PN}}^2 L_{\text{FC}}(F)S_{\text{L}}(F). \quad (7.78)$$

For demonstration of PLL system operation in OEO, below we give descriptions of calculated functions presented in Fig. 7.40a and obtained according Eq. (7.77) and in Fig. 7.40b obtained according to for $K_{2\Gamma\text{PN}}^2$ (Eqs. 6.80, 6.92, 6.93 and 7.78).

For demonstration of the function of PSD of the phase noise of OEO $S(\Delta\nu)$ with the PLL system versus the width of the laser spectral line $\Delta\nu$ in Fig. 7.40a, we present the calculated curves 2–4 for different values of T_{RC}/Ω_0: the ratio of the time constant of the integration filter T_{RC} and the Ω_0 parameter of the PLL system: the curve corresponds to $T_{\text{RC}}/\Omega_0 = 0.0002$, the curve 3—$T_{\text{RC}}/\Omega_0 = 0.02$, the curve 4—$T_{\text{RC}}/\Omega_0 = 2.0$. At that, the curve 1 corresponds to the function of PSD of the phase noise without PLL.

For calculation of theoretical dependences of PSD of the phase noise in OEO (Fig. 7.40), the estimation of the width of the laser spectral line $\Delta\nu = \Delta\nu_{\text{L}}$ is performed according to the appropriation expression for PSD of the laser phase noise $S_{\text{L}} = \Delta\nu_{\text{L}}\frac{D_{\text{Y}}}{2P_{\text{L}}F^2}$. At values $S_{\text{L}} = 10^{-12}$ dB/Hz, $\frac{D_{\text{Y}}}{P_{\text{L}}} = 10^{-10}$, at the offset from the carrier $F = 1$ kHz, the width of the laser spectral line is $\Delta\nu_{\text{L}} = 20 \times 10^3$ Hz.

Presented functions $S(\Delta\nu)$ (Fig. 7.40a) are quadratic functions of the width of the laser spectral line $\Delta\nu = \Delta\nu_{\text{L}}$, and we see that at the ratio $T_{\text{RC}}/\Omega_0 = 0.0002$, the decrease of PSD of the phase noise is more than 20 dB/Hz for OEO with the PLL system compared to OEO without PLL.

In Fig. 7.40b, the presented curve 5 corresponds to the computed PSD of the phase noise of OEO $S(F)$ with the POLL system at the ration $T_{\text{RC}}/\Omega_0 = 0.0002$ for the same laser and OEO elements parameters, as the curves 1–4 (which are in Fig. 7.40b). The benefit in reduction of PSD of the phase noise of OEO with PLL is more than 25 dB/Hz at the offset $F = 1$ kHz, which confirms the effectiveness of utilization of PLL system in OEO.

So, the PLL system in OEO can be successfully used for the decrease of the OEO phase noise. At that, we show that this system can decrease the phase noises by 7–15 dB/Hz in the range offsets from the carrier 1–10 kHz. The presence of PLL system in OEO gives a possibility to decrease the geometrical length of the optical fiber by 1.5–3 times at the same values of PSD of the phase noise.

7.8 Conclusions

We mark out several **main mechanisms for the phase noise** suppression in OEO:

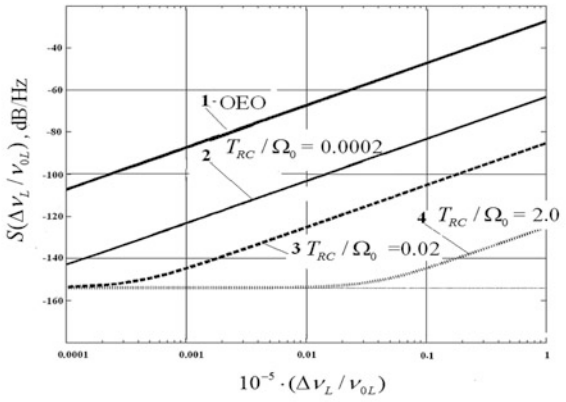

a)

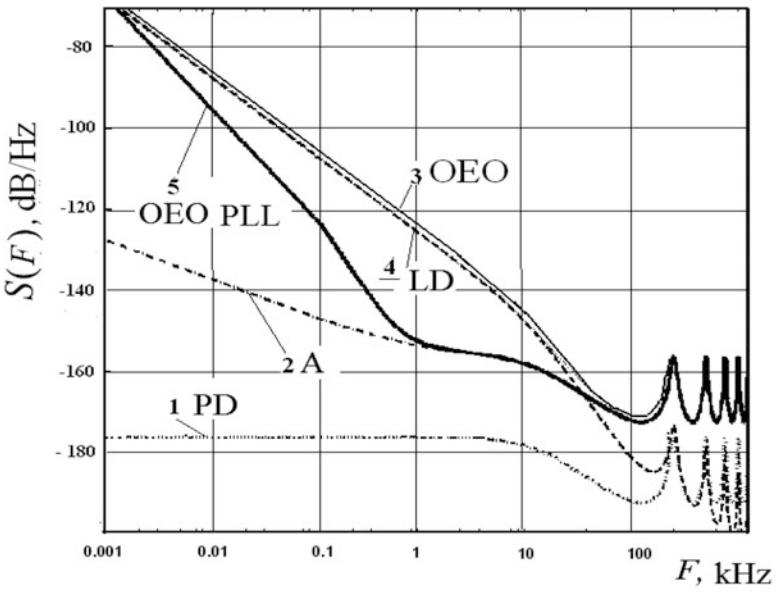

b)

Fig. 7.40 (**a**) Theoretical functions of PSD of the phase noise of OEO $S(\Delta\nu_L/\nu_{0L}) = S_{out}$ with the PLL system versus the width $\Delta\nu = \Delta\nu_L$ of the laser spectral line at different parameters of the system calculated according to Eq. (7.78), ν_{0L} is the average frequency of the laser generation. (**b**) PSD of the phase noise in OEO with the PLL system. Curves 1 "PD" and 2 "A" correspond to minimum possible phase noise of the photodetector and the RF amplifier. The curve 4 "LD" corresponds to detected PSD of the phase noise of the laser diode, and the curve 3 "OEO" corresponds to PSD of the phase noise of OEO without PLL, while the curve 5 "OEO PLL"—with PLL

- Owing to the *fiber-optical delay line with the geometrical length more than 1000 m* (the suppression coefficient due to the length, which was analyzed in Chap. 6).
- Owing to utilization in OEO of *QWLD with ultralow phase noises* (relatively, PSD of the phase noise of QWLD is equal −95 to −120 dBm/Hz at the offset 1–10 kHz from the optical carrier).
- Owing to *suppression of the DC component of the laser emission* passed to the photodetector and, accordingly, the suppression coefficient is equal to 0.01–0.1.
- Owing to the *statistical correlation of noises at combination of the side optical harmonics* in the photodetector (accordingly, the suppression coefficient is equal to 0.001–0.1).

The process of spectra convolution of the detected laser phase noise with the spectrum of the total electronic noise has the new character from the point of view of oscillations theory and the statistical communication theory. We know that the spectrum of the electronic noise is well described (to the accuracy of constants C_{1E}, C_{2E}) by the formula $S_{EPN}(F) \approx \left(\frac{C_{1E}}{F^2} + \frac{C_{2E}}{F^3}\right)$. The convolution of detected laser phase $S_{LPN}(F)$, the view of which can be characterized by the Lorentzian curve with the spectrum of the electronic noise $S_{EPN}(F)$, gives the new type compared to the Lorentzian curve.

The joint suppression factor of the own electronic noises $S_{PNE}(F)$ in OEO varies and takes values $K_{1\Gamma}(F) \cdot K_{2\Gamma}(F) \cdot K_{3\Gamma}(F) = 0.1 - 0.001$.

Besides other, the laser coherence time, the irregularity of excitation coefficient of MZ optical channel effect on the level of PSD of the phase noise in OEO. Limitation in equalization of excitation coefficients of MZ optical channels leads to the limit values of the DC laser emission suppression, which introduce the significant contribution into the level of PSD of the phase noise owing to the nonlinear conversion of phase noises in the photodetector.

The described theory of passive and active waveguides (taking into account of nonsymmetry of optical channels) allows development of the mathematic apparatus for waveguide modeling in modulators and differential delay lines, which are used in OEO MZ and in OEO DM.

The structure of OEO MZ can be treated as the coherent optical processor or the spatial correlator with utilization of spatial filtering. The convolution operations not only in optical and RF ranges, but the spectra convolution operation on the spatial frequencies may be executed in OEO. As spatial filters, we can use the miniature circular and sector spatial filters, which are well-studied in publications on the Fourier optics.

Obtained calculated and experimental variations of PFC and the time constant of QWLD (or the value of PFC on the modulation frequency f_m divided by the value of the given frequency) $T_{LD} = \varphi_{LD}/(2\pi f_m)$ give a possibility to perform measurements of the light time delays (with application of given types of QWLDs as the modulated light source) in FOS and in fiber-optical light guides with the help of self-oscillation methods [30] not worse than 2×10^{-3} ns, which is equivalent, for instance, to

registration of geometrical lengthening of the optical fiber on the level of 0.2 μm. Therefore, such a QWLD is expedient to apply in high-sensitive oscillating fiber-optical sensors, as well as in oscillators with RF FODL for generation of the high-stabilized harmonic radio signal. At small pumping currents, the slope of variations of generation frequency versus the pumping current is 0.3 MHz/mA. At large pumping currents of QWLD (5–8), the slope of variations of OEO DM versus the pumping current is 0.003 MHz/mA.

Discovered experimentally for the first time and explained by our theoretical analysis of the phenomenon for QWLD of polarity change of the LD time constant and the slope inclination S_f of the function $f(I_{pump})$ for OEO with LD gives a possibility to correctly select of the pumping currents of the laser diode in OEO and the amplitude of the modulation signal, and also to optimize the constructions of LD modulator, the matching optical device with the optical fiber, and the thermostabilizing block.

Main determining factors, which affect the process of oscillations formation, are: (1) the value of the reserve in self-excitation $\delta = S_{del}$, (2) the ratio of delay time differences in the light guides (channels) to the time constant of the RF filter $(T_{2FOS} - T_{1FOS})/T_F$, and (3) the excitation coefficients of FOS1 and FOS2 light guides: A and $B = 1 - A$.

Modern technologies of the manufacture of quartz optical fibers with doping by the nitrogen with producing of a variety of high-accurate envelopes give a possibility to produce of optical fibers with low losses at limit bending radii less than 5 mm. To be in sight, at utilization of patented by authors of the high-accuracy technology of optical fiber manufacture with application of the sample heating by the plasma pillar, which created by microwave oscillators, we can develop the optical fibers with ultralow optical losses at small bending radii less than 5 mm. This technology for manufacture of the radiation-resistant optical fiber with the small bending radius in OEO with RF FODL gives a right to state that the limit RF FODL volume with the single lengthy optical fiber is 0.1 cm^3 per 1 km at delay of 5 μs/km.

From the OEO DM analysis, we make a series of remarkable conclusions: PSD of the phase noise in OEO exceeds the amplitude noises (on the frequency offset of 10 kHz) by 10–25 dB/Hz. With the growth of the pumping current, PSD of the phase noise essentially decreases, namely, on the frequency offset from the RF carrier by 10 kHz, PSD is 35–40 dB/Hz, which is caused, on the one hand, by the decrease of PSD of the laser by 25 dB/Hz, but on the other side, by the decrease of PSD of the phase noise of OEO by 10–15 dB/Hz owing to the increase of the RF FODL Q-factor with the optical fiber with the length of 1000 m with the total delay of 5 μs.

The PLL system can be successfully used in OEO to decrease the phase noise. At that, we show that this system is able to reduce the phase noise by 7–15 dB/Hz in the offset range of 1–10 kHz. The presence of the PLL in OEO gives a possibility to decrease by 1.5–3 times of the geometrical length of the optical fiber at the same values of PSD of the phase noise.

References

1. V. Zhalud, V.N. Kuleshov, *Noise in Semiconductor Devices*. Under Edition of A.K. Naryshkin (Sovetskoe Radio, 416 p. (in Russian), Moscow, 1977)
2. J.W. Goodman, *Speckle Phenomena in Optics: Theory and Applications* (Roberts and Company Publishers, Englewood, 2006)
3. B.T. Gorianov, A.G. Zhuravliov, V.I. Tikhonov, *Statistical Radio Engineering. [In Russian]* (Sovetskoe Radio Publisher, Moscow, 1980)
4. T.L. Paoli, Waveguiding in a stripe-geometry junction laser. IEEE J. Quantum Electron. **QE-13**, 662–668 (1977)
5. M.M. Nieto, Exact wave-function normalization constants for the Poschl-Teller potentials. Phys. Rev. A **17**, 1273–1283 (1978)
6. M.A. Man'ko, G.T. Mikaelyan, *Modes and Mode Transformation in Active Semiconductor Waveguides [An Introduction to the Physics of Injection Lasers]* (Nauka Publishing House., 294 p., [in Russian], Moscow, 1983)
7. E. Artin, *The Gamma Function* (Dover Publications, Mineola, 2015)
8. H. Stark (ed.), *Applications of Optical Fourier Transforms* (Academic Press, New York, 1982)
9. S.L. Chuang, *Physics of Photonic Devices* (Wiley, New Jersey, 2009)
10. V.S. Zholnerov, A.V. Ivanov, V.D. Kurnosov, R.V. Chernov, Parameters of a laser diode with a fiber Bragg grating at different fiber lengths. Tech. Phys. **59**, 416–420 (2014)
11. P.V. Gorlachuk, A.V. Ivanov, V.D. Kurnosov, R.V. Chernov, et al., Simulation of power current characteristics of high-power semiconductor lasers emitting in the range 1.5–1.55 μm. Quantum Electron. **44**(2), 149 (2014)
12. C.Y. Tsai, F.P. Shih, T.L. Sung, T.Y. Wu, C.H. Chen, A small-signal analysis of the modulation response of high-speed quantum-well lasers: effects of spectral hole burning, carrier heating, and carrier diffusion-capture-escape. IEEE J. Quantum Electron. **33**, 2084 (1997)
13. Alexander A. Bortsov, Yuri B. Il'in, Laser spectral line widening effect on RF phase and amplitude noises of an optoelectronic oscillator OEO. J. Radio Eng. (2),21-31 (2010), DOI:10.13140/RG.2.2.35665.07527
14. Alexander A. Bortsov and Sergey M. Smolskiy, "Opto-Electronic Oscillator with Mach-Zender Modulator", Infocommunications Journal, Vol. XI, No 1, March 2019, 45-53, (2019),DOI: 10.13140/RG.2.2.20992.69126
15. L. Stolpner, S. Lee, S. Li, A. Mehnert, P. Mols, S. Siala. Low noise planar external cavity laser for interferometric fiber optic sensors, in Proceedings of SPIE 7004, 19th International Conference on Optical Fiber Sensors,700451–700457, (2008)
16. K. Numata, J. Camp, M.A. Krainak, L. Stolpner, Performance of planar-waveguide external cavity laser for precision measurements. Opt. Exp. **18**(22), 22781–22788 (2010)
17. R.E. Bartolo, C.K. Kirkendall, V. Kupershmidt, S. Siala, Achieving narrow linewidth, low phase noise external cavity semiconductor lasers through the reduction of 1/f noise, in Proceedings of SPIE 61333, 6133OI (2006)
18. R.E. Bartolo, C.K. Kirkendall, V. Kupershmidt, S. Siala, Achieving narrow linewidth, low phase noise external cavity semiconductor lasers through the reduction of 1/f noise, in *Novel In-Plane Semiconductor Lasers V*, ed. by C. Mermelstein, D.P. Bour, Proceedings of SPIE, vol. 6133, 61330I (2006)
19. M. Morin, S. Ayotte, C. Latrasse, et al., What narrow-linewidth semiconductor lasers can do for defense and security? in Proceedings of SPIE—The International Society for Optical Engineering 7677, April 2010
20. A.A. Bortsov, *The Influence of the Quality of Laser Resonator to Microwave Phase Noise in Opto-Electronic Oscillator*, Electromagnetic Waves and Electronic Systems, vol 11 (Radiotekhnika, Moscow, 2012), DOI:10.13140/RG.2.2.28352.15361
21. M.T. Sebastian, R. Ubic, H. Jantunen, *Microwave Materials and Applications, 2 Volume Set* (Wiley, Hoboken, 2017)

22. M. Yasin, H. Arof, S. W. Harun (eds.), *Advances in Optical Fiber Technology: Fundamental Optical Phenomena and Applications* (Intech Open, London, 2015)
23. T. Babkina, Alexander A. Bortsov, et al., The fiber optical sensor of physical quantities [In Russian], 8 p, Patent USSR 1,485,750, 1989
24. A.A. Bortsov, Y.B. Il'in, Nanostructured opto-electronic oscillator of frequency-modulated signals, Patent RU: 103431, 2010,DOI: 10.13140/RG.2.2.19544.11524
25. A.A. Bortsov, Y.B. Il'in, V.E. Karasik, A. Karachev, et al., Method of manufacturing of work pieces for opticasing on nitrogen-doped quartz glass, Patent RU 2,537,450, 2015, DOI: 10.13140/RG.2.2.29191.01445
26. K.-H. Lee et al., A 30-GHz self-injection-locked oscillator having a long optical delay line for phase-noise reduction. IEEE Photon. Technol. Lett. **19**(24), 1982–1984 (2008)
27. Alexander A. Bortsov, Y.B. Il'in,Opto-electronic oscillator ,Generator of frequency-modulated signals, 2006-08-20, Patent RU2282302C1,2006, DOI: 10.13140/RG.2.2.29610.44488
28. Alexander A. Bortsov, The low noise laser optoelectronic oscillator with system of phase autofine tuning. Radioengineering (Moscow) **6**, 42–49 (2011)
29. X.S. Yao, L. Maleki, Multiloop optoelectronic oscillator. IEEE J. Quantum Electron. **36**(1), 79–84 (2000)
30. D. Marcuse, *Light Transmission Optics* (Van Nostrand Reinhold, New York, 1972)

Chapter 8
Experimental Investigations and Practical Circuits of Optoelectronic oscillator (OEO) with RF FODL

This chapter organizes as follows.

Its first part is devoted to description of OEO experimental investigations. The aid of these investigations is checking of theoretical calculations fulfilled in Chaps. 3–7 of this book. The other part of this chapter examines the various practical devices of OEO utilization in the modern equipment.

Basically, problems of experimental investigations here are concerned to the bias current influence on the OEO oscillations' frequency and the amplitude (at the closed feedback loop). In the beginning of Sect. 8.1, there is the description of the unified OEO experimental workbench. We study obtained experimental characteristics for variations of the bias current of LED, the laser diode and QWLD for the open feedback loop. Among experimental dependences, we can single out the following: the phase incursion differences and amplitudes of RF FODL output oscillations versus the oscillation amplitude at the modulator input; oscillation amplitude and phase differences at the photoreceiver output for various positions of output laser diode emission selector; amplitude and phase differences at photodetector in the far zone. Then we conduct the comparison of OEO characteristics at utilization of LED, usual (not quantum dimension) laser diodes with high threshold pumping currents and QWLDs with low values of the pumping (or bias) currents on RF and microwave frequencies.

In Sect. 8.2, the reader is supplied by a series of OEO experimental functions for the *closed feedback loop* for variations of DC bias current of LED, the usual laser diode, and QWLD.

Further, we describe the experimental results for OEO with the phased microwave fiber-optical communication line on the base of the powerful laser for the active phased antenna array (Sect. 8.3). Then we discuss the main circuit units including the powerful laser, and examine the specific advantages of OEO application in the system of phased RF signal distribution over various array channels.

Section 8.4 is devoted to OEO experimental investigations in the microwave range 8–10 GHz. We describe the experimental OEO workbench in the microwave

A. A. Bortsov et al., *Laser Optoelectronic Oscillators*, Springer Series in Optical Sciences 232, https://doi.org/10.1007/978-3-030-45700-6_8

range, which is developed and designed in hybrid implementation and realized completely on the Russian element base.

In Sect. 8.5, we examine practical OEO devices of realized microwave and mm-wave oscillators: in tuned low-noise oscillators; in radar stations and in radio-optical radars; in measuring devices for spectral density of the oscillator phase noise; in lengthy fiber-optical lines for secretive communications with increased noise immunity; in devices for formation of optical and electrical pulses with duration less than 1 ps with the low jitter; in fiber-optical sensor of electrical voltage and current; in lengthy radio communication links of the mm-wave range (60–80 GHz) with the high speed of information transmission up to 10 GBt/s.

In the end of this chapter we give the main conclusions.

8.1 Characteristics of Modulated Emission Sources: The Laser Diode and the Light-Emitting Diode in the Microwave Range

An aim of experimental investigations of modulated emission sources included in OEO, namely, laser diodes (LD) and light-emitting diodes (LED), is examination of its main characteristics, dependences of their parameters upon the pumping current, the research of the pumping current influence on the OEO frequency and amplitude at the closed feedback loop. Examination of main LD and LED functions is conducted on the general unified OEO breadboard, which block diagram is shown in Fig. 8.1 (the breadboard content is explained in the below text and in the figure caption). At first, experimental investigations are conducted at the open feedback loop of OEO.

Experimental workbench for our OEO with RF FODL studying is created as the some unified laboratory breadboard and contains:

- OEO with RF FODL with the exchangeable fiber-optical section (with the length 2–4600 m).
- The frequency discriminator (FDisc.).
- The optical tester OT-6 for measurement of the output emission power of light sources.
- The sensor element (Sen).
- Power supply sources for an amplifier and light sources (PS-1 and PS-2).
- The spectrum analyzer C-4-27.
- The oscilloscope C-1-68 for generation signal observation.
- The voltmeter V-7-26.
- The frequency meter Ch-3-54 for generation frequency measurement in OEO with RF FODL.
- The heating lamp and the temperature meter.

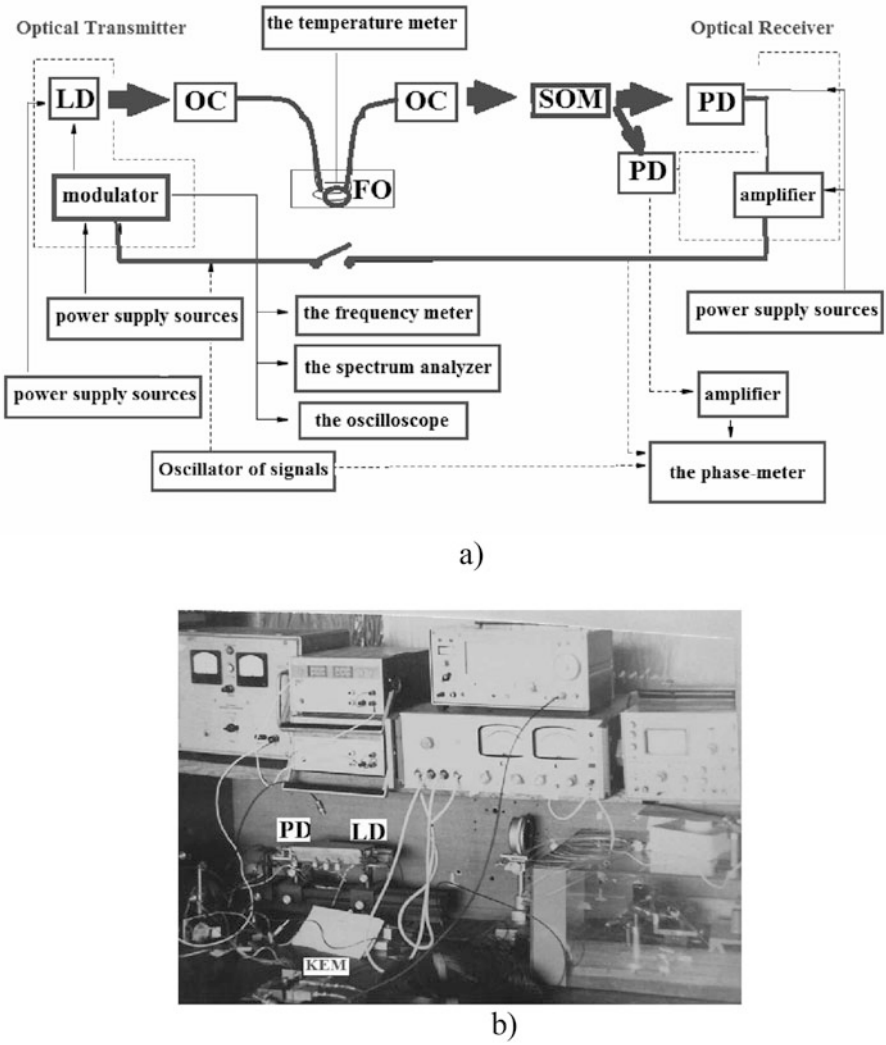

Fig. 8.1 The block diagram of the laboratory breadboard (**a**) and a photo picture of the general view (**b**) of the experimental workbench for OEO investigations. A transmitter and a receiver are performed on the base of quantum-electronic modules (QEM-8). *MD* matching devices, *AD* adjustment devices, *OC* an optical connector, *SOM* a selector of light-emitting modes

On the block diagram (Fig. 8.1a), we see the instruments' connection, and Fig. 8.1b shows the general view of the laboratory workbench.

An experimental breadboard of the optoelectronic oscillator with the fiber-optical delay line in the frequency range 1–10 MHz is performed on the base of the standard available quantum-electronic modules QEM-8 and QEM-34 (Fig. 8.2) and contains of regulation blocks for voltage stabilization for an amplifier and the bias currents of

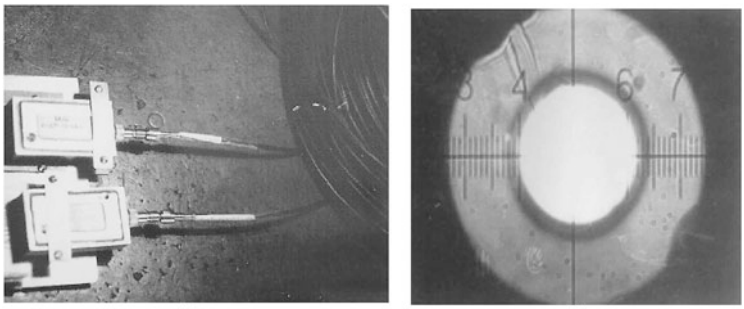

Fig. 8.2 An external view of receiving-transmitting modules (**a**), an enlarged butt of the multimode optical fiber (**b**)

the light source, which are mounted in the mutual case with an active part of OEO with RF FODL.

The experimental sample of OEO with RF FODL in the frequency range 30–40 MHz is developed on the base of the specially created transmitting unit containing of laser diodes of various types (ILPN-204 or 32DL103) on the base of the double hetero-structure with the emission wavelength of 0.85 μm.

The specially developed our receiving unit includes the photodiode LPD-2, the wideband multistage amplifier with the total gain (in AC current) of 10^2–10^3, and the matched (with this amplifier) temperature-controlled tuned circuit: the RF filter (RFF) tuned on the frequency 30–40 MHz. This RFF bandwidth is 1–2 MHz. The large gain of an amplifier gives a possibility to investigate the OEO frequency responses at small general magnitudes of RF FODL transfer functions (much less than 1).

The tuned circuit in OEO is made on the base of KSO capacitors and typical inductors wounded on the ceramic cylinder. For matching and ensure of the small effect of external electric circuits (for example, measuring devices), an oscillator (Osc) contains of the decoupling amplifying stage made on the base of a field-effect transistor.

Figure 8.3 shows the overall views of laser diodes ILPN-204 (a), 32DL-103 (b), and the external view of the laser diode board with an electronic modulator (c). Also Fig. 8.3 shows the laser diode SLT (the emission power is 10–25 mW, the emission spectral line width is 10 MHz, the wavelength is 1.55 μm) (d), the laser diode Dilas (the emission power is 10–15 mW, the wavelength is 1.3 μm, the RF modulation is 12GHz) (e), the photodiode Dilas (RF reception is 12 GHz) (f), the photodiode FRM (RF reception is 15GHz) (g).

During experimental researches, we measured the watt–ampere characteristic (Fig. 8.4) of the LED and the LD with the help of an optical tester OT-6. Figure 8.4c shows experimental characteristics of W-A curves $P_{out}(I_{bias})$ for LD samples of 32D-103 and ILPN-204 types, while Fig. 8.4b presents W-A curves for them of the light-emitting diode included into the quantum-electronic unit QEM-34.

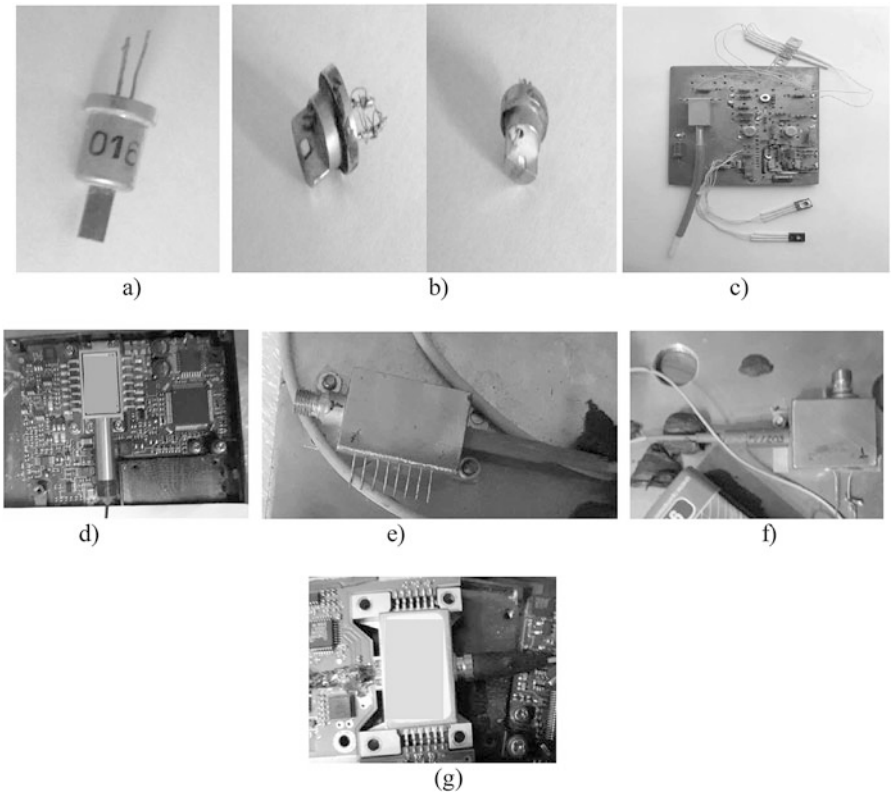

Fig. 8.3 General views of laser diodes ILPN-204 (**a**), 32DL-103 (**b**), and an external view of the laser diode board with an electronic modulator (**c**), laser diode SL T5412 (15 GHz) (**d**), laser diode Dilas (12 GHz) (**e**), photodiode Dilas (12 GHz) (**f**), photodiode FRM5N1 (15 GHz) (**g**)

The nonlinear functions of the emission power obtained by authors and presented in Fig. 8.4 versus the DC pumping current of the LED, the usual LD, and the quantum-well laser diode QWLD have the following qualitative differences. The LED nonlinear characteristics can be approximated by the quadratic function $P_0 = \gamma(I_0)^2$.

The nonlinear characteristic of the usual (non-quantum-well) is approximated by the cubic function $P_0 = \gamma(I_0 - I_{\text{thr}})^2$, while the nonlinear characteristics of QWLD (on the some segments) can be approximated by the linear function $P_0 = \gamma(I_0 - I_{\text{thr}})$, or by the square root function: $P_0 = \sqrt{\gamma(I_0 - I_{\text{thr}})}$. Here I_{thr} is the threshold current.

The QWLD (the laser diode Dilas with the emission power 10–15 mW, the wavelength 1.3 μm, RF modulation is 12 GHz (Fig. 8.3e)) spectra presented in Fig. 8.4 and measured by authors allows the conclusion that the function of the generation wavelength of the QWLD central mode increases monotonically at the pumping DC current growth.

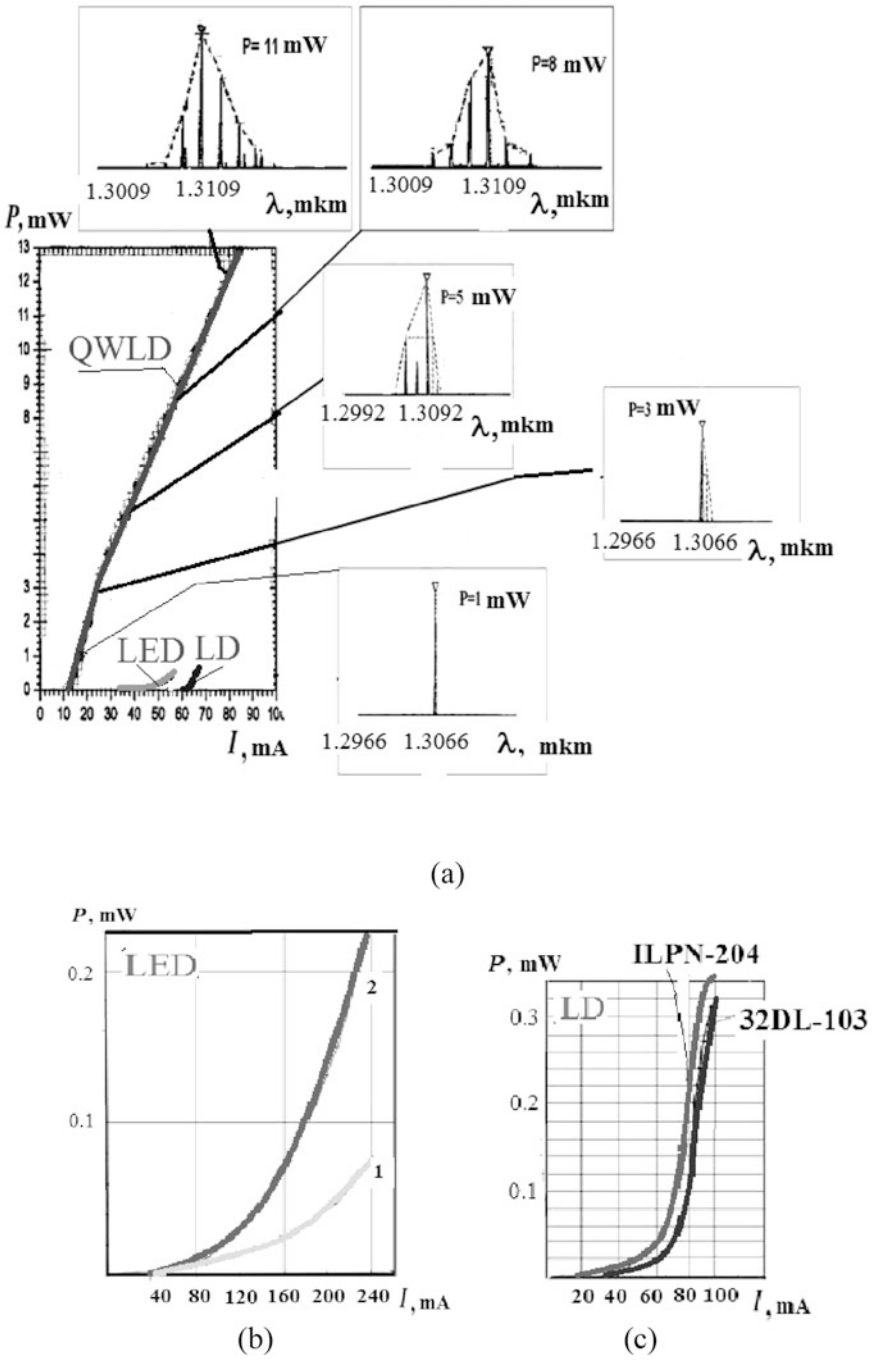

Fig. 8.4 The W-A characteristics of the quantum-well laser diode and spectra of optical emission at various QWLD pumping currents (**a**). The W-A curve of the 3-D usual (non-QWLD) laser diode ILPN-204 (**b**), and the W-A curve of the LED (**c**)

Accordingly, with the pumping current growth, the optical frequency of the laser emission central mode decreases as $\nu = \nu_0[1 - S_\nu(I_0/I_{thr} - 1)]$, where S_ν is a slope of the function of emission optical frequency versus the pumping current, ν_0 is the central mode frequency at the threshold pumping. At that, a slope of the central mode wavelength equaled "on the threshold" to 1.3002 μm versus the DC QWLD pumping current is 0.086 μm/mA or 0.086 mm/A, which corresponds to a slope of the QWLD optical frequency function versus DC pumping current of S_ν = 0.75 THz/(50 mA) = 0.015 THz/mA. Maximal relative deviations of the optical frequency in the current range 20–70 mA are 0.75 THz/229 THz = 0.0032.

The watt–ampere characteristics of QWLD ILPN-204 and 32DL-103 (Fig. 8.4b, c) and LED of the transmitting module KEM (b) for different excitation conditions 1 and 2 are shown in Fig. 8.7b. Functions shown in Fig. 8.4 give a possibility to observe the main difference in watt–ampere characteristics of light-emitting diodes and laser diodes as well as QWLDs. For laser diodes, at exceed of the I_{bias} threshold value ($I_{bias,thr}$), the slope of the emission power function $P_{out}(I_{bias})$ sharply increases, while at bias current values less than the threshold value $I_{bias,thr}$, the watt–ampere curve has a form of a parabola. This relates the fact that at bias currents less than threshold one, a contribution into registered optical emission of spontaneous emission increases. Laser diodes used in breadboards differ in implementation construction of optical matching units of laser diodes with the fiber-optical light guider.

Modulation characteristics of the transition type are investigated for transmitting and receiving modules connected in series through the short piece of the fiber-optical light guider with a length of 2 m in the frequency ranges 0–10 MHz and 30–40 MHz. These functions are shown in Fig. 8.5. Fulfilled measurements allow the correct choice of operation current of emission source and provision of the optical coupling from the output of the reception module KEM to the input of the transmitting module KEM. The function of the output signal amplitude U_{out} at the output of the KEM reception module versus the LED bias current is presented in Fig. 8.5b. From this figure, we see that at the "small" input signal $U_{in} \leq 0.1$ V (at the KEM transmitting module input), the nonlinear function of the signal amplitude $U_{out}(I_{bias})$ "repeats" the watt–ampere characteristic of LED, while at the "large" input signal U_{in} = 1.0 V characteristics $U_{out}(I_{bias})$ are close to linear ones due to arising of "compensation" effects.

Functions $U_{out}(U_{in})$, in which U_{in}, U_{out} are voltage amplitudes of KEM, are experimentally studied. The fiber-optical delay line consists in this experiment of the KEM transmitting module, the optical fiber, and the KEM reception module. At that, the LED bias current is 100 mA, while the frequencies of the sine signal applied to the KEM transmitting module input are 4, 10, and 30 MHz.

The OEO nonlinear characteristic character was determined from functions $U_{out}(U_{in})$. In this case, at small U_{in} signals, the total nonlinear characteristic of KEM modules has a character close to parabolic (i.e., there is a "soft" nonlinearity from the nonlinear oscillation theory point of view).

The average generation frequency of OEO was tuned by a variable capacitor of the RF filter (a tuned circuit) and is equaled for the first breadboard approximately to 6.4 MHz, while for the second breadboard—30 MHz. For these breadboards, the

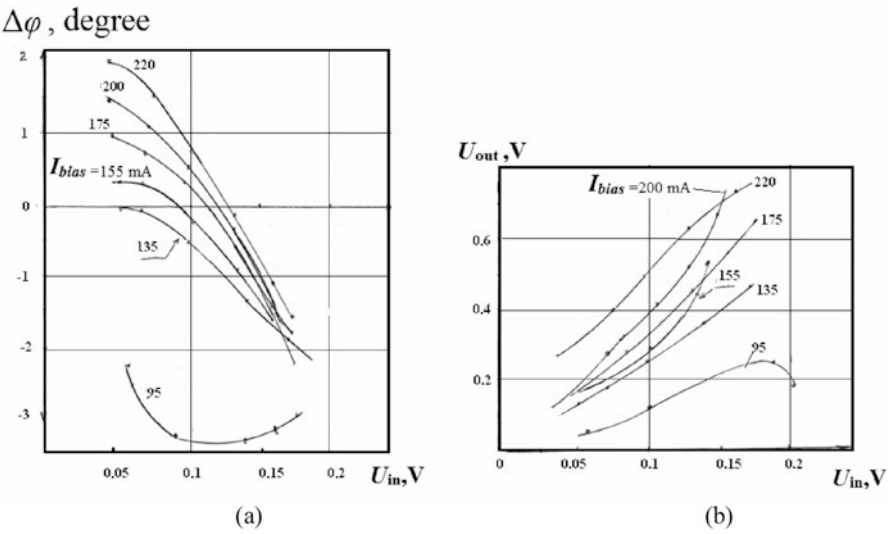

Fig. 8.5 Function of the phase incursions $\Delta\varphi(U_{bias})$ (**a**) and the RF FODL output signal amplitude $U_{out}(U_{in})$ (**b**) versus the signal amplitude U_{in} at the input of the LED modulator for various LED bias current values I_{bias} (at modulation frequency $f = 10$ MHz)

functions of the signal frequency and amplitude are measured in OEO with RF FODL (based on the single fiber-optical light guider) at variation of the bias current of the emission source. These functions are measured for two different RF FODLs on the base of single light guiders with lengths 20 and 300 m.

Figure 8.6 shows experimental functions of amplitude and phase difference of signal modulation at scanning over the "aperture" of the laser diode emission pattern in two different mutually orthogonal X (in the *p-n* junction plane) and *Y* planes.

The signal amplitude U at the output of the scanning photodetector and the phase difference $\Delta\varphi(\theta)$ of signals at input of the laser diode modulator (and measured at the photodetector output) were measured. Measurements of the phase difference are performed with the help of the phase-meter FK-2-12. Figure 8.6a shows the functions of the modulated signal amplitude at the photodetector output $U(\theta)$, where θ is the angle between the laser diode optical axis and a normal to the photodetector light-sensitive area. At that, the sine signal of small amplitude (less than 0.05 V) and at $f = 30$ MHz frequency was applied to the laser diode input.

An analysis of functions $U(\theta)$ and $\Delta\varphi(\theta)$ at different bias currents shows that the emission pattern for the laser diode of 32DL-03 type has a complicate character and complicate non-monotonic dependence upon angular displacements θ at various bias (pumping) currents I_{bias}. At growth of the bias current I_{bias}, the temperature increase occurs in the laser diode optical resonator, and the refraction index in the active area varies. This leads to appearance of longitudinal spatial modes of emission of the higher order in the laser diode optical emission. At that, patterns of output emission

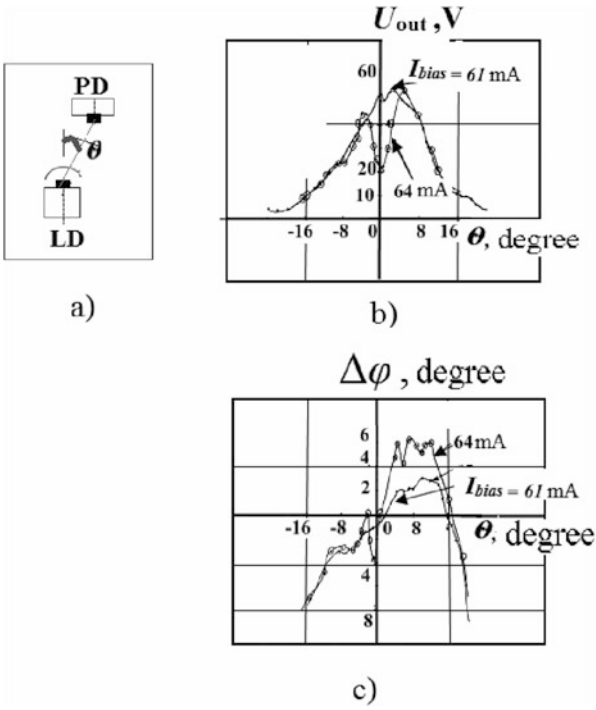

Fig. 8.6 The scheme of the experiment (**a**) and functions of the signal amplitude U_{out} (**b**) and the phase difference $\Delta\varphi$ (**c**) at the photoreceiver output for different selector positions of the laser diode output emission. The frequency is 30 MHz. Functions $\Delta\varphi$ and U_{out} are given for various bias currents in the *Y*-plane

in the optical power have a "dip" which leads to the similar character of the signal amplitude $U(\theta)$ at the output of the scanning photodiode.

Experimental functions of the phase difference $\Delta\varphi$ and the signal amplitude U_{out} on the photodetector output are shown in Fig. 8.7. Angular scanning is performed by variation of the photodetector position (from angular displacement of the PD2 photodiode), placed at the distance of 10 mm from the optical fiber output butt with regard to the optical axis of the optical fiber. RF FODL is formed by the laser diode, the optical fiber, and the photodiode.

Functions of the phase difference $\Delta\varphi$ and the signal amplitude U_{out} at different bias currents of the laser diode (I_{bias} = 66–70 mA) are presented in Fig. 8.7.

On the base of studying of differential modulation characteristics $U(\theta,I_{bias})$ and $\Delta\varphi(\theta,I_{bias})$ at pattern scanning for various laser diodes samples, the conclusion is made that at the optical fiber excitation from the laser diode, the effective signal delay (when this signal passes through RF FODL) varies approximately by 10–15% from the value of the bias current and the appropriate spatial location of the exciting light guider and the laser diode.

Variations of the OEO generation frequency are caused by small offsets of the laser diode bias current and are different for various angular deviations of the optical fiber optical axis from the laser diode optical axis. Thus, measured RF FODL characteristics on the base of KEM and the light guider FLG_0 enable estimation of frequency offsets in OEO with such a RF FODL versus the bias current of the

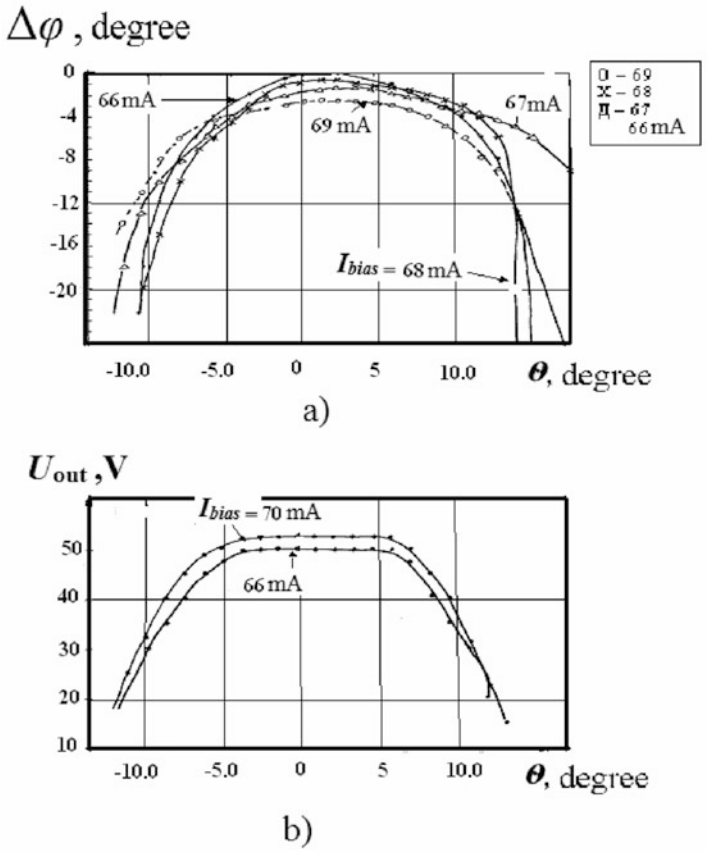

Fig. 8.7 Experimental functions of the phase difference $\Delta\varphi(\theta)$ and the signal amplitude U_{out} at the photodetector output in the far zone

modulated light source, the supply voltages as well as allow the correct choice of the filter natural frequency.

8.2 Influence of DC Bias Current Variations of the Laser Diode Upon the Generation Frequency

One of the goals of experimental investigations is the check of theoretical calculations fulfilled in Chap. 3 concerning the bias current influence upon OEO generation frequency at using the laser diode in OEO. The bias currents in an experiment are varied in the wide range from 0 to 80 mA and correspond to values from the threshold and above the threshold levels of the laser diode emission. The task of

this part of researches is experimental examination of OEO frequency f versus bias current variations I_{bias} of the modulated light source: the laser diode and the light-emitting diode. To solve this task, we use samples of OEO with RF FODL consisting of laser diodes or light-emitting diodes. For the OEO sample with the laser diode the breadboard No2 is used. This includes the following in series ring-connected: the electronic photodetector, an amplifier, the RF filter, and the modulator, the laser diode, the fiber-optical system. As the laser diode, we use the GaAs diode with the double hetero-structure of the 32DL-103 model with the wavelength $\lambda = 0.85$ μm, and ILPN-204 with the wavelength $\lambda = 1.3$ μm. The fiber-optical system in this breadboard consists of the light guider mixer of modes and the interchangeable single multimode light guider with lengths 20, 100, and 300 m. The OEO with RF FODL has the generation frequency which approximately equal to the natural frequency of the RF filter, and it is for various filters $f_{\text{osc}} \approx 8$ MHz, and $f_{\text{osc}} \approx 40$ MHz.

At current values equaled to the threshold value, the frequency function $f(I_{\text{bias}})$ has a minimum. The hysteresis character of the $f(I_{\text{bias}})$ curve at increase or decrease of the pumping current is explained by thermodynamic processes of heating or cooling of the laser diode active area at small variations of an environment temperature.

Theoretical dependences of delay time of RF oscillations for the system "the laser diode–the photodiode" versus the normalized DC bias current are presented in Fig. 8.8a. Figure 8.8b shows experimental functions of the relative frequencies f/f_0, the generation voltage amplitude U of OEO with RF FODL, and the output power P versus the bias current. The laser diode is ILPN-204 type. At that, the average generation frequency f_0 of OEO is 30 MHz.

A gain of an electronic amplifier is $K_{\text{ampl}} \cong 10^3$. The p-i-n diode is used as the photodetector. Experimental functions $f(I_{\text{bias}})$ of OEO with RF FODL are presented in Fig. 8.9a. At that, the laser diode 32DL-103 and the light guider segment with the length $L = 20$ m is used in this OEO breadboard. The laser diode 32DL-103 has no any special optical matching units, and it is joined with the optical fiber directly tightly. At that, the spontaneous emission level (captured by the fiber-optical system) was extremely low, and, as a consequence, RF OEO generation is appeared only for the pumping currents more than the threshold value. At that, the function is monotonically increasing at the bias current growth.

Experimental functions of the OEO generation frequency $f(I_{\text{bias}})$ versus the bias current are described in Chap. 4 for OEO using the laser diode of the ILPN-204 type (in which construction the optical matching system in the form of the "micro-lens" is included). At that, frequency functions $f(I_{\text{bias}})$ have the non-monotonic variation with a change of function slope signs: for bias current increase from 0 to threshold current values these functions are monotonically deceasing, while if the bias current is above the threshold value, these functions are monotonically increasing. In contrast to the previous case, a presence of the matching system in the laser diode allows the OEO generation at currents less than the threshold value. An analysis of the slope polarity change of the phase response at pumping current growth is described in Chap. 4 of this book.

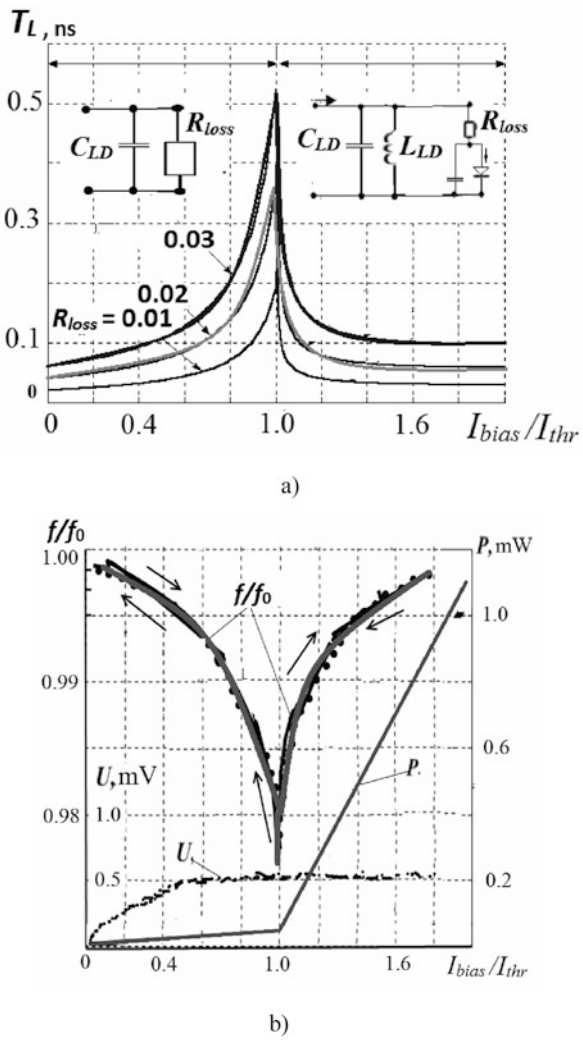

Fig. 8.8 Measurement of delay time T_L of RF oscillations for the system "the laser diode–the photodiode" versus the DC bias current I_{bias}/I_{thr} (I_{bias} is the bias current; I_{thr} is the threshold bias current) for different values of the loss resistance $R_{loss} = 0.01; 0.02; 0.03$ Ω (**a**). Experimental functions of the relative frequency f/f_0, the generation voltage amplitude U of OEO with RF FODL, and the output power P versus the bias current (**b**)

Figure 8.9b shows the oscillation jumps in $f(I_{led})$ for large length (300 m) of the optical fiber. These jumps are caused by oscillation jumps from one type to another in OEO owing to change of the total slope of the LED phase response at growth of the bias current.

These jumps in Fig. 8.9b are typical for OEO wideband frequency tuning by the bias current under conditions that the geometrical length of the optical fiber L_{fiber} is much larger than the wavelength of RF generation. Experimental curves $f(I_{bias})$ are well explained by mathematical models of the modulated light sources introduced in Chaps. 3–5. Measured conversion slopes of frequency variations Δf due to changing of the bias current ΔI_{bias} for LED OEO with RF FODL are: $S_f = 150$ kHz/mA for the optical fiber with length 20 m, and $S_f = 10$ kHz/mA for the optical fiber length

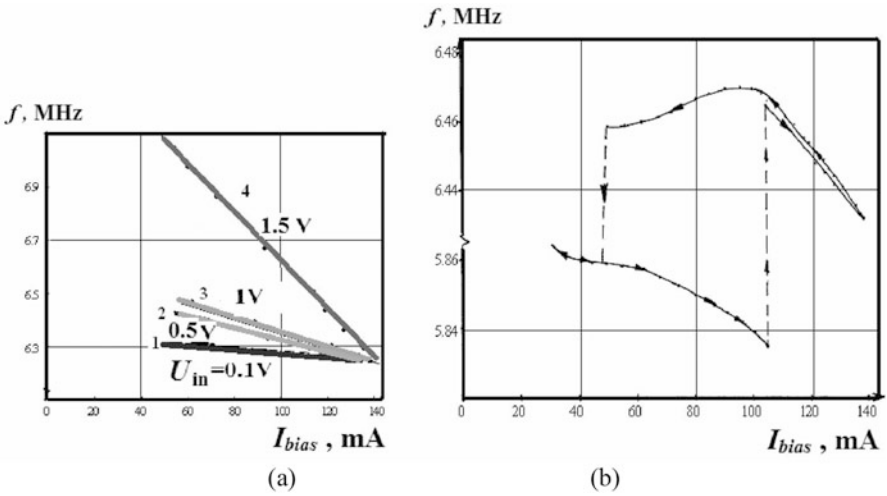

Fig. 8.9 Functions of the oscillation frequency f of OEO versus the bias current of the LED emission source I_{led} at light guider length $L = 20$ m (**a**), at the light guide $L = 300$ m (**b**)

300 m. Thus, this phenomenon was discovered experimentally by authors, for the first time, and explained by our theoretical analysis for laser diodes. According to this phenomenon, the change of polarity of the time constant slope of the laser diode and the slope S_f of the function $f(I_{bias})$ for OEO on the laser diode may be used for the correct choice of the laser diode bias currents in OEO and the modulation signal amplitude, as well as to perform optimization of the modulator structure, the matching optical unit with the light guide and the temperature-controlled unit.

Figure 8.10a, b shows the amplitude U_{out} functions for OEO oscillation versus the bias current I_{bias} of the LED emission source for various lengths of the optical fiber: (a) $L = 20$ m, and (b) $L = 300$ m. It can be seen that for various optical fiber lengths, the plot of these functions has a hysteresis type if the fiber length is more than the wavelength of RF oscillation.

Time-functions of the OEO generation frequency after power supply switching-on (so-called "frequency stopway") are measured. These functions are presented in Fig. 8.10c, d for various light guide lengths (20 and 300 m) and demonstrate the effect of the oscillation frequency stabilization at optical fiber length growth in RF FODL.

8.3 OEO on the Powerful Laser for the Phased Microwave RF FODL for the Active Phased Antenna Array

A goal of this part of our experimental investigations is to study the powerful laser application for the phase synchronization of fiber-optical channels of the distributed active phased antenna array system. The laser type is LTI-501, the laser mode is

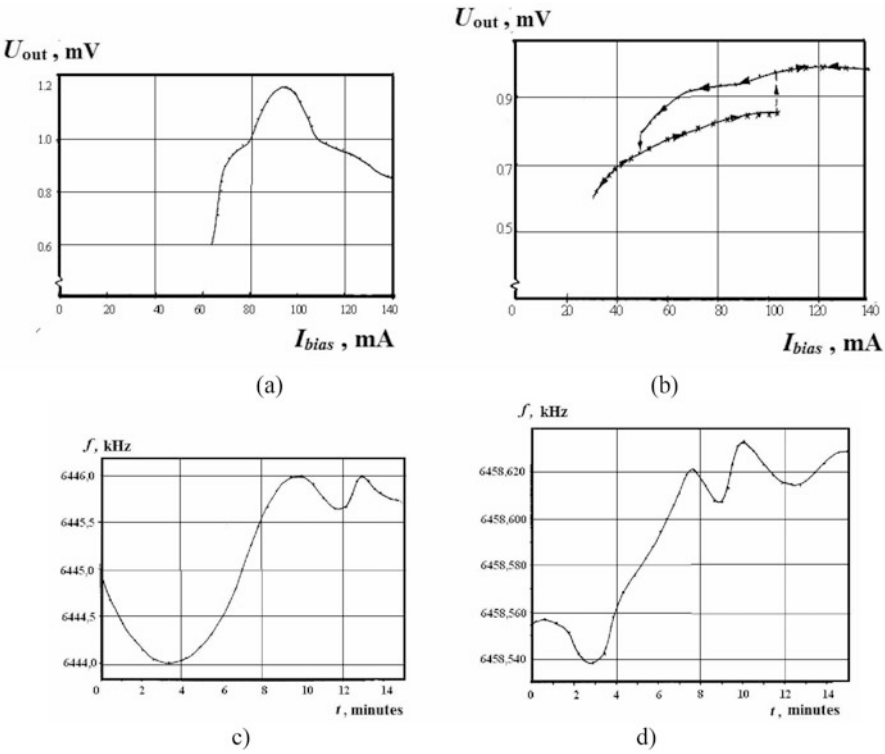

Fig. 8.10 Functions of the oscillation amplitude U_{out} for OEO generation versus the bias current I_{bias} of the LED emission source: (**a**) the fiber length is 20 m, (**b**) the fiber length is 300 m. Frequency stopways at the bias current $I_{bias} = 120$ mA for fiber lengths (**c**) 20 m and (**d**) 300 m

continuous wave, the laser output power is from 1 to 30 W, emission wavelengths are 1.06 and 0.53 μm. We investigated two types of modulators: (1) the acousto-optical modulator (AOM) on the base the para-tellurite crystal, (2) the electric-optical modulator on the base of lithium niobates. The OEO average frequency is 1.0 GHz, the long-term OEO frequency stability per 1 h is 10^{-6}. The phase difference drifts at outputs of the fiber-optical channels offsets are no worse than 2–3°. The dynamic range is 1000.

The optoelectronic oscillator workbench permitting experimental investigations of nonlinear effects in the optical fibers and perform phase measurements using the powerful neodymium-yttrium-aluminum-garnet laser with the power up to 40 W and the electro-optical and acousto-optical modulators in the microwave range is developed at MPEI (Radio-Transmitters Dept) under supervision of Professor V.V. Grigorianz. The structure of this experimental workbench of the phased microwave fiber-optical system on the base of the powerful laser and OEO is presented in Fig. 8.11a. The overall view of the powerful laser and the electric-optical modulator is presented in Fig. 8.11b, c.

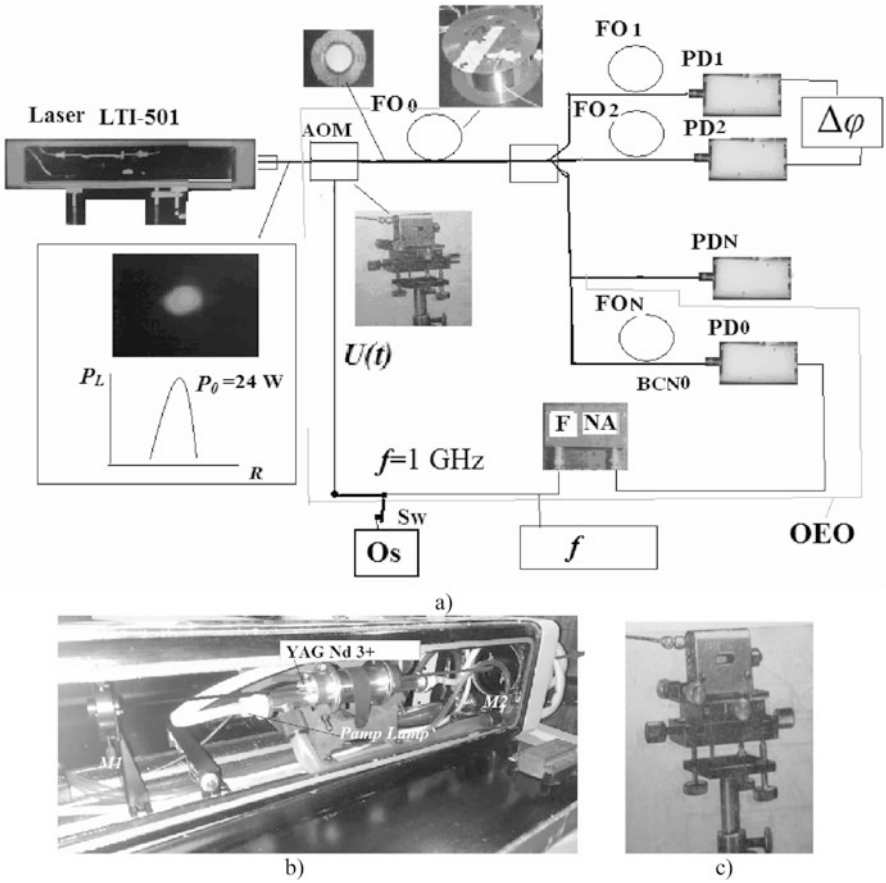

Fig. 8.11 A structure of the phased microwave fiber-optical system (**a**) on the base of the powerful laser and OEO: "Laser LTI-501" = the powerful laser, "AOM" = the acousto-optical modulator, "Os" = oscillator, "*f*" = the frequency-meter, "$\Delta\varphi$" = the phase-meter, "Sw" = a switch, PD0, PD1, PD2, PDN = the respective photodetectors 0,1,2...*N*; FO0, FO1, FO2, FON = the respective optical fiber 0,1,2...*N*; "F" = the RF filter, "NA" = the RF amplifier. General view of the powerful laser LTI-501 (**b**) and the acousto-optical modulator (**c**)

Let us briefly describe the operation of the functional diagram in Fig. 8.11.

Optical continuous emission of the LTI-501 laser, which output power is from 1 to 40 W, and the wavelength 1.06 μm, passes to the AOM modulator input. The sinusoidal voltage with 1 W-power acts at the electric input of AOM from the external oscillator "Os" (with low position of the switch Sw). The coefficient of modulation of the laser emission intensity at AOM output in the main beam on the 1 GHz-frequency is approximately 12%.

Then the optical emission from the modulator output passes to the fiber optical system (FOS) input. FOS consists of the fiber-optical couplers of Y-type and optical fibers FO0, FO1, FO1,...FON with different length—100–4000 m. The modulated

laser emission passes through optical fibers to photodetectors PD0, PD1, PD2,... PDN, and after amplification, it is registered. The amplified electrical sinusoidal oscillation with the voltage amplitude 0.1 V with the frequency 1 GHz (from outputs of two different photodetectors, for example, PD1 and PD2) passes to the phase difference meter. The feature of this structure (see Fig. 8.11) is that at the switch Sw closing in the last right position, the electrical oscillations pass to AOM, which are created by OEO. In this case, OEO is formed by the LTI-501 laser and by (closed in the feedback loop) the AOM modulator, the optical fiber FO0, the photodetector FD0, the RF nonlinear amplifier NA, and the filter F. From the filter F output (at satisfying of excitation conditions in OEO), oscillation with the 1 GHz-frequency pass to the AOM modulator. At that, the gain in power of the NA amplifier is 50–60 dB. The total gain for the OEO open loop depends on the electrical power acting on AOM (1 W), on the optical power passing on the light-sensitive area of the PD0 photodetector (0.01–0.1 mW), the conversion slope of PD (0.5) and optical losses in the channel.

During experiment according to Fig. 8.11, we investigate: the spatial structure of the laser emission for various powers from 1 to 28 W (Fig. 8.12); the watt–ampere laser characteristic; different methods for excitation of optical fibers by the infrared emission with the wavelength 1.06 μm. Functions of OEO oscillation frequency and differential phase incursions in channels are experimentally studied at temperature variations from 0 to 40 °C.

The normal operation of OEO with RF FODL was provided in the single-mode laser generation. During experiments, offsets of the interchannel phase difference are 2–3° at the fixed temperature of optical fibers. So, we prove the perspectiveness of this structure for the active phased antenna array with FOS.

The average modulation frequency of power optical emission is approximately 1 GHz at the entry optical power in the light guide from 1 to 20 W. Intensity distributions at output of the powerful laser in the cross-section and photo-pictures of emission "spots" at different output power values for the wavelength 1.06 μm are presented in Fig. 8.12. Such a structure of the phase-generator method with OEO is experimentally examined for application in modulated signal layout in channels of the phased antenna array.

As the result of this part of experimental investigations, the working capacity and availability are proved for the microwave fiber-optical system on the base of the powerful laser for the active phased antenna array. The measured phase difference drifts in channels on the generation frequency 1 GHz for the single-mode powerful laser are not more than 1°. Recommendations are developed on reduction of phase difference drifts by means of the optical frequency and the laser power stabilization as well as by means of the thermal AOM and fiber-optical channel compensation.

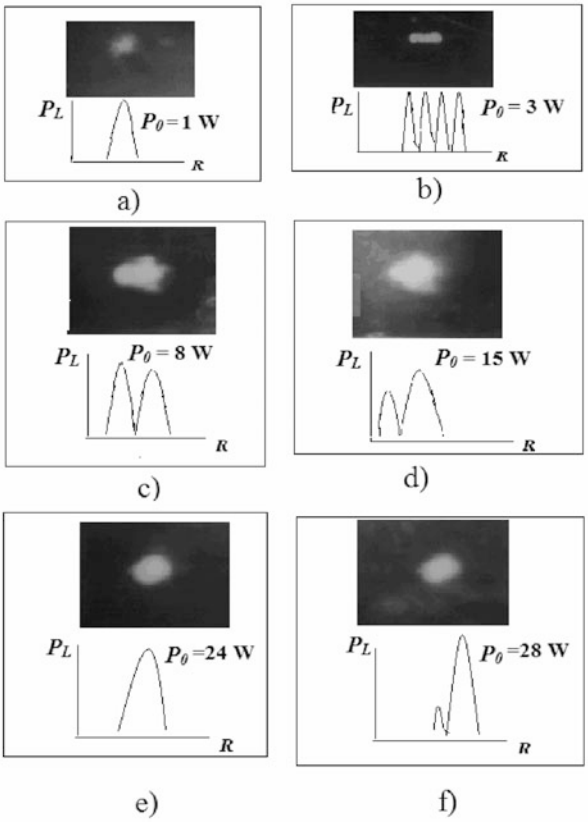

Fig. 8.12 Intensity distributions at the powerful laser output in the cross-section and photo-pictures of emission "spots" at different output power values for the wavelength of 1.06 μm. P_0 is the laser output power, P_L is the power distribution density of the laser emission in the cross section, R is the distance from the current point to the optical axis

8.4 Implementation of OEO in the Microwave Range and Its Experimental Characteristics

This section describes the OEO experimental research results in the microwave range of 8–10 GHz. The experimental OEO breadboard in the microwave range is developed and constructed in the hybrid implementation and created on the completely native element base. A part of experiment plots on the experimental amplitude and phase responses for QWLD, the watt–ampere QWLD characteristics and spectra are presented in Chap. 4 of this book.

For tasks' statement of the experimental investigations, this experimental OEO breadboard is considered as the specific device for creation of available master oscillators and local oscillators for receiving and transmitting sets for radars and optical radars in the microwave range.

The structure of OEO of the microwave range (Fig. 8.13) does not differ (structurally) from the OEO of the RF range. At that, main features are utilization of the quantum-well laser diode as the modulated light source with the modulation bandwidth 12–15 GHz. QWLD is the single-mode single-frequency highly coherent

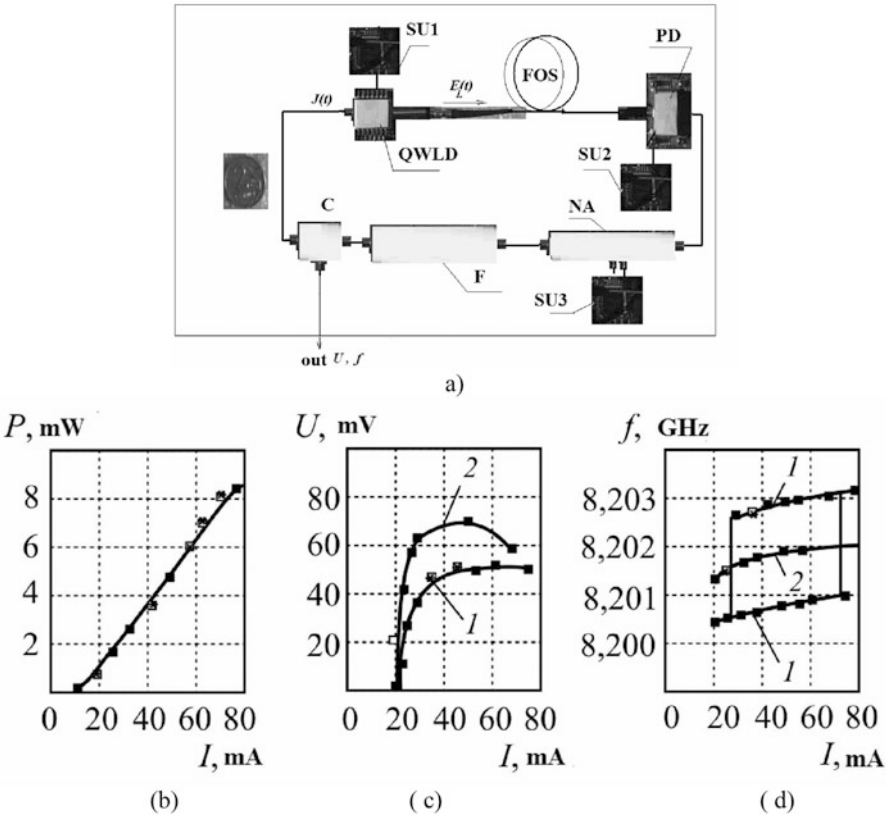

Fig. 8.13 (**a**) The block diagram of the optoelectronic oscillator of the microwave range on the base of OWLD. OWLD = the quantum-well laser diode, PD = the photodetector, FOS = the fiber-optical system, NA = the nonlinear amplifier, F = RF filter, SU1, SU2, SU3 = stabilization units of the pumping current of the laser diode, the bias current of the photodetector, and the supply voltage of the nonlinear amplifier, respectively. Experimental functions in the optoelectronic oscillator versus the bias current I_{bias}: (**b**) the laser diode power P, (**c**) the oscillation voltage amplitude at average RF frequency $f = 8.2$ GHz, (**d**) the oscillation frequency f for various light guide lengths 60 m (1) and 70 m (2)

emission source with the average output power of 3–10 mW. The second OEO feature in the microwave range is utilization of the single-mode low-dispersion fiber light guide as the retarding fiber-optical structure. For photodetection of the optical emission, the modern ultra-wideband (with bandwidth of 12–15 GHz) photodiode is used in OEO. The microwave amplifier with power supply regulation and the bandwidth about 1 GHz and the RF microwave filter on the base of the dielectric cavity with bandwidth about 2 MHz provide amplification and selectivity of microwave oscillations in OEO. The natural frequency of the RF filter is about 8.2 GHz.

In the experimental OEO breadboard according to the structure in Fig. 8.13a, the InGaAlAs/InP quantum-well laser diode is used with the emission wavelength of

1.3 μm. Experimental investigations of the optical spectrum, the watt–ampere characteristics, amplitude and phase responses of the given QWLD sample are conducted on the special experimental workbench and described in Chap. 4.

The maximal QWLD output power of the optical emission is about 10 mW at the wavelength 1310 nm. The width of the laser generation spectral line is about 3 nm.

In the experimental breadboard, the wideband (up to 12 GHz) intensity modulation of laser emission occurs by the QWLD bias current. The photodiode on the base of InGaAsP with the spectral bandwidth of 0.8–1.5 μm is used as the photodetector. The reverse light reflection from the photodiode butt is −40 to −50 dB.

The experimental QWLD used in the experimental sample of microwave OEO with RF FODL combines the following functions:

- The semiconductor optical emission source with the high temporal coherence and the large quantum effectiveness ($S_{LD} \approx 0.5$–0.6 W/A) of the microwave oscillation conversion for the QWLD bias current into oscillations of the output laser emission intensity.
- The ultra-wideband microwave modulator of this emission intensity, which has the large enough (of the order $S_{OM} \approx 0.5$–0.6 W/A) slope of the modulation characteristic.
- The active electro-optical quasi-resonance microwave filter having a capacity to wide frequency electronic tuning by the QWLD bias current.

On these wavelengths, the chromatic dispersion and optical losses in the single-mode fiber light guide from the allotted quartz glass are ps/(nm km) and 0.15–0.25 dB/km, relatively, for the QWLD optical emission with the wavelength of 1.3 μm.

In the OEO structure in Fig. 8.13, an energy of highly coherent optical oscillations (the optical carrier) passes to the photoreceiver (PR) from the QWLD output. Radio-frequency oscillations (subcarrier) obtained in the photoreceiver pass through an amplifier (A), the frequency-selective radio-frequency filter (RFF) (which is the frequency-defining element in the whole range of spectral OEO tuning) and are directed to the QWLD microwave input through the microwave directional coupler (DC) in this closed loop. All functional units of the OEO breadboard, mentioned in Fig. 8.13, are successively and in coordination connected each other into the closed loop of the positive feedback. If excitation conditions in this structure are satisfied, then at microwave output, oscillations occur in the microwave range. Oscillation observation is performed with the help of the C-4-27 spectrum analyzer.

The radio-frequency filter (RFF) represents the dielectric microwave resonator (DR) made on ceramics with the Q-factor $Q \approx 1000$ at average frequency of 8 GHz, which has the high permittivity and low losses in the microwave range. This RFF is tuned on the one of its natural resonance frequencies which is equal to about 8.2 GHz. The narrow RFF bandwidth of about 7 MHz allows obtaining of the single-frequency generation mode of OEO with suppression of the side components better than 49 dB for different light guide lengths from 1 to 4640 m. To ensure the single-frequency generation mode with suppression of side components, the special measures are used. The soft excitation condition is satisfied in the oscillator and the

stable continuous wave mode of autonomous single-frequency steady-state microwave generation of the quasi-harmonic subcarrier on the frequency about 8.2 GHz. The frequency functions of OEO with ordinary single-mode light guides of different lengths (from several meters to 4.6 km) are investigated experimentally in the steady-state mode. For these experiments' fulfillment, we use the "runout" light guide segments with the lengths 1, 3, 60, 70, and 4640 m as the light guides of the fiber-optical system.

For the ordinary low-dispersion optical fiber with lengths up to 65 m, the single-frequency oscillations are excited in the OEO system on the frequency closed to the natural RFF frequency of 8.2 GHz. The measured output power of the microwave subcarrier oscillations at the microwave output is about 0.1–1 mW.

OEO frequency functions are experimentally studied at control from the QWLD bias current (i.e., an operating point on its watt–ampere characteristic). The watt–ampere curve of QWLD is presented in Fig. 8.13a. The QWLD threshold bias current is about $I_{\text{thr}} \approx 12$ mA.

As we see, the QWLD watt–ampere curve in the whole bias current range is closed about to the linear function, but it has a "sharp bend" at the pumping current of about 60 mA, which relates to the generation condition fulfillment of the longitudinal modes of higher orders.

The single-mode optical fibers are selected according to their geometric length with the aid of side component suppression in the frequency spectrum of the generated subcarrier, which allows provision of the microwave single-frequency mode in the whole range of subcarrier frequency control.

Explanation of OEO frequency functions versus the QWLD bias current is described in the Chap. 4 of the present book. In Chap. 4 we can see the joined detailed plots of experimental and theoretical amplitude-frequency and phase-frequency curves for QWLD for various bias currents. At QWLD bias current growth, the generation frequency increases and determines from the phase balance condition by the interception points of the QWLD phase response and the RFF phase response.

At optical fiber length growth (up to 70 m) in experimental curves, we can observe the frequency jumps (Fig. 8.13d), which relates to the OEO frequency tuning to the adjacent oscillation types. If the QWLD bias current increases, the generation frequency essentially grows for small pumping excesses over the threshold value and has the insignificant growth (stabilization from the current) for bias current excesses above the threshold value more than $I_0/I_{0\text{thr}} = 5$–8, which corresponds to QWLD bias currents equaled to $I_0 = 50$–80 mA.

These experimental functions of the frequency f and the amplitude U of OEO microwave generation presented in Fig. 8.13b, d versus the bias current well agree with calculations in Chap. 3.

The frequency of the generated microwave subcarrier can be exactly tuned to the central frequency of the microwave RFF by means of adjustment of the optical phase incursion in the optical phase shifter.

When using the RFF in OEO, the generation frequency determines by the amplitude-frequency curve of the mutual two-port formed by RFF and QWLD.

Amplitude and phase responses of this two-port varies by the QWLD bias current variations. At that, the joined microwave filter "RFF-QWLD" has been formed, and it is controlled by the QWLD bias current. The filter control is performed by displacement of the QWLD amplitude response peak. Therefore, we may speak about new type of the tuned microwave filter. The filter role is played by the known (in the balance theory of laser generation) quasi-resonance peak on the high-frequency edge of the small-signal amplitude-frequency curve of used QWLD.

In the quantum-well laser diodes, as already shown in Chap. 4, this peak is caused by the specific dynamics of electron–photon interaction of the relaxation-reactive character. A position of this peak apex (the natural frequency) on the frequency axis, its height and width depend on many parameters of the active medium and the QWLD optical resonator. The natural frequency of this peak depends on the value of QWLD bias current excess over its threshold value, which is 12 mA in QWLD used in this experiment. The natural frequency of relaxation oscillations corresponding to the peak apex is tuned by the QWLD bias current in very wide limits: from 1 to 9 GHz.

This allows implementation of the OEO generation frequency tuning in the range 8200–8203 GHz at presence of RFF with the natural frequency 8.2 GHz and the bandwidth about 2 MHz in the OEO circuit in Fig. 8.13. Measured experimental function of the generation frequency (Fig. 8.13) versus the bias current, is close to calculated and well approximated by the parabolic function.

At small bias currents, the slope of generation frequency variations versus bias current is 0.3 MHz/mA. At large QWLD bias currents (by 5–8 times) the slope of generation frequency versus is 0.003 MHz/mA. Fulfilled researches allow optimization of the QWLD bias current choice. The optimal bias current is 60 mA.

Investigations of frequency functions (Fig. 8.13) versus the bias current at different light guide length 1, 3, 60, 70, and 4500 m. It is stated that the single-frequency mode of OEO generation in the whole range of bias currents at filter Q-factor close to 1000 may be obtained at definite lengths of the optical fiber. So, for instance, at the optical fiber length of 60 m, the single-frequency mode without jumps occurs in the whole range of bias currents (Fig. 8.13c, the curve 2). At optical fiber length of 70 m, the single-frequency mode is realized with the jump to the adjacent oscillation type (Fig. 8.13c). Owing to narrow bandwidth of RFF and the effect of frequency pulling, the single-frequency mode realizes at the length of 4500 m. Jumps to another type of oscillations at bias current variations are well agreed by the general theory of oscillators (including OEO with RF FODL). The graphical image of amplitude and phase responses of QWLD and RFF, shown in Fig. 7.18 (Chap. 7), well explains a mechanism of the OEO generation frequency control at variations of the bias current.

A hysteresis character (small) of the frequency and amplitude functions versus the bias current (at single-frequency mode without frequency jump) is explained by thermodynamic processes in the active zone of the QWLD at variations of the bias current. At that, the structure of functions of the generation signal amplitude versus the bias current at frequency tuning in this range was different for various lengths of the optical fiber. These experimental functions of frequency and amplitude coincide

(with accuracy of 20%) with calculated functions obtained on the base of the theoretical model of OEO with RF FODL developed in Chaps. 3–7 of this book.

As the result of the experimental data analysis, it is proved that excitation of OEO with RF FODL happens at the bias current about 35 mA, while the QWLD threshold bias current is 12 mA. This is one of features of OEO of the microwave range. Inequality of the QWLD threshold bias current and the bias current, for which the microwave generation arises, is explained by the fact that at small bias currents, the conditions of amplitude and phase balance are not satisfied. At small bias currents (less than 35 mA), the natural frequency of the QWLD resonance peak is 1–6 GHz (Fig. 7.18). At that, for the natural RFF frequency of 8.2 GHz, the amplitude balance condition is not satisfied because the QWLD has in this case the small transfer factor. At the average generation frequency of 8.201 GHz, we obtained the relative frequency instability in the experimental breadboard of OEO not worse than in the time interval of 10 min at room temperature. In OEO of the microwave range, at large delay time from 1 to 25 μs, the stabilization effect arises in the RF FODL of the microwave-modulated optical emission path.

Thus, we considered the specific implementations of fiber-optical systems, QWLD amplitude and phase responses and we described methods of frequency control of the microwave oscillations in OEO by variations of QWLD DC pumping (bias) current because the phase response of the laser diode insignificantly varies with the pumping current.

Theoretically studied and experimentally implemented results of frequency tuning ranges versus the QWLD pumping current in the microwave range on frequency 8.2 GHz were examined. At small pumping current excesses over the threshold value by 1–2 times, the frequency tuning slope is 0.2 MHz/mA, while for excesses by 5–8 times, relatively, the slope is less than 0.01 MHz/mA for the average generation frequency of 8.2 GHz.

Experimental functions of the frequency and amplitude shown in Fig. 8.13, at variations of QWLD DC pumping current, have 10–20%-coincidence with calculated functions, which means that we have the correct choice of QWLD and OEO mathematical models.

Thus, for the first time in Russia, we realized microwave generation in OEO with RF FODL in the microwave range on frequency 8.2 GHz. We proved the possibility of utilization of the native QWLD as the modulated light source with the ultra-wideband modulation frequency as well as the native ultra-wideband photodiode. Measured experimental function of the generation frequency for various bias currents is close to the calculated one and well described by the parabolic function.

At small bias currents, the slope of generation frequency variations versus the bias current is 0.3 MHz/mA. At large QWLD bias currents (by 5–8 times), the slope is 0.003 MHz/mA. Fulfilled examinations allow optimization of QWLD bias current choice. The optimal QWLD bias current for single-frequency mode of the steady-state OEO generation is 60 mA. The general conclusion made about availability of QWLD utilization as the modulated light source in OEO of microwave range on frequencies 8–15 GHz.

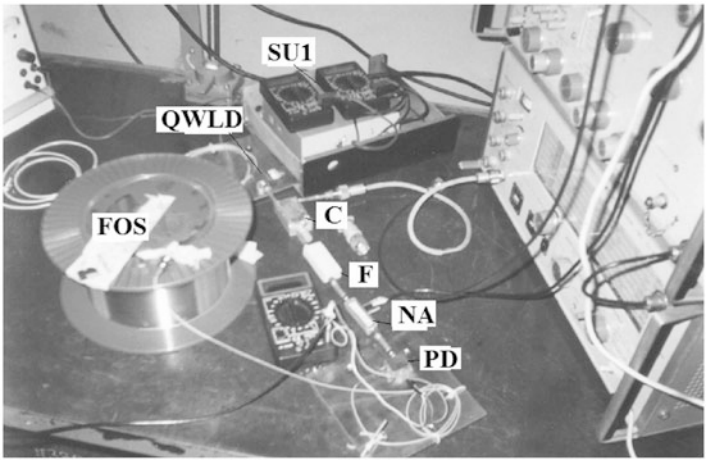

Fig. 8.14 Experimental workbench for investigations of OEO with RF FODL operating in the microwave range of 8–12 GHz with the optical fiber length 4464 m. QWLD (or QWLD) = the quantum-well(dimension) laser diode, PD = the photodetector, FOS = the fiber-optical system, NA = the nonlinear amplifier, F = RF filter, SU1 = stabilization units of the pumping current of the laser diode

Figures 8.14, 8.15 and 8.16 show the experimental workbench and OEO samples with QWLD at direct modulation operating in the microwave range 8.2 GHz with optical fiber length 4464 and 100 m

During experimental works, the operating variant of OEO with the external Mach–Zehnder modulator of the microwave range was developed and examined.

The functional diagram (a) and the general view (b) of experimental sample of the low-noise laser optoelectronic oscillator with the Mach–Zehnder external modulator of microwave range are presented in Fig. 8.16. The operating generated frequencies are 8.2 and 10.1 GHz at application of different radio-frequency high-Q filters. The following abbreviations are introduces in Fig. 8.16: QWLD = a laser diode, MZ = the electro-optical Mach–Zehnder modulator, FOLG = the fiber optical light guide, PD = the photodetector, NA = the nonlinear amplifier, F = the radio-frequency filter, C = the directional coupler.

A wavelength of a laser diode is about 1550 nm. The line width of the laser optical emission is less that 1 MHz. The generated signal power of OEO is 1.8 mW. In OEO, the Mach–Zehnder modulator from Hitachi is used. At that, we use specially developed by authors regulators of the bias current of the laser diode, the temperature laser diode regulator, the bias voltage regulator for the Mach–Zehnder modulator, the supply voltage regulator for an amplifier, and the photodiode current regulator.

With the aim of demonstration of Q-factor influence of the RF filter on the PSD of the phase noise of OEO with the Mach–Zehnder modulator, Fig. 8.17 shows the measurement results of the power spectral density of the phase noise at

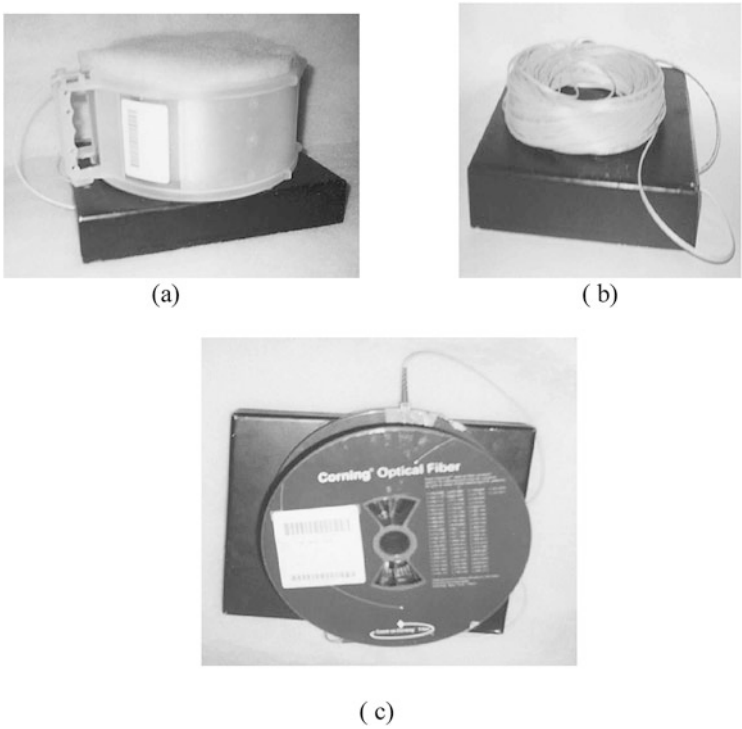

Fig. 8.15 Experimental samples of OEO with RF FODL operating in the microwave range with the optical fiber length of 4464 m (**a**) and 100 m (**b**). The experimental sample of OEO with QWLD for direct modulation operating in the microwave range of 8.2 GHz with optical fiber length of 4464 m (view from above) (**c**)

various Q-factors of the RF filter: 1—the RRF Q-factor is 450, 2—the Q factor is 560, 3—the Q-factor is 900.

The experimental sample of the low-noise differential laser oscillator of the microwave range with operating frequency of 8.2 GHz contains of the QWLD with the line width not more than 1 MHz. QWLD and the photodetector have the specific units for bias currents regulators. QWLD has the additional unit for temperature regulation.

From presented functions, we see that growth of the RF filter Q-factor leads to reduction of PSD of the phase noise, and for the RFF Q-factor of 1000 in OEO with the MZ modulator, the power spectral density of the phase noise on the level -120 dBm/Hz is obtained for the offset 1–10 kHz. At that, we can note that without introduction of special measures, the level of spurious harmonics is from -80 to -30 dBm/Hz and even higher. The frequency difference between harmonics is determined by the geometrical length.

Measures for spurious harmonic level reduction, when using the differential delay line, to the level -100 to -120 dBm/Hz are used with the directional couplers.

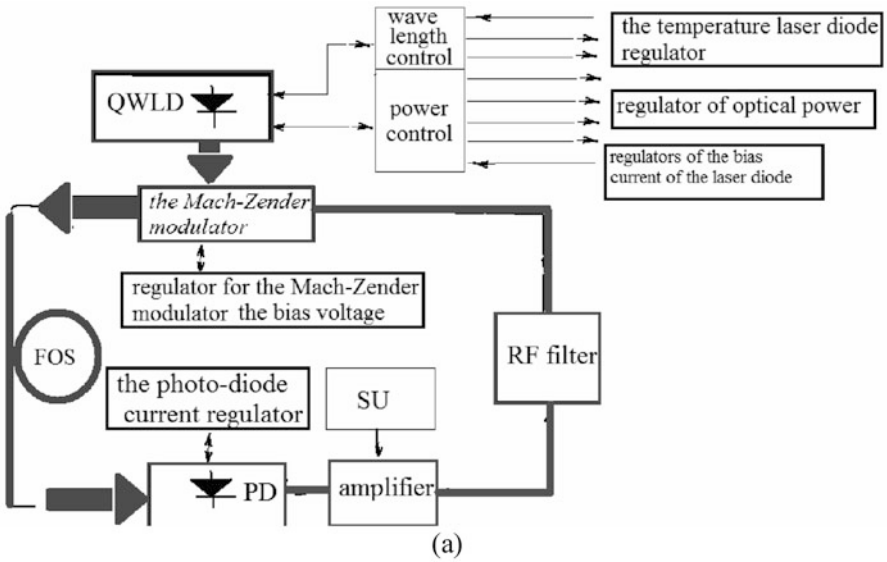

Fig. 8.16 The functional diagram (**a**), the general view (**b**) of the experimental sample of the low-noise laser optoelectronic oscillator with the Mach–Zehnder external modulator of the microwave range. Operating frequencies are 8.2 and 10.1 GHz

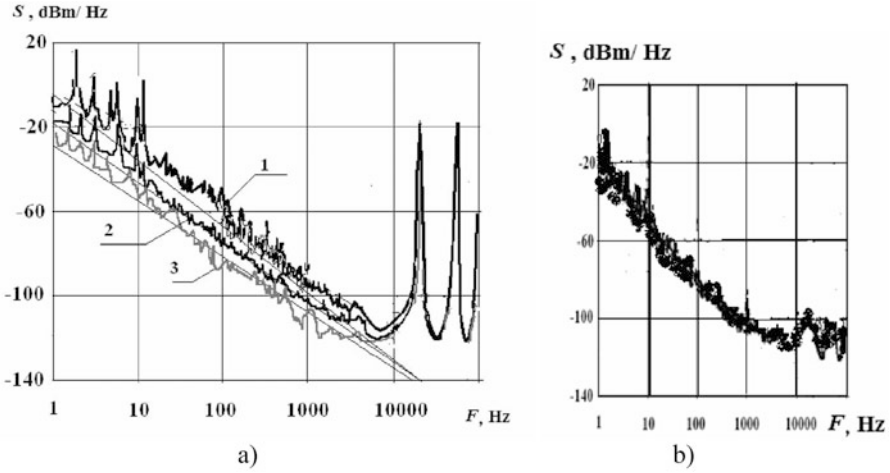

Fig. 8.17 Measurement results of the power spectral density of the phase noise at the various RF filter *Q*-factors: 1—the *Q*-factor is 450, 2—the *Q*-factor is 560, 3—the *Q*-factor is 900 with the ordinary delay line on the base of the single optical fiber (**a**) and with differential RF FODL on the base of two optical fibers of different lengths (**b**)

As the result of measures performed, on average, in the above-mentioned range for offset 5–1000 kHz, the experimentally measured phase noise level is less than −115 dBm/Hz from the microwave subcarrier frequency.

On the base of the experimental data analysis and comparison with calculated values, recommendations are developed on OEO application with the MZ modulator as the low-noise oscillator on the electronic equipment.

There are PSDs of the phase noise of OEO with RF FODL on the base of the Mach–Zehnder modulator, which are presented in many papers by authors: X. S. Yao and L. Maleki (2000) [1], D. Eliyahu and L. Maleki (2003) [2], C. W. Nelson, A. Hati, and D. A. Howe (2007) [3], W.Zhou and G.Blasche (2005) [4], Volyanskiy, J. Cussey (2008) [5], Zhiqiang Fan, Qi Qiu (2019) [6].

From the curve presented, we see that the level less than −140 dB/Hz at offset 1 kHz can be achieved for OEO with the MZ modulator using the high-coherent lasers with the line width of 1 kHz and the phase-locked loop. These OEOs with the MZ modulator are competitive with the traditional oscillators on the leuco-sapphire (Chap. 2) and have a series of advantages: a possibility to withstand the high shocking loads and accelerations at the expense of relatively low weight, small dimensions and the fiber linear structure of RF FODL.

8.5 Practical Circuits of the Optoelectronic Oscillator Implementation

8.5.1 Implementation of Tuned Low-Noise Oscillators in the Microwave and mm-Wave Ranges

OEOs have a series of additional valuable properties for usual and optical radars: the low losses, the low weight, relatively small dimensions (in some cases, they can be done in the integral implementation), the high operation speed, a capability to the remote control of its parameters, the absolute galvanic decoupling with the environment power engineering equipment, the high noise-immunity, and secrecy (electromagnetic compatibility).

In 2019, the commercial sample OE3700 from company OE Waves of the oscillator on the base of OEO with the Mach–Zehnder modulator has the following characteristics: OE3700 specifications: the frequency 10 GHz (Other frequencies available), the RF Output Power + 10 dBm, the Phase Noise −140 dBc/Hz at 10 kHz, Harmonics −40 dBc. [Product Brief. Compact Opto-Electronic Oscillator (OEO). Low Phase Noise Microwave Signal Source Module—Oewaves (www.oewaves.com)].

In spatially spaced and inter-connected coherent usual (RF) and optical radars including Doppler ones, such OEO may be the main functional units of the frequency synthesizers for transmitters and receivers, spatially distributed systems of the remote ultra-noise-immunity synchronization and PLL systems, circuits for frequency stability transfer, transmission sections of the reference, phase-precision oscillations for optical and microwave quantum frequency standards, network nodes for signal layout in active phased antenna arrays.

From the point of view of OEO application as the master reference oscillators of receiving-transmitting devices of the real radar stations of microwave and mm-wave ranges, the extreme interest is caused by utilization of the energy pumping from QWLDs.

8.5.2 OEO in Microwave and mm-Wave Ranges in RF and Optical Radars of On-Board and Ground-Based Stations

Let us consider the prospects of OEO utilization in RF and optical radars.

The radio-optical OEO built with the account of above-listed approaches, have a series of additional valuable properties for RF radars and radio-optical radar (ROR): low losses, the low weight and comparably small dimensions, high operation speed, a capability to the remote control by its parameters, the absolute galvanic decoupling

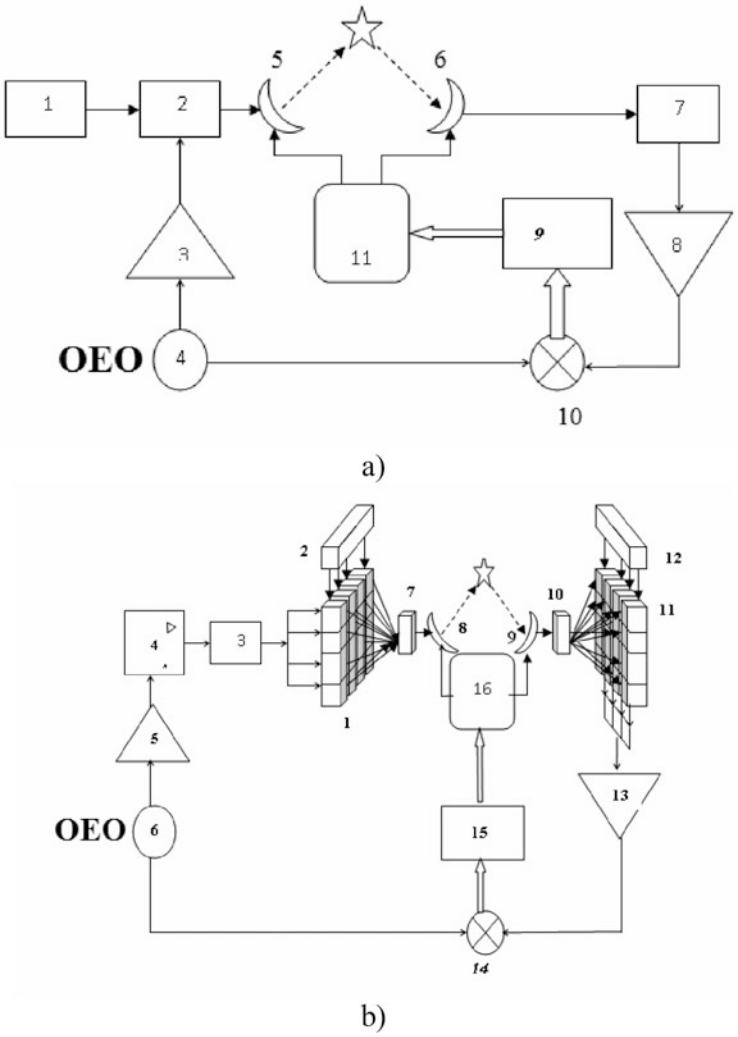

Fig. 8.18 The block diagram of the laser Doppler radar on the base of phased optical arrays with OEO application (**a**). The block diagram of the laser Doppler radar systems on the base of the single powerful laser (**b**)

with environment power engineering equipment, the high noise-immunity, and secrecy (electromagnetic compatibility).

Let us describe the block diagram of the laser Doppler radar (LDR) system on the base of the optical phased antenna array (OPAA) (Fig. 8.18).

In the block diagram of Fig. 8.18a the following units are included: 1 = the powerful continuous-wave (or pulse) laser, 2 = the external electro-optical microwave modulator of the laser emission intensity, 3 = the electronic microwave driver, 4 = the reference optoelectronic oscillator in the microwave range, 5 = the transmitting optical antenna, 6 = the receiving optical antenna, 7 = the photoreceiver, 8 = the microwave amplifier, 9 = the processing unit, 10 = the mixer, 11 = the system for laser beam guiding for spatial detection and guiding of the moving target.

To create the LDR on the native element base in the IR range with the operating distance from 3 to 70 km and more, which have the microwave in the 25 GHz range (in prospect in 50 GHz and higher), we can use the structure in Fig. 8.18b.

The following unit are included in the block diagram in Fig. 8.18b: 1—the microwave phased array from laser diodes (continuous-wave or pulse) with the direct internal modulation of their intensity, 2—the supply unit for laser diodes of the array, 3—the divider of microwave power, 4—the powerful microwave driver, 5—the microwave preamplifier, 6—the reference optoelectronic oscillator, 7—the noncoherent optical combiner-collimator of microwave-modulated of emission intensity of laser diodes in the array, 8—the transmitting optical antenna (the lens system), 9—the receiving optical antenna (the lens system), 10—the optical intensity divider of received optical emission, 11—the receiving array from high-operation-speed photodiodes, 12—the unit of the bias voltage to receiving array photodiodes (not always necessary), 13—the microwave amplifier of the photoreceiver, 14—the microwave mixer, 15—the processing unit, 16—the system for laser beam pointing, spatial detection and tracking of the moving target.

LDRs with the microwave subcarrier offered for development and implementation, allow measurements of target radial velocities in the real time scale and with high accuracy at target and emitter movement in any direction. These measurements can be performed owing to the large energy brightness of the high-intensity laser quasi-continuous emission obtained at the output of the optical transmitter, as well as owing to the high value of modulation frequency. Such laser Doppler radars are able to measure of the small radial velocity of the moving targets of the order of 0.1 m/s for large distance of 50 km and more, which becomes possible at the short-term frequency instability of the order of 10^{-10} to 10^{-11}. Fulfillment of hard requirements to the high-frequency oscillator in the transmitter and the to the microwave local oscillator in the receiver concerning the short-term frequency instability is realizable, when the quasi-harmonic OEO is applied with the unique transfer function of RF FODL in the microwave loop of the positive feedback. Sensitivity and the dynamic range of the LDR with the microwave subcarrier are higher by several orders than characteristics of traditional Doppler radars because in LDR we provide measurement of the Doppler shift for subcarrier oscillations, which have high frequency (10–25 GHz and higher) and the phase noise level is low: −130 to −150 dB/Hz. We should note that the priority of the creation idea of the laser Doppler radar on the

OEO base belongs to authors of this book and it was mentioned for the first time in publication in 2004 and 2005 on the international conference "Radio-optical technologies-2004" [7].

8.5.3 OEO Utilization for Measurement of PSD of Phase Noises in Oscillators, Microwave and mm-Wave Devices and Lasers with the Narrow Spectral Line Below 100 kHz

One of the OEO application (with the close and open feedback loop) is in the measuring workbenches for the phase noise analysis in microwave and mm-wave oscillators with the extremely low level of minimally measured noises of −130 dB/Hz at 10 GHz-frequency and 1 kHz-offset. At that, OEO is used as the reference oscillator with low phase noises, and in this case, the OEO feedback loop is closed.

One of OEO advantages, which have optical and electronic outputs, is application of the low-noise fiber-optical retarded system with the time delay more that 50 μs without the additional electro-optical converter in devices of the phase noise measurement. Prospects of this method utilization for phase noise measurements are improved with development of the wideband Mach–Zehnder modulators with bandwidth up to 50 GHz. The potential measurement limit with the help of composite compensating Mach–Zehnder modulators and utilization of lasers with the line width less than 1 kHz can be decreased down to −160 dB/Hz.

From commercial point of view, this method is more beneficial compared to application of expensive low-noise oscillators with the sapphire resonator.

8.5.4 OEO Application in Lengthy Fiber-Optical Links of the Secretive Communication with the Increased Noise Immunity

The main principle of these systems' construction consists in the masking of message transmission with the help of useful information introduction into chaotic carrier [8]. The reverse information extraction at the unauthorized access, i.e., at absence of a-priori data about the initial dynamic system, is quite difficult, and in some condition, is practically impossible. Thus, the chaotic signal is indistinguishable with high probability from the random interference for the external observer, which allows hiding of the transmission fact itself. At detection, the procedure of information extraction itself essentially complicates by the traditional methods, which provides high confidence of transmitted data.

Application of OEO chaotic oscillations for information transmission through the fiber optical communication links is defined, firstly, by relative simplification of the

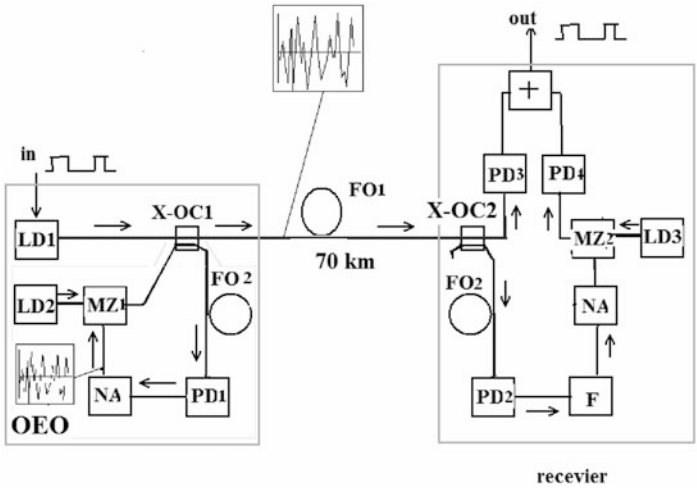

Fig. 8.19 The block diagram of fiber optical communication link with masking message transmission with OEO as the chaotic source

chaotic oscillator creation of the RF and microwave ranges on the OEO base, and secondly, there is a possibility to have the electronic and fiber-optical outputs in the chaotic OEO, and thirdly, there as a possibility of the electronic and optical synchronization of chaotic oscillations in the transmitter and in the receiver. The block diagram of the lengthy (more than 70 km) fiber-optical communication link with masked message transmission with OEO as the chaotic oscillation source is shown in Fig. 8.19 [9]. OEO in this system operates in the chaotic mode and is synchronized on the optical communication by the external laser diode LD_2 using the directional coupler DC_1. OEO is formed by in series closed into a loop by the modulated light source MLS, consisting of the laser diode LD and the external Mach–Zehnder modulator, the light guide LG, the photodiode PD_1, and the radio-frequency amplifier NA. Notably, that in this structure, the external Mach–Zehnder modulator acts as the nonlinear element. The average frequency of radio-frequency subcarrier is 10 GHz. The frequency of the optical carrier is approximately 128 THz (the wavelength of optical emission is 1.55 μm).

For informational message extraction in the receiving section, the optical signal is divided with the help of the directional coupler X-OC2 and passes on photodiodes PD2 and PD3. From the photodiode PD2, the RF signal passes to the first input of the mixer M_1. The signal from the PD4 output passes to the second input of the CM_1 mixer. The signal of original information message is extracted at the output of the CM1 mixer. Application of the nonlinear processing of the chaotic signal with delay is a peculiarity of the structure of the secretive RF FODL. This signal channel contains of the additional laser diode LD3, the modulator MZ2, and the photodiode PD4.

8.5.5 OEOs for Formation of Optical and Electric Pulses with Durations Less than 1 ps with the Low Jitter

OEO of the microwave range with the Mach–Zehnder modulator can be used for formation of optical pulses with the duration of 1 ps with the low jitter [10].

The OEO formed by in-series closed into a loop, the modulated light source (Fig. 8.20) consisting of the laser diode (LD) and the MZ modulator, the fiber light guide (FLG), the photodiode (FD), the wideband amplifier and a filter, constitute the formation unit. With the help of directional couplers DC_1 and DC_2, the optical emission formed by the fiber-optical ring laser (FORL) with the erbium active medium, passes through the MZ modulator in opposite direction from its output to its input. When OEO excitation condition satisfies, the electric voltage of precision oscillations with the frequency about 10 GHz acts on the modulator. Owing to this, the optical emission circulated in the ring FORL is also modulated in intensity, and FORL synchronization is performed. At FORL synchronization, the optical pulse duration at its output decreases to $T_i = 1$ ps, and the jitter value is several femtoseconds.

The simpler variant of the short pulse formation with duration of tens picoseconds with the relatively low jitter is the formation circuit using OEO with the MZ modulator or with the absorptive electro-optical modulator. OEO formed by in series closed into a ring the modulated light source consisting of the laser diode and the absorptive electro-optical modulator, the fiber light guide with the length up to 2 km,

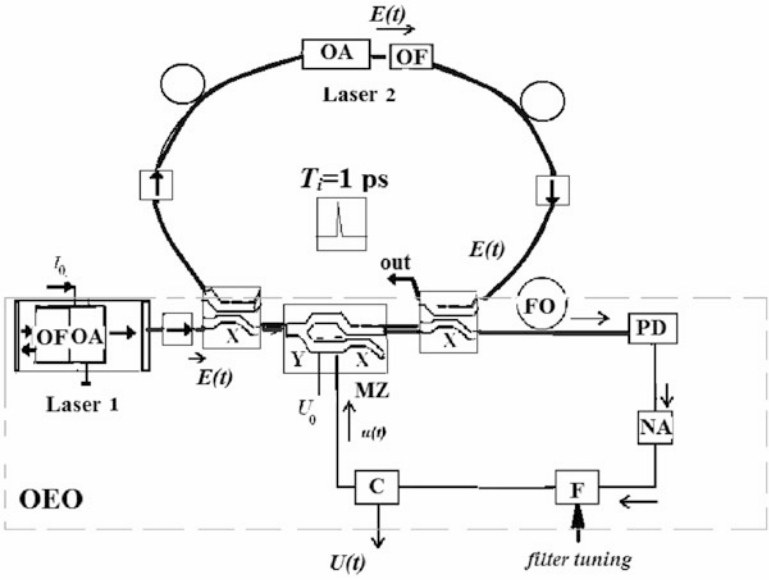

Fig. 8.20 The block diagram of OEO with the ring laser operating in the mode of longitudinal mode synchronization

and the photodiode, an electronic amplifier, and a filter with the Q-factor of 1000 are included in this circuit. At large reserve in excitation, the OEO ring structure forms the optical pulses with duration of 10–20 ps. The pulse jitter in not more than 0.1 ps.

8.5.6 Implementation of Fiber-Optical Sensors of Physical Quantities on the OEO Basis

Experimental testing of the functional converters (FC) of the electric voltage and current on the base of OEO with RF FODL is conducted by authors for the first time. Measurements of FC main characteristics show an expediency of OEO application for measuring of electrical voltages with large and small values in the difficult in access places with the strong external spurious electromagnetic fields. In the experimental breadboard of FC on the OEO base, the conversion slope of "electric current-to-frequency" and "voltage-to-frequency" are relatively 3 kHz/A and 1 kHz/V, which allows effective registration of voltages, currents, and electromagnetic fields in the wide range of amplitude values with the large dynamic range 10^3–10.

In the OEO breadboard of the electric current sensor, the maximal OEO frequency deviations are measured. They are $\Delta f = 5.0$–10.0 kHz at variations of the AC electric current amplitude $I_c = 750$–1500 A. We proved theoretically and experimentally a possibility of physical influence conversion into the OEO frequency.

It is shown that variations of mechanical displacement at measurement of two parameters of OEO with RF FODL—the frequency f and the signal amplitude—increase the measurement accuracy and reliability of mechanical displacements. Double-parameter measurements allow the conduction of the complex compensation against interference caused, for example, by a temperature or a pressure affecting to the light guides. The minimal registered level (sensitivity) of such a converter of "acoustic oscillations-to-OEO frequency"-type is about 30 mPa.

Authors conducted experimental investigations (of displacement, temperature, electrical voltages, and currents) on the OEO base. In addition, experimental investigations are fulfilled during a creation of the breadboard on the OEO base for studying of the light guide temperature influence on its parameters. Experimental measurement breadboards and sensor characteristics are discussed below. This section also contains description of the promising sensors on the OEO base using the sensor "FBR-technology," which allows conversion of the micro-displacement variations in the material structure into variations of the light intensity. This technology of OEO with the differential delay line utilization as the converter on the light intensity variations into the oscillation of radio-frequency allows development of effective strain sensors. The application area of these strain sensors is vast. First of all, this is fiber- and plastic aircraft construction and shipbuilding, the alternative energy sources—turbines of wind generators, monitoring of oil and gas pipe lines, manufacturing of the plastic pipes, bridge engineering, underground construction,

etc. Authors had got authors certificates and patents on many constructions of sensors on the OEO base.

8.5.6.1 Sensor for Mechanical Micro- and Nano-Displacement

The fiber-optical sensor on the OEO of RF and microwave ranges created as the fiber-optical interferometer gives a possibility to monitor the structural surface variations with the accuracy of 0.1 nm. The measurement principle of relative variations of geometrical dimensions is based on the light reflection from the monitored surface. This accuracy achieves by utilization of four wavelengths of the laser diode optical emission in the nanoscope, the frequency registration of the OEO precision oscillation signal and further computer processing. The foreign prototype operates on the principle of phase measurement of microwave subcarrier (instead of frequency measurement in our sensor).

8.5.6.2 Sensors of Electric Voltage

The functional diagram of the OEO fiber-optical sensor is shown in Fig. 7.24 (Chap. 7). The block diagram of the high-voltage sensor (more than 25 kV) is shown in Fig. 8.21. It contains of separate controllers C_1–C_3 and frequency indicators with the ring fiber-optical transfer module of information transmission from each sensor of the high pulse voltage at each net conductor (Fig. 8.21).

Experimental characteristics of the electrical voltage sensor are presented in Figs. 8.22 and 8.23 and show its effectiveness. Figure 8.24a shows the general view of experimental unit of this sensor.

8.5.6.3 The Magneto-Gorge Sensor of Electric Current

Authors fulfilled investigations of the experimental sample of the magneto-gorge sensor (Fig. 8.24b, c) of the AC electric currents with the amplitude of 100–2000 A. At that, we use the OEO with the single fiber light guide in the indicator. The sensor construction, which view is shown in Fig. 8.24b, c, represents a toroid with external diameter of 10 cm made from the magneto-gorge material (ferromagnetic). The fiber light guide with the length of 100 m had wounded in special manner to the external side of the toroid and this fiber was pasted to the toroid case by the epoxy adhesive. The copper wire, through which the AC electric current with amplitude 100–2000 A flows, is placed into the internal cavity of the toroid.

The relative total longitudinal stretching-compression of the optical fiber in the coil is approximately one hundred thousandth part (1.2×10^{-5}) at wounding length of 100 m for the amplitude of the registered AC electric current about 1.5 A.

Relative variations in the oscillation frequency of the laser oscillator are values of the order of 1×10^{-5} according to calculation and experiment results. The effect on

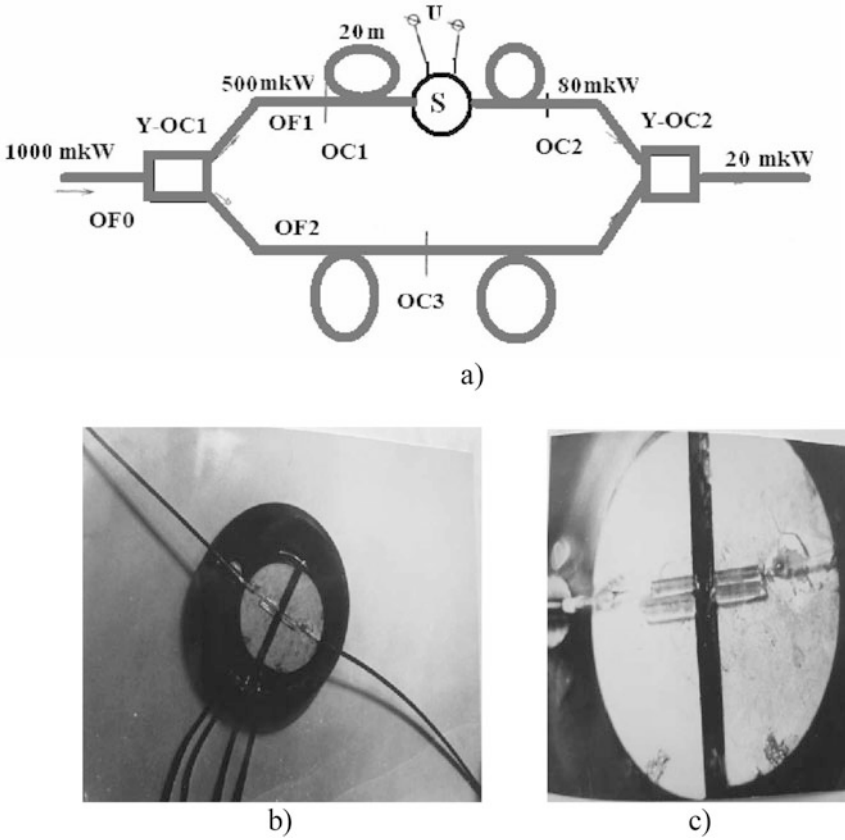

Fig. 8.21 The block diagram of piezo-electric sensor (S) connection into the fiber-optical delay line. OC1, OC2, and OC3 are optical connectors; optical fiber OF0, OF1, OF2 (**a**). The general view of the piezo-elecric sensor (S) (**b**), enlarged view of the piezo-sensor (**c**)

current variation conversion into the indicator frequency is weak at wounding length of 100 m, while, if the current is more than 1000 A, passes through, we could clearly register of variations of the OEO indicating frequency.

8.5.7 OEO Application in Lengthy Communication Links of mm-Wave Range of 60–80 GHz with Large Speed of the Information Transmission Up to 10 Gbit/s

The important application of OEO is in the lengthy radio communication channels (including space communications) of mm-wave range (60–80 GHz) with high speed of information transmission of 10 Gbit/s. Figure 8.25 shows experimental spectra of

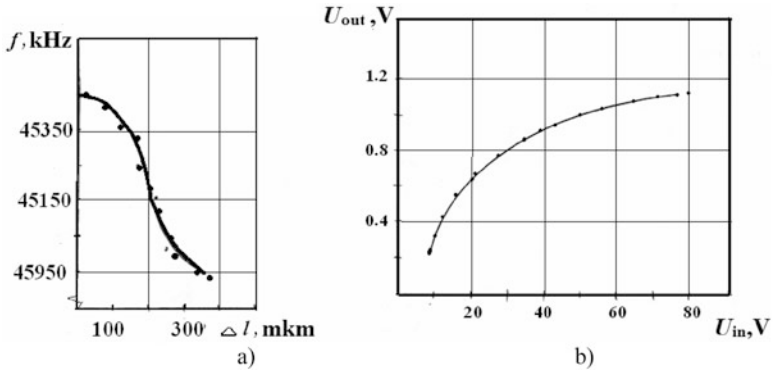

Fig. 8.22 Variation of generated frequency at misalignment of the optical connector OC_3 (**a**). The amplitude characteristics of the piezoelectric sensor for the resonance frequency of 5 kHz of acoustic influences (**b**)

the output optical emission, while Fig. 8.26 presents the experimental block diagram of formation and transmission of the RF signal with the carrier of 60 GHz and the modulation bandwidth of 1 GHz. As we see, the structure in Fig. 8.26 has OEO with the direct QWLD modulation [11]. The central wavelength is 1.55 μm in Fig. 8.25, experimental spectra of optical emission at output of LD_1 (c) and at output of the optical filter (d) in OEO with the frequency 30 GHz (Fig. 8.25). The central wavelength is 1.55 μm. The modulation frequency is 30 GHz. Before the optical filter, the levels of optical components are −25 dBm, 5 dBm, −25 dBm. After optical filter these levels are −17 dBm,12 dBm, 8 dBm.

An analysis of experimental results shows the OEO utilization (the average generation frequency is 30 GHz) with the QWLD direct modulation allows not only obtaining of low value of PSD of phase noise −100 to −110 dB/Hz at offset of 10 kHz (at average generation frequency 60 GHz), but achieving of the high-quality oscillation transmission from the central station to the basing station on the distance of more than 10 km through the fiber-optical communication link.

8.6 Conclusions

We make the general conclusion about promising utilization of QWLD as the modulated light source in OEO in microwave range on the generation frequencies of 8–15 GHz. We offer to use OEO with RF FODL in microwave and mm-wave ranges in onboard of usual stations and the optical radar stations.

As the results of fulfilled experimental investigations of RF and microwave ranges, the following conclusions are made.

On the base of studying of differential modulation characteristics $U(\theta,I_{bias})$ and $\Delta\varphi(\theta,I_{bias})$ during emission pattern scanning for different samples of laser diodes,

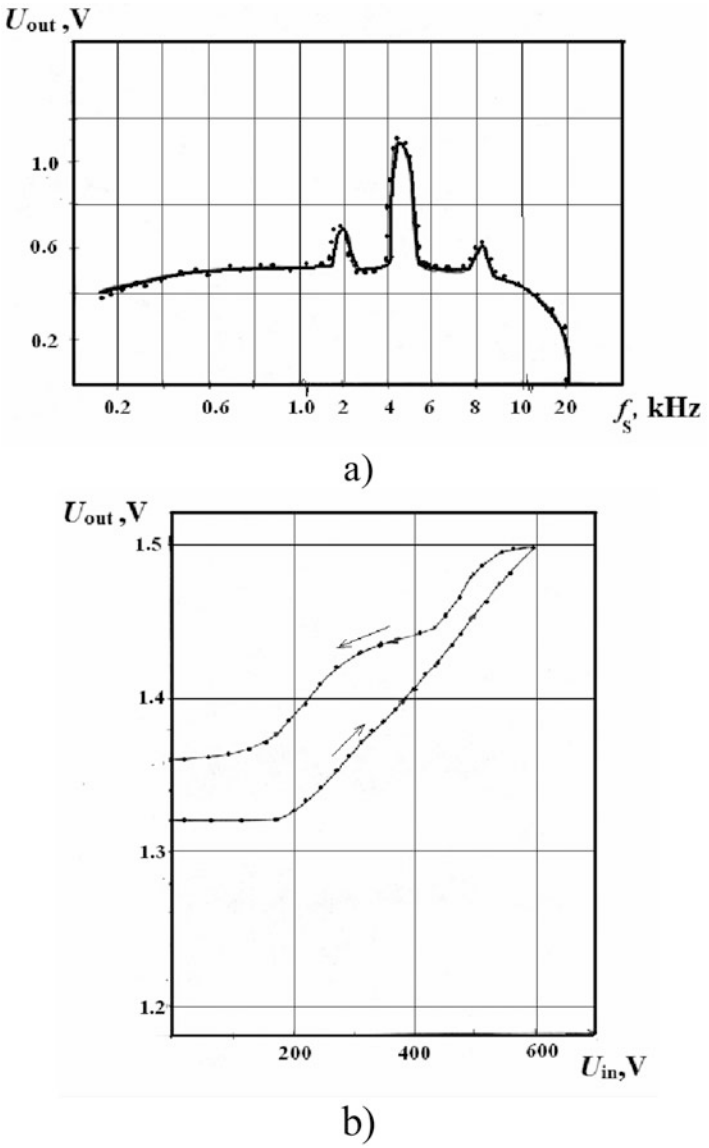

Fig. 8.23 The amplitude-frequency characteristics of the piezoelectric sensor (**a**). Functions of the constant amplitude $U_{out}(U_{in})$ at the output of the OEO frequency detector with the differential fiber-optical delay line versus the constant electric voltage постоянного электрического напряжения U_{in}, applied to the sensor piezoplate (**b**)

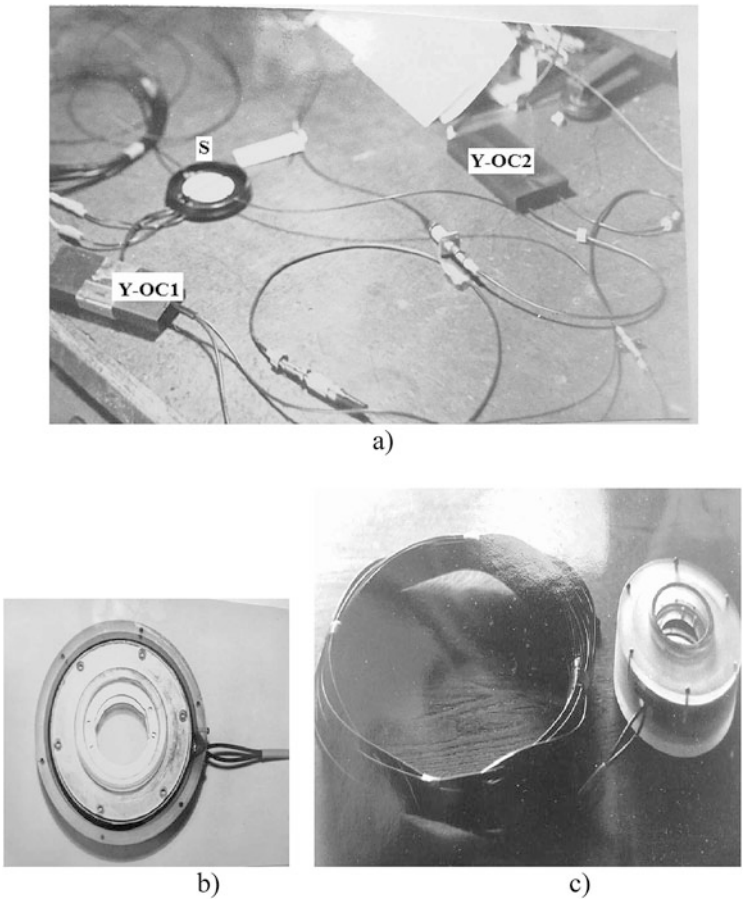

Fig. 8.24 The general view of the electrical voltage indicator with OEO and the piezoelectric sensor S and optical connectors Y-OC1, Y-OC2 (**a**). The inductive magneto-gorge sensor of AC electric current (**b**) and general view of the electric current sensor with the optical cable (**c**)

the conclusion is deduced that at light guide excitation from the laser diode, the effective signal delay (passed through RF FODL) varies approximately by 10–15% from the bias current value and relative spatial location of the exciting light guide and the laser diode.

Utilization of the selector of optical modes in OEO in input of the exciting light guide is necessary since small variations of the signal delay in RF FODL formed by the laser diode, the fiber-optical system, and the phase detector, lead to 10–15%-variations of generation frequency in OEO. Variations of the OEO generation frequency are caused by small bias current drift in the laser diode and are different for various angular deviations of the optical axis of fiber optical system from the optical axis of the laser diode.

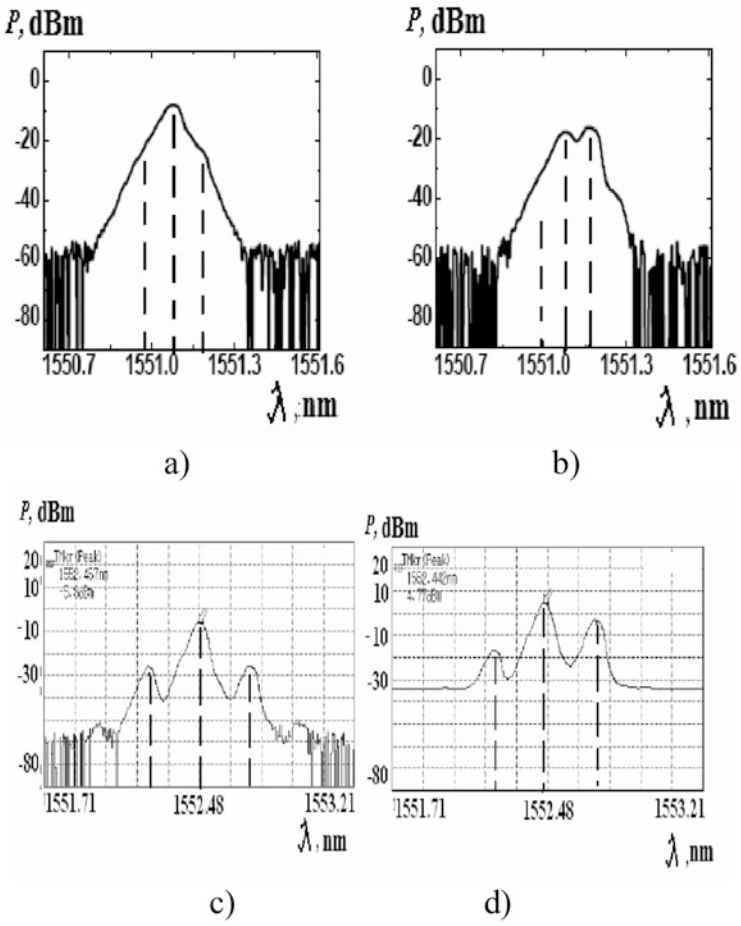

Fig. 8.25 Experimental spectra of output optical emission of LD1 (**a**) and at output of the optical filter (formed by LD2) (**b**) in the OEO with the frequency of 10 GHz. Experimental spectra of output optical emission of LD1 (**c**) and at output of the optical filter (formed by LD2) (**d**) in the OEO with the frequency of 30 GHz

On the base of data obtained, we may make a conclusion about necessity of bias current regulation for the light-emitting diodes and laser diodes used in OEO with RF FODL to values 10^{-4} to 10^{-3}. Measured average slopes S_f of the function $f(I_{bias})$ (at the same offsets $|I_{bias} - I_{thr}|$ from the threshold value I_{thr}) in areas of current variations upper and lower of the threshold value, are approximately equal for OEO with RF FODL and the laser diode are $S_f = \Delta f / \Delta I_{bias} = 15$ kHz/mA.

A phenomenon of polarity change of the laser diode time constant slope and the S_f slope of the function of $f(I_{bias})$ for OEO with the laser diode gives a possibility to select correctly the bias operating currents of the laser diode and the amplitude of the modulation signal as well as to optimize constructions of the laser diode modulator,

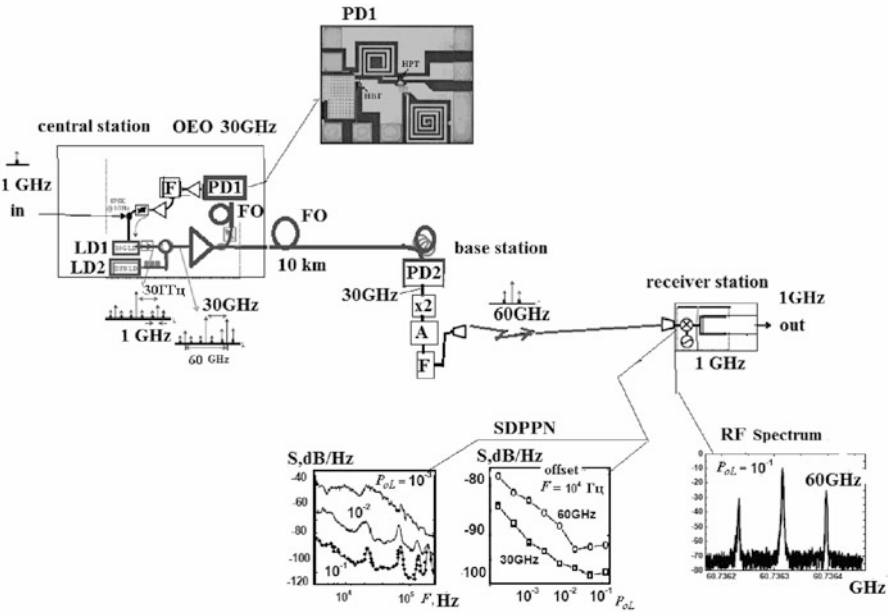

Fig. 8.26 Experimental diagram for radio signal formation on the OEO base (mean frequency 30 GHz) with QWLD direct modulation, and the signal transmission on the carrier 60 GHz and with modulation bandwidth 1 GHz. The optical fiber length in OEO is 2 km. The following abbreviations are introduces: LD1, LD2 = a laser diodes, FO = the fiber optical light guide, PD1, PD2 = the photodetectors, A = the RF amplifier, F = the radio-frequency filter

the matching optical device for the fiber optical system and the temperature-regulated unit. Measured in experiments average slopes S_f of the function $f(I_{bias})$ (at equal offsets $|I_{bias} - I_{thr}|$ from the threshold value I_{thr}) in areas of current variations upper and lower of the threshold value, are approximately equal for OEO with the laser diode and are $S_f = \Delta f/\Delta I_{bias} = 15$ kHz/ma.

The optical coupling arising in the directional coupler of X-type, as shown in Chap. 4, makes the frequency response $f(r)$ periodical with significant values of the conversion "control radial displacement–frequency" slope. Depending on the choice of the "average operating point," the conversion "radial displacement–frequency" slope essentially changes and for maximal values is 0.1 MHz/μm for the experimental sample of OEO with RF FODL.

An influence of optical coupling arising in the directional coupler, as shown in Chap. 4, makes the function $f(r)$ periodical with significant values of the conversion "radial displacement–frequency" slope. On the other hand, for tasks of development of frequency stabilized OEO and the frequency control in its electronic part, it is necessary to use in OEO of the differential RF FODL for coupling of optical channels of directional couplers of Y-type, in which the longitudinal optical coupling is absent of less by several orders.

For the first time, experimental investigations of functional converters of the electric voltage and current on the base of OEO with RF FODL are fulfilled. Measurements of its main characteristics show an expedience of its application at measurement of electrical voltages on large and small values in difficult of access places with strong external spurious electromagnetic fields. In experimental breadboard of the functional converter of "electrical current–frequency" and "voltage–frequency" type are, relatively, 3 kHz/A and 1 kHz/V, which allows effective registration of voltages, currents, and electromagnetic fields in the wide range of amplitudes with a large dynamic range of 10^3–10^4.

In the OEO breadboard of the electric current sensor, the maximal deviations of OEO frequency were measured. They are $\Delta f = 5.0$–10.0 kHz at variation of AC electric current amplitudes $I_c = 750$–1500 A. A possibility of physical impacts conversion to the OEO generation frequency is proved theoretically and experimentally.

As we show, measurements of mechanical displacement during measurement of two parameters of OEO with RF FODL: the frequency f and signal amplitude, increases an accuracy and reliability of mechanical displacement measurements. Double-parameter measurements allows fulfillment of complex compensation against interference caused, for instance, by a temperature and a pressure affecting on the optical fiber. Minimal registered level (sensitivity) of such functional converter of "acoustic oscillation–OEO generation frequency" type is approximately 30 mPa.

Main mechanisms of physical quantities into the frequency and into the phase difference of OEO oscillation are discussed. The functions of OEO frequency for variations of the light guide length and owing to the light guide mode selection on the output are analyzed.

For the first time in Russia, we realized the operating structure of the optoelectronic oscillator in the microwave range at the frequency of 8.2 GHz. A possibility is proved of utilization in OEO with RF FODL in the microwave range of the quantum-dimension laser diode with the ultra-wideband modulation bandwidth as the modulated light source, and also the native ultra-wideband photodiode.

The measured experimental frequency function versus the bias current is closed to the calculated one, and well approximated by the parabolic function. At small bias currents, the variation slope of the generation frequency is 0.3 MHz/mA. For large bias currents of QWLD (by 5–8 times), the slope of frequency variations versus the bias current is 0.003 MHz/mA.

Investigations of frequency functions versus the bias current for different light guide lengths, formed the fiber-optical system, of 1, 3, 60, 70, and 4500 m is performed. We proved that the OEO single-frequency mode of generation in the whole range of bias currents for the filter Q-factor closed to 1000, can be realized at definite light guide length. So, for instance, at fiber length of 60 m, the single-frequency mode without jumps occurred in the whole range of bias currents, while at fiber length of 70 m, the single-mode realized with the jump to adjacent oscillation type. We made to general conclusion about promising of QWLD application as the modulated light source in OEO in the microwave range at frequencies 8–15 GHz.

We offer to use OEO with RF FODL in the microwave and mm-wave ranges in onboard usual radar and optical radar systems.

References

1. X.S. Yao, L. Maleki, Multiloop optoelectronic oscillator. IEEE J. Quantum Electron. **36**(1), 79–84 (2000)
2. D. Eliyahu, L. Maleki, Low phase noise and spurious level in multiloop optoelectronic oscillator, in Proceedings of IEEE International Frequency Control Symposium (2003), p. 405
3. C.W. Nelson, A. Hati, D.A. Howe, Microwave optoelectronic oscillator with optical gain, in Proceedings of the IEEE International Frequency Control Symposium (FCS '07), vol. 31 (7) (2007), pp. 1014–1019
4. W. Zhou, G. Blasche, Injection-locked dual opto-electronic oscillator with ultra-low phase noise and ultra-low spurious level. IEEE Trans. Microwave Theory Tech. **53**(3I), 929–933 (2005)
5. K. Volyanskiy, J. Cussey, H. Tavernier, P. Salzenstein, G. Sauvage, L. Larger, E. Rubiola, `Applications of the optical fiber to the. generation and measurement of low-phase-noise microwave ,J. Opt. Soc. Am. B **25**(12), 2140–2150 (2008)
6. Z. Fan, Q. Qiu, S. Jun, T. Zhang, Tunable low-drift spurious-free optoelectronic oscillator based on injection locking and time delay compensation. Opt. Lett. **44**(3), 534–537 (2019)
7. A.A. Bortsov, Y.B. Il'in, New low-noise UHF oscillator with the pumping by the quantum-well laser diode. Radio-optical technologies in instrumentation: (In Russian), in Proceedings of II Scientific Conference, 14–21 of September 2004,Sochy,70-71,(2004)
8. G.D. Van Wiggeren, R. Roy, Optical communication with chaotic waveforms. Phys. Rev. Lett. **81**(16), 3547–3550 (1998)
9. C.R. Mirasso, I. Fischer, L. Larger, D. Syvridis, Chaotic optical communications. OSA Technical Digest Series, Optical Society of America, 2005, paper FTuA6 (2005)
10. N. Yu, E. Salik, L. Maleki, Ultralow-noise mode-locked laser with coupled optoelectronic oscillator configuration. Opt. Lett. **30**(10), 1231–1233 (2005)
11. K.-H. Lee et al., A 30-GHz self-injection-locked oscillator having a long optical delay line for phase-noise reduction. IEEE Photon. Technol. Lett. **19**(24), 1982–1984 (2008)

Conclusion

To authors' opinion, this book is the new theoretical contribution to investigations of the optoelectronic oscillator with the fiber-optical delay line. The significance of new theory of OEO is determined by the fact that together with many interesting reviews of experimental researches of OEO, for example, prepared by P. Devgan [1], in reviews and manifold papers and reports, extremely small attention is paid to theoretical explanation of formation of small phasenoises in OEO. Methods and the analysis of the amplitude and phase noise described in this book can be used to many systems of the quantum electronics, which are intended for generation of RF oscillations of microwave and mm-wave ranges, and which operation principle is based on heterodyning of two spaced in frequency optical harmonics.

Owing to the new nontraditional approach both for radio engineering and for optics and quantum electronics, authors could discover the main mechanisms of amplitude and phase noise formation in the optoelectronic oscillator. For this, the oscillator under investigation was considered as the unified device, in which two oscillating processes in optical and radio-frequency ranges are developed on frequencies respectively about 129 THz and 10 GHz. The notation of the differential equation system for the optical quantum oscillator (or the laser), which is spanned by the positive feedback, permits to obtain in an explicit form the necessary functional dependences of the power spectral density of the RF noise of OEO as a function of the power spectral density of the spontaneous noise of the laser emission.

To our opinion, this book presents an interest not only as the description of fundamentals of the optoelectronic theory. It contains the rich material on the experimental investigations of OEO.

In Chap. 2 we performed a comparison of many types of RF oscillations sources in microwave and mm-wave ranges with the ultralow phase noise level. We noted that OEO takes the own definite place among known modern RF oscillators. At the necessary choice of parameters of all OEO components, the OEO phase noise are comparable with the phase noise of the least low-noise RF oscillator with the

A. A. Bortsov et al., *Laser Optoelectronic Oscillators*, Springer Series in Optical Sciences 232, https://doi.org/10.1007/978-3-030-45700-6

resonator on the leuco-sapphire crystal as well as the femto-second optoelectronic frequency synthesizer of the RF range.

Authors repeatedly note that the main advantage of OEO and optoelectronic methods of RF oscillations generation is not only a presence of the optical delay line (up to 50 μs at total losses in FODL of −15 to −20 dB) or the optical resonator, but the utilization of heterodyning methods of two spaced in frequency (by 10–80 GHz) optical harmonics, for example, 129 and 139 THz. Exactly statistical averaging at the same amplitude of harmonics and at their photodetection allows achievement of the ultralow values of the phase noise (−130 to −147 dBm/Hz at 1 kHz-offset from the carrier of 10 GHz). In OEO, as in the femto-second synthesizer in the RF range, there is a possibility to extract among initially generated optical harmonics of two optical harmonics. At that, the harmonic difference can be, for instance, 20 or 80 GHz, i.e., is the multiple of the final frequency of RF oscillations in 2 or 8 times. We know that at frequency division by 2 or by 8, we can achieve of the additional benefit in reduction of the phase noise.

In Chap. 3 we examined the modulation and heterodyning methods in OEO. At that, authors placed in the OEO fiber-optical system of the optical filter, which is capable to filter out or to reject of two optical harmonics. The optical filter, which plays an important role, can be placed both in the positive feedback loop and outside of it. We proved that the optical harmonic filtering can be performed by several methods: of the main (central) and the side harmonic, or two side harmonics with the main harmonic suppression. Another important conclusion of the modulation methods' analysis of the laser emission is the fact that in OEO DM and in OEO MZ, the mode of radio frequency doubling is possible. In this mode, the significant possibility of suppression is provided of the DC optical component, which essential noise level worsens the suppression of the OEO phasenoises.

We stated that it is necessary to introduce in OEO of the optical rejection filter tuned on the central optical frequency and to achieve of DC component suppression. In OEO MZ, as authors show, we can achieve the effective suppression of the DC optical carrier at the value of the ratio of the first harmonic voltage amplitude in the MZ input to the amplitude of the DC bias in MZ in the mode "180°", at that, the ratio $U_{1MZ}/U_{0MZ\pi}$ should be $x = U_{1MZ}/U_{0MZ\pi} = 2.4$.

The special pole in Chap. 3 is paid to laser representation in OEO as the main source of fluctuations, which has the quantum nature. We show that the phase noise dispersion of the laser σ_E^2 is defined by the dispersion of carriers noise ξ_N and depends upon the life timeT_1 on the excited level. The phase noise level of OEO is determined by the phase noise of the laser, which depends on the noise time T_1.

In Chap. 4 authors investigate the laser (or QWLD) included in the OEO structure with utilization of the classic methods of the oscillation theory. We developed the quantum generator theory, from the point of view of radio physics. This approach is described by V. Shtykov and S. Smolskiy in the excellent textbook on quantum electronics [2].

In our book, at derivation of the constitutive equations of the laser in the semiclassical approximation, we reduced the system from three differential

equations (complicated for analysis) to the single differential equation of the fourth order. At that, the inertial nonlinear element was extracted and analyzed, its mathematical model is examined. We used for the QWLD analysis methods, which are widely applied in the oscillations theory; we investigated the stability of the steady-state modes of QWLD. The special attention was attracted to the laser operation on the boundary of the stable mode ultrahigh power density of the laser optical resonator. Original results of the laser investigation described in this book are relevant, because in many labs of the world, at present, the application ideas of optical micro-tori or the micro-resonators have got the development in the laser systems. We would like to note that first investigations of micro-tori application in quantum systems were made by Soviet and Russian physicist V.B. Braginsky [3] and they are seriously advanced by researches of his pupil M.L. Gorodetsky [4], as well as the teams of A.B. Matsko, L. Maleki, V.S. Ilchenko [5], and by others.

The second, third, fourth, and fifth chapters of this book are devoted to the methods to obtain of differential "abbreviated" equations on the base of Evtianov approach [6] for OEO with external and direct modulation of the laser. In fourth, fifth and sixth chapters, relying on the Evtianov–Kuleshov method [7] for the noise analysis in traditional electronic oscillators, as well as on researches of Tikhonov [8] and Goodmen [9] on the statistical analysis, relatively, RF and optical systems, we developed the main methods for the amplitude and phase noise analysis in OEO MZ and OEO DM. We could obtain the strict mathematically well-found formulas for amplitude and phase noises in OEO depending on the spontaneous laser noise, the delay time in the optical fiber, the laser coherence time, and its power. At that, formation of the final phase RF noises of OEO is examined as the result of the convolution operation of the laser optical spectrum and the RF spectrum of the oscillation acting in the Mach–Zehnder modulator input. One of the results of our analysis is that we could show how the PSD level of the "resonance peak," which is caused by the relaxation electron–photon resonance in the laser, influences on PSD of the phase noise in OEO. The influence of the ratio of the laser coherence time to the delay time in the optical fiber upon the OEO phase noise is another important result, as well as the influence of the amplitude levels of optical harmonics in the structure of the single-channel modulation in the MZ modulator. We noted that equalization of the optical power in different optical channels allows the significant suppression of the optical carrier, which leads also to reduction of the OEO phase noise level.

In Chap. 6, we discuss the detailed description of the modulation methods and constructions of the modern Mach–Zehnder modulators. This gives us a possibility to show that utilization of the double-channel modulation (or RF modulation of two "parallel-coupled" modulators, which are mounted on the single substrate) not only increases the amplitude level of RF output oscillation in OEO MZ, but, at that, phasenoises caused by the laser, the photoreceiver, the RF amplifier are significantly suppressed. We note that in the double-channel structure, the essential role in noisesuppression is played also by the "absolute" equalization of the optical power passed in different MZmodulators.

The sixth chapter describes the calculation approach of the nonsymmetrical optical channel included in the OEO structure. The beginning of Chap. 7 has something in common with Chap. 4 in the description style because we perform in it the investigation of the waveguide section. We showed that methods of the OEO phase noisesuppression are not exhausted by development of the high-coherent lasers, wideband modulators and photodetectors (with the modulation band 10–60 GHz), but widen with utilization of the spatial methods of laser emission selection. At that, we can use of different filters and optical Fourier transforms [10], which are known from the adaptive optics and are successfully suppressed of the optical carrier, noises and extracting the useful signal.

To the one of advantage of Chap. 7 we can attribute the fact that we considered methods of the phase and frequency automatic control systems, which are capable to decrease the OEO phase noise by 10–15 dBm/Hz.

The large section in Chap. 7 is devoted to experimental investigations of the long-term frequency stability in OEO and the parametric frequency stability of OEO from temperature of the optical fiber. Described results of temperature researches within the limits of 0–120 °C allow development of the thermal-stabilized optical fiber for FODL in OEO, as well as the patented OEO system with two optical resonators, which is stable to temperature variations. On the base of the model of optical mode coupling, we explain of the observed in the experiments the oscillating character of the temperature dependence in the multi-mode optical fibers and in systems of coupled optical fibers.

The description of several patents developed by authors is presented in Chaps. 7 and 8: the OEO sensor with division of the frequency measurement and the phase difference measurement, OEO with differential delay line with application of Y- and X-fiber-optical couplers. We think that frequency and amplitude functions in OEO at variations of the excitation conditions of optical fibers in different branches will be interesting for readers. The special interest is represented of the oscillating functions of the OEO frequency with the differential FODL with the X-coupler.

Original results of experimental amplitude, frequency and phase responses in OEO of the microwave and mm-wave ranges are described in Chap. 8. We would like to specially emphasize of the hysteresis frequency functions in OEO with the "spasmodic transition" at the single-frequency generation. Frequency jumps are caused by the fulfillment of the excitation conditions for many types of oscillations at increase of the geometrical length of the optical fiber, and the hysteresis character is defined by the inertial nonlinear characteristic of OEO nonlinear elements.

We would like to note that conducted tedious laser investigations, which are included in the OEO structure, permits to reveal the interesting physical phenomena. The bifurcation of the laser directional pattern is one of such phenomena. Theoretical explanation of this phenomenon is presented in Chap. 7, at the examination of nonsymmetric active and passive waveguide optical structures. The phenomenon of the slope polarity sign change in the frequency response of OEO at variation of the pumping current can be attributed to another new physical phenomenon, which are discussed in Chaps. 7 and 8.

In Chap. 8, we describe in brief the various structures of OEO applications as the source of microwave and mm-wave oscillations with the ultralow PSD level of the phase noise of −130 to −147 dBm/Hz at 1 kHz-offset from the carrier of 10 GHz [11]. We discuss structures and systems, in which OEO performs the role of the master oscillators and local oscillators in optical and RF radar systems, in systems of information transmission with masking at utilization of the stochastic methods; in sensors of various physical quantities.

We can for sure certify that the further progress in direction of phase noisesuppression in OEO, which operate in microwave and mm-wave ranges, relates with development of manufacture technologies of commercially available low-noise single-frequency QWLDs, MZmodulators, photodetectors, low-noise amplifiers. The development of technologies directed on manufacture of micro- and miniaturization of the fiber-optical delay lines with the delay times of 1 – 20 μs are promising as well. We noted in the book that appearance in the market of modern perforated optical fibers with optical losses less than 0.001 dB per one band of optical fiber with the bend radius of 1–5 mm, facilitates to investigations of compact OEO MZ and OEO DM.

References

1. P. Devgan, *A Review of Optoelectronic Oscillators for High Speed Signal Processing Applications. ISRN Electronics,V. 2013* (Hindawi Publishing Corporation, London, 2013)., Article ID 401969, 16 pages
2. V.V. Shtykov, S.M. Smolskiy, *Introduction to Quantum Electronics and Nonlinear Optics. Lectures for University Students* (Springer, New York, 2020), 341 p
3. V.B. Braginsky, M.L. Gorodetsky, V.S. Ilchenko, Quality-factor and nonlinear properties of optical whispering gallery modes. Phys. Lett. A. V. **137**, 393–397 (1989)
4. M.L. Gorodetsky, A.A. Savchenkov, V.S. Ilchenko, Ultimate Q of optical microsphere resonators. Opt. Lett. **21**, 453–455 (1996)
5. V.S. Ilchenko, M.L. Gorodetsky, Y.X. Steve, L. Maleki, Microtorus: a high finesse microcavity with whispering-gallery modes. IEEE Photon. Technol. Lett. **26**(5), 256–258 (2001)
6. I.V. Komarov, S.M. Smolskiy, *Fundamentals of Short-Range FM Radar* (Artech House, Norwood, 2003)
7. V. Zhalud, V.N. Kuleshov, *Noise in Semiconductor Devices. Under Edition of A.K. Naryshkin* (Sovetskoe Radio, 416 p. (in Russian), Moscow, 1977)
8. B.T. Gorianov, A.G. Zhuravliov, V.I. Tikhonov, *Statistical Radio Engineering. [In Russian]* (Sovetskoe Radio Publisher, Moscow, 1980)
9. J.W. Goodman, *Speckle Phenomena in Optics: Theory and Applications* (Roberts and Company Publishers, Englewood, 2006)
10. H. Stark (ed.), *Applications of Optical Fourier Transforms* (Academic Press, New York, 1982)
11. A.A. Bortsov, S.M. Smolskiy, Optoelectronic oscillator as the time correlator with ultralow phase noise. Opt. Eng. **59**(6), 061618 (2020). https://doi.org/10.1117/1.OE.59.6.061618

A. A. Bortsov et al., *Laser Optoelectronic Oscillators*, Springer Series in Optical Sciences 232, https://doi.org/10.1007/978-3-030-45700-6

Index

A. A. Bortsov et al., *Laser Optoelectronic Oscillators*, Springer Series in Optical Sciences 232, https://doi.org/10.1007/978-3-030-45700-6